

Geological Characterization of Cataclastic Rock Samples Using Medical X-ray Computerized Tomography: Towards a Better Geotechnical Description

THÈSE N° 4316 (2009)

PRÉSENTÉE LE 19 JUIN 2009

À LA FACULTÉ ENVIRONNEMENT NATUREL, ARCHITECTURAL ET CONSTRUIT
Laboratoire de géologie de l'ingénieur et de l'environnement
SECTION DE GÉNIE CIVIL

ÉCOLE POLYTECHNIQUE FÉDÉRALE DE LAUSANNE

POUR L'OBTENTION DU GRADE DE DOCTEUR ÈS SCIENCES

PAR

Pierre Guillaume **CHRISTE**

acceptée sur proposition du jury:

Prof. A. Schleiss, président du jury
Prof. A. Parriaux, Dr V. Labiouse, directeurs de thèse
Prof. P. Marinos, rapporteur
Prof. G. Viggiani, rapporteur
Prof. J. Zhao, rapporteur



ÉCOLE POLYTECHNIQUE
FÉDÉRALE DE LAUSANNE

Lausanne, EPFL
2009



ABSTRACT

Technical difficulties associated with tunnelling operations in tectonized geological settings are frequently encountered. They may include instantaneous and delayed cavity convergence, sudden collapse of walls or roof of a gallery, outpouring of fault-filling materials and water inflows. These phenomena may negatively affect economical and safety aspects of construction sites. The present study refers to two previous research projects conducted at the EPFL addressing the problem of an improved geological and geomechanical characterization of weak cataclastic rocks in underground excavation works (*Cataclastic fault rocks in underground excavations, a geological perspective*, Bürgi, 1999; *Caractérisation géomécanique de roches cataclastiques rencontrées dans des ouvrages souterrains alpins*, Habimana, 1999).

Cataclasis is an evolutionary rock degradation process in time and magnitude related to fault zone activity in the Earth's crust. A conceptual model describing the occurrence and variability of cataclastic rocks at shallow crustal conditions is proposed in this research. It describes environment of fault zones based on both theoretical considerations and field experiences collected during self-realized short-drilling operations performed in contrasted petrological settings. The model considers cataclasis from a regional perspective (macroscopic scale) down to its microscopic manifestations on rock materials. Cataclastic rock characteristics are strongly influenced by the degree of tectonic solicitation and the initial rock composition. Guidelines about specific damage microstructures diagnostic of the cataclastic intensity and function of the initial rock protolith can meaningfully assist the interpretation of rock specimens recovered from reconnaissance drilling operations. Despite the poor mechanical quality often observed for such samples and their readiness to collapse, this study demonstrates that the *in situ* extraction of cataclastic specimens can be largely improved with the use of a high-quality drilling equipment. Accordingly, with the availability of representative materials for subsequent studies, the uncertainties affecting the geological prognosis can be strongly limited at a preliminary stage of geotechnical studies.

It is shown that the geotechnical characterisation of cataclastic rock cores by means of laboratory investigations requires combining information about rock microstructure and mineralogy with strain-stress relationship derived from triaxial compression tests. Such a framework makes it possible to interpret and explain the specific mechanical behavior of heterogeneous-anisotropic rock materials in a much more coherent manner. With this regard, the approach followed by Bürgi (1999) with a mineralo-structural index (MSI) determined on 2D thin sections and proposed to predict cataclastic rock strength based on geological evidences, is found to have potential for geotechnical studies. However, Bürgi's approach still faces heavy criticism in the light of the practical application. Its limitations are detailed and discussed in this study.

Accounting for both aspects of the rock characterization procedure, an operational methodology is therefore proposed aiming at its application in geotechnical studies. The medical X-ray computerized tomography (XRCT) has been specifically implemented in this context for the analysis of geotechnical rock cores, as a non-destructive technique which allows a rapid indirect imaging of the rock core structure before any further analytical manipulations are conducted. The technique is found facilitating to a great extent the study of cataclastic materials.

An irradiation protocol has been defined and an acquisition strategy minimalizing inherent artifacts of the XRCT technique has been tested. Obtained results are highly encouraging. Moreover, an image analysis tool has been developed in order to improve the segmentation of geological damage features from indirectly recorded X-ray models. As discussed in details within this study, a critical analysis of 3D segmented models corresponding to sample structures *before* and *after* mechanical tests is thought to be capable to improve the triaxial test interpretation. The XRCT is therefore envisaged as a bridge technique permitting an improved correlation between specific properties of cataclastic rocks based on indirect evidences. With it, the geological and mechanical characterizations can be performed on the exactly same samples, reducing uncertainty in the characterization procedure. This step goes towards the development of a precise geotechnical classification for cataclastic rocks. Based on the XRCT technique, it is also discussed how Bürgi's approach could be translated in a three-dimensional form to reach a wider agreement.

Based on a database of carbonatic cataclasites, it is evidenced that cataclastic strength and deformation properties are strongly influenced by textural and structural characteristics of pre-existing damage microstructures. Strength

data obtained in this research show that in the same fault zone environment, different mode of deformations affect cataclastic rocks and that peak triaxial strength can vary significantly. Heterogeneity and material anisotropy are prime factors affecting specific behaviors of cataclastic rocks. Therefore, it is suggested to incorporate geological features into constitutive frameworks which describe mechanical behavior of such materials. This last aspect constitutes a very stimulating research field where further work is needed today.

Key words: Cataclasis, rock cores, characterization, damaged structure, texture, triaxial tests, fracturing, XRCT

RÉSUMÉ

Les difficultés techniques associées aux opérations en tunnels dans des milieux géologiques tectonisés sont fréquemment rencontrées. Celles-ci concernent des convergences instantanées ou différées de la cavité, des écroulements soudains des parois ou du toit de la galerie, des déboulements de failles et des venues d'eau. Ces phénomènes sont susceptibles d'affecter négativement les aspects économiques et la sécurité des chantiers de construction. La présente étude se réfère à deux précédents projets de recherche conduits à l'EPFL questionnant l'amélioration de la caractérisation géologique et géomécanique de roches cataclasées en travaux souterrains (*Cataclastic fault rocks in underground excavations, a geological perspective*, Bürgi, 1999; *Caractérisation géomécanique de roches cataclastiques rencontrées dans des ouvrages souterrains alpins*, Habimana, 1999).

La cataclase est un phénomène évolutif de dégradation du matériel rocheux en temps et en intensité qui est lié à l'activité de failles affectant la croûte terrestre. Un modèle conceptuel décrivant l'apparition et la variabilité de roches cataclasées dans la partie supérieure de l'écorce terrestre est proposé dans cette recherche. Il décrit les environnements de failles sur la base de considérations théoriques et d'expériences récoltées sur le terrain lors de la réalisation de forages courts dans des contextes pétrologiques variés. Le modèle considère la cataclase en partant d'un point de vue régional (échelle macroscopique) jusqu'à ses manifestations microscopiques sur les matériaux rocheux. Les caractéristiques des roches cataclasées sont fortement influencées par le degré de la sollicitation tectonique ainsi que par la composition initiale de la roche. Des directives sur des microstructures d'endommagement diagnostiques de l'intensité de cataclase et fonction de la protolite rocheuse initiale peuvent assister d'une manière significative l'interprétation d'échantillons récupérés durant des forages de reconnaissance. Malgré la qualité mécanique médiocre affectant souvent de tels échantillons ainsi que leur propension à la désintégration, cette étude démontre que l'extraction *in situ* de roches cataclasées peut être largement améliorée au moyen d'un équipement de forage de haute qualité. Conformément à cela, en disposant de matériaux représentatifs pour des études ultérieures, l'incertitude qui affecte le pronostic géologique peut être fortement réduite à un stage préliminaire des études géotechniques.

Il est démontré que la caractérisation géotechnique en laboratoire de carottes de forages cataclasées demande à ce que des informations relatives à la microstructure et la minéralogie soit mises en lien avec les relations de contrainte-déformation dérivées de tests de compression triaxiale. Un tel cadre rend possible d'une manière beaucoup plus cohérente l'interprétation et l'explication du comportement mécanique spécifique relatif aux matériaux rocheux hétérogènes-anisotropes. En ce sens, l'approche poursuivie par Bürgi (1999) au moyen d'un indice minéralo-structural (MSI) déterminé sur lames minces 2D et proposé pour prédire la résistance de roches cataclasées en fonction d'évidences géologiques semble prometteuse dans le cadre d'études géotechniques. Cependant, l'approche de Bürgi se confronte toujours à une forte critique en vue d'une application pratique. Les limitations de cette approche sont détaillées et discutées dans cette étude.

En intégrant les deux aspects de la procédure de caractérisation, une méthodologie opérationnelle est ainsi proposée visant son application dans les études géotechniques. La tomographie médicale par rayons-X (XRCT) a été spécifiquement implémentée dans ce contexte pour l'analyse de carottes de forages géotechniques en tant que méthode non-destructive permettant une imagerie indirecte rapide de la structure de la carotte avant la conduite de procédures analytiques ultérieures. La technique est démontrée faciliter grandement l'étude de matériaux cataclasés.

Un protocole d'irradiation a été défini et une stratégie d'acquisition qui minimise les artefacts inhérents à la technique XRCT testée. Les résultats obtenus sont hautement encourageants. Parallèlement à cela, un outil d'analyse d'images a été développé qui permet sur la base des modèles indirects enregistrés la segmentation améliorée d'évidences géologiques d'endommagement. Tel que discuté en détail au sein de cette étude, une analyse critique des modèles 3D segmentés correspondant aux structures d'échantillons *avant* et *après* test mécanique est estimée capable d'améliorer l'interprétation des tests triaxiaux. La XRCT constitue en ce sens un pont qui permet une corrélation améliorée entre des propriétés spécifiques de roches cataclasées sur la base d'évidences indirectes. Grâce à elle, les caractérisations géologique et mécanique peuvent se faire sur les mêmes échantillons, réduisant de ce fait l'incertitude de la procédure de caractérisation. Ce pas va dans la direction du développement d'une classification géotechnique détaillée pour roches cataclasées. Sur la base de technique XRCT, il est également discuté comment l'approche de Bürgi pourrait être

retranscrite dans une forme tridimensionnelle afin d'obtenir son accord plus large.

Une base de données produites sur des cataclasites carbonatées démontre que la résistance et la déformation cataclastiques sont fortement influencées par les caractéristiques texturales et structurales de microstructures d'endommagement préexistantes. Les données de résistance obtenues dans cette recherche indiquent qu'au sein d'un même environnement de faille, différents modes de déformation affectent les roches cataclasées et que la valeur de résistance triaxiale de pic peut varier de manière significative. L'hétérogénéité et l'anisotropie du matériel sont des facteurs de première importance influençant les comportements spécifiques de roches cataclasées. Il est ainsi suggéré d'introduire des éléments de géologie dans les modèles constitutifs décrivant le comportement mécanique de tels matériaux. Ce dernier aspect constitue un domaine de recherche très stimulant dans lequel des investigations supplémentaires demandent à être réalisées aujourd'hui.

Mots clés: Cataclase, carottes de forage, caractérisation, structure d'endommagement, texture, tests triaxiaux, fracturation, XRCT

TABLE OF CONTENTS

| | | |
|----------|--|----|
| 1 | ENGINEERING UNCERTAINTY RELATED TO WEAK ROCK MASSES | 1 |
| 1.1 | CATACLASIS IN ENGINEERING GEOLOGY | 3 |
| 1.2 | COMMON PROBLEMS ENCOUNTERED IN TUNNELLING | 4 |
| 1.3 | A RATIONAL APPROACH FOR A GEOLOGICAL QUALITY INPUT IN UNDERGROUND CONSTRUCTIONS | 6 |
| 1.4 | AN INTERDISCIPLINARY RESEARCH FIELD | 7 |
| 2 | THE CATACLASIS – STATE OF THE ART | 9 |
| 2.1 | GENETIC CONSIDERATIONS..... | 11 |
| 2.1.1 | Mechanisms Of Brittle Deformation | 12 |
| 2.1.1.1 | Cataclastic flow or cataclasis..... | 13 |
| 2.1.1.2 | Crystal plasticity | 14 |
| 2.1.1.3 | Other mechanisms..... | 14 |
| 2.1.2 | Implication For Fault-Zone Generation | 16 |
| 2.1.3 | Rheological Implications | 17 |
| 2.2 | INFLUENCE OF THE INITIAL PROTOLITH COMPOSITION..... | 19 |
| 2.3 | TERMINOLOGY FOR TECTONIZED ROCKS | 21 |
| 2.4 | GLOSSARY OF TERMS RELATED TO CATACLASTIC MATERIALS..... | 22 |
| 2.4.1 | Primary Rock Matrix..... | 22 |
| 2.4.2 | Cataclastic (Damaged) Rock Matrix..... | 23 |
| 2.4.3 | Blocks & Clasts..... | 23 |
| 2.4.4 | Fractures..... | 23 |
| 2.4.5 | Damage Indicators | 24 |
| 2.5 | CONCLUDING REMARKS | 24 |
| 3 | PREVIOUS RESEARCH AT EPFL | 27 |
| 3.1 | CONSIDERATIONS ON ROCK MASS CHARACTERIZATION..... | 28 |
| 3.1.1 | Why Rock Mass Characterization?..... | 28 |
| 3.1.1.1 | The Q-system of Barton..... | 29 |
| 3.1.1.2 | The RMR of Bieniawski..... | 30 |
| 3.1.1.3 | The GSI of Hoek | 31 |
| 3.1.2 | How to Translate Geology into Numbers?..... | 33 |
| 3.2 | THE APPROACH OF BÜRGI & HABIMANA (1999)..... | 35 |
| 3.2.1 | A Combined Geological and Geomechanical Approach | 35 |
| 3.2.2 | Geological Investigations..... | 36 |
| 3.2.3 | A Mineralogical and Structural Index for Cataclastic Rocks..... | 37 |
| 3.2.4 | Geomechanical Investigations | 38 |
| 3.2.5 | Rupture Criterion For Cataclastic Rocks | 39 |
| 3.3 | CORRELATION BETWEEN GEOLOGICAL CHARACTERISTICS AND GEOMECHANICAL ... PROPERTIES | 42 |
| 3.3.1 | Correlation Chart Between MSI and Triaxial Data (1999) | 42 |
| 3.3.2 | Limitations and Perspectives..... | 43 |
| 3.3.3 | MSI Evidences From New Petrological Contents (2007)..... | 43 |
| 4 | CURRENT PROJECT DESCRIPTION | 47 |
| 4.1 | PURPOSE OF THIS RESEARCH | 48 |
| 4.2 | ECHO OF THE RESEARCH FROM 1999..... | 48 |
| 4.3 | A CONCEPTUAL MODEL FOR THE OCCURRENCE OF CATACLASTIC ROCK MASSES ... | 50 |
| 4.4 | GENERAL METHODOLOGY | 53 |
| 4.5 | METHODOLOGICAL INSIGHTS | 53 |
| 4.5.1 | Sampling..... | 53 |
| 4.5.2 | Sample Preparation | 53 |
| 4.5.3 | Geological Characterization | 54 |
| 4.5.4 | Mechanical Characterization | 54 |

Table of contents

| | | |
|----------|---|------------|
| 4.6 | CONSIDERATIONS ABOUT HETEROGENEITY AND ANISOTROPY..... | 56 |
| 4.7 | FROM 2D TO 3D EVIDENCES | 57 |
| 5 | SAMPLING SITES..... | 59 |
| 5.1 | PETROLOGICAL VARIETY | 60 |
| 5.2 | GEOTECHNICAL ROCK CORES | 60 |
| 5.3 | SAMPLING SITES..... | 63 |
| 5.3.1 | N16 Highway Moutier Tunnel..... | 63 |
| 5.3.2 | Tridel Gallery Lausanne..... | 66 |
| 5.3.3 | Belmont Landslide Area | 66 |
| 5.3.4 | N16 Highway Roche St Jean Tunnel | 67 |
| 5.3.5 | A9 Highway Glion Tunnel | 69 |
| 5.3.6 | A9 Highway Eyholz Tunnel..... | 71 |
| 5.3.7 | Hongrin Dam Site | 71 |
| 5.3.8 | AlpTransit Gotthard Base Tunnel, Amsteg..... | 72 |
| 5.3.9 | AlpTransit Ceneri Base Tunnel, Sigirino | 74 |
| 6 | SAMPLING TECHNIQUE..... | 77 |
| 6.1 | DESIGN OF THE SYSTEM | 78 |
| 6.2 | EXPERIENCE | 81 |
| 6.3 | FURTHER DEVELOPMENTS | 81 |
| 7 | METHOD OF GEOLOGICAL CHARACTERIZATION..... | 83 |
| 7.1 | BULK APPARENT CHARACTERIZATION..... | 84 |
| 7.1.1 | Direct Evaluation | 84 |
| 7.1.2 | Indirect Evaluation..... | 86 |
| 7.2 | DETAILED GEOLOGICAL CHARACTERIZATION | 87 |
| 7.2.1 | Mineralogical Analyses | 87 |
| 7.2.1.1 | X-Ray Diffractometry (XRD) | 88 |
| 7.2.1.2 | Electron Microscope Techniques..... | 88 |
| 7.2.2 | Microstructural Analyses | 89 |
| 7.2.2.1 | Impregnation of cataclastic rocks for thin section preparation..... | 89 |
| 7.2.2.2 | The texture coefficient TC | 90 |
| 7.2.2.3 | The matrix coefficient MC..... | 91 |
| 8 | X-RAY COMPUTERIZED TOMOGRAPHY (XRCT) APPLIED TO ROCK CORE | 95 |
| | SAMPLES | 95 |
| 8.1 | PRINCIPLES OF XRCT ACQUISITION | 96 |
| 8.2 | OVERVIEW OF CT-TECHNIQUES APPLICATION TO ROCK SAMPLES | 99 |
| 8.3 | ROCK CORES OF GEOTECHNICAL DIMENSIONS vs. XRCT | 99 |
| 8.3.1 | XRCT Equipment Used in this Study | 101 |
| 8.3.2 | X-Ray Interactions With Rock Materials | 101 |
| 8.3.3 | Elimination of Beam Hardening Effects | 103 |
| 8.3.4 | Signal Reconstruction over Extended Range of HU Units..... | 103 |
| 8.4 | 3D RECONSTRUCTIONS | 105 |
| 9 | METHODS FOR A GEOMECHANICAL CHARACTERIZATION OF CATACLASTIC ROCK CORES | 107 |
| 9.1 | Characterization by Means of Strength Data | 108 |
| 9.1.1 | Triaxial Tests..... | 109 |
| 9.1.2 | Evaluation of Mechanical Behaviors | 111 |
| 9.1.3 | Complementary Mechanical Investigations | 112 |
| 9.1.3.1 | Uniaxial Compression..... | 112 |
| 9.1.3.2 | Direct Shear Test..... | 113 |

Table of contents

| | | |
|-----------|---|------------|
| 9.1.3.3 | Tensile Strength | 113 |
| 9.1.3.4 | Impregnation of Triaxially Deformed Rock Core | 114 |
| 9.2 | Characterization Using Indirect Techniques | 114 |
| 9.2.1 | XRCT Recording of Rock Samples Before and After Triaxial Test | 114 |
| 9.2.1.1 | Back-Analysis of Triaxial Data Based on XRCT Evidence of Fracture Patterns | 115 |
| 9.2.1.2 | Evolution of Damage Indicators Under Triaxial Deformation | 117 |
| 10 | METHOD OF CATACLASTIC ROCK CORE CHARACTERIZATION..... | |
| | IMPLEMENTING MEDICAL XRCT | 119 |
| 10.1 | IMAGE ANALYSIS TECHNIQUE – CARact 3D METHOD..... | 120 |
| 10.1.1 | Detection Principles and Geological Features of Interest..... | 121 |
| 10.1.2 | Segmentation Method and Application | 121 |
| 10.1.3 | Primary Segmentation (global) | 124 |
| 10.1.4 | Secondary Segmentation (local)..... | 125 |
| 10.1.4.1 | Mathematical Formulation of the Secondary Segmentation | 127 |
| 10.1.5 | Noise Elimination | 129 |
| 10.1.6 | Overdensity Elimination | 130 |
| 10.1.7 | Results and Preliminary Discussion | 130 |
| 10.2 | CATACLASTIC ROCK CORE CHARACTERIZATION USING MEDICAL XRCT | 132 |
| 10.2.1 | Derivation of TC & MC from XRCT slices | 132 |
| 10.2.2 | Study of Damage Indicators from XRCT | 134 |
| 10.2.2.1 | Quantification of Damage Indicators..... | 134 |
| 10.2.2.2 | 3D Visualization of Damage Indicators..... | 134 |
| 11 | RESULTS OF THE GEOLOGICAL CHARACTERIZATION | 137 |
| 11.1 | RESULTS OF THE BULK CHARACTERIZATION | 138 |
| 11.1.1 | Definition of Quality Classes for the RSJ Samples | 138 |
| 11.1.2 | Comparison with GSI criteria..... | 140 |
| 11.1.3 | Quantification of Damage Indicators | 140 |
| 11.1.3.1 | Best-fit segmentation of XRCT data | 140 |
| 11.1.3.2 | Confrontation with visual classes | 143 |
| 11.2 | RESULTS OF THE DETAILED CHARACTERIZATION: MSI DETERMINATIONS FROM THIN SECTIONS & AXIAL CT-SLICES..... | 143 |
| 11.2.1 | Mineralogical Composition (mwVh Parameter) | 144 |
| 11.2.2 | Structural & Textural Characterization (TC & MC Parameters)..... | 145 |
| 11.3 | RESULTS FROM THE INDIRECT XRCT CHARACTERIZATION..... | 146 |
| 11.3.1 | TC & MC Determinations Using XRCT Data | 146 |
| 11.3.2 | Observed Variability on Frontal & Sagittal Planes | 149 |
| 11.3.3 | XRCT-Derived MSI Determinations..... | 149 |
| 11.4 | 3D RECONSTRUCTIONS OF SEGMENTED MODELS..... | 151 |
| 11.5 | PETROGRAPHICAL DIAGNOSTIC BETWEEN THIN SECTIONS & XRCT DERIVED ANALYSES | 154 |
| 11.6 | DISCUSSION..... | 154 |
| 12 | RESULTS FROM MECHANICAL TESTS | 157 |
| 12.1 | TEST RESULTS: STRENGTH DATA..... | 159 |
| 12.1.1 | Evaluation of Triaxial Stress Data: Peak & Residual Behaviors | 159 |
| 12.1.2 | Mechanical Behaviors of RSJ Samples | 161 |
| 12.1.3 | Re-Interpretation of Rupture Angles by Means of XRCT | 163 |
| 12.1.4 | Analysis of Mohr Residual Circles | 166 |
| 12.2 | RESULTS OF XRCT CHARACTERIZATION AFTER DEFORMATION | 169 |
| 12.2.1 | Damage Index Determinations After Triaxial Test..... | 169 |
| 12.2.2 | Reconstruction of Segmented XRCT Stacks After Test | 171 |
| 12.2.3 | Comparison with Models Before Tests: Test Induced Fracturation | 171 |
| 12.3 | DISCUSSION..... | 174 |

Table of contents

| | | |
|-----------|---|-----|
| 13 | TOWARDS A BETTER GEOTECHNICAL DESCRIPTION? | 177 |
| 13.1 | GEOLOGICAL ROCK CORE CHARACTERIZATION | 178 |
| 13.1.1 | MSI-Determinations from XRCT Data..... | 179 |
| 13.1.1.1 | Parameters constitutive of the TC | 179 |
| 13.1.1.2 | Parameters constitutive of the MC | 181 |
| 13.1.1.3 | Synthesis from TC & MC determinations | 184 |
| 13.1.1.4 | Implications of a cataclastic gradient for MSI determinations | 186 |
| 13.1.1.5 | Attempt of correlation between the MSI and triaxial strength..... | 189 |
| 13.2 | MECHANICAL ROCK CORE CHARACTERIZATION | 192 |
| 13.2.1 | Use of XRCT Models Before and After Triaxial Tests | 193 |
| 13.2.2 | Relevance of a Rupture Angle Determined by XRCT | 196 |
| | | |
| 14 | CONCLUSIONS & PERSPECTIVES | 199 |
| 14.1 | INPUTS FROM THE THESIS | 200 |
| 14.2 | TOWARDS A CHARACTERIZATION OF CATACLASTIC ROCK PROPERTIES BASED ON 3D XRCT DATA..... | 203 |
| 14.2.1 | Parameters of the MSI vs. Damage Indicators from XRCT | 204 |
| 14.2.2 | Inputs for a XRCT Formulation of the MSI..... | 206 |
| | | |
| | ACKNOWLEDGEMENTS | 209 |
| | | |
| | BIBLIOGRAPHY | 211 |
| | | |
| | APPENDICES I-V | |

1

ENGINEERING UNCERTAINTY RELATED TO WEAK ROCK MASSES

Homme! libre penseur – te crois-tu seul pensant
Dans ce monde où la vie éclate en toute chose :
Des forces que tu tiens, ta liberté dispose,
Mais de tous tes conseils l'univers est absent.

Gérard de Nerval, *Vers Dorés*

The high density of occupied land, the increasing environmental and economical constraints force engineers to build under the ground surface. This growing need for underground structures requires tunnelling and excavation through increasingly difficult geological conditions.

Excavations through hard solid rocks independent of depth frequently encounter zones of weaker mechanical properties that despite of their general small extent can be very difficult to overcome and require unconventional engineering techniques. Contradictorily, most effort is devoted today to technological developments but not on a reliable methodology to better characterize tectonized weak rocks. The unpredicted difficulties in tunnelling are however often a function of an incomplete understanding of rock mass architecture on both the regional and local scales. Therefore the occurrence of weak rock masses in underground projects is still synonym of a risk factor and of discomfort among engineers.

Strong constraints (mostly economical) tend to minimize the time and means devoted to the geological prognosis during preliminary site studies. As a result, often too much free room is left to geological uncertainties that seem quite ambiguously accepted and tolerated in a preliminary stage of project realization. In cases, difficult geological occurrence encountered during ongoing excavation can be properly managed with a flexible adaptation of the excavation method/sequence so as to minimize at most serious delays in the project realization. However, extreme rock occurrences can cause serious problems. Thus, heavy and expensive consolidation measures result before excavation can be re-initiated, stopping the works for several weeks or even months.

Finding the proper balance between not exaggerating preliminary studies due to a too conservative attitude vs. not shortcutting the critical information required for a safe excavation sequence in a given geological setting is indeed not an easy task. From the eyes of a geologist it is said that every underground setting bears characteristic particularities affecting its rock mass structure that have to be each time thoroughly assessed. Accordingly, it is a geologist opinion that a successful underground project management cannot only be interpreted on the base of past experiences. Most important, when weak rock masses are considered, it is obvious that efforts have to be given today for the development of specific geotechnical classifications capable to integrate the specific effect of the (progressive) tectonization process in terms of rock strength.

Many recent researches deal with the geological and mechanical characterisation of so-called cataclastic rocks, to define a group of tectonized rocks through brittle processes that preferentially favors the apparition of weak rock masses at shallow crustal conditions (up to 10 km depth). Accordingly, new data about their structural properties, their genesis and their geomechanical properties could be gained (*Russo, 1994; Wyder, 1997; Hoek & Brown, 1997; Hoek et al., 1998; Wyder & Mullis, 1998; Bürgi, 1999; Habimana, 1999; Laws, 2001; Lützenkirchen, 2002; Heilbronner & Keulen, 2006*). A proper geotechnical classification of weak rock masses is however still missing and attempts are controversial. Genetically-based classifications (*Wise et al., 1984; Schmid & Handy, 1991*) coexist with more descriptive approaches (*Higgins, 1971; Sibson, 1977; Heitzmann, 1985*).

Facing the structural complexity and great variability of such materials, a combined approach including geological and mechanical evidences as well as a clear conceptual model of the occurrence and mechanisms leading to weak rock formation seems appropriate to find practicability. Great emphasis will be put in this work on the possible improvements regarding cataclastic rock characterization.

Weak rocks introduce a problem of stability during tunnel excavation. They are susceptible to produce permanent deformations through visco-plastic processes and creep. Such permanent

deformations have to be properly defined in the preliminary phase of work realization, monitored and tracked during the entire maintenance cycle of the tunnel over its service life. In the case of underground works, the behavior of the surrounding rock must be controlled for different timescales. Temporary worksite road tunnels may have a short service life, mining tunnels usually should be designed for 5-30 years, but deep repositories (i.e. for nuclear waste) should be designed for thousand of years. For conventional modern tunnels in the domain of civil engineering, design life ranges between 75 and 120 years (*Bakoyannis, 2005*). A detailed study of tunnel pathologies and their effects on tunnel degradation and maintenance requirements can be found in *Sandrone (2008)*.

1.1 CATACLASIS IN ENGINEERING GEOLOGY

A rock mass is a picture of geological history. The effect of tectonic forces accumulated in different rock masses over geological time leads to the transformation of the original rock material into a tectonized one. At shallow crustal level, brittle deformation processes are dominant and lead independent of the petrological content to cataclasis, a type of metamorphism involving purely mechanical forces causing crushing and granulation of the rock fabric (*Bucher & Frey, 1994*). Cataclastic metamorphism is favoured by high strain rates under high shear stress at relatively low temperatures. Cataclasis is confined to the vicinity of faults and overthrusts and are an important component of the underground structure to take into account in civil engineering projects.

As stated in *Schubert (2006)*, the problems assimilated to faulted rock masses already start with the difficulty in investigating, testing and characterizing them. Weak rock masses inherited from brittle tectonic processes depict highly contrasted properties (**Fig. 1.1**). This variety can be explained by consideration of the initial rock composition (petrological content) and by differential strain accumulation inside fault zones which is reflected by a heterogeneous rock mass structure. Accordingly, correct interpretation of punctual samples as obtained in boreholes is difficult to assess if the drilling density is low. Thus any geotechnical prediction in such context is affected by a large degree of uncertainty. Moreover, as a result of intense fracturation processes over geological time, cataclastic samples are difficult to recover from drilling operations what explains that a certain lack of knowledge still prevails regarding their geological and mechanical properties, due to limited possibilities of testing representative samples in a laboratory.

Summarizing the available geotechnical knowledge, weak rocks are characterized by a low mechanical strength situated somewhere between that of rocks and soils (*Habimana, 1999*). Expressed in terms of uniaxial compressive strength, the domain of weak rocks is reported by *Russo (1994)* varying between ~ 1 MPa (transition to soils) and ~ 25 MPa (transition to strong rocks). Weak rocks are characterized additionally by high deformability involving non-linear constitutive laws, strong strength dependence on water saturation and temperature, and by their susceptibility to weathering. The observed micro-structural and mineralogical changes within a fault zone development lead to subsequent modifications in mechanical properties.

Thus a geotechnical classification for cataclastic rocks aiming a prediction in terms of strength and deformability to be used in geotechnical applications has to consider relevant parameters able to:

- understand the effect of the excavation-related disturbances on such heterogeneous rock masses (material nature);
- consider the increased alterability that such rocks introduce on the tunnel structure compared to intact rocks (material behavior).

Because the inherent randomness and discontinuity in cataclastic textures introduces a weak coupling between microstructural and mechanical analysis of rocks in the brittle regime (*Hadizadeh & Johnson, 2003*), amount of cataclastic samples from one location must absolutely be maximized in order to establish the most comprehensive framework of rock mass behavior variability in function of geological heterogeneity.

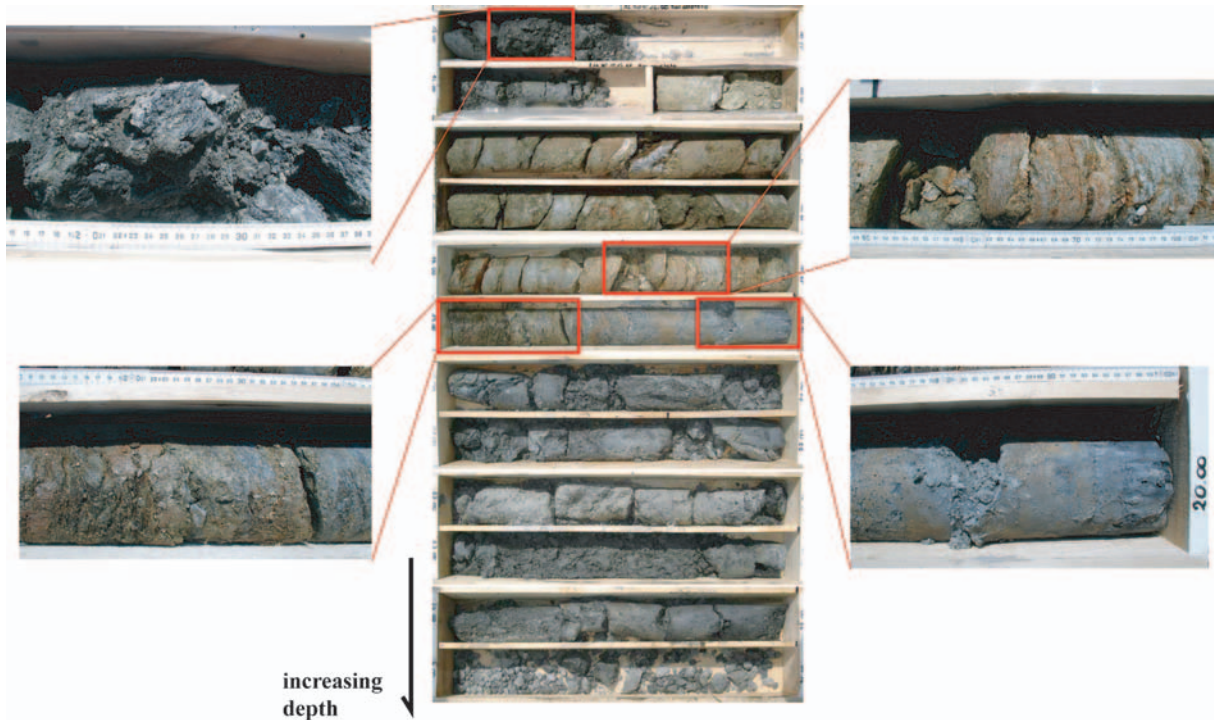


Fig. 1.1 Results from a drilling operation performed with the triple tube core barrel technique at the Ceneri base tunnel site in August 2004. This technique allows nowadays the most optimized sample recovery in their natural structural state even in difficult geological contexts. This example makes clear that cataclastic samples can be recovered for further analytical procedures in the laboratory. Note the important and rapid variations in rock structures, reflecting the natural heterogeneity of tectonized rock horizons. Drillhole San Antonino/"Vigana" CB 116, inclination 45°, coord. 719°542/112°457. Courtesy of Dr Baumer SA, Ascona, Ticino, Switzerland.

1.2 COMMON PROBLEMS ENCOUNTERED IN TUNNELLING

Fault zones crossed by underground civil engineering project introduce potential hazards that must be considered during overall project management. These hazards can be sudden or delayed. Problems related to collapses (roof and walls) and face instabilities due to geological uncertainties are typical of the tunnel construction process.

Because the strength of fault rocks is strongly dependent on effective pressure, fault rock behavior may change at depth and behave in an unexpected manner. Thus depth of the excavation is an important parameter to be taken into account. As stated by *Kaiser (2006)*, understanding of real rock behavior is often not available prior to real-time experiences underground. Accordingly, successful constructions must operate in a flexible, risk-sharing framework as unexpected conditions can only be managed once they are actually encountered and understood. Applied to the potential presence of weak rock masses in underground work, this consideration highlights the relevance of a tunnelling strategy and philosophy based on anticipation that should rely on a firm theoretical rock mass behavior background. *Lombardi (2006)* summarizes the following:

- Absolute geological prediction can't be awaited, but the best-possible should be done.

Chap. 1 Engineering uncertainty related to weak rock masses

- Security issues should take into account the potential variability of parameters derived from geological preliminary studies.
- In a new tunnelling operation, the unexpected should be expected; therefore it is a responsibility to be prepared for it.
- Constant observations of rock behavior during excavation have to be done and used as forecast of probable rock mass behavior to expect and respect.
- Facing uncertainties, sufficient flexibility in design and construction techniques should be ensured.

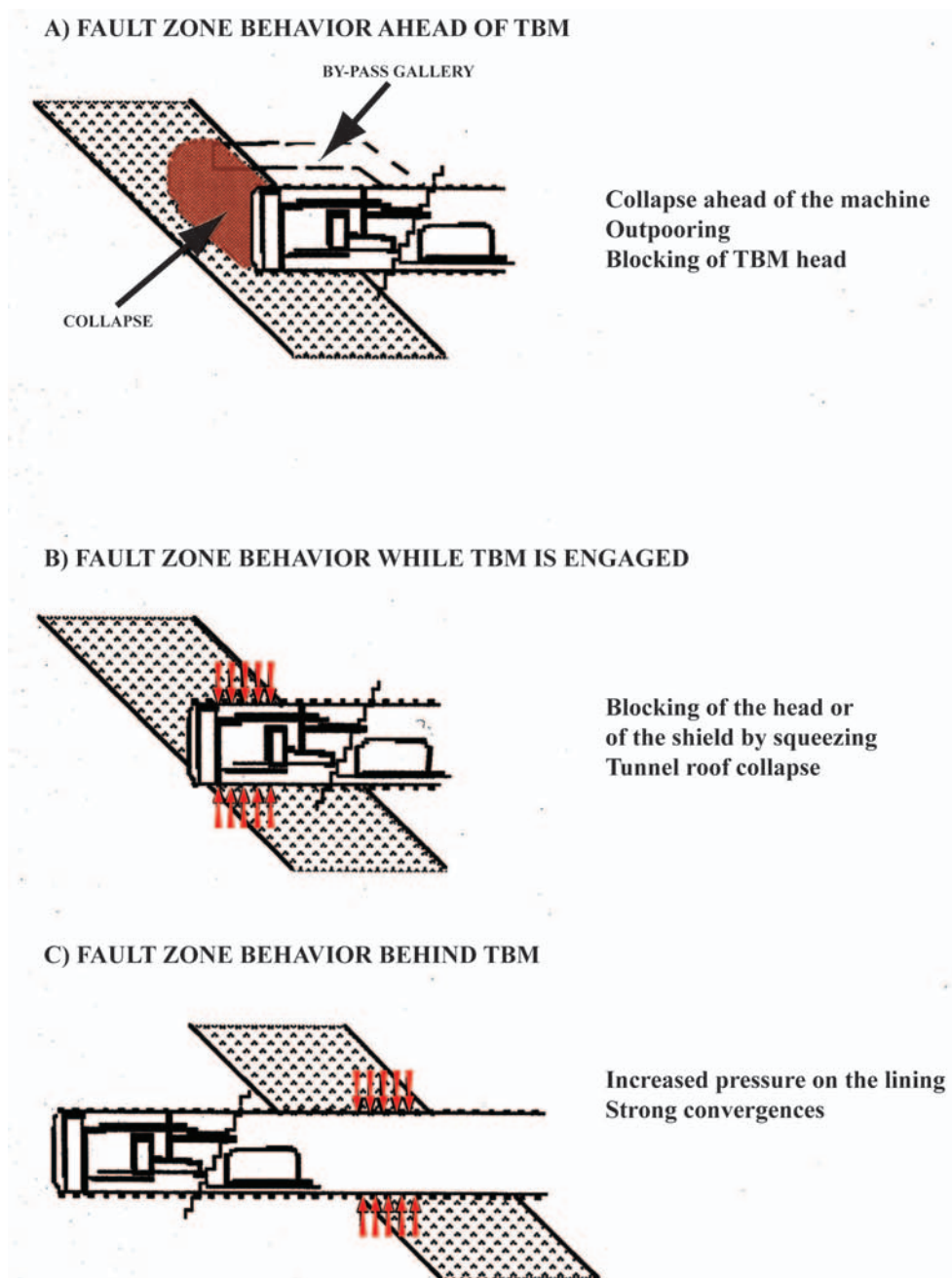


Fig. 1.2 Illustration of typical problems impairing on TBM advance in relation with the occurrence of a fault zone characterized by weak mechanical properties. Effect on TBM A) when the fault zone is still ahead, B) when the fault zone is crossed, and C) when the fault zone is behind. After *Habimana* (1999).

Based on considerations about the properties of cataclastic fault rocks, some relevant major problems encountered in tunnelling are summarized in **Fig. 1.2**.

1.3 A RATIONAL APPROACH TO A GEOLOGICAL QUALITY INPUT FOR UNDERGROUND CONSTRUCTIONS

Several guidelines and norms agree on the fact that successful tunnelling strongly depends on the quality of preliminary geological information. They have developed over the years a normative basis for underground constructions and allow the sharing and exchange of experiences. In Switzerland, the SIA norms 198 (*Travaux souterrains – Exécution, 2004*) & 199 (*Etude du massif encaissant pour les travaux souterrains- Description du massif, Appréciation du massif, Rapports géologiques, hydrogéologiques et géotechniques, 1998*) give a global framework for all types of underground structures and are specifically designed to help in the realization phase, but should already be taken into account during the design phase. In particular, norm 199 describes the determination of rock mass conditions (with a distinction made between “hard rocks” and “soft grounds”), the integration of such informations in the predictive geological profile, the evaluation of potential risks & hazards, and refers to the different methods for *in situ* and laboratory measurements of rock mass properties.

According to *AFTES* (2003), the essential goal of rock mass characterization is to *provide the engineer the qualitative and quantitative data that are necessary for the proper description of the structure and evaluation of mechanical and hydraulic properties of the rock mass at the scale of the volumes affected by the works*. It includes the preliminary geological investigations (“geological model”) and the identifications of homogeneous geotechnical units of consistent mechanical and hydraulic properties. Fault zones are recommended to be treated as units on their own. Each geotechnical unit is further characterized by considering the:

- 1) *Rock matrix* properties and their subsequent mechanical characteristics.
- 2) *Discontinuities* properties and their subsequent mechanical characteristics.

The *rock mass* (i.e. rock matrix + discontinuities) is further identified by means of its mechanical characteristics, hydrogeological conditions, initial *in situ* stress field, and temperature.

Points 1) & 2) derive mainly from laboratory analyses. Investigations at the rock mass scale include *in situ* measurements and the use of referenced geotechnical classifications. Accordingly a translation of parameters determined on rock samples is made to the scale of the rock mass by means of empirical correlations, so as to facilitate the choice over the most adequate realization techniques (excavation + support design). Support classes are accordingly defined during the tunnel feasibility study and these classes can be reajusted if needed during ongoing excavation. The general idea of the characterization is therefore to limit uncertainty. It considers a set of major parameters affecting rock mass behavior that can be integrated into a “check-list” based on deemed-to-satisfy rules of prescriptive character (*Bakoyannis, 2005*).

This largely empirical approach proved very efficient for rocks of relative good mechanical performance. However the field of weak rock masses and the type of related deformations introduce a limitation to their direct applicability. In particular, models of rock failure used in established standards are not appropriate to simulate weak rock mass deformability so that the ground model in such context contains a high degree of uncertainty. In practical studies, paradoxically, *in situ* measurements on weak rock masses are often let aside not primarily because of their high cost but

more because of the risk to destroy the measuring device itself (*Bussard*, pers. comm.).

The adopted approach for tunneling in difficult geological setting is based today on risk assessment. As stated in *Bakoyannis* (2005), risk and safety perception have to do with expert and scientific knowledge. Further, risk assessment and management starts with risk identification which is largely function of professional judgement (*Kaiser*, 2006). Numerical analysis is the ultimate tool able to deal with complicated problems but requires high quality input data. With such techniques, extensive stress redistribution at the stage of excavation, prediction on the deformability of critical rock masses and installation of primary support can be estimated. For engineers, an important responsibility will be to manage objective safety margins.

With this regard, *Bakoyannis* (2005) points out the importance of the dual role of ground as load imposing and load bearing element which must be assessed in detail for the short- and long-term integrity of the underground structure. Therefore, a sound risk evaluation and assessment during design is an essential basis for a successful construction. For tunnelling applications, the particularity of faulted rock masses (heterogeneity, structural development, alteration, contrasting ground water flow) induces big variation on stresses and displacements of the tunnel and the surrounding ground within short sections (*Schubert*, 2006). As a consequence, in terms of rationality, proper models of fault zones mechanisms, resulting structures and subsequent physico-chemical rock damage should be studied from a genetic point of view and confronted with their particular implications in current rock mass behavior accomodating a tunnel.

1.4 AN INTERDISCIPLINARY RESEARCH FIELD

Land planning management nowadays - because of the actual demographic and economic growth - considers more and more the need to go underground. An interdisciplinary project is currently active at EPFL on that subject (Deep City-SNF 54). The difficulties associated with a 3D land planning require proper understanding of the underground structure on two levels:

- 1) The stability, rock properties, excavability, long-term evolution of rock behavior and hydrogeological conditions must be known.
- 2) The interaction of the rock environment with the construction materials must be taken into account for time scales up to thousand of years (i.e. storage of nuclear waste).

A presentation of major underground structures worldwide can be found on the website of the International Tunnelling and Underground Space Association (ITA-AITES, www.ita-aites.org).

Weak rock masses are a particularity of the underground space for which engineering predictability face uncertainty. The conception and projection of ground-breaking underground constructions over the past decade showed that the chance to cross complex geology increases together with project complexity. The geotechnical problems induced by weak rocks are huge and involve a multi-disciplinary approach to optimize project realization. Several perspectives at different scales must be considered for tunnelling applications:

- *Genetic processes*: evidences from regional stress field, extent and width of fault zones, rock composition involved, strain indicators, and weathering.
- *Failure processes and deformability*: fault rock volume, amount of fracturing and shear influencing rock mass structure (heterogeneity), tunnel depth, effect of mineralogy,

presence of clay, permeability, structural singularities, and risk assessment.

- *Excavation techniques*: excavation sequence, abrasivity and/or plasticity of the faulted rock, structural stability, reinforcing requirements (bolting, forepoling, fiber glass, injections, freezing), and risk management.
- *Natural environment*: sustainable management of the natural resources, hydrological regime, ground surface monitoring above excavation, choice of construction materials, recycling of excavated materials for further civil engineering use.
- *Human resources*: work security measures for miners and technical staff.

Project success in complex geological setting and optimal management of costs is a function of the positive interaction between engineers, geologists, material scientists, hydrologists, technicians and miners. Experience and professional judgement is a prerequisite for underground works. However, the uncertainty regarding weak rock masses shows that a lot has still to be learned. Accordingly, the specific challenges that such rocks introduce require in the future a close link between fundamental and applied researches and constitute a particularly stimulating field for the rock scientific community in its broadest sense.

2

THE CATACLASIS – STATE OF THE ART

« Il a d'étranges possibilités dans chaque homme. Le présent serait plein de tous les avènements, si le passé n'y projetait déjà une histoire. Mais, hélas ! un unique passé propose un unique avenir – le projeté devant nous, comme un point infini sur l'espace. On n'est sûr de ne jamais faire ce que l'on est incapable de comprendre. Comprendre, c'est se sentir capable de faire. ASSUMER LE PLUS POSSIBLE D'HUMANITÉ, voilà la bonne formule. »

André Gide, *Les Nourritures Terrestres*

Cataclasis is a degradational tectonically induced process affecting rocks by brittle fracturing, grinding, crushing and rotation of rock components. Cataclasis is therefore preferentially favored along active fault zones. Cataclasis can be accelerated by interaction with hydrothermal fluids that circulate preferentially in the rock mass as a response to the increased fracture density. In this chapter cataclastic rock masses are described and an observation of cataclasis at different scales is described. The processes leading to and controlling cataclasis are defined and resulting rock masses presented. A discussion is conducted about how initial petrology exerts a control on fault development influencing textural, structural and mineralogical properties of the resulting cataclastic rocks. As observed in this research and as well documented in the literature (see references herein), cataclastic rocks resulting from ongoing stress/strain activity over time are highly heterogeneous, leading to a widespread variability in rock materials and rock material properties.

Stress regime, width of the fault zone and initial rock composition explain this wide variety of cataclastic materials, with extreme alteration occurring in fault cores (so-called *kakirites*, a rock material completely lacking cohesion, see below). In contrast with brittle fracturing processes affecting to some extent all (uncataclastic) rock masses at shallow crustal conditions, cataclasis requires a critical confining pressure to occur, determining a regime where continuous fracturing becomes the energetically most favorable mode of deformation and for which movements along preexisting discontinuities (governed by a frictional sliding criterion) are made impossible (**Fig. 2.1**). To describe the effect of cataclasis on rock mass properties, the damage produced by tectonic stress should be accurately depicted and translated quantitatively in terms of their influence on rock rheology and mechanical behavior. Regarding the wide range of cataclastic materials and because cataclasis is a gradational process in fault zone function of stress accumulation and strain localization (defining a cataclastic gradient), a way to look at cataclastic rocks is to separate between “hard” and “soft” rock components. Classical models of rock mechanics are widely used to describe hard rocks in general. It is therefore expected that introducing parameters from geology accounting for the structural and mineralogical properties of the softer rock fraction into mechanical models can lead to the formulation of a more appropriate mathematical description of cataclastic rock behavior (see the considerations of *Habimana*, 1999).

The study of cataclastic rocks is directly applicable to underground engineering projects where damaged rock mass can cause severe technical, economical and safety issues. Reconnaissance

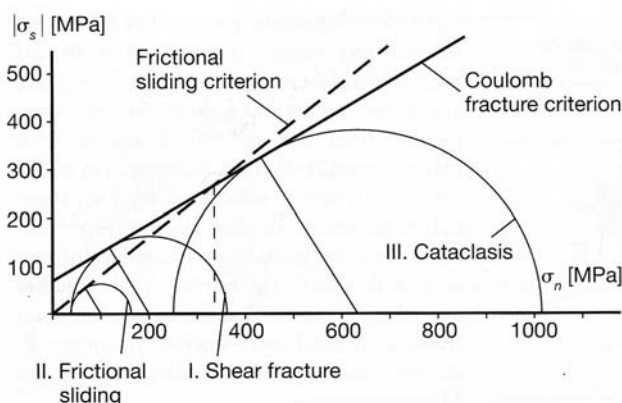


Fig. 2.1 Representation of Coulomb fracture criterion and frictional sliding criterion for sliding on a preexisting fracture on a normal vs. tangential stress diagram. Mohr circles indicating critical stress conditions for shear fracture (circle I), frictional sliding on a fracture plane at constant confining pressure (circle II) and cataclastic flow during which fracturing requires a lower differential stress than frictional sliding at the same confining pressure (circle III). After *Twiss & Moores* (1992).

drilling operations provide the ability to infer on the presence of cataclastic rocks. Upon encountering cataclastic materials, particular care should be taken in the proper recovery of such rock core samples to derive representative data in the laboratory. During ongoing excavation, additional samples can be punctually taken in the tunnel under construction to increase the effective amount of information on a particular faulted rock mass and its expected development and geotechnical implications beyond the tunnel face. Because of the overall fragility of such rock materials and difficulty in performing standard tests on them, a general lack of high quality data affect the geotechnical study of cataclastic rocks. Increasing the amount of sampling

from reconnaissance drilling operations is an important task in geotechnical applications to improve the general knowledge about cataclastic materials. Moreover, high-end drilling techniques should be used if the occurrence of fault-rocks is expected at the level of the underground excavation.

2.1 GENETIC CONSIDERATIONS

The study of the lithosphere involves considering characteristic domains of rock properties that differ according to depth (**Fig. 2.2**). Elastic rheologies prevail at shallow conditions and permanent deformation results in the form of brittle fractures. Tectonic breccias are generally formed at temperatures $< 300\text{ }^{\circ}\text{C}$ (*Mancktelow*, 1985). Deformation changes from brittle fracturing to plastic flow at crustal levels $> 10\text{ km}$ that involves higher temperatures and pressures (*Wyder & Mullis*, 1998). Plastic rheologies are appropriate below this depth and permanent deformation is in the form of creep and ductile behaviour. Indicatively the plasticity limits of two main mineral phases constitutive of the earth crust are reached at temperatures between 300 and 400°C for quartz and 550 to 650°C for feldspar. At higher temperatures in the range of 1000°C , creep processes become dominant, including diffusion and dislocation creeps. Therefore, partial melting of the rock mass is likely to occur. As stated in *Manaker et al.* (2006), the transition from brittle to ductile behavior occurs over a wide range of pressure and temperature conditions.

Another consideration for cataclastic materials is that of fracturation. Fracturation spans a wide range

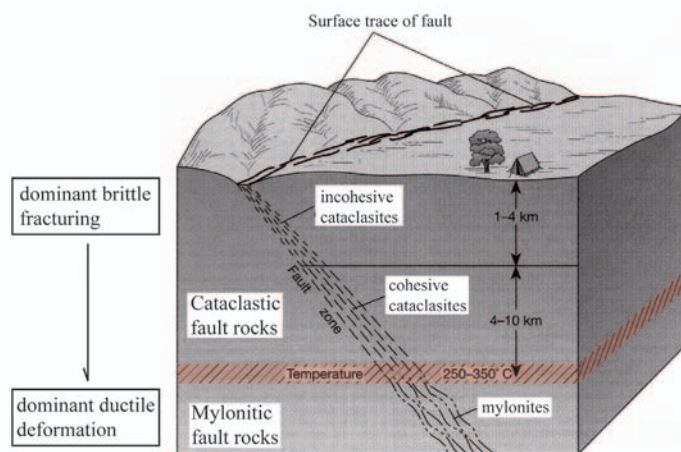


Fig. 2.2 Rheological stratification of the Earth's lithosphere. Implication for fault rock occurrence: incohesive cataclasites (e.g. kakirite), cohesive cataclasites and mylonites. Mylonitization of the original rock protolith marks the transition between brittle fracturing and generalized ductile deformation. This transition varies according to rock composition but is generally accepted at crustal depths $> 10\text{ km}$. Modified from *Twiss & Moores* (1992).

of scales from (micro)- fractures, fault bands to regional joint systems and fault zones. Cataclastic processes are responsible for the brittle deformation of the crust on a regional scale. At a smaller scale, brittle processes and consequent fracturation produces cataclastic rocks in fault zones. Seen as a whole, the increased damage of a rock mass by brittle processes at low temperatures leads to ductile behaviour through cataclasis (including fragmentation, fragment rotation). The term cataclastic flow is used to describe such a behavior (*Sibson 1977; Paterson 1978*) (**Fig. 2.3**). Cataclastic flow is generally obtained without creep and plasticity if the confining pressure of the rock approaches the brittle strength (e.g. critical confining pressure as

indicated on **Fig. 2.1**). It is also reported that cataclastic flow can be the primary process responsible for the deformation in folding (*Ismat & Mitra*, 2005). The importance of brittle mechanisms in folding through elastic-plastic and visco-elastic processes have been further documented (*Manaker et al.*, 2006). From a rheological perspective, the generalized formation of microfractures through cataclasis reduces the elastic strength of the material. Accordingly, as fractures initiate, grow and coalesce with other fractures, the material becomes weaker.

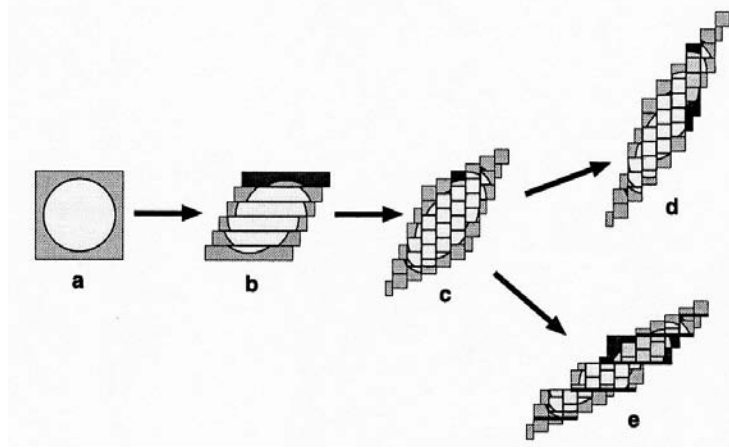


Fig. 2.3 Model for large-scale cataclastic flow resulting from a generalized (small-scale) brittle fracturing leading in overall ductile rock mass behavior at the scale of the fault zone. Undeformed rock protolith is represented as a square with a circle inside it (a). As a result of cataclastic deformation, the circle deforms progressively to an ellipse depicted in (b) through (e). Strain accommodation is realized with slip on two sets of surfaces, horizontal (b) and vertical (c). After stage (c), different paths of deformation can be observed, resulting in unique strain ellipses. Stage (d) presents the case where only the vertical slip surfaces remained active. In stage (e), selected horizontal fracture sets (thick black lines) grew with renewed slip (i.e. reactivation). This model clarifies the idea that a collection of small amounts of slip on just two sets of slip surfaces (vertical and horizontal) can result in a significant amount of strain. It shows also that the fracture bound blocks do not require independent rotation about their own axis to produce significant amounts of strain. After *Ismat & Mitra* (2005).

2.1.1 Mechanisms Of Brittle Deformation

Cataclasis produces a fragmentation of the rock protolith and is described by grain rotation and sliding as well as grain interactions. The mechanism of deformation is strongly dependent on the effective stress (difference between lithostatic and interstitial pressure, *Schmid*, 1982). The progressive and sustained fragmentation of a rock mass is characterized by grain comminution (*Billi et al.*, 2003) and overall decrease in grain size distribution. Particle size distribution in cataclasite is affected by the fragmentation process, the initial size distribution, the number of fracturing events, the energy input, the effective strain, and the confining pressure (*Blenkinsop*, 1991). As a function of initial rock mineralogy, initial rock fabric and stress conditions, the geometry of resulting grains -and at a bigger scale of clasts- can take many forms. Many studies use the concept of fractal dimension to describe particle size distribution in brittle fault rocks (see *Blenkinsop*, 1991; *Storti et al.*, 2003; *Billi*, 2005; *Hayman*, 2006). The fractal dimension can be considered as a measure of the relative abundance of small and coarse grains in each sample, with values increasing together with the relative abundance of small grains. High fractal dimension values involving both constrained comminution and selective fracture of large particles are general features of experimental and natural cataclasis (*Blenkinsop*, 1991).

Cataclasis is a chaotic degradation process and cataclastic deformation manifests itself differently according to the level of confining stress: the higher the confining stress the higher the tangential stress needed to activate the deformation (**Fig. 2.1**). Therefore, optimal cataclasis conditions take place at low confining stress and high interstitial pressure. Temperature and strain rate appear to have a negligible influence on the cataclastic process (*Schmid & Handy*, 1991). Two main mechanisms of deformation interact within cataclastic fault zones: *cataclastic flow* and *crystal plasticity*, mechanically corresponding to brutal failure over stress through the fracturation process or to strain accommodation by internal plastic deformation. Cataclastic flow tends to decrease the cohesion of the material whereas crystal plasticity preserves it and can in some case even increase cohesion (**Fig. 2.4**). In rock mechanics, these two deformation mechanisms define brittle and

ductile behaviors. According to *Hoek & Brown* (1997), brittle rocks accommodate tectonic stress by reducing strain (fracturation) whereas ductile rocks accommodate permanent deformation without losing their ability to resist stress. More generally, brittle deformation is associated with localized dilatancy and faulting, whereas ductile deformation is associated with non-localized macroscopic flow (*Evans and Kohlstedt, 1995*).

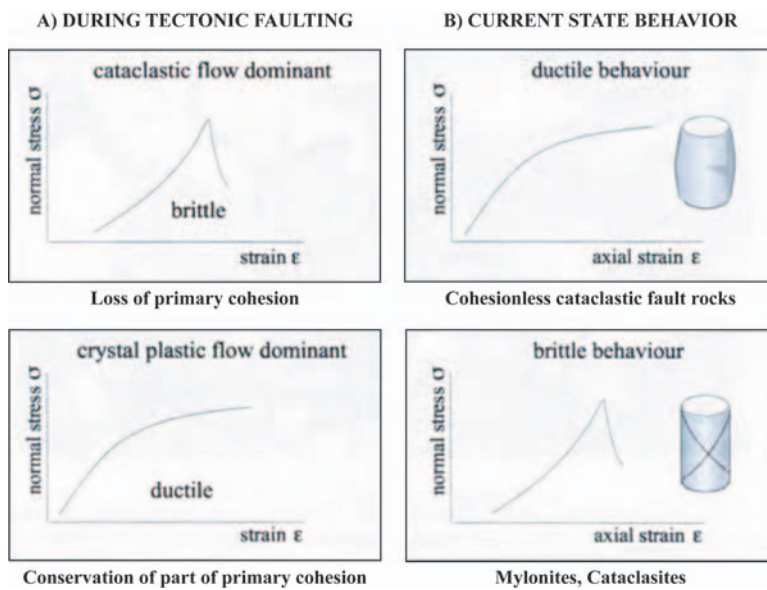


Fig. 2.4 Concurring mechanisms of cataclastic flow and crystal plasticity affecting to various extents the damaged rock mass. For fault rocks classification, see **section 2.3**. Effects on current state rock cohesion and deformation behavior are schematically highlighted. After *Bürgi* (1999).

2.1.1.1 Cataclastic flow or cataclasis

Cataclastic flow or cataclasis is a type of ductile flow that refers to a purely mechanical low-temperature deformation process involving brittle fragmentation of grains by micro-cracking, frictional grain boundary sliding, dilatancy and rigid-body rotation of crystal and grain fragments (see also *Passchier & Trouw, 1996; Schmid & Handy, 1991; Sibson, 1977; Bürgi, 1999*). Fracturing takes place by nucleation, propagation and displacement along newly formed cracks. It is accompanied by frictional grain-boundary sliding. The individual grains and crystals endure in general no intracrystalline deformation (*Knipe, 1989*). Cataclastic flow is the dominant deformation process at non- to low-grade metamorphic conditions and at relatively high strain rates. It is favored by high fluid pressures. Cataclastic rock fabrics will be a function of the rock composition but common fabrics contain fractured angular rock and grain fragments that vary greatly in size range. Open spaces are expected to be subsequently filled by quartz or carbonate precipitation and re-fractured by further cataclasis.

Cataclastic flow is generally defined for thin, confined zones, where deformation and flow lead progressively to grain size reduction. The resulting rock has a fine-grained matrix surrounding larger grains/fragments. With continued shearing, the cataclasite may form disjunctive foliations with elongated matrix- and framework grains showing preferred alignment (**Fig. 2.5**). This type of deformation is referred to as **matrix-controlled cataclastic flow** (*Ismat & Mitra, 2005*). Cataclastic flow that is not confined to thin zones can best be defined as a continuous deformation, which is accomplished by many slip events on a network of faults, where the overall deformation is much larger than the slip on individual faults (*Hadizadeh & Rutter, 1983; Ismat & Mitra, 2001*). In other words, the deformation is mesoscopically brittle and macroscopically ductile. A collection of small amounts of slip on just two sets of slip surfaces can produce a significant amount of strain, without requiring independent rotation of the fault-bound blocks with respect to each other. This type of deformation is referred to as **block-controlled cataclastic flow** because it does not require a fine-grained matrix for macroscopic flow to be accomplished. During block-controlled cataclastic

flow, deformation takes place dominantly by fracturing and sliding along a population of fractures (**Fig. 2.5**), the material eventually forming a well-developed, stable fracture-network (*Ismat & Mitra, 2001*). These networks form fault-bound blocks of various sizes and shapes, defining block-subsystems that can optimally fill void spaces at fold hinges (*Laubscher, 1979*). The fracture-bound blocks slide past each other, maintaining contact during flow, so that there is minimal dilatancy and the rock body as a whole undergoes ductile deformation. When deformation takes place by block-controlled cataclastic flow, the material behavior of the rocks is no longer like that of the original homogeneous lithology. Block controlled cataclastic flow is influenced by micro-scale variables because the growth and linkage of micro-fractures form larger-scale fractures (*Ismat & Mitra, 2005*). Micro-fractures nucleate and grow at heterogeneities, such as impurities (iron oxide, calcite), grain boundary-overgrowth contacts and grain boundaries, especially if there is a large grain-size variation. Continued growth of micro-fractures also depends on average grain size and the amount of matrix inter-connection. Because larger grains have lower fracture strength, fractures typically propagate through larger grains. Fractures can also propagate along well-connected overgrowths and/or impurities (*Schmid & Handy, 1991*). The fracture networks produce an induced anisotropy, which can continuously evolve with new fracture growth and/or reactivation; thus, the rock now has a 'fractured rock' rheology (see rock mass in the damaged zone on **Fig. 2.5**).

2.1.1.2 Crystal plasticity

An important deformation mechanism coming along with brittle deformation and known as *crystal plasticity* is realized when metamorphic conditions exceed those of cataclasis *s.str.* Crystal plasticity corresponds to a deformation regime where permanent strain is accommodated in crystals without loss of cohesion by intracrystalline deformation processes based on the migration of lattice defects inside crystallographic structures (*Twiss & Moores, 1992*). Important lattice defect migration includes *dislocation glide*, *dislocation creep*, and *twinning*, all of which are accompanied by dynamic recovery and recrystallisation. They are strongly a function of temperature, strain rate and grain size, whereas effective pressure is of minor importance. Effects of intracrystalline deformation are characterized in thin sections by undulose extinction, formation of subgrains, deformation lamellae and tapered twins (*Passchier & Trouw, 1996*).

At a further stage of deformation under ongoing metamorphic conditions, strain energies stored in crystals are mostly released through dynamic recrystallization, which accommodate a large amount of strain without strain hardening. The driving force of dynamic recrystallisation is thought to be a gradient of strain energy across grain boundaries (*Nishikawa et al., 2004*). Strain free grains preferentially grow at the expense of highly strained grains, which changes microstructures and average crystallographic orientations rapidly in steady state. Therefore, the strain accommodation process and grain growth are essential in dynamic recrystallization, and are considered to control the evolution of microstructure and texture, and also deformation behaviors of minerals (*de Bresser et al., 1998, 2000*).

2.1.1.3 Other mechanisms

Other important deformation mechanisms that can affect cataclastic deformation when interaction with hydrothermal fluids gets important are *pressure solution* and *diffusion creep*. In these cases, deformation is achieved by mass-transfer through an intergranular fluid by dissolution-precipitation processes, respectively by solid-state diffusion (e.g. *Schmid & Handy, 1991; Knipe, 1989*). Pressure solution is localized at grain contacts where crystal lattices are under high stress and solubility of minerals in aqueous phase increased. The dissolved material is redeposited at the grain boundaries adjacent to pore spaces where stress in the crystal lattice is lower. Pressure solution processes are therefore important under low-grade metamorphic conditions in porous materials with abundant pore fluids. Solid-state diffusion creep in contrast becomes important at relatively high temperatures with respect to the melting temperature of the involved minerals. Crystals deform by diffusion of

vacancies through the crystal lattice, respectively along the grain boundaries (*Passchier & Trouw, 1996*).

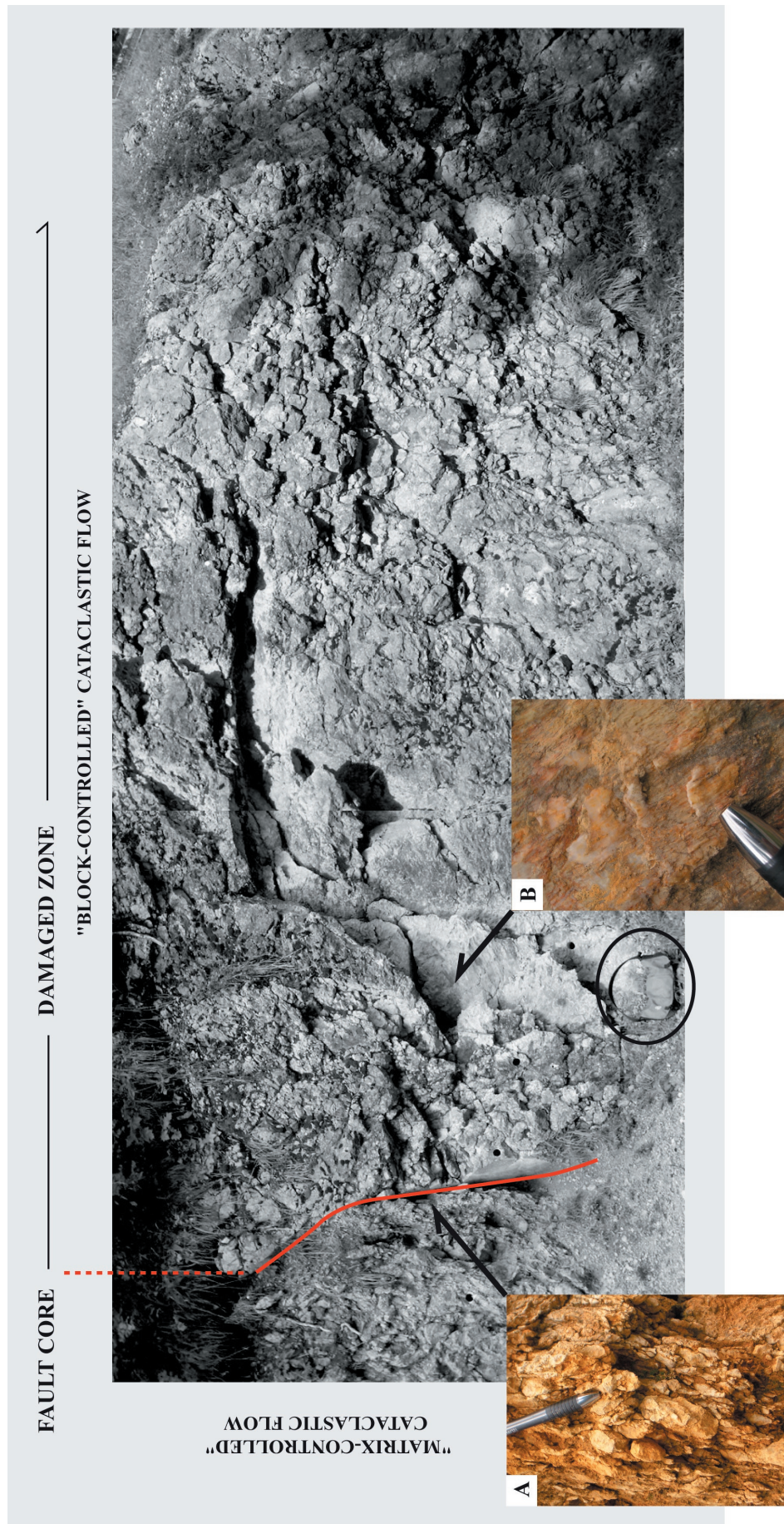


Fig. 2.5 Example of fault zone in carbonatic rocks, Vallorbe, Jura Mountains, Switzerland. The overall damaged rock mass is particularly nicely outcropped. Transition between damaged zone and fault core is sharp. The fault core develops a rough disjunctive foliation with mm- to cm-wide microlithons (A). Structure of the fault core is indicative of *matrix-controlled* cataclastic flow. The damaged zone is characterized by several sets of slip surfaces and is indicative of *block-controlled* cataclastic flow. Dynamic recrystallizations are observed on slip surfaces (B). Scale is given by the bag on the bottom part of the picture. Modified from *Christe (2004)*.

2.1.2 Implication For Fault-Zone Generation

A fault zone is a source that generates permanent stress perturbation in rocks. Cataclastic fault zones can vary from millimetrical scales up to a thickness of several kilometers. It is expected that grain size in rocks will decrease together with an increase in fault zone width, which reflects more important displacement accumulated along the fault. Some studies (*Homberg et al.*, 2004; *Hayman*, 2006) tried to relate the thickness of a cataclastic zone with the displacement accumulated along the corresponding fault over geological time, using evidence from textural, structural and geochemical data. A fault zone is a four-dimensional system involving slip along the main fault surface and deformation within a volume around that surface, both of which accumulate through time. This accumulation through time is, however, difficult to characterize, even when cross-cutting relationships are available to constrain relative timing. *Micarelli et al.* (2006) make the assumption that faults with small displacements represent the early stages of growth of larger faults, e.g. that the combined study of faults of different magnitude affecting similar lithologies in the same geological context can provide clue over fault zone development through time in terms of width and structural complexity.

A discontinuous transition is often observed between intact and damaged rock mass causing a stress deflection. Stress states in the fault zone and surrounding rock are therefore characteristic and a complex transmission of stress is likely to occur at the transition zone, leading to a possible fault growth with time. Fully developed fault zones are structurally characterized by a damage zone and a fault core. Fault cores and damage zones show contrasting rheological relationships as well as evolving permeability properties that relates to a gradient of stress-strain responses within the fault zone. This results in characteristic structures function of the original protolith composition. The damage zone consists of rock volumes affected by fault-related fracturing and can be further separated into a weakly deformed damage zone (with properties close to the intact rock mass) and an intensely deformed damaged zone (where fracturation, fragmentation and crushing processes conduct to the production of more and more fine-grained matrix) (*Micarelli et al.*, 2006). In damage zones, bedding surfaces and inherited structural fabrics are commonly preserved (*Billi et al.*, 2003). Fault core nucleation is influenced by the structural fabric developed at the transition between the intensely deformed damage zone and the fault core. A fault core is characterized by a high amount of fine-grained matrix in comparison to clasts, leading at the end to a homogeneous fault rock with structural properties comparable to soils. The degree of fracture connectivity strongly increases from the protolith-damage zone boundary towards the fault plane (*Micarelli et al.*, 2006), thus influencing fluid flow properties inside the fault. Fault cores consist therefore of low permeability cataclastic rocks where slip is localized and pre-existing, sedimentary and tectonic structures are fully obliterated by cataclastic flow (e. g. *Sibson*, 1977). An extremely sheared rock mass can lead to the development of natural flow barriers (see example in *Bürgli*, 1999).

Fault activity involves composite deformation mechanisms at various time scales (**Fig. 2.6**). Frictional sliding on a plane occurs theoretically as a result of two forces controlling the static and dynamic conditions over the surface of the plane (*Paterson*, 1978; *Twiss & Moores*, 1992). This means that once the movement is initiated on a shear plane the friction coefficient of the plane will tend to decrease allowing the velocity of shear to increase, whereas during inactivity along the plane, the friction coefficients will increase again as a result of confining stress which leads to a hardening of the shear zone (i. e. densification of the fault rocks). As a function of tectonic activity, several critical aspects of fault activity evolve through time, like the stress distribution in the crust and the fault-shear strength. Various mechanical approaches, such as dislocation model or crack theory, concur that slip on a fault induces significant changes of the static stress field (in both magnitude and direction) in the surrounding rock volume (*Homberg et al.*, 2004). Fault zones are therefore systems that mature through times and a categorization of fault zones based on field evidence can benefit applied studies (see for example *Neubauer*, 2005).

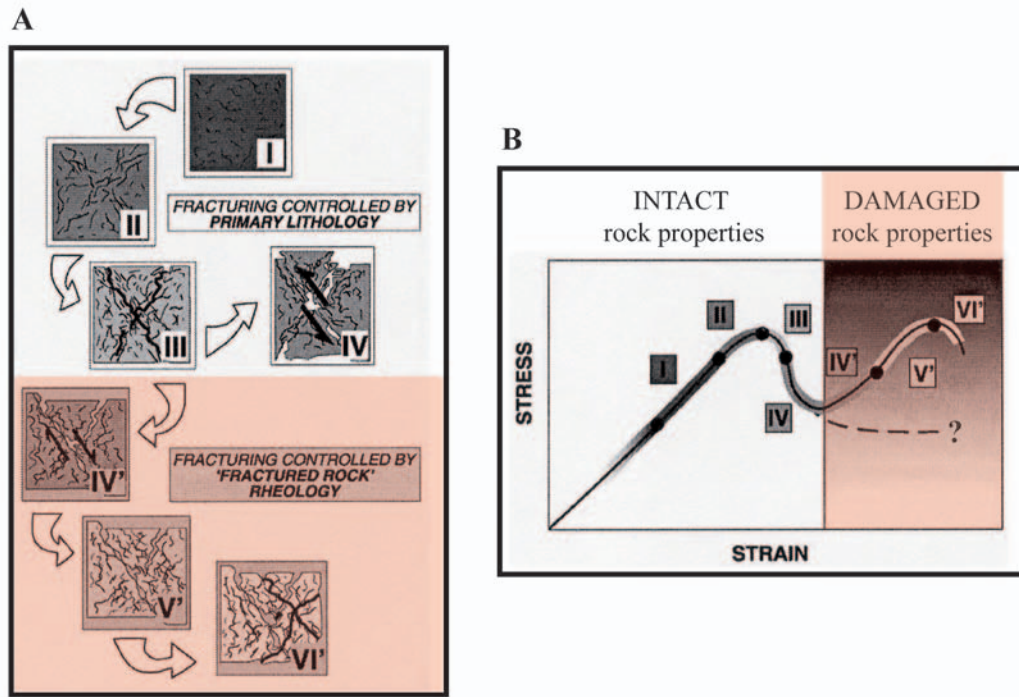


Fig. 2.6 Schematic model to illustrate the composite mechanisms active in brittle fault zones and the change in rock rheology expected over time. The evolution of strain localization and shear fracturing leading eventually to cataclasis is represented on a reference rock mass unit that is increasingly deformed under vertical stress application. Primary rock lithology controls deformations in stages I-IV. Fractured rock rheology influences the deformation in stages IV'-VI'. **A)** Stages I-III present the development of shear bands across the rock mass that can produce outcrop scale features through growth and linkage of initial microfractures. Once these fractures are formed, deformation can continue in a cyclic manner through sliding mechanisms during periods of strain softening (IV). If movements along the shear band cannot be activated (stages IV'-VI'), strain hardening will result and new (micro-)fractures will have to propagate through the already fractured rock mass leading to an evolution of the outcrop scale feature. This evolution is influenced in this case by the fractured rock rheology from stage III. **B)** Stress-strain relationship for the stages described in **A)**. Illustration of strain softening and strain hardening in fault zone. After *Ismat & Mitra* (2005).

2.1.3 Rheological Implications

Ongoing fracturation means accommodation of three-dimensional penetrative strain in the rock mass, resulting in a damaged rheology that will be a function of the cataclastic intensity and the mechanical specificities of the intact rock material. The resulting cataclastic rocks offer mechanical properties that will be proportional to the extent of damage present. Damage can be described by structural, textural and mineralogical evidences. Cataclastic rock materials from brittle fault zones are highly complex and variable, and detailed models of fault rock deformation have been documented (see references below). Based on a conceptual approach, cataclastic fault rocks correspond to a mixture of "hard" and "soft" parts, for which the definition of a damaged rock rheology applies best. Hard parts correspond to blocks and clasts of different size and shape inside the fault zone. The softer parts are characterized by the altered rock matrix. A bimodal approach is therefore appropriate to describe fault zone materials. An indicative simplistic comparison can be made between cataclastic rocks and reinforced concrete: the angular cataclastic blocks are comparable to metallic fibers in concrete, which have a strengthening effect on the rock mass. However, average mechanical behavior is controlled by the matrix properties that result from the complex interaction between fracture localization and chemical weathering.

Fault zones *s. str.* form by strain localization and initiate by the development of shear bands. Shear

bands can be seen as resulting from the spatial development of a crack population and correspond in this sense to the larger scale manifestation of a fracture as made up of many small fracturation events. The basic approach to understanding the occurrence (localization) of deformation bands draws from the application of soil mechanics to porous rock deformation (see *Bésuelle & Rudnicki, 2004*). The formation of bands in a sheared rock is similar to the phenomenon of yielding in soils (*Roscoe, 1958, 1963*) and corresponds to the stress level marking the transition from elastic to permanent (plastic) deformation. From a theoretical point of view a modified Cam cap approach can be adopted to describe yielding in rocks. This corresponds basically to an improvement of the Mohr-Coulomb approach for intact rock that considers normal and tangential stresses on a single fracture plane to describe rock failure (e.g. σ & τ , **Fig. 2.7**) by using instead the first stress invariant p and the deviatoric stress q accounting for the deformation by concurrent multiple fracture “planes”. A one-to-one correspondence between certain terms and concepts of Cam cap models for soils and rocks is not considered to be established because homogeneous deformation and continuum flow are implied in critical state soil mechanics and the classical Cam cap model, whereas strain localization is of more importance in rocks (*Schultz & Siddharthan, 2005*). It is reported that yielding (formation of bands) is a function of hostrock’s porosity, grain packing geometry, pore-water content, depth of burial (i.e., confining pressure), the differential stress that drives the deformation, and the stress path that the rock has taken to get from its undeformed state to its yielding state (*Schultz & Siddharthan, 2005*). Surfaces resembling critical state lines in porous rocks are reinterpreted in this context as either the peak or residual frictional sliding criteria that represent the stress states for which yielded rock (damage zones composed of dilational or compactional deformation bands) changes its deformation style from distributed strain hardening

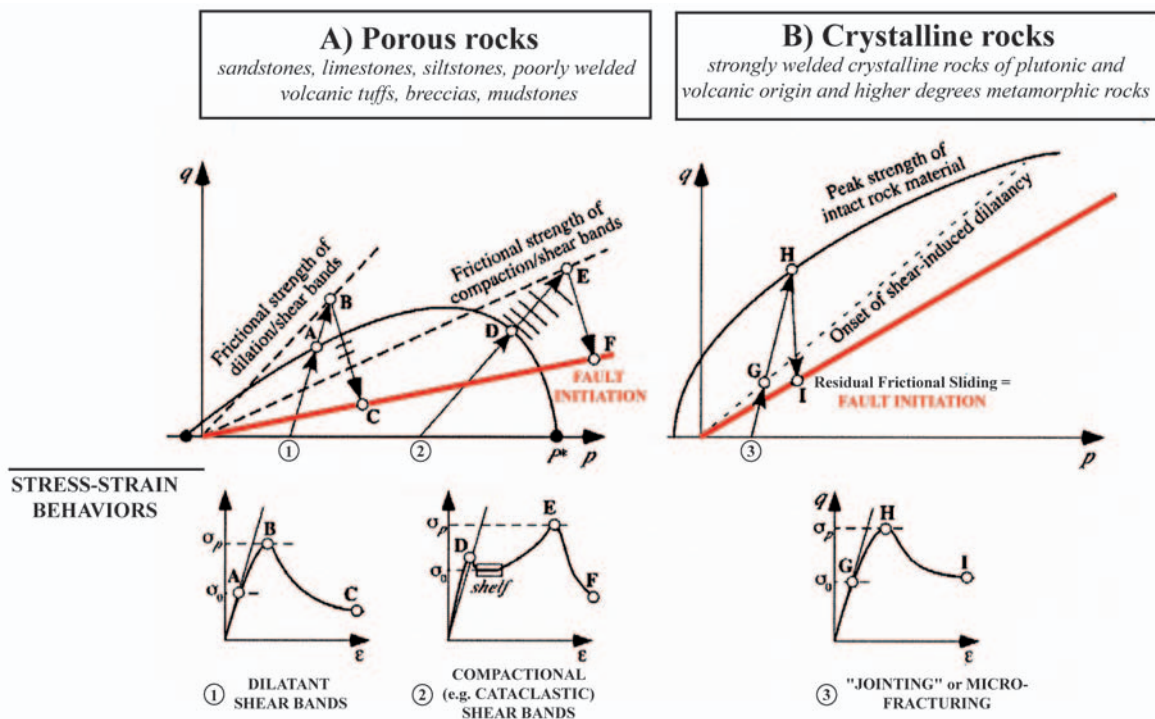


Fig. 2.7 Comparison of fault growth in porous rocks (A) and crystalline rocks (B) for a compressive remote stress state. Path 1, 2 and 3 corresponds to different fault initiation in function of the mode of “fracturing” or “failure” of the rock. Cam cap model to describe yielding in rocks, using the two stress invariants q (“deviatoric stress”) and p (first stress invariant $I_1 = \sigma_1 + \sigma_2 + \sigma_3$). In the context of porous rock deformation, yielding may occur somewhat sooner than band localization in rock. Much of the standard literature on rock deformation and fault formation centers on Coulomb frictional sliding on a preexisting “zone of weakness” such as cracks and joints. While Mohr Coulomb approach may be relevant to faulting in crystalline rocks having very low porosity, such as granite, basalt, welded tuff, and highgrade metamorphic rocks, it does not adequately describe the faulting process in e.g., sedimentary rocks having higher porosities, as are commonly found in continental interiors and at plate margins (such as accretion prisms and continental rifts). Modified from *Schultz & Siddharthan (2005)*.

to focused strain softening behavior. Both the individual elements (e.g., bands, cracks) and the total assemblage (e.g., damage zone, large-offset fault zone with linked slip surfaces) must now be considered as “fractures” in the broadest sense of the term.

The structural model of fault zones mentioned in **section 2.1.2** involves different types of deformation bands that involves or not a shear component (**Fig. 2.8**). *Schultz & Siddhartan* (2005) make in this respect a difference between *compactional* and *cataclastic* bands. They include *dilation bands*, mainly equivalent to a “crack”, just involving more porous rock inside the band than outside, *dilation bands with shear* that are effective fluid conductor, *shear bands* accommodating shear with no volume change (compaction or dilation) within the band, *compaction bands with shear*, and *compaction bands without shear*, forming barriers to subsurface fluid flow. Dilation bands do not have cataclasis and likely serve as efficient conduits for fluid flow in the subsurface due to their enhanced porosity relative to the host rock. Compaction bands with shear lead to cataclasis and include grain crushing which reduces the average grain size within a growing band, produces a tighter packing geometry (porosity reduction), and makes the grains more angular and consequently less able to roll under shear stress. As a result it becomes more difficult to accommodate shearing displacements resulting from progressive strain hardening in these bands and favored cataclasis. As seen in **Fig. 2.8**, the creation of a spatially distributed network of fractures/bands is responsible for the development of an extremely damaged zone (e.g. that precedes faulting, strongly reducing permeability producing seals to fluid circulation, *Schultz & Siddhartan*, 2005). According to these authors, all five kinematic varieties of bands can be understood using the framework of a Cam cap model as applied to porous granular rocks. This approach provides a simple yet powerful unifying framework for understanding the genesis and developmental sequence of deformation bands, damage zones, and attendant faulting.

2.2 INFLUENCE OF THE INITIAL PROTOLITH COMPOSITION

The occurrence of damaged rock mass is irrespective of the initial rock composition that undergoes deformation and faulting. In porous media (e.g. in the range of 5% porosity or more), including sandstones, limestones, siltstones, poorly welded volcanic tuffs, breccias, as well as poorly indurated (“soft”) sediments like mudstones, deformation bands lead to the nucleation of fault by progressive strain localization and ongoing yielding (**Fig. 2.7 A**). In these rocks, deformation occurs by grain shifting (i. e. shearing, dilatation and compaction) and spatial rearrangements of these grains follow (i. e. modification in grain packing and grain size reduction by crushing of individual grains). The degree of grain shifting defines the classes of deformation bands mentioned above. In low porosity rocks (< 1% porosity), including strongly welded crystalline rocks of plutonic and volcanic origin and higher degree metamorphic rocks constituting solid crystalline aggregates, deformation and strain localization occur in a different way and faulting results more as a response of “failure” than of initial yielding of the rock (**Fig. 2.7 B**). *Schultz & Siddhartan* (2005) explain this difference in deformation behavior by the fact that cracking in crystalline rock (i. e. moving the grain apart) requires less energy than does shearing, implying either the creation of joints as preexisting planes of weakness leading to faulting by frictional sliding, or the nucleation of microcrack swarms that condense and form a weak zone as an early stage of the same deformation event leading eventually to shearing. In both cases, the deformation of crystalline rocks involves dilatant cracks and local volume increase that subsequently shears.

Cracks, faults and deformation bands all lead at the end to the development of fault zones and follow as a response of strain localization (**Fig. 2.8**). The homogeneity of the model presented in **Fig. 2.7** is accordingly highly interesting to provide a coherent framework in the combined geological-geomechanical approach of cataclastic fault rocks. The conditions for localization of either type of

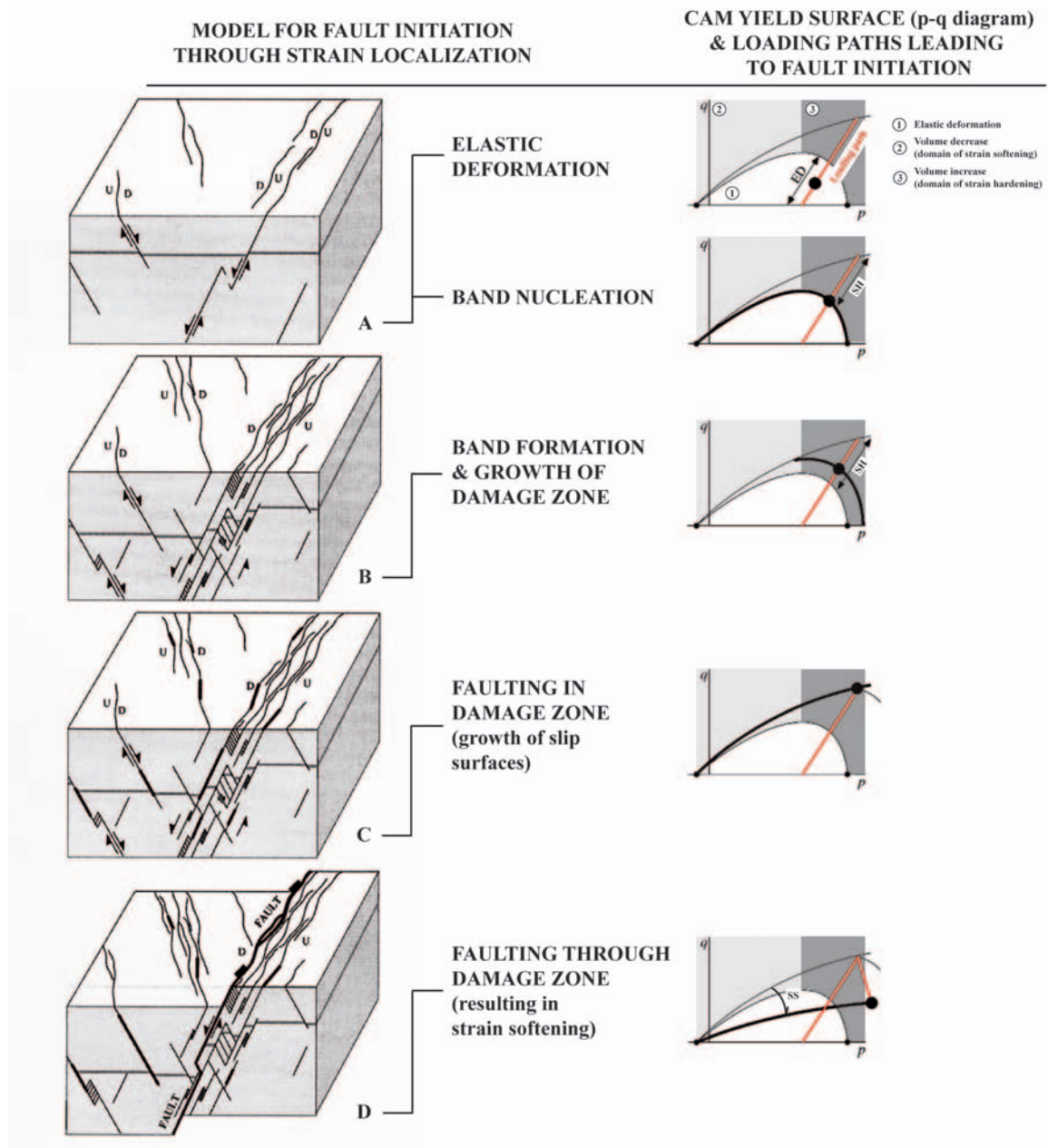


Fig. 2.8 Initiation of fault zone through progressive development and interaction of deformation bands including compaction (no shear) and cataclastic (shear) bands. Corresponding Cam yield surfaces defining the limit of elastic deformations are given. Stages of strain hardening (volume increase) and strain softening (volume decrease) are indicated. Cataclasis of initial rock masses involve a succession of these two mechanisms over geological time, leading to the progressive damaging and apparition of fractured rock rheology. Modified from *Schultz & Siddharthan* (2005).

deformation mode in a pressure-sensitive, dilatant/frictional material are quite similar (*Borja, 2002*) but are achieved differently as a result of initial rock composition. Therefore, *Schultz & Siddharthan* (2005) propose to extend the term “fracture” as a generic name for such processes. In this regard, fault zones that nucleate either by a progressive building of shear bands leading to a continuous change in normal and shear strain or by brutal step-wise changes in the displacement gradient (e.g. failure) involving a discontinuous shear should be regarded as the large-scale manifestation of “fracture”.

Accordingly, a key for the geological and geomechanical characterization of the resulting fault rocks will be the study of the textures and structures development in function of initial rock composition,

as well as the mineralogical and geochemical modifications occurring from the damage zone toward the fault core, mostly as a result of the general increase in fracture density (*Escuder-Virueite et al.*, 2004). *Hayman* (2006) shows that a coupled study of fault rock integrating geochemical, mineralogical and structural techniques is of great advantage in understanding the nature of the rock outcropped in such context and in inferring on its actual alteration state.

2.3 TERMINOLOGY FOR TECTONIZED ROCKS

The classification of fault rocks is either made through descriptive (*Higgins*, 1971; *Heitzmann*, 1985) or genetic classification systems (e.g. the review in *Twiss & Moores*, 1992). An evolution of terminology and definitions of (cataclastic) fault rocks has been observed as a result of the better understanding of rock deformation mechanisms but some confusion still exists between geologists and practitioners in engineering geology (*Bürgi*, 1999). Therefore, **Table 2.1** presents a combined classification for fault rocks based on **A**) structural geological considerations and **B**) geomechanical implications in terms of expected material performance. A detailed discussion of the origin of the names given to fault zone rocks can be found in *Bürgi* (1999).

All fault rocks result from strain localization leading to formation of fault zones and are ductile on a regional scale. Kakirite and cataclasite result from brittle processes that were extensively described in this chapter. They are often subject to weathering and alteration due to interaction with fluids (e.g. *Passchier and Trouw*, 1996). Kakirite corresponds to materials likely to be found in fault cores and are stable only under confining pressure conditions, with properties similar to soil materials (*Habimana*, 1999). Additional names involve fault breccia and fault gouge (*Davis & Reynolds*, 1996). Fault breccia and fault gouge can be differentiated by the amount of matrix material. In this respect, fault breccias are composed of angular and rounded clasts in a finer matrix, where the amount of matrix constitutes less than 30% of the rock mass volume. Fault breccia fabric is usually random. In fault gouge the entire mass, including the mineral grains, is heavily fragmented (microbreccia) and the matrix makes up more than 30% of the rock mass volume. Fault gouge may depict a crude foliation.

Observed in thin-sections, the diagnostic character of brittle fault rocks is the clast-in-matrix texture wherein clasts, or survivor grains, are surrounded by a matrix of comminuted material and secondary minerals (*Hayman*, 2006). The clast-in-matrix texture can be further subdivided into cataclastic and granular textures (*Twiss & Moores*, 1992). Cataclastic textures, found primarily in the breccias, are distinctive for contacts between clasts, and transgranular fractures that cross grain boundaries or radiate from grain contacts. Granular textures, found mostly in the gouges, are distinctive for clasts that are separated by a finer grained matrix and, where present, have transgranular fractures that do not cross grain boundaries (i.e. predate gouge deformation). Some gouges, and granular gouges in particular, have compositional banding, referred to as microbands.

The occurrence of mylonite involves higher metamorphic conditions and induces the production of dynamically recrystallized mineral assemblages that are indicative of greenschist facies conditions. Mylonite will not be considered further in this work.

A

| CATACLASTIC ROCKS | | | | |
|--|---|--------------------------|-------------------------------|-------------------|
| Fabric | Texture | Name | Clasts | Matrix proportion |
| No macroscopic preferred orientation, chaotic fabric | Cataclastic texture, angular and obtuse fragments | Tectonic breccia: | | |
| | | <i>Megabreccia</i> | > 0.5 m | < 30 % |
| | | <i>Breccia</i> | 1 – 500 mm | < 30 % |
| | | <i>Microbreccia</i> | < 1 mm | < 30 % |
| | | Kakirite | < 0.1 mm | < 30 % |
| | | Cataclasite | ≤ ~10 mm | > 30 % |
| | | Pseudotachyllite | Glassy or granulometry ≤ 1 μm | |
| MYLONITIC ROCKS | | | | |
| Fabric | Texture | Name | Granulometry | Matrix proportion |
| Foliated or lined | Metamorphic texture, crystalline aggregates | Mylonitic gneiss | > 50 μm | |
| | | Mylonitic serie : | | |
| | | <i>Protomylonite</i> | < 50 μm | < 50 % |
| | | <i>Mylonite</i> | < 50 μm | 50 - 90 % |
| | | <i>Ultramylonite</i> | < 10 μm | > 90 % |

B

| CATACLASTIC FAULT ROCKS | | | |
|------------------------------------|---------------------------|----------------------|-----------|
| UNCOHESIVE CATACLASTIC FAULT ROCKS | | COHESIVE FAULT ROCKS | |
| KAKIRITES | | CATACLASITES | MYLONITES |
| Fault Breccia (>30% clasts) | Fault Gouge (<30% clasts) | | |

Table 2.1 Classification of fault rocks according to **A**) a genetic classification in terms of grain size (adapted from *Twiss & Moores, 1992*) and **B**) a more geotechnical classification of fault rocks inferring on rock cohesion (adapted from *Bürgi, 1999*).

2.4 GLOSSARY OF TERMS RELATED TO CATACLASTIC MATERIALS

Considering two domains of intact and damaged rock mass, resulting rock mass elements have to be defined to address characterization purposes. The idea is to obtain a general framework of terms and a conceptual view that can be adopted for any brittle fault rocks regardless of their initial petrological content. With this glossary, it is expected that an improved communication basis between geologists and engineers can be promoted and that a better geotechnical characterization of rock cores realized in the future.

The terms presented hereafter refer to observations at the sample scale, by means of direct or indirect techniques (see later **Chap. 4 & Fig. 4.2**). A protocol of geological characterization based on these considerations will be presented accordingly in **Chap. 7 to 10**.

2.4.1 Primary Rock Matrix

Primary rock matrix is the “rigid body” of the initial rock protolith making up the intact rock mass. It corresponds to the “block material” of the classification of *Hoek & Brown (1997)* based on a block-discontinuity model. Primary rock matrix defines the raw strength of the intact rock material and can be related to typical textures that are a function of the petrology and its corresponding mineral paragenesis (magmatic, metamorphic or carbonatic). Over geological history, textural, structural and possible mineralogical modifications can affect the primary rock matrix.

In general, macroscale discontinuities (e.g. joints, stratification) that do not involve a shear component do not change rock matrix composition. Diagnostic elements of such primary discontinuities can be found at the sample scale. Other primary discontinuities concerns void

spaces (e.g. pores). A geomechanical characterization of the intact rock mass through investigations at the sample scale requires therefore defining the strength properties of the primary rock matrix and to take into account the strength reduction expected from such discontinuities at a more regional scale (block-discontinuity model).

2.4.2 Cataclastic (Damaged) Rock Matrix

The cataclastic or damaged rock matrix results from a dynamic alteration that has modified a primary rock matrix as a result of tectonic activity. Alteration related to tectonics is responsible for fault zone development and can take several degree and intensity. It produces the general heterogeneous and structurally complex nature of damaged rock masses. Such alteration results from both mechanical and chemical processes. Mechanical processes are characterized by stress & strain localization that is responsible for fracturation at different scales. A shear component is often involved. Chemical processes transform the primary rock composition and lead to the development of secondary mineral phases (phyllosilicates, clay minerals). Chemical alteration is increased in case of a high degree of fracturation and favors rock interaction with hydrothermal fluids.

Damaged rock matrix corresponds to the fine-grained component of fault rocks. Textural remnants of an intact rock matrix can be preserved but major structural & mineralogical modifications are expected as a result of tectonic activity. Discontinuities affecting the damaged rock matrix are mostly observed at the microscale. They can be open, sealed or recrystallized, the respective presence of which complexifies the overall damaged rock rheology.

Precise determination of the strength properties of a damaged rock mass at the regional scale is therefore more difficult to establish due to the great heterogeneity observed at the sample scale. For a geomechanical characterization, a mineralo-structural analysis has first to be conducted at the microscopic level. Second, by combining the derived informations from representative and contrasted samples, an evaluation of the heterogeneity at the rock mass scale can be addressed to develop the best mechanical understanding of the probable behavior of a damaged zone.

2.4.3 Blocks & Clasts

Blocks and clasts are the result of intact rock mass fragmentation by tectonic processes. Blocks are the largest fragments that can be observed both on regional and outcrop scales. Clasts are the equivalent at the sample scale and are observable down to the microscopic level. Study of blocks and clasts can be directly linked to a degree of damage that has affected initial rock mass. Blocks and clasts form either by static or dynamic fracturing.

Accordingly, two categories of blocks and clasts have to be determined. The first develops fragments that still correspond to the composition of the intact rock matrix (*blocks/clasts of intact rock matrix*). The second category corresponds to rock fragments having properties of the damaged rock matrix (*blocks/clasts of damaged rock matrix*).

For the improved geomechanical characterization of a damaged rock mass, strength determination can consider the relative proportion of blocks and clasts of an intact or damaged rock matrix as well as their respective shape and orientation.

2.4.4 Fractures

Fractures are used as a generic term describing the discontinuities affecting a rock mass at all levels of observation. They can be micro-cracks, cracks, joints, veins, deformation bands, fault zones, and shear zones. All are constituents affecting the rock mass and resulting from strain localization expressed as compressive, dilatant or shear efforts. The occurrence of fractures changes

the mechanical properties of the rock mass by modifying its textural, structural and mineralogical properties to produce a fractured-rock rheology.

Fracturing is the result of tectonic efforts and deformations and is responsible for the development of a heterogeneous rock material involving complex relationships between different fracture populations. Fractures are defined by their extent, persistence, orientation, and rugosity. They favor fluid circulation and can be additionally characterized by variable surface conditions.

2.4.5 Damage Indicators

The term *damage indicator* is introduced in this study to characterize all structural, textural and mineralogical elements that are diagnostic of the cataclastic process when observed at the sample scale. The concept can be however translated to the outcrop and regional scales to better describe a given rock mass architecture. With the concept of *damage indicators* an attempt is made to characterize the particular zones of weakness inside a damaged rock. It is chosen in reference to the terminology for fault zone description proposed by *Micarelli et al.* (2006), evolving from a weakly deformed damage zone (low damage) towards an intensely deformed damage zone (high damage) and a fault core (maximum damage).

As used in the present work, *damage indicators* relate to observations at the microscopic level. They regroup evidences from secondary (weak) mineral phases, from damage micro-structures (e.g. fractures) and from specific rock textures indicative of rock fragmentation at different levels (progressive clast and grain comminution). *Damage indicators* provide accordingly a mean to evaluate the specific modifications underwent by a given rock mass during tectonic activity which will affect its properties compared to a corresponding intact rock composition. Thus it is expected that *damage indicators* observed at the sample scale can assist in evaluating a degree of tectonic alteration underwent at a given sample locality.

Evidences from various and contrasted samples coming from a same tectonized zone can further be brought in relationship with typical modes of mechanical deformations that will concurrently affect a cataclastic horizon.

2.5 CONCLUDING REMARKS

As presented throughout this chapter, cataclasis is a complex process affecting all rock types at shallow crustal conditions. It involves complex mechanisms reflecting the effect of stress & strain accumulation and release over time. Both mechanical and chemical alterations influence cataclasis. Resulting rocks represent therefore many qualities of materials, with strength properties varying from near intact rock strength down to values similar to soil materials.

Tunnelling projects regularly encounter cataclastic materials underground; therefore a proper rock mass characterization as well as its translation in terms of strength will be crucial for the most appropriate choice of excavation techniques. Because tunnels represent a disturbing feature corresponding to the opening of a “discontinuity” in the underground space, knowledge of the response of both intact and damaged rock masses is most important for the proper design of the engineering structure. Accurate mechanical models exist for intact rock masses. Due to the heterogeneity of damaged rock masses, such models are more difficult to establish in this domain. Therefore combining knowledge from fundamental research on fault zone development and its implications on rock textures, structures and mineralogy can add many useful constraints for a better rock mass characterization based on rock core samples from reconnaissance drilling operations. Observations made at that level can be transposed in their meaning for the large-scale

picture of fault zones. Geomechanical models could most probably be improved in that way.

This research attempts at interpreting the modifications that rocks undergo during tectonic activity and subsequently quantify these modifications by means of *damage indicators*. Methodological implementations of damage indicators for the geological and geomechanical characterizations are described in **Chap. 10**.

3

PREVIOUS RESEARCH AT EPFL

Peu à peu, ma vie
s'empara du monde
que je croyais aux autres.
Les images de mes livres
devinrent mer, terre, ciel,
naviguée, foulée, pénétré
par moi. Le lent dimanche – rue solitaire –
du village nostalgique, fut un dimanche
universel et plein de joie.

Juan Ramón Jiménez, *Piedra y Cielo*

A research project on the behavior of cataclastic rocks encountered in underground excavations through the Alps was started at EPFL in the late nineties under the financial support of the Swiss National Science Foundation. It questions the possible correlation between geological and geomechanical properties of cataclastic rocks for their improved geotechnical characterization.

A first research conducted at GEOLEP was entitled *Cataclastic fault rocks in underground excavations: a geological characterization* (Bürgi, 1999). A second research dealing with more mechanical aspects of cataclastic rocks was realized at LMR under the name *Caractérisation géomécanique de roches cataclastiques rencontrées dans des ouvrages souterrains alpins* (Habimana, 1999). Promising results were obtained from the study of quartzo-phyllic rocks sampled in the hydraulic gallery of Cleuzon-Dixence in the Swiss Alps in terms of the mentioned correlation. The present project is a continuation of these two studies; it constitutes in this sense an interdisciplinary research.

As part of this new research, two Master theses have been realized at GEOLEP (Veuve, 2007; Chaignat, 2007) and presented in 2007 at the University of Lausanne in the framework of the Master Program in Engineering Geology (partnership UNIL-EPFL).

3.1 CONSIDERATIONS ON ROCK MASS CHARACTERIZATION

To introduce the characterization methodology for cataclastic rocks, a first review of current geotechnical classifications is presented. Specific problems related to the occurrence of cataclastic rocks in underground engineering projects are presented. In particular, the reasons why classical schemes are limited for the study of tectonized rocks is highlighted.

3.1.1 Why Rock Mass Characterization?

Rock mass characterization represents an entire part of the preliminary studies investigating the feasibility of an underground construction project. Based on experience, rock mass characterization is an empirical reference tool that helps designing an underground excavation by determining global rock quality characteristics. Such a characterization permits to establish international comparison standards and provides geologists and engineers with a common language (Habimana, 1999).

Geotechnical rock description is based on geomechanical properties of rock materials building up geotechnical units that are translated in terms of strength characteristics. Uniaxial compressive resistance determined from laboratory tests on rock cores was used by many authors to define mechanical domains of rock conditions and stability for tunnelling applications. A synthesis of rock properties in terms of strength has been conducted by Russo (1994) and is presented in **Fig. 3.1**.

In the last fifty years, several rock mass characterization schemes have been developed and used worldwide for tunnelling applications. They gained international recognition and define common practice in modern projects. Triaxial mechanical tests became an important aspect of rock characterization because of their ability to reproduce *in situ* stress conditions (e.g. effect of confining stress on rock strength & failure). Experience and increasing complexity in tunnelling showed however limitations of applicability, in particular when weak rocks (see **Fig. 3.1**) are encountered. Many modifications of classical rock mass characterization have therefore been proposed and implemented with more or less success.

Rock mass characterization is required to limit uncertainties for a proper project realization. Based on a purely mechanical approach, weak rocks are classified in such schemes regardless of origin, lithological, textural or mineralogical differences (Bürgi, 1999). However, since rock mass characterization has a direct impact on the choice of the excavation method, the tunnel support, the

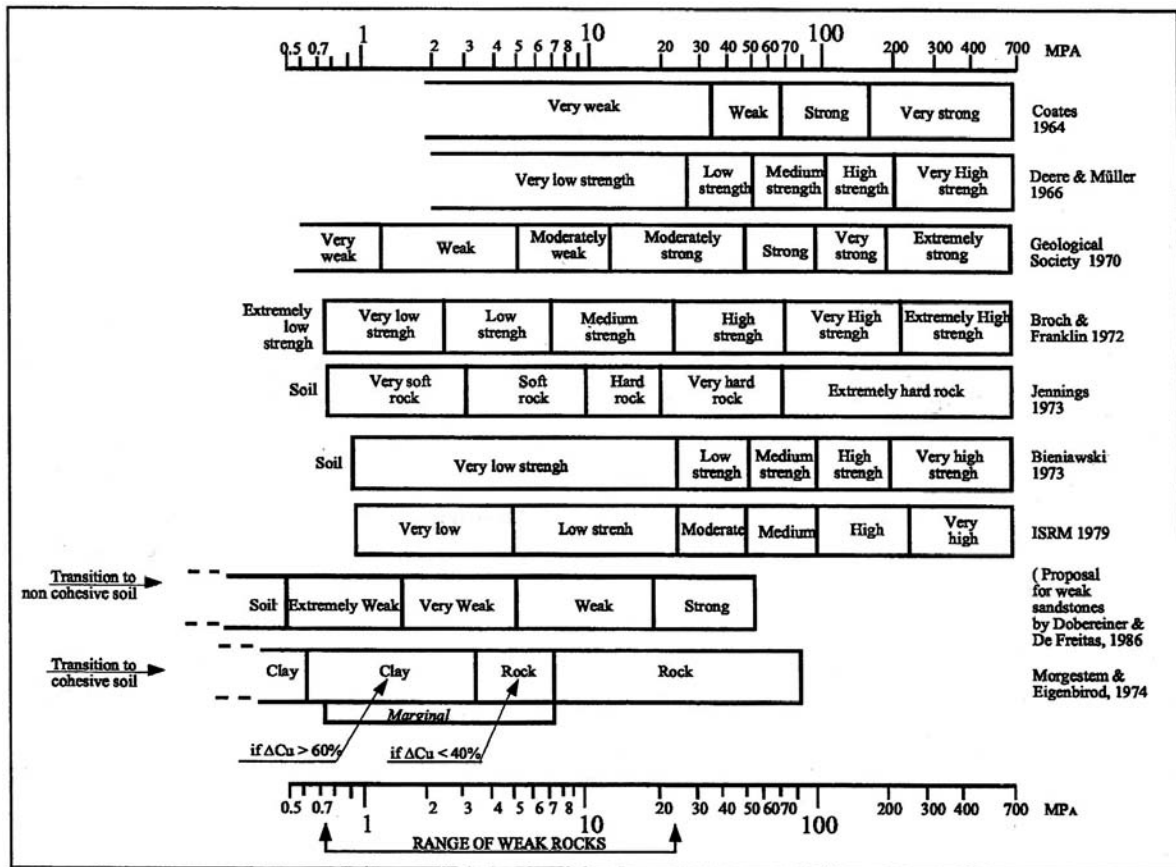


Fig. 3.1 Description of rocks based on the uniaxial compressive strength. After Russo (1994).

safety on the working site, the duration of the works, the long-term behavior and finally the cost of the construction, it is necessary to develop a correlation basis in between geological rock parameters and their objective control on rock strength.

Within standard rock mass classifications, material properties determined from selected samples have to be related with macroscopic evidences. Laboratory determinations address the characterization of rock matrix and joint conditions (families of joints, their spacing, their orientation and their surface conditions). Further, hydrological conditions in the rock mass are assessed from field investigations. Based on these inputs, a global picture of rock mass properties is drawn. The reliability of rock mass classification used in underground excavation and support design has been discussed in Palmstrom *et al.* (2001).

3.1.1.1 The Q-system of Barton

This system proposed by Barton *et al.* (1974) at the Norwegian Geotechnical Institute (NGI) is originally based on about 200 case histories of tunnels and caverns (Singh & Goel, 2006). It considers 6 parameters of rock properties (e.g. 2 for rock strength, 3 for fracturation and joint conditions and 1 for water incomes) from which a rating Q is determined accounting for the global quality of the rock mass. Numerical values of Q have been tested and introduced in empirical charts for the most appropriate design of support systems in function of the size of the tunnel (height or width). Accordingly, 38 support types are defined and since the original study of Barton (1974), more than 1260 records of tunnel construction having used this design approach are available nowadays. Based on experience, the Q-system is considered the best among all the classification systems for support in tunnels (Singh & Goel, 2006). The general scheme of the Q-system for tunneling applications is given in **Appendix I-I**.

In terms of rock mass characterization, the Q-system can be used to determine 9 classes of rock masses (Fig. 3.2). Furthermore, many empirical correlations have been proposed between the Q-value and additional parameters critical for the design of the underground structure. To name a few, relationships are reported between Q and the modulus of deformation, the P-wave velocities and in some extent the *in situ* permeability (Barton, 2002).

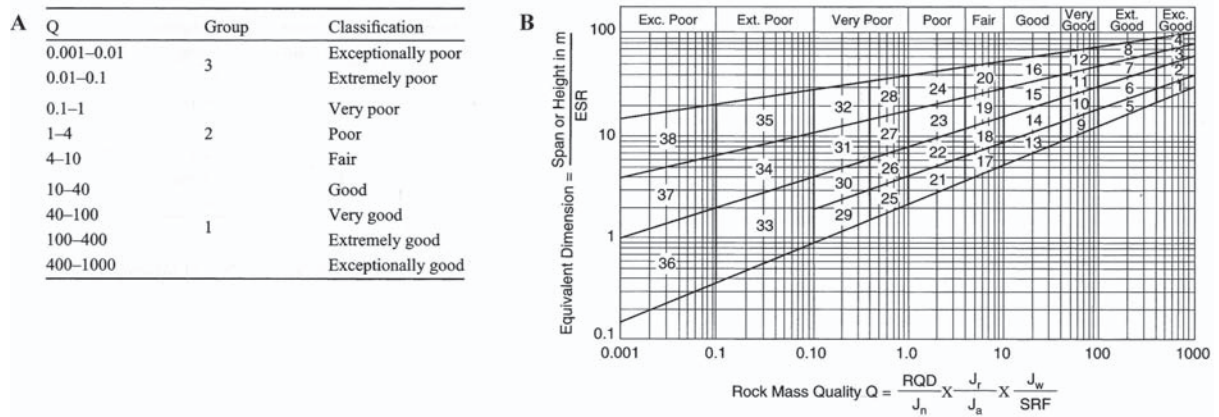


Fig. 3.2 A) Classification of rock mass based on Q-values. B) Tunnel support chart showing 38 categories according to the determined Q-values and in function of the excavation size (ESR = excavation support ratio). After Singh & Goel (2006).

3.1.1.2 The RMR of Bieniawski

Bieniawski rock mass classification is based on the concept of rock mass rating (RMR) and has seen many developments since its initial definition in 1973 (Bieniawski, 1973, 1976, 1978, 1979, 1984). Rock mass rating defines a value of expected rock mass quality and properties for each geotechnical unit under which a specific underground space is subdivided for design assessments. In a similar way than for the Q-system, 6 parameters are taken into account and for each of them a quality factor is attributed. The sum of these factors allows determining the global parameter RMR for the rock mass (e.g. the geotechnical unit) under investigation. When Q-values give a mean to decide which tunnel support will be more appropriate, RMR is more indicative of an estimation of the stand-up time of an underground opening. Design parameters and engineering properties of rock mass obtained via RMR are presented in Fig. 3.3. Accordingly, guidelines for selection of tunnel supports applicable to tunnels excavated with conventional and blasting methods are determined as shown in Table 3.1 (see also Appendix I-II).

| S. No | Parameter/properties of rock mass | Rock mass rating (Rock class) | | | | |
|-------|--|-------------------------------|-----------------------|---------------------|---------------------|----------------------|
| | | 100–81 (I) | 80–61 (II) | 60–41 (III) | 40–21 (IV) | <20 (V) |
| 1. | Classification of rock mass | Very good | Good | Fair | Poor | Very poor |
| 2. | Average stand-up time | 10 years for 15 m span | 6 months for 8 m span | 1 week for 5 m span | 10 h for 2.5 m span | 30 min. for 1 m span |
| 3. | Cohesion of rock mass (MPa)* | >0.4 | 0.3–0.4 | 0.2–0.3 | 0.1–0.2 | <0.1 |
| 4. | Angle of internal friction of rock mass | >45° | 35°–45° | 25°–35° | 15°–25° | <15° |
| 5. | Allowable bearing pressure (T/m ²) | 600–440 | 440–280 | 280–135 | 135–45 | 45–30 |

Fig. 3.3 Rock mass classification into five classes of rock quality according to RMR values. After Bieniawski (1979).

* These values are applicable to slopes only in saturated and weathered rock mass.

Note: During earthquake loading, the above values of allowable bearing pressure may be increased by 50 percent in view of rheological behavior of rock masses.

| Rock mass class | Excavation | Supports | | |
|--------------------------------|---|--|--|--|
| | | Rock bolts (20 mm diam. fully grouted) | Conventional shotcrete | Steel sets |
| Very good rock RMR = 81–100 | Full face 3 m advance. | Generally, no support required except for occasional spot bolting. | | |
| Good rock RMR = 61–80 | Full face. 1.0–1.5 m advance. Complete support 20 m from face. | Locally, bolts in crown 3 m long, spaced 2.5 m, with occasional wire mesh. | 50 mm in crown where required. | None |
| Fair rock RMR = 41–60 | Heading and bench. 1.5–3 m advance in heading. Commence support after each blast. Complete support 10 m from face. | Systematic bolts 4 m long, spaced 1.5–2 m in crown and walls with wire mesh in crown. | 50–100 mm in crown and 30 mm in sides. | None |
| Poor rock RMR = 21–40 | Top heading and bench. 1.0–1.5 m advance in top heading. Install support concurrently with excavation 10 m from face. | Systematic bolts 4–5 m long, spaced 1–1.5 m in crown and wall with wire mesh. | 100–150 mm in crown and 100 mm in sides | Light to medium ribs spaced 1.5 m where required. |
| Very poor rock RMR < 20 | Multiple drifts 0.5–1.5 m advance in top heading. Install support concurrently with excavation. Shotcrete as soon as possible after blasting. | Systematic bolts 5–6 m long spaced 1–1.5 m in crown and walls with wire mesh. Bolt invert. | 150–200 mm in crown 150 mm in sides and 50 mm on face. | Medium to heavy ribs spaced 0.75 m with steel lagging and forepoling if required. Close invert |

Shape: Horseshoe; Width: 10 m; Vertical stress < 25 MPa; Construction: Drilling & blasting.

Table 3.1 Guidelines for excavation and tunnel support following recommendation by *Bieniawski* (1984).

Similar to Q, empirical relationships integrating the RMR have been proposed to evaluate optimal tunnel design (see for example equations used to estimate support pressure, unsupported span time of underground openings, efficiency of rock bolts and required rock bolt length, type and amount of sprayed concrete needed, etc.). As stated by *Hoek & Marinos* (2006) and *Singh & Goel* (2006), RMR system is however unreliable in very poor rock masses and care should be taken when applying such an approach in unfavorable context. Based on experience, the Q-system of Barton is reported more accurate when having to deal with weak rock masses.

3.1.1.3 The GSI of Hoek

As an alternative to Barton’s and Bieniawski’s rock mass classifications, *Hoek* (1994) envisaged a *Geological Strength Index* (GSI) for intact and jointed rock masses that has been developed in order to avoid the double accounting of parameter in the analysis of rock structures and estimating rating of a rock mass. By double accounting it is meant that the particular effect of a specific parameter can be redundantly considered in either the analysis of a specific rock structure or its formulation in terms of the RMR (for example effect of pore water pressure or orientation of joint sets).

Based initially on RMR or Q-values, *Hoek & Brown* (1997) established a methodology for GSI determination relying on field observations. Using the concept of a rock mass strength dependent on “intact block” properties and concurrent effect of discontinuities, a characterization chart taking into account structure of the rock mass and surface conditions of discontinuities was developed to define ranges of GSI values for the average *in situ* retranscription of rock mass properties. **Fig. 3.4** presents the GSI chart in the form published by *Hoek et al.* (1998) taking into account practical recommendations made by these authors for tectonically sheared rock masses.

Even if often seen as a simplification by design engineers, GSI-based approaches have the advantage of being closer to the geological observations than are Q- or RMR classification systems that rely more on “numbers” (*Hoek & Marinos*, 2006). This aspect is particularly important when having to deal with weak rock masses in underground excavations (e.g. GSI < 25) and it is reported by several authors that the use of the Q-system or RMR, developed for applications in hard rocks and jointed rock masses bear many disadvantages and can lead to erroneous determination of design

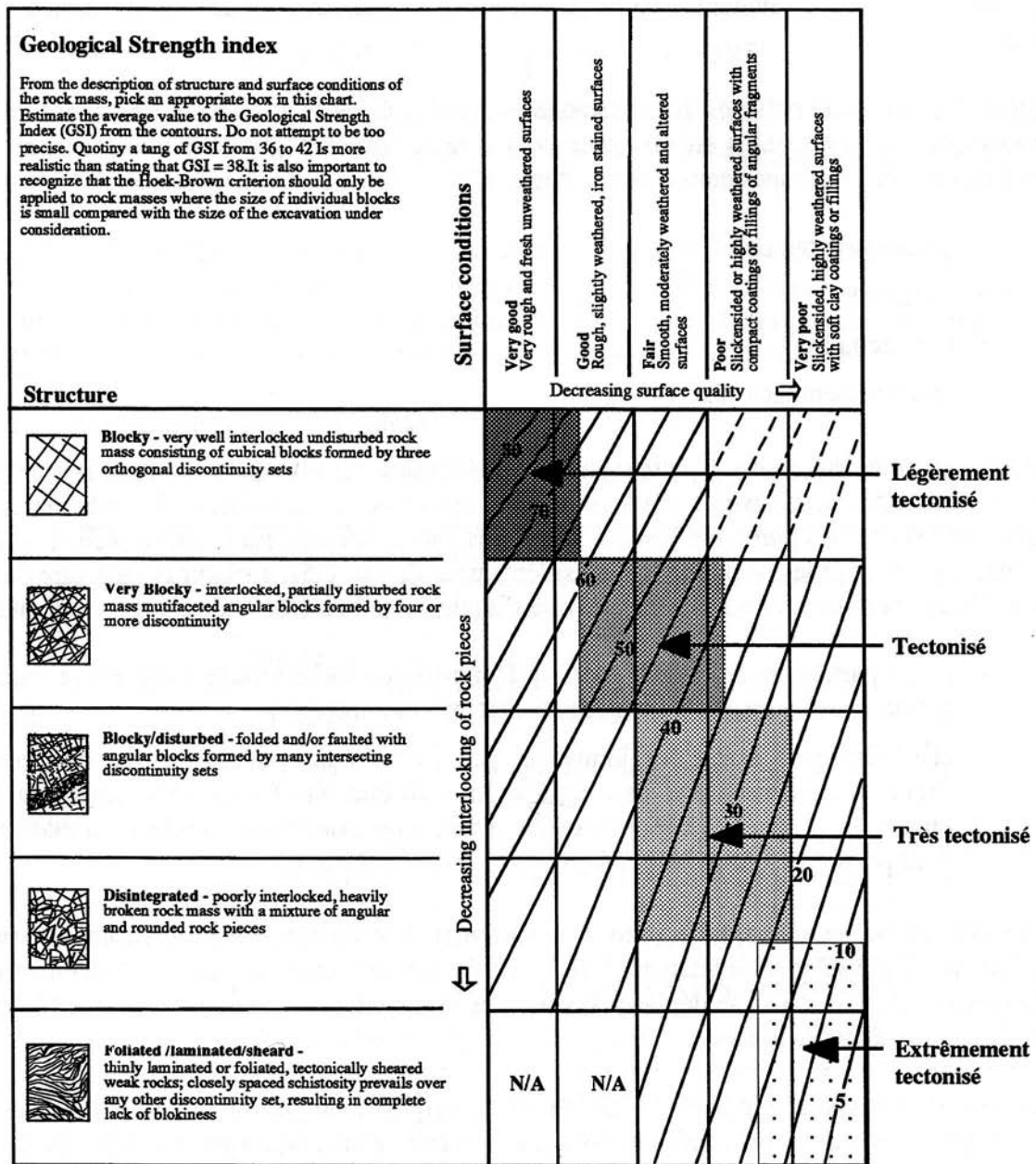


Fig. 3.4 GSI chart for rock mass characterization of jointed rock masses proposed by Hoek et al. (1998) and used by Habimana (1999) for the definition of four tectonization degrees for cataclastic rock materials. See also Appendix I-III.

parameters (Russo, 1994; Hoek et al., 1997, 2005, 2006; Kavvas, 1996; Bürgi, 1999; Habimana, 1999; Dalgıç, 2003). A critical approach for the geotechnical characterization of (weak) rock masses is still awaited and based on the current evidence, it seems important to introduce micro-structural and mineralogical considerations in such a classification. A better characterization of tectonized rock mass features at the scale of the work could accordingly be obtained that would relate genetic aspects of the cataclastic deformation (e.g. result of fault zone activity) with specific damage structures to be assessed during preliminary studies and proper excavation.

Since the original publication by Hoek & Brown (1997), the GSI chart have seen several modifications in the past years to correspond to more complex structural types such as laminated and sheared rock masses, heterogeneous rock materials such as flyschs, confined and fissile molasse (Hoek et al., 1998; Hoek & Marinos, 2000; Marinos & Hoek, 2000; Hoek et al., 2005, see Hoek &

Marinos, 2006 for a summary and Appendix I-III). Table 3.2 presents estimates for geomechanical parameters indicative of very good, average and very poor rock masses as mentioned in Hoek & Brown (1997).

| | | Symbol | Very Good quality hard rock mass | Average quality rock mass | Very Poor quality rock mass |
|---------------------------|--------------------------------|----------------------|-------------------------------------|------------------------------|--------------------------------|
| INITIAL CHARACTERISTICS | Intact rock strength | σ_{ci} [MPa] | 150 | 80 | 20 |
| | Hoek-Brown constant | m_i | 25 | 12 | 8 |
| | Geological Strength Index | GSI | 75 | 50 | 30 |
| | Friction angle | ϕ' | 46° | 33° | 24° |
| | Cohesive strength | c' [MPa] | 13 | 3.5 | 0.55 |
| | Rock mass compressive strength | σ_{cm} [MPa] | 64.8 | 13 | 1.7 |
| | Rock mass tensile strength | σ_{tm} [MPa] | -0.9 | -0.15 | -0.01 |
| | Deformation modulus | E_m [MPa] | 42'000 | 9000 | 1400 |
| | Poisson's ratio | ν | 0.2 | 0.25 | 0.3 |
| | Dilation angle | α | 11.5° ($\phi'/4$) | 4° ($\phi'/8$) | 0 |
| POST-PEAK CHARACTERISTICS | Friction angle | ϕ_f' | 38° | - | - |
| | Cohesive strength | c_f' | 0 | - | - |
| | Broken rock mass strength | σ_{fcm} [MPa] | - | 8 | 1.7 |
| | Deformation modulus | E_{fm} [MPa] | 10'000 | 5000 | 1400 |

Table 3.2 Practical estimates for the evaluation of geomechanical parameters used in the assessment of rock mass quality. After Hoek & Brown (1997).

3.1.2 How to Translate Geology into Numbers?

Based on a stimulating Summerschool performed in 2005 (Rational Tunnelling, Kolymbas & Laudahn, 2005), a little excursion is made in this section to introduce some of the limitations involved with the above presented rock mass classifications as well as to develop relevant aspects for this current research.

It has to be noted that none of the rock mass classification schemes presented above considers tectonically disturbed rock units from a genetical point of view (Bürgi, 1999). Pragmatical approaches are documented by Hoek et al. (1998), Marinos & Hoek (2001) or Marinos et al. (2005). They provide engineers with a more appropriate investigation protocol to assess rock mass quality in complex geological environment. However no proper geotechnical parameters describing quantitatively the expected strength reduction of a rock mass in function of tectonization (microstructural and mineralogical evidences) are currently in use. This results often in an incomplete characterization of damaged rock masses.

To summarize, the Q- and RMR-systems provide numerical values to the engineers from a purely effect-related perspective. They both have a subjective character. The GSI is on the contrary more of a causal approach based on pure geological observations. This would be actually appropriate to take into account tectonization, however it is often seen as a simplified model for the design of underground structure since this approach delivers *only* one value for rock mass friction, cohesive strength and elastic modulus (e.g. no strain softening and no anisotropy is taken into account, Fellner, 2005).

Extensive use of the presented geotechnical classifications is made in tunnelling projects and - without better alternative- weak rock mass characterization is performed accordingly. Thus, the geotechnical prognosis face many unknowns related to the geological uncertainty. Currently the

problem is overcome by introducing high security factors in the design calculations. This means that the common practice is based on risk reduction. As discussed in **Chap. 1**, risk assessment and management can only be achieved if a proper risk identification and understanding is previously available. This requires a proper scientific knowledge. **Chap. 2** makes clear that cataclastic fault zones represent 3D structures forming geotechnical units on their own. The width of a fault zone is with this regard a decisive control factor on resulting cataclastic rock fabric (*Fellner, 2005*). A successful characterization approach needs therefore determining critical parameters inherent to cataclastic rock structure and composition that have to be introduced as such in stability calculations to quantitatively account for geological factors.

As tunnelling methods rely strongly on initial rock mass characterization, a tendency of developing “recipes” for tunnelling has been seen over the years. The Norwegian Method of Tunnelling (NMT) makes extensive use of the Q-system and provides a clean design framework for good (hard) rock masses. The New Austrian Tunnelling Method (NATM) is based on the philosophy of “build as you go” and constantly confront expectation in terms of rock mass behavior with real-time observation through monitoring of the excavation. Unfortunately, such (empirical) recipes can lead to a disadvantageous black-box approach. In a slightly extreme manner, heavy criticism has even been expressed towards the NATM because the method is reported to mix scientific knowledge with pseudo-scientific postulates what led to confusion among professional engineers, which was further increased by an aggressive marketing approach (*Kovari, 2003*).

In our sense, in order to establish an effective rock mass characterization in the wide variety of geological conditions at shallow crustal conditions, two distinct rock domains function of geological history have to be assessed (*intact* and *damaged* domains, **Chap. 2**). The Q-, RMR- or GSI-systems have been developed initially based on considerations from the intact rock domain. The GSI, being closer to geological considerations, introduces already pragmatic extensions of the characterization procedures to describe *weak, laminated/sheared* and *tectonically* disturbed rock masses (**Appendix I-III**). A rational tunnelling approach requires the ability to predict potential risk and shouldn't rely (only) on adaptive strategies or past experiences. Positive identification of fault zones and their effect on rock mass characteristics constitutes an important potential risk for which assessment possibilities must be developed. In terms of design, a descriptive characterization of tectonized rock masses at the scale of the work is often not sufficient as critical elements able to explain their (large-scale) behavior are found through mineralo-structural studies at the microscopic scale.

In terms of hazard scenarios (short- and long-term), *Fellner (2005)* recommends considering anisotropic constitutive material behaviors, axisymmetric or 3D modelisation of wall effects on fault zones and strain softening or non-linear constitutive equations to study the influence of non-ideal plastic behavior on deformations.

The “hazard approach” has been implemented in the case of the 57 km long Gotthard Base Tunnel in Switzerland (*Fellner, 2003; Ehrbar, 2004; Amberg, 1999*). Previous research conducted at EPFL by *Bürgi & Habimana (1999)* delivers geological and geomechanical input parameters that could be considered in the risk assessment, modelisation and management of cataclastic rocks in underground works. Their respective works are now considered in the next two sections.

3.2 THE APPROACH OF BÜRGI & HABIMANA (1999)

A characterization methodology for cataclastic rocks based on mineralogical-structural parameters and mechanical evidences was developed at EPFL based on two PhD projects.

The *geological part* (Bürgi, 1999) gives an improved definition of weak rocks and a comprehensive method for their geological characterization. The application of objective and quantitative criteria, based on a clast-matrix model, leads to characterize cataclastic rocks by the combined influence of mineral phases (mean weighted Vickers hardness), arrangement of clasts (given by a texture coefficient) and matrix conditions (given by a matrix coefficient). By correlating the results from this geological classification with the geomechanical parameters of the studied cataclastic rocks, the method was found to have possibilities.

The *geomechanical part* (Habimana, 1999) points out the significant influence of the tectonisation intensity on both failure criterion and stress-strain relationship of cataclastic rocks. An adaptation of the Hoek & Brown failure criterion is suggested that takes into account the progressive damage undergone by cataclastic rocks during the tectonisation process. Parameters for this modified criterion are bounded by an upper limit corresponding to the original untectonised rock and a lower limit corresponding to a soil-like extremely tectonized material.

The two respective studies of Bürgi & Habimana (1999) represent a first effort in confronting geological and geomechanical evidences to improve the characterization possibilities of weak cataclastic fault rocks. Samples from different fault zones location have been studied and special care was accorded to the quality of the samples. With this regard, appropriate techniques of rock extraction have been developed to gain samples in their *in situ* conditions for both the geological and geomechanical investigations.

3.2.1 A Combined Geological and Geomechanical Approach

The study of rock cores from prospective drilling operations is an important input for the decision regarding the method of excavation and further design calculations. Data from rock core analyses together with consideration of the site conditions and *in situ* observation define a bundle of parameters that serve to establish a model of the underground structure and of its mechanical properties.

Two distinct approaches are required for rock core analysis:

- 1) For the **intact rock domain**, effective rock strength used for design purposes is controlled by the discontinuities affecting the rock mass, therefore laboratory strength values should be regarded as optimistic, since the sample scale is often not representative of the discontinuity spacing at the rock mass scale. General recommendations are made to reduce a laboratory determined strength value by 70% for practical applications. Additionally, in case of anisotropic rocks, the orientation of the weakness zones should be taken into account (oriented rupture criterion).
- 2) For the **damaged rock domain**, deformation of rock cores in the laboratory is controlled by the properties of the damaged rock matrix that can only be analyzed from a microstructural and mineralogical perspective. Laboratory data of damaged rock mass is here too pessimistic as the structural particularities of brittle fault zones influence effective rock strength at a larger-scale (e.g. for example blocks with angular shapes that can increase rock mass strength in analogy with metallic fibers in reinforced concrete, with the difference that rocks depict very low tensile strength compared to metallic fibers).

In the study of cataclastic fault rocks, a combined geological-geomechanical approach makes therefore particular sense. The reliability of laboratory tests can be evaluated on the base of an adequate conceptual model for the rock mass. Moreover, extensive laboratory determinations on cataclastic materials allow to test a large scatter of geological and geomechanical properties represented by this type of rocks as a result of their inherent heterogeneity.

3.2.2 Geological Investigations

According to *Bürgi* (1999), mineralogical composition and rock fabric define the main internal controls of mechanical properties. Rock fabric includes texture (geometrical aspects of grains/clasts, i.e. relative proportions, size, shapes packing and angularity) and structure (e.g. type of discontinuities, discontinuity orientation and density).

Rock fabric is best studied by means of thin section analyses for which image analysis techniques have been widely developed for quantitative structural/textural determinations from photomicrographs (*Howarth & Rowlands*, 1986; *Heilbronner*, 2000; *Stipp et al.*, 2002; *Wheeler et al.*, 2003; *Billi*, 2005; *Heilbronner & Keulen*, 2006). Mineralogical composition can be derived from different techniques: semi-quantitative X-ray diffractometry (XRD) provide a determination of the main mineral assemblage. If particular physico-chemical processes affecting rocks need to be investigated (rock alteration and weathering), electron microscopy techniques are required, as they allow inferring on chemical reactions affecting mineral phases by tracking their variation in mineral chemistry.

Geological investigations on about 40 cataclastic fault rocks of mainly quartzo-phylitic composition have been performed aiming the derivation of a textural, structural and mineralogical index (MSI). The respective influence of textural and structural parameters on rock strength is taken into account by a texture and matrix coefficient (texture coefficient TC, *Howarth & Rowlands*, 1986; matrix coefficient MC, *Bürgi*, 1999). They have been determined on digitalized thin sections at a standardized magnification of 8x. The strength control exerted by the mineral assemblage is expressed by its corresponding Vickers hardness (mwVh, *Calembert et al.*, 1980; *Bürgi*, 1999). A mean weighted Vickers hardness mwVh is accordingly determined by weighting the respective Vickers hardness of the mineral phases in presence according to their proportion determined by XRD.

The use of textural-structural considerations for fault rocks description defines two extreme cases of rock materials which refer to the deformation mechanism for cataclastic rocks (**Chap. 2 & Fig. 3.5**):

- 1) Cataclasite with a **granular (clastic) fabric** characterized by angular clasts of different dimension in a fine-grained cataclastic rock matrix made of a high proportion of weak minerals (e.g. *matrix-controlled cataclastic flow*);
- 2) Cataclasite with a **discontinuity fabric** where the general fracturation framework affects rock mass structure on a global scale (e.g. *block-controlled cataclastic flow*).

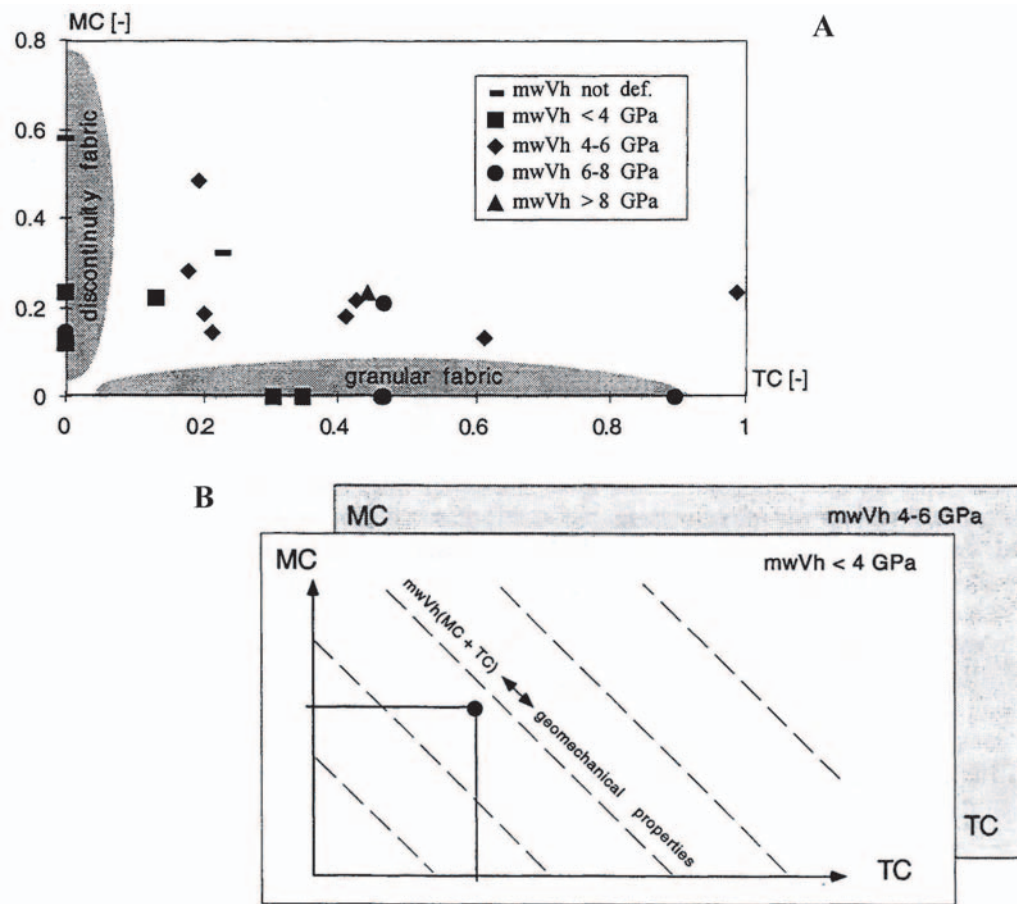


Fig. 3.5 A) MC-TC fabric diagram presenting the range of variability of quantified kakirite rock fabrics from Cleuzon-Dixence. B) Conceptual method for the characterization of weak cataclastic fault rocks taking into account their mineralogical composition (mwVh) and rock fabric (MC, TC). After Bürgi (1999).

3.2.3 A Mineralogical and Structural Index for Cataclastic Rocks

The mathematical formulation of the geological parameters supposed to control primarily cataclastic rock deformation and rock strength is given by Bürgi (1999) as the *Mineralogical and Structural Index* (MSI). In its actual form and as evaluated in this research, the MSI is defined as follow:

$$\text{Eq. 3.1} \quad \text{MSI} = \text{mwVh} (\text{MC} + \text{TC})$$

with

mwVh mean weighted Vickers hardness of mineral phases constitutive of the rock

MC matrix coefficient reflecting the effect of « discontinuities »

TC texture coefficient reflecting the effect of « clasts »

Observations on the rocks from Cleuzon-Dixence led to the idea that cataclastic rock strength is controlled at first by the mineralogical composition and that rock structure and texture represent “correction factors” accounting for a particular rock fabric inherited from tectonic movements. In which extent this correction has to be performed remained an open question in the work of Bürgi (1999). Similarly, the relationship between textural, structural and mineralogical properties of cataclastic rocks with selected geomechanical parameters has to be identified.

Compared to classical rock mass characterization schemes (RMR, Q-system, GSI) this index has the particularity of establishing a quantification of the rock mass based on rock evidences from the microscopic scale. Material heterogeneity and anisotropy are quantified with spatial & directional analysis tools. This quantification is based on the orientation of the thin section, generally taken perpendicular to the schistosity plane (if present or still visible). This point has therefore to be taken into account when the correlation between the geological and geomechanical properties of cataclastic rocks is addressed (orientation of thin section vs. rock core orientation used for triaxial test).

A detailed description of the parameters constitutive of the MSI will be made in **Chap. 7** as part of the geological characterization used in this research.

3.2.4 Geomechanical Investigations

A program of mechanical tests on cataclastic materials including uniaxial, triaxial, shear, traction and creep tests have been carried out by *Habimana* (1999). Two aspects were followed:

- 1) Characterization of the strength of cataclastic materials by determining an adequate rupture criterion ;
- 2) Characterization of their deformability through stress-strain relationships and marginally test the time dependency of the cataclastic deformation through creep experiments.

Considering a review of ten different rupture criteria for fractured rock masses found in the rock mechanical literature, *Habimana* (1999) suggests that the rupture criterion of *Hoek & Brown* (1997) is by far the more appropriate. Nevertheless the specific effect of tectonization isn't introduced in such a formulation.

Based on a statistically supported idea that tectonized rock masses can have properties varying from intact rock to soil properties, *Habimana* (1999) has modified the Hoek & Brown rupture criterion by introducing consideration from soil mechanics (Mohr-Coulomb criterion, **Fig. 3.7 A**). To account for the progressive transformation of an initial rock protolith into a soil-like material (i.e. kakirite), a parameter referring to the degree of tectonization is proposed. This parameter t is estimated visually using the GSI (Geological Strength Index, *Hoek et al*, 1998, see **Fig. 3.4**). Four tectonization states are accordingly defined (*lightly tectonized*, *tectonized*, *highly tectonized* and *extremely tectonized*) and characteristic stress-strain responses for these different degrees are summarized in **Fig. 3.6**.

As discussed in *Habimana* (1999), rock strength is expected to decrease significantly with increasing tectonization degree. Post-failure behavior of cataclastic rocks is supposed to be a function of the initial intensity of tectonization affecting the sample. Post-failure behavior is highly plastic for extremely tectonized materials whereas it tends to be fragile for slightly tectonized ones, reflecting the new adjustment of rock fragments after initial failure that imbricate so as to produce the most stable network. It has been further suggested that deformability close to rupture is more intense in the case of highly and extremely tectonized materials, reflecting in our sense a probable switch in rupture mode from brittle fracturing, to sliding and crushing towards progressively more dominated crystal plastic deformations (Chap. 2). Interestingly, extreme tectonization is referred to by *Habimana* (1999) as the process leading to an entirely fragmented and crushed rock material that has mechanical properties comparable to soil. This is in agreement with the idea of a cataclastic intensity gradient in fault zone from the damage zone towards the fault core, with fault core accommodating kakiritic rock types.

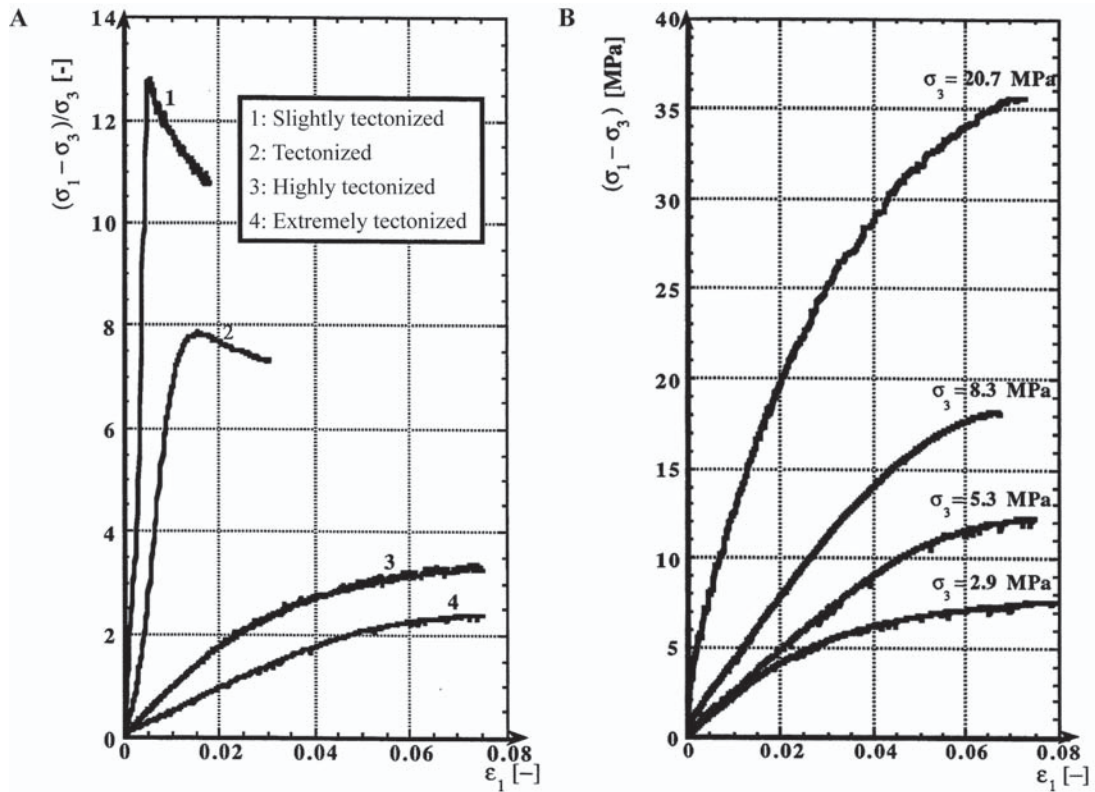


Fig. 3.6 A) Influence of the degree of tectonization on the mechanical behavior of cataclastic quartzites. Deviatoric stress has been normalized to allow triaxial data comparison. B) Influence of the confining pressure on the deformation for cataclastic of a same tectonization degree. Case of extremely tectonized quartzites. After *Habimana (1999)*.

3.2.5 Rupture Criterion For Cataclastic Rocks

Habimana (1999) observed that cataclastic strength doesn't increase proportionally with confining stress, involving a non-linear rupture criterion function of the degree of tectonization. Non-linearity is expected to decrease with increasing tectonization. The modified rupture criterion for cataclastic rocks is of the form (**Fig. 3.7 A**):

$$\text{Eq. 3.2} \quad \sigma_1 = \sigma_3 + t\sigma_{ci} \left(m_b \frac{\sigma_3}{t\sigma_{ci}} + s \right)^a$$

with

σ_1, σ_3 maximum and minimum principal stresses

$t\sigma_{ci}$ uniaxial compressive strength of intact rock affected by a reduction factor taking into account the degree of tectonisation based on visual examination of the rock sample using the GSI approach ($1 \geq t \geq 0$)

a curvature of the rupture envelope ($0.5 \leq a \leq 1$) for the evolution of an intact rock to an extremely tectonized rock comparable to a soil

m_b slope of the rupture envelope, accounting for the shear characteristics of the studied material ($m_b = m_i$ for slightly tectonized rocks, $m_b \approx k_p - 1$ for extremely tectonized materials)

s y-coordinates of rupture envelope at origin on a $\sigma_1 - \sigma_3$ plot ($1 \geq s \geq 0$) for the evolution from an intact rock to a soil

| | Limits | Suggested relationships |
|---|--|---|
| A | $0.5 \leq a \leq 1$ | $a = 0.5 [1 + \exp (\frac{-GSI}{20})]$ |
| B | $m_i \geq m_b \geq (k_p-1)$ | $m_b = k_p - 1 + (m_i - k_p + 1) \exp (\frac{GSI - 100}{28})$ |
| C | $1 \geq s \geq 0$ | $s = \exp (\frac{GSI - 100}{9})$ |
| D | $1 \geq t \geq 0$ | $t = (\frac{GSI}{100})^{0.55}$ |
| | <div style="display: flex; justify-content: space-between; width: 100%;"> hard (intact) rock soil-like material </div> | |

Table 3.3 Relationships between the suggested failure criterion of *Habimana et al.* (2002) and the GSI. **A)** Concept of a continuous increase in the curvature a of the failure envelope with the tectonization degree. The upper and lower bound values of parameter a correspond to the two extreme states for cataclastic rocks. **B)** Similar relationship than *Hoek & Brown* (1997) except that the lower bound value reaches (k_p-1) to take into account the nature of the filling material with increasing tectonization. **C)** Relationship for s is kept identical with the one proposed by *Hoek & Brown* (1997). **D)** Equation for t accounting for the progressive damage of the rock matrix with the tectonic process from an intact state ($t = 1$) to a completely crushed soil-like material ($t \approx 0$). After *Habimana et al.* (2002).

The influence of the degree of tectonization reflects itself on the shape of the rupture criterion (**Fig. 3.7 B**). The a parameter reflects the curvature of the envelope and integrates the effect of the rapid strength increase with confining stress for low stress levels. It can be seen as associated to the degree of fracturation and alteration of the rock mass. In function of a , the failure envelope changes progressively from a parabolic failure curve for lightly tectonized rocks ($a = 0.5$) to a more linear criterion for extremely tectonized rocks ($a = 0.75$) (*Habimana et al.*, 2002). The m_b parameter is sensitive against the level of imbrication of geological components as well as on the granulometry and mineralogy. It is bounded between m_i for an intact rock and (k_p-1) for a soil-like material (where k_p is the passive earth pressure coefficient, $k_p = \tan^2(45^\circ + \varphi/2)$). Accordingly, it accounts for the shear characteristics of the filling material, which influence becomes more and more important as the tectonization degree increases. Finally, the s parameter is linked with the quality of the overall rock mass and describes the state of degradation of this rock mass estimated on the base of the block size and joint density. It reaches the value of ~ 0 for an extremely tectonized rock.

To conform to the observed behavior of cataclastic rocks, the relationships between GSI and the a , m_b and s parameters have been accordingly modified compared to the empirical original relationships proposed in *Hoek & Brown* (1997). **Table 3.3** presents these new relationships between the suggested failure criterion of *Habimana et al.* (2002) and the GSI.

Note: In terms of deformability (not addressed in this study), *Habimana* (1999) implemented following constitutive laws (compare with **Fig. 2.7**):

- elastic perfectly plastic or an elasto-plastic with strain hardening for extremely tectonized materials;
- elasto-plastic with strain softening for slightly tectonized materials.

The non-linearity of the proposed stress-strain relationship for cataclastic rocks has been tested through relationships

between the initial deformability modulus E_i ($\neq E_{50\%}$) and the stress level for each tectonization degree. For a same degree of tectonization, increase in deformability modulus is observed with increasing confining stress. Based on the stress-strain relationship for non-linear soil and rock behavior (Duncan & Chang, 1970; Kulhawy, 1975), the cataclastic behavior of extremely tectonized materials (GSI < 20) seems accurately reproduced. The effect of the fragile deformation component affecting slightly tectonized cataclasites is however more difficult to reproduce (combined effects of yielding and fragile failure). Moreover, the effect of a same tectonization degree on rocks from different petrologies is reported by Habimana (1999) being inconsistent what can lead to contradictory observations.

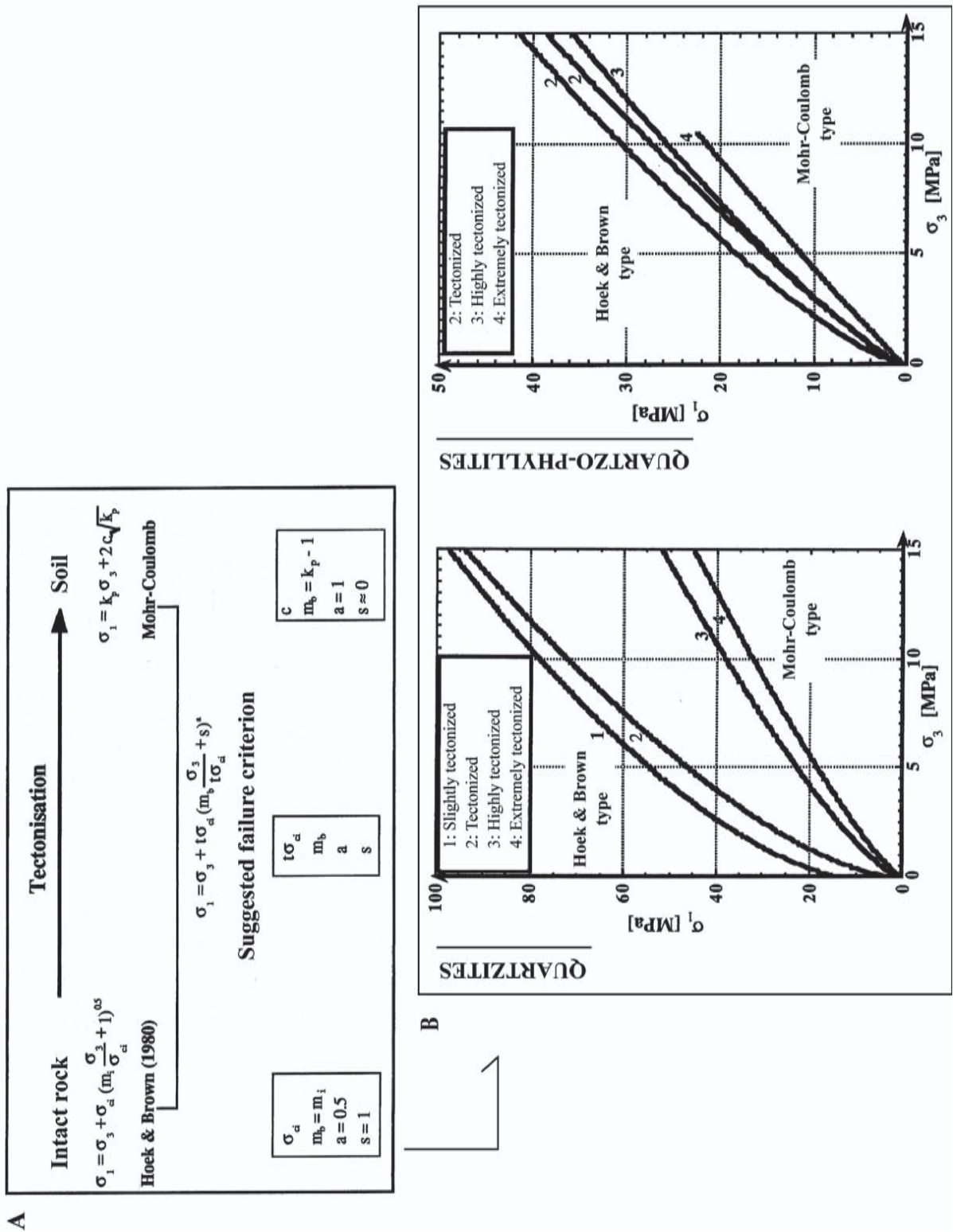


Fig. 3.7 A) Progressive evolution of the rupture criterion proposed by Habimana (1999) for the mechanical characterization of cataclastic fault rocks. B) Effect of the degree of tectonization on the rupture envelope for quartzite and quartzo-phyllite from Cleuzon-Dixence, unit D, Zerjona. Data from Habimana (1999).

3.3 CORRELATION BETWEEN GEOLOGICAL CHARACTERISTICS & GEOMECHANICAL PROPERTIES

The combined geological and geomechanical approach followed in two previous research projects on cataclastic rocks at EPFL have proposed a correlation between the MSI and results from triaxial tests.

3.3.1 Correlation Chart Between MSI and Triaxial Data (1999)

By comparing MSI values determined on 12 cataclastic and kakiritic samples from Cleuzon-Dixence and Goltschried in the Swiss Alps (quartzite, quartzo-phylite, carbonatic breccia) with the triaxial results obtained on samples from the same localities, a positive correlation between geological and geomechanical properties has been proposed by *Bürgi* (1999) (**Fig. 3.8**). In order to take into account the non-linearity of the strength criterion of *Habimana* (1999), values of principal stresses at rupture taken for two different levels of confinement ($\sigma_3 = 5$ and resp. 10 MPa) were determined by regression on the triaxial test data.

It has to be said that this apparent positive correlation is restricted to a small amount of samples and requires to be validated in other petrological content. Accordingly, if a geological understanding of cataclasis in function of rock types results (microscopic level), the mechanical parameter t used in **Eq. 3.2** to account for the degree of tectonization (GSI-type determination) could be more objectively determined by getting closer to the real material nature. It could be further brought in adequation with specific cataclastic rock properties (genetical interpretation of type-microstructures and their translation in predictive cataclastic behaviors defined according to the mechanical implications related to such microstructures). Parameters of interest in the description of cataclastic materials susceptible to influence rock rheology are: granulometry, angularity of clasts, specific mineralogy, hardness of mineral phases, chemical alteration of rock mass, and microfractures accounting for rock anisotropy.

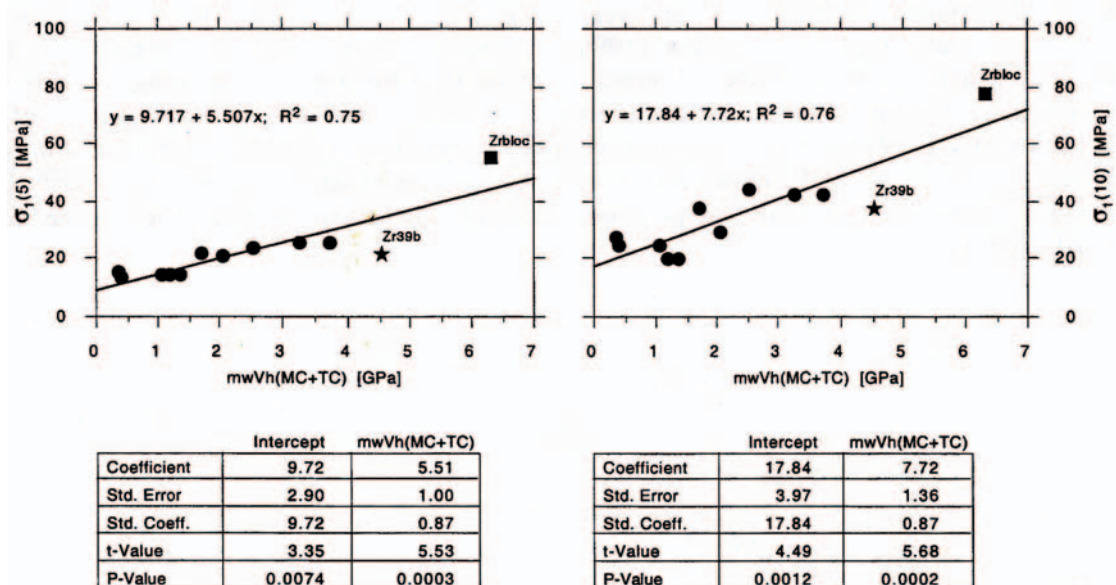


Fig. 3.8 Correlation of geological and geomechanical properties of 12 kakirites studied respectively by *Bürgi* and *Habimana* (1999). Mechanical rupture values are given for two level of confining stress ($\sigma_3 = 5$ and 10 MPa), in order to take into account the non-linearity of the rupture criterion proposed for cataclastic rocks by *Habimana* (1999).

3.3.2 Limitations and Perspectives

Information from different scales of observation is needed to assess rock mass quality. The approach and results of *Bürgi & Habimana* (1999) was a first step in the improved characterization at the sample scale. A more global approach still need however to be developed for the proper rock mass characterization of fault zones in tunnelling. Techniques allowing outcrop and regional survey should be used together with laboratory procedures to depict a best picture of the underground structure. Accordingly, transition paths between the different scales of investigation have to be established. Only a close collaboration between researchers and practitioners can provide a proper answer to this point (*Habimana*, 1999).

To assist in the determination of critical aspects and properties of cataclastic materials at the sample scale, the chart of **Fig. 3.8** has several practical applications. Based on geological evidences, the determination of a domain of rock strength for cataclastic samples can be expected. This is helpful as rock core recovery from exploration drillings in tectonized settings is often limited. Accordingly, if no rock cores are available for mechanical tests, an evaluation in terms of strength can be done by means of the MSI, as only very little undisturbed kakirite material is required for the realization of thin sections.

Bürgi (1999) explains that the MSI is based on “mean weighted” parameters. The presence of a structural singularity in a cataclastic rock core sample submitted to a triaxial test will therefore most likely prevent any possible correlation between σ_1 and either MC, TC or mwVh by taking a too important control on the sample deformation in the cell. Accordingly, the application of the proposed characterization method is restricted to kakirites with a certain structural and mineralogical homogeneity at the scale of thin sections and triaxial tests. As a result of geological and mechanical analyses performed on different samples, the exact correspondence between the geological and geomechanical determinations is further questioned. Moreover, the information on rock fabric anisotropy is lost due to the use of 2D thin sections.

Observations realized by *Habimana* (1999) show moreover that creep is an important mechanism in cataclastic behavior and should be considered for the practical applications. The microscopical aspects and material internal controls leading to creep should accordingly be investigated. An objective picture of damaged rock mass rheology involves therefore genetical and mechanical evidences and confrontations. A more genetical description of the cataclastic degree would benefit the establishment of accurate constitutive laws which further can be implemented in numerical codes used for tunnel planning in preliminary studies.

3.3.3 MSI Evidences From New Petrological Contents (2007)

In the framework of this research project, new MSI data on cataclastic rocks from contrasting petrological content have been produced in the framework of two supervised Master theses (*Veuve and Chaignat*, 2007). Petrologically contrasted samples from the N16 Roche St Jean tunnel (*RSJ*, tectonized limestone), the AlpTransit Ceneri Sigirino gallery (*CBT*, Giumello gneiss), the A9 Glion tunnel (*GL*, tectonized dolomite), and the A9 Eyholz tunnel (*Eye*, polygenic breccia) have been investigated (see further **Chap. 5** for the respective site descriptions). Results are presented in this short section for indication and confronted with the correlation proposed between the MSI and triaxial strength data by *Bürgi* (1999) on quartzo-phyllitic rocks. The mechanical tests were conducted at EPFL on two samples of each locality, one tested at a confinement σ_3 of 5 MPa and the other at 10 MPa, so as to permit a proper comparison with results from the research of 1999.

Results support the proposed correlation of *Bürgi* (1999) between MSI and triaxial strength data (**Table 3.4 & Fig. 3.9**), at least they show that some logic is respected between the geological and

mechanical parameters. It has to be noted that TC & MC coefficients for the samples investigated by *Chaignat* and *Veuve* (2007) have been determined either on thin sections or on axial CT-slices from medical X-ray Computerized Tomography (XRCT). The XRCT analytical method will be described in details in **Chap. 8** and its extended implementation for rock core characterization in **Chap. 10**.

Results of the Master theses show moreover that the calculated MSI data are in close agreement between the two analysis support (thin section or XRCT) despite of the contrasted resolutions affecting the techniques. It suggests that for a proper evaluation of the sample structure the lower XRCT resolution is compensated by the more representative field of view compared to thin section. In particular, *Eye* exhibits structural properties at a feature scale inaccurately depicted by means of the single thin section quantified by *Chaignat* (2007), with an obtained MSI that is interpreted not representative. In this case, the advantage of investigating the entire sample structure by means of medical XRCT limits uncertainty by providing a more objective reproduction of the feature scale (**Fig. 3.10**).

Taking a closer look at the determinations of *Chaignat* and *Veuve* (2007), it is however evident that the mineralogical composition expressed by means of the mwVh has currently the strongest influence on the MSI-value (see for example *RSJ* with TC & MC parameters from XRCT twice bigger than corresponding thin section determinations despite of MSI values staying in a close interval). Therefore, the observed variations in determined TC & MC between a thin section and an XRCT slice are somehow compensated in resulting MSI by the weight accorded currently to the effect of the mineralogical composition.

| Petrology | Samples | XRD mwVh (MPa) | Thin section | | XRCT (xy slice) | | MSI | MSI _{XRCT} | Triaxial strength | |
|-------------------------------------|-----------------|-------------------|--------------|-------|-----------------|-------|--------|---------------------|----------------------|-----------------------|
| | | | MC | TC | MC | TC | | | σ_1 (5) (MPa) | σ_1 (10) (MPa) |
| <i>(Bürgi & Habimana, 1999)</i> | | | | | | | | | | |
| CRYSTALLINE | | | | | | | | | | |
| Quartzo-phyllite | CLEUZON-DIXENCE | 6.700 | 0.209 | 0.465 | | | 4.516 | | 22.000 | 38.000 |
| | | 5.200 | 0.188 | 0.202 | | | 2.028 | | 21.000 | 30.000 |
| | | 4.700 | 0.141 | 0.213 | | | 1.664 | | 22.000 | 38.000 |
| | | 3.400 | 0.117 | 0.000 | | | 0.398 | | 14.000 | 25.000 |
| | | 2.900 | 0.223 | 0.130 | | | 1.024 | | 15.000 | 25.000 |
| | | 2.700 | 0.121 | 0.000 | | | 0.327 | | 16.000 | 28.000 |
| | | 5.000 | 0.132 | 0.614 | | | 3.730 | | 26.000 | 43.000 |
| | | 5.000 | 0.217 | 0.428 | | | 3.225 | | 26.000 | 43.000 |
| | | 3.800 | 0.000 | 0.306 | | | 1.163 | | 15.000 | 20.000 |
| | | 3.800 | 0.000 | 0.349 | | | 1.326 | | 15.000 | 20.000 |
| 4.300 | 0.177 | 0.410 | | | 2.524 | | 24.000 | 44.000 | | |
| <i>(Chaignat & Veuve, 2007)</i> | | | | | | | | | | |
| Giumello gneiss SIGIRINO | | | | | | | | | | |
| | | 6.305 | 1.845 | 1.409 | 1.780 | 1.793 | 20.519 | 22.528 | 65.900 | 112.400 |
| CARBONATIC | | | | | | | | | | |
| Dolomite | GLION | 2.733 | 0.808 | 1.634 | 1.221 | 1.659 | 6.675 | 7.872 | 38.869 | 61.240 |
| Limestone | ROCHE ST JEAN | 1.720 | 1.531 | 1.343 | 0.858 | 0.723 | 4.941 | 2.719 | 18.447 | 31.633 |
| POLYGENIC | | | | | | | | | | |
| Breccia | EYHOLZ | 4.129 | 6.629 | 1.308 | 0.972 | 0.267 | 32.771 | 5.116 | 35.600 | 48.100 |

Table 3.4 Input data for the petrological correlation MSI vs. strength for rocks studied by *Bürgi & Habimana* (1999) and *Chaignat* and *Veuve* (2007). This study considers using both thin sections and XRCT to derive the structural and textural TC & MC parameters constitutive of the MSI. XRCT determinations have been realized by *Chaignat* (2007) using axial (xy) CT slices (i.e. perpendicular to the applied triaxial load). Values are listed in the table. Further determinations for the *RSJ* samples made within this research have implemented the frontal (xz) and sagittal (yz) planes, which correspond to the planes parallel to applied triaxial load, as recommended by *Bürgi* (1999). These more detailed determinations will be presented later in **Chap. 11**. Mineralogical compositions used for the determination of the mean weighted Vickers hardness (mwVh) correspond to XRD analyses by *Veuve* (2007).

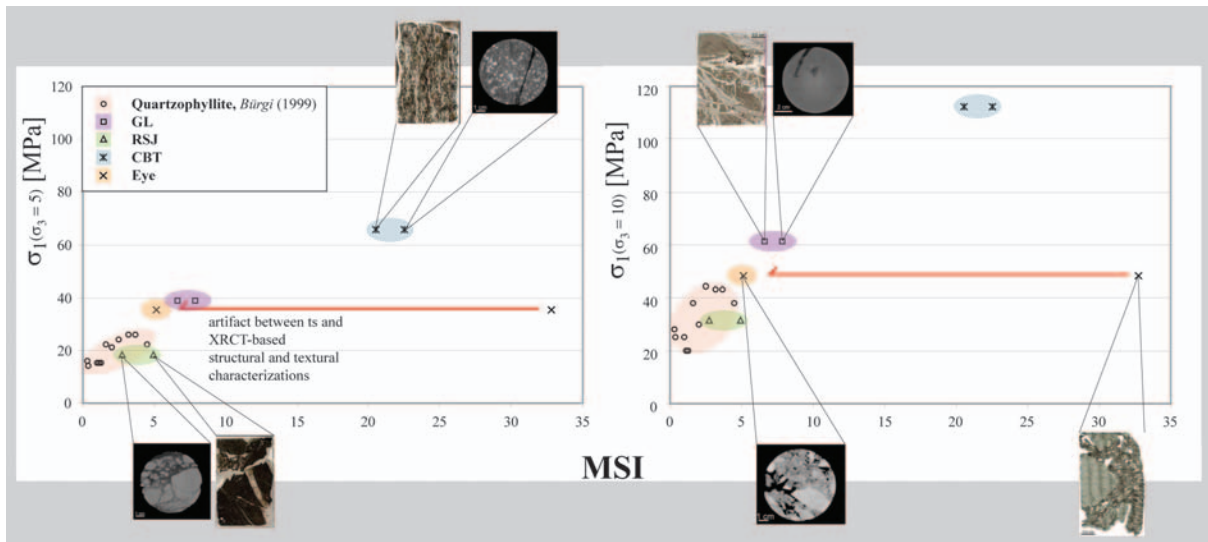


Fig. 3.9 Petrological correlation MSI vs. triaxial strength for cataclastic rocks studied by *Bürgi* (1999) and *Chaignat* and *Veuve* (2007). Petrological domains are highlighted. Mechanical data are taken from *Habimana* (1999) for the quartzophyllite and from this study for the other petrologies. They are presented for two levels of confining stresses σ_3 (5 & 10 MPa) in order to take into account the non-linearity of the strength criterion proposed for cataclastic rocks (see *Bürgi*, 1999). Structural and textural analyses of *Chaignat* have been performed either on thin sections or axial (xy) XRCT images. Despite of the different resolutions represented by both techniques, MSI derived values are in good agreement between both analyses supports. An exception is represented by the *Eye* sample, for which average rock structures are more objectively depicted by means of XRCT (red arrow). Such a confirmation from the correlation envisaged by *Bürgi* (1999) is highly encouraging in continuing with the efforts of developing a geological analytical protocol based on structural and mineralogical evidences. In the future, a versatile conversion chart between geological evidence and mechanical resistance could be developed.

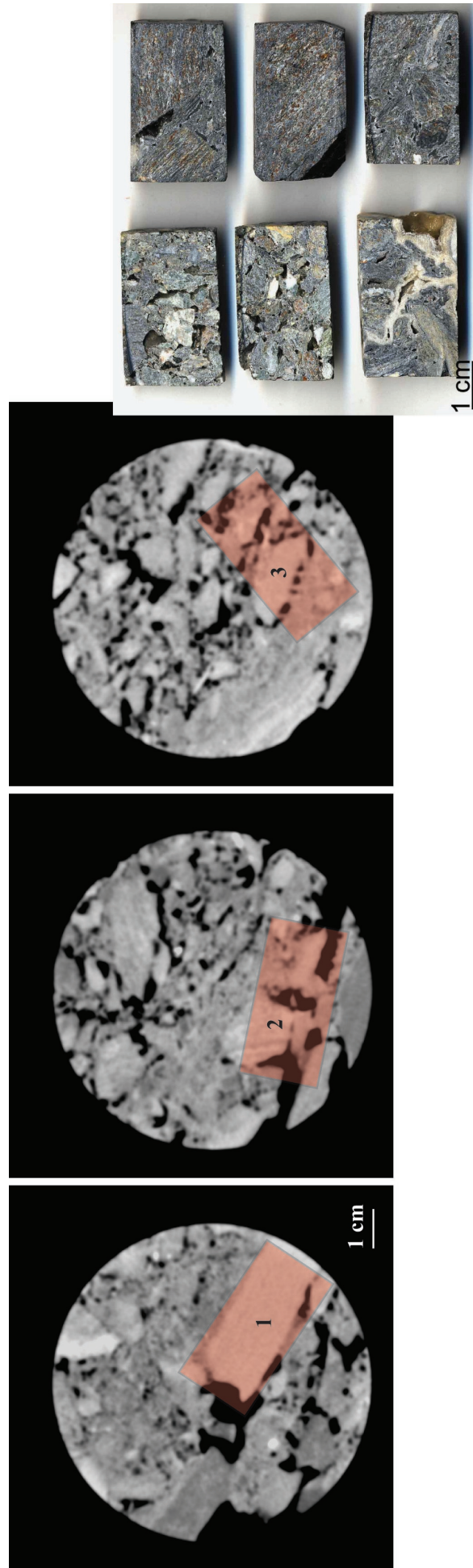


Fig. 3.10 Contrasting field of view between thin section and XRCT for *Eye* sample. See also later **Fig. 10.4**. On each axial CT slices, a window representing the thin section size is highlighted (about 4 x 2 cm). **1)** Case where the thin section depicts fairly homogeneous rock portions. In this case, MC and TC are expected to be unrealistically high compared to the averaged rock core structure. **2)** Thin section covering big sized features resulting in excessively low MC and TC values. **3)** Thin section in a rock portion representative of overall *Eye* structure. MC and TC values between thin section and XRCT determinations are expected in this case to be comparable. Right are the rock plates from which thin sections have been realized by *Chaignat* (2007). Note the resulting structural contrasts according to the sawing orientation. In order to obtain structural representativity, several thin sections from such contrasted samples should be considered. In this sense, the field of view represented by XRCT is more objective, despite of an effective lower resolution.

4

CURRENT PROJECT DESCRIPTION

O Mort, vieux capitaine, il est temps ! levons l'ancre !
Ce pays nous ennuie, ô Mort ! Appareillons !
Si le ciel et la mer sont noirs comme de l'encre,
Nos cœurs que tu connais sont remplis de rayons !

Verse-nous ton poison pour qu'il nous réconforte !
Nous voulons, tant ce feu nous brûle le cerveau,
Plonger au fond du gouffre, Enfer ou Ciel, qu'importe ?
Au fond de l'Inconnu pour trouver du *nouveau* !

Charles Baudelaire, *Le Voyage*

This new project addresses the continuation of the geological and geomechanical research on weak rock mass characterization initiated by *Bürgi & Habimana* (1999).

Motivations, philosophy and general methodological aspects of this study are presented hereafter.

4.1 PURPOSE OF THIS RESEARCH

This research project attempts at better characterizing cataclastic fault rocks from a geological perspective to question the possibilities to effectively correlate mineralo-structural evidences determined on representative rock cores from reconnaissance drilling operations with specific mechanical aspects inherent to the cataclastic nature. In particular, following considerations will be treated:

- 1) Perform a genetical description of cataclastic rocks based on fundamental aspects of fault zone development and activity at shallow crustal conditions.
- 2) Demonstrate that for geotechnical studies the proper assesment of cataclastic rocks and the understanding of their implications in engineering projects require a close link between the geological and mechanical characterization procedures.
- 3) Test the potential of a characterization methodology developped at EPFL in 1999 that from a micro-structural perspective (thin section, 2D) considers cataclastic rocks as corresponding to bimodal materials affected by different degree of tectonization which are found closely related to material resistance and deformability.
- 4) Faced with the often very bad rock core qualities obtained during drilling operations, improve any possibilities to sample cataclastic rocks in their representative *in situ* conditions with a portative rock core extractor. Explore in this context different tectonized settings underground that outcrop contrasted cataclastic petrological contents.
- 5) Test the medical X-ray computerized tomography (XRCT) to indirectly evidence in 3D the structural and textural characteristics of cataclastic rock cores in standard dimensions for geotechnical studies. Recognize its big advantage to permit a geological and mechanical characterization derived from the exactly same rock cores.
- 6) Develop specific image analysis tools for the improved numerical treatment and analysis of rock core XRCT-acquisitions so as to obtain a possibility to explore micro-structural studies from a 3D perspective and aliment the mechanical interpretation performed on cataclastic rocks after they have been the object of triaxial deformation tests.
- 7) Based on the structural-textural study of a serie of contrasted cataclasites, develop a conceptual model for their occurrence and development in a rock mass architecture susceptible to assist geotechnical preliminary studies.

4.2 ECHO OF THE RESEARCH FROM 1999

Scientific results from the previous geological and geomechanical studies have been published in selected journals (*Bürgi et al.*, 2001; *Habimana et al.*, 2002). Communications presented by the applicants during conferences or symposium, in or outside Switzerland, were largely appreciated by both scientific and professional communities and pointed out the necessity to improve the basic

knowledge in that domain.

It is clear that the genetic and geotechnical understanding of cataclastic rocks constitutes a highly complex puzzle that requires a close link between applied and fundamental researches to be satisfactorily resolved. The promising correlation found between MSI and triaxial strength shows that geologically based parameters can assist the mechanical interpretation made on cataclastic rocks. With the MSI, estimates of expected strength can be derived from geological observations. Due to the mineralo-structural particularity of cataclastic materials, the MSI approach that quantifies rock microstructures and mineralogy is found less subjective to properly characterize fault rocks than a GSI-type determination extended to the sample scale. It has however to be said that mechanical parameters constitutive of the modified rupture criterion proposed by *Habimana* (1999) can be estimated on the base of the indicative GSI determination (see **Table 3.3**).

Anticipating from current evidences, the development of a conversion chart between geological and mechanical properties of cataclastic rocks in function of petrology (**Fig. 4.1**) is expected to have a strong practical interest for tunneling applications in tectonized settings. It constitutes a first step in the operational characterization methodology for weak rock masses.

With more numerous strength and deformability data (wide variety of petrological samples and of cataclastic degrees) proper design parameters accounting for the effects of tectonization could be proposed to the design engineers. Such parameters derived from the diagnosis of cataclastic microstructures and their translation in mechanical control factors are seen to integrate numerical calculation based on constitutive laws appropriate for heterogeneous rock mass behavior. As a result, this approach should help with time better taking following tunnel design-related decisions:

- effects of stress field modification induced by the excavation on a given cataclastic rock mass;
- choice over the more rational sequence of excavation;
- expected time-dependent degradation of the rock mass surrounding the tunnel;
- appropriate and rational hazard assessments.

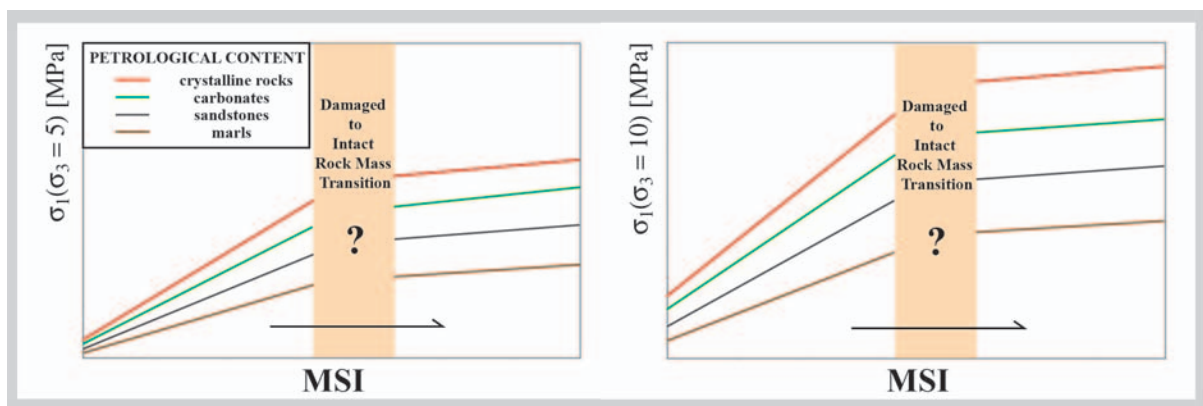


Fig. 4.1 Suggested petrological MSI- σ_1 chart for the prediction of cataclastic strength based on geological parameters. Two levels of confining pressure are considered to take into account the non-linearity of the rupture criterion for cataclastic rocks presented by *Habimana* (1999). Correlation curves are envisaged between strength and MSI-determinations from cataclasites of contrasted petrological contents. Accordingly, MSI values have to be tested in function of petrology for different cataclastic degrees so as to characterize the transition from damaged to intact rock masses that is expected to be either continuous or discontinuous.

4.3 A CONCEPTUAL MODEL FOR THE OCCURRENCE OF CATACLASTIC ROCK MASSES

Taking into account both the genetic considerations of depth and fracturation presented in **Chap. 2**, a conceptual model of cataclastic rocks at shallow conditions is developed in this section (**Fig. 4.2**). Respective occurrence of *intact* and *damaged* rock masses is presented (*domains A & B*). Such a model is expected to aid in understanding the nature of the rock mass and its implication for geological-geomechanical studies. **Fig. 4.2** highlights moreover the scale correspondence that prevails for the fractured nature of a damaged rock mass which is further responsible for ductile behavior of cataclastic fault zones whereas cataclasis is a strictly brittle process.


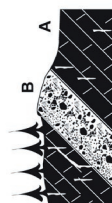



Domain A has the largest geographical extent and can refer to all primary rock-forming environment (e.g. sedimentary, magmatic and metamorphic). Rocks from *domain A* are named *intact* and their rheological properties are governed by their primary mineral assemblage defining rock strength. Intact rock strength takes into account discontinuities that can affect rock mass and that are characterized by their surface conditions and orientation. The description of intact rock mass in mechanical models is made by an *intact rock-discontinuity model*. Rock mass is assumed isotropic and homogeneous and its rheological behavior is elastic unless rock strength is exceeded.

Domain B refers to the occurrence of cataclastic rocks in a fault zone. Such rocks are named *damaged* because they result from a generalized brittle degradation process function of stress & strain accumulation into the fault zone over geological history causing fracturing, shearing and chemical alteration. They represent materials of a more chaotic nature than rocks from *domain A* and their strength can no longer be described by the rock composition itself. Cataclastic rocks instead represent a spectrum of materials of contrasting properties that require an alternative approach to the model mentioned above. From a mechanical point of view, cataclastic rocks must be described by a fractured rock rheology that involves anisotropy and heterogeneity resulting from the progressive degradation of the original intact rock mass. A description of damaged rock mass leads to the concept of a *clast in fine-grained matrix model* that defines further the *clast-controlled* and *matrix-controlled* cataclastic flows (see **section 2.1.1.1**). Rheological behavior is elasto-plastic for the clasts embedded in the cataclastic horizon but the whole rock mass is expected to behave in a visco-plastic manner.

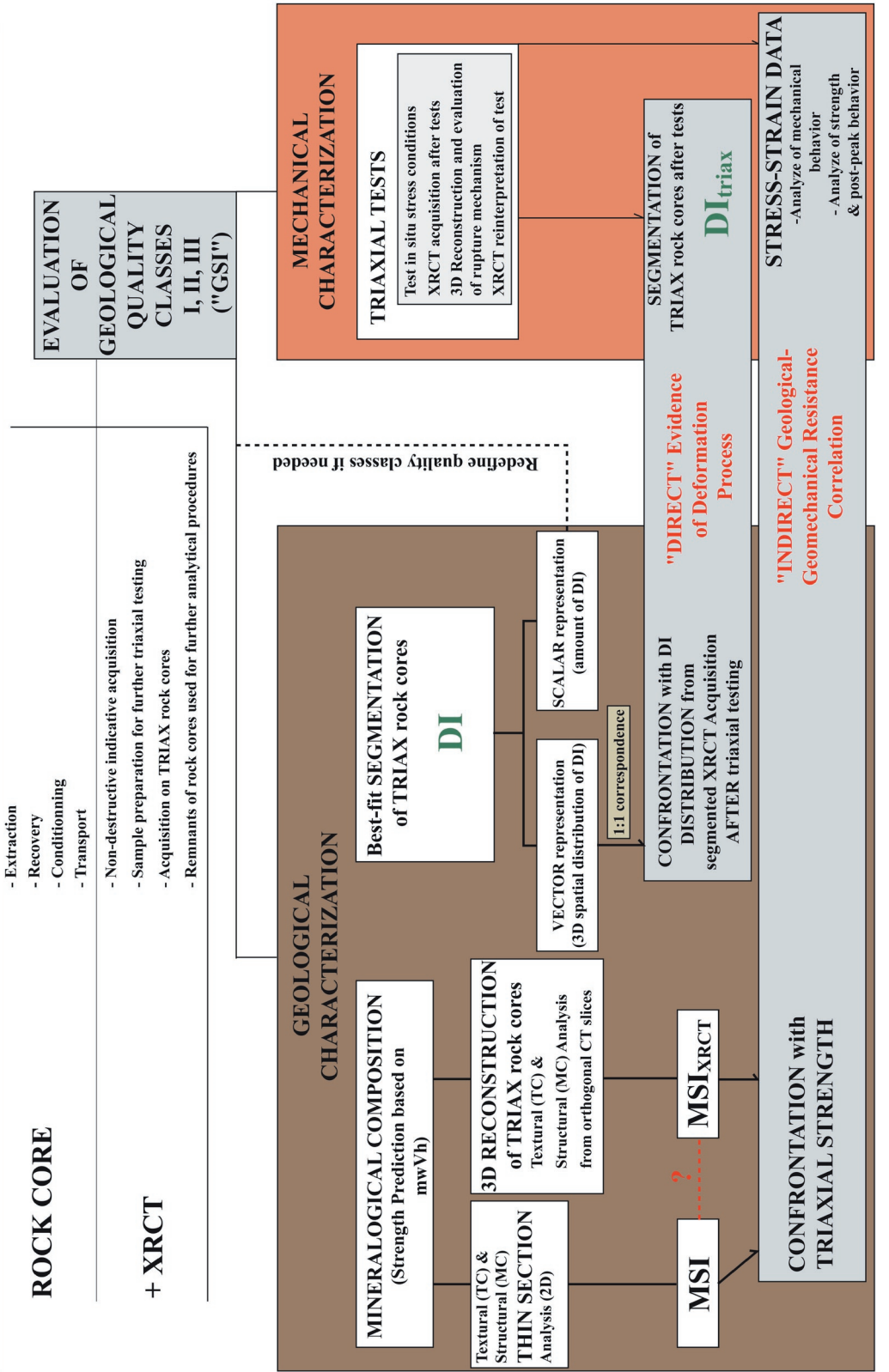
Note: The binary representation of **Fig. 4.2** shows that the generic name “fracture” can be used for all structural manifestation of brittle processes independent of scale. Rock mass elements (relevant parameters) to be taken into account for a proper geomechanical description of *intact* and *damaged* rock samples are accordingly given. These parameters are referred to as *damage indicators* (**Chap. 2**) and they regroup in this sense different structural, textural and mineralogical evidence describing the development and nature of a damaged rock mass. Damage in a general sense is associated with the reduction of frictional strength through wear of asperities, fracturing and comminution. Damage indicators are expected to be helpful for cataclastic rock mass characterization as well as in the definition of improved mechanical models of cataclastic behavior as they can be determined from the analysis of cataclastic samples (e.g. rock cores from drilling operations) and quantitatively translated further into *strength reduction criteria*.

Fig. 4.2 (next page) Scale-independent binary representation of fault zone at shallow crustal conditions. Conceptual model for the illustration of the fracture analogy from the regional to the microscopic scales. The figure shows that the occurrence of cataclastic rocks is restricted to a specific domain characterized by a damaged rock rheology (i.e. cataclastic flow) no more comparable with the original intact rock rheology. Damage manifests itself as a function of tectonic processes (*fracturing*, i.e. development of fault zone, fault, fault band or fault plane according to the scale of observation). As a function of the petrology of the intact rock protolith, resulting texture, structure and mineralogy of cataclastites can take several forms. A list of characteristic parameters leading to the determination of damage indicators is presented and should be used for their translation into strength reduction criteria for an improved geomechanical characterization of damaged rock mass. Differentiation of two domains of intact and damaged rock mass leads to the definition of two models of rock structure influencing deformation. In the *block-discontinuity model*, deformation is assumed being controlled mainly by the discontinuities. In the *clast in fine-grained matrix model*, the property of the damaged rock matrix is the most critical parameter that controls deformation. A terminology for the specific characterizations of intact and damaged rock masses is given in **Chap. 2**. Further explanations in text.

Fault-Zones at shallow crustal condition, brittle deformation & cataclastic flow. SCALE-INDEPENDENT BINARY REPRESENTATION OF FRACTURATION PROCESS. COMPARATIVE CHART.

| REGIONAL | MODEL | LEVEL OF OBSERVATION (FAULT PROCESS DIAGNOSIS) | PARAMETERS (DAMAGE INDICATORS) | IMPLICATION FOR ROCK MASS | TERMINOLOGY FOR ROCK MASS ELEMENTS |
|--------------|---|--|--|---|--|
| kilometers |  | <p>FRACTURE = FAULT ZONE.</p> <ul style="list-style-type: none"> - Fault Zone Type - Fault Zone Anatomy - Fault Zone Thickness & Depth - Fault Zone Composition - Fault Zone Mechanisms - Tectonic Evolution of Fault Zone - Implication of Fault Zone on the hydrological & hydrothermal regime - Relationships to Host (intact) Rock Mass | <ul style="list-style-type: none"> - Compressional vs. Extensional Setting - Shear Rate - Shear Amount - Shear Conditions - REGIONAL Stress Field - Offsets - Strain Level, Localization & Accommodation - Type of Deformations - Implications of Deformations (Stability, Fluid Circulation, Large-Scale Inhomogeneities) | <p>A) INTACT Rock Mass (Peripheral Strain)</p> <p>HOMOGENEOUS</p> <ul style="list-style-type: none"> - brittle deformation - Fracturing <p>B) DAMAGED Rock Mass (Penetrative Strain)</p> <p>HETEROGENEOUS</p> <ul style="list-style-type: none"> - brittle deformation - cataclastic flow through fracturing, crushing and rotation of rock fragments | <p>A) INTACT Rock Mass ("petrogenetic")</p> <p>B) DAMAGED Rock Mass ("detritic")</p> |
| OUTCROP |  | <p>FRACTURE = FAULT</p> <ul style="list-style-type: none"> - Fault Type - Fault Geometry & Structure - Fault Variability, Fault Core vs. Damaged Zone, Gradational Profile - Composition of Fault Materials - Dry vs. Wet Faults, Weathering - Relationships to Host (intact) Rock Mass | <ul style="list-style-type: none"> - Shear vs. Rock Mass - Density/Persistence of Discontinuities - LOCAL Stress Field - Offsets - Degree of Structural Complexity - Type of Deformations - Implications of Deformations (Stability, Fluid Circulation, Small-Scale Inhomogeneities) | <p>INTACT Rock Rheology</p> <p>FRACTURED Rock Rheology (e.g. no more direct function of lithological composition)</p> | <p>ROCK MATRIX</p> <p>FINE-GRAINED MATRIX (e.g. Cataclastic Matrix)</p> <p>DISCONTINUITIES / FRACTURES</p> <p>DISCONTINUITIES / FRACTURES</p> |
| SAMPLE |  | <p>FRACTURE = FAULT BAND, FAULT PLANE.</p> <ul style="list-style-type: none"> - Intact Rock Materials vs. Damaged Rock Materials - Categorization of Structural State of Rock Materials - Structural and Textural Evidence of Fracture Types - Other Structures - Assumptions on Isotropic/Anisotropic Nature of Material <p>INDIRECT OBSERVATION (X-ray irradiation):</p> <ul style="list-style-type: none"> - on Intact or Damaged Rock Material - BEFORE or AFTER mechanical testing - Based on Density Contrasts (Features Of Interest (FOI) vs. Undifferentiated Matrix) - 2D & 3D Visualization of Structural/Textural Relationships | <ul style="list-style-type: none"> - Cracks (open, filled, recrystallized) - Joints, Joint surfaces - Veins, Anastomosing Fractures - Shear Bands - Slip/Slith (transpressive) - Slickenside (transpressive) - Schistosity - Foliation - Breccia Texture - Gouge Texture - Grain Size Variability - Clay content <p>ADDITIONAL</p> <ul style="list-style-type: none"> - Primary Pores, Voids - Determination of Porosity/Permeability - Consistency - Alteration Zone, Physico-Chemical Weathering, Mineral Grains Zonations - Density Contrasts - Preferred Orientation of Mineral Grains (for example Quartz c-axis) | <p>ELASTIC & PLASTIC DEFORMATIONS</p> <p>VISCO-ELASTIC & VISCO-PLASTIC DEFORMATIONS</p> <p>"BLOCK - DISCONTINUITY" Model</p> <p>"CLASTS IN FINE-GRAINED MATRIX" Model defining</p> <ol style="list-style-type: none"> "MATRIX - CONTROLLED" Cataclastic Flow "BLOCK - CONTROLLED" Cataclastic Flow | <p>BLOCKS / CLASTS / FRAGMENTS OF</p> <p>BLOCKS / CLASTS / FRAGMENTS OF</p> <p>INTACT Rock (e.g. Intact Blocks, no internal deformation)</p> <p>DAMAGED Rock (e.g. Cataclastic Blocks, internally disturbed)</p> <p>INTACT Rock (e.g. Intact Blocks, no internal deformation)</p> |
| XRCT |  | <p>MICROSCOPIC OBSERVATION (polarized light):</p> <ul style="list-style-type: none"> - on Intact or Damaged Rock Material - Petrographical Nature of Materials - Equilibrium/Disequilibrium Mineral Assemblages - Interpretation of Microstructures - 2D Visualization of Structural/Textural Relationships | <p>To be translated into STRENGTH REDUCTION PARAMETERS Mechanical Strength Analysis (Compressive vs. Extensive Strength)</p> | | |
| THIN SECTION |  | | | | |

GENERAL METHODOLOGICAL CHART FOR THE GEOTECHNICAL CHARACTERIZATION OF CATACLASTIC ROCK CORE SAMPLES



TRANSLATION TO THE GLOBAL FAULT ZONE SCALE

Fig. 4.3 Proposed methodological chart for the combined geological and geomechanical characterization of cataclastic rock cores.

4.4 GENERAL METHODOLOGY

Based on this highlighted philosophy, a general methodological chart for cataclastic rock core characterization is presented in **Fig. 4.3**. It schematically illustrates the path followed from rock core sampling on site to its objective and successful characterization in terms of geotechnical prediction. The geological and geomechanical analyses are presented in their complementarity with medical XRCT establishing a bridge between the two characterizations procedures.

A first aspect of this project is related to cataclastic sample extraction from characteristic outcrops and the establishment of a sampling strategy (**Chap. 5 & 6**).

Based on the encouraging results in terms of a combined geological-geomechanical approach (*Bürgi et al.*, 2001), MSI type determinations and triaxial testings are proposed to further investigate the proposed combined characterization of cataclastic rock cores (**Chap. 7 & 9**).

A specificity of this research is to implement medical X-ray computerized tomography (XRCT) in order to adapt the methodology envisaged by *Bürgi* (1999) and perform the geological and mechanical investigations on the exactly same rock core. This approach is expected limiting the uncertainties between the respective parameters studied and proposed for a geological-geomechanical correlation (**Chap. 8**).

Further, XRCT derived data are considered for the possibility to adapt the MSI for its potential extension to a three-dimensional characterization index. Specificity of XRCT data are tested and investigated for their visualization capacities and possible implementation into a numerical code of 3D petrography (**Chap. 10**, discussed in **Chap. 13**).

The specific results from the geological and geomechanical characterization will be presented in **Chap. 11 & 12** and further discussed in terms of a potential correlation in **Chap. 13**.

4.5 METHODOLOGICAL INSIGHTS

4.5.1 Sampling

The necessity to obtain samples in the form of rock cores in dimensions as obtained from reconnaissance drilling operations is recognized for a practical methodological applicability.

Given a particular petrological content, assessment of the extent of cataclasis and how it manifests through the original rock mass is important. Thus sampling along a gradational profile of cataclastic intensity from the damaged zone towards the fault core (see **Fig. 2.5**) would constitute the ideal approach. The idea is to obtain a full range of materials from intact rock towards fully damaged rock zones.

4.5.2 Sample Preparation

To optimize at most the sampled rock core serie it is decided to use medical XRCT to perform a first non-destructive acquisition of the collected materials prior to any geological or geomechanical investigations. Visualization of the rock core structure on a 3D basis is made possible. This preliminary test performs an assessment of sample quality based on the 3D indirect evidence. Accordingly, comparison with field observations and derived rock quality impressions can be made. Moreover an initial categorization of the collected samples is done to better orient further analytical procedures.

4.5.3 Geological Characterization

The general idea for the geological characterization of cataclastic rocks is to further develop the MSI of Bürgi (1999) by testing its applicability and validity on contrasting petrologic series. This is a necessary step to dissociate the effect of the bulk mineralogical content on the geomechanical properties of a cataclastic rock from its textural and structural effects, and therefore to better quantify the influence of mineralogy on the mechanical behaviour.

From a general perspective, it has to be said that a scale-effect will inevitably have to be considered for the global understanding and description of cataclastic rock behavior, leading to the possibility of an improved prognosis for underground works. As presented in **Fig. 4.2**, the cataclastic process finds an analogy on scales differing by orders of magnitude. Petrologic, structural and mineralogical observations should be done at the scales of the rock mass, of the outcrop, of the sample and of the thin section. Critical mineralogical species inherited from cataclasis have to be especially considered as they are primary *damage indicators*.

Bürgi (1999) mentioned specifically that the grain size would have to be taken into account to determine the influence of the finest granulometric fraction in the mineral transformation processes. From another perspective surface analysis along specific failure planes could provide rheological constraints on the observed deformational behavior. This is an important aspect to integrate in the confrontation of geological and geomechanical data. With this regard, using XRCT acquisitions of rock cores is seen as a bridge technique in between geological and geomechanical investigations providing the possibility to confront a particular 3D structure indicative of the cataclastic process with the effective deformation observed during subsequent mechanical test.

Geological investigations are expected to provide a key to relate genetical information with their meaning in terms of actual rock quality and deformability. In this step, the definition of which relevant parameters should be taken into account to ponder and better explain the observed mechanical behavior is required (see **section 3.1.2**).

Material obtained during field work and available for geological investigations corresponds to:

- Remnants from rock cores after preparation to the standard dimension for triaxial tests;
- Impregnated rock cores after they underwent triaxial deformation;
- Additional hand samples that are collected separately on the field;
- “Indirect samples” as recorded by medical XRCT.

4.5.4 Mechanical Characterization

Mechanical tests performed in this research were first envisaged to determine whether the suggested failure criterion for cataclastic rocks and the related stress-strain relationships for quartzo-phyllic cataclasites can be used, or should be adapted, for tectonised rocks from other petrologic series. Proper answer to this question would have required performing multiple mechanical procedures on a large amount of samples to get reliable results. Facing the problem of a limited sample quantity per locality (see **Chap. 5**), a focus has been given to the realization of triaxial deformation tests in order to obtain prioritarily strength values on cataclasites from different petrological contents. These data have been produced in the framework of two supervised Master theses to assess the pertinence of Bürgi's correlation between geological and mechanical data (*Chaignat and Veuve, 2007, Table 3.4*). Moreover, a serie of structurally contrasted carbonatic samples has been mechanically tested with more details to evidence the effect on strength of specific geological features inside a sample and

to investigate the resulting variation in mechanical responses. In parallel, these samples were the object of a detailed characterization by means of the MSI approach to define its possible limitations. Results constitute the main object of this research.

In practical engineering, the use of basic models like the Mohr-Coulomb fracture criterion is advantageous when a limited sample quantity can be characterized by means of triaxial tests. Such an approach involves namely only two parameters of rock mass characterization: angle of internal friction φ and cohesion c . These two parameters can be determined relatively easily by few laboratory tests.

More elaborated models using numerous parameters to account for the specificity of a given rock mass lead to two problems. First, the amount of laboratory analyses have to be increased to constrain these parameters (see for example the a , m , s parameters of the Hoek & Brown approach). Empirical determinations have been accordingly proposed to facilitate in this step (see the relationships between the GSI and the a , m , and s parameters). Second, because rock mass description is addressed through a multi-parameter formulation, the source of errors in such a calculation increases concurrently. Thus increasing security factors in the stability calculations seem to be the common practice in underground engineering. It is rapid, effective in the majority of cases and cost-efficient.

With the use of recorded triaxial deformation by means of XRCT, a rapid and advantageous technique can however be provided for an improved interpretation of triaxial tests. In particular, critical evidences of the sample structure can be adequately related to the observed mechanical behavior and mode of deformation (see **Chap. 10**). It is therefore suggested that a more structurally based definition of the “tectonization degree” of *Habimana* (1999) would be welcome. Doing so, a better accounting of the effect of specific textural, structural and mineralogical modifications inherited from cataclasis can be reached in terms of their respective control on rock core deformation.

In this research, the stress-strain behavior of cataclastic rocks could only be qualitatively addressed by means of a conceptual model (**Fig. 4.2**) from which particular considerations about damaged rock rheology have been summarized based on the work of several authors (e.g. *Bésuelle & Rudnicki*, 2004; *Billi et al.*, 2003; *Billi & Storti*, 2004; *Billi*, 2005; *de Bresser et al.*, 2001; *Hadizadeh & Rutter*, 1983; *Hadizadeh & Johnson*, 2003; *Hayman*, 2006; *Ismat & Mitra*, 2001, 2005; *Lee & Kim*, 2005; *Micarelli et al.*, 2006; *Schultz & Siddharthan*, 2005).

Note: As stated in *Rudnicki* (2000) it is considered that the mechanical interpretation from laboratory analyses allows inferring on microscale processes. However the specific question of how these processes affect the macroscale behavior is still incomplete and goes beyond the scope of this research. A limitation is certainly that triaxial tests produce an axi-symmetric loading in which two of the main principal stresses (σ_2 & σ_3) are equal. However the effect of the intermediate principal stress is known controlling strongly deformation of the material. Results from triaxial tests on cataclastic and interpolation of these results at a larger scale corresponding to the damaged rock mass are therefore subject to caution. Profiting from advances in computing power, multi-axial experiments could provide an important input to test more elaborate constitutive models and better succeed in translating data from laboratory experiments in their ability to accurately describe and predict natural processes. However, this means implementing facilities that are not standard but belongs to fundamental research. Moreover, such studies involve a time- and cost-effort that goes beyond the purpose of geotechnical studies.

4.6 CONSIDERATIONS ABOUT HETEROGENEITY AND ANISOTROPY

Heterogeneity affects geological formation by nature. It has a methodological implication on both the geological and the geomechanical characterizations. As a matter of fact it is a difficult parameter to assess at the scale of the rock sample. As a consequence, geotechnical descriptions of rock masses are mostly based on homogeneous models.

Heterogeneity refers to the variations observed inside a rock material in terms of structure and composition and can be characterized through the analysis of different distinct components. Such components can correspond to grain size variation, void repartition, zones of alteration, development of microcracks and resulting preferred orientation of fracture networks, among many others. Heterogeneity in rocks may define a directional anisotropy, e.g. a preferred spatial distribution of one or several distinct components leading to a variation of rock physical properties in function of its spatial orientation. In this sense, *structural* and *compositional* anisotropies can develop.

For intact rocks (broad term), anisotropy is best represented in foliated rocks (slates, schists) that are characterized by closely spaced planes of weakness, cleavage or schistosity, which makes the determination of uniaxial compressive strength difficult. Visual impression of the quality of such rock types is always very subjective to determine on the sole base of field observation. For damaged rocks (*sensu* **Fig. 4.2**), anisotropy results from sustained shearing and crushing in fault zones. Heterogeneity and anisotropy are a main cause why classical mechanical models are often invalid to properly describe cataclastic rocks.

To aid in the critical interpretation of triaxial test data, rock core samples have to be evaluated in terms of their (heterogeneous) structural and compositional characteristics and how these characteristics interact under applied triaxial load and eventually influence the axi-symmetric deformation pattern. This is an especially important parameter and was mentioned as a deficit in the study by *Habimana* (1999). As mentioned, the use of indirect XRCT provides an interesting mean to obtain awareness of the rock core structures and their orientation prior to the realization of triaxial tests.

Based on the conceptual model of **Fig. 4.2**, following general assumptions can be made in terms of the evaluation of heterogeneity affecting rock cores and its influence on triaxial data:

- *Intact domain* (domain A): rock samples exhibit a structural consistency over a large scale. Strength and deformability data determined in the laboratory can be evaluated at the scale of the rock mass assuming homogeneity of rock mass properties. Quality of the model for the rock mass will benefit from analyses on samples taken in different locations, to obtain the most global picture of the rock mass and infer on realistic geomechanical values to describe its characteristics.
- *Damaged domain* (domain B): rock samples are affected by the extreme action of cataclasis on the initial rock protolith, causing important mineralogical and structural variations. Strength and deformability data from experiments have to consider microscopic evidences to infer on rock rheology and characterize adequately such materials. Seen as a whole, extremely damaged materials are affected by time-dependent deformations in the form of creep. Occurrence of such rocks is limited to the narrow zone corresponding to the fault core.

- *Intermediate domain* (A + B): rock samples present a mixture of intact and damaged rock characteristics. Rock mass has a chaotic nature leading to strong structural and compositional contrasts inside the damaged rock mass that cause a structural heterogeneity to develop. Microscopic parameters influencing rock deformation have to be taken into account (e.g. *damage indicators*) and a quantitative description of heterogeneity has to be addressed. To develop a proper understanding on such intermediate rock mass properties, sampling should be densified in a same location to account for heterogeneity (*Gunsallus & Kulhawy, 1984*) and performed in as much location as possible throughout the damaged rock mass to depict the most representative picture of heterogeneous rock mass variability and find an appropriate constitutive law to describe its behavior.

4.7 FROM 2D TO 3D EVIDENCES

A limitation to the geological approach of *Bürgi* (1999) to correlate mineralo-structural parameters with mechanical evidences is the fact that the characterization index MSI is derived from thin section analyses that represent a 2D observation support. As stated in *Escuder-Viruete et al.* (2004), traditional 2D fracture spacing measures have inherent geometric biases, which can lead to inaccurate representations of the true fracture pattern. From the microscopic perspective, an objective translation between geological and geomechanical properties that takes into account the effect of heterogeneity would require realizing multiple thin sections in at least 2 orthogonal directions at different levels of the rock core used for triaxial testing. Major problems to be named here are:

- Realizing thin sections implies destruction of the rock core. Accordingly the geological and geomechanical characterization cannot be performed on the same rock core sample;
- To confront geological and geomechanical data from a same sample involves using an alternative non-destructive technique for the determination of the structural and textural parameters included in the formulation of the MSI.

The medical XRCT resolution, although limited and not able to rivalize with the level of petrographic details observed from thin sections, permits a complete 3D view of the sample. The relevance of particular structural characteristics (the determination of which can be aided by thin sections realized on an impregnated triaxially deformed rock core) can be accordingly better assessed. Thus medical XRCT acquisitions are seen as an ideal numerical support for cataclastic rock core characterization and modelisation of their deformation. Accordingly, a geological characterization implementing XRCT and based on the MSI approach will be addressed. Moreover, the interest of the XRCT visualization for an improved understanding of the triaxially induced ruptures will be illustrated.

5

SAMPLING SITES

“Ce n’est pas notre petitesse qui fait notre passivité,
c’est au contraire notre passivité qui fait notre
petitesse.»

Charles-Ferdinand Ramuz

In order to test the geological-geomechanical correlation proposed by *Bürgi* (1999) the study of cataclastic rocks from various petrological contents has been undertaken. Contacts have been taken across Switzerland to find out sampling sites with a particular emphasis on current tunnelling projects in difficult geological conditions.

Next to the possibility to obtain a widespread petrological variability, an important site selection criterion that has been retained was to dispose of good outcrop accessibility for quality sampling, as the sampling campaigns have been made with a prototype of portative drilling equipment implementing the triple tube core barrel technique. The details of the sampling device are presented later in **Chap. 6**.

Field campaigns have been performed between November 2004 and March 2006 in relation with ongoing engineering projects. A total amount of 32 samples could be obtained from self-realized short drilling operations (max. 1 m depth). About 120 additional rock cores from official drilling operations realized in relation with ongoing site works have been moreover collected. Not all samples could be integrated in the current research project for a geotechnical characterization. Preferentially, a serie of 12 samples of tectonized limestones has been considered for the combined geological-geomechanical approach. The remaining rock material is stored at EPFL in a humid room (marl samples are stabilized in paraffine) and available for further studies.

The stage of calibration of the medical XRCT for rock core investigations (**Chap. 8**) profited moreover greatly from acquisitions performed on the wide variety of petrological contents collected during this study.

5.1 PETROLOGICAL VARIETY

Rock core samples have been obtained in 5 tectonic units of Switzerland corresponding to the folded Jura Mountains, the Molasse basin near Geneva Lake, the Prealps of Vaud, the crystalline basement of Aar massiv and the metamorphic series of the Southern Alps near Locarno. Accordingly, rock core material from 6 different petrologies has been collected: limestones, dolostones, sandstones, marls, crystalline metamorphic rocks and polygenic assemblages. **Fig. 5.1** shows the location of the different sites that has been the object of a sampling field campaign. **Table 5.1** is a general table indicating the petrological variety of the collected rock cores, general site informations, and amount of samples obtained.

5.2 GEOTECHNICAL ROCK CORES

A geotechnical characterization of cataclastic materials for underground engineering projects is best done using fresh material from reconnaissance drilling operations. Special care is required after extraction from the rock mass to maintain sample structure and avoid contact with ambient air so as to prevent alteration and sample loss.

The temporary storage of cataclastic samples in the commonly used wooden boxes is inappropriate. Cataclastic samples should be confined just after extraction under hermetic conditions. Carefull packaging of the rocks and stabilization with paraffine is a widely adopted technique. Using a triple tube core barrel, confinement of the rock cores directly during ongoing drilling in a PVC inner tube is very advantageous. As such, rock cores are subjected to minimal manipulation and remain representative of structures that are indicative of rock mass conditions at a larger scale (definition of domains A & B on **Fig. 4.2**). Moreover it allows retaining the natural humidity levels of the materials and prevents alteration of critical mineralogical components, making these the optimal

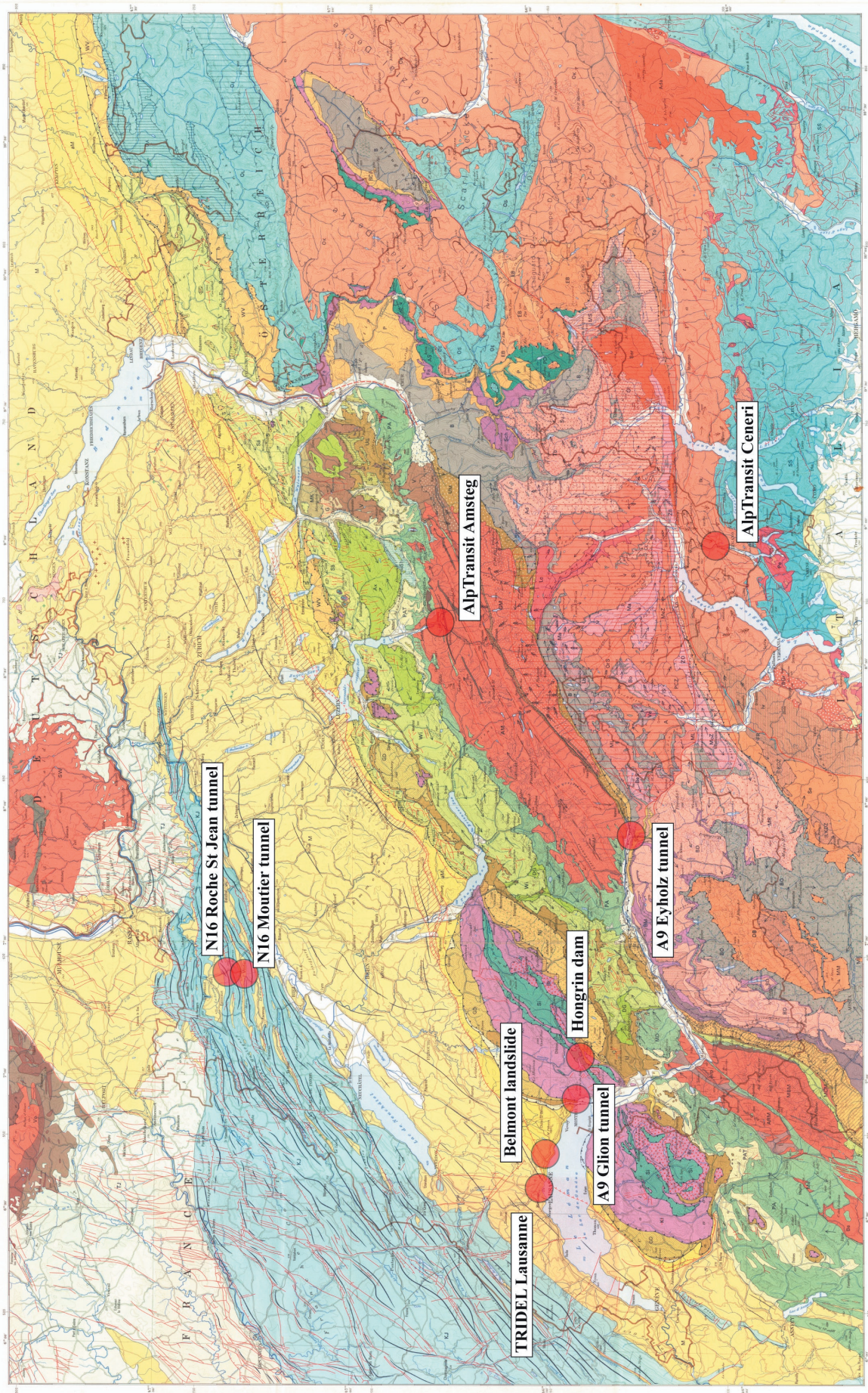


Fig. 5.1 Tectonic map of Switzerland and location of selected sites where the different sampling campaigns aiming the collection of cataclastic rock cores of various petrological contents have been realized in this study.

| PETROLOGICAL CONTENT | SITE | TECTONIC CONTEXT | SAMPLING CONDITIONS | SAMPLING TECHNIQUE | COLLECTED SAMPLES | DENOMINATION |
|-------------------------------|--|--|--|------------------------------------|-------------------|--------------|
| TECTONIZED MARLS & SANDSTONES | N16 Moutier tunnel, BE | MOLASSE BASIN, OBERRHINGGRABEN, Tertiary Elsäßer Molasse | Horizontal drilling in tectonized marls ahead of tunnel face, 30-35m overburden | double tube core barrel | 15 | TM |
| | TRIDEL gallery, Sébeillon access, Lausanne, VD | SUBALPINE MOLASSE, Tertiary grey molasse of Lausanne (+ marls) | Drilling of tectonized marls on side walls behind tunnel face, average of 50 m overburden | single tube core barrel | 4 | TR |
| | Belmont landslide, VD | THRUSTED SUBALPINE MOLASSE | Differently oriented drilling in slightly cataclased sandstones along road outcrop | single and triple tube core barrel | 8 | BEL |
| LIMESTONES & DOLOSTONES | N16 Roche St-Jean tunnel, Choindex, JU | FOLDED JURA, tectonized limestones, Kimmeridgian, Upper Malm Formation | Horizontal and vertical drilling of tectonized limestone with numerous clay-bearing zones below N-portal, 30 m overburden | double and triple tube core barrel | 12 | RSJ |
| POLYGENIC ASSEMBLAGE | A9 Glion tunnel, VD | PENNINIKUM, MEDIAN PLASTIC FOREALPS, Triassic carbonates | Drilling of tectonized dolomites on side walls of upper tube, 50 m overburden | triple tube core barrel | 3 | GL |
| | A9 Eyholz tunnel, Visp, VS | PENNINIKUM, ZONE OF BRIG- SION-COURMAYEUR, undifferentiated | Recuperation of rock cores from reconnaissance drilling operation (contact with bureau Norbert SA), max. 800 m overburden | double tube core barrel | 15 | Eye |
| CARBONATIC METAMORPHIC SERIE | Hongrin dam site, VD | PENNINIKUM, MEDIAN PLASTIC FOREALPS, Jurassic metamorphosed Carbonates | Recuperation of rock cores from reconnaissance drilling operation (dam foundation, contact with bureau Norbert SA) | double tube core barrel | 90 | HO |
| | AlpTransit Gotthard BT, Amsteg, UR | AUTOCHTON, AAR MASSIV, Gasterm Granite (300Ma) and associated migmatites | Drilling attempts on tunnel side walls in W-tube (hydrothermally altered zone) and in E-tube just behind TBM (sheared granite and migmatites), 2000 m overburden | triple tube core barrel | 0 | |
| CRYSTALLINE METAMORPHIC SERIE | AlpTransit Ceneri BT, Sigrino, TI | SOUTHERN ALPS, INSUBRIC CRYSTALLINE, Giuvello gneiss & gneiss misti | Drilling of variably kairitized gneiss on side walls of the Sigrino access gallery, 600 m overburden | triple tube core barrel | 5 | CBT |

Table 5.1 Presentation of sampling sites, petrological attribution, indication of tectonic context and details of cataclastic rocks sampling. The different sampling techniques used are indicated. A total of 152 samples have been collected and are deposited currently at EPFL and available for further study. As will be presented later, this research focuses in particular on 12 samples obtained at the N16 Roche St Jean site of the Jura Mountains as highlighted in the table.

representative samples of *in situ* conditions to be studied in a laboratory.

On the contrary to the works of *Bürgi & Habimana* (1999), both the geological and geomechanical studies have been performed during this same research. Accordingly, sampling directly into cylindrical shapes has facilitated further material preparation for mechanical tests. Moreover, as this research implements medical XRCT as an additional characterization tool, it has been recognized that rock cores are particularly appropriate over X-ray irradiation (shape homogeneity, minimization of artifacts).

5.3 SAMPLING SITES

The different sites listed in **Table 5.1** are presented shortly in the following. They are described with details even in case where samples were not directly or only partly integrated in the geological and geomechanical approach, as they bear information about different cataclastic contexts and manifestations in a variety of petrological environments.

5.3.1 N16 Highway Moutier Tunnel

The construction of the new N16 highway through the Jura Mountains of Switzerland involves since a couple of years the construction of several tunnels through a succession of anticlines and synclines structures affecting jurassic limestone beds over 10 km in the Moutier Gorges (**Fig. 5.2**).

Excavation of the Moutier tunnel started in 1999. It corresponds to a 1.6 km long tunnel at shallow conditions. The Moutier tunnel represents a particular case, because of unexpected difficulties associated with tectonized tertiary sediments (Elsässer Molasse Formation) constituting the plain of Moutier. Initial decision to excavate the tunnel using a soft-rock TBM revealed quite inappropriate as documented by the blocking of the machine on 27.02.2003, i.e. 4 months after beginning of the works and after only 189 m of excavation. A subvertical fault zone constituted of clay-rich materials that strike approximately parallel to the tunnel axis caused the blocking of the TBM head. Consequently, an adaptative strategy had to be adopted (excavation by means of divided sections).

Based on additional geological site investigations, a highly complex rock mass structure characterized by localized highly ductile deformations has been revealed (**Fig. 5.3**). Main structure is a 50 m wide zone of tectonized, brecciated marls (zone D2a) oriented 320/90 with smaller sized replicas. On 08.05.2003 excavation of the southern tube began and a by-pass gallery soon permitted the connection between the two tubes. Arch excavation by means of drill and blast technique started backwards in the northern tube towards the TBM head. The machine could be freed and invert excavation in the southern tube has been realized with the reactivated TBM. The complete excavation in this tube has been finally succeeded in December 2006, more than 3 years after beginning of the works. Full implementation of the Moutier tunnel is expected for 2011.

Profiting from reconnaissance drilling operations performed between April and July 2005 ahead of the tunnel face into zone D2a (Stump Foratech SA), 15 samples of tectonized marls have been collected. They are composed of more than 50 vol% clay (chl-ill-sm±ka) and characterized by very low permeabilities ($k = 1.79 - 2.79 \times 10^{-12}$ m/s). They exhibit contrasting water contents varying between 10.1 and 18.8%, which have been documented directly influencing rock strength on site (the “dry” marls being more competent). Atterberg limits have been calculated and a plasticity index of 29.52 % was determined. The oedometer test gave a value of pre-consolidation of 1000 kPa. Dilatometric tests performed on sites in zone D2a gave values of deformation modulus ranging between $E = 13 - 58$ MPa.

Chap. 5 Sampling sites

Indicative mechanical tests on the Moutier marls have been performed within this research. Uniaxial compressive strength indicated a value of 0.6 MPa. Triaxial strength has been found at 2.1 MPa for 400 kPa confinement in a rock triaxial cell. The very low permeabilities encountered introduced however a difficulty for the realization of consolidated-drained triaxial tests due to excessive loading speeds. 3 other samples have been therefore drilled in the laboratory using a dry single tube barrel (no water injection to prevent sample wash out) in smaller diameters of 55 mm to be tested in soil triaxial cells that allow a better control of the loading speed (consolidated-drained tests). Results are estimated however not significant as they evidence an important variability. Significant determination of intrinsic parameters from such rocks requires a high density of tests which fell outside the possibilities of this study.

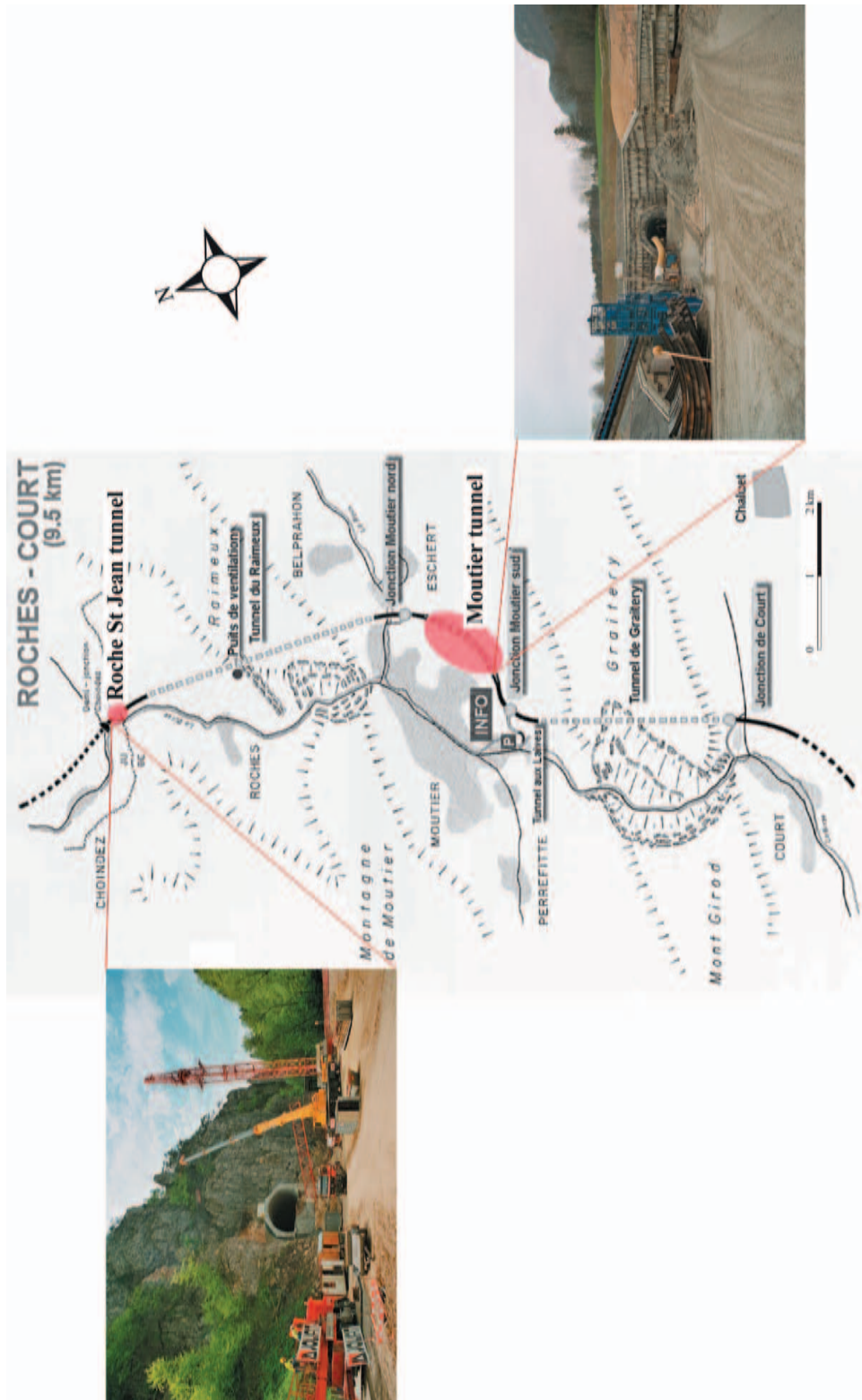


Fig. 5.2 Geographical context of the N16 highway under construction between the Bern and Jura cantons of Northern Switzerland. Location of the Moutier and Roche St Jean tunnels is indicated. The Moutier tunnel cross tertiary sandstones that has been deposited in the Moutier syncline. Note the shallow tunnelling situation, although numerous problems related to difficult geological conditions have been encountered. The Roche St Jean tunnels presented later in **section 5.1.4**.

Interestingly, pilot XRCT acquisitions on the redrilled samples of Moutier marls showed that the laboratory drilling induced a radial cracking of the rock core, affecting the natural properties of the tested materials. It was therefore decided to use the Moutier marl materials for methodological purposes only (mostly related to indirect imaging and implementation of medical XRCT in a triaxial test procedure).

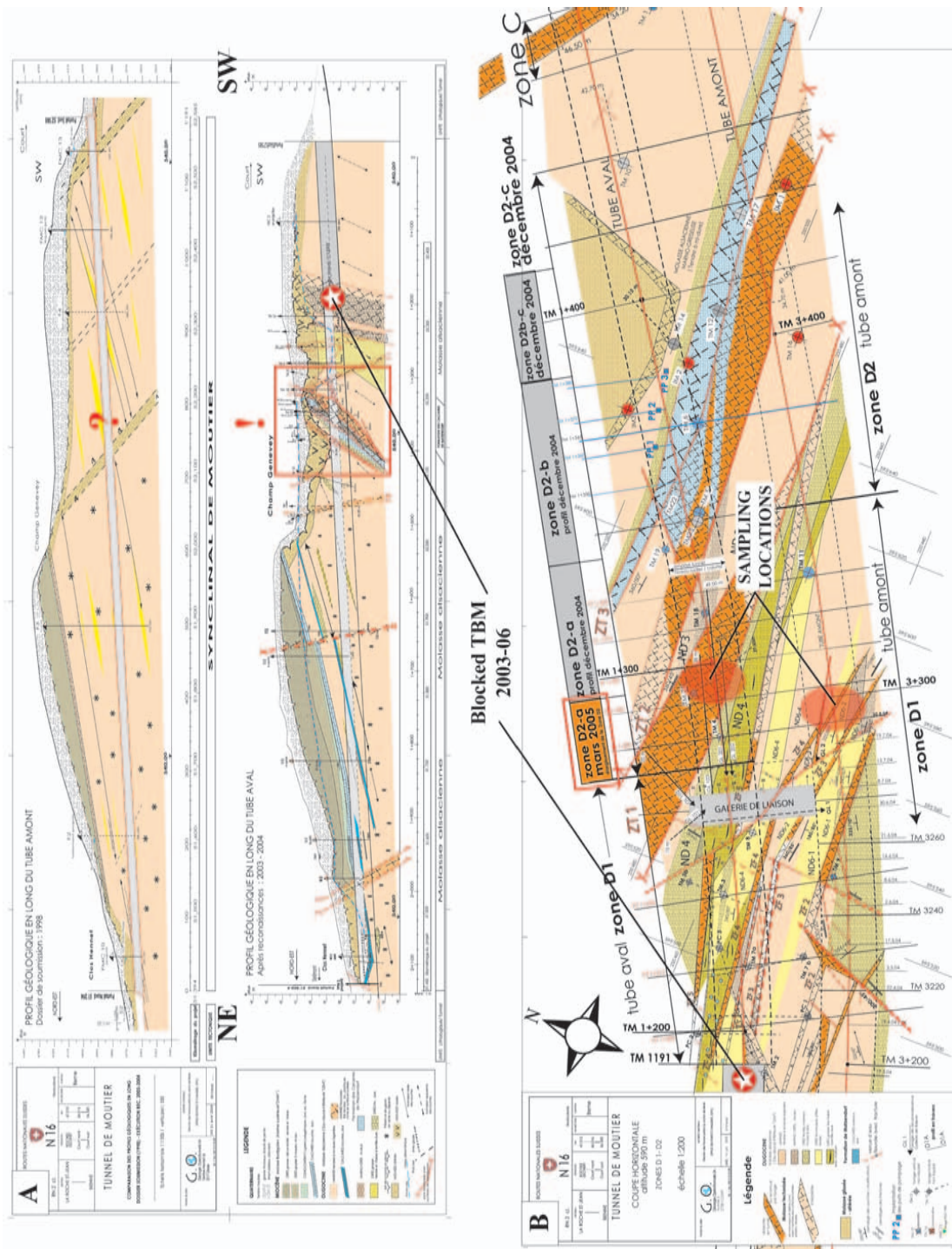


Fig. 5.3 A) Vertical profiles on site of the Moutier tunnel. Comparison between the initial prognosis of 1998 and the structure in subvertical position depicted after realization of complimentary geological field investigations in 2003. The tectonized zone D2a is characterized by similar weak mechanical properties than the horizons responsible for the blocking of the TBM head in 2003. B) Horizontal profile of the Southern end of the Moutier tunnel. Position of blocked TBM is indicated. Additional geological field and drillhole investigations have evidenced a complex fractured structure characterized by subvertical tectonized marls alternating with weathered sandstone beds. Two subhorizontal reconnaissance drillings in tectonized zones (ZT) of various extents have been performed in spring 2005. The tectonized marls depict different values of water content that are directly related with rock strength properties. The TBM was eventually freed by the end of 2006. With the authorization of G. O. Géologie Opérationnelle, Court.

5.3.2 Tridel Gallery Lausanne

In order to limit the truck traffic related to the waste treatment in the agglomeration of Lausanne, a concept has been created in 2002 to connect the station of Sébeillon with the TRIDEL incineration plant by mean of a 3.8 long railway tunnel under the city (average slope of 5%). Accordingly, the transport of about 60 % of waste products send for incineration at TRIDEL can be realized. The first waste transport by train in the gallery has been done in April 2007.

During excavation of the gallery in March 2005, few samples have been collected by hand drilling operations with a portative single tube core barrel equipment. The technique showed to be quite inappropriate to ensure extraction of the drilled cores without breaking them (no core lifter). Accordingly, only 4 samples of highly tectonized marls have been collected. They are characterized by various amount of graphite and numerous shear surfaces.

Samples are stored at EPFL and were not integrated in the program of geological and geomechanical investigations. In a same way than for the Moutier marls, such clay-rich rocks are difficult to characterize on the base of a too limited amount of samples for mechanical tests.

Outcrop conditions are presented in **Fig. 5.4**.

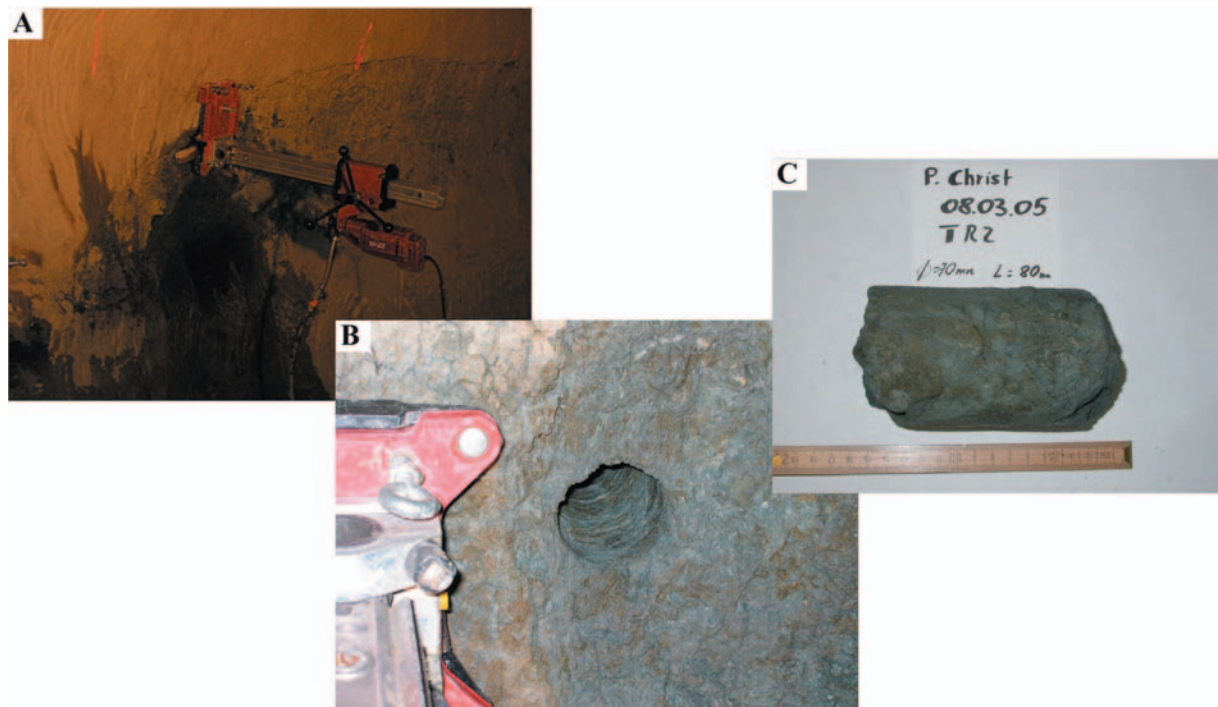


Fig. 5.4 Outcrop conditions at TRIDEL implementing the single tube core barrel technique (A & B). After this experience in winter 2005, the development of a more appropriate sampling device has been addressed (see **Chap. 6**). Note interesting rock mass and sample texture (B & C).

5.3.3 Belmont Landslide Area

During spring and fall 2005, field campaigns along a road outcrop near Belmont (VD) have been performed. The site is located on a landslide and the sandstone is found accordingly with different levels of fracturation. Collected samples show evidence of open or clay-sealed fractures, some traces of graphite, as well as grain size variability along micro-shear planes.

The BEL samples listed in **Table 5.1** have been the object of a Master Thesis performed at GEOLEP (*Sené*, 2006). They have been characterized texturally and structurally and triaxial tests have been realized. They are not used not discussed here.

The site of Belmont with its easy accessibility served optimally to the development and test of the portable triple tube core sampler that has been implemented in this research (see **Chap. 6**).

5.3.4 N16 Highway Roche St Jean Tunnel

To the North of Moutier, another N16 tunnel has been under construction at the Roche-Saint-Jean site close to Choindez in the Jura canton (**Fig. 5.2**). The tunnel is 211 m long and cross the reversed anticlinal of Envelier at 330/02. A sinistral main fault is cutting the tunnel axis at 80/115 right at the North portal. The overall stratigraphy is oriented NE-SW and layers have a dip of 90/200. Many fracture systems are visible at preferentially 80/285 and 35/320. Numerous open cracks have been noticed (0.1 à 10 mm) during tunnel construction with water outflow of 100 to 150 l/min (*Bugnon*, pers. comm.). During field work siderolitical filling material has been observed next to marls and fine-grained tectonic breccias.

Rocks correspond to a white micritic limestone of Oxfordian-Kimmeridgian age (Malm) that is highly fractured, crushed, tectonized and karstified (some conduits > 1 m have been found during excavation of the tunnel). Rockfall protection measures have been addressed to secure the N-exit of the tunnel that will connect in the future with the Verrerie viaduct.

Self-realized drillings have been undertaken in Mai 2005 just below the N-portal in an axis more or less parallel to the tunnel axis (**Fig. 5.5**). The nature of the rock showed to be highly complex and brittle to securely fix the sampling device at the outcrop. As a consequence, only 3 rock cores could be gained in adequate dimensions for triaxial tests. Additional rock cores have been recovered from 2 vertical drilling operations in the Verrerie plain by Zchokke SA in Mai 2005 aiming the determination of rock conditions to accomodate the piles of the projected viaduct (**Fig. 5.6**). At the end, 12 samples depicting interesting textural and structural evidences could be integrated in this research.

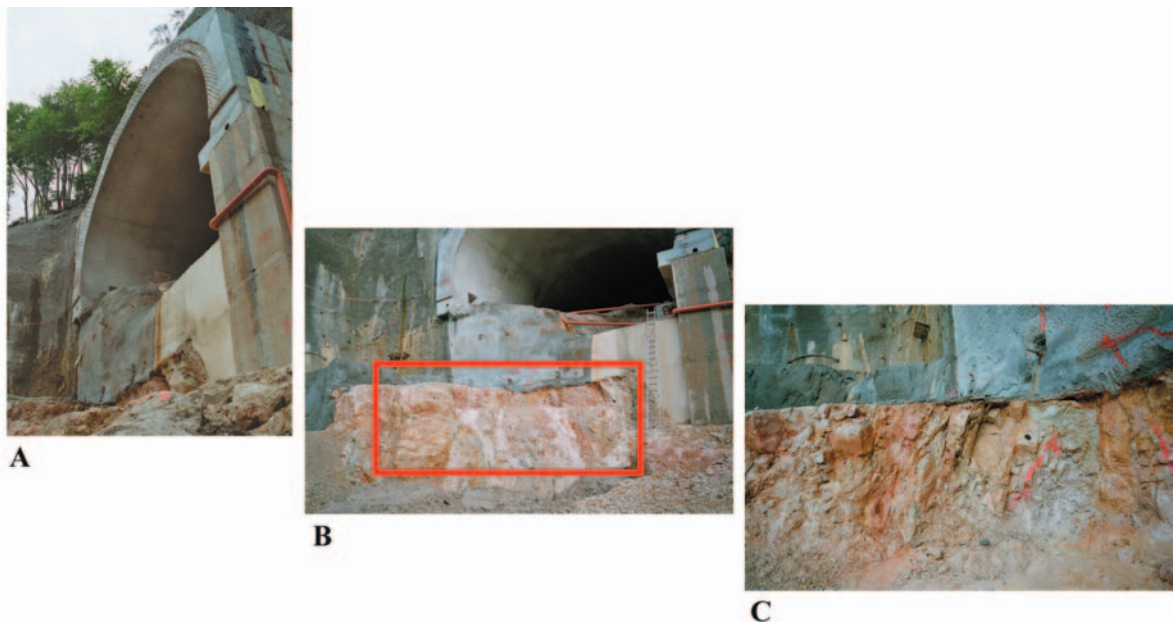


Fig. 5.5 Roche St Jean tunnelling site under construction in spring 2005. **A)** View of the N-portal from where the Verrerie viaduct above the Choindez basin is under construction, to connect the Roche St Jean with the La Verrerie tunnel. **B)** Area where drilling operations have been performed. **C)** Outcrop conditions and damaged rock mass.

The *RSJ* samples have been interpreted as reflecting the progressive development of a damaged zone characterized by a re-calcified tectonic limestone matrix affected by numerous fractures of different shapes and sizes. Fault core material is further made of limestone clasts in a clay matrix (fault

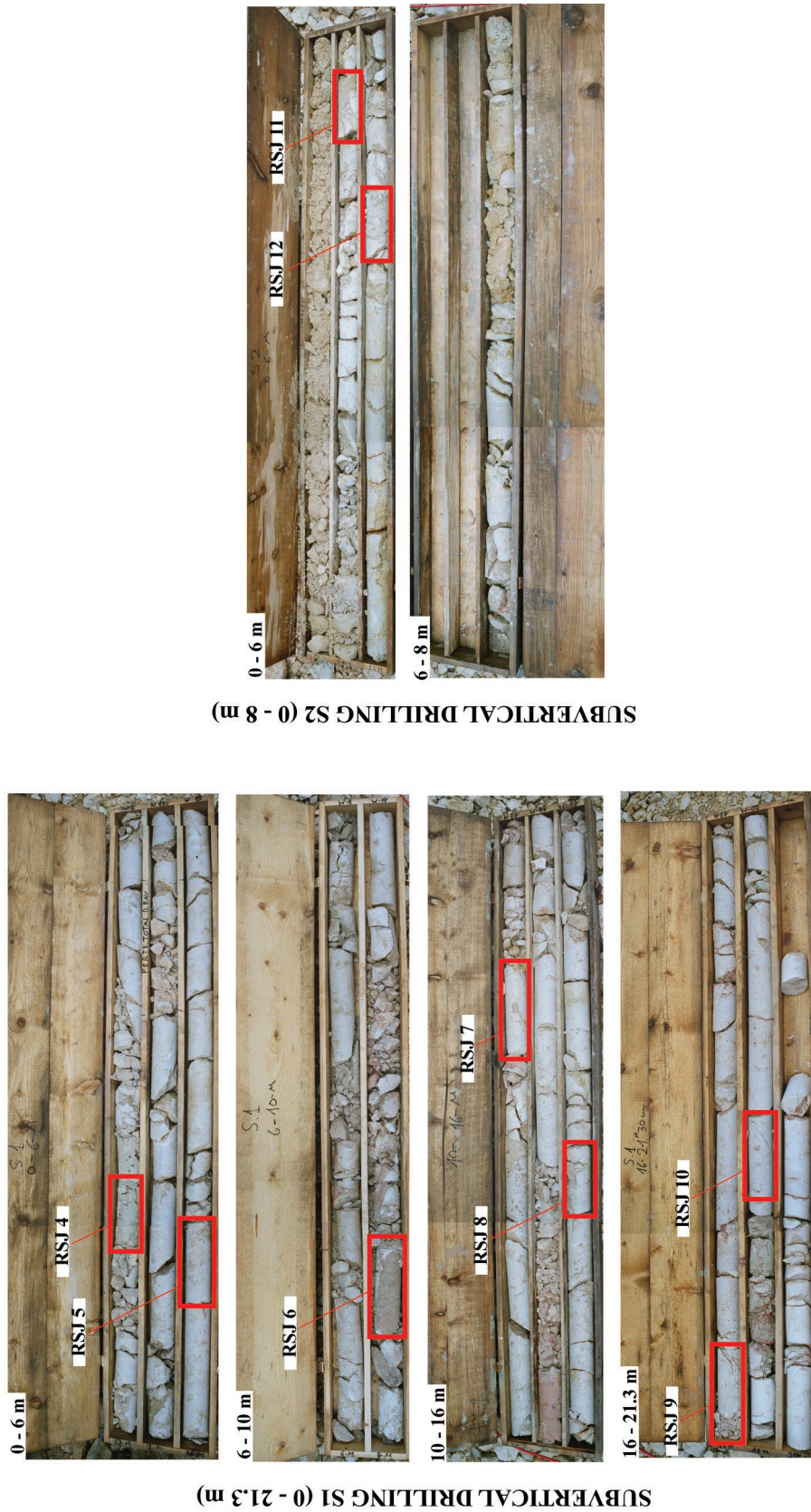


Fig. 5.6 Drillings S1 and S2 by Zschokke SA and recuperation of selected samples for this research. A wonderful opportunity.

breccias). Contrasting types of fractures coexist ranging from open, filled to fully recrystallized subtypes. **Fig. 5.5** shows evidences from site condition and outcrops where the sub-horizontal tunnel-axis parallel drillings have been realized.

The *RSJ* samples have been the object of both detailed geological and mechanical investigations. They have been considered preferentially for this research as they were found depicting the widest

scatter in structural relationships to assess the contrasted cataclastic intensity inside a fault zone compared to the observations made during the other sampling campaigns. They will be discussed in **Chap. 11, 12 & 13**.

5.3.5 A9 Highway Glion Tunnel

The Glion tunnel between Montreux and Villeneuve is well known in Switzerland by skiers because it is part of the A9 highway portion connecting Vaud with Valais where important traffic congestions happened regularly during its refection in 2004-05. Refection works addressed the structure readjustment to new fire security norms. It is about 1 km long and has been build between 1968 and 1971 through the Triassic dolomites of the Median Plastic Prealps (**Fig. 5.7**). The rock mass is fractured and folded as a result of the last alpine deformation stages (*Mosar et al.*, 1996). The dolomite is cataclastic and karstified with minute crystals filling the pore cavities. Several generations of discontinuous and accidented fractures coexists and cross the micritic texture (**Fig. 5.8**).

A sampling campaign has been performed on the 4th of June 2005 during refection works in the upper tube (mountain side). Successful extraction of 3 samples could be taken at SOS post M3 with the freshly developped portative triple tube core driller (**Fig. 5.8**). SOS post M3 is a 2.5 m wide & 3 m deep security slot. Main measured discontinuities at outcrop define a conjugate system in orientation 352/65 and 308/85.

A geological and mechanical characterization on one of the extracted rock core sample has been done in relation with this research by *Chaignat & Veuve* (2007).

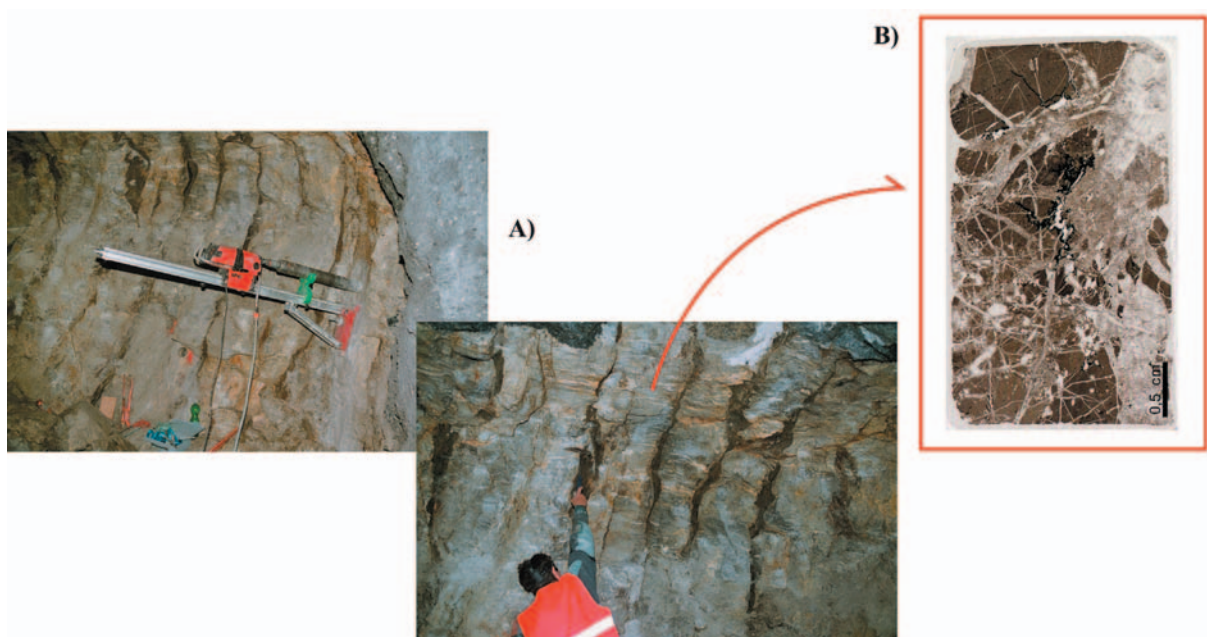


Fig. 5.8 Sampling conditions at SOS keyway M3 in the upper tube of the A9 Glion tunnel. **A)** Outcrop structure. **B)** Thin section realized in sample GL 3 depicting the numerous fractures in complex structural relationship.

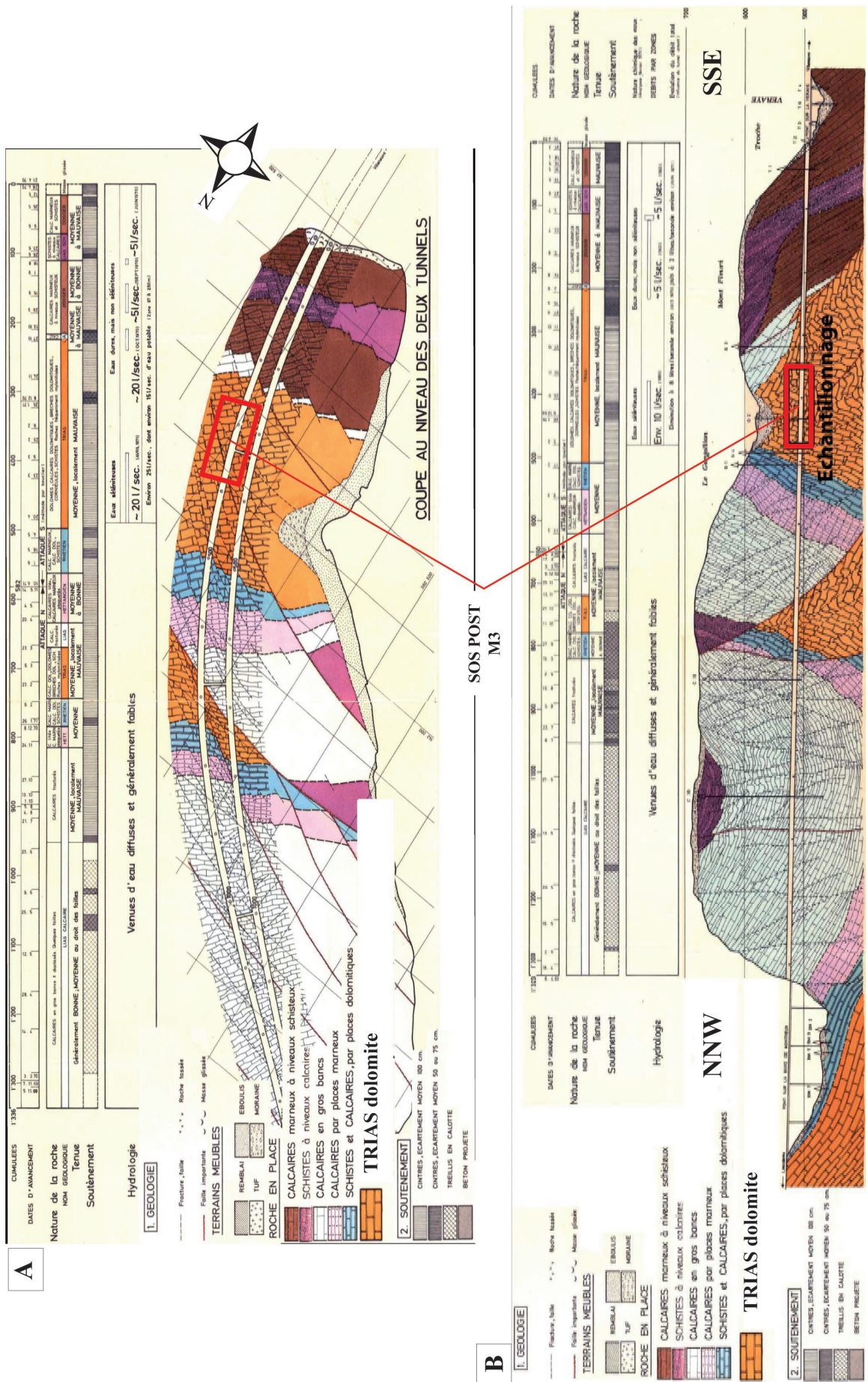


Fig. 5.7 Horizontal (A) and vertical (B) profiles of the A9 Glion tunnel and indication of sampling locations in triassic cataclastic dolomites. With the authorization of Bureau Norbert SA, Lausanne.

5.3.6 A9 Highway Eyholz Tunnel

Rock cores from reconnaissance drillings at Eyholz tunnel in Valais have been the object of a geomechanical characterization for a mandatory contract at LMR in fall 2005. Even if not corresponding to cataclasites *s.str.*, the Eyholz samples indicate a quite exotic structure (**Fig. 5.9**) characterized by the complex arrangement of rock clasts from different petrological content (calcshists, quartzite, prasinite and dolomite) and concurrent cementation by calcite-rich fluids. The breccia is moreover defined by an important porosity making them particularly interesting for medical XRCT imaging (**Fig. 5.9** and further **Chap. 10**). Clasts size varies strongly from millimetrical size up to angular components of decimetrical dimensions. Average cohesion is good and an important secondary crystallization of calcite is evident in void spaces.

The collected Eyholz material has been interpreted as corresponding to the geological record of an important quaternary landslide probably related with earthquakes activity at that time. Fragmented rock material (Saint-Christophe strata) collapsed and has been washed out by streams, to be deposited and finally cemented in the Vispa valley. The area still depicts today a relatively high seismicity in Switzerland, as a result of movements along one of the major alpine fault zone affecting valley floor (Rhône-Simplon line).

The Eyholz tunnel under construction is part of the A9 highway continuation between the cities of Sierre and Brig. It will be 4 km long with a maximal rock overburden of 820 m. It is expected to reduce massively the road traffic through the city of Visp by establishing a transit by-pass to the South.

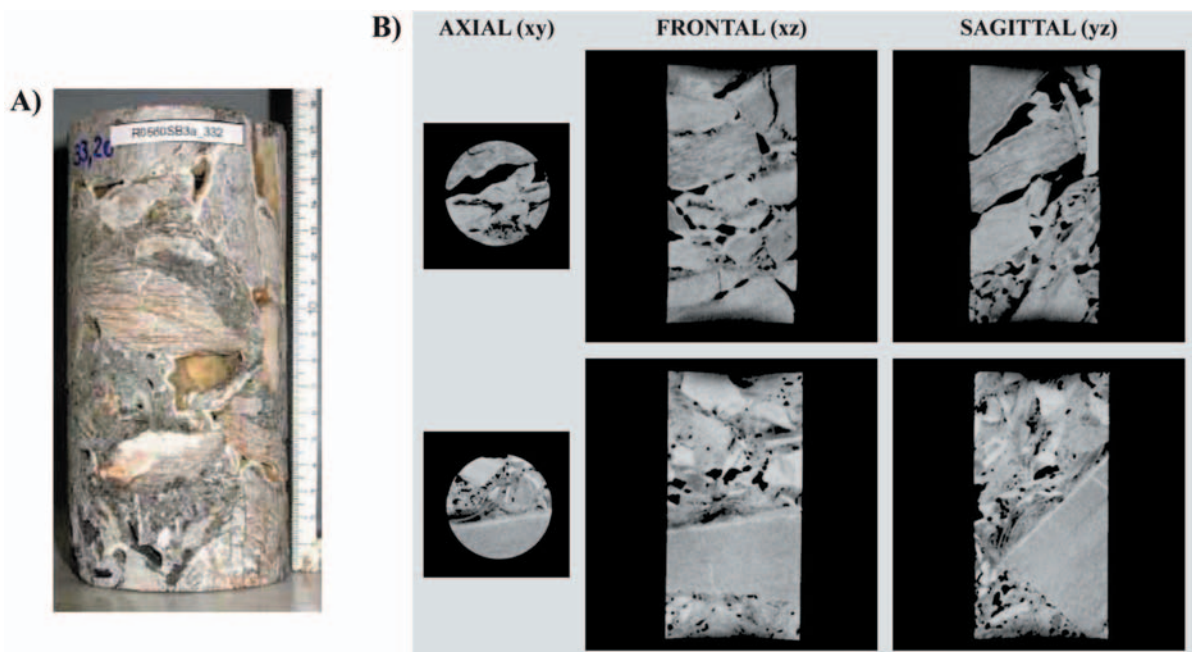


Fig. 5.9 A) Indicative structural evidence of Eyholz samples. Sample height is 170 mm. B) Preliminary acquisitions by medical XRCT. The Eyholz rock material has been the object of an extensive use to callibrate the XRCT technique for rock core characterization (see later **Chap. 10**). The darker tones correspond to components of lower mineralogical density, with black zones referring to void spaces. Note the contrasted components size and shape.

5.3.7 Hongrin Dam Site

The Hongrin is for hikers a well-known mountain lake in the Alpes vaudoises. It has been formed as a result of the construction of a double-arched dam in 1969. Dam height is 123 and 93 m and the crown is 325 m. The developed power is 240 MW that are distributed in the Rhône plain to aliment households and industries. The lake is naturally alimented in its upper part by the river

Hongrin which belongs to the catchment area of the Rhine through the river Sarine. Hydroelectric plants perform pumping in Lake Geneva (Rhône catchment area) to maintain a constant level in the Hongrin Lake and ensure the activity of the turbines by gravitary flow. The total catchment area of the dam corresponds to 90.8 km². Lake volume is about 52 mio m³ and its surface is 160 hectares.

A hundred of rock cores from the Hongrin dam site could be gained profiting from a contact with Bureau Norbert SA, Lausanne after a drilling campaign had been performed in December 2006 for the evaluation of the stability of the dam. The collected samples show interesting structural/textural relationships and correspond to calc-schists. Samples have been stored after attribution in 3 quality classes of increasing tectonization degree at EPFL for further research. Two samples have been tested by XRCT and indicated that the Hongrin rock cores represent a material of choice for a combined geological-geomechanical characterization. Mechanical tests have only been realized in the framework of a mandatory contract at LMR and are not discussed here.

These samples came unfortunately too late to address a complete geological-geomechanical characterization in the framework of this research. They are implemented currently in a new research project at GEOLEP addressing the characterization of rock core alteration using X-ray Computerized Tomography (*Farine*, in prep.).

5.3.8 AlpTransit Gotthard Base Tunnel, Amsteg

The Gotthard base railway tunnel (**Fig. 5.10**) corresponds to one of the biggest civil engineering construction in the world with a length of 57 km through the alpine orogeny connecting southern with northern Switzerland at a depth below surface reaching 2500 m in places. Consortia of different contractors are responsible for the construction works under the supervision of AlpTransit Gotthard Ltd (wholly owned subsidiary of Swiss Federal Railways (SFR) with headquarters in Lucerne, www.alptransit.ch). The Gotthard Base Tunnel should become operational at the end of 2016.

In the framework of this research, an authorization from the authorities in charge of the subsection Amsteg could be obtained to perform sampling in January 2006 on the walls of the W-tube. There a 50 m wide hydrothermally weathered zone caused difficulties during TBM excavation due to the strong contrast encountered in rock properties compared to the dominant Gastern granite. These rocks seemed therefore interesting for the purpose of this research. At times of field work, the TBM that stood still for 5 months just could cross the weathered rock mass after its proper consolidation through pressurized injections.

Experience on the field with the triple tube core barrel device was in term of rock core recovery quite frustrating. Sampling attempts have been realized at km 114.960 in a slot just at the level of the altered rocks. The slot was unfortunately covered with sprayed concrete that made the drillings with the portative machine difficult, the metallic fibers of the concrete causing rapid overheating of the drill bit. After several attempts in drilling directions parallel and perpendicular to W- tube axis, only ridiculously small rock core specimen of a white migmatite could be extracted. Despite interesting mineralogical properties (indicative of the hydrothermal alteration pattern of sensitive silicate minerals by degradation of biotite into chlorite, K-feldspar into sericite, and plagioclase into a fine-grained saussuritic assemblage of albite ± epidote ± calcite) the logistical constraints involved in hand drillings made better result impossible.

Another attempt of sampling has therefore been conducted the next day in the E-tube at km 116.180 just below the backtrain of the working TBM. There, some shear zones of small extent

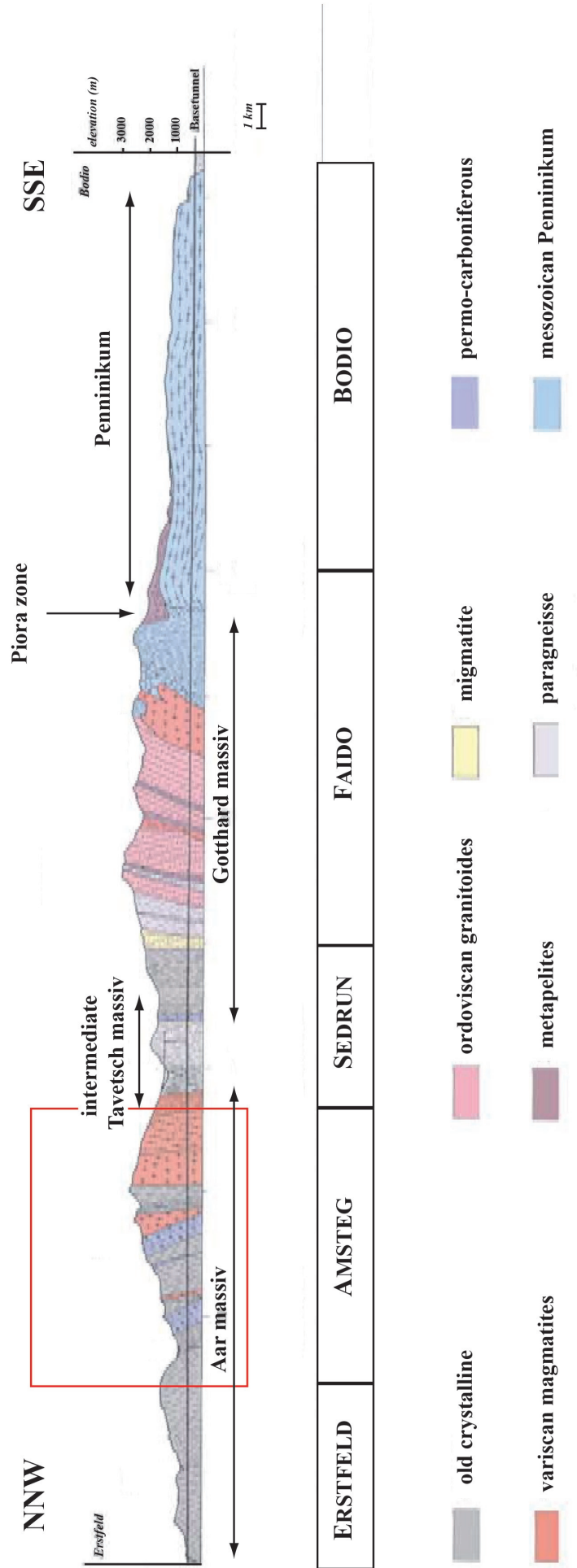


Fig. 5.10 Cross section of the projected Gotthard Base Tunnel, attribution of main geological zones and position of Amsteg subsection. Modified after Alp Transit documents.

just had been documented the day before. They were corresponding to structures related with tectonic activity in the Intschi zone. Also this attempt has been unsuccessful in terms of rock core recovery. Positioning of the drilling device on the freshly excavated concave tunnel surfaces was quite difficult. In such conditions, the drilling axis in a perpendicular direction to the tunnel axis correspond often to the shear plane induce by the zone, making sample recovery really problematic without better equipment. Moreover, considering the fact that about 2000 m of rocks cover the tube in that place and that the tunnel face are still in a stress disequilibrium state as a result of the excavation, this result is also interpreted as reflecting rock unstabilities. Conditions of the two sampling attempts are visible on **Fig. 5.11**.



Fig. 5.11 Sampling conditions in the Gotthard base tunnel at Amsteg. Field work has been performed together with Laurent Chaignat and Christophe Veuve in January 2006. **A)** Material transport. **B)** Just behind the TBM head. **C)** Drilling on freshly excavated walls.

5.3.9 AlpTransit Ceneri Base Tunnel, Sigirino

The Ceneri base tunnel is the southern continuation of the 57 km long Gotthard base tunnel striking more or less N-S through the Swiss Alps (**Fig. 5.12**). It is 15.4 km long deep-seated tunnel (600 m overburden) and represents the third largest railway tunnel project of Switzerland. After preliminary studies proper excavation works started in March 2006 and the tunnel is planned to be finished by 2019.

An exploration tunnel near Sigirino has already been excavated between 1999 and 2003 to gain geological data on the rock formations at the base tunnel's level. Due to the information that was gathered it has been decided that only a small part can be drilled using a tunnel boring machine, the rest will be excavated with traditional blasting methods. Due to space limitations in place of the N- and S-portals, it has been decided to use the Sigirino access to constitute the attack point for south- and north-wards excavations.

Overall tectonic context is complex in the geographic area of Monte Ceneri. Many major accidents and related fault zones (synthetic Riedel shears) characterize the Southern Alps, from which the Insubric line is a famous example (**Fig. 5.12**). Lithospheric brittle deformations inherited from dextral activity along the Insubric line influences rock architecture on site of the Ceneri base tunnel. Movements have been accommodated probably along the Val Colla line what gave raise to an alternance of mixed gneiss, schistose rocks and amphibolites. Numerous occurrences of kikirite and cataclasite have been documented during excavation of the Sigirino gallery (*Pozzorini, pers. comm. 2006*).

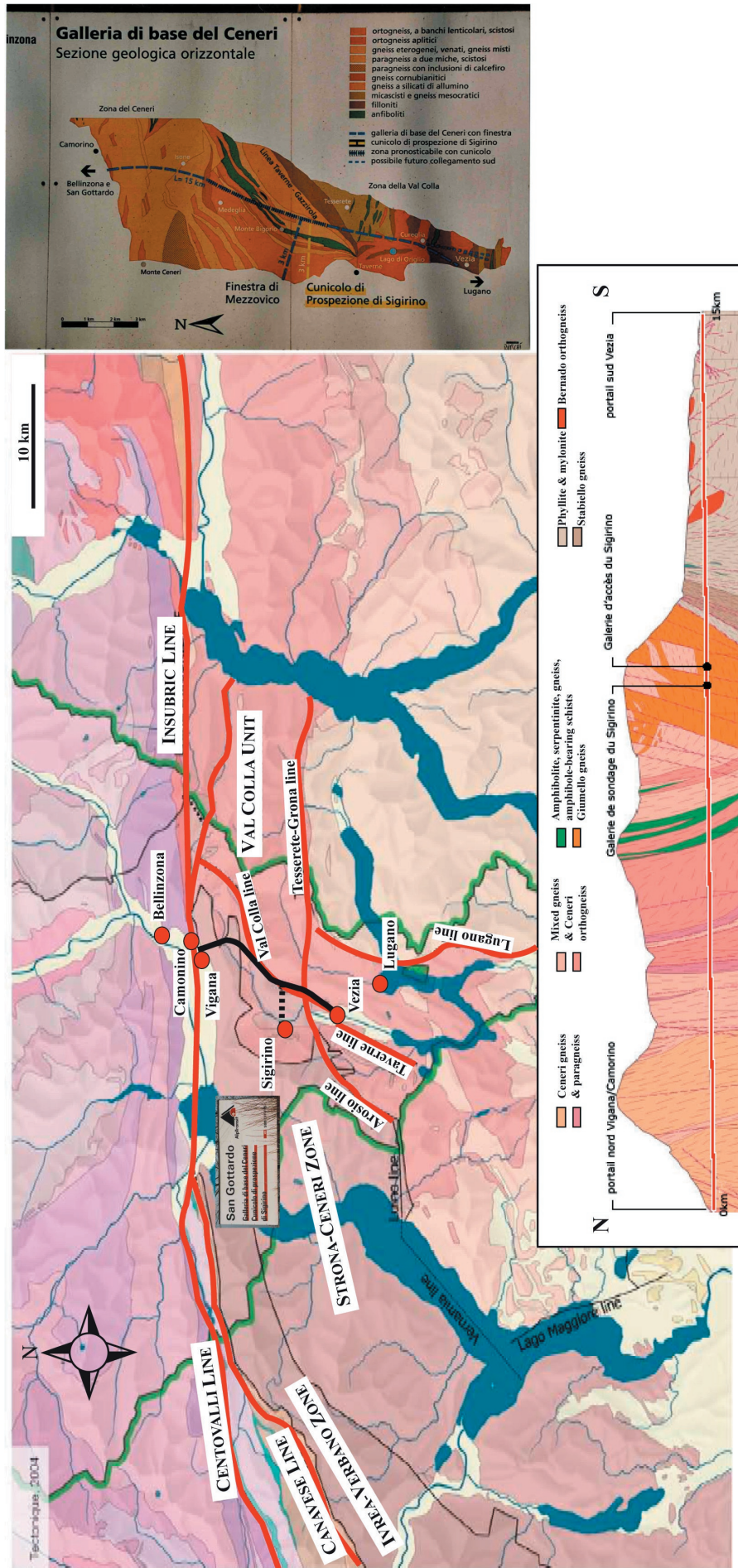


Fig. 5.12 Situation of the Ceneri base tunnel between Vigana/Camonina to the North and Vezia to the South. Due to access difficulties in the portal area, excavation is realized from the station built at Sigirino. Relation with the general tectonic context of the Southern Alps. Transition from the Insubric to the Centovalli line marks a transition from dominant ductile to predominantly brittle deformations in the alpine edifice. Modified from the tectonic Atlas of Switzerland 2004.

A possibility to perform field work with the triple tube core drilling device has been obtained in March 2006 through contacts with Dr Baumer SA in Locarno. After one week of work between km 2'340 and 2'406 5 samples of different degree of cataclase could be obtained. The transition between the bt+ms Giumello gneiss and kakiritized gneissi misti (plasticity = 80%) could be accordingly sampled along a profile of increasing cataclasis. Additional informations about the reconnaissance works at Sigirino can be found in the Master theses of *Chaignat* (2007) and *Veuve* (2007).

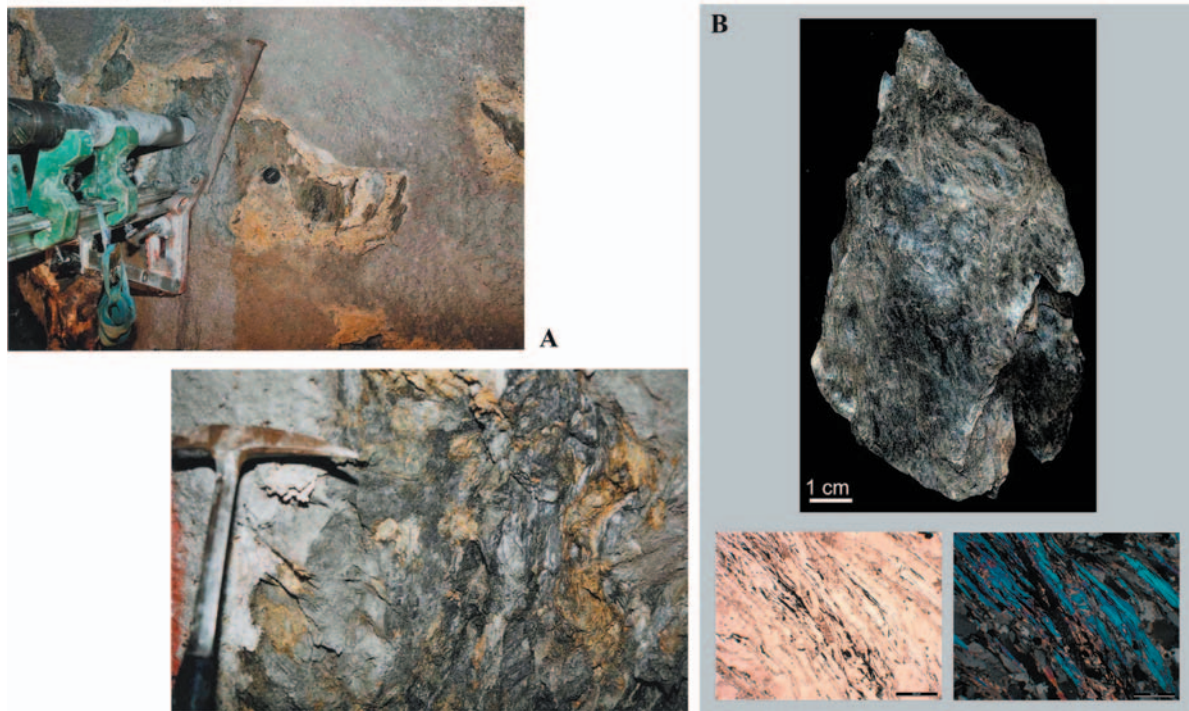


Fig. 5.13 **A)** Outcrop conditions in the Sigirino gallery at km 2340. **B)** Evidence from a handspecimen of cataclased gneissi misti depicting important shear planes characterized by white micas. Small pictures are a photomicrograph in plane and polarized light evidencing the presence of white micas in shear planes. Bar is 500 μm . Sampling at Sigirino was greatly aided by the presence of Laurent Chaignat and Christophe Veuve. Geological and mechanical investigations have been realized in their respective Master theses (2007).

6

SAMPLING TECHNIQUE

« Chaque usage a sa raison et chacun appelle
barbarie ce qui n'est pas de son usage. »
Montaigne, *Les Essais*

Rocks affected by cataclasis are very variable regarding their strength characteristics and state of alteration/weathering. The possibility to obtain fresh samples constitutes a difficulty as cataclastic rocks will rapidly desolidarize, once extracted from their *in situ* confinement conditions. Moreover, their inherent nature makes them particularly sensitive when brought in contact with ambient air. Thus proper sample recovery is often affected by strong limitations in cataclastic rock formations.

An important aspect of this research has been related to the development of an appropriate sampling technique for cataclastic rock material. In particular an effort has been conducted to obtain a method offering the greatest versatility for different petrological context. Considering the rock types investigated by *Bürgi & Habimana* (1999), e.g. highly cataclased samples characterized by a soft fine grained matrix, it has soon been recognized that the sampling techniques used in their respective studies would not be appropriate in cataclastic formations characterized by stronger competence contrasts between rock components. Namely, the U-shaped box driven with the geological hammer into the rock formation as envisaged by *Bürgi* (1999) is effective only in case of extremely cataclased formations (e.g. kakirites) that are soft enough to permit penetration. In the same way, the portable sampler of *Habimana* (1999) that is driven in the rock mass using a hydraulic jack face limitations in heterogeneous formations where harder blocks coexist next to a soft matrix.

Accordingly, the development of an alternative core sampler has been considered and tested. After discussions with professional drillers, it was namely clear that triple tube core drillings constitute today the most effective sampling method for a widespread type of difficult rock conditions when sample recovery has to be maximized. From case to case, it has been advised to test different drilling bits specifically designed for soft, medium or hard formations so as to optimize core cutting conditions.

Sampling by means of drilling was moreover interesting for two reasons:

- 1) First, rock cores as obtained in this research represent ideal samples for a combined geological and geomechanical characterization. They are of standard dimensions for the realization of triaxial tests, they correspond to undisturbed cataclastic structures, and the remaining rock portions after concurrent preparation for mechanical tests can be valorized for the realization of geological analyzes.
- 2) Second, rock cores have been evaluated representing an ideal shape for medical XRCT investigations, allowing recording indirectly sample structure before any manipulation in the laboratory. This point is particularly interesting for cataclastic rocks since their inherent fragility complicates the proper and optimized sample preparation in a laboratory.

6.1 DESIGN OF THE SYSTEM

After preliminary studies devoted to the evaluation of cataclasite sampling possibilities with a conventional single tube sampler for drillings in concrete (*Christe, 2004*), the problem of insufficient rock core recovery has been encountered. In order to reduce the technical difficulties associated with the extraction of cataclastic fault rocks at the outcrop, adaptation of the triple tube drilling technique to a hand-motor for short drilling operations has been considered.

A portative rock core sampler has accordingly been developed between 2004 and 2005 in close collaboration with Hilti SA (www.hilti.ch) and TechniDrill DGA (www.technidrill.com). On one hand, a hand motor developing sufficient power to support drilling at a diameter corresponding

Chap. 6 Sampling technique

to geotechnical rock cores could be found (contact Hilti SA). On the other hand, a triple tubing manufactured in dimensions that allow transportation at outcrop by hand was required (contact with TechniDrill DGA).

Accordingly, an operational equipment for short-drilling operations in cataclastic formations could be designed as illustrated in **Fig. 6.1**. With this system, drillings reaching a depth of maximum 1 m inside the rock mass have been realized. After a serie of preliminary tests on natural outcrops, the performance of the sampler has been recognized. Technical data of the portative rock core sampler can be found in **Table 6.1**.

| PORTATIVE TRIPLE TUBE CORE EXTRACTOR | | | | |
|--------------------------------------|-------------------------|----------------|----------------------------------|--------------------------------------|
| TUBE | COOLING | INNER DIAMETER | DRILLING DEPTH | |
| T6 101 mounted for Triplex | Water through hand pump | 76 mm | 2 x 50 cm using prolongation bar | OVERALL WEIGHT about 90 kg |
| MOTOR | NOMINAL POWER | FREQUENCY | ROTATION SPEED | |
| Hilti DD-200 | 2250 W | 50 Hz | 320 trs/min | 200 daN.m |

Table 6.1 Technical data related to the portative triple tube core extractor for cataclastic rocks.

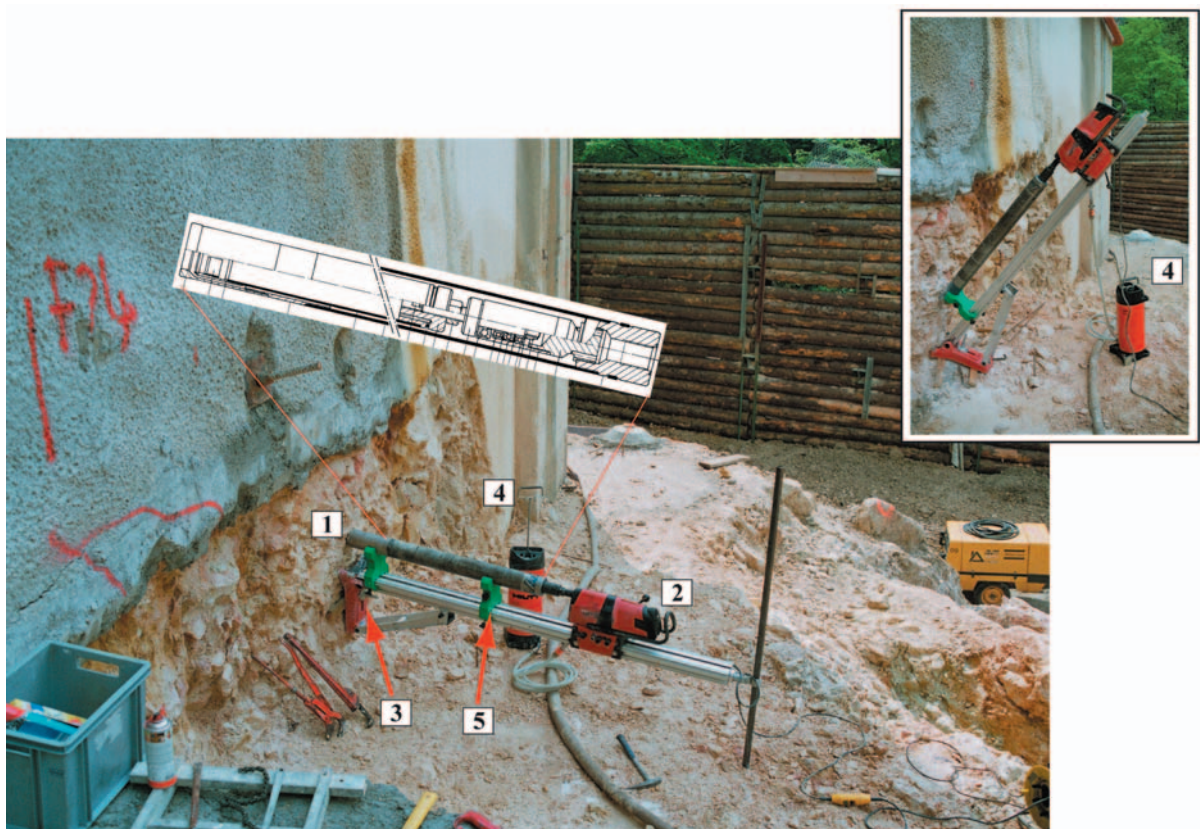


Fig. 6.1 Triple tube core barrel device for short drilling developed at the GEOLEP in collaboration with HILTI SA and TechniDrill DGA. A maximum depth of one meter (i.e. 2 times 50 cm) can be reached by using a prolongation bar after the first 50 cm of rock have been drilled. **1)** Double tubing implementing a triplex inner tube for increased sample recovery. **2)** Hand motor controlling advance of the drill head in the rock mass. **3)** Anchoring of the system at the outcrop by means of a single expansion bolt. **4)** Hand-pump injecting cooling water in the tube during ongoing drilling operation. **5)** Stabilization guides to position the drilling tube parallel to the rotation axis of the motor, minimizing momentum and ensuring a proper attack of the drill head in the rock. As seen from the small picture, orientation of the drill axis can be controlled in a range of $\pm 45^\circ$.

Chap. 6 Sampling technique

In order to improve recovery of intact cores in soft, non-homogeneous or fractured formations, triplex inner tubes in transparent plastic material have been used as recommended by the manufacturer. Core barrels adopting the triplex tubes allow enhanced fluid ejection in place of the drill-head (i.e. “drill-water” ensuring cooling of the tube barrel and drill bit). This has the positive effect to considerably reduce erosion of the core during ongoing operation. The triplex tube, not creating friction with the inner tube of the core barrel, is also removed easily, decreasing the time of core extraction. For cataclastic samples, this has further the advantage of permitting an efficient and rapid conditioning of the extracted samples so as to ensure their safe transport to the laboratory (**Fig. 6.2**).

First drilling operations using the newly developed core sampler have been initiated by spring 2005 in contact with tunneling sites across Switzerland (**Fig. 5.1** & **Table 5.1**). Although the aim of our research almost always received a positive echo, the logistical organization of the sampling campaigns on active tunnelling sites was not easy to organize. The risk represented by our presence in the galleries under construction had to be evaluated carefully and no perturbations on the ongoing tunneling operations could be accepted. Given this stiff framework for the sampling campaigns underground, the success obtained with the portable sampler makes clear that the technique is operational and could be further adopted for difficult sampling conditions in virtually any petrological cataclastic context.

To obtain best efficiency, a team of 3 people has been judged optimal to ensure rapid transportation of the material at outcrop (3 bags of about 25-30 kg can accordingly be attributed to each of the member of the team). During ongoing drilling operations, 2 persons can then monitor drill-head advance in the rock formation (1 person taking care of the tube driving and the other controlling the injection of cooling water by mean of the hand pump). During that time the third person can already further explore the outcrop development in order to select the next sampling location and prepare for the ulterior mounting of the core sampler.

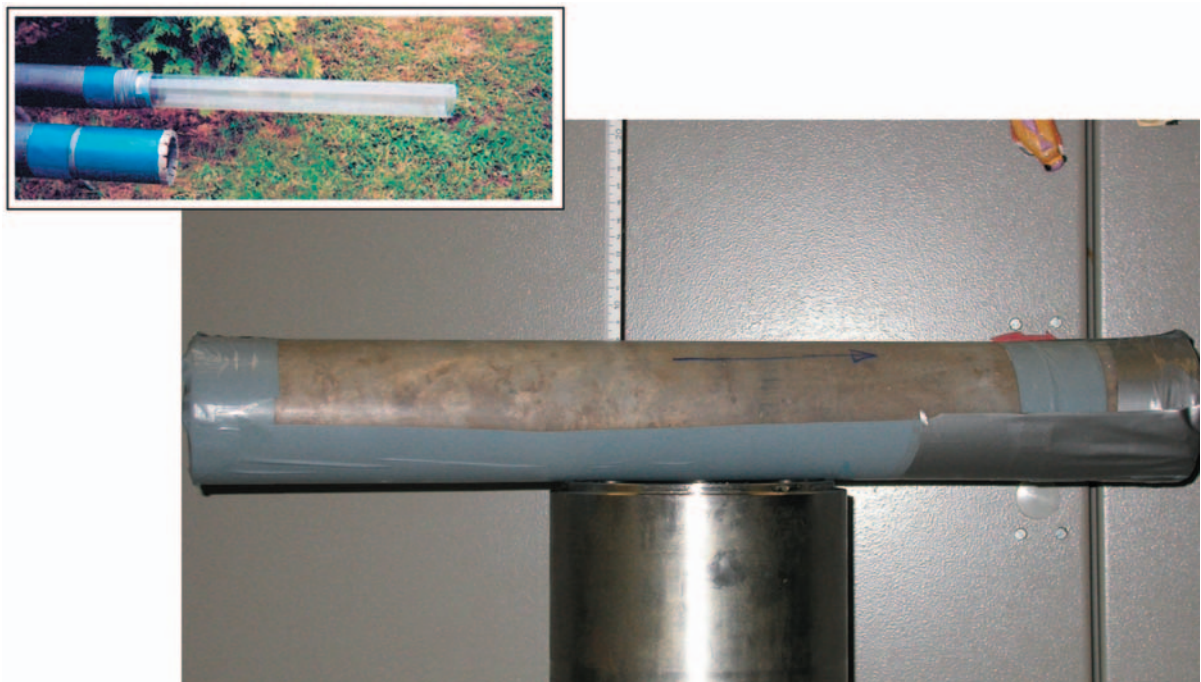


Fig. 6.2 Sample conditioning in the triplex plastic tube (see inset, www.technidrill.com), collecting and maintaining rock core structure directly during ongoing drilling operation. Once extracted, the triplex tube is hermetically sealed to prevent sample degradation and alteration at the contact with ambient air.

6.2 EXPERIENCE

The rock core extractor has been tested during this research in an already quite representative amount of contrasted outcrop conditions. Sampling has been performed from road outcrops down to deep seated tunnels. Accordingly, more or less success has been obtained. Two particular problems have been noticed in the current development of the technique. They are presented in this section (**Fig. 6.3**).

One problem concerns the onset of vibrations during ongoing drilling (**Fig. 6.3 A**). It had to be recognized that the anchoring of the drilling guide to the outcrop is quite minimalistic in its current form. Namely only one expansion bolt has to support the momentum induced by the core extractor (90 kg, see **Table. 6.1**). When drilling starts, the transmission of effort from the drill head along the guide cause vibrations that can in cases exceed the strength of the cataclastic rock in which the anchoring is performed. This problem has been recognized as the most recurrent source of difficulties associated with the extraction of cataclastic rock samples during field campaigns. As a matter of fact, the more time-consuming action on the field has been the stage of mounting of the core extractor, which could take several hours.

Once the extractor mounted and a drilling operation initiated, advancement of the head in the rock is controlled by a hand-wheel controlling advancement of the tube along the guide. It has been experienced that the right amount of pressure to add on the drilling head constitutes a difficult balance to find. Moreover, the control of injected cooling water during ongoing operation is also difficultly made by means of the hand pump (see **Fig. 6.1**). As a result, in cataclastic rock formation affected by a strong proportion of weak minerals, often too much water was injected and/or not appropriately dissipated from the drilling head (**Fig. 6.3 B**). Thus, clogging of the head happened several times, making the readjustment of the drilling operation often problematic (difficulty in releasing a clogged drill bit, adding additional stress on the anchoring point, which in the most negative experiences caused the rupture of the rock where the extractor had been mounted).

As an end result, the developed sampling technique proved to be efficient for the extraction of cataclastic samples in case of solid anchoring of the drilling device but was several time put at its limit in difficult outcrop conditions. We estimate that the validity of the technique doesn't have to be questioned but that important improvements of the anchoring technique are required. Put in situation during field work at Sigirino together with Laurent Chaignat and Christophe Veuve (who have performed their Master theses in the framework of this research), we have tried to stabilize the drilling machine with wood logs and palettes and different spansets. This has lead to strong drilling improvements and extraction of quality rock cores for laboratory studies could be obtained.

6.3 FURTHER DEVELOPMENTS

Rock core drilling is an art in itself. To ensure quality drilling, experience from professional drillers can provide many useful ideas for improvements on the proposed cataclastic rock core sampler. In particular, the interpretation of drill behaviors to be related with given rock structures and qualities seem to be often very indicative. This is of particular interest for drilling in heterogeneous materials. This can also avoid “overstressing” a sampling location when obviously something goes wrong. Another aspects concern the possibilities to adapt the drill bit chosen for an operation according to outcrop evidences.

Ameliorations to name in relation with the sampling device are:

- 1) Avoiding vibrations of the guide by improving stabilization of the anchoring and ensuring

a smooth axial progression of the tube in the rock mass;

- 2) Improving the hand motor to dispose of a broad spectrum of drilling power and speed. Accordingly a possibility to adapt drilling conditions at each manually noticed transition in rock response can be obtained;
- 3) Disposing of several types of drilling bits according to given cataclastic conditions (increased water transit through the head to prevent clogging, soft and hard teeth, ...);
- 4) Performing possible dry drilling operation in particular cases when water rock interaction has to be avoided to obtain representative samples.

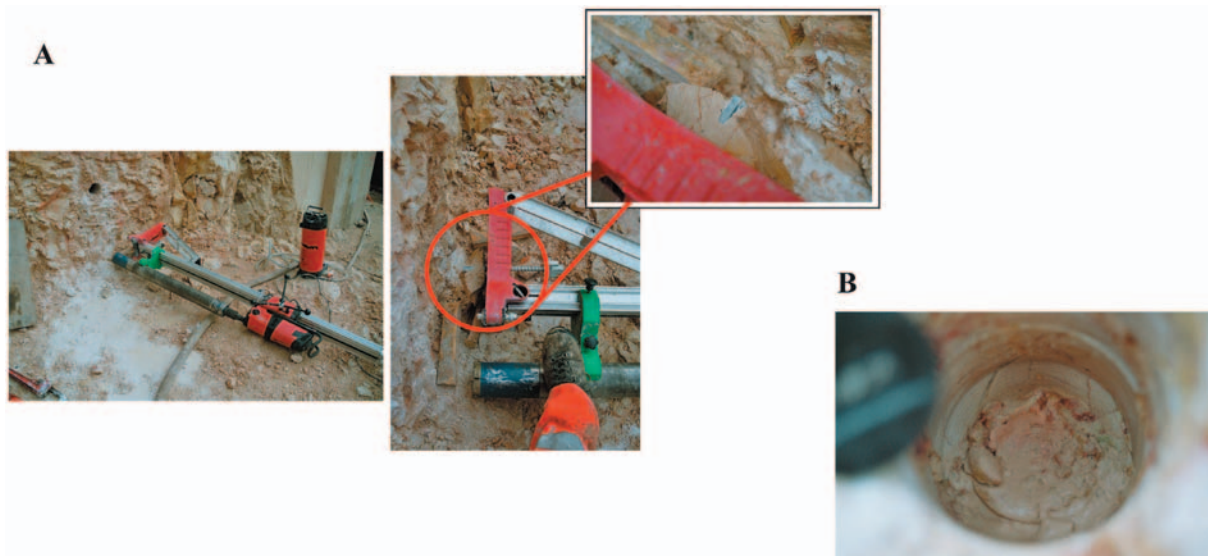


Fig. 6.3 Example of two typical difficulties encountered during field work with the triple tube core extractor. **A)** Weakness of the anchoring point at outcrop by means of a single expansion bolt. In the case depicted on the picture, the stress produced by the tension of the bolt exceeded rock strength and caused the collapse of the core extractor during ongoing drilling, due to system vibrations. **B)** When a high amount of clay is present in the rock formation, the complex interaction of clay minerals with the injected cooling water occasions often a clogging of the drill head, producing strong efforts on the hand motor. Removal of the drill bit after clogging is made difficult.

7

METHOD OF GEOLOGICAL CHARACTERIZATION

« Im Augapfel kollidieren Sicht und Einsicht, Schöpfung und spätere Überlegung. Die Janusfrüchte des Sehens sind eine magische Schwingtür, wo der erschaffende Geist sich selber im Erschaffenen begegnet. Das Auge, das ins Universum schaut, ist das Auge des Universums selbst. »
Jostein Gaardner, *Maya*

The geological characterization of rock core samples is carried out at two distinct levels:

- A bulk apparent characterization of the degree of damage of the rock based on direct and indirect evidences;
- A detailed characterization including mineralogical and structural evidences as determined from X-ray diffractometry (XRD) and thin section analyses.

The bulk apparent characterization is performed initially by adapting the evaluation parameters of the Geological Strength Index (GSI, *Hoek et al.*, 1998) to the rock core sample scale. Accordingly, a first classification of rock core qualities is realized based on observation of their structure and discontinuity conditions.

The detailed characterization is basically founded on the Mineralogical and Strength Index (MSI) proposed by *Bürgi* (1999, 2001). As shown in **Chap. 3**, it aims to quantify the mineralogical, textural and structural features of cataclastic rock samples. It permits the consideration of compositional and microstructural constraints to better explain cataclastic rock strength and deformability.

A particularity of this research, next to the use of medical XRCT for rock core investigations, was to implement electron microscopy for the high-resolution mineralogical analysis of the investigated samples and infer on alteration processes affecting the rock materials (e.g. *Veuve*, 2007).

In order to provide the reader with a synthetic view of the geological characterization, **Table 7.1** lists the different methods implemented for cataclastic rock core analysis. Derived structural and mineralogical parameters are given. Relevance for the determination of structural and compositional anisotropies (**Chap. 4**) is indicated.

7.1 BULK APPARENT CHARACTERIZATION

Facing the structural nature of fault zones, an effective geological characterization would benefit from the possibility to dispose of samples covering the entire rock mass quality spectrum from the external part of the fault zone (*intact* domain) to the very internal part (fault core, *extreme* domain). An ideal methodology of sampling has accordingly been presented in **section 4.3.2**.

7.1.1 Direct Evaluation

Provided a given rock core set, it is useful to perform a preliminary categorization of the apparent quality of rock materials. For these purpose, based on the theoretical considerations discussed in **Chap. 4**, a good approach is to determine 3 initial quality classes.

This classification is seen as pertinent to perform since weakly (*class I*) and strongly (*class III*) cataclased sample types are quite objectively identified. Samples corresponding to *class II* exhibit therefore a mixture of weak and strong cataclastic features (e.g. transitional samples in between the *intact* and *extreme* domains, often showing the most complex structural states). Referring to the fault zone architecture presented in **Chap. 2**, following relationships can be expected:

- *Class I*: weakly deformed damage zone.
- *Class II*: intensely deformed damage zone.
- *Class III*: fault core.

| ANALYTICAL METHOD | DETERMINATION | RESOLUTION | DERIVED PARAMETERS |
|--------------------------|----------------------|-------------------|---|
| PETROGRAPHY | Thin section | 50 μm | Shape, orientation and density of grains and discontinuities = 2D structural anisotropy |
| | XRCT | 500 μm | Shape, orientation and density of grains and discontinuities = 3D structural anisotropy |
| GEOCHEMISTRY | XRCD | > 500 ppm | Evaluated hardness of mineral assemblage |
| | Electron Microscopy | 100 ppm | Precision on mineral assemblage from XRD (if needed) Repartition of chemical elements indicative of alteration processes = 2D compositional anisotropy |
| | | | |

Table 7.1 Analytical methods from petrography and geochemistry for the structural and mineralogical description of cataclastic rock cores. Indication of relevant parameters for a geological characterization is given.

Based on defined geological quality classes I-III, further analytical procedures can be adequately oriented.

Adaptation of the Geological Strength Index (GSI, *Hoek et al.*, 1998, see **Chap. 3**) to the sample scale provides good pragmatic means in evaluating rock mass structure and joint conditions observable on rock cores.

It must be mentioned that true applicability of the GSI is for the quantitative assessment of rock mass characteristics and rock mass behavior at the outcrop level; thus an application at the sample scale is only envisaged to help in the visual classification of rock cores prior to any further investigations. Such an application was also envisaged by *Habimana et al.* (2002) for a mechanical characterization to help in defining the parameters constitutive of the modified rupture criterion for cataclastic rocks and relationships between the GSI and the a , m , and s parameters have been proposed (**Table 3.3**).

A rock core attribution in 3 quality classes is seen as a valid approach independent of which petrological content is investigated. However, definition of quality classes will vary strongly from case to case, in function of rock compositions and representativity of the rock core set obtained on the field. By applying GSI considerations on cataclastic materials, it becomes obvious that the *intact rock – discontinuity* model on which the GSI is based is hardly valid for tectonized materials and that microstructural and mineralogical considerations are required in order to precise the specificity of the fractured (cataclastic) rock mass.

7.1.2 Indirect Evaluation

The pertinence of the classification performed on the base of *direct* visual rock core evidences is then confronted with an *indirect* whole-volume imagery obtained by means of medical X-ray computerized tomography (XRCT). Because this step required adapting the technique for the analyses of rock core samples, it will be presented in a subsequent chapter (**Chap. 8**). Quantification of rock core structures and their consequent 3D reconstructions needed moreover the development of specific image analysis tools that will be described in **Chap. 10**.

Medical XRCT as an indirect technique still doesn't allow interpretative petrographical determinations due to its limited spatial resolution and unknown interactions between particular rock constituents and X-rays, meaning that only density contrasts are recorded.

Accordingly, the indirect cataclastic rock core evaluation and subsequent characterization will be made by analyzing resolved geological features based on the concept of *damage indicators* as described in **Chap. 2** (see **section 2.4.5**). In this approach, both the shape and orientation of petrographical elements indicative of the cataclastic process will be evidenced in 3D. At the medical XRCT resolution, these elements correspond to a major extent to crack patterns (fractures), voids and zones of predominant cataclastic rock matrix. With such visualizations, an improved determination of the parameter t of *Habimana* (1999) accounting for the degree of tectonization could be most probably expected. In any cases, with a characterization of cataclastic rocks based on the study of *damage indicators*, a better account of the geological particularities affecting rock cores can be expected in their mechanical description by means of triaxial tests.

A detailed discussion of the XRCT-visualized *damage indicators* will be conducted within **Chap. 13**.

7.2 DETAILED GEOLOGICAL CHARACTERIZATION

A general presentation of *Bürgi's* characterization methodology for cataclastic rocks based on mineralogical (XRD) and microstructural (thin section) analyses has been addressed in **Chap. 3**. It is given by the MSI relationship (**Eq. 3.1**). Its relevance for a geotechnical rock mass characterization was discussed by confrontation with mechanical triaxial data provided by *Habimana's* thesis work (see **Fig. 3.9**).

In this section the details of the parameters constitutive of **Eq. 3.1** will be given as well as the techniques providing the input data for their calculation.

7.2.1 Mineralogical Analyses

To take into account the effect of a given mineral paragenesis in terms of strength, *Bürgi* (1999) proposed to use the concept of the mean weighted Vickers hardness (mwVh) of mineral phases, e.g. the weighted hardness of mineral phases with regard to their weight proportions inside a sample (*Calembert et al.*, 1980). In terms of rock core characterization a good correlation is reported between the calculated mwVh and the compressive uniaxial strength by *Calembert et al.* (1980). Thus, the strength control of mineralogical composition during a triaxial test can be adequately described in a similar manner. The mean weighted Vickers hardness is given by following relationship:

$$\text{(Eq. 7.1)} \quad \text{mwVh} = \sum_i v_i \cdot Vh_i$$

with

mwVh = mean weighted Vickers hardness [MPa]

v_i = weight proportion of mineral phase i

Vh_i = Vickers hardness of mineral phase i [MPa]

The Vickers hardness of common rock forming minerals has been studied by *Tourenq* (1966) and is

| Mineral | Vickers hardness [MPa] |
|------------|------------------------|
| Quartz | 9807 |
| Albite | 7679 |
| Chlorite | 1147 |
| Biotite | 1147 |
| Calcite | 1638 |
| Muscovite | 1304 |
| Dolomite | 2697 |
| Andalusite | 9807 |
| Sphene | 5335 |
| Staurolith | 9807 |
| Pyrite | 7679 |
| Rutile | 7679 |
| Garnet | 8826 |

Table 7.2 Vickers hardness in MPa of specific mineral species encountered in samples from this study. Vickers hardnesses are used to define the mean weighted Vickers hardness of cataclastic samples to account for the effect of mineralogy on rock strength. Vickers hardness has been determined according to the Tabor relationship between Mohs and Vickers hardness (*Wenk & Bulakh*, 2004) to derive values for mineral phases determined on rocks from this study. Values from the Tabor relationship vary slightly from the values found in *Tourenq* (1966) and used by *Bürgi* (1999) After *Veuve*, 2007.

a more precisely defined parameter than Mohs hardness (scratch resistance of minerals as compared to ten reference minerals). It is determined by measuring the impact of a small diamond bit on the polished surface of the tested mineral. It is defined as the ratio of the applied load to the square of the measured indentation diameter. **Table 7.2** presents the Vickers hardness for different mineral species encountered in samples from this research.

As proposed by *Bürgi* (1999), determination of the mineralogical composition of cataclastic rocks is realized by means of X-ray diffractometry. However this method is limited in terms of resolution and it is expected that critical mineral phases in small amount can't be inferred properly. Thus, in the framework of this research, *Veuve* (2007) tested the implementation of the electronic microscopy for the increased mineralogical characterization of cataclastic rock samples. Both methods are shortly presented hereafter.

7.2.1.1 X-Ray Diffractometry (XRD)

X-ray diffractometry (XRD) is based on the measurements of the diffraction pattern resulting from scattering of the incoming rays in successive planes of atoms and recorded as an interference pattern. XRD uses monochromatic X-rays of known wavelength λ . When targeted on a crystal or cluster of crystals, the X-ray beam undergoes diffraction to form a diffraction pattern function of various angles of diffraction θ . Measurements of these various angles can be used to determine the inter-planar spacings d characteristic of the diffracting crystal. Crystals can be seen as the repetition of a three-dimensional ground structure acting as a three-dimensional diffraction grating. Using Bragg's equation, main mineralogical phases can be determined semi-quantitatively in a sample by comparing their resulting diffraction patterns with a reference standard database for mineralogical determination.

XRD is used in this study to quantify the main mineral assemblage of cataclastic rocks in order to determine the mean weighted Vickers hardness $mwVh$ proposed by *Bürgi* (1999) to account for the indicative mineralogical strength offered by a cataclastic rock of a given composition.

XRD measurements are realized on rock powders of homogeneous granulometry of about 10 μm grain size prepared from at least 200 g representative sample material to account for material heterogeneity. In the framework of this research XRD was performed by *Veuve* (2007) at the cement plant Jura Cement Cornaux on a D4 ENDEAVOR X-ray Diffractometer. Detection limit of quantitative XRD is 5 Vol% of the mineral phase to detect inside the sample. Trace elements and alteration products are not detectable by XRD.

7.2.1.2 Electron Microscope Techniques

Electron Microscopy allows performing indirect imagery of a sample as well as chemical analysis at a high resolution. It is based on the interaction of a high energy electron-beam with the sample placed in vacuum conditions. Low-energy electrons are first accelerated to kinetic energies of 15-30 keV and preliminary focused to a beam of 50 μm . Additional lenses in the microscopic column can reduce the beam focus to sizes $< 1 \mu m$ according to which probe current is chosen. Electron beam can be used in raster mode to image sample surface and get information on its topography and composition, or it can be used in spot mode to excite various effects inside the sample.

When targeted on a sample of given mineralogical composition, the electron-beam is scattered in different ways and different interactions of the high-energy electrons with matter will result. Part of the beam will be reflected with different photon intensities at the surface of the probe (back-scattered and secondary electrons) and will result in an indirect imagery of the probe surface (*Scanning Electron Microscopy*, SEM). Such imagery permits the inference of the chemism of the sample by tracking a given chemical element and producing a surface map of that element when the

back-scattered signal is analyzed by a spectrometer. A remnant beam enters the probe and excites X-ray with characteristic wavelengths that can be analyzed with different spectrometers to determine mineralogical phases (*Transmission Electron Microscopy*, TEM typically in an electron microprobe column).

For cataclastic samples that underwent alteration phenomena, electronic microscopy in scanning mode is an ideal tool to provide a means for quantitative analysis of the extent and degree of alteration. Maps of chemical elements indicative of alteration processes can be used for the determination of compositional anisotropies inside the sample. With the principle of TEM, main and trace compositions of minerals can be inferred and element repartition inside of minerals can be assessed (e.g. mineral zonations). Mineralogical analyzes performed with the electron microprobe are expected to vary slightly from analyzes performed with XRD and to be more accurate. In particular, when the determination of mineral phases present in small quantity in a sample (e.g. alteration products, secondary mineral phases ...) is desired, the electron microprobe would deliver the most useful information.

SEM and TEM measurements by *Veuve* (2007) have been realized at the University of Lausanne on a Camscan 4 microprobe and a Jeol 8200 Superprobe respectively.

7.2.2 Microstructural Analyses

Microstructural analyses aiming the derivation of the TC & MC parameters were performed by means of thin sections (20-30 μm thickness in standard dimensions of 2.5 x 4.5 cm) realized from impregnated cataclastic rocks at GeoPrep Basel. Applied to cataclastic rocks, 2D petrographical analysis under a polarizing light microscope permits to specify the distribution of clast and matrix, the extent of weathering and shearing and the fracturing. Such determinations can be related to brittle deformation processes underwent by the samples and used for the determination of a textural/structural anisotropy. Moreover, fractures condition can be analyzed and evidence of recrystallized, sealed or open cracks can be found and used for the improved rheological characterization of the cataclastic material. Due to the inherent heterogeneity of cataclastic rocks, mineralogical determinations from thin sections are expected not precise enough and therefore mineralogical composition has been derived from the above mentioned XRD and/or electronical microscope analyses.

Remnants of sample preparation into the dimension of standardized rock cores for triaxial testing (see **Chap. 9**) were used for thin section realization as well as additional samples collected on the field.

7.2.2.1 Impregnation of cataclastic rocks for thin section preparation

Thin section realization from cataclastic rock cores is a difficult task because of sample fragility. Fragile rock core specimens require stabilization by impregnation with a low viscosity resin to ensure proper penetration into the fine-grained rock fraction. Resin penetration will be optimal if the rock material is dried before the impregnation process. In this research a resin composed of 40% Laromin C 260 and 60% Araldit DY 026SP that has best fluidity at a temperature of 50°C was used. The impregnation is performed in a pre-heated vacuum cell into which the rock core, previously encapsulated in a wire mesh, is placed (**Fig. 7.1**). The wire mesh allows preliminary stabilization of the rock core during diving inside the cell. The quantity of liquid resin must be sufficient to allow adequate penetration into the rock volume but a proper balance must be found as strong unwanted exothermic reactions can occur ($T > 100^\circ\text{C}$!), resulting in the irreversible hardening of the fluid inside the cell and sample loss. Once the cell is sealed, an electric pump is activated to produce vacuum conditions. The sample is maintained there for about 15 minutes after which air

pressure is released again. Another vacuum cycle is then started for another 15 minutes to ensure optimal resin penetration into the geotechnical rock core. The cell is then opened and the sample

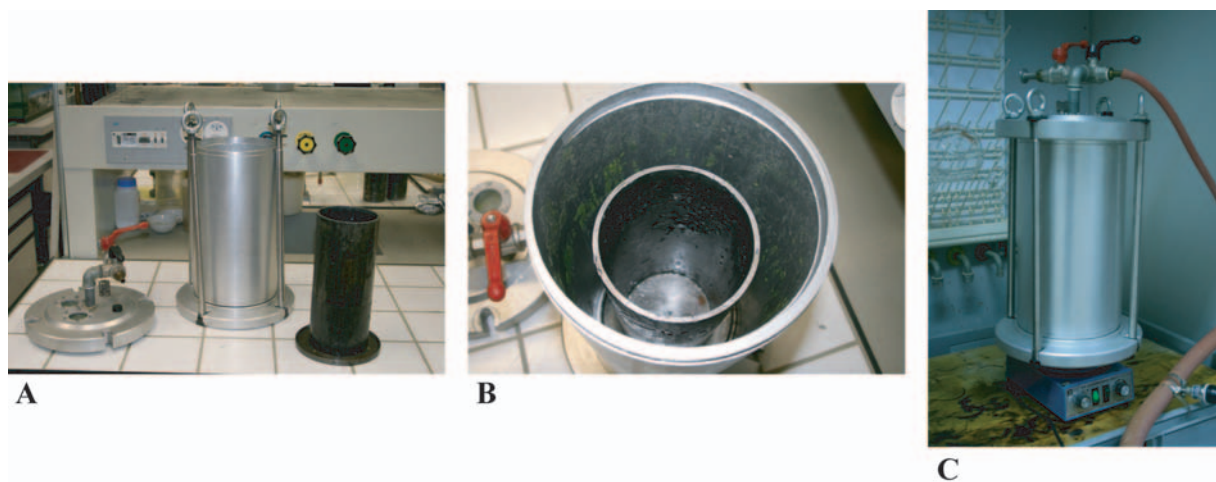


Fig. 7.1 Equipment used for the impregnation of cataclastic rock cores with a low-viscosity resin. **A)** Components of the impregnation cell. **B)** Double piston. The sample is placed inside the inner piston where the impregnation resin is added. **C)** The cell is sealed and placed on a heated plate. Vacuum conditions are realized inside the cell with an electric pump connected to the cell by a tube.

can be easily extracted from the resin bath with the aid of the wire mesh. Once extracted from the piston, it is placed in the oven overnight at a temperature of 60-80°C what allows proper hardening of the resin. Resulting impregnated rock cores are highly resistant and can be handled like healthy rock samples. Sawing of rock plates for thin section realization can be made in any wanted spatial direction.

7.2.2.2 The texture coefficient *TC*

With the texture coefficient *TC* an attempt is made to translate how a particular rock texture affects geomechanical properties of intact rocks. Texture is defined by the spatial arrangement of grains/clasts and 3 parameters are considered: the grain shape, the grain orientation, and the grain density. From the literature (see references in *Bürgi*, 1999), it is documented that a negative linear correlation exists between grain size and rock strength, whereas a positive one prevails between grain packing density and rock strength. Moreover, a random orientation of grains tends to be more resistant against stress than a preferred grain arrangement which is susceptible to develop planes of weakness more easily.

In order to quantify rock texture from a thin section, a texture coefficient *TC* can be expressed in following form (**Fig. 7.2 A**), as proposed by *Howarth & Rowlands* (1986) and further used by *Bürgi* (1999):

$$(Eq. 7.2) \quad TC = CD \left[\left(\frac{N_o}{N_0 + N_1} \frac{1}{\overline{FF}_o} \right) + \left(\frac{N_1}{N_0 + N_1} \overline{AR}_1 \overline{AF}_1 \right) \right]$$

where

| | | |
|----------------------|---|---|
| <i>TC</i> | = | texture coefficient [-] |
| <i>CD</i> | = | clast density |
| <i>N_o</i> | = | number of isometric clasts (aspect ratio < 2) |
| <i>N₁</i> | = | number of elongated clasts (aspect ratio > 2) |
| \overline{FF}_o | = | mean form factor of isometric clasts |
| \overline{AR}_1 | = | mean aspect ratio of elongated clasts |
| \overline{AF}_1 | = | angular factor of elongated clasts |

Howarth & Rowlands (1986) report TC values for metamorphic, magmatic and sedimentary (healthy) rocks to range from 0.5 to 3, what correspond to low, respectively high rock strength. Values of TC derived from cataclastic quartzo-phyllic rocks of Cleuzon-Dixence by *Bürgi* (1999) are comprised between 0 and about 0.7. From that evidence, it is said that rock strength increases generally together with clast density, and specifically when the clasts at high angular differences get more elongated (high AF and \overline{AR}_1). Moreover, an increase in the amount of rounded clasts (meaning a high \overline{FF}_o) is expected to influence rock strength negatively.

Form and shape of clasts are determined from a digitalized binary thin section image on which automatic measurements can be performed with the use of image analysis software. In this research, ImageJ™ has been used and clast parameters include clast area, clast perimeter, lengths of major and minor axes of a best fitting ellipse, angular orientation α of major axis to a chosen reference line and total clast area per reference area. They are taken into account by the parameters AR (aspect ratio, ratio of major to minor axis of the best-fitting ellipse) and FF (form factor, e.g. the measure of the grain's deviation from circularity) (**Fig. 7.2 A**).

Orientation of clasts is determined for grains with an aspect ratio > 2 and follows the description made by *Howarth & Rowlands* (1986). Angular difference between the major axes of the best-fitting ellipses for elongated grains are measured and classified into 9 orientation classes of 10° width ($0-10^\circ, 10-20^\circ \dots 80-90^\circ$) that are weighted with a factor i varying from 1 to 9. The angle factor AF is then calculated by summing the products of the class weightings and the fractions of the total number of angular differences in each class. AF is a dimensionless parameter that varies according to *Bürgi* (1999) between 0.2 for oriented clasts and 1.0 for unoriented ones. In order to get reliable result on effective clast orientation, a minimum of 30-50 clasts should be analyzed.

Clast density is a measure of clast packing and corresponds to the total clast surface per reference area. It can be determined on ImageJ™ by dividing the calculated clast surface (in mm^2) by the total surface of the binary image.

7.2.2.3 The matrix coefficient MC

The matrix coefficient was developed by *Bürgi* (1999) to quantify structural discontinuities estimated to represent potential shear-zones inside the sample and exerting an important control on the mechanical strength of cataclastic rocks. It is given by following relationship:

$$\text{(Eq. 7.3)} \quad MC = \frac{R_L}{\overline{T_{LL}} \cdot T_{LD}} \frac{1}{\delta}$$

where

| | | |
|---------------------|---|--|
| MC | = | matrix coefficient |
| R_L | = | linear roughness [mm/mm] |
| $\overline{T_{LL}}$ | = | mean trace line length [mm] |
| T_{LD} | = | trace line density [mm/mm^2] |
| δ | = | orientation factor [-] |

Fig. 7.2 B illustrates the procedure for the MC calculation. First a mask is drawn by hand so as to isolate all the features interpreted as discontinuities. Each drawing is scanned and converted to a binary mask from which the dimension in mm^2 is calibrated with the use of ImageJ™. Traces of discontinuities are reduced to a width of 1 pixel (function “skeletonize”). Using the analysis functions implemented in the program, the calculation of the factors constituting the MC (Linear Roughness R_L , Mean Trace Line Length $\overline{T_{LL}}$, Trace Line Density T_{LD} , and Orientation Factor δ)

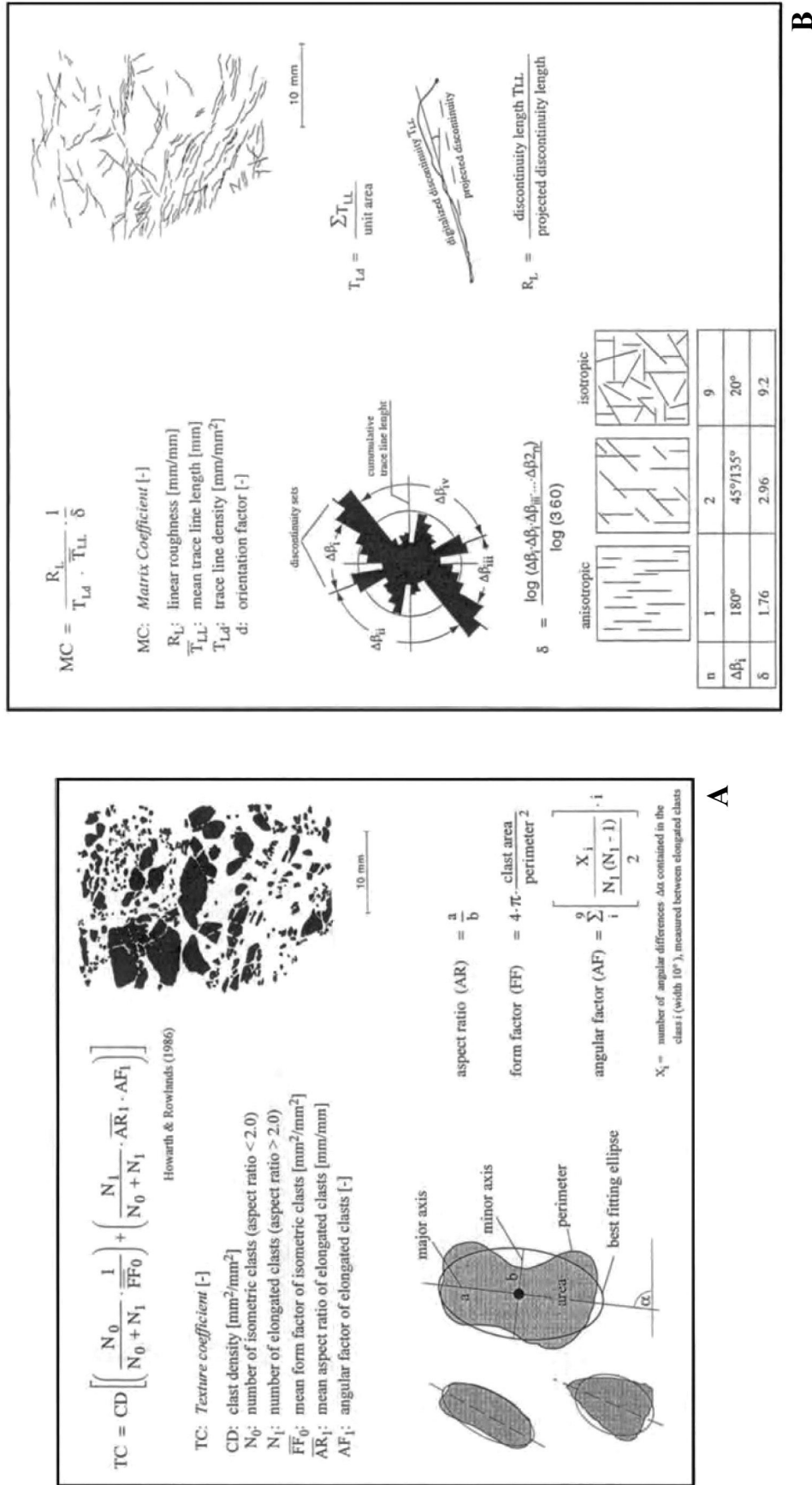


Fig. 7.2 Principles of TC & MC determinations as performed from 2D binary images highlighting clasts and discontinuity proportions inside the sample. **A)** The TC considers clasts shape, orientation and density following considerations by *Howarth & Rowlands, 1986*. **B)** MC determination involves quantifying rock fabric anisotropy by consideration of discontinuity lines that are regrouped and plotted in 18 families of 10° each on a rose diagram. Length, roughness and density of discontinuities are considered. After *Bürgi (1999)*.

is readily done. R_L is calculated by dividing the T_{LL} of a discontinuity by the regression line of that feature, from which the angle β to the horizontal is measured in order to further calculate the orientation factor δ . The different R_L are then averaged over the values obtained for the different features in a slice. T_{LL} is obtained by taking half of the perimeter given for the feature during calculation on $Image^{TM}$, from which the pixel size is subtracted in order to get the effective length of that feature. T_{LD} is derived from the surface area represented by the features in the considered binary image that is divided by the total surface area of that image. The sum of T_{LL} (cumulative lengths) sorted according to their orientation β (taken from horizontal reference line) in 18 classes of 10° each are plotted in a rose diagram so as to read the discontinuity orientations $\Delta\beta_i > 1/36$ (Fig. 7.2 B, inner boundary of rose diagram defining the limit of isotropy, see Bürgi, 1999). The orientation factors are calculated using following relationship:

$$\delta = \frac{\log(\Delta\beta_i \cdot \Delta\beta_{i+1} \cdot \dots \cdot \Delta\beta_{2n})}{\log(360)} \text{ with } \sum_i^{2n} \Delta\beta_i = 360^\circ$$

The orientation factor δ will have a low value for rocks affected by few discontinuities and will reach the value of 1 for a perfectly fractured rock mass. An increase of the linear roughness R_L will have a positive effect on rock strength, implying stronger friction conditions on preexisting discontinuities. An increase in all other parameters ($\overline{T_{LL}}$, T_{LD} and δ) will be reflected by a decrease in rock strength.

8

X-RAY COMPUTERIZED TOMOGRAPHY APPLIED TO ROCK CORE SAMPLES

« Toute connaissance doit mener au mystère, elle part de
l'étonnement pour aboutir à l'ahurissement. »
Edgar Morin

Medical X-Ray Computerized Tomography (XRCT, **Fig. 8.1**) was studied to:

- 1) Test its visualizing and volume rendering capacities when applied on rock core specimens of decimetrical sizes as obtained from reconnaissance drilling operations (3D indirect petrography);
- 2) If pertinent to be integrated for both the geological and geomechanical characterizations of cataclastic samples.

Accordingly, the question of image analysis possibilities at the medical scanner resolution had to be evaluated. Alternative techniques have consequently been evaluated.

Motivated by discussions with the paleontological research group of the University of Basel (*Schwarz et al.*, 2005; *Meyer*, pers. comm.), the resolution potentials obtained between XRCT- and neutron-derived irradiations have been investigated. Neutron tomography is implemented at the Radiography Facility *NEUTRA* at SINQ of the Paul-Scherrer Institute in Villigen (PSI) (*Lehmann et al.*, 1996, 1999). A test on 4 petrologically contrasting samples was performed in 2005 to be compared with the corresponding XRCT acquisitions realized previously at CHUV.

Results from this work were subject of a research paper that has been published in *Acta Geotechnica* (*Christe et al.*, 2007). The XRCT was concurrently evaluated to be more versatile for the indirect visualization of rock cores than the neutron tomography despite of the fact that irradiation with neutrons could be very interesting in evaluating the presence of hydrated mineral species like clay on discontinuity surfaces. A copy of this article can be found in **Appendix II**.

8.1 PRINCIPLES OF XRCT ACQUISITION

Medical XRCT is based on the cross-sectional imaging of an opaque object from transmission data collected by illuminating the object from different directions using an X-ray radiation modality. X-ray computerized tomography was developed by *Hounsfield* (1972) for medical applications and 3D rendering of the human body internal parts. The general interest of XRCT investigations is their indirect non-destructive character and low-time consumption. Diagnoses of human pathologies are readily made in medical research using specific protocols for scan interpretations.

An XRCT scanner records attenuations of an incident beam through a material of given composition and converts them on a linear scale of tomodensities (Hounsfield units, HU). Beer's law relates the final intensity I to the initial intensity I_0 via a linear attenuation coefficient μ . Mass attenuation coefficients for typical rock constituents are given for energy of 120 keV in **Table 8.1** (as evaluated the most efficient for rock core acquisition on decimetrical dimensions) and attenuation coefficients μ at that energy are derived when multiplying by mineral density ρ . They are plotted in **Fig. 8.1** along a trend of increasing mineral densities.

Recording of intensity signals from different angles of projections (e.g. sinograms) and combination of these projections all together allows with the use of filtered back projection (FBP) algorithms the reconstruction of a 3D tomographic image of the investigated structure (*Jain*, 1989; *Wellington & Vinegar*, 1987). Signal reconstruction is performed over 360° using a FBP in the Fourier domain. To satisfy the needs of medical research in heart imagery (XRCT records in between single pulses), modern medical CT apparatus implement reconstructions using a FBP over 180° using a so-called Walsh transform which reduces computing time significantly (*Thomas & Govindan*, 2006). Such developments are compatible with the geo-scientific research addressing the real-time monitoring

of particular processes (for example rock deformation). Thus, from a physical and signal processing perspective, medical and material researches go hand in hand. Because of its early implementation and subsequent numerous developments, medical XRCT is able to deliver many insights to develop specific protocols for quantitative analysis of rock materials comparable to those used for the diagnosis of human pathologies.

Reconstructed XRCT images from inert materials like rocks provide insights on their 3D structure

| Material | Chemical Formula | Crystal system | Mineral Density (g/cm ³) | X-ray mass attenuation coefficient (cm ² /g) 120 keV | X-ray attenuation coefficient (cm ⁻¹) 120 keV | Tomodensity (HU) 120 keV | Image pixel value | Theoretical 16bit grey value |
|-------------|--|----------------|--------------------------------------|---|---|--------------------------|-------------------|------------------------------|
| Air | O ₂ | - | 0 | 0.000 | 0.000 | -1000 | 24 | 32792 |
| Water | H ₂ O | - | 1.00 | 0.161 | 0.161 | 0 | 1024 | 33792 |
| Microcline | KAlSi ₃ O ₈ | trkl | 2.56 | 0.158 | 0.404 | 1512 | 2536 | 35304 |
| Kaolinite | Al ₂ Si ₂ O ₅ (OH) ₄ | trkl | 2.60 | 0.153 | 0.398 | 1471 | 2495 | 35263 |
| Albite | NaAlSi ₃ O ₈ | trkl | 2.62 | 0.152 | 0.398 | 1474 | 2498 | 35266 |
| Quartz | SiO ₂ | trig | 2.65 | 0.154 | 0.408 | 1535 | 2559 | 35327 |
| Chlorite | (Mg,Fe,Al) ₂ (Si,Al) ₈ O ₂₀ (OH) ₁₆ | mkl | 2.65 | 0.187 | 0.496 | 2078 | 3102 | 35870 |
| Smectite | (Na,Ca)Al ₄ (Si,Al) ₈ O ₂₀ (OH) ₄ ·2(H ₂ O) | mkl | 2.70 | 0.155 | 0.419 | 1599 | 2623 | 35391 |
| Calcite | CaCO ₃ | trig | 2.71 | 0.170 | 0.461 | 1861 | 2885 | 35653 |
| Illite | (K,H ₃ O)[(Si,Al) ₃ O ₁₀ (OH) ₂ | mkl | 2.75 | 0.157 | 0.432 | 1682 | 2706 | 35474 |
| Anorthite | CaAl ₂ Si ₂ O ₈ | trkl | 2.76 | 0.160 | 0.442 | 1743 | 2767 | 35535 |
| Biotite | K ₂ (Mg,Fe) ₆₋₄ (Fe,Al,Ti) ₂₋₂ (Si ₆₋₅ Al ₂₋₃ O ₂₀)(OH,F) ₄ | mkl | 2.82 | 0.183 | 0.516 | 2205 | 3229 | 35997 |
| Muscovite | KAl ₃ Si ₃ O ₁₀ (OH) ₂ | mkl | 2.83 | 0.156 | 0.441 | 1742 | 2766 | 35534 |
| Dolomite | CaMg(CO ₃) ₂ | trig | 2.87 | 0.160 | 0.458 | 1847 | 2871 | 35639 |
| Apatite | Ca ₅ (PO ₄) ₃ (OH,F,Cl) | hex | 3.19 | 0.172 | 0.549 | 2408 | 3432 | 36200 |
| Ky-Sil-And | Al ₂ SiO ₅ | trkl-orth | 3.20 | 0.151 | 0.483 | 2001 | 3025 | 35793 |
| Grossular | Ca ₃ Al ₂ Si ₃ O ₁₂ | kub | 3.57 | 0.166 | 0.593 | 2681 | 3705 | 36473 |
| Staurolite | H ₂₋₃ (Fe,Mg,Zn)(Al ₁₇₋₁₆ Fe ₀₋₂₅ Fe ₀₋₂₅ (Si _{7-6.5} Al _{0-3.5})O ₄₈)* | mkl | 3.71 | 0.167 | 0.620 | 2848 | 3872 | 36640 |
| Pyrope | Mg ₃ Al ₂ Si ₃ O ₁₂ | kub | 3.74 | 0.152 | 0.568 | 2531 | 3555 | 36323 |
| Spessartine | Mn ₃ Al ₂ Si ₃ O ₁₂ | kub | 4.18 | 0.184 | 0.769 | 3777 | 4801 | 37569 |
| Almandine | Fe ₃ Al ₂ Si ₃ O ₁₂ | kub | 4.19 | 0.191 | 0.800 | 3971 | 4995 | 37763 |
| Rutile | TiO ₂ | tetr | 4.25 | 0.185 | 0.786 | 3884 | 4908 | 37676 |
| Ilmenite | FeTiO ₃ | trig | 4.79 | 0.212 | 1.015 | 5307 | 6331 | 39099 |
| Pyrite | FeS ₂ | kub | 5.01 | 0.218 | 1.092 | 5784 | 6808 | 39576 |
| Magnetite | Fe ₃ O ₄ | kub | 5.20 | 0.235 | 1.222 | 6590 | 7614 | 40382 |
| Hematite | Fe ₂ O ₃ | trig | 5.30 | 0.232 | 1.230 | 6637 | 7661 | 40429 |

* Holdaway et al. (1986), Am. Mineral. 71, 1142-1159

Table 8.1 Presentation of some common mineral phases found in rocks and classified by density. Crystal systems are given for all phases. X-ray attenuation coefficients calculated for X-ray energies of 120 keV. Corresponding tomodensities are indicated. CT signals (pixel values) as observed on the software ImageJ™ are listed and corresponding 16bit grey level given. These grey levels are theoretical and should be used as reference only. Such a degree of precision will never be achieved on medical XRCT images from rocks, but these grey values are used for consideration about the development of the segmentation procedure presented in **Chap. 10**. It is therefore important to keep in mind that such grey values would vary on effective scans due to the limited resolution potential of the XRCT, the size of the sample investigated and according to the corresponding object dimension inside the rock sample. All attenuation coefficients calculated from XCOM, *National Institute of Standards and Technology, Berger et al., 1998.*

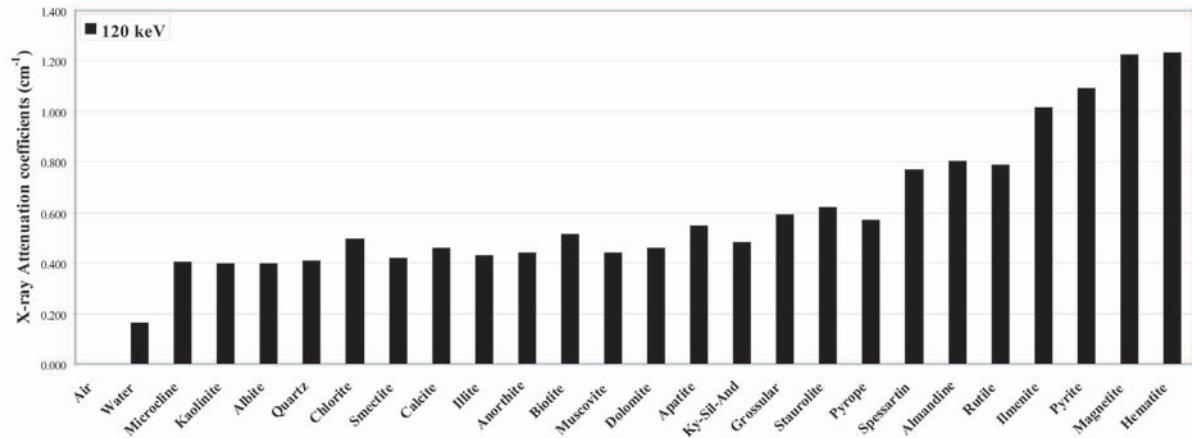


Fig. 8.1 Attenuation coefficients for some common rock-forming minerals calculated from mass attenuation coefficient at an X-ray energy of 120 keV. Coefficients calculated from *Berger et al.*, 1998.

in minimal time by highlighting contrasts linked to the spatial variation of linear attenuation coefficients, that are a function of the given mineralogical assemblage and specific structural or textural elements. 3D data from XRCT and its resolution are characterized by the voxel size, which is the 3D equivalent of the pixel size in 2D.

Note: Old-generation CT apparatus where confronted with the problem of producing a slice thickness exceeding the voxel size, leading to an imprecision when considering single CT slices. Modern medical XRCT apparatus allow a smaller voxel size and a smaller slice thickness and benefit from high-quality detectors providing a sub-millimetrical isotropic 3D imagery. As a general rule, one should keep in mind that the quality of a given acquisition is function not only of the emitting source, but vary strongly in function of the detector quality and signal processing techniques. Medical XRCT use electric current to produce polychromatic X-rays (e.g. containing a spectrum of energies) and modern scanners allow efficient adjustment of the parameters controlling the radiation modality. Polychromatism of the source means a large fluence (also called *integrated density* describing the strength of the radiation field per unit area, m⁻¹) which allows investigation over a wide range of contrasting material densities (cf. soft tissues of human body vs. hard rock minerals). On the other hand, polychromatism is the reason of beam hardening effects, meaning a non-uniform attenuation of the different energies composing the X-ray beam while crossing matter (**Fig. 8.2**). Beam hardening involves a preferred attenuation of “soft” X-rays in comparison to “hard” X-rays that are more penetrative. The amount of beam hardening is function of the initial X-ray spectrum as well as the composition of the material traversed. As a result of beam-hardening, the effective attenuation coefficient of a material depends on the *thickness* of material traversed. Therefore, a protocol of geological analyses should be able to introduce the expected variability in tomodensity for a given component in function of known sample thickness.

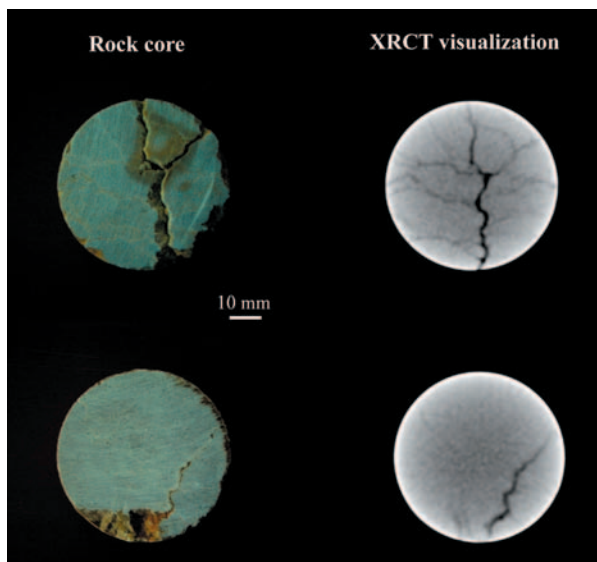


Fig. 8.2 First acquisitions performed with medical XRCT on a cataclastic limestone set (Sequanian limestone sampled along the Pontarlier fault system at Vallorbe, Jura Mountains, Switzerland) that provided XRCT resolved images containing a strong artifact. XRCT acquisition was performed without sample conditioning causing a strong beam hardening artifact (see **section 8.3.2**) while traversing from air to rock media and producing the characteristic white halo on the XRCT images. Such blurred images were not effective for a further numerical treatment. Adapted from *Christe*, 2004.

8.2 OVERVIEW OF CT-TECHNIQUES APPLICATION TO ROCK SAMPLES

Irradiation by X-ray sources for material visualization became in recent years widely used in several research fields (*Conroy & Vannier, 1984; Holler & Kögler, 1990; Carlson & Denison, 1992; Verhelst et al., 1996; Olsen & Børresen, 1997; Re & Scavia, 1999; Nakashima, 2000; Ketcham & Carlson, 2001; Pandita & Verpoest, 2003; Muzi et al., 2004*).

Next to medical scanners, industrial XRCT scanners were widely developed for specific rock science applications (see for reference the *GeoX CT center at Kumamoto University, Japan* or the *High-Resolution X-ray Computerized Tomography Facility at the University of Texas at Austin (UTCT), USA* a. o.) and most powerful sources are found today at synchrotron radiation facilities (*Paul Scherrer Institute (PSI), Switzerland; European Synchrotron Radiation Facility (ESRF), Grenoble, France* or *National Synchrotron Light Source (NSLS) at Brookhaven National Lab, New York USA*).

To fix orders of magnitude, the X-ray beam from synchrotron radiation is a thousand billion times “brighter” than the beam produced by a hospital X-ray machine (*Bésuelle et al., 2006*). Synchrotron-derived irradiation makes use of monochromatic and monoenergetic X-rays that are very efficient for microtomographic investigation on small rock samples (diameter < 5 cm) but lack fluence for the proper investigation of larger sample sizes comparable to geotechnical rock cores.

An often limiting factor in indirect X-ray analysis is therefore the sample size, as the highest resolutions are achieved on the smallest samples with acquisition times of several hours. New possibilities seem offered by the synchrotron irradiation with reports from experiments that could combine both fast tomography and high resolution micro-tomography (*Viggiani et al., 2004*). A stimulating research field profiting from the technical scanner improvements is the *in situ* tomography, e. g. the continuous time-resolved tomographic record of a process simulated by a specifically designed experiment, as already tested by *Vinegar et al. (1991), Alshibli et al. (2000), Schreurs et al. (2003)* or *Hirono (2005)*.

In all given tomography application, data processing time will increase concurrently with increasing resolution. **Table 8.2** presents an overview of the different techniques in application.

8.3 ROCK CORES OF GEOTECHNICAL DIMENSIONS vs. XRCT

Geotechnical rock cores have a dimension that makes the uniform penetration of the X-ray beam through the sample often difficult. The cylindrical shape ensures on the contrary the most homogeneous irradiation over the irradiating field. Specific laboratories for material investigation have developed industrial scanners that permit microstructural rock core investigations for diameters up to 500 mm (**Table 8.2**). However such facilities are not easily available and analysis are provided at high costs. At a lesser resolution, medical XRCT is a very convenient facility that can be accessed in most medical research centers and is more and more implemented at different geological and engineering research institutes. The rapidness of an analysis and the quality of the data obtained based on medical reconstruction protocol makes it a technique of choice to be used for geotechnical rock cores characterization.

As developed by pioneer authors in 3D indirect rock petrography (*Van Geet et al., 2000 & 2001; Ketcham, 2005 a. o.*), medical XRCT provides petrographical informations at a transitional resolution in between microscopical investigations and outcrop scale observations. Structural and textural 3D elements linked to primary rock-forming processes (chemical composition, i.e. material density, crystalline vs. diagenetic origin, mono- vs. polygenetic assemblage) or to secondary

| Tomography type | Technique | X-ray irradiation | X-ray beam geometry | Acquisition time | Diameter of investigated samples | Scale of resolution |
|-----------------|--|--|---------------------|---------------------|--|---------------------------|
| Medical CT | XRCT | helical <i>(constant motion of source-detector pair around the sample)</i> | fan - cone | < 1 min | up to 200 mm <i>(no length limitation)</i> | 500 μm |
| Industrial CT | high-resolution CT ultra-high resolution CT | stationary <i>(incremental motion of sample in the irradiation field)</i> | highly-collimated | 1 min - > 1 hour | 25 - 500 mm <i>(limited length)</i> | > 10 - 200 μm |
| Synchrotron CT | micro CT | stationary <i>(incremental motion of sample in the irradiation field)</i> | parallel | 1 min - > 1 hour | 25 mm <i>(limited length)</i> | < 50 nm - 1 μm |

Table 8.2 X-ray computerized tomography techniques in use. Respective acquisition mode and X-ray beam geometry are given. The more parallel the beam, the less rebinning will have to be done in order to render the fan beam parallel before the use of the filtered back projection, meaning less interpolation and a better reliability. Indicative times of sample irradiation are given and demonstrate that medical XRCT is very efficient due to the low-time consumption related to an investigation. Sample sizes readily investigated by each technique are indicated and an advantage of medical XRCT is its ability to scan samples with no limitation in length, as theoretically rock core as tall as the human body could be investigated by the technique, provided enough time for X-ray tube cooling would be available. Concurrent resolutions of each CT technique are given and place XRCT as an interesting complimentary analytical method for rocks, at a transitional level between micro- and macroscopic investigations.

processes (tectonic damage, dissolution, and weathering) are readily visualized by XRCT. Although one order of magnitude bigger than classical thin section analysis, XRCT determinations have the advantage of being fully 3-dimensional. This becomes particularly interesting for the evaluation of rock anisotropy and heterogeneity.

8.3.1 XRCT Equipment Used in this Study

The scanner used at CHUV is a LightSpeed VCT from GE Medical Systems (www.gehealthcare.com) (Fig. 8.3).



Fig. 8.3 Illustration of the third-generation XRCT scanner used at the service of radiodiagnostic and interventional radiology, CHUV, Lausanne. Although XRCT techniques are nowadays widely used in material sciences and designed for high-resolution imaging, the sample size is still a limiting factor. For samples corresponding to geotechnical rock cores dimensions (76-85 mm diameter and 150-170 mm length) the medical XRCT remains a fast and accurate technique for indirect imaging of whole rock structures even though limited to an effective resolution of 0.5 mm. **A)** General view of the CT scanner, X-ray tube and table. **B)** A geotechnical rock core placed in a rubber membrane as used for triaxial mechanical testing. The membrane is then placed into a PVC cylinder covered by a thin copper sheet in order to prevent beam hardening effects. **C)** End positioning of the sample at the middle of the CT gantry just before completion of the scan. For more details on the acquisition technique, see **sections 8.3.2-4**.

Detector is a 40 mm-wide HiLight® Matrix III Scintillator with an isotropic design. It contains 64-channel detector rows made of 58368 cells (912 detectors per row) with a thickness in the z-direction of 0.625 mm each, providing an isotropic resolution of 0.6 mm. Lighting angle of the detector is 56 degrees. Dynamic range is 16 bit (accommodating 65'536 grey values) and reconstructed density maps are 512 x 512 pixels. To analyze rock core samples of geotechnical dimensions and highlight optimally specific rock constituents in a range of 2.5 up to 5.3 g/cm³, X-ray parameters were set to 120 keV voltage and 640 mA tube current for a focal spot size of 1.2 mm. Acquisition on 80 mm diameter rock cores was achieved in helicoidal mode corresponding to the displacement of the sample at a constant speed of 25.8 mm/s in the X-ray field produced by the continuous rotation of the CT gantry (X-ray source and detector). A full rotation was performed in 0.8 seconds and image reconstruction step was set to 0.31 mm corresponding to half of the detector size (Nyquist theorem for optimal signal processing). A voxel size of 0.6 x 0.215 x 0.215 mm is obtained. A reconstruction algorithm with a medium edge enhancement effect was used.

Data from XRCT scans are collected as image sequences in the DICOM format (Digital Imaging and Communications in Medicine, *American College of Radiology & National Electric Manufacturers Association*, 1985). Scans of geotechnical rock cores with 76 mm diameter produce about 500 CT images and 3D reconstruction of a whole CT stack involves processing 256'000 KB concurrently.

8.3.2 X-Ray Interactions With Rock Materials

X-rays, emitted as a polychromatic beam, interact mainly with the electron shells of atoms (*Hubbell et al.*, 1975). This leads to a CT map of attenuation coefficients that are dependent on material density, isotope composition and radiation energy. At medical XRCT energies, photoelectric absorption (function of atomic number Z) and Compton scattering (function of mineral density ρ) influence the result of the irradiation, and low-energy X-rays are more sensitive to differences

in composition than higher energy ones, allowing better differentiation of attenuation contrasts in materials. However, at low energies, elements like Ca and K having a large Z (and present in large amount in some rock-forming minerals) will produce more photoelectric absorption, causing additional image artifacts.

In radiation protection science, the half value layer (HVL) is used to design appropriate shields against electromagnetic radiations of a given energy. It corresponds to the thickness of material needed to reduce the radiation by half and is closely linked to the attenuation coefficient by following relationship:

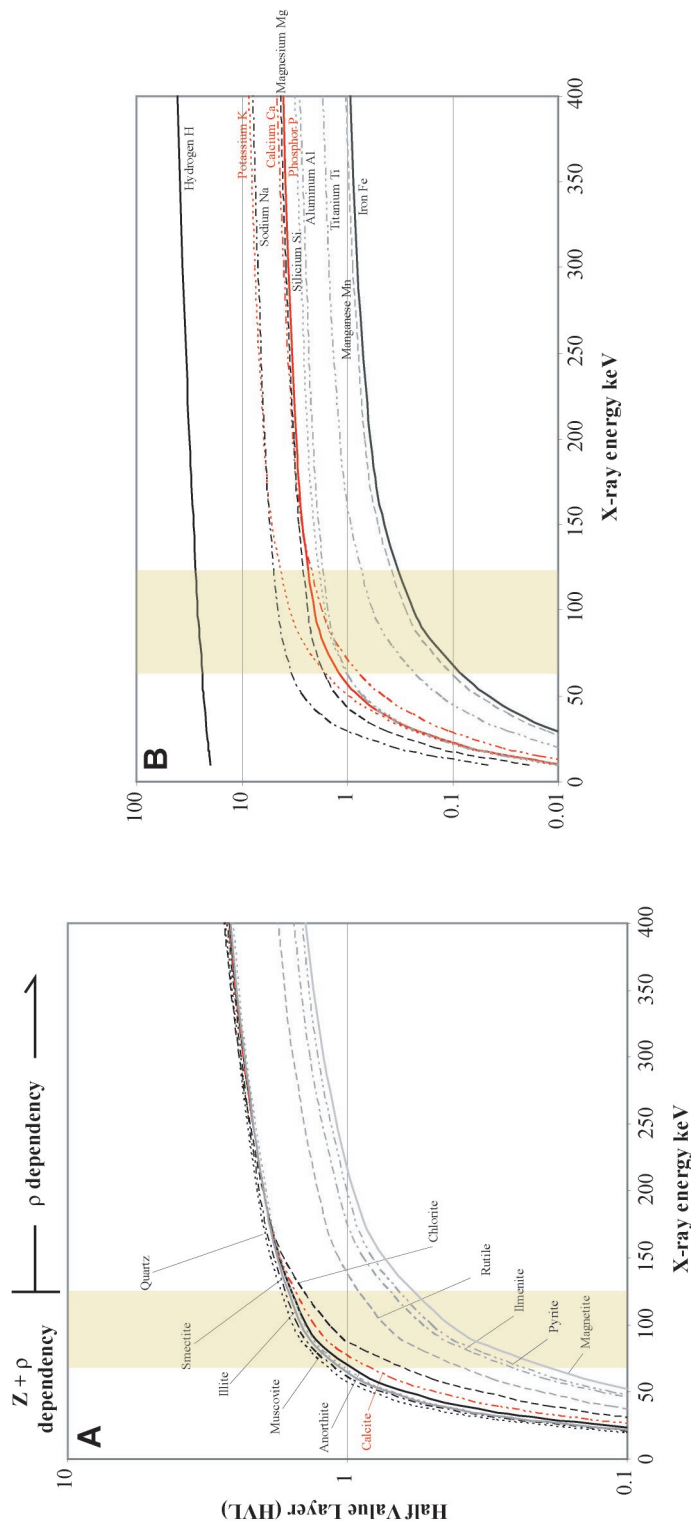


Fig. 8.4 Plots of half value layer (*HVL*) vs. X-ray energy range of 0 to 400 keV for **A**) different rock-forming mineral species and **B**) typical chemical compounds. The domains of a *composition* oriented tomography (e.g. sensitive on atomic number Z and mineral density ρ) and an essentially *density* oriented tomography (mainly function of mineral density ρ) are given, with an optimal compositional sensitivity of X-rays in the range of 60-120 keV. Indirect mineral phase differentiation could be expected from XRCT acquisition in the range of 60-120 keV, meaning probably an adaptation of the acquisition protocol (longer acquisitions, optimized sample thickness for a given mineral paragenesis, no limitations due to overheating of the X-ray tube ...). Such considerations would open the path to a real 3D petrography comparable to thin section analysis and need to be addressed in the future.

Eq. 8.1
$$HVL = \frac{\ln 2}{\mu}$$

Transferred to rock analysis, the concept of *HVL* could be used to find out the most proper range of irradiation needed for the optimized analysis of a given mineral assemblage in function of sample thickness and grain size. In a same way, it could delimit the critical sample thickness above which no information would be obtained from XRCT irradiation.

Fig. 8.4 presents *HVL* calculated for some important rock-forming minerals as well as for typical chemical compounds encountered in rocks over the energy range 0-400 keV. A rapid increase of *HVL* is generally observed up to an energy level of 60 keV, describing the rapid diminution of the effective section for photoelectric absorption. Thus attenuation below 60 keV can be understood as a mixture of photoelectric absorption and Compton scattering effects, whereas above that value Compton scattering becomes more and more predominant. Above 120 keV, the different *HVL* of chemical compounds stay almost constants and increase slightly in the case of minerals, reflecting the more complex attenuation paths endured by X-rays in complex atomic structures. The shift in *HVL* curves above 120 keV defines a transition between a *composition* oriented tomography (e.g. sensitive on atomic number *Z* and mineral density ρ) and an essentially *density* oriented tomography (mainly function of mineral density ρ), with an optimal X-ray mineral sensitivity in the range of 60-120 keV. This corresponds to the irradiation range of medical XRCT.

8.3.3 Elimination of Beam Hardening Effects

In order to minimize beam hardening effects and improve the initial image quality obtained in 2004 (**Fig. 8.2**), a sample holder made from a Cu-sheet surrounding a 2 cm thick PVC cylinder was used to physically pre-filter X-rays before entering the sample so as to enhance reconstructed image quality and –by extension- improve the segmentation possibilities of geological features of interest (**Fig. 8.5**).

X-ray energy entering the proper rock volume was evaluated being concurrently reduced by about 50 keV due to the effect of the sample holder, producing an effective analysing beam of 70 keV, e.g. in an adequate range to differentiate between the main rock constituents (predominance of Compton effect defining the domain of tomodensities).

8.3.4 Signal Reconstruction over Extended Range of HU Units

Medical XRCT investigations of the human body are confronted with density values ranging from 0 g/cm³ (air density) up to about 1.35 g/cm³ (mean human bone value) and involve a HU range of -1000 to 3096 HU, based on the tomodensity of water set as 0 HU. Standard medical measurements focus on a signal reconstruction up to 4096 HU to optimize contrast visualization. In order to depict properly surgery elements like screws or metallic plates (densities of about 4.5 g/cm³), medical HU coverage can be extended to allow proper signal reconstruction.

Rock materials, with typical densities of 2.3 up to 6 g/cm³ depending on their mineral constituents, are strongly attenuating compared to a human body. They introduce important scattering effects and differential attenuations when analyzed under the standard HU coverage, leading to an exaggeration of detected feature sizes. This observation was made during acquisition of a garnet-bearing gneiss sampled during field work at the AlpTransit Ceneri base tunnel site (**section 5.3.9**). The single garnet grains produce strong attenuations in comparison to the overall rock matrix constituents what results in an important loss of photons for subsequent CT-image reconstruction (“starving

effect” of the detector). This results in the apparition of artifacts.

In order to obtain an adequate imagery from rocks, use of the scanner in extended HU mode (increasing the level of interpretation of the incoming signal, e.g. more bits) was decided for the most realistic signal reconstruction (**Fig. 8.6**).

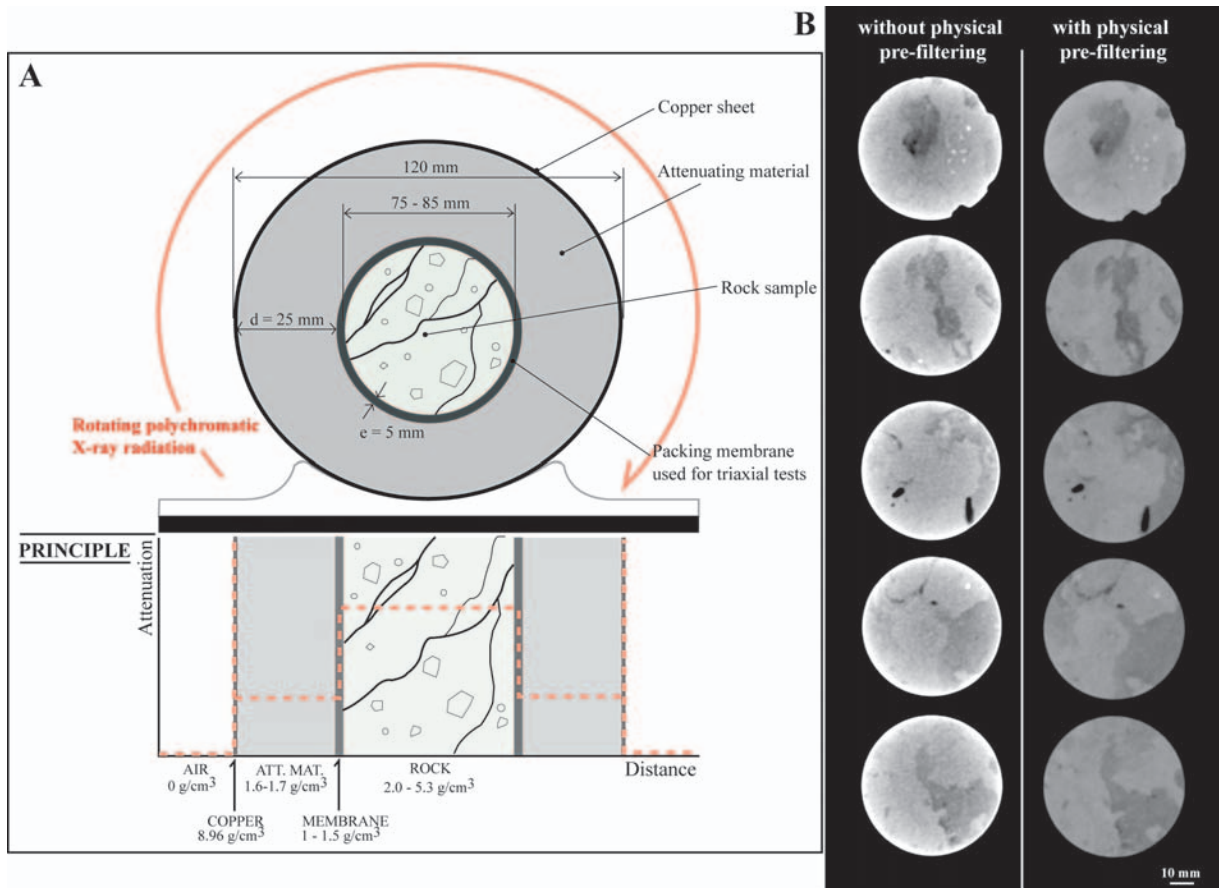


Fig. 8.5 A) Schema of the rock core holder made of a PVC-type material having a density in between air and average rock density as described in the text. The effect on the X-ray beam is qualitatively depicted on a graph of attenuation vs. distance. **B)** Illustration of acquisition artifacts (mostly beam hardening) illustrated by single CT slices from a limestone sample (Sequanian limestone sampled along the Pontarlier fault system at Vallorbe, Jura Mountains, Switzerland). The left views are direct XRCT acquisitions from the sample that was scanned without any particular preparation. In that case, the artifacts are represented by brighter halos at the outer margin of each of the slices. Right and next to them are the correspondent slices from a scan that tested the efficiency of the sample holder presented in A). Sample diameter is 55 mm.

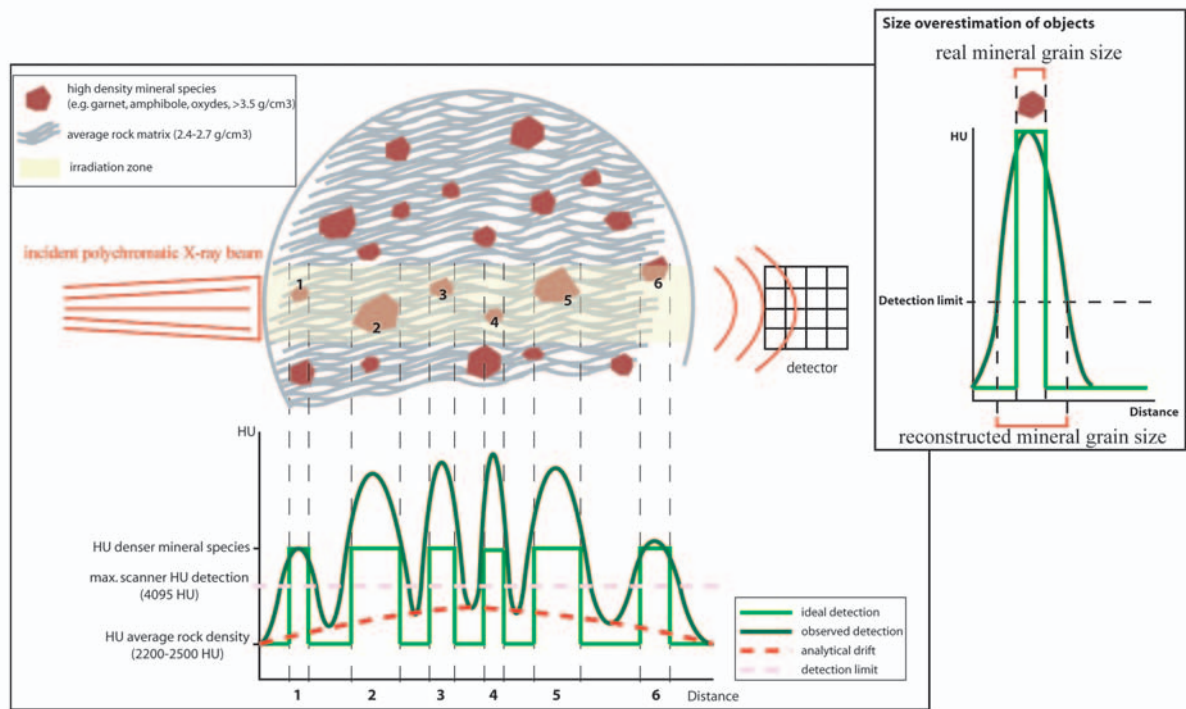


Fig. 8.6 Analytical drift observed without the use of the extended HU function on the medical X-ray scanner. In the case of strongly attenuating components having excess densities, a limitation in the HU reconstruction range introduce a bias in the reconstructed object size, as exemplified here by the garnet mineral grains.

8.4 3D RECONSTRUCTIONS

Medical XRCT is expected to aid in the initial characterization and quality assessment performed on geotechnical rock cores from drilling operations (see **Chap. 7**). This is in particular interesting in the case of cataclastic rock cores due to their fragility and difficult manipulation. **Fig. 8.7** shows the example of two samples extracted at the N16 Roche St Jean tunnel in Jura canton and confronts the visual aspects of the rocks by means of direct and indirect evidences.

3D tomographic reconstructions were realized in this study with the use of VGStudioMAX software (www.volumegraphics.com). Based on the original .dicom data or any further transformation data format (.tiff, .bmp ...) the software reconstructs the recorded xy CT-slices composing the XRCT stack into a whole-volume model. For geotechnical rock cores analyzed under the scanning parameters defined in **section 8.3.1**, about 500 CT slices per sample are accordingly recorded and reconstructed. Functions implemented in VGStudioMAX allow further realizing virtual slicing inside the rock volume inferring on the spatial development of structural elements. Preferential slices in the xz- and yz-planes can be obtained but the arbitrary definition of a clip plane is made possible with adjustment tools.

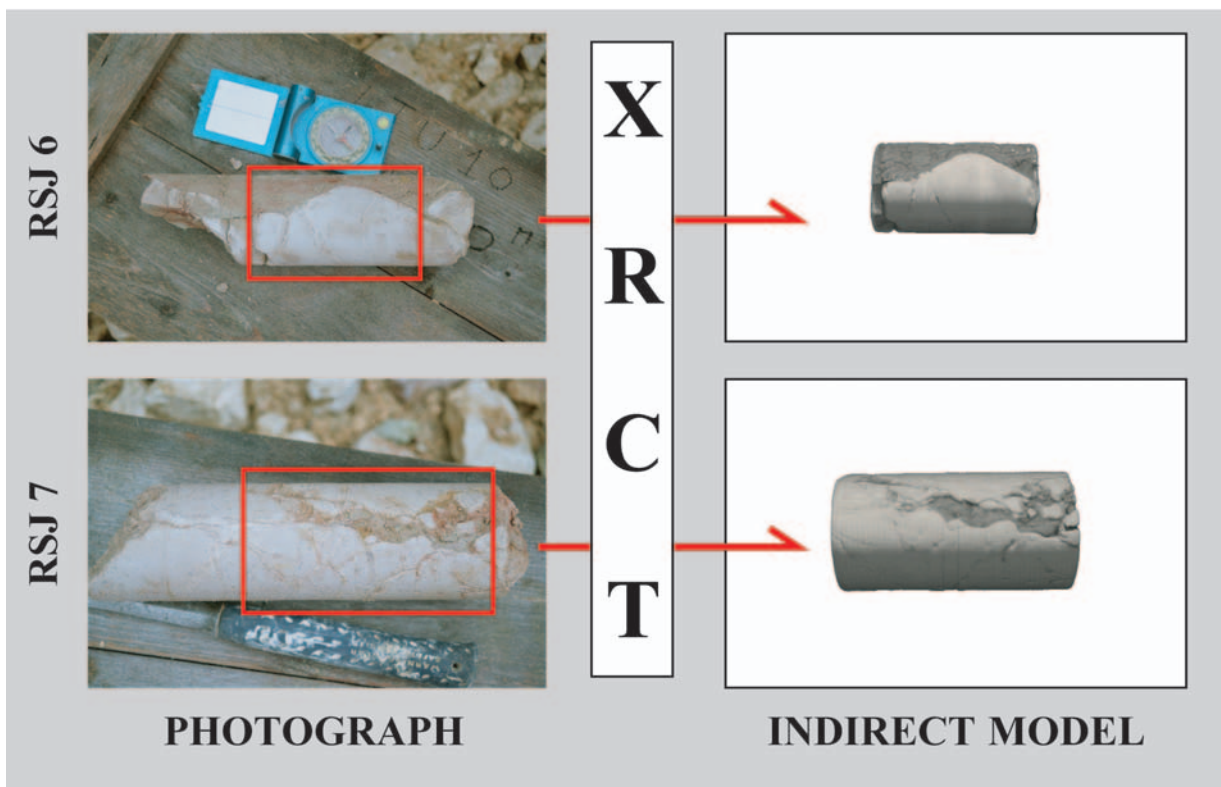


Fig. 8.7 Confrontation of direct and indirect views of geotechnical rock core samples (N16 Roche St Jean Tunnel). The quality of medical XRCT models can deliver many additional insights on rock core structures. Scale given by the compass and geological hammer.

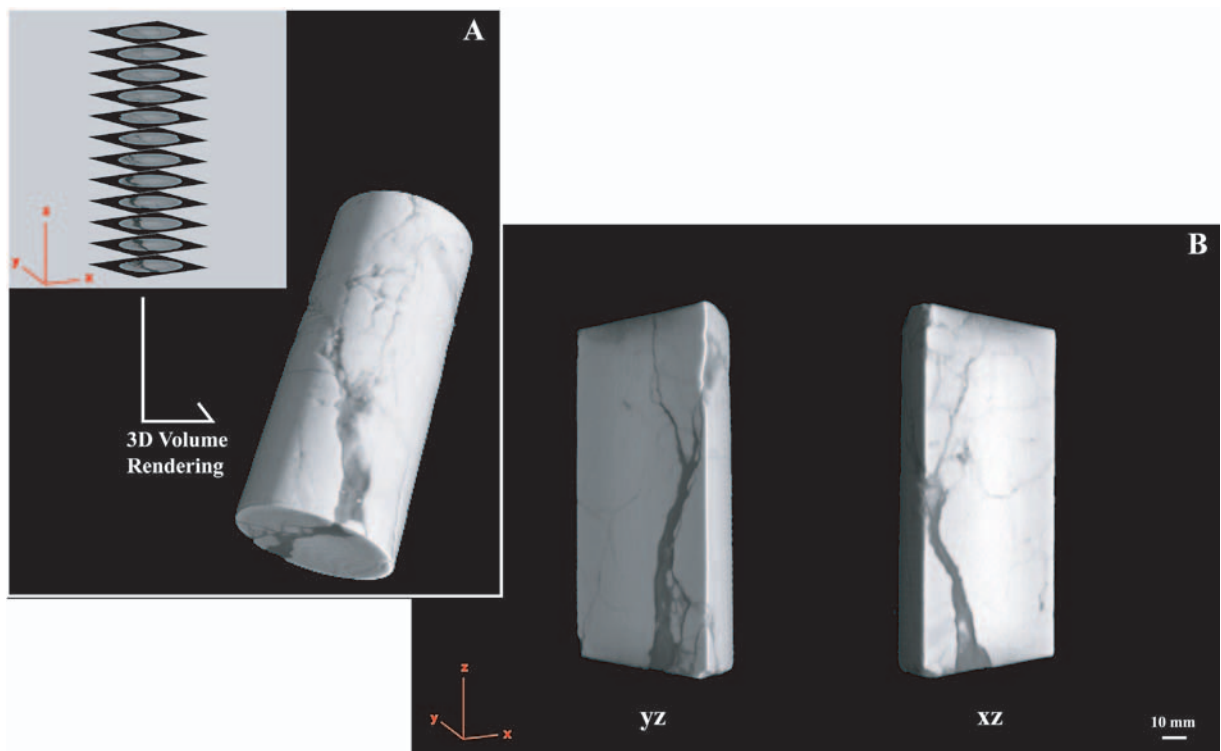


Fig. 8.8 Principle of 3D indirect reconstruction of rock cores from XRCT xy-data. With the use of appropriate softwares, virtual slicing can be performed inside the rock material in xz- and yz-directions or any arbitrary adjusted clip plane.

9

METHODS FOR A GEOMECHANICAL CHARACTERIZATION OF CATACLASTIC ROCK CORES

“We need to succeed; otherwise we run the risk of failure.”

A former US president

In a similar way than the geological characterization, the geomechanical characterization of geotechnical rock cores is performed from two perspectives:

- A *direct* analysis aiming the study of triaxial strength at determined confining levels σ_3 in agreement with *in situ* conditions (description of mechanical behavior);
- An *indirect* analysis using XRCT aiming the back-analysis of triaxial test data based on the visualized structural evidence of fracturation (improved understanding of damage inherited from the deformation).

Rock cores are tested by means of triaxial tests in a Hoek cell under standard analysis of peak and residual strength. Accordingly, a mechanical classification of the sample based on their deformational behavior is realized. Three rock core families are determined and confronted with the geological quality classes I-III of the bulk apparent geological characterization (**Chap. 7**). A first potential correlation is then tested and the complexity of the deformation response inside a given rock core set assessed. For this step, particular attention is given to the determination of geological micro-structures able to explain a given stress-strain response.

XRCT has been presented in **Chap. 8** as a technique of choice for the indirect 3D reconstruction of rock cores and the possibility to perform virtual slicing through their structure. Consequently XRCT acquisitions are realized on rock cores *before* and *after* triaxial deformation. Critical evidences of fracturation modes and an objective quantitative evaluation of the triaxially induced damage structures have been assessed.

Within this research, triaxial strength data could be gained on cataclastic rock cores as well as evidences of their modes of deformation. The aspect of the stress-strain constitutive relationships of cataclastic materials from different petrologies had however to be left aside. Also no creep tests were undertaken in the methodological development of this research.

9.1 CHARACTERIZATION BY MEANS OF STRENGTH DATA

Mechanical tests have been conducted at the Laboratory of Rock Mechanics from EPFL (LMR) following accredited standard test procedures. A particularity of this research is to use XRCT for cataclastic rock core imaging prior to any laboratory manipulation. Accordingly, preliminary indirect recording of the geotechnical rock cores permits to evaluate sample conditions and structures which facilitate optimal sample preparation for triaxial tests by minimizing the potential control of the mechanical behavior by singular preexisting discontinuities (**Chap. 4**).

The preliminary XRCT imagery is only indicative and not used for image analysis determinations.

Following questions based on the XRCT preliminary evidence have been retained during the production of rock core for triaxial testing (e.g. reshaping of the drilled rock cores into cylinder characterized by a diameter/length ratio of 1:2):

- What are the best portions of the drilled rock cores to be used to obtain test representativity?
- Are there zones of particular interest inside the rock core volume (e.g. presence of important voids, contrasting rock matrices, unfavorably oriented fractures) susceptible to strongly control the test-induced deformations?

- In which extent is the heterogeneous structure of a cataclastic rock core susceptible to introduce a source of error in the interpretation of triaxial data by means of classical models (see **section 9.2**)?

In the case of cataclastic rock cores, deformation of samples is realized under application of the minimal possible displacement rate of the piston into the Hoek cell. No monitoring of the build up of interstitial pressures has been made within this study. Stress determinations correspond therefore to total stress conditions.

Chap. 2 showed that cataclasis is strongly function of the level of deviatoric stress and the strain rate. Effects of confining level on cataclastic failure involve a non-linear rupture criterion (*Habimana, 1999*). Mechanical tests aiming the detailed study of the cataclastic mechanism would moreover require proper considerations of the presence of water and pore pressures (Terzaghi's principle of effective stress).

Analyses of triaxial total stress data by means of the Mohr-Coulomb theory as made in this research introduce therefore a strong interpretative simplification of the effective monitored ruptures from cataclastic materials. Nevertheless, a realistic mechanical description could be obtained provided a large amount of tests on cataclasites from a same provenance (statistical relevance). As it was decided to focus in this research on only 12 specific structurally contrasted rock cores, the interpretation of triaxial tests could not provide an elaborated intrinsic curve for the mechanical behavior. The purpose of the mechanical characterization will accordingly be to obtain mechanical evidences to be confronted with the geological characterization. Accordingly, the feasibility of triaxial test interpretation introducing considerations from structural analysis of rock cores by means of XRCT is addressed.

9.1.1 Triaxial Tests

One of the most important characteristics of rock, from the design engineer's point of view, is the significant increase in strength with increasing confining pressure (*Hoek & Franklin, 1968*). Adequate description of this strength behavior can be analyzed in the laboratory with triaxial tests performed on geotechnical rock cores over a range of confining pressures.

A triaxial test corresponds to the loading of a sample under constant confining stress σ_3 . The rock core is isolated by a rubber membrane and further positioned into a Hoek cell able to build up internal (isotropic) confining pressure σ_3 (**Fig. 9.1**). Vertical stress σ_1 is increased by axial compression of a piston at constant speed on the upper face of the sample and raised until material failure. Thus for a given confining stress σ_3 the evolution of the principal stress σ_1 is recorded in function of axial deformations ε_1 . Each sample undergoes 3 loading cycles following a linear ramp of confining stress conditions. The maximal value of deviatoric stress $\sigma_1 - \sigma_3$ at rupture (e.g. main principal stresses) can be determined from the first loading cycle (peak strength). When the residual strength value is obtained, the lateral stress σ_3 is modified to a higher value until the axial stress σ_1 stabilizes to that new confinement conditions. Residual stress states (e.g. deviatoric stresses $\sigma_1 - \sigma_3$ controlling shear movements on the rupture plane) are recorded and used for the determination of an indicative Mohr-Coulomb criterion for each tested sample.

In general, mechanical parameters from triaxial tests are:

- The *elastic modulus* $E_{50\%}$ (MPa) measured during the first loading cycle as the slope of the deviatoric stress/axial deformation curve at half of the maximum deviatoric stress level.

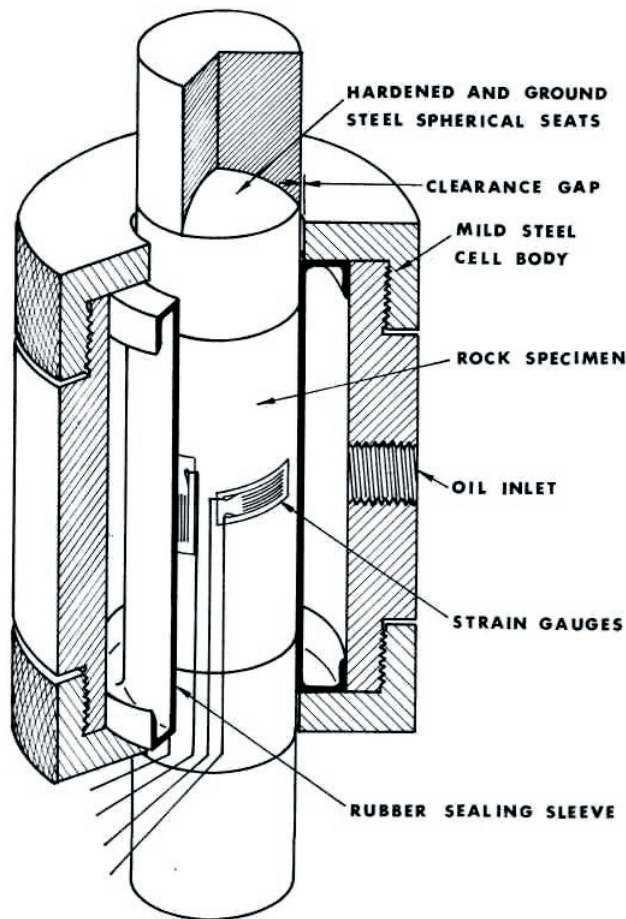


Fig. 9.1 Principles of the Hoek triaxial cell. After Hoek & Franklin, 1968).

stresses (τ) on the assumed rupture plane and relates them by following equation:

$$(Eq. 9.1) \quad \tau = c + \sigma_N \cdot \tan \phi$$

with

σ_N = normal stress on rupture plane

τ = tangential stress on rupture plane

ϕ = internal friction angle

The determination of normal (compressive) and tangential (shear) stresses on the assumed rupture plane can be calculated from the Mohr circle analysis (Fig. 9.2, presentation of worst case where α corresponds to $45^\circ - \phi/2$). Based on residual stress data and a determination of the Mohr rupture angle α they become:

$$(Eq. 9.2) \quad \sigma_N = \frac{\sigma_1 + \sigma_3}{2} - \frac{\sigma_1 - \sigma_3}{2} \cdot \cos 2\alpha$$

and

$$(Eq. 9.3) \quad \tau = \frac{\sigma_1 - \sigma_3}{2} \cdot \sin 2\alpha$$

A high value of elastic modulus means a steep loading curve which corresponds to a stiff material. Stiffness is defined as the inverse of deformability. For uniaxial loading, deformability δ of rock cores at a given stress σ can be expressed with consideration of elastic modulus E by following relationship:

$$\delta = \frac{\sigma}{E}$$

- The *cohesion* c (MPa) of rock cores which corresponds to the ordinate τ -value of the adjusted Mohr-Coulomb criterion when $\sigma = 0$.

- The *angle of internal friction* ϕ corresponding to the slope of the adjusted Mohr-Coulomb criterion. It can be understood as the ease with which sliding is initiated along a rupture plane. Theoretical most unfavorable joint orientation when submitted to axial stress is given for $45^\circ - \phi/2$.

The classical Mohr-Coulomb criterion used in soil mechanics at rupture considers the normal (σ_N) and shear

An expression of the Mohr-Coulomb criterion for the strength limit of material can be given by consideration of the main principal stresses. This criterion has only limited validity since it constitutes a simplification of effective rock behavior (linearization of a parabolic criterion, see for example the Hoek & Brown rupture criterion for rocks). It is given by following equation:

$$(Eq. 9.4) \quad \sigma_1 = \frac{\sigma_3(1 + \sin \phi) + 2c(\cos \phi)}{1 - \sin \phi}$$

Note: Triaxial tests are generally performed under estimated *in situ* stress conditions. A scale-effect affects however determined strength values between laboratory and *in situ* measurements. It is reported that short-term laboratory tests on very hard brittle rocks tend to overestimate the *in situ* rock mass strength (Hoek & Brown, 1997). This is due to damage resulting from micro-cracking processes inside the rock. Accordingly, critical intensities for fracturing initiate and develop at lower stress levels in the field than in laboratory tests that are carried out at higher loading rates on smaller specimens. For geotechnical applications, a value reduced to 70% of the measured triaxial strength at failure is therefore recommended.

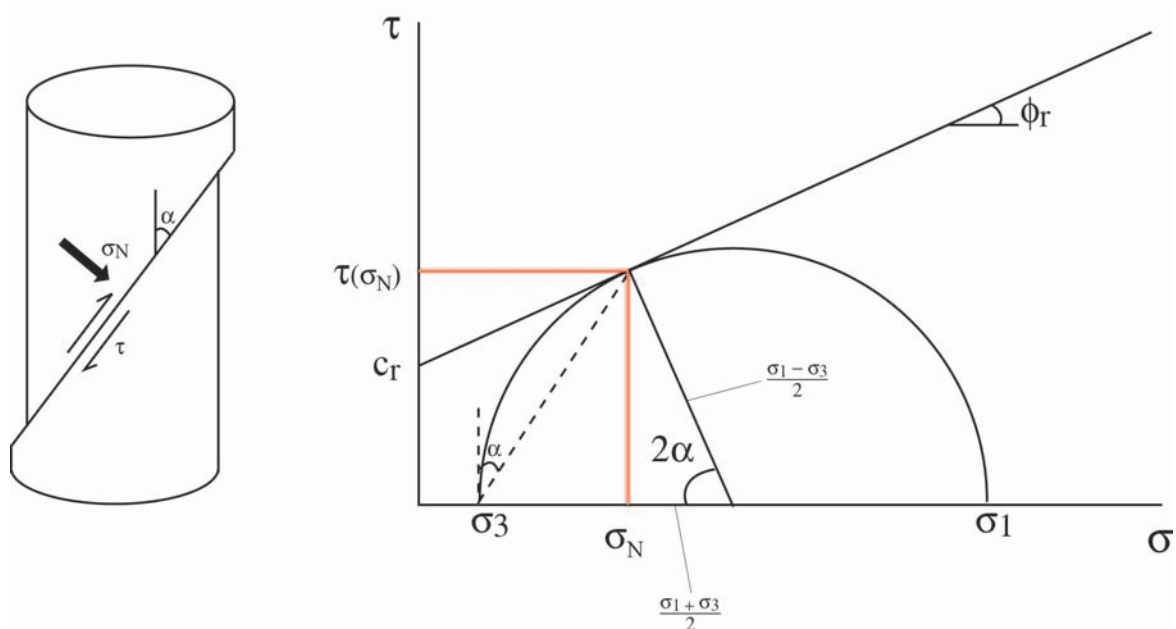


Fig. 9.2 Geometrical principles based on the Mohr circles for the reconstruction of normal and tangential stresses acting on the assumed rupture plane. Theoretical worst rupture case where α corresponds to $45^\circ - \phi/2$. This scenario assumes rock core homogeneity, e.g. it doesn't consider the influence of singular discontinuities in orientations susceptible to influence triaxial test result. When such a discontinuity is evidenced inside the sample its orientation has to be assessed and an oriented Mohr Coulomb criterion adopted. Based on *Twiss & Moores* (1992).

9.1.2 Evaluation of Mechanical Behaviors

Next to strength data, triaxial tests provide evidences of overall fragile or ductile sample behavior by evidences depicted on the stress-strain curve. Recorded evidences constitute a central aspect in the evaluation of rock mass properties. Accordingly, the direct mechanical characterization of cataclastic rock cores in this research aims to perform a classification according to their mode of deformation. With this regard, following mechanical classes have been considered (**Fig. 9.3**):

- 1) *Brittle* samples: most competent rock cores in an investigated sample set characterized by a steep triaxial deformation curve that leads to the value of maximum deviatoric stress (peak

strength). Samples preferentially developing a well-defined rupture plane.

- 2) *Ductile* samples: weakest rock cores characterized by a flat triaxial curve that never reaches a peak. Accordingly, no difference can be made here between peak and residual strength values. Generally, samples are made of large proportions of soft mineralogical components or controlled by a preexisting rupture plane free to be activated under load.
- 3) *Intermediate* samples: rock cores depicting a mixture of fragile and ductile mechanical elements that produce a complex triaxial deformation path evidencing numerous ruptures in different orientations and subsequent adjustment of desolidarized and remobilized contrasted rock parts up to peak strength.

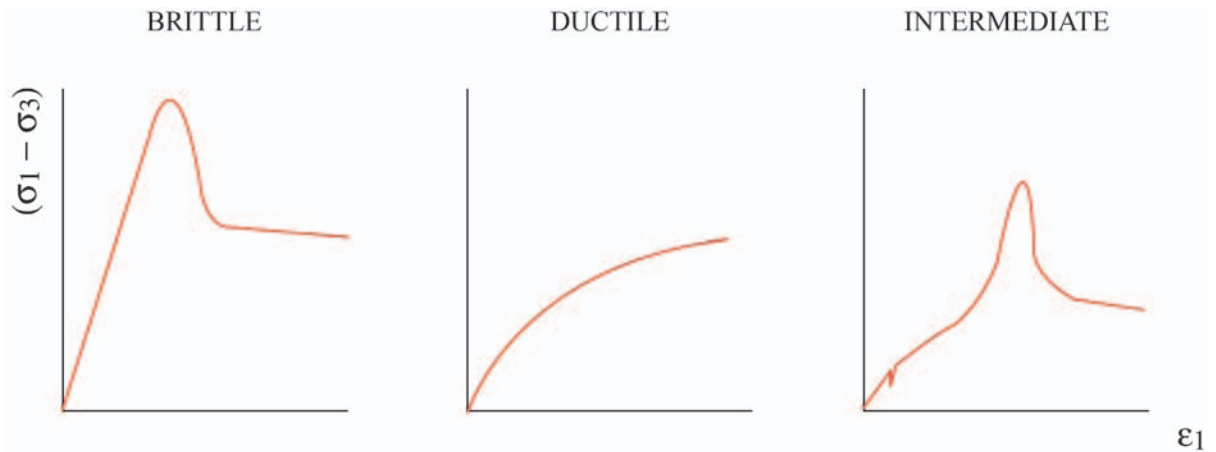


Fig. 9.3 Three mechanical families determined on the base of triaxial testing. A) Overall fragile behavior. B) Ductile behavior. C) Intermediate behavior.

9.1.3 Complementary Mechanical Investigations

Next to triaxial tests, additional mechanical procedures deliver useful data that helps in the mechanical interpretation of triaxial test. In this research, the limited quantity of samples led to consider an optimum rock core set valorization. Thus, following additional mechanical procedures have been realized on excess materials that remained from the preparation of the rock cores into standard dimensions from triaxial tests.

9.1.3.1 Uniaxial Compression

Uniaxial compression corresponds to the deformation of a rock core under an axial load applied on top of the core at constant speed. No confining stress is applied on the sample. The test is finished once the sample reaches failure. Rupture stress is labeled σ_c (MPa) and elastic modulus E is read similar to triaxial tests from the deformation curve (σ - ϵ) at $\sigma = 50\% \sigma_c$. Deformation speed in UCS is maintained at a value of 0.1 mm/min. Rupture stress σ_c is given by consideration of maximal obtained axial force F_{max} and rock core maximum cross section A:

$$(Eq. 9.5) \quad \sigma_c = \frac{F_{max}}{A}$$

Tested rock cores have the same diameter/length ratio as triaxial rock cores. In this research, rock cores for UCS are of smaller dimension as they had to be produced from re-drilling in the hardest remaining parts of the rock cores used for triaxial tests (rock core set valorization). Accordingly, only “hard clasts” from the cataclastic rock cores have been valorized in that way, as the damage inherited from cataclasis makes the re-drilling procedure in heterogeneous samples extremely difficult and

precarious.

9.1.3.2 Direct Shear Test

Shear tests are realized according to the Casagrande procedure and aim to determine mechanical properties of joints (fractures) and discontinuities.

Basic principle of the shear test is to let two surfaces slide on each other. The test is performed by putting the sample into a box split in 2 compartments along which the sample is sheared back and forth at a constant speed of $v = 0.5$ mm/min under an applied normal load. Variation of the force that is needed to shear the sample is recorded next to the dilatancy that is caused by the rugosities of the shear plane during displacement along the surface. The test is performed in 3 cycles corresponding to normal loads of 586, 1172 and 1758 N. Finally, determination of the friction angle φ for the joint is made by taking the average of values obtained in both senses of shear.

Shear along an ideally planar and smooth surface is given by the Mohr-Coulomb criterion assuming a cohesion $c = 0$.

The pertinence of shear tests from rock core remnants partly reconstituted is low and accurate data of joint conditions would require an elaborated program of tests based on petrographic evidences from especially prepared samples. Accordingly, data derived from shear tests in this research are only indicative of potential main joint behavior.

Based on petrographic evidences of cataclastic rock cores, a general remark has to be done according to preexisting structures and discontinuities. As a result of the generalized fracturing induced by cataclasis, several discontinuities affect the rock mass. These discontinuities depict at least 3 joint surface conditions:

- *open* discontinuities, characterized mainly by their surface condition (roughness);
- *sealed* discontinuities, characterized mainly by the rheological properties of the filling materials;
- *recrystallized* discontinuities, characterized mainly by the texture and composition of the mineral assemblage, which further influence discontinuity strength.

Accordingly, a modelisation of the cataclastic behavior should be able to integrate mechanical constraints to each of these discontinuity types and evaluate the effect of their spatial distribution against an imposed stress field. Contrasting rock discontinuities have to be evaluated in terms of their influence on stress transmission and deflection inside the cataclastic material, as they are a source of answers for the unexpected behaviors frequently observed in heterogeneous media. Moreover, cataclastic fractures exert a preferential control on rock matrix alteration, negatively influencing sample strength.

9.1.3.3 Tensile Strength

Tensile strength can be indirectly assessed by the so-called “Brazilian” test (Fairhurst, 1964a).

A thin circular disc is compressed to failure across a diameter. The compression induces tensile stresses normal to the diameter, which are sensibly constant over a region about the centre. The tensile strength (σ_T) is calculated on the assumption that failure occurs at the point of maximum tensile stress (i.e. at the center).

Combining value of σ_T with results from UCS allows the determination of an empirical intrinsic curve of mechanical behavior. The σ - τ relationship based on σ_c and σ_T is given by (Fairhurst, 1964b):

$$\text{(Eq. 9.6)} \quad \tau = \sigma_T \cdot (m - 1) \cdot \sqrt{1 + \frac{\sigma}{\sigma_T}}$$

with

$$m = \sqrt{\left(\frac{\sigma_c}{\sigma_T} + 1\right)}.$$

9.1.3.4 Impregnation of Triaxially Deformed Rock Core

Triaxially tested rock cores can be impregnated to allow preparation of thin sections accurately corresponding with the geomechanically tested materials. Impregnation follows the protocol given in the note of **section 7.2.2**.

Although not done to evaluate strength properties, this step is envisaged for two reasons mainly addressing considerations about discontinuities of contrasting mechanical properties :

- Evaluate how thin sections could provide petrographic constraints for the evaluation of fractured rock rheology based on triaxial tests (e.g. determine an indicative rheology for fracture types, take into account evidences of alteration);
- Be able to confront thin sections taken on the same sample that effectively underwent triaxial deformation to investigate further preferential mode of failure (see **Chap. 4**).

The second point has been considered in particular for the confrontation of the contrasting resolution potentials between thin sections and XRCT and will be discussed later in **Chap. 11 (Fig. 11.7)**.

9.2 CHARACTERIZATION USING INDIRECT TECHNIQUES

In the geomechanical characterization of cataclastic rock cores, XRCT has been envisaged as an alternative technique able to minimize uncertainties in triaxial test interpretation. It delivers many useful evidences of the effective fracturation processes induced in mechanical tests. Effects of preexisting geological features inside samples can be qualitatively assessed and the control of rock core heterogeneity and anisotropy on resulting strength potentially investigated.

In **Chap. 8**, references have been given of studies implementing XRCT for the monitoring of rock deformation by means of X-ray tomography (e.g. *Alshibli et al.*, 2000; *Viggiani et al.*, 2004). In this research, evaluation of effective fracturation modes has been addressed through comparison of medical XRCT models recorded *before* and *after* the completion of the mechanical tests.

9.2.1 XRCT Recording of Rock Samples Before and After Triaxial Test

Cataclastic rocks are characterized by strong heterogeneities. Thus complex deformation patterns are most likely to occur. Based on methodological considerations expressed in **Chap. 4**, deformation of a rock core under triaxial conditions can be qualitatively analysed by confronting XRCT rock core acquisitions *before* and *after* realization of the mechanical test. Each triaxially deformed sample is accordingly carefully removed from the cell after test and maintained in the rubber membrane to ensure sample integrity. A new XRCT acquisition can then be realized and compared with the initial structural/textural evidence from XRCT.

Within this research, XRCT data recorded *before* and *after* triaxial tests are used to:

- 1) Better interpret triaxial failure by effectively visualizing rock core deformation. Accordingly, a rupture angle α_{XRCT} is determined to re-interpret test results based on the Mohr Coulomb theory (see below).
- 2) Quantify the development of damage inside the rock core volume by comparison with initial sample structure, which permits optimal confrontation between the geological and geomechanical observations.

Such considerations have been motivated at the beginning of the project on observation from a marl sample from a subhorizontal drilling operation performed in 2005 ahead of the face in the N16 Moutier tunnel (TM 6). Sample heterogeneity is very difficult to assess from such clay rich materials, e.g. a visual inspection can't deliver objective information on material structure. After completion of a triaxial test, it has been realized from the study of the indirect XRCT acquisition *before* and *after* test that the sample was characterized by an important preexisting structure. This structure appeared further to control rock core deformation under triaxial load. **Fig. 9.4** depicts the 3D reconstructed XRCT acquisitions *before* and *after* triaxial test of sample TM 6 as obtained on the AdvantageWindows facility for Linux at the radiodiagnostic institute in CHUV.

9.2.1.1 Back-Analysis of Triaxial Data Based on XRCT Evidence of Fracture Patterns

This step is used to confront the Mohr-Coulomb analysis made on the residual Mohr circles by integrating the XRCT visual evidence of the rupture geometry. Accordingly, a more realistic translation of the fracture geometry can be introduced in the Mohr Coulomb description. This is expected to help in improving triaxial test interpretation for heterogeneous materials based on the Mohr-Coulomb approach, e.g. when the amount of rock cores available for test is limited.

Fig. 9.4 presents the proposed visualization support for the re-interpretation of triaxial test data based on XRCT. Analysis of rupture angles on orthogonal clipped planes inside the rock core volume is made on a pseudo-3D basis. Angular relationships in the frontal plane are confronted with determinations on the sagittal plane by tracking the trace line of the obviously *main structure* influencing rupture. The XRCT reinterpretation of triaxial data considers therefore only one plane of rupture, what is consistent with the Mohr-Coulomb theory.

Using the stereographic projection, the maximum dip direction of the main structure can be reconstructed. Average of angular measurements on the 2 selected trace lines in frontal and sagittal views are reported as points on the stereoplot and the best-fit great circle containing both trace lines can easily be drawn. Accordingly, the rupture angle α_{XRCT} for the improved Mohr-Coulomb interpretation of triaxial data from heterogeneous samples is determined. *Rockware StereoStat 1.4.2* has been used for this determination (www.rockware.com). With the development of proper numerical tools for the 3D analyses of XRCT models at the medical scanner resolution, it is expected to perform such determinations in the future on the whole volume data, which is expected increasing precision by considering the topography of the rupture surface in its entire complexity. To offer such a tool at the end of this research was unfortunately premature as it would have required the development of a full 3D directional analysis code specifically designed for tomographic images. At this stage, only the improved segmentation of medical XRCT data could be addressed (see **Chap. 10**).

The determination of a rupture angle by XRCT as made in this research stays somehow subjective (i.e. the fracturation observed on the XRCT imagery after test results from 3 loading cycles, with

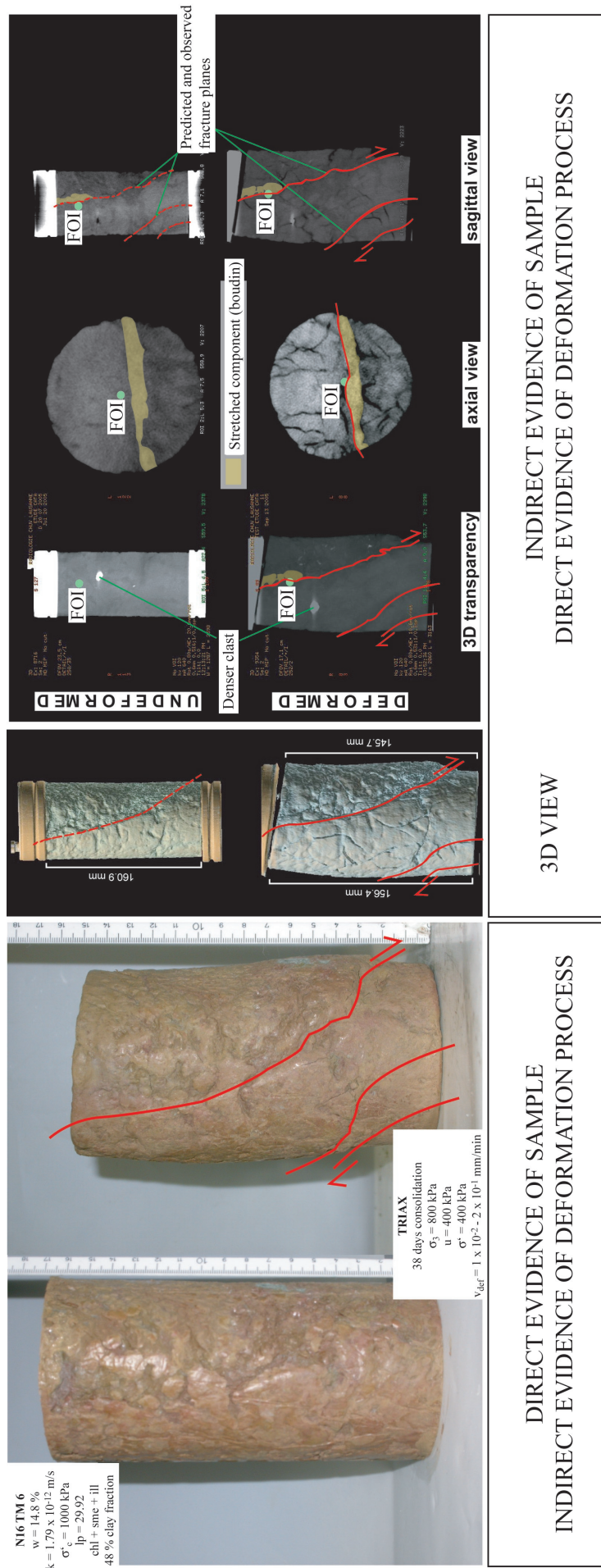


Fig. 9.4 First example of XRCCT acquisitions *before* and *after* completion of a triaxial test conducted in this research. Reconstructions performed on AdvantageWindows at CHUV in 2005. This example strongly motivated the use of indirect imagery techniques for the improved interpretation of triaxial data. Sample TM 6 is a tectonized marl from the N16 Moutier tunnel, Bern canton, Switzerland. Such materials are very difficult to handle and direct visual observations don't offer much interpretative possibilities. By means of XRCCT, the evaluation of the fracturation mechanism induced from loading at constant confining stress became visible through the presence of a denser component (boudin) in the upper part of the rock core (FOI, feature of interest). This geological feature, not visible by eye on the natural specimen, exerts an obvious control on the resulting shear failure of the sample. By means of such imagery, internal evidences of fracture conditions can be inferred and the control of preexisting geological features evaluated. XRCCT visualization capacities provide mechanical procedures with an important additional control technique that has the potential to profoundly influence the derived interpretation made from stress data.

residual cycles 2 & 3 modifying somehow the structural relationship of the peak fracture stage). Nevertheless, positive identification of a preferential rupture plane can be obtained on the base of rational geological considerations (see examples in **Chap. 12**). Moreover, following remarks seem pertinent:

- The question on “how to introduce the visualization advantages of XRCT into a triaxial test interpretation for heterogeneous materials” has potential for an improved geomechanical characterization based on geological evidences;
- Even if not absolutely precise in its current determination, α_{XRCT} defined as the angle of maximum dip based on trace line evidences from two orthogonal planes might be more significative than a rough angle taken from residual Mohr circle analysis since it considers the visualized geometry of the rupture plane;

Based on α_{XRCT} , normal σ_{N} and tangential τ stresses are then recalculated using **Eq. 9.2** and **9.3** to determine new values for the cohesion and the angle of internal friction (c_{XRCT} & φ_{XRCT}). A confrontation with σ_{N} - τ stress values obtained from analysis of the residual Mohr circles is then conducted. It has to be said that this procedure assumes stress uniformity on the rupture plane, which is simplistic with regard to the heterogeneous nature of cataclastic materials.

9.2.1.2 Evolution of Damage Indicators Under Triaxial Deformation

The indirect XRCT characterization of rock cores based on the quantification of *damage indicators* (see **section 7.1.2** & **Chap. 10**) can be similarly addressed on the XRCT models *after* triaxial test. Derived determinations are used to:

- Visualize fracture propagation inside rock cores and interaction with preexisting geological features when submitted to a deformation experiment under a given confining stress;
- Quantify the amount of triaxially induced *damage indicators* to be compared with the initial (already damaged) rock core structure;
- Determine a rock core fracturing susceptibility, implying the determination of rock matrix degradation vs. reactivation of preexisting fractures.

Image analysis tools for such determinations and their implementation will be presented in the next chapter.

10

METHOD OF CATACLASTIC ROCK CORE CHARACTERIZATION IMPLEMENTING MEDICAL XRCT

« Un camino no es más que un camino. Que lo abandones cuando tu corazón así te lo indique no significa ningún desaire a ti mismo ni a los demás. Pero tu decisión de seguir esa senda o apartarte de ella no debe ser producto del temor ni la ambición. Te advierto: examina cada camino atentamente. Luego hazte esta pregunta: ¿Tiene corazón este camino? Todos los caminos son iguales, no llevan a ningún lado. Si ese camino tiene corazón, entonces es bueno. De lo contrario, no te servirá de nada. »
Carlos Castaneda, *Les Enseignements de Don Juan*

The methodological aspects of a geotechnical rock core analysis and characterization based on medical XRCT is presented in this chapter.

It is subdivided into two parts:

- 1) Development of a new segmentation tool for rock core analysis at the obtained medical XRCT resolution (CARact3D).
- 2) Implementation of segmented XRCT stacks in the geological and mechanical characterization of geotechnical rock cores.

The second point can be understood as an attempt to evidence control parameters influencing rock deformation, from both a structural and genetic perspective (i.e. effect of preexisting discontinuities, obvious propagation of deformation in the rock structure by comparing rock cores *before* and *after* triaxial loading).

10.1 IMAGE ANALYSIS TECHNIQUE – CARact 3D METHOD

Tomography produces images where the voxel (3D pixel) intensity is roughly proportional to the density of the material at that point. A histogram of voxel intensities of a porous or fractured material shows distinct peaks at intensities representing the solid material and the void space (Landis, 2006). As such, a simple way to separate the two is to establish a threshold intensity at the minimum between the two peaks (Jain, 1989). If the voxel intensity is above the threshold, it is considered solid while voxel intensities below the threshold are considered void. Accordingly a binary image is produced that can be used for further numerical treatment.

The possibility of performing direct thresholding increases together with decreasing voxel size, as the problem of partial volume effects will be reduced. Optimum voxel sizes are obtained nowadays from high-resolution CT images (Ketcham, 2005; Landis, 2006). Medical XRCT used in this research on geotechnical rock cores limits the spatial resolution to about 0.5 mm. Therefore a same type of geological features can produce inconsistent attenuation contrasts depending on their size, shape and location inside the sample. Rock constituents have densities up to five times above human tissues, organs and bones (**Table 8.1**). Recorded contrasts from rocks are therefore often blurred and partial volume effects complicate the segmentation procedure. The problem of inaccurate direct thresholding of geological features at the resolution of the medical XRCT is visible on **Fig. 10.1**.

To overcome these difficulties and get the most valuable information from XRCT scans on geotechnical rock cores, a specific segmentation technique taking advantage of the raw data, minimizing the use of preliminary mathematical filters and avoiding in this way modifications of the initial raw voxels relationships is envisaged. Accordingly, more grey dynamic is contained in the CT data, no recalculation of the pixel distribution is made and a more precise criterion based on variation in CT signal intensity is possibly adjusted. Using standard image analysis tools, it has been found that filtering processes convert 16 bit files into 8 bit files and suppress therefore a large degree of freedom to adapt local segmentation calculations. The proposed segmentation procedure was implemented as a plugin for the freeware ImageJ™ (rsbweb.nih.gov/ij). The program code CARact3D can be found in **Appendix III**.

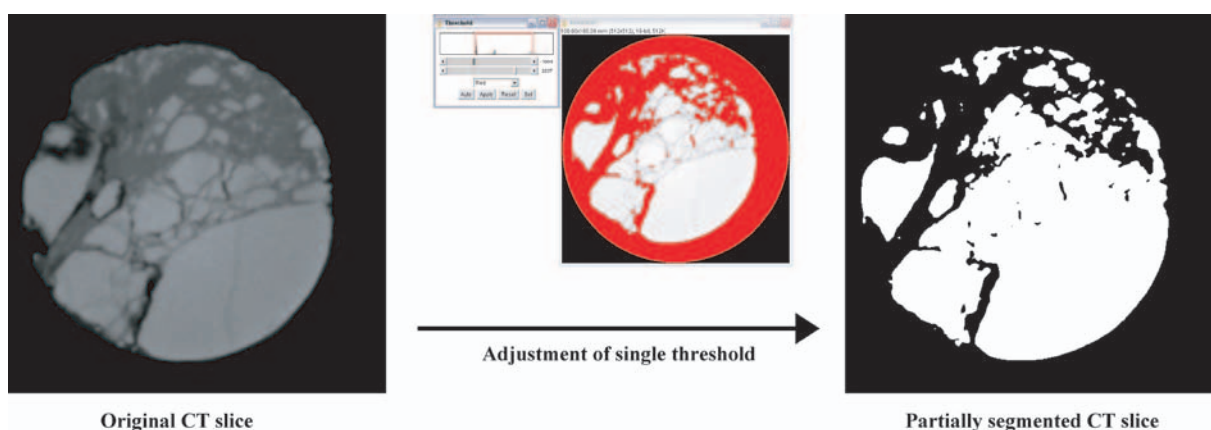


Fig. 10.1 Result of single thresholding performed on a CT slice taken from the medical XRCT acquisition of sample *RSJ 11* (kimmeridgian tectonized limestone, N16 Roche St Jean tunnel, Jura canton, Switzerland). Single thresholding (illustrated by the threshold adjustment windows of ImageJ™) fails to reproduce accurately the structures depicted inside the rock and result in a partially segmented binary image. This is unsatisfactory in terms of rock core characterization. An alternative segmentation technique is proposed in this research under the name CARact3D. Rock core diameter is 81.7 mm.

10.1.1 Detection Principles and Geological Features of Interest

The problem of quantitative image analysis is a prolific subject in the field of geology. From the many analysis facilities in use, thin sections are of particular interest for quantitative petrography (see **Chap. 3**). With the progress of indirect imaging using irradiation techniques, precise 3D segmentation tools for object-based analysis became essential (*Aguet et al.*, 2005; *Ketcham*, 2005).

3D grain fabrics measurements envisaged by *Ketcham* (2005) involve high-resolution tomographic images as it is based on contrasts in voxel intensities between adjacent objects. The use of steerable filters as proposed by *Aguet et al.* (2005) is based on specific shapes to detect (e.g. curve and surface detectors based on second-order Gaussian derivatives). However, segmentation procedures based on 3D steerable filters unsatisfactorily reproduce geological features in their shape and size variations inside a sample. In particular interconnected objects like fractures are isolated as segments, impairing on the geological relevance of the quantitative analysis.

A technique to segment typical rock features as they appear on medical CT-scans, e.g. as imperfectly voxelized objects, has been specifically developed in this research. This technique is based on a *first global segmentation* procedure isolating all features of interest having well resolved dimensions. A *second local segmentation* is further implemented which refines the detection by tracking the considered feature at sizes close to the detection limit. Typical features of interest (FOI) from rocks of various petrologies investigated by medical CT scans are summarized in **Fig. 10.2**.

Note: To be resolved, a feature within the sample volume must typically span several voxels in at least one dimension, and more favourably in two or three (*Ketcham*, 2005). Positive identification and measurement of objects is therefore a matter of object form and size. For clasts, approximately 3 voxel widths in diameter are required to produce a detectable contrast from the surrounding matrix. For fractures, detectable widths can be less than one voxel because it is extended by several voxels in the other two dimensions.

10.1.2 Segmentation Method and Application

To define segmentation criteria, the study of intensity profiles from single CT-slices together with their second derivative sensitivity has been found very powerful. Accordingly, ranges of grey values corresponding at best to the FOI to detect can be extracted. **Fig. 10.3** illustrates the general methodology of the proposed segmentation principles for rock analysis as depicted by medical XRCT.

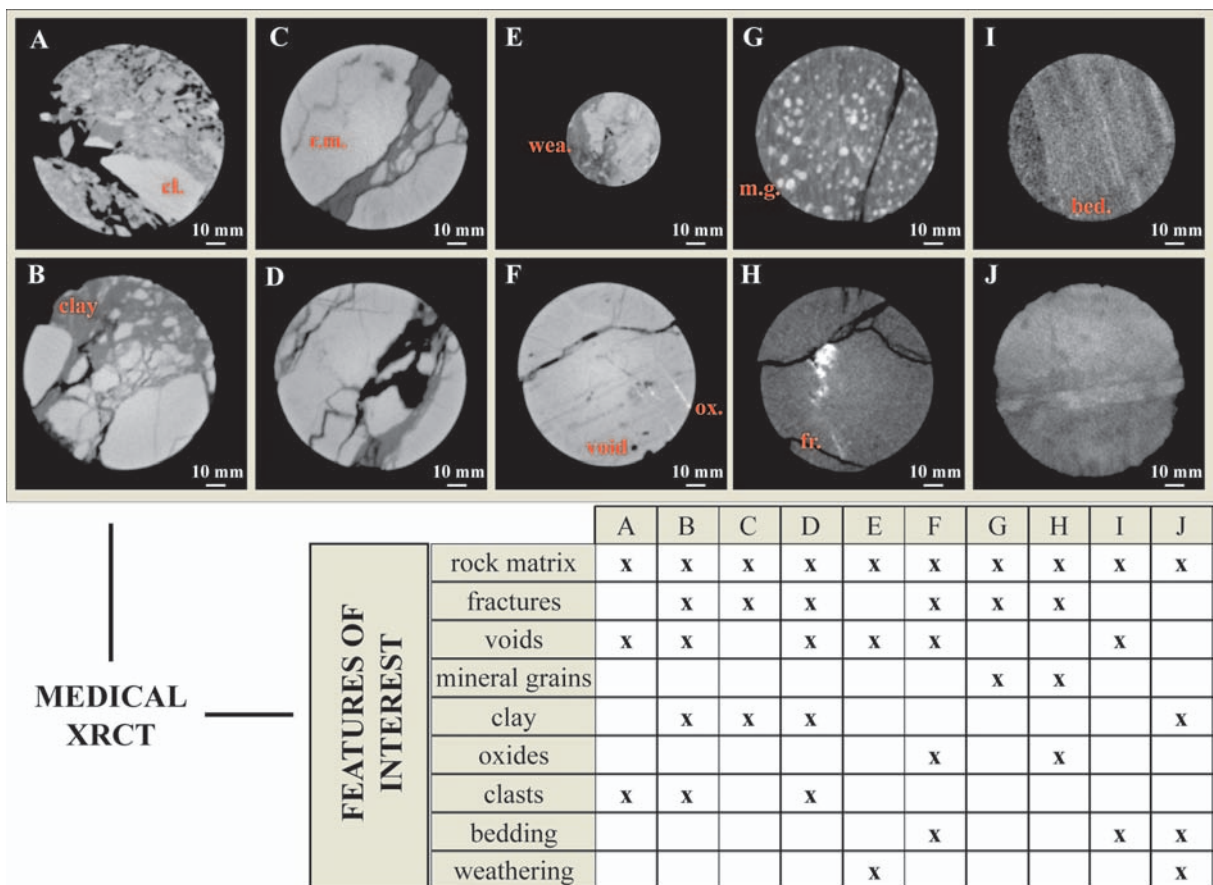


Fig. 10.2 Visual appreciation of the application domain of medical XRCT for rock imaging. Illustration of single CT-slices from rock samples of different petrologies after medical XRCT investigation, depicting the geological features of interest (FOI) analyzable and resolvable with this technique. Resolution of such features is related to density contrasts produced by void spaces inside the rock mass, e.g. pores and fractures or density contrasts produced by the rock composition itself, e.g. alteration zones, presence of phenocrysts, grains or clasts as well as weathered zones and bedding discontinuities. Each rock core has a diameter of 80 mm except rock core **E**) having a diameter of 55 mm. **A**) Polygenic breccia made of metamorphic clasts cemented by calcite. **B**) Carbonatic breccia of tectonic origin. **C**) & **D**) Fractured limestone, open and sealed fractures. **E**) Limestone showing evidence of matrix alteration. **F**) Dolostone showing pyritisation. **G**) Garnet and mica gneiss. **H**) Medium-grained sandstone depicting graphite inclusions. **I**) Medium-grained sandstone showing bedding planes. **J**) Marl made of more than 50% clay showing weathered zones inside the matrix. On the CT-slices, labels mean: cl. – clasts; clay – damaged rock matrix; r.m. – primary rock matrix; wea. – weathering; void – primary or secondary porosity; ox. – oxides; m.g. – mineral grains; fr. – fractures; bed. – bedding.

The segmentation method has been calibrated based on a medical XRCT acquisition of a brecciated rock core denominated Eye 1 (A9 Eyholz tunnel in canton Wallis, Switzerland, **Chap. 5**). Sample diameter is 76 mm for a length of 90 mm. This sample has been chosen because it exhibits a geological feature size accurately detected by the medical XRCT. Accordingly it was estimated as an ideal material for calibration purposes of the method. It consists of millimetrical to centimetrical angular clasts of polygenic origin that were cemented by strongly mineralized water circulation and concurrent calcitic precipitation into important void spaces. Mineralogy of the clasts has been determined on the base of thin section analysis and indicates mus+chl+qtz+fsp-tlc paragenesis with single quartzite-, calcschist- and gneiss-pebbles. Small clasts tend to be monocristalline. A very fine-grained undifferentiated matrix is also visible but was not further quantified (**Fig. 10.4**).

The proposed FOI considered to study the improved segmentation of the CT data corresponds in the case of Eye 1 to the void space defining a macro-porosity. Indicative sample porosity has been determined by picnometry at a value of 10.5%. This value will be used to confront the accuracy of the indirect void space detection. Even if no determination of the microporosity will be possible

at the medical XRCT resolution, the nature of the sample and the size of void spaces were judged appropriate to perform such a confrontation for calibration purposes of the detection method, e.g. the value of 10.5% being assumed produced mainly by the macropores.

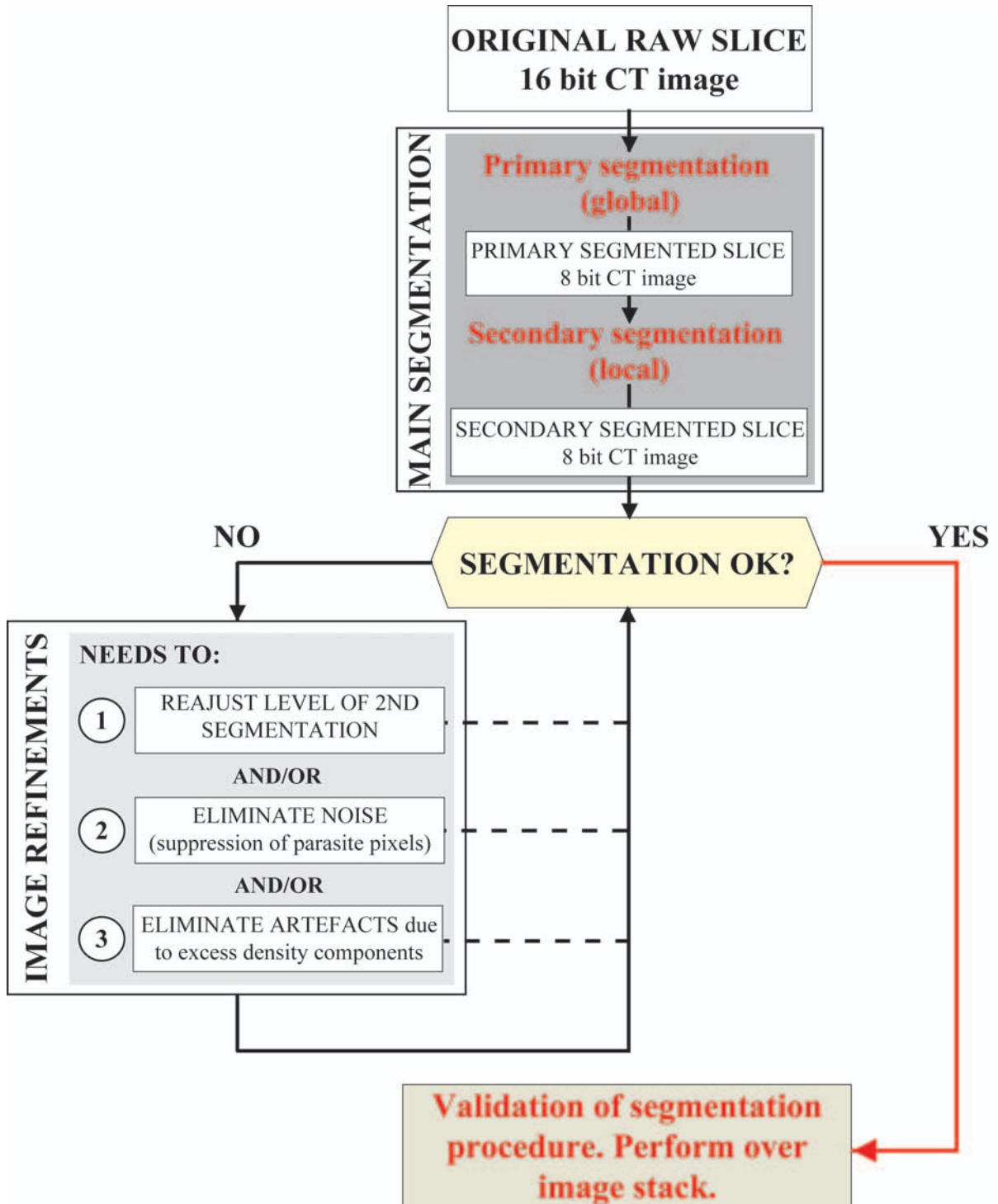


Fig. 10.3 Segmentation procedure for the improved detection of geological features from XRCT raw data acquisition. Main segmentation implies the primary (global) and secondary (local) segmentations. Image refinements are possible if needed and provide 2 tools for the correction of the segmented data concerning the removing of isolated parasite pixels and the elimination of typical artifacts induced by the presence of components displaying excess densities in regard to a particular segmentation task.

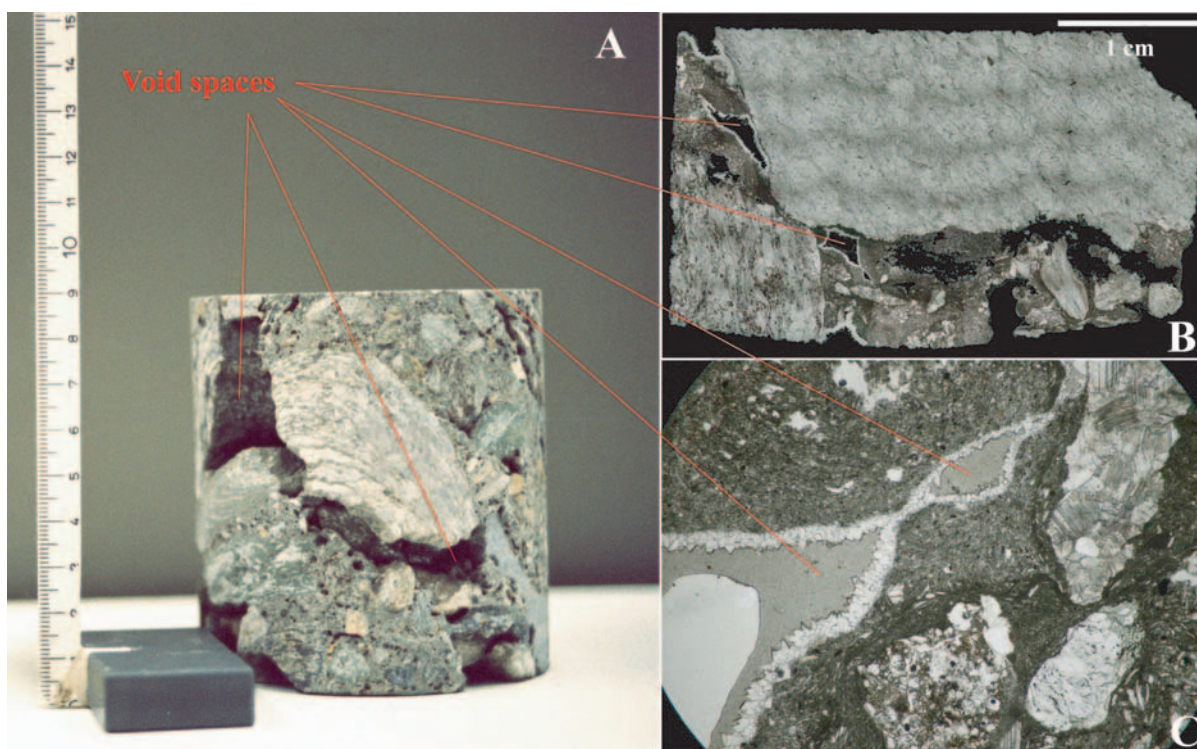


Fig. 10.4 Sample Eye 1 used in this study as calibration material for the development of the segmentation routine based on its geological features (voids) of important dimensions and adequate rendering on XRCT images. See text for explanation. **A)** Hand specimen. **B)** Typical thin section view. Scale given by the bar. **C)** Thin section under light microscope, magnification 25x.

10.1.3 Primary Segmentation (global)

Primary segmentation means the rough elimination of grey values above a given threshold corresponding to the void space to be detected. In general, void spaces should give CT values of -1000 to 0 HU, which corresponds to the Hounsfield units as defined for air (0 g/cm^3) and water (1 g/cm^3) and corresponding theoretically to 31768 grey unit for air and 32768 grey unit for water (16 bit grey scale). Optimal values for a primary segmentation not overestimating the effective void space but being a best-fit in regard to the CT-data resolution and consequent voxel size are therefore required to perform the first step in the FOI detection. With this procedure, all features of interest clearly above the detection limit (features $> 5 \text{ mm}$) are detected.

By applying different thresholds to a representative CT slice from the Eye 1 XRCT stack (slice 100), a variation of the segmented void space is obtained (**Fig. 10.5**). An inflection point is delimited at a grey value of 816 HU (33584 grey level) which is namely the mean value in between air density (-1000 HU, 31768 grey level) and undifferentiated rock matrix (2632 HU, 35400 grey level). The primary segmentation threshold is accordingly fixed as the mean grey value between the average rock matrix (in the studied case 35400) and a slightly conservative value for the FOI (e.g. voids set at 32000 instead of ideally 31768, to take into account the imperfect resolution of the medical CT scan).

Result of the segmentation performed with a threshold set at 33700 is depicted on **Fig. 10.6 A**, together with the original raw 16 bit CT slice and the grey value histogram evidencing two maxima for the void and average rock matrix CT signals. As observed, only the biggest void spaces are detected, but smaller voids visible by eye on the raw data fail to be reproduced. Nevertheless, the selected primary segmentation doesn't overestimate the size of the feature to detect giving free room to adapt the detection for smaller sized void spaces.

When performing the primary segmentation at the 33700 threshold all over the XRCT stack represented by sample Eye 1, total void space value lies by about 6% (**Fig. 10.5 B**), which is clearly under the value of 10.5% determined by picnometry.

After completion of a primary segmentation, the detection therefore underestimates the spatial distribution of the FOI as only the objects having sizes far above the scanner resolution will be adequately depicted. By getting closer to the detection limit, e.g. towards smaller feature sizes, the object would be less accurately depicted (e.g. partial detection) and the smallest void spaces would not be displayed on the segmented image (see **Fig. 10.6 A**).

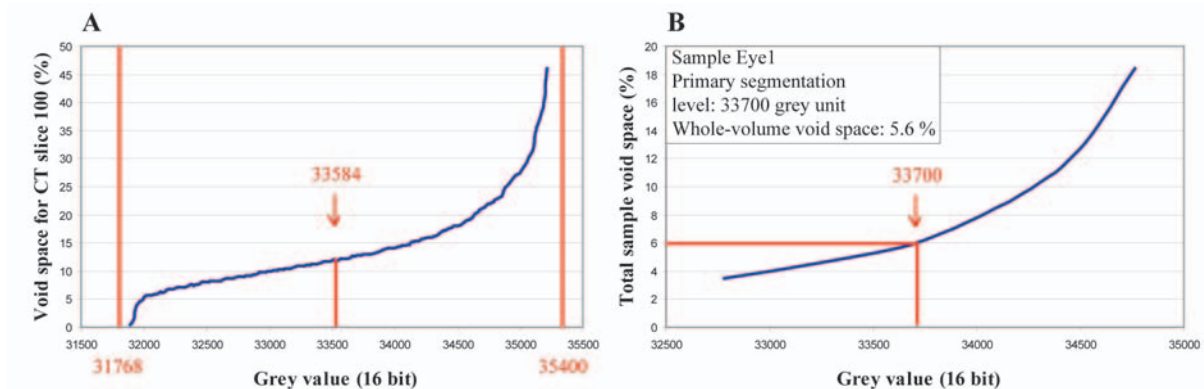


Fig. 10.5 A) Evolution of void space percentage according to the segmentation level for a single CT slice of sample Eye 1. Theoretical void space would display a value of 31768 (corresponding to -1000 HU) and the average rock matrix of Eye 1 is 35400 (2632 HU). The inflection point of the curve is given at a grey value of 33584 which is the mean value between the FOI (void space) and the average rock matrix. **B)** Considering the primary segmentation at a slightly conservative threshold of 33700 and performing a void space calculation over the entire XRCT stack represented by sample Eye 1, the porosity value lies by 6%, which is far below the real value calculated in the lab by picnometry at 10.5%.

10.1.4 Secondary Segmentation (local)

For small sized objects close to the resolution potential of the medical CT, partial volume effects arise and the FOI is found sharing common voxels with the surrounding rock matrix, increasing the apparent grey value displayed, e.g. giving a void grey level signal in between the primary segmentation level (33700) and the value for average rock matrix (35400). In order to refine the detection process, an argument to decide which intensity deflections should be interpreted as FOI or rejected as matrix during a secondary segmentation must be defined.

Fig. 10.6 B illustrates the procedure for secondary segmentation based on Eye 1 CT slice 100. Three profile lines across contrasting portions of the slice are presented:

- **Profile 1:** characterized by the homogeneous rock matrix (e.g. average rock matrix). The variations of the second-derivative are small and stay in a density range of $[-500; 500]$. Little fluctuations (“noise”) in CT intensities is assumed reflecting the medical XRCT resolution.
- **Profile 2:** profile line through a void of about 1 cm width (e.g. far above the detection limit of the scanner). The CT intensity makes a strong deflection passing from the average rock matrix into the void (e.g. -6000 grey levels). Such strong contrasts are readily detected with the primary global segmentation.

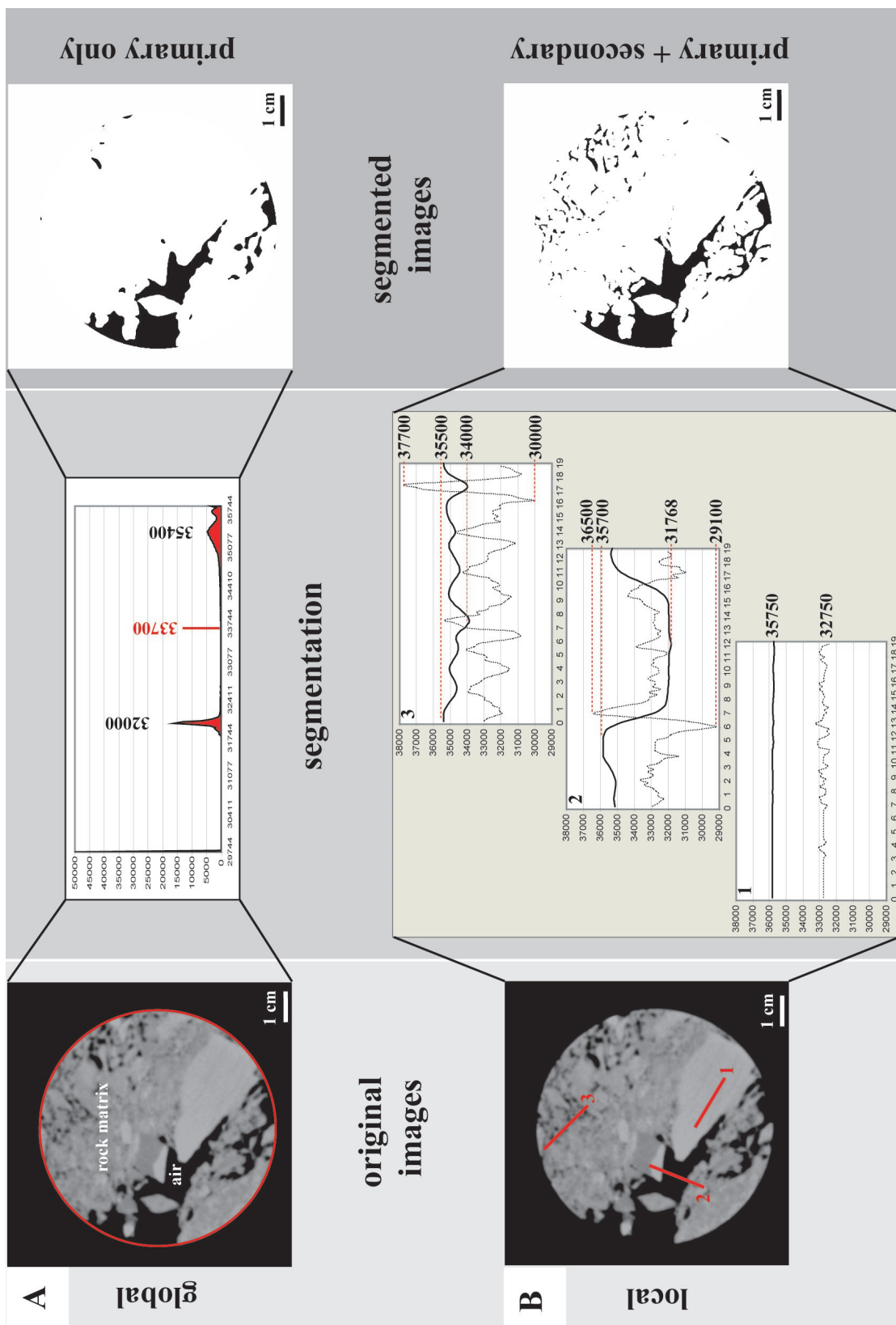


Fig. 10.6 Single CT slice of sample Eye 1 displaying important void spaces and used to illustrate the primary and secondary segmentation procedures envisaged in this study. **A)** Raw data, global consideration, general histogram and segmented slice at the primary threshold value set as the mean grey value between average rock matrix and best-fit value of the feature to detect. **B)** Raw data, local consideration depicted by CT-profile lines and segmented slice after primary + secondary segmentation. For the 3 CT-profiles across the image surface, CT-intensity curves (black) and corresponding second derivative curves (dotted black) are plotted. A local secondary segmentation can be adapted with a criterion based on the second derivative, which allows detection of void features having sizes close to the medical XRCT resolution. See text for further explanations.

- **Profile 3:** profile across small sized voids clearly visible by eye on the raw CT data but not detected during the primary segmentation. Such feature sizes produce more subtle intensity deflections of about 500-1200 grey levels that are too close from the average rock matrix value to be segmented using single threshold intensity. The observed signal deflections induce however strong second-derivative variations.

Introducing a criterion onto the second derivative permits accordingly to fix secondary local threshold values permitting a refinement of the detection procedure that includes the smaller void spaces.

10.1.4.1 Mathematical Formulation of the Secondary Segmentation

Fig. 10.6 B shows that for Eye 1 a local secondary detection requires detecting CT intensity deflections in the order of 500-1200. Such deflections produce characteristic second-derivative peaks of 1000-7500 grey level/mm². A positive detection can therefore be envisaged once the second-derivative exceeds a defined value that is related to the form and the depth of the CT intensity deflection.

To exemplify this, advantage is taken from a simple sinusoidal model proposed to simulate such intensity deflections (**Fig. 10.7**). A deflection produced by a local evolution of the CT intensity is therefore taken corresponding to:

$$(Eq. 10.1) \quad f(x) = f_0 + A \cos\left(\frac{2\pi}{l} x\right),$$

with

f_0 = mean CT intensity along a given profile line,

A = half-depth of the intensity deflection,

l = influence length, e.g. function of the given FOI width.

From (**Eq. 10.1**) it follows that:

$$f''(x) = -\frac{4\pi^2}{l^2} A \cos\left(\frac{2\pi}{l} x\right) = -\frac{4\pi^2}{l^2} (f(x) - f_0).$$

Given C , the detection criterion imposed on the second-derivative, following condition can be set:

$$|f''(x)| > C \quad \Leftrightarrow \quad f(x) < f_0 - \frac{Cl^2}{4\pi^2}.$$

Local void space detection is given for:

$$(Eq. 10.2) \quad C < \frac{4\pi^2}{l^2} A,$$

The second-derivative criterion acts therefore as a detection parameter evaluating the properties of the CT intensity deflection being proportional to its depth and inversely proportional to its length.

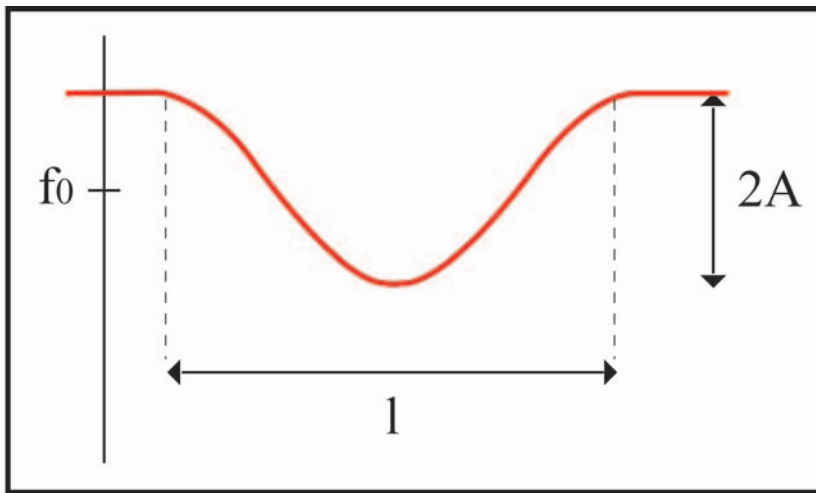


Fig. 10.7 Sinusoidal curve taken as mathematical model for the local segmentation of grey level drops induced by small-sized features that are not detected when a primary global segmentation is performed. Form, depth and aperture of the curve are parameters of importance in the selection of the secondary segmentation level. See text for explanation.

Following relationship is further established to introduce the implementation parameter c permitting adaptation of the level of secondary segmentation in CARact3D. The improved detection is accordingly realized for intensity deflections in the order of 1000 CT units based on a given CT intensity difference Δ between the CT signals corresponding to **a)** average rock matrix and **b)** the chosen FOI:

$$\text{(Eq. 10.3)} \quad C = c \frac{\Delta}{1000} \quad \text{and} \quad \frac{C}{\Delta} = \frac{c}{1000}$$

Taken $\Delta = 4000$ in the case of Eye 1 for the intensity difference between average rock matrix (36000 CT units) and void spaces (32000 CT units), adaptation of the parameter c for a given secondary segmentation can be realized in CARact3D with regard to detection of CT deflections corresponding to 1000.

A calibration chart for the secondary segmentation in function of different values of c is presented in **Fig. 10.8**. Accordingly, any secondary segmentation can be adjusted to the voxel size of the FOI causing an observed intensity deflection on the CT data. In the case of Eye 1, a given void space would then *at least* be detected if it induces a CT deflection corresponding to the value indicated by the criterion curve (note that y-values correspond to the half-depth of the intensity deflection, i.e. A).

Note: As an indication for typical contrast of tomodensities observed on rock materials, taking for c of 10 to 20 allows detecting numerous small features visible on the CT scan by eye. A too small c would however produce noise, as small fluctuations inside the matrix itself (e.g. textural inhomogeneities) would be detected as well. Therefore, initial inspection of the CT intensity levels represented by the stack to analyze and the FOI to detect is required before performing the calculation. This can be achieved easily by producing a histogram of grey level distribution represented by the XRCT stack. Accordingly, a best-fit c -value can be defined.

In order to take into account the variable geometry of a given FOI and to permit an accurate detection of rounded as well as linear features, secondary segmentation is performed along 4 cardinal directions over the CT slices constituting the XRCT stack (e.g. *N-S, NE-SW, E-W, SE-NW*). Brought in relation with the resolution obtained for rock core analyses from medical XRCT, this has been assumed precise enough. Moreover the approach has the advantage not to excessively slow down the calculation time by the computer.

Amelioration in FOI detection is visible on **Fig. 10.6 B** for the same CT slice from sample Eye 1 on which the primary segmentation was performed. The whole volume voids calculation performed on the segmented stack give now a value of 10.3%, being therefore quasi identical with the picnometry

determined value (10.5%).

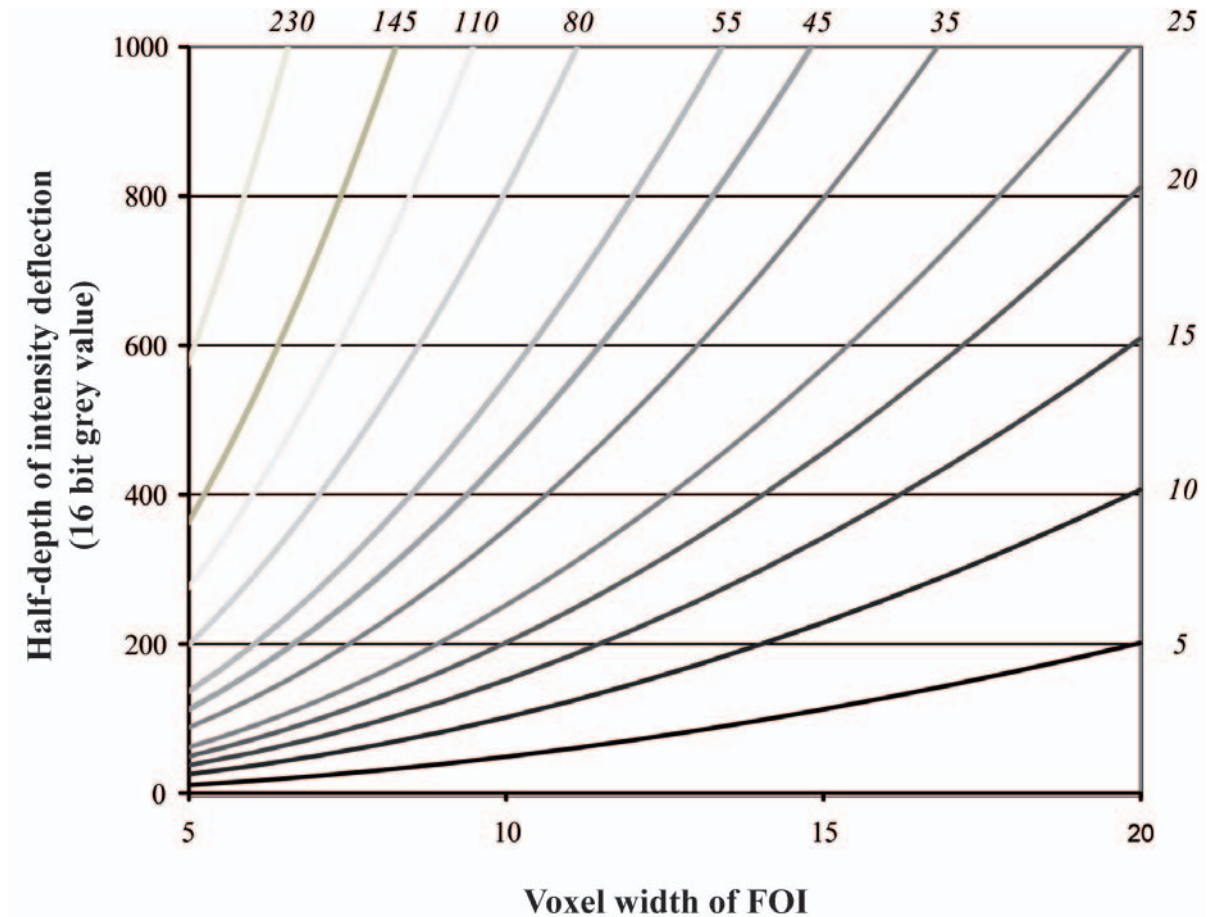


Fig. 10.8 Chart used for the calibration of the local secondary segmentation based on local evolutions of the CT intensity curve and sensitivity of its second-derivative (Eq. 10.3). All detection criterion c are taken assuming a difference Δ of 4000 between average rock matrix and the FOI to detect. Detection curves are accordingly represented for c taken in between 5 and 230. Reading is as follow: FOI detection for a 10 voxel wide feature with a criterion $c = 35$ requires a theoretical CT intensity deflection of at least $2 \times 360 = 720$ grey levels. With a criterion $c = 15$, the same FOI would be detected by producing only a difference of about 300 grey levels between FOI and average rock matrix.

10.1.5 Noise Elimination

The problem of noise appearance is related to the reduction of the secondary segmentation value c when the FOI gets very close to the XRCT detection limit. Noise is expected to arise for small values of c (i.e. between 5 and 15). When a local threshold is performed at that level, isolated or small groups of voxels <10 will appear.

In order to “clean” the segmented image from this resulting noise a specific function has been added to the detection procedure (Fig. 10.3). It offers the possibility to choose how many isolated voxels must be removed from the resulting detection according to the number of neighbors under which it is assumed that the detected voxel is clearly not belonging to void spaces. In this process, values of noise elimination are set between 0 and 7. A value of 0 means that each isolated detected voxel is removed from the segmented image. The other extreme value of 7 produces the elimination of any detected voxels having at most 7 void neighbors.

Note: Applying this function improves the quality of the segmented stack by cleaning it from detection artifacts reflecting the medical XRCT resolution. In ideal cases, noise elimination values should stay in the range 0-2, as such values have low impact on the already detected features. When initial image quality is so that higher noise elimination values should be adopted, the user must be aware that the noise removing process would affect the detected features

from the primary and secondary segmentations. However, when segmented XRCT stacks are reconstructed in 3D, the quality of the visualization will benefit from noise-free single CT-slices. Examples of 3D reconstructed segmented stacks will be presented in **Chap. 11** & **12** and further discussed in **Chap. 13**.

10.1.6 Overdensity Elimination

The last feature of the detection procedure concerns the elimination of artifacts produced by components having excess tomodensities in regard to the values presented by the average rock matrix and the FOI. Excess tomodensities are related to high-density components $>4 \text{ g/cm}^3$ as represented by some mineral grains. Such grains displays CT intensities in the order of 37000 (see **Table 8.1**). Such local excess intensities give rise to abnormal second derivatives that are taken into account and influence local secondary segmentation.

As exemplified by a single CT slice taken from a gneissic rock sampled at the Ceneri Base Tunnel site (**section 5.3.9**), the idiomorphic garnet grains affect the primary and secondary segmentations aiming the detection of a transversal fracture. The typical segmentation pattern produced by such heavy mineral grains corresponds to voxel groups displayed as small circles on the segmented images (**Fig. 10.9**).

Given the known grey value of these local overdensities, the function developed here allows removing these unwanted detected voxels from the final segmented image (**Fig 10.9**). It acts therefore as a kind of detection prohibition level that would be respected while performing the local secondary segmentation without influencing the principles of primary and secondary segmentations.

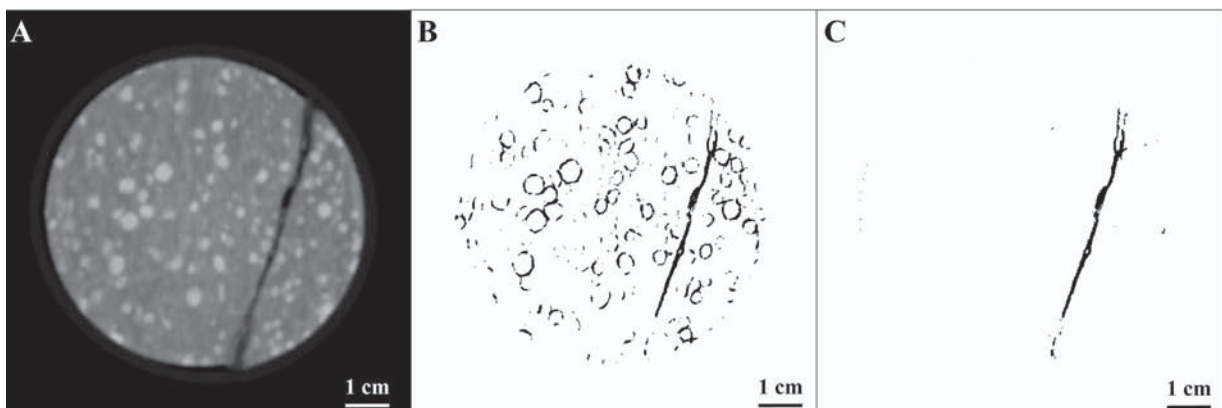


Fig. 10.9 Single CT slice of sample CBT 2 displaying important proportion of garnet mineral grains having density far above the average rock matrix. **A)** Raw data. **B)** Result of fracture detection after the primary and secondary segmentations, using the mean value between average rock matrix and ideal value of the feature to detect for the global detection and a criterion $c = 20$ for the local detection. Important artifacts produced by the garnet grains are noticed. **C)** Same primary and secondary segmentation as for **B)** but using this time the function for overdensity elimination.

10.1.7 Results and Preliminary Discussion

The segmentation tool developed for ImageJTM has been tested on a serie of rock CT slices taken from XRCT acquisitions on geotechnical rock cores of contrasting petrologies. **Fig. 10.10** presents different segmentation tasks. They range from void and crack detections (**Fig. 10.10 A, B, C, D, & E**), to clast, matrix and single mineral grains detections (**Fig. 10.10 A, C, E & F**), and even an attempt of bedding detection on a sample of medium-grained sandstone was performed (**Fig. 10.10 G**). Depending on the type of rocks and structural variability, different segmentation tasks on the same slice can be performed.

For geological applications at the resolution of a medical CT scanner, the detection of such elements

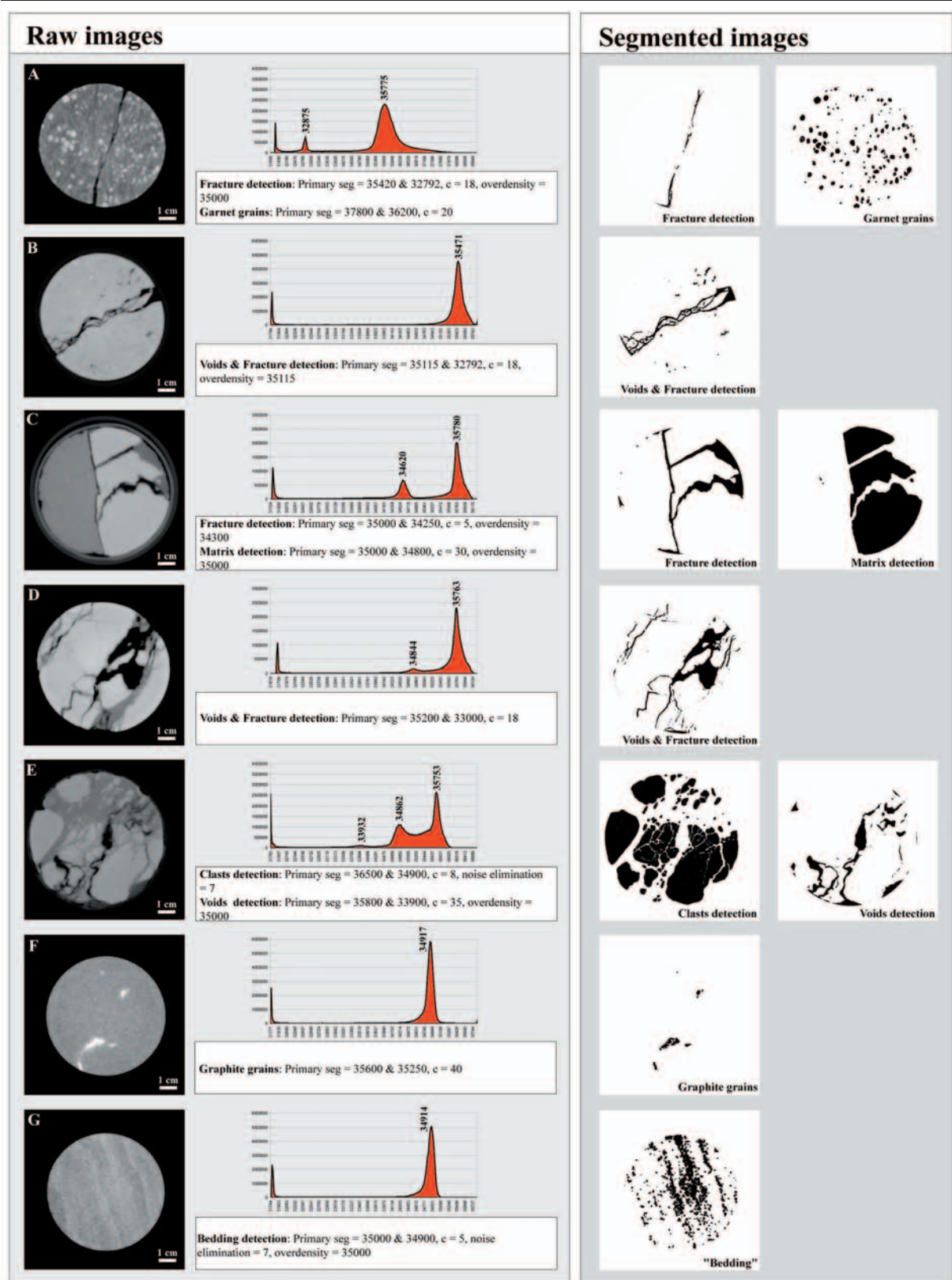


Fig. 10.10 Single CT slices from different rock core samples before and after particular feature detection using the segmentation tool developed for ImageJ™. For each presented CT slice, the grey level histogram (16 bit) is depicted together with retained segmentation parameters. Different segmentation tasks can be performed on a same single slice (or entire image stack). **A)** Deformed garnet gneiss sampled on the AlpTransit site of the Ceneri Base Tunnel, Switzerland. **B)** Triaxially deformed dolomitic limestone from the Glion tunnel, A9 highway, Switzerland. **C), D) & E)** Tectonic limestone from the Roche-St-Jean tunnel, N16 highway site, Switzerland. **F) & G)** Sandstone from Belmont landslide, Switzerland.

is clearly improved by our segmentation method and a better rock mass characterization of the rock cores under study can be expected. A limitation concerns certainly the fact that the segmentations performed with CARact3D regroups contrasted petrographical entities due to the difficulty in assessing each geological feature separately as a result of the medical XRCT resolution.

At this stage, we are conscious that CARact3D is still too much user dependent and that improvements have to be made in this sense to facilitate its implementation. The presented segmentation procedure has however the advantage to be rapid and functional on any PC platform. Moreover, with better resolved images (e.g. scans from industrial scanners producing a smaller voxel size), the detection based on the developed methodology would gain in accuracy and improve rock mass prognosis based on critical 3D evidences obtained from XRCT acquisitions at the geotechnical rock core scale.

10.2 CATACLASTIC ROCK CORE CHARACTERIZATION USING MEDICAL XRCT

As presented in the methodological chart of **Fig. 4.4**, both the geological and geomechanical characterizations of cataclastic rock cores are performed with a specific implementation of medical XRCT. Next to its visualizing capacities that have been presented in **Chap. 8 & 9** for indirect rock core imaging, two specific quantitative procedures have been developed within this research.

The first aims to derive the TC & MC parameters of the MSI equation (**Eq. 3.1**) directly from the XRCT data. Accordingly, an evaluation of the MC and TC variability inside a same sample can be obtained. Moreover, the determination of these parameters on the same rock core used for triaxial testing introduces an advantageous 1:1 confrontation between the MSI and the mechanical data.

The second implements more specifically the segmentation procedure presented above and addresses the 3D reconstruction of segmented XRCT stacks obtained on rock cores. At the medical XRCT resolution this approach corresponds to an attempt of bringing in relation 3D resolved geological features with a particular deformation process that results from a triaxial loading experiment (see **Fig. 9.4**). Based on such models, the quantitative analysis of 3D petrographical elements can be envisaged and the effect of their spatial distribution on rock deformation most possibly assessed.

These two procedures envisaged for characterization purposes are described hereafter.

10.2.1 Derivation of TC & MC from XRCT slices

Evidences from cataclasites of different petrological contents indicate that their structural relationships often requires a bigger field of view than thin sections to be accurately assessed in a geotechnical characterization. According to petrology and its influence on cataclasis, a clear separation of clast and matrix phases can become in particular difficult. To overcome this problem, slices from medical XRCT one order of magnitude below the thin section resolution but allowing a full coverage of the rock core structures can be used to derive the TC & MC parameters.

Studying CT slices in orientations parallel to the rock core axis is estimated a powerful approach to confront with result of triaxial tests, as the spatial orientation of pre-existing geological structures can be directly related with the apparition of rupture planes. This consideration was already followed by *Bürgi* (1999) for the MSI determination. Special focus is therefore put in this study on the xz- and yz-CT slices.

As the XRCT acquires raw data corresponding to the xy-view, CT slices in the frontal (xz) and sagittal (yz) planes (e.g. parallel to rock core axis) have to be produced with VGStudioMAX

(Chap. 8). CT slices in xz - and yz -directions are therefore taken at regular increments through the volume what permits a good coverage of the structural and textural evolution inside a rock core (Fig. 10.11).

The TC & MC parameters are defined on binary masks in the same way as described in section 7.2.2, replacing the numerized thin section masks with CT masks. In comparison with *Bürgi* (1999), where one cataclastic sample was characterized by means of a single thin section, this approach allows performing several TC & MC determinations per sample, what is expected to improve the reliability of the derived parameters, making them more “volumetric”. Accordingly, the derived parameters are averaged to determine a MSI_{XRCT} and the specific constituents of the TC & MC parameters can be compared with each other to aid in the improved geological characterization of rock cores (structurally homogeneous vs. heterogenous rock cores).

Note: For the MC calculations, orientation factors δ have been determined slice by slice (local orientation factors) but a determination involving the representation of all discontinuity trace lines for the studied xz - and yz -views (cumulative length T_{LL} over the xz - and yz -slices in function of the measured orientations β) has been addressed to define global xz and yz orientation factors, in order to be more representative of the main orientation of discontinuities over the sample volume in these planes.

Moreover, in samples displaying a clastic nature, side of clasts were taken as discontinuities in MC determinations. Using both a local and global orientation factor, a mean local MC and a global MC in xz - and yz -directions has been calculated. This is done in order to evaluate how a MC parameter can vary when determined on orthogonal planes, providing a pertinent measure of sample heterogeneity & anisotropy.

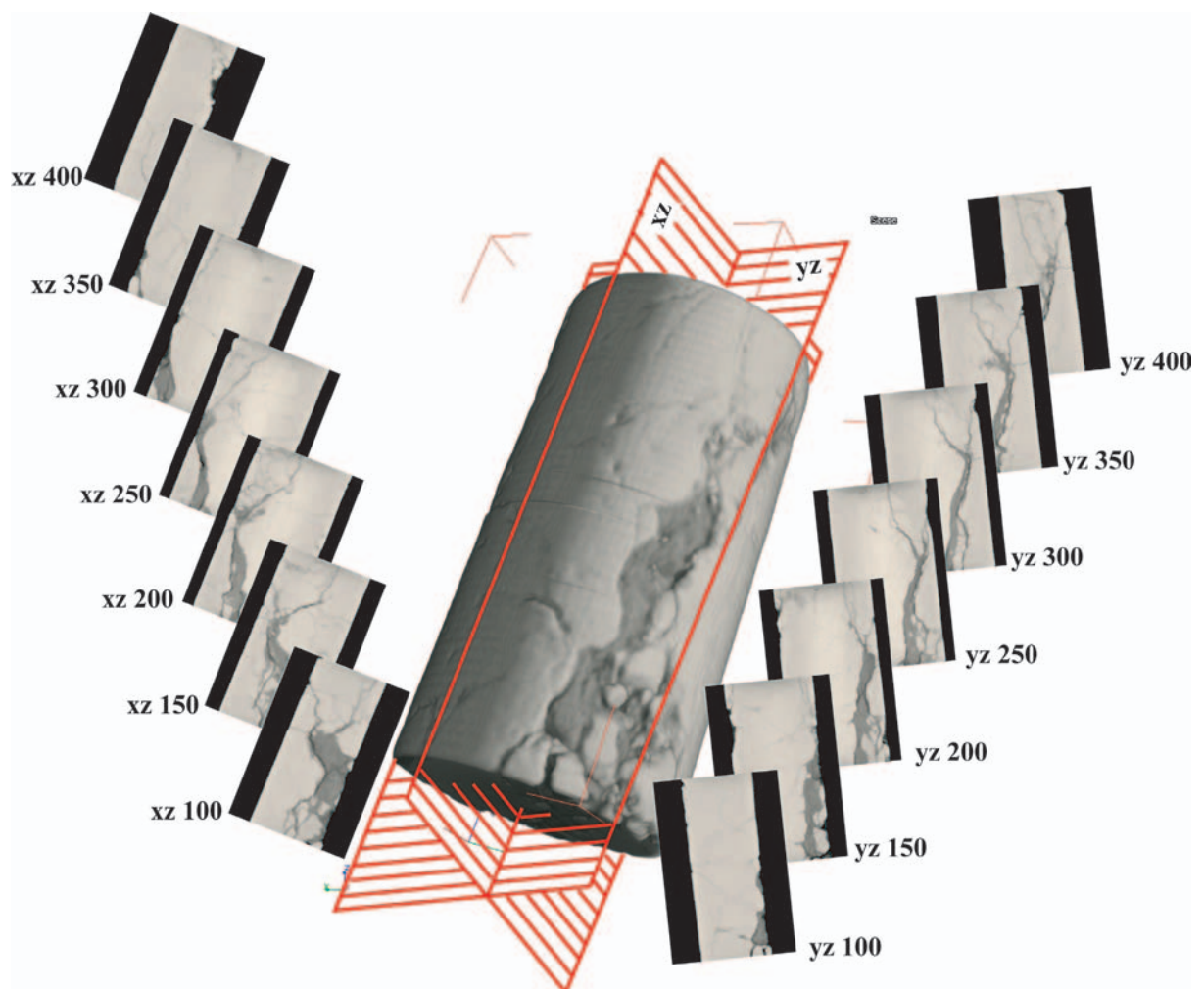


Fig. 10.11 Selection of CT slices for TC & MC determinations on a rock core acquisition by XRCT. In comparison to the methodology implemented by *Bürgi* (1999), this procedure is expected to be more representative of the true sample structure, e.g. summing up 2D TC & MC parameters from a same sample has “volumetric” character.

10.2.2 Study of Damage Indicators from XRCT

The concept of *damage indicators* has been introduced in **Chap. 2 (section 2.4.5)** and is used for the indirect characterization of cataclastic rock cores through a best-fit segmentation of geological features corresponding to damage structures (**Chap. 7, section 7.1.2**). Results of such segmentations can then be reconstructed and visualized in 3D. With such an approach, important consideration about rock heterogeneity and anisotropy can be made. A full quantitative numerical treatment of the structural information depicted by the 3D volume is however still in need of development.

In the present stage, two implementations of damage indicators are realized referred to as *scalar* and *tomographic* representations on **Fig. 4.3**.

10.2.2.1 Quantification of Damage Indicators

To conform to the bimodal “clast-matrix” approach envisaged by *Bürgi* (1999), segmented damage indicators are called the *XRCT-matrix* (i.e. the “weak” rock components). The remaining portions of the indirect rock core that are above the segmentation threshold correspond to the *XRCT-clasts* (i.e. the “hard” rock components). The prefix *XRCT* is used to remind us that these determinations are based on medical XRCT data and correspond to best-fit detections using CARact3D for the improved segmentation of geological features at the resolution potential of the technique.

For this task, 4 slices per sample representative of the structural size variation inside the rock core were selected and best-fit segmentation parameters are determined (**Fig. 10.12**). After this calibration step, segmentation is realized over the entire XRCT volume and the proportion of damage indicators can be calculated as well as their geometrical arrangement visualized. To characterize a degree of tectonic alteration, the damage index *DI* is used as a measure of damage inside the sample by comparison with sample volume ($XRCT_{\text{volume}}$):

$$(Eq. 10.6) \quad DI = \frac{XRCT_{\text{matrix}}}{XRCT_{\text{volume}}}$$

By using such a ratio, it is possible to perform an indirect assessment of rock core quality (quantification of damage indicators) and to compare it with the quality assessment made visually on the sample periphery (see **Fig. 4.3**). Moreover, for a given sample, the ratio can be recalculated using identical segmentation parameters from the XRCT acquisition after triaxial test and used in the confrontation of the geological and geomechanical characterization procedures.

10.2.2.2 3D Visualization of Damage Indicators

Segmented XRCT stacks –when reconstructed in 3D– highlight the structural complexity of cataclastic samples as represented by *damage indicators*. Such 3D reconstructions are realized on the acquisitions *before* and *after* triaxial tests. Accordingly, they are expected helping in the interpretation of triaxial data and overall cataclastic rock core characterization as they allow the critic of pre-existing rock structures in terms of their influence on rock deformation (**Fig. 10.12 B**). In particular, deformation mechanisms could be better explained by confrontation with evidences from the indirect geological characterization. With such tomographic models, geological structures could be spatially analyzed in 3D and input parameters from the geological characterization could be accordingly determined as tensors (for example preferred orientations defined by the fractures or the clast agencement). This last aspect is thought capable to reduce optimally the uncertainty when a correlation in between geological and mechanical characteristics of cataclastic rocks is addressed.

Based on the feature detection method described in this chapter, 3D reconstructions of segmented stacks will be presented in **Chap. 11 & 12** *before* and *after* they underwent triaxial deformation. A general discussion about the possibilities to adapt the characterization procedure envisaged by

Bürgi (1999) from 2D thin section to a fully three-dimensional characterization is addressed in Chap. 13 and put in perspective in Chap. 14.

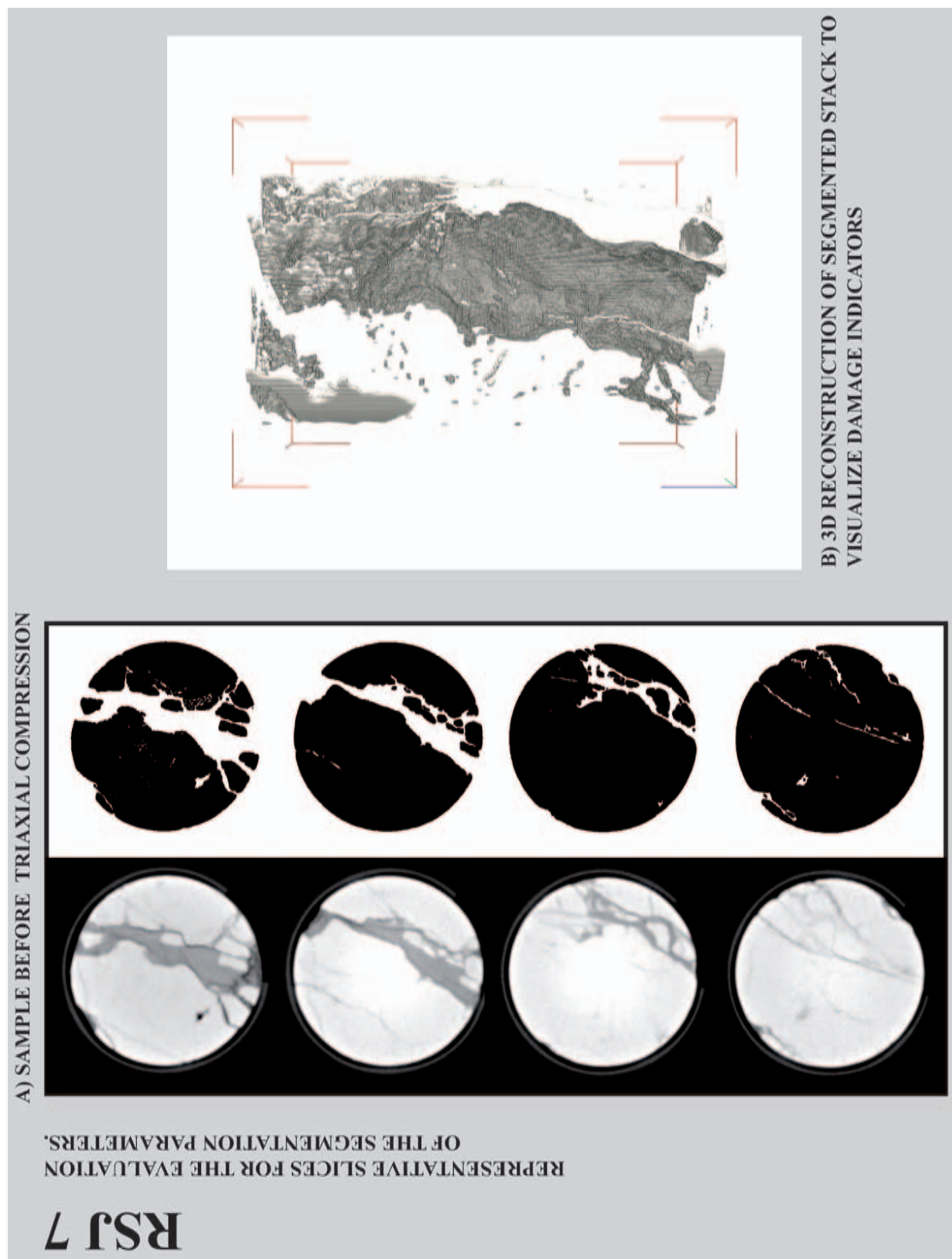


Fig. 10.12 A) Principles of the study of damage indicators from XRCT acquisition of cataclastic rock cores of geotechnical dimensions. Example of sample *RSJ 7*. A full acquisition represents about 500 xy-images. In order to find best-fit segmentation parameters, 4 calibration slices per sample are selected and best-fit segmentation parameters are defined. On these slices, segmentation parameters are adjusted to find out best results. Primary segmentation is calibrated in regard to the grey level histogram distribution over the sample. Secondary segmentation is then tested for different values of the detection criterion c (trial and error process). In order to prevent segmentation bias induced by top and base of the rock core against XRCT irradiation, the 10-20 first and last slices are suppressed from the XRCT stacks. B) A 3D reconstruction of the segmented damage indicators. Such a view is interesting in evaluating possible structural controls provided by the rock structure prior to the realization of mechanical tests. See **Appendices IV-III & V-II**.

11

RESULTS OF THE GEOLOGICAL CHARACTERIZATION

« Si tu es visionnaire à la lumière - ô Mer - de chaque jour
et chaque nuit,
Dis,
qu'est-ce que tu lis dans le courant qui fait ma vie? »
Scourie, septembre 2006

Based on the methodological considerations presented in **Chap. 7**, the protocol of geological characterization has been implemented on a rock core set sampled at the N16 Roche St Jean tunnelling site in the Jura Mountains of Switzerland (see **section 5.3.4** for the geological site description). The set is composed of 12 samples corresponding to tectonized limestones and breccia, denoted in the following *RSJ 1-12*. *RSJ* samples were found exhibiting the widest range of structural states, and as such offer a good scope for examination under the proposed combined geological and geomechanical approach.

All samples were prepared according to standard sample size recommendations for the realization of triaxial tests. XRCT acquisitions were performed on each rock core at CHUV to address the geological characterization on the base of the 3D data. Concurrently, the *RSJ* samples underwent triaxial deformation and a new acquisition by XRCT has then been realized. The description of the mechanical test procedure and further implementation of the XRCT models after deformation in the triaxial cell has been made in **Chap. 9**.

11.1 RESULTS OF THE BULK CHARACTERIZATION

The first step in the geological characterization of geotechnical rock cores is to establish a preliminary classification of the samples based on a visual inspection of their average structure. In the case of fragile samples that don't allow manipulation easily, using in addition the indirect evidence from the raw XRCT acquisition on unprepared samples is helpful.

11.1.1 Definition of Quality Classes for the *RSJ* Samples

Table 11.1 presents the collected *RSJ* samples and describes their structural properties and the visual geological categorization that has been made on them. Cataclastic degrees have been qualitatively assessed and 3 visual classes have been defined:

- **Class I: *Low cataclasis*.** Relative “healthy” rock material, rock matrix mostly defined by hard limestone cement, discontinuities showing calcite recrystallization; samples *RSJ 1*, *RSJ 5*, *RSJ 10*.
- **Class II: *Medium cataclasis*.** The rock cores exhibit evidence of at least one big discontinuity that is of important dimension and/or in unfavorable orientation according to rock core axis. Moreover rock cores exhibit important competence contrasts; samples *RSJ 2*, *RSJ 3*, *RSJ 7*, *RSJ 8*, *RSJ 9*.
- **Class III: *High cataclasis*.** Rock materials showing strong structural variations, as well as mineralogical contrasts between “hard” and “soft” components, and/or showing a clastic nature, indicative of the most tectonized horizons in presence; samples *RSJ 4*, *RSJ 6*, *RSJ 11*, *RSJ 12*.

In the preparation process of the rock cores for triaxial mechanical testing, sample *RSJ 1* allowed the realization of two rock cores in adequate dimensions, denominated *RSJ 1a* and *RSJ 1b*. Due to an important preexisting transversal fracture, *RSJ 1b* was re-affected to *Class II*.

This preliminary classification based on visual assessment will be criticized on the light of micro-structural (this chapter) and mechanical (**Chap. 12**) evidences, and accordingly will provide a reflexion basis on how to possibly improve the geotechnical characterization of heterogenous rock structures at the sample scale.

| PETROLOGY | LOCALITY | TECTONIC CONTEXT | SITE CONDITIONS | SAMPLES | DRILL-AXIS | ROCK MASS DESCRIPTION | GSI (estimated) | GEOLOGICAL QUALITY CLASS |
|-----------|---|--|---|---------|------------|--|-----------------|--------------------------|
| CARBONATE | ROCHE ST JEAN N16 Tunnel, Choindex, Jura Mountains, Switzerland | FOLDED JURA, Malm Formation, Okfordian-Kimmerid- gian micritic limestone, tectonically disturbed during folding of the Envelier anticlinal | Sub-surface tunnel through anticlinal structure. Fault zone striking more or less E-W (115/80), cross-cutting tunnel axis at N-portal Orientation of rock layers: 200/90 Orientation of main joints: J1 = 115/80 (main fault) J2 = 285/80 J3 = 320/35 | RSJ 1 | (322/08) | Relatively homogeneous and competent rock cores, recrystallized rock matrix, important evidence of fracturation in the rock mass, important recrystallization with calcite in fault planes, presence of clay minerals in some fractures and pores that induces preferred planes of weakness, traces of Fe-alteration at the periphery of cracks Heterogeneous sample, important amount of green clay, evidence of numerous fractures affecting the tectonized limestone matrix, clasts of limestone in clay dominated rock core portions. Relatively homogeneous and competent rock core, numerous fractures through the rock matrix mostly recrystallized with calcite in fault planes Highly heterogeneous sample, strong competence contrast between clay-dominated and limestone parts, building two domains in the rock core, presence of green and brown clay Relatively homogeneous rock core of tectonized limestone matrix, rock core affected by one fracture of important dimension in subvertical orientation, filled in parts by a clastic mixture of limestone fragments in soft green clay prograding into calcite recrystallization. Heterogeneous sample, numerous evidence of fracturing through the rock mass, presence of clay minerals in some fracture planes and in void spaces, important recrystallization with calcite Heterogeneous sample, numerous evidence of fracturing through the rock mass, presence of clay minerals in some fracture planes and in void spaces, important recrystallization with calcite, important evidence of Fe-alteration at the periphery of cracks Relatively homogeneous and competent rock core, fracture planes recrystallized with calcite, small amount of green clay in pores and some cracks, important Fe-alteration at the periphery of cracks. Matrix supported fault breccia with mm- to cm-sized angular limestone clasts in a clay matrix, strong heterogeneity and competence contrasts expected in the rock core Very damaged sample, described as elast-supported fault breccia, fractures planes through the tectonized limestone matrix filled with clay material, strong heterogeneity and competence contrasts expected through the rock core | 50 | I |
| | | | | RSJ 2 | (336/00) | | 35 | II |
| | | | | RSJ 3 | (336/00) | | 35 | II |
| | | | | RSJ 4 | | | 20 | III |
| | | | | RSJ 5 | | | 50 | I |
| | | | | RSJ 6 | | | 20 | III |
| | | | | RSJ 7 | | | 35 | II |
| | | | | RSJ 8 | | | 30 | II |
| | | | | RSJ 9 | | | 35 | II |
| | | | | RSJ 10 | | | 50 | I |
| | | | | RSJ 11 | | | 15 | III |
| | | | | RSJ 12 | | | 20 | III |

Table 11.1 Visual geological descriptions of *RSJ* samples collected at the N16 Roche St Jean tunneling site under construction during spring 2005.

11.1.2 Comparison with GSI criteria

To introduce a first quantitative support to the often subjective rock core quality evaluation, the above defined quality classes have been translated in terms of the Geological Strength Index (GSI) at the sample scale following the considerations presented in **Chap. 7**. The chart of GSI values used for this purpose is taken from *Hoek et al.* (1998) (**Fig. 3.4** & **Appendix I-III**).

Table 11.2 presents the evaluation of rock mass structure according to fracture density and joint surface qualities (here the fractures at the sample scale) that has been obtained on the *RSJ* samples. GSI values are found to range between 50 and 15, the values of 50 corresponding therefore to geological quality *class I*, 35-30 to *class II*, and 20-15 to *class III*. Diminution of the GSI from 50 to 15 corresponds to a decrease in rock mass interlocking from *VERY BLOCKY* to *BLOCKY/DISTURBED/SEAMY* to *DISINTEGRATED* and an associated decrease in joint surface qualities from *FAIR* to *POOR* up to *VERY POOR*. Descriptive GSI estimations performed on the 12 *RSJ* samples together with sample photographs can be found.

This preliminary classification of the *RSJ* samples allows the recognition of particular discontinuity types (e.g. *recrystallized, open, clay-coated*) that will be demonstrated having a control and influence in the mechanical deformation of such heterogeneous rock cores.

11.1.3 Quantification of Damage Indicators

To test the accuracy of the visual classification, the different *RSJ* samples have been further characterized by means of the damage index DI (**Eq. 10.6**) to evaluate the amount of *damage indicators* present in each rock core and relate them with sample properties. Segmentation has been performed using CARact3D.

The characterizations by means of *damage indicators* is confronted with the initial visual characterization made on the rock cores (geological quality classes I-III) and used to define a quantitative mean to support preliminary sample classification.

11.1.3.1 Best-fit segmentation of XRCT data

In general, beam hardening and ring artifacts are generally stronger at the base and top of a rock core acquisition, resulting in averaged slightly lower CT values in these portions than in the middle of the core. To process a full XRCT stack (over the 500 CT views), a “best-fit” detection is therefore required. Best-fit detection means the ability to segment the range of grey values produced by *damage indicators* over the entire stack without excessive exaggeration or underestimation, so as to give a result close to reality.

Table 11.3 regroups the parameters that have been used for best-fit segmentation of the XRCT stacks corresponding to the *RSJ* samples. Even if from a same petrology and same provenance, the different *RSJ* samples require each time an adjustment of the segmentation parameters as their structural characteristics differ, e.g. they depict geological features of different dimensions and types, influencing the distribution of CT values recorded during scan. These parameters will be used later in **Chap. 12** for the segmentation of the XRCT stacks after triaxial test. **Appendix IV-III** presents for each of the *RSJ* samples the raw CT slices that have been used for calibration of the best-fit detection parameters. Resulting segmented binary images are given for reference and evaluation.

Note: For each of the *RSJ* samples, 4 slices have been selected for calibration of the segmented parameters. Primary segmentation has always been defined in regard to the grey level histogram distribution over the sample. This is successful in keeping the primary segmentation at a conservative threshold value. The secondary segmentation is adjusted progressively so as to refine the primary detection still in a conservative manner. Secondary segmentation has been tested between some extreme minimal and maximal values for local XRCT-matrix detection. This trial and error process rapidly leads to an acceptable result for the validation of the level of secondary segmentation to perform.

The functions “noise elimination” and “overdensity elimination” are used for noise reduction and improvement of reconstructed segmented stacks.












| SAMPLES | PHOTOGRAPH | STRUCTURE | SURFACE CONDITIONS | GSI |
|---------|---|---|---|-----|
| RSJ 1 |  | Blocky interlocked partially disturbed rock mass, leading to angular blocks | Poor surfaces, slickensided highly weathered surfaces with compact coatings | 50 |
| RSJ 2 |  | Blocky interlocked partially disturbed rock mass, leading to angular blocks, one unfavorably oriented structure/discontinuity recognized in rock core | Poor to very poor surfaces, slickensided, highly weathered surfaces with alternance of compact and soft clay coatings or fillings | 35 |
| RSJ 3 | RSJ 3 missing | | | |
| RSJ 4 |  | Disturbed poorly interlocked heavily broken rock mass, leading to angular and rounded blocks, important clay content | Poor to very poor surfaces, slickensided, highly weathered surfaces with alternance of compact and soft clay coatings or fillings | 20 |
| RSJ 5 |  | Blocky interlocked partially disturbed rock mass, leading to angular blocks | Poor surfaces, slickensided highly weathered surfaces with compact coatings | 50 |
| RSJ 6 |  | Disturbed poorly interlocked heavily broken rock mass, leading to angular and rounded blocks, important clay content | Poor to very poor surfaces, slickensided, highly weathered surfaces with alternance of compact and soft clay coatings or fillings | 20 |
| RSJ 7 |  | Blocky interlocked partially disturbed rock mass, leading to angular blocks | Very poor surfaces, slickensided, highly weathered surfaces with alternance of compact and soft clay coatings or fillings | 35 |
| RSJ 8 |  | Very blocky interlocked partially disturbed rock mass, leading to angular blocks | Poor to very poor surfaces, slickensided, highly weathered surfaces with alternance of compact and soft clay coatings or fillings | 30 |
| RSJ 9 |  | Blocky interlocked partially disturbed rock mass, leading to angular blocks | Very poor surfaces, slickensided, highly weathered surfaces with alternance of compact and soft clay coatings or fillings | 35 |
| RSJ 10 |  | Blocky interlocked partially disturbed rock mass, leading to angular blocks | Poor surfaces, slickensided highly weathered surfaces with compact coatings | 50 |
| RSJ 11 |  | Disintegrated poorly interlocked heavily broken rock mass, leading to angular and rounded blocks | Poor to very poor surfaces, slickensided, highly weathered surfaces with alternance of compact and soft clay coatings or fillings | 15 |
| RSJ 12 |  | Disintegrated poorly interlocked heavily broken rock mass, leading to angular and rounded blocks, less clay than in RSJ 11 | Poor to very poor surfaces, slickensided, highly weathered surfaces with alternance of compact and soft clay coatings or fillings | 20 |

Table 11.2 Photographs of the 12 *RSJ* rock cores and GSI characterization applied to the sample scale. Although GSI is initially designed to describe rock mass quality at another level of observation (rock mass), use of GSI (Hoek *et al.*, 1998) has been made here to confront derived values with the geological quality classes I-III. This approach is only done to facilitate sample classification prior to further analytical procedures.

Detections of *damage indicators* made on the *RSJ* samples are estimated being realistic and brought in relation with a degree of heterogeneity of the rock core. This degree of heterogeneity can be defined as the structural evidence of damage in presence based on the indirect resolution of feature-induced density contrasts inside the sample. The heterogeneity and anisotropy of rock cores can then be analyzed in terms of the 3D geometry of the segmented *damage indicators* (see **section 11.4**).

| Samples before triaxial test | Representative CT slices for calibration of segmentation | Primary segmentation: XRCT _{clasts} | Primary segmentation: XRCT _{matrix} | Secondary segmentation | Noise elimination | Overdensity elimination | % XRCT _{clasts} | % XRCT _{matrix} | DI |
|------------------------------|--|--|--|------------------------|-------------------|-------------------------|--------------------------|--------------------------|-------|
| RSJ 1a | 75, 195, 300, 446 | 35815 | 35145 | 15 | 7 | 35815 | 99.35 | 0.73 | 0.007 |
| RSJ 1b | 128, 298, 360, 529 | 35590 | 34200 | 10 | 5 | no | 96.5 | 3.53 | 0.035 |
| RSJ 2 | 16, 107, 253, 498 | 35800 | 35400 | 25 | 7 | 35800 | 95.74 | 4.29 | 0.043 |
| RSJ 3 | 50, 200, 336, 469 | 35900 | 35450 | 20 | 7 | 35900 | 93.23 | 6.82 | 0.068 |
| RSJ 4 | 31, 238, 343, 494 | 35400 | 34945 | 20 | 7 | no | 78.52 | 21.51 | 0.215 |
| RSJ 5 | 65, 194, 429, 445 | 35700 | 35500 | 35 | 7 | 35700 | 98.71 | 1.32 | 0.013 |
| RSJ 6 | 30, 66, 119, 228 | 35390 | 34750 | 20 | 7 | no | 63.05 | 37.09 | 0.371 |
| RSJ 7 | 20, 74, 169, 236 | 35500 | 35300 | 5 | 7 | 35500 | 89.34 | 10.68 | 0.107 |
| RSJ 8 | 20, 90, 361, 455 | 35420 | 34900 | 35 | 7 | no | 93.41 | 6.61 | 0.066 |
| RSJ 9 | 30, 104, 160, 248 | 35250 | 34950 | 35 | 7 | no | 94.33 | 5.69 | 0.057 |
| RSJ 10 | 77, 226, 380, 454 | 35590 | 35300 | 45 | 7 | no | 99.41 | 0.7 | 0.007 |
| RSJ 11 | 93, 166, 313, 404 | 35580 | 35150 | 25 | 7 | no | 60.22 | 39.87 | 0.399 |
| RSJ 12 | 86, 210, 254, 510 | 35140 | 34750 | 30 | 7 | no | 85.98 | 14.11 | 0.141 |

Table 11.3 Best-fit segmentation parameters for the RSJ rock cores and evaluation of damage index DI (Eq. 10.6). These same parameters will be used later in **Chap. 12** for the segmentation of the XRCT models recorded after deformation of the samples in the triaxial cell. Having to deal concurrently with 500 images per sample implies an automatization of the segmentation procedure over the stack in order to produce efficient work. Therefore, the best-fit segmentation had to be evaluated for each XRCT stack and results are a good but not a perfect determination.

11.1.3.2 Confrontation with visual classes

Fig. 11.1 is a graphic presentation of the damage index DI used to evaluate the pertinence of the categorization of the *RSJ* samples into the geological quality classes I, II, III. Such a plot support with a strong concordance the determined quality classes defined for each sample. It confirms the medical XRCT as a technique of choice for a rapid and accurate cataclastic rock core characterization.

An input for the classification of carbonatic altered rock cores can be proposed with DI values between 0.005 and 0.015 for *Class I*, 0.030 and 0.110 for *Class II* and 0.140 and 0.400 for *Class III*. These limits are indicative and correspond to observations on a very limited amount of rock cores. Accordingly, it is expected that these ranges should be investigated with more details by introducing observations on additional carbonatic rock core samples affected by a high structural variability.

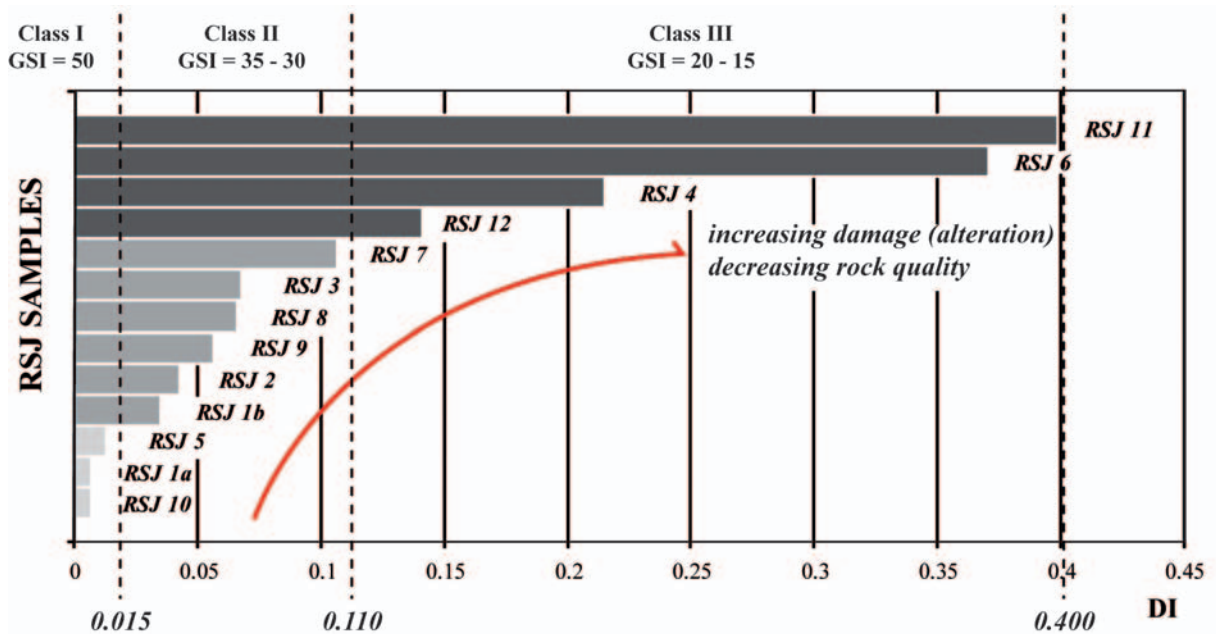


Fig. 11.1 Graphical representation of *RSJ* rock cores classified according to increasing damage index DI. Confirmation of the geological visual classes presented in section 11.1.1. Note the increase in damage indicators from samples of *Class I* towards samples of *Class III*. The same graphic will be presented within Chap. 12 based this time on a sample classification by means of observed types of mechanical behaviors within the *RSJ* samples. The relationship with GSI determinations on the different rock cores are given.

11.2 RESULTS OF THE DETAILED CHARACTERIZATION: MSI DETERMINATIONS FROM THIN SECTIONS & AXIAL CT-SLICES

In this section, the details of the MSI-determinations on remnants of *RSJ* material (corresponding mainly to the “primary matrix” material) performed by *Veuve* and *Chaignat* (2007) in their Master theses that have been supervised within this research project are presented (see also section 3.3.3). These data are given to provide an additional discussion basis for the critics of the MSI determinations on 13 *RSJ* samples implementing XRCT data that constitute the main focus of the current work.

The mineralogical analyses of *RSJ* remnants were conducted by *Veuve* (2007) and two analytical procedures were mainly tested. They are mentioned in section 11.2.1 and details can be found in Chap. 7. The determined *RSJ* “main” composition has then been adapted in this research to calculate mwVh for the 12 *RSJ* samples by taking into account the proportion of clay minerals (e.g. the “damaged matrix” material) estimated on the base of XRCT data segmentation using CARact3D.

The microstructural analyses of the TC & MC parameters by *Chaignat* (2007) have been made using thin sections (**section 11.2.2**). An attempt of determinations implementing axial CT-slices (e.g. raw data perpendicular to rock core axis) has also been conducted to indicatively confront the resolutions obtained between the direct (thin section) and indirect (XRCT) petrographical analytical methods. These data can be found in **Table 3.4**. Later in the chapter (**section 11.3**), a more elaborated use of the XRCT data for the microstructural analysis is presented profiting from frontal (xz-) and sagittal (yz-) CT slices (e.g. tomographically reconstructed orthogonal projections parallel to rock core axis, made possible with VGStudioMAX software).

MSI determinations by *Veuve* and *Chaignat* (2007) led to interesting considerations about the mineralo-structural approach proposed by *Bürgi* (1999) that are summarized in **Appendix IV-IV**.

11.2.1 Mineralogical Composition (mwVh Parameter)

Mineralogical composition of the Roche St Jean limestone has been determined by *Veuve* (2007) using XRD and electron microscopy analytical techniques (SEM). **Table 11.4** presents the results obtained. SEM determination corresponds to an average of two sites taken on a same thin section as shown in **Fig. 11.2**. Results between XRD and electron microscopy are in good agreement, with SEM detecting an additional mineral phase due to its more precise resolution than XRD.

Two values of mean weighted Vickers hardness (mwVh) are accordingly determined from mineralogical compositions using Vickers hardness given in **Table 7.2**.

The mineralogy determined by *Veuve* (2007) will be used to approximate the mineralogical compositions of the 12 *RSJ* samples under particular investigation and provide input for the MSI_{XRCT} calculation of these samples proposed in this study.

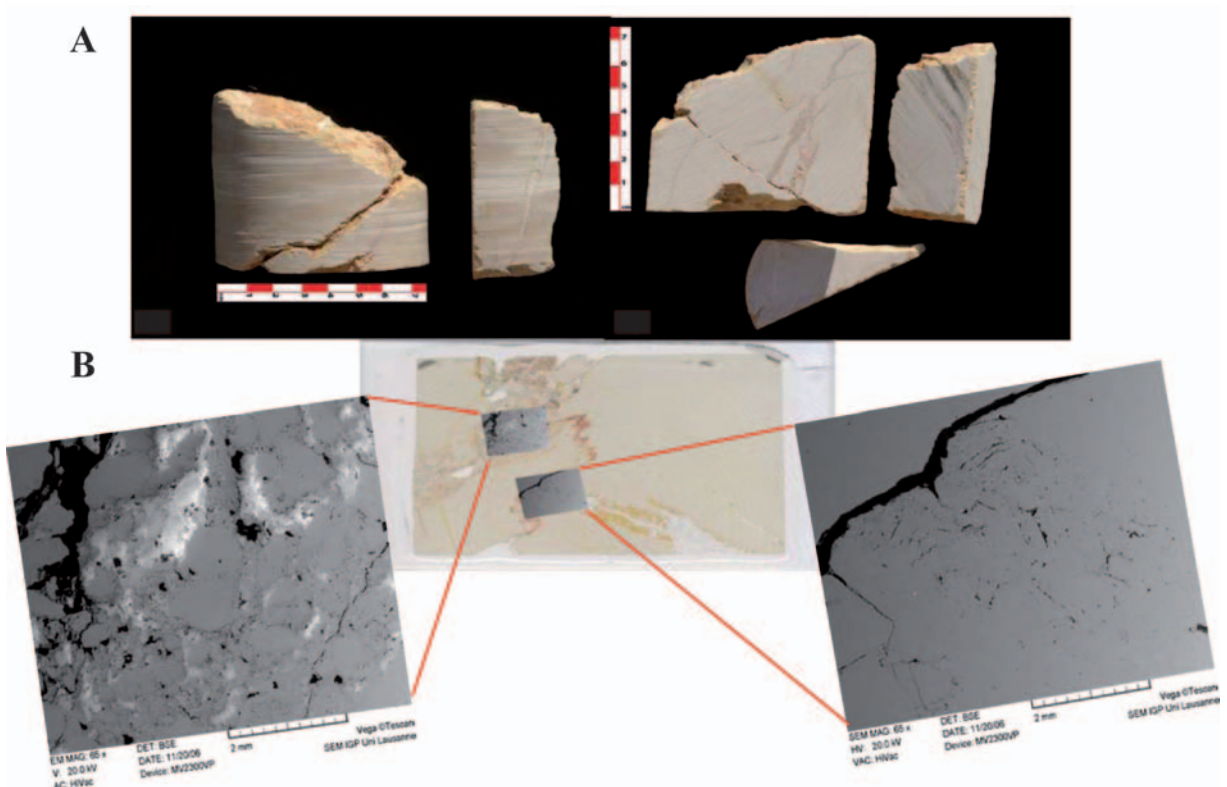


Fig. 11.2 A) Rock core remnants after preparation of sample *RSJ 1* for triaxial testing. B) Presentation of the SEM sites (backscatter electron view) used for mwVh derivations next to XRD analyses, as investigated by *Veuve* (2007).

11.2.2 Structural & Textural Characterization (TC & MC Parameters)

Four thin sections from two rock core remnants of the *RSJ* limestone have been studied by *Chaignat* (2007) to determine the TC & MC parameters and test their validity in carbonatic petrology. **Fig. 11.3** presents the corresponding *RSJ* photomicrographs together with the derived binary masks for TC and MC determinations.

Results of the microstructural characterization performed by *Chaignat* (2007) are presented in **Table 11.4**.

It has to be noted that the thin sections used by *Chaignat* (2007) question a first time the applicability of the bimodal clast-matrix approach of *Bürgi* (1999), as the TC determinations are made quite subjective (lack of fine-grained damaged matrix, therefore quantification of texturally welded grains instead of clasts, see **Fig. 11.3**). It suggests therefore that an improper characterization might result in terms of TC and that the MSI index face potential limitations to describe any type of cataclastic rocks (in particular slightly tectonized ones). Namely, when the degree of tectonization is still low, the fracturation in the material has not generalized yet, and the progressive evolution towards a crushed rock (cataclasite s.str.) is still incomplete (outside domain of the clast-matrix approach). In terms of characterization by means of the MSI (i.e. wish of a geologically-based prediction in terms of strength) this is an important observation that will be discussed more in details profiting from the observations on the 12 specific *RSJ* rock cores performed in this research.

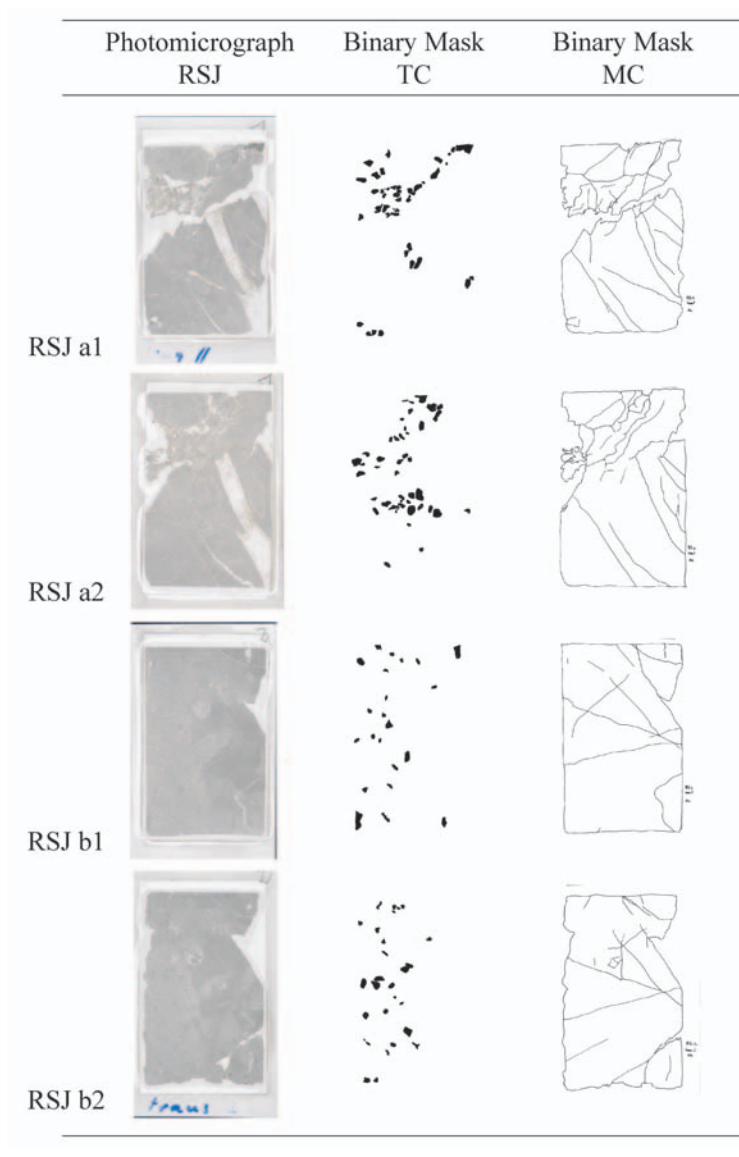


Fig. 11.3 Thin sections of samples *RSJ a & b* (rock core remnants) from the A16 Roche St Jean Tunnelling site studied by *Chaignat* (2007) in his Master thesis. Photomicrographs are given as well as the binary images for the calculation of the TC & MC parameters. Note the subjectivity in defining the TC parameter, as the bimodal clast-matrix approach envisaged by *Bürgi* (1999) is in the context of carbonatic cataclasite difficult to adopt as such. Numerical values are given together with values of mwVh in **Table 11.4**.

| Petrology | Samples | XRD | | SEM | | Thin section | | MSI | |
|--|--------------------------|--------------|--------------|----------|--------|--------------|-------|---------------|-------|
| | | mwVh (MPa) * | mwVh (MPa) * | TC | MC | XRD | SEM | Average value | |
| CARBONATIC (Chaignat & Veuve, 2007) | | | | | | | | | |
| Roche St Jean limestone | | | | | | | | | |
| | RSJ 1 (rock powder) | 1.76 | | | | | | | |
| | RSJ 1 (uncovered TS) | | 1.68 | | | | | | |
| | RSJ a1 (TS) | | | 1.160 | 1.260 | 4.259 | 4.066 | | |
| | RSJ a2 (TS) | | | 1.162 | 1.991 | 5.549 | 5.297 | | |
| | RSJ b1 (TS) | | | 1.354 | 1.689 | 5.356 | 5.112 | | 4.941 |
| | RSJ b2 (TS) | | | 1.694 | 1.180 | 5.058 | 4.828 | | |
| * Results of mineralogical analyses: | | | | | | | | | |
| | Mineral | Calcite | Quartz | Dolomite | Albite | mwVh (MPa) | | | |
| | Vickers hardness (MPa) | 1638 | 9807 | 2697 | 7679 | | | | |
| | RSJ 1 _{XRD} (%) | 96.87 | 1.29 | 1.85 | - | 1.76 | | | |
| | RSJ 1 _{SEM} (%) | 97.54 | 0.61 | 0.3 | 0.21 | 1.68 | | | |

Table 11.4 Results of the mineralogical and structural characterization for the *RSJ* limestone. Corresponding parameters mwVh, TC & MC are given together with calculated values of MSI using **Eq. 3.1**. Three values of MSI are accordingly determined: MSI based on XRD mineralogy, MSI based on SEM mineralogy and an average MSI for the rock core remnant of *RSJ 1*. Modified after *Veuve* and *Chaignat* (2007).

11.3 RESULTS FROM THE INDIRECT XRCT CHARACTERIZATION

The next sections deal first with the determination of TC & MC parameters from CT-slices as proposed in **section 10.2.1**. Second, the evaluation of *damage indicators* inside the rock cores is performed (**section 10.2.2**). Their ability to quantitatively support the definition of geological quality classes is presented.

11.3.1 TC & MC Determinations Using XRCT Data

Results of TC & MC determinations on the RSJ samples are found in **Table 11.5**. Binary masks according to frontal (xz-) & sagittal (yz)-reference planes that have been used for the different determinations are listed in **Appendices IV-I & II**. These masks were produced by hand involving a high time consumption and introducing a relative imprecision at the medical XRCT resolution.

Unfortunately, in the current stage of developments in relation with image analysis of XRCT acquisitions on rocks, CARact3D works only with raw CT-data (axial slices, 16 bit). The frontal and sagittal CT-slices, being produced in VGStudioMAX from the tomographic reconstruction of the raw CT-data, correspond therefore only to “virtual views” that can be saved in common numerical image formats (.bmp, .tif, .jpg ... all 8 bit formats). It is therefore currently not possible to take advantage of CARact3D on such tomographic projections, as it would require the possibility to convert the default axial raw stack (xy) into a frontal (xz) and sagittal (yz) raw stack. This point requires further research.

Analysis of the different hand-derived binary images has then been performed using “standard” image analysis tools implemented in ImageJTM. Due to the structural particularities of carbonatic cataclasites, not every rock core has permitted the definition of a clast and matrix phase (see also **section 11.2.2**). Thus, TC determinations for the RSJ samples concern only samples *RSJ 1b*, *4*, *6*, *7*, *8*, *9*, *11* & *12*. For the other samples, extreme value of TC accounting for the absence of clasts

| Rock core | Visual characterization | View | T_{LL} | R_L | T_{LD} | δ_{global} | MC_{global} | CD | N_1 | N_0 | \overline{FF}_0 | \overline{AR}_1 | AF_1 | TC_{global} |
|---------------|-------------------------|-----------|----------|-------|----------|-------------------|---------------|-------|-------|-------|-------------------|-------------------|--------|---------------|
| RSJ 1a | I | xz | 22.438 | 1.111 | 0.036 | 4.989 | 0.279 | | | | | | | |
| yz | | 25.167 | 1.273 | 0.055 | 6.862 | 0.181 | | | | | | | | |
| xz | | 24.372 | 1.116 | 0.051 | 4.041 | 0.223 | | | | | | | | |
| yz | | 24.986 | 1.145 | 0.070 | 4.050 | 0.162 | | | | | | | | |
| RSJ 10 | II | xz | 29.387 | 1.126 | 0.033 | 6.040 | 0.194 | | | | | | | |
| yz | | 42.635 | 1.154 | 0.038 | 1.764 | 0.405 | | | | | | | | |
| xz | | 24.035 | 1.101 | 0.045 | 4.050 | 0.252 | | 0.028 | 3 | 7 | 0.722 | 3.241 | 0.722 | 0.060 |
| yz | | 21.087 | 1.098 | 0.050 | 3.057 | 0.341 | | 0.017 | 2 | 6 | 0.371 | 2.352 | 0.411 | 0.042 |
| xz | | 26.002 | 1.114 | 0.042 | 5.054 | 0.202 | | | | | | | | |
| yz | | 27.987 | 1.087 | 0.043 | 4.877 | 0.186 | | | | | | | | |
| xz | | 25.323 | 1.115 | 0.029 | 4.065 | 0.370 | | | | | | | | |
| yz | | 21.888 | 1.118 | 0.032 | 4.921 | 0.322 | | | | | | | | |
| RSJ 7 | III | xz | 17.389 | 1.149 | 0.095 | 3.057 | 0.228 | 0.121 | 5 | 11 | 0.689 | 2.581 | 0.389 | 0.180 |
| yz | | 19.805 | 1.163 | 0.102 | 1.764 | 0.326 | | 0.204 | 8 | 17 | 0.705 | 2.478 | 0.280 | 0.242 |
| xz | | 21.226 | 1.138 | 0.071 | 4.112 | 0.184 | | 0.099 | 3 | 4 | 0.713 | 2.894 | 0.624 | 0.182 |
| yz | | 21.711 | 1.140 | 0.063 | 5.152 | 0.161 | | 0.112 | 4 | 3 | 0.692 | 2.381 | 0.427 | 0.154 |
| xz | | 21.071 | 1.159 | 0.088 | 4.099 | 0.152 | | 0.284 | 6 | 14 | 0.716 | 3.042 | 0.245 | 0.327 |
| yz | | 20.119 | 1.180 | 0.089 | 4.084 | 0.161 | | 0.112 | 10 | 12 | 0.719 | 3.352 | 0.197 | 0.121 |
| xz | | 28.408 | 1.128 | 0.040 | 2.983 | 0.334 | | 0.099 | 4 | 15 | 0.720 | 2.443 | 0.980 | 0.145 |
| yz | | 24.271 | 1.127 | 0.044 | 1.764 | 0.602 | | 0.102 | 3 | 5 | 0.480 | 2.222 | 0.327 | 0.118 |
| xz | | 27.873 | 1.122 | 0.049 | 4.115 | 0.200 | | 0.038 | 1 | 3 | 0.600 | 1.701 | 0.133 | 0.061 |
| yz | | 21.444 | 1.127 | 0.050 | 3.041 | 0.347 | | 0.014 | 2 | 3 | 0.723 | 1.621 | 0.100 | 0.013 |
| xz | | 8.806 | 1.112 | 0.121 | 5.061 | 0.206 | | 0.312 | 18 | 74 | 0.746 | 2.497 | 0.084 | 0.350 |
| yz | | 9.190 | 1.135 | 0.115 | 2.807 | 0.382 | | 0.313 | 38 | 60 | 0.717 | 2.833 | 0.042 | 0.295 |
| RSJ 12 | | xz | 10.458 | 1.106 | 0.084 | 5.091 | 0.247 | 0.232 | 21 | 55 | 0.766 | 2.724 | 0.068 | 0.232 |
| | | yz | 10.101 | 1.112 | 0.087 | 6.057 | 0.208 | 0.200 | 27 | 48 | 0.748 | 2.912 | 0.046 | 0.190 |

Table 11.5 Global values of microstructural TC & MC parameters based on oriented CT-slices. See **Appendices IV-I & II** for the corresponding CT views, binary masks and results of the local determinations (e.g. slice by slice). Only eight samples permitted a TC determination. For the other samples, TC is assumed equal 0, corresponding to an extreme case where the “physical meaning” of the bimodal approach of *Bürgi* (1999) is not appropriate to describe accurately rock mass properties (see **Chap. 13**). Values listed correspond to averaged data for the frontal (xz-) and sagittal (yz-) binary masks considered for each sample (3+3 for TC; 7+7 for MC).

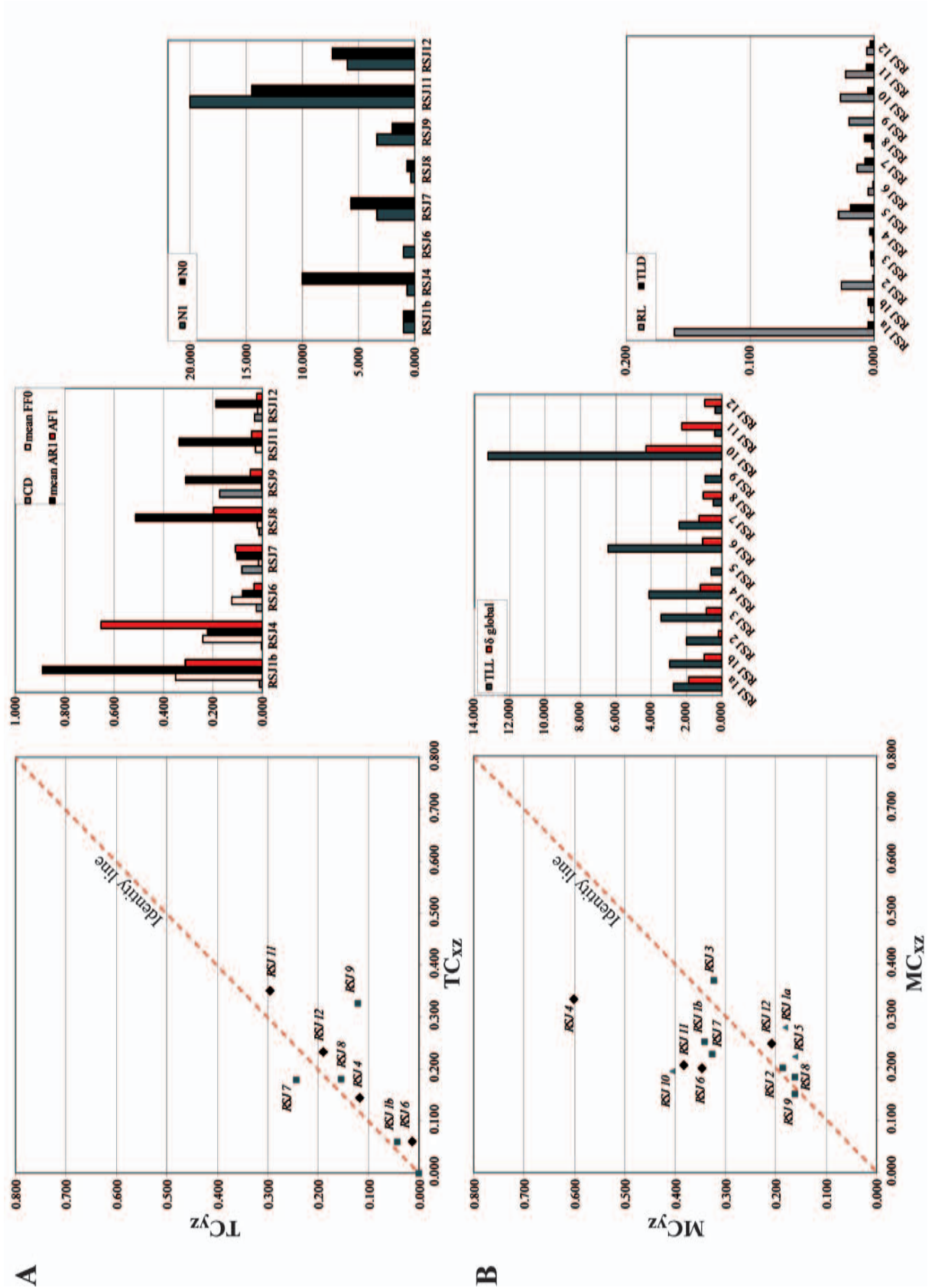


Fig. 11.4 Plots of $TC_{xz} - TC_{yz}$ (A) & $MC_{xz} - MC_{yz}$ (B) introducing an identity line referring to textural and structural homogeneity of rock cores. *Small triangles*: rock cores of *Class I*. *Squares*: rock cores of *Class II*. *Diamonds*: rock cores of *class III*. Differences in TC & MC constitutive parameters according to frontal (xz-) or sagittal (yz-) determinations are depicted for the RSJ rock cores. Strongest variations affecting TC are the relative proportions of isometric and elongated clasts. Other parameters are consistent over the analyzed CT-slices. In case of MC, the most sensitive parameters seem to be the trace line length T_{LL} and the orientation factor δ . Note different plot scales.

in the studied image has been taken (e.g. TC = 0, which will be shown having a strong impact on the resulting MSI-data of these samples, leading to a detailed discussion within **Chap. 13**). TC determinations have been made using 6 binary masks per sample. On the contrary, MC parameters could be calculated for all 12 rock cores. For each sample, 14 binary masks have been used for their calculations. For MC, a global orientation factor has been calculated in xz and yz. This has been estimated more logical than taking an average of the orientation factor determinations from both the frontal and sagittal CT slices. Namely, it permits a better characterization of the discontinuity distribution and orientation on the two considered orthogonal planes (e.g. recalculation of a rose diagram based on all cumulative trace line lengths in xz or yz to define δ_{global}).

TC & MC parameters have been determined slice by slice (e.g. *local* determinations) and they are separated into TC_{xz} - TC_{yz} & MC_{xz} - MC_{yz} parameters, according that they correspond to the frontal (xz) or sagittal (yz) planes across the XRCT volume (**Appendices IV-I & II**). To characterize the different rock cores from a *global* perspective, values of TC & MC in **Table 11.4** correspond to the averaged parameters for the two orthogonal planes considered. *Local* variations of the different parameters constitutive of TC and MC inside the *RSJ* samples will be closely studied in **Chap. 13**.

11.3.2 Observed Variability on Frontal & Sagittal Planes

Based on **Table 11.5**, **Fig. 11.4** presents a graphic confrontation of the TC & MC values and resulting differences in constitutive parameters according to frontal or sagittal determinations. The direct confrontation of TC_{xz} - TC_{yz} & MC_{xz} - MC_{yz} defines an identity line on which microstructural homogeneity can be assumed. Deviation from the diagonal supports the assumption of preferred orientation and anisotropy inside the rock samples. Thus this figure provides a quantitative estimate of rock core heterogeneity by considering the variations in clasts and discontinuities as observed on two orthogonal planes.

From **Fig. 11.4 A & B**, it is found that no *a priori* relation exists with the defined geological classes I-III. In terms of TC, values from *Class III* seem more homogeneous between the frontal and sagittal determinations than values obtained on samples from *Class II*, reflecting the more pronounced clastic nature that results as a function of increasing cataclasis. In terms of MC, all determinations made on *Class I* to *Class III* samples lead to consider structural heterogeneity as affecting the *RSJ* rock cores. Such considerations demonstrate that provided the possibility to get a 3D visualization by means of medical XRCT, the development of image analysis tools for the volumetric structural and textural analysis of rock cores would be welcome. Accordingly, a more realistic quantification of rock core heterogeneity can be expected and incorporated as a strength reduction parameter in the mechanical interpretation. Such tools could be probably best implemented on the reconstructed segmented models in terms of DI (tomographic representation of DI, **section 10.2.2.2**).

It is reminded that values presented with **Fig. 11.4** correspond to averaged determinations in the frontal and sagittal planes (average from 3 resp. 7 CT slices per orientation). A detailed study of *local* variations (e.g. comparison slice by slice within one plane of view) will be conducted in **Chap. 13** with a great emphasis on evaluating the possibility to characterize heterogeneous samples by means of an MSI-type index.

11.3.3 XRCT-Derived MSI Determinations

MSI values in xz- and yz-directions (MSI_{xz} and MSI_{yz}) for the 13 *RSJ* samples of Roche St Jean have further been determined based on the values of TC & MC of **Table 11.5**. Mineralogical compositions have been taken from XRD data by *Veuve* (2007) from which slight adaptations have been performed to account for evidence of clay minerals inside the *RSJ* sample (**Table 11.6**).

| RSJ samples | Vickers Hardness (GPa) <i>Veuve</i> , 2007 | | XRD composition, main elements <i>Veuve</i> , 2007; evaluation of clay content: <i>Christe</i> , this study) | | | | mmVh (GPa) | average IC | | | average MC | | | MSI _{XRCT} (GPa) | | |
|-------------|--|-------|--|-------------------------|-------|-------|------------|------------|-------|-------|------------|-------|----|---------------------------|----|--|
| | cal | qtz | dol | "clay _{XRCT} " | | | | xz | yz | yz | xz | yz | xz | yz | yz | |
| | 1.638 | 9.807 | 2.697 | 0.2 | | | | | | | | | | | | |
| RSJ 1a | 95.86 | 1.29 | 1.85 | 1.00 | 1.749 | 0.000 | 0.000 | 0.000 | 0.279 | 0.181 | 0.487 | 0.316 | | | | |
| RSJ 1b | 95.86 | 1.29 | 1.85 | 1.00 | 1.749 | 0.060 | 0.042 | 0.252 | 0.341 | 0.670 | 0.546 | 0.670 | | | | |
| RSJ 2 | 95.86 | 1.29 | 1.85 | 1.00 | 1.749 | 0.000 | 0.000 | 0.202 | 0.186 | 0.325 | 0.354 | 0.325 | | | | |
| RSJ 3 | 91.86 | 1.29 | 1.85 | 5.00 | 1.691 | 0.000 | 0.000 | 0.370 | 0.322 | 0.544 | 0.626 | 0.544 | | | | |
| RSJ 4 | 71.08 | 1.29 | 1.85 | 25.78 | 1.392 | 0.145 | 0.118 | 0.334 | 0.602 | 1.002 | 0.666 | 1.002 | | | | |
| RSJ 5 | 95.86 | 1.29 | 1.85 | 1.00 | 1.749 | 0.000 | 0.000 | 0.223 | 0.162 | 0.283 | 0.390 | 0.283 | | | | |
| RSJ 6 | 60.53 | 1.29 | 1.85 | 36.33 | 1.241 | 0.061 | 0.013 | 0.200 | 0.347 | 0.446 | 0.323 | 0.446 | | | | |
| RSJ 7 | 81.86 | 1.29 | 1.85 | 15.00 | 1.547 | 0.180 | 0.242 | 0.228 | 0.326 | 0.879 | 0.632 | 0.879 | | | | |
| RSJ 8 | 86.86 | 1.29 | 1.85 | 10.00 | 1.619 | 0.182 | 0.154 | 0.184 | 0.161 | 0.511 | 0.593 | 0.511 | | | | |
| RSJ 9 | 91.86 | 1.29 | 1.85 | 5.00 | 1.691 | 0.327 | 0.121 | 0.152 | 0.161 | 0.477 | 0.809 | 0.477 | | | | |
| RSJ 10 | 95.86 | 1.29 | 1.85 | 1.00 | 1.749 | 0.000 | 0.000 | 0.194 | 0.405 | 0.709 | 0.340 | 0.709 | | | | |
| RSJ 11 | 51.98 | 1.29 | 1.85 | 44.88 | 1.118 | 0.350 | 0.295 | 0.206 | 0.382 | 0.756 | 0.621 | 0.756 | | | | |
| RSJ 12 | 76.86 | 1.29 | 1.85 | 20.00 | 1.475 | 0.232 | 0.190 | 0.247 | 0.208 | 0.588 | 0.707 | 0.588 | | | | |

Table 11.6 Mineralogical compositions of the *RSJ* samples based on *Veuve* (2007) and adapted after determination of a clay-percentage inside the *RSJ* rock cores as visualized by means of XRCT and quantified using the detection method presented in Chap. 10. Determinations of MSI_{XRCT} are accordingly given using the microstructural parameters listed in Table 11.5.

An estimation of the percentage of clay present in a sample has been realized based on the indirect XRCT volumes by means of segmentation (determination of a fraction “clay_{XRCT}”). For all samples it was assumed that at least 1% clay is affecting the rock mass. A Vickers hardness of 200 MPa has been taken for the undefined clay component. It corresponds to the value for talc given in *Bürgi* (1999) and has been assumed realistic for hydrated clay as present in the *RSJ* samples.

Table 11.6 regroups the approximated mineralogical compositions of the different *RSJ* samples that together with the structural & textural parameters lead to the values of MSI_{xz} and MSI_{yz} .

Fig. 11.5 A confronts MSI in the same way as for TC & MC parameters (**Fig. 11.4**). Only one sample has consistent MSI values between the frontal and sagittal determinations (i.e. *RSJ 2*). This is an additional argument supporting the idea to perform the MSI calculation on a full 3D basis for more reliability. **Fig. 11.5 B** presents the obtained differences in TC, MC and MSI parameters. Again no *a priori* relation is found with the geological classes.

An average MSI value of 4.941 has been found by *Chaignat* and *Veuve* (2007) based on thin section analysis (**Table 11.4**). This is clearly above the values of MSI_{XRCT} . Assuming that the TC parameter for the thin sections studied by *Chaignat* (2007) are not indicative in terms of the MSI approach (see **Fig. 11.3**) and setting $TC = 0$, the MSI from thin section is reduced to 2.632. At this point and provided only few data, it is difficult to say if the differences between MSI and MSI_{XRCT} is due to the contrasting field of view between thin section and CT-slices or to the difference in resolution impairing the exact diagnostic of discontinuities on medical CT-slices compared to thin section (see later **Fig. 11.7**).

Again, as mentioned above, the study of local variations observed slice by slice according to TC & MC determinations provides a strong additional input for the MSI validity and meaning based on the detailed study of the *RSJ* samples.

11.4 3D RECONSTRUCTIONS OF SEGMENTED MODELS

The spatial representation of *damage indicators* (e.g. tomographic representation of DI) inside the *RSJ* rock cores has been performed using VGStudio MAX by reconstruction of the different segmented XRCT stacks in 3D. All reconstructions have been made after having performed previously an overall noise reduction manipulation on the different XRCT stacks (*despeckle function* implemented in ImageJ™). At the medical XRCT resolution, some noise is inevitably introduced during image segmentation what will alter the 3D image reconstruction. In order to better visualize the structures corresponding to effective *damage indicators*, noise reduction has proved to be beneficial.

Fig. 11.6 presents the 3D spatial distribution of *damage indicators* inside the *RSJ* rock cores. Such indirectly resolved 3D structural models allow consideration about the effective topography and morphology of preexisting structures inside rock cores (e.g. DI). As such they can provide a strong input for mechanical test interpretation by taking into account the respective effects of *shape* and *orientation* of DI on concurrent sample deformation and recorded material resistance. The conceptual mathematical representation of fractures as planes or some simple geometry is also proved to be not realistic for an objective rock core characterization in cataclastic materials. Qualitative assessment of rock core *types* (e.g. in function of DI geometry) can be made based on the 3D visualization of *damage indicators*. Indicatively the 3D *RSJ* models are ordered on **Fig. 11.6** according to their belonging to classes I-III.

Provided such visualization capacities, the 3D structural models of reconstructed DI provide important stimulating evidences and possibilities for the characterization of heterogeneous rock

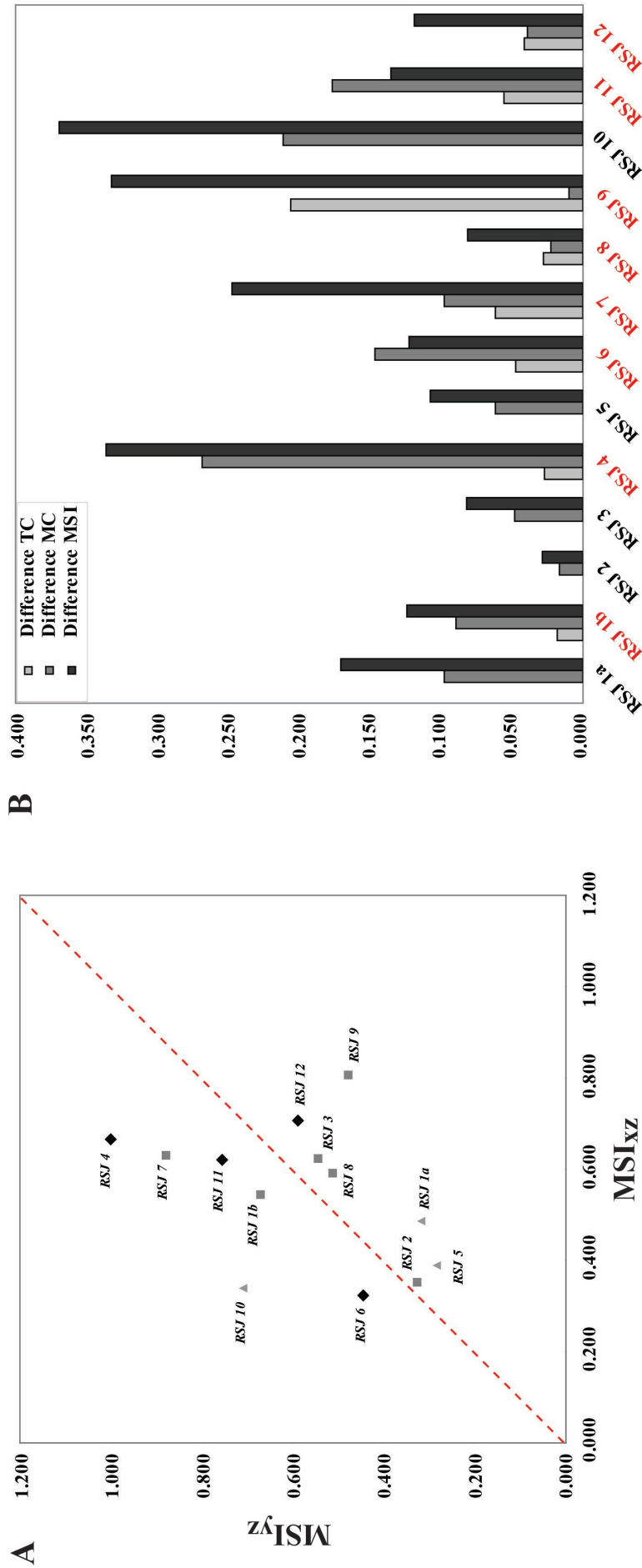


Fig. 11.5 A) Plots of MSI_{xz} and MSI_{yz} showing the relation of the different *RSJ* rock cores with the identity line. A mineralo-structural “isotropy” is found for sample *RSJ 2*. B) Differences in TC, MC & MSI parameters obtained between frontal (*xz*) and sagittal (*yz*) determinations. Samples labeled in red are the samples that have allowed a TC calculation. Rock core *RSJ 8* depicts the less overall variation. Again, full 3D numerical treatment would affect the MSI with more objectivity and reliability. Symbols referring to the geological classes I-III are the same as on **Fig. 11.4**.

samples. They will be discussed more in details in **Chap. 13 & 14.**

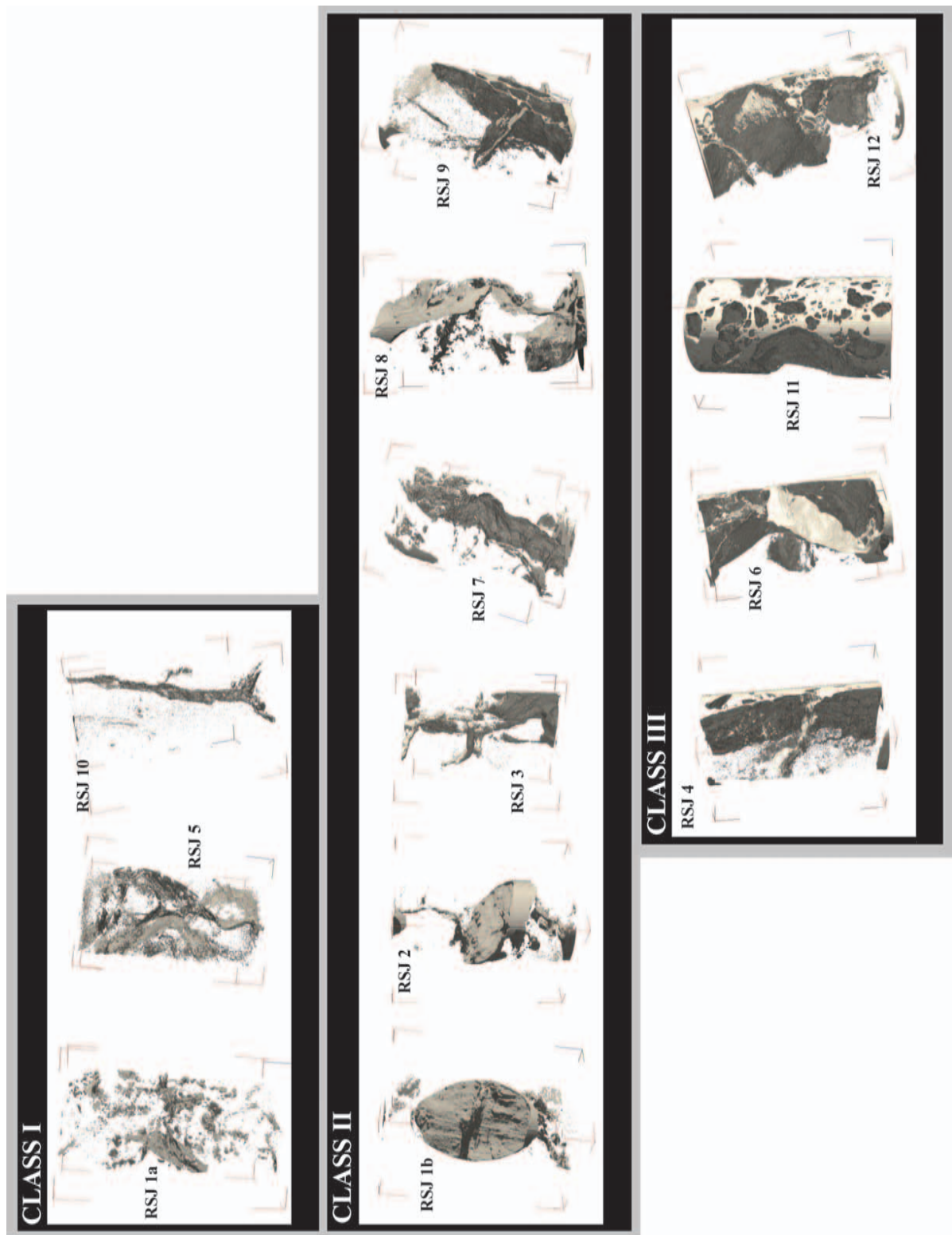


Fig. 11.6 Reconstructed 3D segmented XRCT models of the investigated *RSJ* samples. Such 3D information, including evidences from mechanical data can strongly assist an objective geological and geomechanical characterization of rock mass.

11.5 PETROGRAPHICAL DIAGNOSTIC BETWEEN THIN SECTIONS & XRCT DERIVED ANALYSES

In this section a confrontation of thin section and XRCT views is performed to evaluate the inherent petrographical uncertainty affecting the analysis by XRCT based on the concept of *damage indicators*.

Fig. 11.7 depicts the XRCT model of sample *RSJ 11* after its triaxial deformation (see **Chap. 12**) which was concurrently impregnated with the low viscosity resin described in **Chap. 7**. Several thin sections at different levels through the volume have been realized to be compared with the XRCT indirect imagery. Relationships between geological structures in the size domains represented by XRCT and thin sections are evaluated.

As evidenced by the thin sections of sample *RSJ 11*, different discontinuity types are observed in carbonatic rocks, namely:

- *open discontinuities* (to be evaluated by their surface conditions and rugosity);
- *clay coated discontinuities* (for which clay rheology must in particular be taken into account);
- *calcite recrystallized discontinuities* (that requires an evaluation in terms of resistance compared to the carbonatic rock matrix), and
- *mixed discontinuities* (for which a “rheological discretization” of the discontinuity surface would be needed).

Based on the sole XRCT visualization, discrimination of discontinuity types is difficult. A geological characterization seeking geotechnical relevance will therefore gain in accuracy if these evidences could be taken into account in the mechanical analysis of the fractured rock rheology.

Such considerations should in particular be taken into account for the MC type determinations as done in this research (see **Appendix IV-II**). Even if the spatial distribution of 2D *damage indicators* can be accurately determined, the MSI determination will benefit from the knowledge about discontinuity conditions. In this sense and as presented in **Fig. 11.7**, XRCT and thin sections should be regarded today as complimentary techniques. The general rock core characterization can obviously be better done with the advantage of the XRCT as a 3D technique but the meaning of the $XRCT_{matrix}$ should still be properly addressed by integrating petrographical evidences from thin sections.

Based on 3D visualized DI, morphological considerations will be introduced in **Chap. 13** and assessed in terms of their possible petrographical relevance.

11.6 DISCUSSION

A cataclastic rock characterization has to consider rock heterogeneity and structural/mineralogical complexity. As presented in **Chap. 2**, the geotechnical characterization of materials involving a fractured rock rheology requires constraints imposed on discontinuity types and knowledge about mineralogical alteration/weathering (see also **Fig. 4.2**). In particular, the study of different petrological contents can provide specific *damage indicators* to be considered in function of initial rock composition. Accordingly, the understanding of cataclastic processes in a particular context

can be addressed in terms of rock mass characterization.

Mineralogical constraints can be added with high-resolution analytical techniques compared to XRD, as demonstrated by *Veuve* (2007) or *Hayman* (2006). Moreover, a 3D petrography of the quality of thin section analyses is envisaged to become possible in the future, as demonstrated by pioneer work like *Ketcham et al.* (2001, 2005), *Van Geet et al.* (2001), *Viggiani et al.* (2004) or *Desrues et al.* (2006).

MSI derivations for the *RSJ* samples have been determined in this chapter based on global TC & MC parameters from frontal (xz-) and sagittal (yz-) CT slices (**Table 11.5 & 11.6**). No *a priori* relation with the geological classes is found at this point. Contradictions are even detected. For example, samples *RSJ 4, 7, 9, 11 & 12* (all *Class II* or *III*) depict the highest value of MSI. Moreover, samples of *Class I* seem to have generally lower MSI values than *Class II & III*. This is of course introduced by the fact that for them, no TC could be derived and the MSI calculation has then been performed in a conservative manner (e.g. TC = 0 to account for the absence of clasts and to demonstrate the limitations of the MSI to properly characterize slightly cataclased materials due to the inappropriate TC approach). However, when no clasts are observed, an extreme TC value could be taken (upper bound, for example TC = 1). As will be shown later in the discussion (see in particular **Fig. 13.5** and **Table 13.1**), this would actually better correspond to the logic of the MSI as envisaged by *Bürgi* (1999). The low MSI values obtained on *Class I* samples is however also related to the fact that for them the analyzed discontinuities from the CT-slices are mostly calcite recrystallized fractures having high strength. Thus accounting for them in a MC determination is pessimistic, leads to inaccurate low MSI what at the end is not objective for a prediction of rock mechanical properties. Facing such observations confront us with the question to adapt the index according to the level of cataclastic intensity experienced by a given rock core. In function of cataclasis, an evolution of micro-structural and mineralogical relationships is namely observed inside fault zones that probably cannot be assessed and quantified by means of a unique index.

Evidences from a local confrontation of TC & MC inside the investigated *RSJ* rock cores (e.g. slice by slice) will therefore be conducted within **Chap. 13** to establish a detailed conceptual model that depicts the structural variability observed in cataclastic samples and more generally the progressive rock material evolution inside fault zones. Accordingly, a domain of validity for the MSI in the formulation proposed by *Bürgi* (1999) will be established.

It is evident that MSI determinations from XRCT data introduce the advantage of working on the same rock material that is effectively tested mechanically, improving the reliability to correlate geological with geomechanical properties.

Even if developments are in great need today, the determination of a MSI type index based on 3D structural evidences such as the DI models are expected becoming increasingly relevant for a geotechnical characterization of heterogeneous rock cores. This is most of all to explain by the fact that the index will be global and accurately fitting the material on which further mechanical tests will be performed. Moreover, considering higher resolution XRCT acquisitions, the possibility to perform a specific segmentation for contrasted petrographical elements might become possible, introducing an important improvement for the correlation between geological and geomechanical properties of cataclastic rock samples.

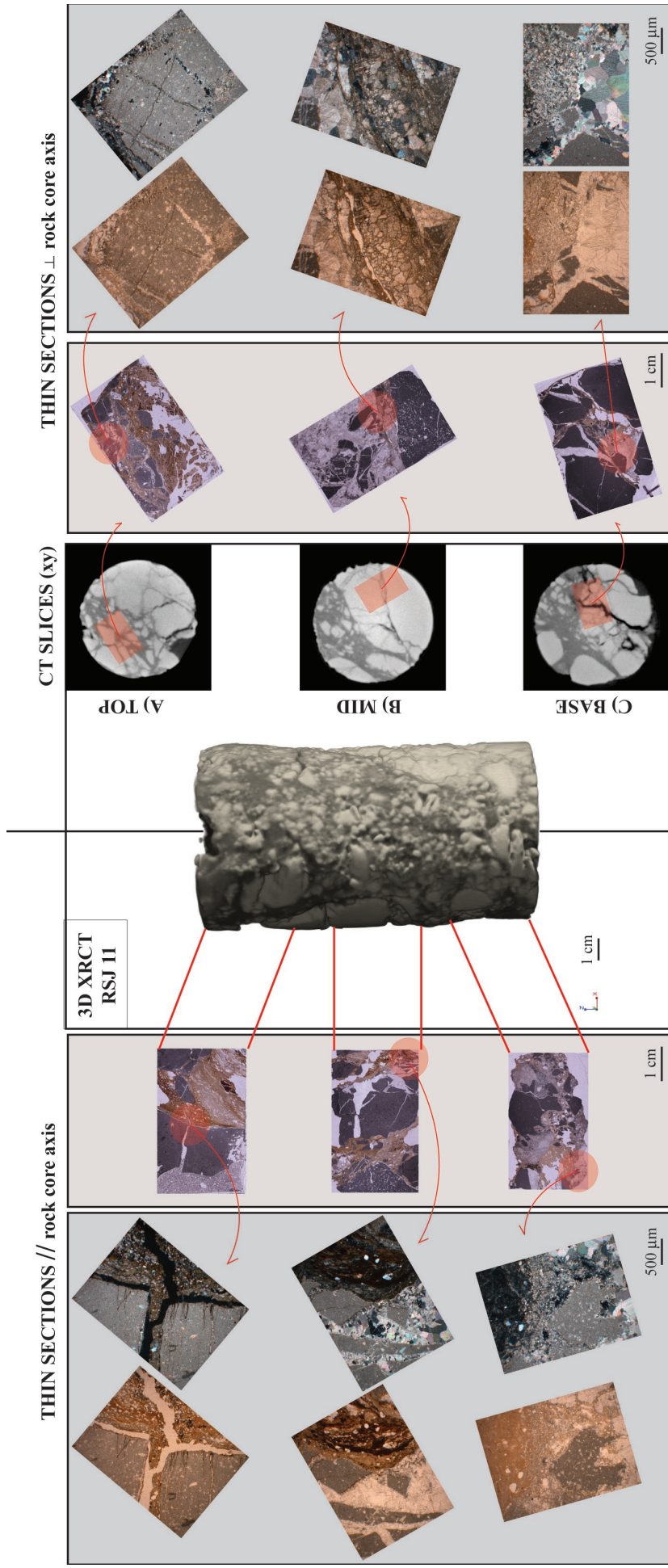


Fig. 11.7 Illustration of the domain of resolution defined by thin section and XRCT analyses based on evidence of deformation of sample *RSJ 11* after it underwent triaxial deformation. XRCT resolved structures are confronted with thin sections realized from the deformed volume once extracted from the membrane used for triaxial testing and impregnated with low viscosity resin. Thin sections parallel (left) and perpendicular (right) to rock core axis are presented. Next to the XRCT volume, 3 slices (axial *yz*-view) are depicted corresponding approximately to the original rock core slices from which thin sections have been realized. Three sections inside the rock core volume have been considered: **A)** TOP: Parallel to rock core axis, complex fracture relationship with incomplete clay coating is evidenced. Perpendicular to rock core axis, the thin section shows intra-clasts fracturing. **B)** MID: left is a view of two types of discontinuities of contrasting mechanical behavior (calcite recrystallization vs. clay). Right presents a detail of an important recrystallized fracture with clay stripes and dissolution cavities. **C)** BASE: Left evidences an altered clast surrounded by calcite recrystallization and clay filling. Right shows contrasting calcite grain size in calcite recrystallizations. Thin section views make it obvious that the “package of discontinuities” highlighted by means of XRCT stack segmentation (e.g. the XRCT matrix translated in terms of *damage indicators*) corresponds actually to a complex mixture of structural and mineralogical entities affected by strong rheological contrasts. A precise description of cataclastic behavior should therefore be able to take into account the different response to stress of such various discontinuity types.

12

RESULTS FROM MECHANICAL TESTS

« Il y a deux catégories d'hommes dans l'existence, ceux qui toute leur vie poursuivent un but sans jamais l'atteindre et ceux qui l'ayant atteint ne s'en satisfont pas. Alors être une moitié des deux est un fardeau très lourd à porter. »

Gilbert Sinoué, *Avicenne où la route d'Ispahan*

The *RSJ* rock cores characterized in the previous chapter from a geological perspective have further been investigated mechanically. Triaxial tests have been undertaken on the 13 samples under study. Accordingly, a comparison between the evidence of triaxial deformation with results from the geological characterization is attempted.

Strength data and deformation results are presented in this chapter. Triaxial tests have been complemented by additional mechanical procedures on excess material that remained after rock core preparation into standardized dimensions.

- 3 uniaxial compressions (UCS) on 2.5 x 5 cm re-drilled cores from excess material of samples *RSJ 2* and *RSJ 3*;
- 3 shear tests on reconstituted materials of sample *RSJ 6* estimated representative of main discontinuity types (calcareous, clay, and mixed joints);
- 1 indirect tensile test (“Brazilian” test) on a re-drilled core from sample *RSJ 5* (25 x 25 mm) used in combination with UCS to determine an indicative intrinsic curve for the *RSJ* samples.

Based on mechanical test evidences, a confrontation with the textural and structural data available from the geological characterization is attempted in order to investigate the proposed translation of *damage indicators* (described by means of shape and orientation) into *strength reduction criteria* for an improved mechanical interpretation. A detailed discussion will be conducted in **Chap. 13**.

The mechanical study performed in this research corresponds to an analysis of residual triaxial strength values based on the Mohr-Coulomb approach. It takes advantage of the XRCT visualization capacities to indirectly confront the *undeformed* and *deformed* rock cores, e.g. *before* and *after* they underwent triaxial deformation. Accordingly, a reinterpretation of the rupture angle, the cohesion and the angle of internal friction is made on the base of indirect evidences. Two points have to be mentioned in this context:

- 1) The approach that has been followed corresponds to the usual soil mechanics approach for homogeneous isotropic geomaterials, e.g. the interpretation of rupture angles derives from an analysis of the residual Mohr circles on which a best-fit Mohr-Coulomb regression curve has been determined. It is a strong simplification of the true rupture conditions and has only been adopted to evaluate the different *RSJ* samples on a common basis. It is however evident that the structural variability affecting these samples would require a more detailed analysis of the rupture conditions (control of pre-existing discontinuities or not and adoption of an *oriented* failure criterion). In case of carbonatic cataclasites, the rock material is of a chaotic nature and it is thus difficult to define a relationship between applied stress σ and rupture angle α . Moreover the existence of contrasted types of discontinuities introduces an additional complication since they can be characterized by very different strength properties (see **section 11.5**). Accordingly it was questioned how the visual capacities of medical XRCT could potentially improve the mechanical understanding of such heterogeneous tectonized materials and how XRCT data could be implemented for their geotechnical characterization.
- 2) Based on the *RSJ* triaxial strength data, and with the use of GSI determinations made on the different rock cores in **Chap. 11**, it would have been theoretically possible to go one step further and to test at least on some samples the rupture criterion proposed by *Habimana*

(1999, **Eq. 3.2**). Namely, profiting from data of the uniaxial compression and Brazilian tests to define the σ_{ci} and m_i parameters for the intact rock, together with data of the shear tests to determine the shear strength of the discontinuities, the constitutive parameters of the modified criterion for cataclastic rocks could have been estimated from the relationships proposed in **Table 3.3**. However, aware that available data from *RSJ* were limited, this determination in terms of an intrinsic *RSJ* behavior has been estimated affected by a too strong level of uncertainty. Therefore it has been decided to focus only on how to potentially better interpret complex rupture conditions from a structural perspective (e.g. XRCT-based arguments), in order to explore the possible improvements in any correlation attempts between the geological and geomechanical evidences. This has been done accordingly on a pure qualitative perspective to stimulate ideas for further research.

In this chapter, it is demonstrated that the possibilities offered by the medical XRCT places it as a bridge analytical technique permitting a direct confrontation of geological and geomechanical observations on identical cataclastic rock cores. Eventually quantification and visualization of the triaxially induced damages is made by comparison with the 3D segmented models presented in **section 11.3.2**. These observations are proposed to evaluate the susceptibility to fracture of the different rock cores under study and to evidence structural controls related to pre-existing discontinuities influencing triaxial response.

On a more general perspective, the different parameters discussed in the current and preceding chapters are envisaged for their interest in improving the determination of a tectonization degree for cataclastic rock cores. Accordingly, the quantification of the parameter t of the modified rupture criterion proposed by *Habimana* (1999) could be probably enhanced in the future based on a thorough morphological and topographical analysis of 3D *damage indicators*. A determination of t on the base of microstructural and mineralogical quantitative evidences is expected more realistic than its GSI-derived estimation.

12.1 TEST RESULTS: STRENGTH DATA

The different results of mechanical tests that have been realized on the *RSJ* rock cores are presented in **Table 12.1**. **Table 12.1 A** is a compilation of triaxial strength data. **Table 12.1 B** shows the valorization of excess rock core materials providing additional reference values for the mechanical interpretation.

12.1.1 Evaluation of Triaxial Stress Data: Peak & Residual Behaviors

The evaluation of the triaxial tests carried on the *RSJ* rock cores is made from two perspectives:

- Classification of the *RSJ* rock cores into the 3 mechanical families *brittle*, *ductile* and *combined* by consideration of the stress-strain triaxial curve σ - ε (for the definition of these families see **Chap. 9, section 9.1.2**).
- Using triaxial residual strength, computation of the normal and tangential stresses (σ_N and τ) on the rupture plane from **Eq. 9.2 & 9.3** (Mohr circle).

Fig. 12.1 is the results obtained in terms of peak and residual strength and regroups the different Mohr circles in a normal-deviatoric stress space (σ - τ). Based on the results for uniaxial and tensile strengths (**Table 12.1 B**), estimation of an *indicative* intrinsic curve for the *RSJ* samples («*RSJ*») has been made and is represented on the graph. Using values for Kimmeridgian limestone from the LMR database, a second intrinsic curve is drawn («*kimmeridgian LMR*»). These curves have

A)

| SAMPLE | dimensions (mm) | TRIAXIAL PEAK VALUES (MPa) | | | E _{50%} | TRIAXIAL RESIDUAL VALUES (MPa) | | | | | |
|--------|--------------------|----------------------------|------------|------------|------------------|--------------------------------|-------|------------|-------|-------------|--|
| | | σ_1 | σ_3 | σ_3 | | Loading I | | Loading II | | Loading III | |
| RSJ 1a | 166 x 75 | 90.9 | 4 | - | 43.3 | 4 | 52.9 | 6 | 63.1 | 8 | |
| RSJ 1b | 164.5 x 75.5 | - | - | - | 14.6 | 2 | 22.4 | 4 | 28.8 | 6 | |
| RSJ 2 | 161 x 75.6 | 157 | 2 | 14800 | 102.7 | 2 | 143.3 | 4 | 178.8 | 6 | |
| RSJ 3 | 148 x 75.7 | 96.4 | 2 | 22000 | 37.7 | 2 | 50.4 | 4 | 61.5 | 6 | |
| RSJ 4 | 155 x 80.1 | 54.2 | 2 | 13300 | 24.2 | 2 | 34.8 | 4 | 44.7 | 6 | |
| RSJ 5 | 166.5 x 80.6 | 73 | 4 | 16000 | 37.1 | 4 | 47.7 | 6 | 59.9 | 8 | |
| RSJ 6 | 163 x 80.9 | - | - | - | 24.7 | 2 | 36 | 4 | 45.9 | 6 | |
| RSJ 7 | 161 x 80.9 | 55.3 | 4 | 14600 | 39.4 | 4 | 49.5 | 6 | 59.6 | 8 | |
| RSJ 8 | 166 x 80.6 | 64.1 | 8.3 | 10800 | 57.2 | 8.3 | 33.7 | 4.3 | 21.2 | 2.2 | |
| RSJ 9 | 157 x 80.9 | 33.4 | 2 | 8500 | 30.2 | 2 | 42.4 | 4 | 53.4 | 6 | |
| RSJ 10 | 163 x 80.6 | 93.7 | 2.2 | 20000 | 28.5 | 2.2 | 44.1 | 4.4 | 56.5 | 6.6 | |
| RSJ 11 | 158 x 81.7 | - | - | - | 11 | 2.2 | 17 | 4.4 | 22.6 | 6.6 | |
| RSJ 12 | 159.5 x 80.6 | - | - | - | 27.7 | 4.4 | 38.1 | 6.6 | - | - | |

B)

| SAMPLE | COMPRESSIVE STRENGTH (MPa) | | | DIRECT SHEAR STRENGTH | | | TENSILE STRENGTH (MPa) | |
|------------|----------------------------|------------|------------------|---------------------------------|-------------------|----------------|------------------------|------------|
| | dimensions (mm) | σ_c | E _{50%} | dimensions (mm) | c_{res} (MPa) | Φ (°) | dimensions (mm) | σ_T |
| RSJ 2a | 40 x 25 | 70.9 | 13600 | 40 x 25 52 x 25 50.8 x 25 | 0.65 0 1.79 | 38 20 28 | 25 x 25 | 5.6 |
| RSJ 2b | 52 x 25 | 40.6 | - | | | | | |
| RSJ 3 | 50.8 x 25 | 79.8 | 22850 | | | | | |
| RSJ 5 | - | - | - | - | - | - | - | - |
| RSJ calc | - | - | - | - | - | - | - | - |
| RSJ 6 clay | - | - | - | - | - | - | - | - |
| RSJ mixed | - | - | - | - | - | - | - | - |

Table 12.1 Results of mechanical tests performed on the *RSJ* rock cores. **A)** Results from triaxial tests. Samples *RSJ 1b*, *6*, *11* & *12* exhibit ductile behavior, e.g. no peak strength is reached. Rock cores have been tested at three levels of confining pressures: $\sigma_3 = 2; 4; 6$ MPa, $\sigma_3 = 4; 6; 8$ MPa and an inverse $\sigma_3 = 8; 4; 2$ MPa. Evaluation of rupture conditions in the investigated rock cores is made through a confrontation of classical Mohr-Coulomb residual circles vs. XRCT-derived observations. **B)** Valorized excess materials from preparation into standardized dimensions of triaxial samples. Results from uniaxial compression (intrinsic resistance of hard rock matrix), direct shear tests (joint strength), and “Brazilian” test (tensile strength of hard rock matrix).

been defined based on the empirical relationship of *Fairhurst* (1964b) (Eq. 9.6). As stated in the beginning of this chapter, an estimation of the modified rupture criterion of *Habimana* (1999) has not been addressed but would have been theoretically possible with considerations of the proposed relationships between the GSI and the a , m_p , s and t -parameters.

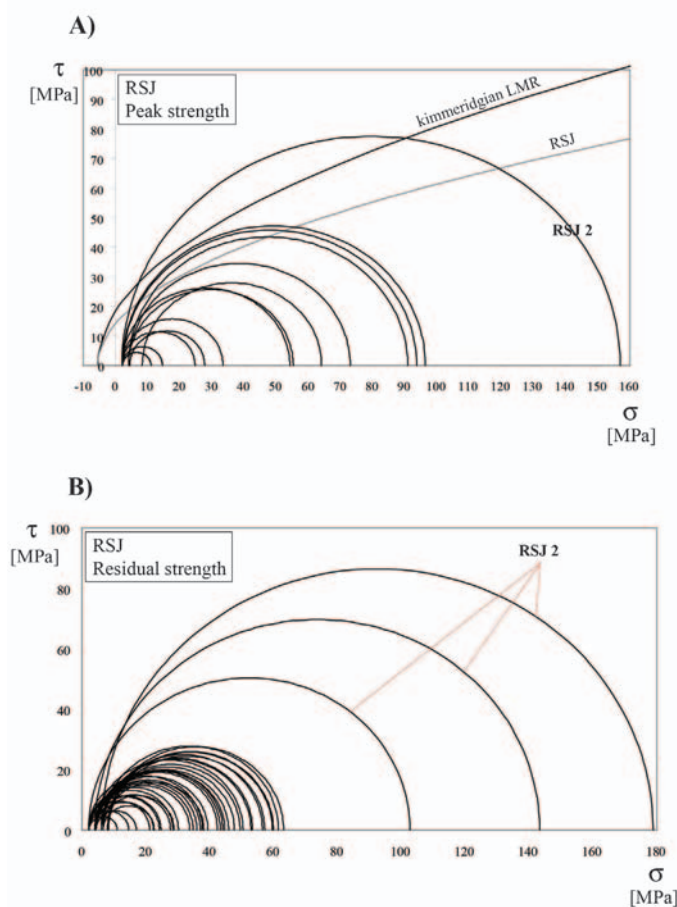


Fig. 12.1 Results of triaxial tests performed on the RSJ rock cores. A) Peak strength. B) Residual strength (3 residual Mohr circles for each rock core). On A), 2 evaluated intrinsic curves for kimmeridgian limestone are evidenced («RSJ» & «kimmeridgian LMR», see text). Note the special position on B) of sample *RSJ 2* (3 outermost circles). As will be presented later on, an oriented preexisting discontinuity affects the triaxial response of *RSJ 2*, preferentially stimulating a fracturation in the primary rock matrix during test.

12.1.2 Mechanical Behaviors of RSJ Samples

Due to the strong heterogeneity of the tectonically deformed limestone and as a result of variable amounts of soft components inside the *RSJ* samples (e.g. clay), 3 different mechanical behaviors have been observed during triaxial deformation. They have been classified according to the criteria presented in **section 9.1.2**.

Table 12.2 presents the different mechanical behaviors observed on the *RSJ* samples. Reference to the determined geological quality classes is made. The different triaxial stress-strain curves (σ - ϵ) of the *RSJ* rock cores can be found in **Appendix V-I**. **Table 12.2** further introduces evidences from pre-existing discontinuities susceptible to control with more or less importance the triaxial deformation of the *RSJ* rock cores. It is observed that the modes of deformation recorded on the *RSJ* samples are in no direct relationship with the visually assessed and XRCT confirmed geological classes (I-III). This is to explain by the fact that such a confrontation remains at a simplistic level of correlation between geological and mechanical parameters, i.e. no considerations about the spatial orientation of pre-existing discontinuities with regard to rock core axis have been made yet (which would imply a tensor determination of geological parameters instead of the current scalar approach by means of the quantified DI or the MSI; this is potentially to improve on the base of the tomographic DI reconstructions, see **section 12.2.2** and later **Chap. 13**). Taking into account the spatial orientation of pre-existing discontinuities and a precise determination of the nature of such discontinuities, a

| SAMPLE | GEOLOGICAL CLASS | POTENTIAL CONTROL OF PREEXISTING DISCONTINUITIES DURING TRIAXIAL TEST | OBSERVED MECHANICAL BEHAVIOR | ESTIMATED MODE OF DEFORMATION |
|--------------|------------------|--|------------------------------|-------------------------------------|
| RSJ1a | I | relative homogeneous rock core, low potential control from preexisting discontinuities | brittle | plane |
| RSJ5 | I | relative homogeneous rock core, low potential control from preexisting discontinuities | intermediate | plane |
| RSJ10 | I | relative homogeneous rock core, low potential control from preexisting discontinuities | brittle | plane |
| RSJ1b | II | high potential control from a preexisting active fracture plane at 45° | <i>ductile</i> | plane |
| RSJ2 | II | high potential control from a preexisting discontinuity in singular orientation | intermediate | combined (plane + fragmentation) |
| RSJ3 | II | high potential control from a preexisting subvertical structure on top of rock core | brittle | combined (plane + fragmentation) |
| RSJ7 | II | high potential control from a preexisting subvertical structure filled with clay-material across rock core | intermediate | fragmentation |
| RSJ8 | II | high potential control from a preexisting subvertical structure on top of rock core | intermediate | plane |
| RSJ9 | II | high potential control from a preexisting subvertical structure on base of rock core | intermediate | fragmentation |
| RSJ4 | III | strong competence contrast between soft and hard rock components in subvertical orientation, high potential control | brittle | combined (plane + internal) |
| RSJ6 | III | strong competence contrast between soft and hard rock components in unfavorable orientation, high potential control | ductile | internal |
| RSJ11 | III | heterogeneity, strong competence contrast between soft and hard rock components in random orientation, low potential control | ductile | internal |
| RSJ12 | III | heterogeneity, strong competence contrast between soft and hard rock components in random orientation, low potential control | ductile | combined (fragmentation + internal) |

Table 12.2 Presentation of the observed mechanical behaviors from the *RSJ* rock cores and confrontation with the determined geological quality classes (**Chap. 11**). No direct relationship is found, see text for a discussion. Indication is made about potential test control from pre-existing discontinuities. Additional evaluations of the mode of deformation are made. For the estimation of single vs. multiple plane fracturing and/or of internal deformation (e.g. no development of a rupture plane), XRCT visualization on reconstructed volumes *before* and *after* tests has been used. This corresponds to a qualitative procedure that mainly consists in reevaluating the development of localized (e.g. development of a single rupture plane) vs. more generalized rupture conditions of the rock material. Note that prediction of brittle behavior is difficult to assess, while the other mechanical behaviors seem more obviously related to the predicted geological class (in particular a good correspondence is found between *Class III* and ductile behavior). Sample *RSJ 1b* is an exception for ductile behavior but as will be evidenced later, deformation corresponds to pure frictional sliding on a pre-existing cohesionless discontinuity.

better correspondence between geological classes and their expected mechanical behavior could be possibly obtained. Interestingly, due to the effect of the orientation of pre-existing discontinuities with regard to the load application in triaxial tests, the prediction of brittle mechanical behavior is made difficult (see for example samples *RSJ 3* and *RSJ 4*). On the other hand, it is found that the best correspondence is observed between samples of *Class III* that are ideally expected to behave in a ductile manner (see *RSJ 11 & 12*, and also *RSJ 6*).

Structural and textural factors control obviously the deformation of heterogeneous materials. These have to be properly assessed before any robust correlation in between geological and mechanical parameters can be expected. The MSI is in this sense an attempt based on oriented thin sections; however many critics are expressed by rock mechanicians on the effective applicability of the index to accurately predict strength (2D approach, determination not realized on the sample that is effectively triaxially tested). With the implementation of 3D segmented models as shown later in the chapter, new considerations can be drawn on how to introduce morphological and topographical properties of damage indicators in terms of their effect on rock deformation. With additional petrographical constraints (nature of damage indicators) this could permit a 1:1 confrontation between a given heterogeneous rock structure and its control on resulting mechanical behavior and mode of failure.

12.1.3 Re-Interpretation of Rupture Angles by Means of XRCT

XRCT scans have been performed on each sample before completion of the triaxial test and a second imagery realized after removal from the triaxial cell. Based on the XRCT recording of *undeformed* and *deformed* states, the classical triaxial evaluation (residual Mohr-circle analysis) has been confronted with an interpretation taking advantage of the indirectly evidenced main discontinuity that has most likely controlled sample deformation during test.

For each *RSJ* rock core, a thorough analysis of the XRCT imagery *before* and *after* test has been conducted in order to define rupture conditions during triaxial deformation. From this qualitative assessment, the main geological structure has been defined and its orientation measured on six plane views across the sample, corresponding to 3 xz- and 3 yz-clipped positions at regular increments inside its volume (positions 150, 250 and 350, see **Appendix V-I**). On each clipping plane, the angular variability of the main structure (susceptible to cause a dilatancy effect during deformation) has been assessed by numerous measurements using the angle measurement tool implemented in VGStudioMAX. Averaged frontal and sagittal discontinuity traces allow reconstructing the maximum dip orientation (e.g. α_{XRCT}) of the assumed rupture structure using the stereographic projection.

With this methodology, an attempt is made to consider the true rupture geometry in the triaxial test interpretation. It is however affected by potential bias, since the acquisition *after* triaxial test is done after removal of the rock core from its confining environment, meaning that the XRCT-visualized structures are most probably exaggerated as a result of sample decompression. In the context of this research, the best possible has been made by keeping the samples in the test membrane and by performing the second XRCT acquisition at CHUV straight after test completion. Therefore, in terms of the determination of the orientation of the main geological structure, the approach is found promising. Some improvements could be considered in the future (such as to scan the sample directly in the triaxial cell under confining pressure and after the first failure has been recorded) in order to prevent the complications introduced by **1**) secondary rupture structures and **2**) the effect of rock decompression.

| XRCT EVIDENCE FOR DAMAGE DEVELOPMENT IN ROCK CORES | | RUPTURE ANGLE | |
|--|---|--|----------------------|
| | | Mohr analysis (derived) | XRCT (stereographic) |
| | Major structure | Secondary structures | |
| FRAGILE | | | |
| RSJ1a | Localized conjugate fracturing | Subvertical fracturing + subhorizontal fracturing | 30 |
| RSJ3 | Localized conjugate fracturing | Subvertical fracturing + central dislocation (progressive fragmentation) | 26 |
| RSJ4 | Subvertical fracturing in hard rock components + clast rotation | Central dislocation (progressive fragmentation) | 26 |
| RSJ10 | Compaction band with shear + associated fracturing, bending | Minor fracturing | 30 |
| INTERMEDIATE | | | |
| RSJ2 | Sliding along the preexisting transversal surface + corner development (progressive fragmentation) | Subvertical fracturing | 13 (55) |
| RSJ5 | Compaction band with shear + associated fracturing | Progressive fragmentation | 30 (45) |
| RSJ7 | Influence of preexisting discontinuities of contrasting properties, complex stress accumulation, transversal rupture ("lightening fracture"), preferential fragmentation in bottom part | | 30 |
| RSJ8 | Settling + initiation of shear band + activation of shear band | Progressive fragmentation | 26 |
| RSJ9 | Shear band along preexisting discontinuity inducing a sustained preferential fragmentation in bottom part | Development of a conjugate subhorizontal crack system | 30 |
| DUCTILE | | | |
| RSJ1b | Sliding along a preexisting transversal surface, clast rotation + dilatation | Slight comminution of clasts (progressive fragmentation) | 35 (45) |
| RSJ6 | Subvertical fracturing in hard rock components, reactivation of a major structure at 45°, progressive fragmentation | | 30 |
| RSJ11 | Fracturing in bigger clasts | Comminution + rotation (sustained fragmentation) | 30 |
| RSJ12 | Fracturing in bigger clasts | Comminution + rotation (sustained fragmentation) | 30 |

Table 12.3 Comparison between rupture angles determined from the Mohr circle analysis (according to the usual soil mechanics approach) or by mean of XRCT. In the Mohr circle analysis, samples *RSJ 1b, 2 & 5* are typical specimens for which an oriented failure criterion should be adopted (visual evidence of a failure plane on the rock core after test, values of α in bracket). Next to it, definition of a rupture angle α_{XRCT} is made from an interpretation of the rupture conditions based on structural XRCT-evidences visualized on a selection of orthogonal clipping planes taken parallel to rock core axis (see **Appendix V-I**). At this stage, α_{XRCT} is affected by a certain level of subjectivity, function of the «geological eye». Nevertheless, adequate image analysis tools for 3D XRCT data analysis can lead in the future to a more robust angle determination, by integrating the topography and morphology of the effective rupture plane(s) (see tomographic DI reconstructions in **section 12.2.2**).

The different α_{XRCT} that have been taken for the re-calculation of normal and tangential stresses are listed in **Table 12.3**, together with the geological interpretation of rupture conditions. Resulting stress data can be further found in **Table 12.4**. A graphical analysis will be conducted in the next section.

It has to be pointed out again that in case of the Mohr-Coulomb analysis, due to the often complex rupture geometries, failure has been considered as corresponding to the rupture orientation given by the tangence point between the Mohr-Coulomb criterion and the residual Mohr circles (corresponding to the usual soil mechanics approach, see **Fig. 9.2**). This is incorrect in the sense that the spatial orientation and control of pre-existing discontinuities are accordingly not assessed (e.g. oriented failure criterion for rock mechanics). Two samples were particularly influenced by singular pre-existing discontinuities (*RSJ 1b* and *RSJ 2*) and it is thus to expect that the derived mechanical analyses are affected by errors. Moreover sample *RSJ 5* has been a typical example where failure conditions could be determined visually after removal of the specimen from the triaxial cell (development of a singular shear plane). For these 3 specific samples, an angle determined visually has been retained (value in brackets in **Table 12.3**).

| A) | | Mohr rupture angle α | Mohr parameters | | Normal & tangential stresses [MPa] | | | | | |
|--------------|--------|-----------------------------|-----------------|----------|------------------------------------|--------------|------------------|--------------|------------------|--------------|
| | | | c_r [MPa] | ϕ_r | σ_N triax | τ triax | σ_N triax | τ triax | σ_N triax | τ triax |
| Brittle | RSJ 1a | 30 | 5.1 | 40.7 | 13.8 | 17.0 | 17.7 | 20.3 | 21.8 | 23.9 |
| | RSJ 3 | 26 | 5.3 | 45.0 | 8.9 | 14.1 | 12.9 | 18.3 | 16.7 | 21.9 |
| | RSJ 4 | 26 | 3.1 | 42.1 | 6.4 | 8.9 | 10.1 | 12.3 | 13.7 | 15.5 |
| | RSJ 10 | 30 | 2.7 | 44.6 | 9.0 | 11.5 | 14.6 | 17.4 | 19.5 | 21.8 |
| Intermediate | RSJ 2 | 55 | 2.3 | 32.0 | 70.4 | 47.0 | 98.6 | 65.0 | 123.4 | 80.7 |
| | RSJ 5 | 45 | 2.1 | 35.1 | 20.5 | 16.5 | 26.8 | 20.8 | 33.9 | 25.9 |
| | RSJ 7 | 30 | 4.1 | 40.9 | 13.1 | 15.5 | 17.2 | 19.0 | 21.3 | 22.6 |
| | RSJ 8 | 26 | 1.7 | 44.7 | 18.0 | 19.5 | 10.2 | 11.7 | 6.0 | 7.6 |
| | RSJ 9 | 30 | 3.7 | 43.2 | 9.3 | 12.3 | 13.9 | 16.8 | 18.2 | 20.7 |
| Ductile | RSJ 1b | 45 | 1.7 | 29.3 | 8.3 | 6.3 | 13.2 | 9.2 | 17.4 | 11.4 |
| | RSJ 6 | 30 | 3.0 | 41.9 | 7.7 | 9.8 | 12.0 | 13.9 | 16.0 | 17.3 |
| | RSJ 11 | 30 | 1.6 | 26.7 | 4.5 | 3.8 | 7.6 | 5.5 | 10.7 | 7.0 |
| | RSJ 12 | 30 | 1.5 | 39.7 | 10.4 | 10.2 | 14.7 | 13.8 | | |

| B) | | XRCT rupture angle α_{XRCT} | XRCT Mohr parameters | | Normal & tangential stresses [MPa] | | | | | |
|--------------|--------|------------------------------------|----------------------|----------|------------------------------------|-------------|-----------------|-------------|-----------------|-------------|
| | | | c_r [MPa] | ϕ_r | σ_N XRCT | τ XRCT | σ_N XRCT | τ XRCT | σ_N XRCT | τ XRCT |
| Brittle | RSJ 1a | 30 | 5.1 | 40.7 | 13.8 | 17.0 | 17.7 | 20.3 | 21.8 | 23.9 |
| | RSJ 3 | 42 | 4 | 37.4 | 18.0 | 17.8 | 24.8 | 23.1 | 30.8 | 27.6 |
| | RSJ 4 | 30 | 3 | 41.3 | 7.5 | 9.6 | 11.7 | 13.3 | 15.7 | 16.8 |
| | RSJ 10 | 36 | 2.5 | 41.8 | 11.3 | 12.5 | 18.1 | 18.9 | 23.8 | 23.7 |
| Intermediate | RSJ 2 | 83 | 0.1 | 6.6 | 101.2 | 12.2 | 141.2 | 16.9 | 176.2 | 20.9 |
| | RSJ 5 | 49 | 1.9 | 32.3 | 22.9 | 16.4 | 29.8 | 20.6 | 37.6 | 25.7 |
| | RSJ 7 | 34 | 3.9 | 39.6 | 15.1 | 16.4 | 19.6 | 20.2 | 24.1 | 23.9 |
| | RSJ 8 | 28 | 1.6 | 44.3 | 19.1 | 20.3 | 10.8 | 12.2 | 6.4 | 7.9 |
| | RSJ 9 | 30 | 3.7 | 43.4 | 9.0 | 12.2 | 13.6 | 16.6 | 17.8 | 20.5 |
| Ductile | RSJ 1b | 55 | 1.3 | 23.9 | 10.5 | 5.9 | 16.3 | 8.6 | 21.3 | 10.7 |
| | RSJ 6 | 63 | 1.3 | 21.5 | 20.0 | 9.2 | 29.4 | 12.9 | 37.7 | 16.1 |
| | RSJ 11 | 39 | 1.6 | 25.9 | 5.7 | 4.3 | 9.4 | 6.2 | 12.9 | 7.8 |
| | RSJ 12 | 52 | 1 | 28.6 | 18.9 | 11.3 | 26.2 | 15.3 | | |

Table 12.4 Residual mean normal and tangential stresses acting on the assumed rupture planes based on **A)** a residual Mohr circle analysis and **B)** an analysis of the XRCT models *before* and *after* test (α_{XRCT}). For each samples, σ_N and τ values for 3 residual Mohr circles are given, except for sample *RSJ 12* that only underwent 2 loading cycles. The determination procedure of α_{XRCT} from frontal and sagittal CT views is discussed in **Chap. 9** and further detailed in this section. Note samples *RSJ 1b*, *2* & *5* for which the usual Mohr circle analysis has been made implementing a value of rupture angle visually assessed on the sample once extracted from the triaxial cell. These samples represent a typical case in rock mechanics where an oriented failure criterion should be adopted; see text for limitations of the approach.

12.1.4 Analysis of Mohr Residual Circles

To interpret stress conditions on the rupture plane, an analysis of the residual Mohr circles determined after completion of triaxial tests on the *RSJ* rock cores has been conducted. **Table 12.4** presents the results of the Mohr-Coulomb analysis for the 3 mechanical families corresponding to the *RSJ* samples. Values of normal and tangential stresses (σ_N and τ , i.e. tangence point between the Mohr Coulomb line and the Mohr circles according to the usual soil mechanics approach for homogeneous and isotropic materials) have been determined using **Eq. 9.2** and **9.3**. Then, parameters of the Mohr-Coulomb criterion (c_f and ϕ_f) have been calculated for each mechanical behavior depicted by the *RSJ* rock cores. As mentioned in the previous section, 3 samples have been interpreted based on visual evidences of rupture geometry after removal from the triaxial cell (*RSJ 1b, 2 & 5*). Next to it, the same determination has been conducted when the different rupture angles interpreted by means of XRCT are used (α_{XRCT} , **Table 12.3**).

Fig. 12.2 is a graphical representation of the obtained results. **Fig. 12.2 A** shows a plot of the mean residual normal and tangential stresses on the failure plane (σ_N and τ) for the *RSJ* samples classified by mechanical behavior as obtained by taking into account the determined rupture angle from the residual Mohr circle analysis. **Fig. 12.2 B** shows the same plot but with the values of σ_N and τ calculated by taking this time the XRCT derived angle into account. **Fig. 12.3** highlights next the difference obtained between the two determined Mohr-Coulomb criteria for the three mechanical families. In comparison with the classical approach, the XRCT determination of the failure plane allows an interpretation of the triaxial tests that is somewhat improved compared to the standard procedure, especially for samples behaving in a plastic manner. Discrimination of brittle and intermediate behaviors are more problematic and a more detailed investigation of the nature of pre-existing discontinuities should be addressed for them. In this context, it is interesting to notice the isolated position of sample *RSJ 5* of combined behavior, clearly separated from the other samples of this category that are difficult to distinguish from the brittle mechanical family. To deliver an explanation for the position of sample *RSJ 5* would require a specific examination of pre-existing discontinuities, in terms of their orientation and petrographical properties. Sample *RSJ 5* is in addition indicative of the need to introduce geological considerations in a mechanical interpretation of heterogeneous already weakened geomaterials. Some comments will be attempted in the next chapter (see in particular **Fig. 13.7**). All these results show the interest of implementing an indirect visualization to interpret the deformation mechanism of particularly altered samples, as it provides the ability to evidence deformation structures that would stay unresolved in a classical approach. More generally, with a visualization support able to more objectively evaluate the effective fracture geometry resulting from the complex interaction of cataclastic rock elements (XRCT), indications are obtained in this way concerning the structural control of pre-existing discontinuities (e.g. *damage indicators*) on rupture conditions.

At this stage, only a residual strength analysis of the *RSJ* samples has been conducted. In order to improve the exercise of confrontation between two determinations of main rupture angle, a peak strength analysis implementing the oriented failure criterion should be adopted together with a more detailed petrographical analysis of the indirect XRCT data, so as to define conditions for failure and shear inside a given rock core. This last aspect is thought capable to provide engineers with more confident data on material (and fracture) characteristics and to improve accordingly any mechanical interpretation performed on heterogeneous cataclastic materials. The 3D segmented models (tomographic DI reconstructions) that will be presented in the next section can moreover assist greatly an improved mechanical analysis that would take into account the petrographical and structural reasons why a preferential mode of deformation is found affecting a given rock core.

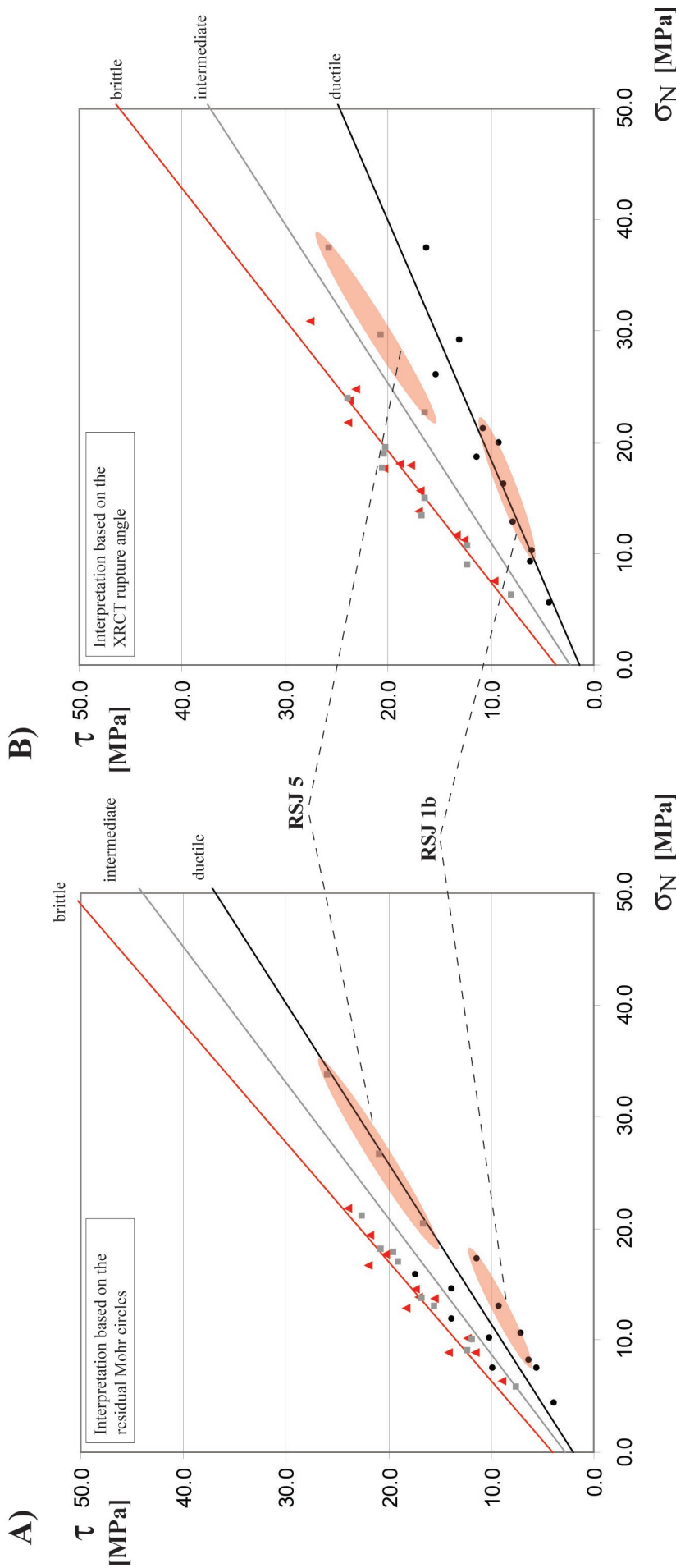


Fig. 12.2 Residual mean normal and tangential stresses [in MPa] on the rupture plane determined from **A**) the triaxial protocol with an estimation of rupture angle based on linear regression on residual Mohr circles, and **B**) a reinterpretation using α_{XRCT} . See text for considerations about the validity of such an approach. Mohr-Coulomb criteria have been determined for each mechanical behavior described in the previous section. Mechanical families are: red triangles: brittle; grey squares: intermediate; black dots: ductile. Note the interest of XRCT to more accurately analyse rock cores affected by ductile behavior. Samples of intermediate behavior seem closely related to the brittle samples in terms of stress conditions after rupture. Only sample RSJ 5 of intermediate behavior is clearly isolated from an undifferentiated brittle-intermediate cloud of values, which would require more detailed petrographical and structural investigations to be explained. Results of samples RSJ 2 are outside the plots due to a much higher strength than the other RSJ samples (see Table 12.4). Position of sample RSJ 1b for which a visual rupture angle determination after removal from the triaxial cell has been conducted is also highlighted. Despite a limited amount of data, evidences of **A**) and **B**) is encouraging in generalizing the use of XRCT in mechanical test procedures to better account for fracture conditions in heterogeneous rock materials.

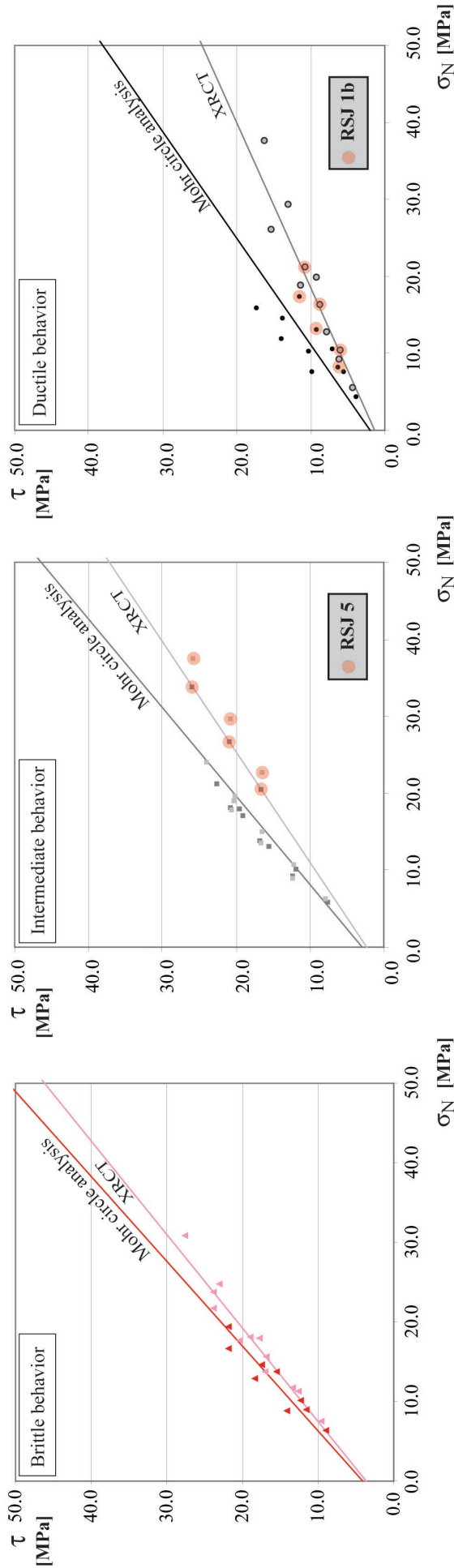


Fig. 12.3 Mohr-Coulomb criteria for the different *RSJ* mechanical families as determined from the Mohr circle analysis or using XRCT evidence. In each plot, light toned symbols correspond to the XRCT derived data. Note that derived c_r and ϕ_r differ more strongly in ductile behavior, with a better material description based on α_{XRCT} (indirect evidence of deformation patterns made possible with XRCT but hardly made by eye after removal of the rock core from the triaxial cell). Note again the isolated position of sample *RSJ 5* in the intermediate family. For this category of samples, it seems that the α_{XRCT} determination is not effective (difficulty in isolating clearly one main rupture structure due to sample heterogeneity and complex deformation pattern, involving numerous sub-ruptures in different orientations). Sample *RSJ 1b* of ductile behavior is also highlighted as it was the object of a visual rupture angle determination in the Mohr circle analysis, see text. Values of normal and tangential stresses are in MPa.

12.2 RESULTS OF XRCT CHARACTERIZATION AFTER DEFORMATION

This section performs the study of *damage indicators* on the *RSJ* samples (see **Chap. 11**) based on the XRCT acquisitions *after* triaxial tests. Accordingly, a confrontation between the two detections of damage indicators *before* and *after* triaxial deformation will be performed. This is done to objectively evaluate the control of preexisting discontinuities on resulting deformations and in particular to present the advantages of the XRCT technique for a combined geological and geomechanical rock core characterization.

12.2.1 Damage Index Determinations After Triaxial Test

The damage index *DI* of the geological characterization (**Eq. 10.6**) has been renamed DI_{triax} and calculated for the *RSJ* rock cores after their deformation in the triaxial cell. To determine DI_{triax} , the segmentation parameters of **Table 11.6** have been used. To ensure a volumetric correspondence between XRCT stacks *before* and *after* tests and avoid at most errors induced by sample shape distortion during test, calculation of DI_{triax} has been performed using the same region of interest (ROI) that has been implemented for the indirect geological characterization. **Table 12.5** presents numerical values of DI_{triax} that are further plotted in **Fig. 12.4**.

Note: The region of interest is simply the circular window adjusted on the axial CT slices constitutive of an XRCT stack defining the effective image field of view from which the volume calculation is performed. As experienced with rock core CT data, sample shape after triaxial deformation can strongly differ from circularity. In order not to introduce artifacts during segmentation (e.g. detection of the CT contrast caused by the rubber membrane or detection of additional void space resulting from dislocation of rock core parts), a conservative ROI has been defined to proceed to the *DI* determinations to be sure that segmentation is performed *only* on rock components. These conservative ROI have been adjusted on both the XRCT data *before* and *after* test, to ensure consistence between determined *DI* and DI_{triax} (e.g. same “virtual” rock core volume considered in both case).

A geological-mechanical correlation requires obviously more than just the consideration in terms of *DI*. As will be discussed later on, damage indicators from brittle and ductile samples correspond to petrographical entities of contrasted mechanical properties (recrystallization of calcite vs. clay proportion). It is expected that combining the parameters *DI* (heterogeneity & anisotropy), MSI_{XRCT} (mineralo-structural characterization), and a parameter FI_{triax} (ponderation factor accounting for the structural control of pre-existing discontinuities in triaxial deformation and rock core unicity, see below) can provide a pertinent approach to define a tectonization degree for rock cores, following the consideration of *Habimana* (1999). See **Chap. 13** for a detailed discussion.

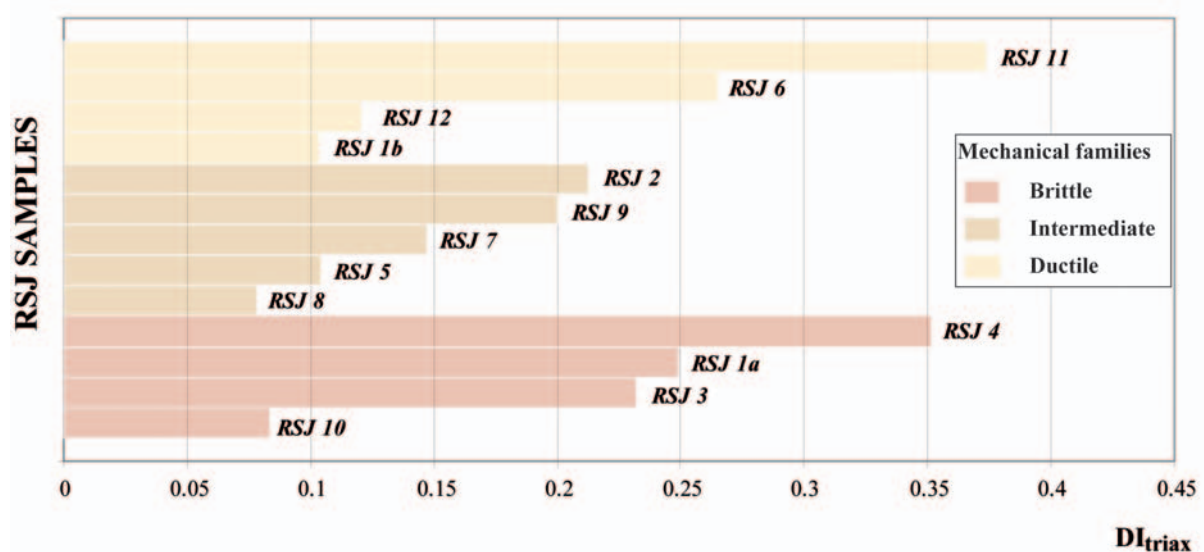


Fig. 12.4 *RSJ* rock cores classified according to increasing damage index DI_{triax} for each mechanical family. Compare with **Fig. 11.1**. Note the similarity in DI_{triax} between brittle and ductile behaviors.

| Samples after triaxial test | Representative CT slices for calibration of segmentation | Primary segmentation: XRCT _{clasts} | Primary segmentation: XRCT _{matrix} | Secondary segmentation | Noise elimination | Overdensity elimination | % XRCT _{clasts} | % XRCT _{matrix} | DI _{triax} |
|-----------------------------|--|--|--|------------------------|-------------------|-------------------------|--------------------------|--------------------------|---------------------|
| RSJ 1a | 64, 190, 314(?), 485 | | | | | | 75.16 | 24.94 | 0.249 |
| RSJ 1b | 126, 296, 382, 559 | | | | | | 89.78 | 10.39 | 0.104 |
| RSJ 2 | 3929, 4019, 4171, 4395 | | | | | | 78.9 | 21.29 | 0.213 |
| RSJ 3 | 48, 188, 322, 459 | | | | | | 77.08 | 23.2 | 0.232 |
| RSJ 4 | 552, 758, 935, 1069 | | | | | | 65.04 | 35.19 | 0.352 |
| RSJ 5 | 2286, 2410, 2619, 2632 | | | | | | 89.62 | 10.43 | 0.104 |
| RSJ 6 | 3394, 3482, 3569, 3794 | | | | | | 73.66 | 26.53 | 0.265 |
| RSJ 7 | 3306, 3187, 2999, 2857 | | | | | | 85.32 | 14.71 | 0.147 |
| RSJ 8 | 30, 100, 350, 440 | | | | | | 92.3 | 7.81 | 0.078 |
| RSJ 9 | 1697, 1849, 1990, 2169 | | | | | | 80.01 | 20.04 | 0.200 |
| RSJ 10 | 1177, 1327, 1477, 1530 | | | | | | 91.86 | 8.39 | 0.084 |
| RSJ 11 | 642, 715, 867, 929 | | | | | | 62.79 | 37.42 | 0.374 |
| RSJ 12 | 643, 760, 809, 1042 | | | | | | 88.21 | 12.06 | 0.121 |

Same segmentation parameters as in Table 11.6

Table 12.5 Best-fit segmentation parameters for the *RSJ* rock cores and evaluation of damage index DI_{triax} (Eq. 10.6). The same detection parameters of Table 11.6 for the determination of DI have been used. The CT-slices for the different *RSJ* rock cores after triaxial deformation can be found in Appendix IV-III next to the corresponding initial CT slices. An uncertainty on slice correspondences results in some cases, which is due to the sample dislocation between acquisitions *before* and *after* test (see *RSJ 1a*, comparison between the last 2 slices). This illustrates the problem of sample decompression mentioned in section 12.1.4 that results from performing the XRCT acquisition *after* test once the tested rock core is extracted from the triaxial cell.

12.2.2 Reconstruction of Segmented XRCT Stacks After Test

Based on the segmented XRCT stacks of the *RSJ* samples *after* triaxial deformation, 3D reconstructions of DI_{triax} have been performed and are presented in **Fig. 12.5**. For indication, the 3D rendering of initial DI (**Fig. 11.6**) has been superimposed for each rock core.

Provided such models, following improvements for triaxial test interpretation can be seen:

- Critical evaluation of fracturation and fracturing mechanisms inside a given cataclastic rock core as a result of triaxial deformation (damage propagation);
- Evaluate the presence and causes of obvious test particularities such as the presence of a pre-existing discontinuity;
- Determine directional parameters for the preferred weakness orientations related to rock core heterogeneity and anisotropy;
- Provide the triaxial test interpretation with information on the natural variability of cataclastic rock masses and their related diagnostic elements, based on objective mineralo-structural observations.

Detailed and bigger sized 3D models of DI_{triax} can be found in **Appendix V-II** together with clipped DI_{triax} in position 150, 250 and 350 inside the considered volume, so as to better highlight the relationship with initial DI.

In the future, an upscaling of the two models (i.e. adaptative coordinate system and calibration of DI_{triax} based on DI) based on selected markers inside the volume should be performed, in order to take the volumetric change of the rock cores into account and permit detailed spatial analysis of structural DI models. It should be kept in mind that detected damage indicators correspond to a mixture of different petrological entities. At this stage, without the ability to differentiate between types of structures using medical XRCT, the DI analysis is mostly interesting for directional analysis to be related with rock core anisotropy and heterogeneity. Data from thin sections are still required to correctly interpret the mechanical implications of a given DI configuration. However, petrographical arguments can already be found when the shape and morphology of DI is considered, together with a conceptual model for the development of cataclastic rock fabric in fault zone. This point will be discussed in **Chap. 13**. All samples have a height of about 160 mm, impression of size variations between rock cores is due to the different adjustments of the camera on the scene window in VGStudioMAX.

12.2.3 Comparison with Models Before Tests: Test Induced Fracturation

Based on the possibility to visualize the fracturation process by means of XRCT *before* and *after* triaxial test, comparison between *damage indicators* (i.e. $XRCT_{\text{matrix}}$) has been envisaged as indicative of rock fracturation. Such a confrontation leads to following considerations:

- Evaluation of material competence with regard to its ability to produce new fracture (high variation in DI) vs. to use pre-existing discontinuities (low variation in DI).
- Evaluation of structural control from preexisting discontinuities in triaxial tests.

To take into account the structural entity of each rock core, an additional parameter has been envisaged and defined as the *triaxially induced fracturation index* FI_{triax} . It is defined based on the possibility to visualize a rock core *after* triaxial deformation and is used to evaluate the effect of an

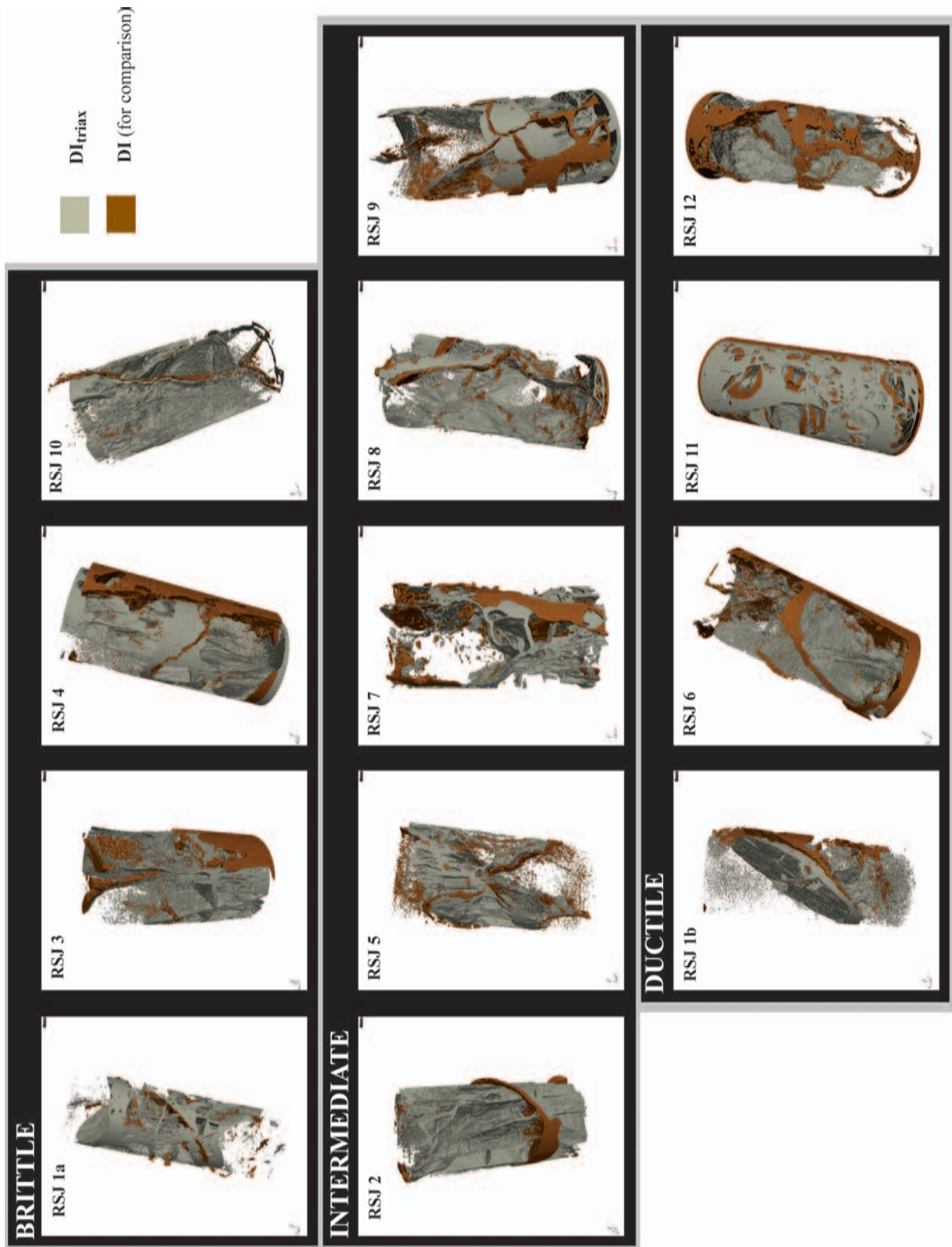


Fig. 12.5 3D reconstruction of DI_{triax} and superposition of initial DI for indication. Rock cores are classified according to mechanical behavior. Clipping parallel to rock core axis highlighting propagation of damage due to triaxial test can be found in Appendix V-II for positions 150, 250 & 350 inside the volumes. Sample *RSJ 2* is indicative for triaxial test affected by a singular pre-existing discontinuity. Accordingly, *damage indicators* develop perpendicular to a structure in unfavorable orientation. Note slight imprecisions in the superimposed segmented XRCT stacks resulting from induced distortion and/or dislocation during triaxial test (also decompression).

initial structural configuration in its respective influence on the deformation. It corresponds to:

$$(Eq. 12.1) \quad FI_{triax} = \frac{(XRCT_{matrix, TRIAX} - XRCT_{matrix})}{100}$$

Amount of $XRCT_{matrix}$ before and after test are the values in % of the segmentation results during both determination of *damage indicators*. Values obtained from the RSJ rock cores are listed in **Table 12.6**. With FI_{triax} , a possibility seems offered to investigate the inconsistent geological and mechanical characterizations (**Fig. 11.1 & 12.4**). Values of FI_{triax} can accordingly be used as an indication of preferential modes of deformation affecting cataclastic rock cores. Based on the RSJ evidence, two main deformation mechanisms are defined:

- 1) Domain of **preferential rock fracturing and splitting**, leading to a progressive fragmentation of the rock material. A production of new $XRCT_{matrix}$ («cataclastic rock matrix» characterized preferentially by lower CT intensities) is therefore observed that results from stress accumulation in the hard rock components (i.e. the « $XRCT_{clasts}$ », to be related with a «primary rock matrix»). As a consequence positive FI_{triax} are obtained. Such a mechanism concerns the fragile and intermediate mechanical behaviors.
- 2) Domain of **preferential compaction favorising comminution**, where a decrease in $XRCT_{matrix}$ is observed leading to a lower proportion of DI after test. This situation causes negative FI_{triax} and evidences this time the preferential deformation into the «cataclastic rock matrix». It concerns principally the ductile mechanical behavior. As will be shown in **Chap. 13 (Fig. 13.6)**, the inverse segmentation of DI should be considered for these types of samples, as it bears more useful information in terms of rock structures and textures.

These two domains are highlighted in **Fig. 12.6**. FI_{triax} , together with DI and MSI_{XRCT} will be discussed in **Chap. 13** and brought in perspective in **Chap. 14** with regard to their practical ability to be integrated into standard triaxial test interpretations.

| | SAMPLES | $XRCT_{matrix}$ (%) | $XRCT_{matrix, triax}$ (%) | DI | DI_{triax} | FI_{triax} |
|--------------|---------|------------------------|-------------------------------|-------|--------------|---------------|
| Brittle | RSJ 1a | 0.73 | 24.94 | 0.007 | 0.249 | 0.242 |
| | RSJ 3 | 6.82 | 23.20 | 0.068 | 0.232 | 0.164 |
| | RSJ 4 | 21.51 | 35.19 | 0.215 | 0.352 | 0.137 |
| | RSJ 10 | 0.70 | 8.39 | 0.007 | 0.084 | 0.077 |
| Intermediate | RSJ 2 | 4.29 | 21.29 | 0.043 | 0.213 | 0.170 |
| | RSJ 5 | 1.32 | 10.43 | 0.013 | 0.104 | 0.091 |
| | RSJ 7 | 10.68 | 14.71 | 0.107 | 0.147 | 0.040 |
| | RSJ 8 | 6.61 | 7.81 | 0.066 | 0.078 | 0.012 |
| | RSJ 9 | 5.69 | 20.04 | 0.057 | 0.200 | 0.144 |
| Ductile | RSJ 1b | 3.53 | 10.39 | 0.035 | 0.104 | 0.069 |
| | RSJ 6 | 37.09 | 26.53 | 0.371 | 0.265 | -0.106 |
| | RSJ 11 | 39.87 | 37.42 | 0.399 | 0.374 | -0.025 |
| | RSJ 12 | 14.11 | 12.06 | 0.141 | 0.121 | -0.021 |

Table 12.6 Input data for the determination of the triaxially induced fracturation index FI_{triax} following Eq. 12.1. RSJ rock cores classified according to mechanical behaviors.

12.3 DISCUSSION

Cataclastic rock cores are highly heterogeneous and correspond to complex structural entities (**Fig. 12.5**). It has been shown in **Chap. 11** that micro-structural determinations can greatly vary inside a same rock core depending on which thin sections (MSI) or CT slices (MSI_{XRCT}) are considered. In order to reach a prediction of mechanical behavior based on geological evidences this study considers 2 aspects of prime importance:

- 1) Provided the advantages of the indirect visualization by means of XRCT, an objective combined geological and mechanical characterization of cataclastic rock cores, or any heterogeneous materials, benefits from the possibility to work on the exact same rock core.
- 2) Provided the quality of the XRCT rendering obtained from geotechnical rock cores, a 3D mineralo-structural analysis by means of segmentation (CARact3D) delivers important improvement possibilities in the understanding of cataclastic mechanical behaviors.

Accordingly, the control exerted by pre-existing geological structures on the observed mechanical response (e.g. *shape* and *orientation* of tomographically reconstructed *damage indicators*) can be assessed and quantified as *strength reduction parameters* for triaxial test interpretation (in a similar manner than the quantification of a tectonization degree t as proposed by *Habimana et al.*, 2002). Based on CARact3D, the implementation of XRCT for cataclastic rock core characterization has introduced for this purpose the parameters DI, DI_{triax} and FI_{triax} .

In a less elegant way (pseudo-3D approach), it has been shown that α_{XRCT} can be determined from analysis of orthogonal frontal and sagittal planes. As presented in this chapter, determination of a rupture angle by means of visual XRCT evidence is encouraging in better taking into account the complex fracturing of cataclastic rock cores. In the future, adequate 3D analysis tools should permit a full 3D determination of α_{XRCT} (and also of MSI_{XRCT} , with probable adaptations of the formulation for MSI proposed by *Bürgi*, 1999).

An attempt to relate and confront these parameters is addressed in **Chap. 13**. Currently, a correlation between geological and mechanical properties of cataclastic rocks from different petrological content is expected possible with 3 types of strength reduction criteria expected to modify intact rock properties:

- 1) Criterion for *rock core alteration*, e.g. control of the mineralogical content over fracture initiation.
- 2) Criterion for *rock core heterogeneity*, e.g. control of the initial material fragmentation (textural evidence of DI, i.e. SHAPE).
- 3) Criterion for *rock core anisotropy*, e.g. control of the spatial arrangement of damage indicators (structural evidence of DI, i.e. ORIENTATION).

Moreover, the determination of a *rock core fracturability* described by the triaxially induced fracturation index FI_{triax} should be introduced as a ponderation factor. It takes into account the particularity of each single rock core (consideration of structural singularities and of the natural variability found in cataclastic horizons).

In general, it should be kept in mind that any improvement in the understanding of the cataclastic rock mass behavior requires numerous samples from a cataclastic fault zone to be integrated in

the combined characterization procedure. The parameters proposed for cataclastic rock core characterization based on XRCT data have therefore to be tested on the base of case studies, but results from only 13 *RSJ* rock cores are according to us encouraging.

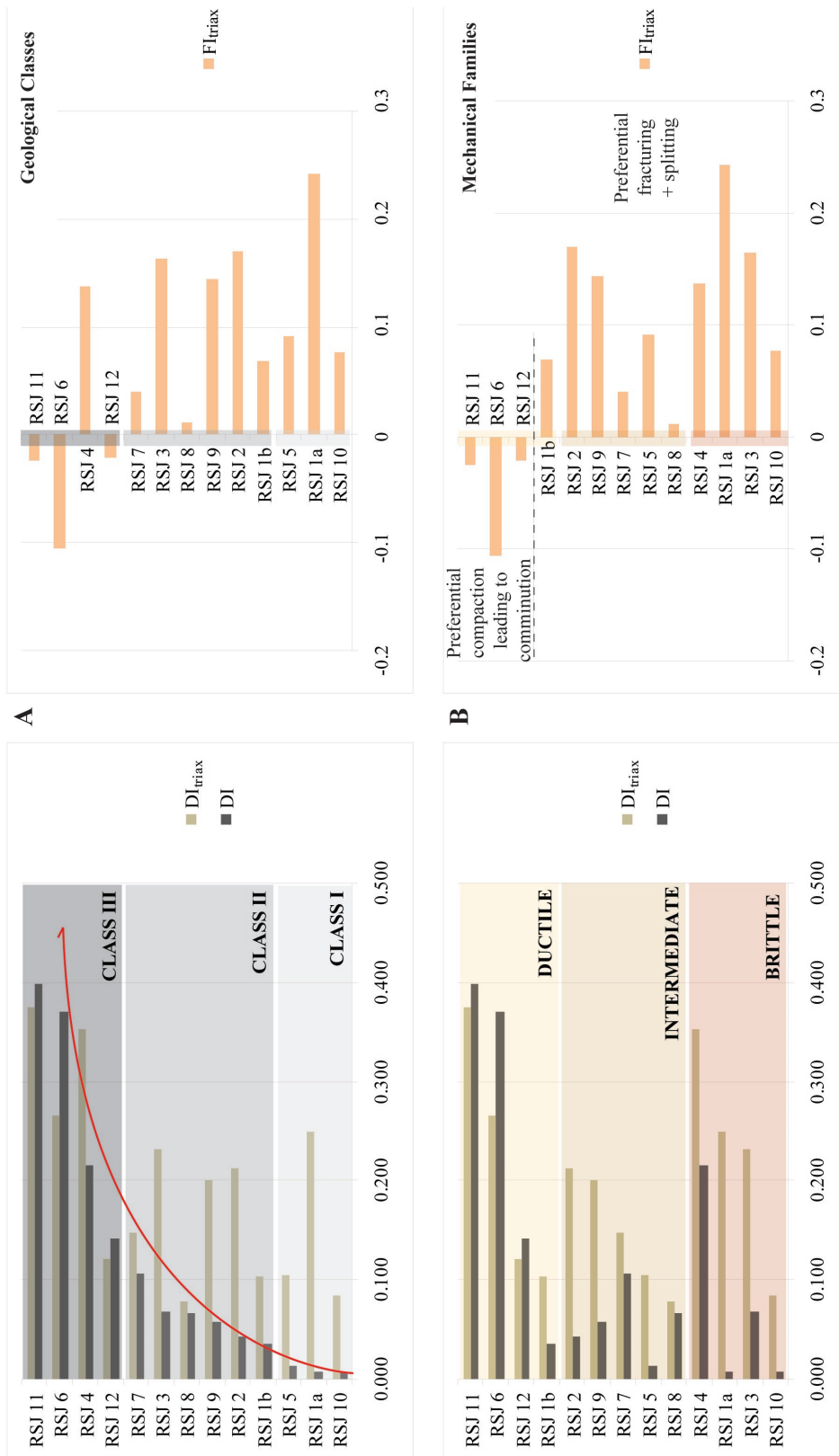


Fig. 12.6 Graphic representation of the triaxially induced fracturation index FI_{triax} for the *RSJ* rock cores based on **A**) the geological classes and **B**) the mechanical behaviors. The DI increase with geological quality classes (red arrow, see also **Fig. 11.5**) is not able to predict mechanical behavior. By introducing additional considerations (e.g. FI_{triax} but also MSI_{XRCT}) important interpretation constraints based on a 3D structural analysis considering structural heterogeneity and anisotropy could be found. Accordingly, the translation of the concept of *damage indicators* in terms of *strength reduction criteria* for mechanical interpretation can be greatly improved. As seen from **B**) distribution of FI_{triax} based on the mechanical families shows a better trend than when considered on the base of the geological classes. An evolution path from fracturing, progressive fragmentation and comminution is evidenced from brittle to ductile samples, with a general decrease in FI_{triax} from preferentially fractured towards perfectly clastic materials for which negative values are observed.

13

TOWARDS A BETTER GEOTECHNICAL DESCRIPTION?

« Never Give Up
No matter what is going on
never give up
develop the heart
too much energy in your country
is spent developing the mind
instead of the heart.
Be compassionate
not just to your friends,
but to everyone.
Be compassionate.
Work for peace in your
heart and in the world
work for peace and I say again
never give up
no matter what is happening
no matter what is
going on around you
never give up. »

His Holiness the XIVth Dalai Lama

A methodological concept has been envisaged within this research to potentially improve cataclastic rock characterization. This concept combines geological and geomechanical determinations and expects to find appropriate correlations between them. Such an approach is thought able to deliver important additional data when the characterization of heterogeneous geomaterials is addressed. Not only the results of mechanical tests can be better interpreted by taking advantage of a more detailed petrographical knowledge but also the implications of diagnostic geological features at the sample scale can be assessed and further related to a probable mode of rock mass behavior. For geotechnical studies in tectonized settings, both the prediction of material strength based on the geological properties of representative samples and the effect of heterogeneity and anisotropy on the mechanical behavior are important inputs that should be determined with best confidence. Thus the proposed approach is seen as a pragmatic strategy to improve the geotechnical characterization of weak rock masses by adding geological evidences as observed at the sample scale.

Cataclastic structures are complex geological entities. It is shown in *Bürgi* (1999) that cataclasis correspond to a broad spectrum of material states and that structural homogeneity can be accepted only for very damaged and altered specimens. Samples investigated within this study are however mostly heterogeneous. Accordingly, a general synthetic characterization scheme has been presented in **Fig. 4.3** to objectively evaluate the influence of initial geological structures in a mechanical characterization of cataclastic rocks by means of triaxial tests. From geology, the mineralogical and structural index MSI and newly the quantification of *damage indicators* using the indirect XRCT technique are of particular interest.

Geological and geomechanical results obtained on a set of 13 rock cores at different degree of cataclasis from the N16 Roche St Jean tunnel in the Jura Mountains of north-western Switzerland have been presented in **Chap. 11 & 12**. They demonstrate the advantage of performing the geological and mechanical studies on the exact same samples based on 3D evidences.

Accordingly this discussion has been separated in 2 parts:

- First, a discussion addressing the characterization of rock cores using the MSI-approach is conducted. The TC & MC constitutive parameters of the MSI are discussed based on their respective determinations from medical XRCT data. A general evaluation of the characterization procedure is conducted. The specific influence of each parameter regrouped in the TC & MC determinations is presented. Accordingly, the validity domain of the MSI is discussed.
- Second, the implementation of XRCT in mechanical triaxial test procedure for a more objective test interpretation is discussed. Rock core rupture and deformation are considered based on the XRCT visualization of a cataclastic sample *before* and *after* it undergoes triaxial deformation. Both the pertinence of the rupture angle α_{XRCT} and its pseudo-3D relevance are discussed.

13.1 GEOLOGICAL ROCK CORE CHARACTERIZATION

The geological characterization implements the MSI as a *strength prediction index* for cataclastic rocks (*Bürgi*, 1999). With this regard, inherent fault rock parameters are determined (mineralogical composition and rock fabric, translated as *damage indicators* in this study). Moreover, cataclastic intensity (e.g. degree of tectonization) should be defined to obtain a diagnostic regarding material evolution from the damage zone to the fault core.

In this section, a critic of the MSI determinations based on textural and structural determinations from CT slices taken in the frontal and sagittal planes is made. From them, both the validity domain of the MSI and the respective weight of the different parameters constitutive of the TC and MC are discussed. Accordingly, a conceptual model of cataclasis diagnosis in rock cores is proposed.

13.1.1 MSI-Determinations from XRCT Data

Global MSI values for the *RSJ* samples have been determined implementing frontal (*xz*) and sagittal (*yz*) CT slices, as presented in **Chap. 11**. As already mentioned, these orientations are in a parallel direction to the applied load of geomechanical tests, e.g. they provide a plane of view rich in information to evaluate the triaxially induced deformations. Since the geological and geomechanical characterizations are performed in this study using the exact same rock cores, this allows estimating how the TC & MC parameters might relate with observed mechanical rock properties.

For carbonatic cataclasites, the development of schistosity from tectonic efforts is theoretically only valid for fault cores materials (see **Fig. 2.6**). Direct arguments for the determination of a maximal anisotropy are difficult to find without proper directional analysis of the preexisting structures and textures. For microstructural studies in schistose rocks, the orientation perpendicular to textural anisotropies is generally recommended for the realization of thin sections (see *Bürgi*, 1999). For carbonatic rocks, state of the art microstructural studies should be based on the study of the crystallographic preferred orientation of calcite-*c*-axis, which was outside the scope of this study.

In this section, a close look at the *local* variations of the TC & MC constitutive parameters across a same plane view is performed (3 CT slices for TC and 7 CT slices for MC, see **section 11.3.1-2** and **Appendices IV-I & II**). The followed approach can therefore be understood as pseudo-3D, with an estimation of the spatial variations of structure made possible by considering different levels inside the rock core. Accordingly, structural and textural heterogeneity of the *RSJ* samples can be estimated and the domain of validity of the MSI assessed.

Fig. 13.1 and **13.2** presents the frontal and sagittal confrontation of the TC & MC constitutive parameters that has been observed (see also Frontispiece of **Appendices IV-I & II**). *RSJ* samples are evaluated according to the determined geological classes introduced in **Chap. 11**. As will be demonstrated, textural and structural observations on the *RSJ* samples require separating between 3 main rock types: *fractured*, *fragmented* and *clastic* rocks. Accordingly, argument can be found concerning the validity domain of the MSI by *Bürgi* (1999).

Note: All this discussion is affected by the uncertainty introduced by hand drawing of the binary masks that is often imprecise from CT-slices at the resolution of medical XRCT. For example, the drawing of the clast angularity at that resolution is difficult and probably exaggerates the effective roundness of the considered clasts. Therefore this discussion has mainly a didactic character. It permits an evaluation of the philosophy behind the MSI as proposed by *Bürgi* (1999) and highlights the structural variety represented by the *RSJ* samples that are affected to different extent by fracturing and fragmentation. It shows also that the geological characterization of cataclastic rock cores based on medical XRCT will require in the future proper numerical developments to permit a full 3D structural and textural analysis of *damage indicators*. In this way, their quantification as tensor entities instead of the current scalar approach could be realized and most objectively integrated in a modified MSI-formulation for 3D data.

13.1.1.1 Parameters constitutive of the TC

After the detailed study of numerous CT slices taken on structurally and texturally contrasted cataclastic rock cores, it is found that parameters constitutive of the TC (**Eq. 7.2**) can be regrouped in 3 categories:

- 1) "*Characteristic parameters*": represented by the clast density CD, which is a parameter accounting for the overall rock texture. CD has a meaning for clastic materials only, and

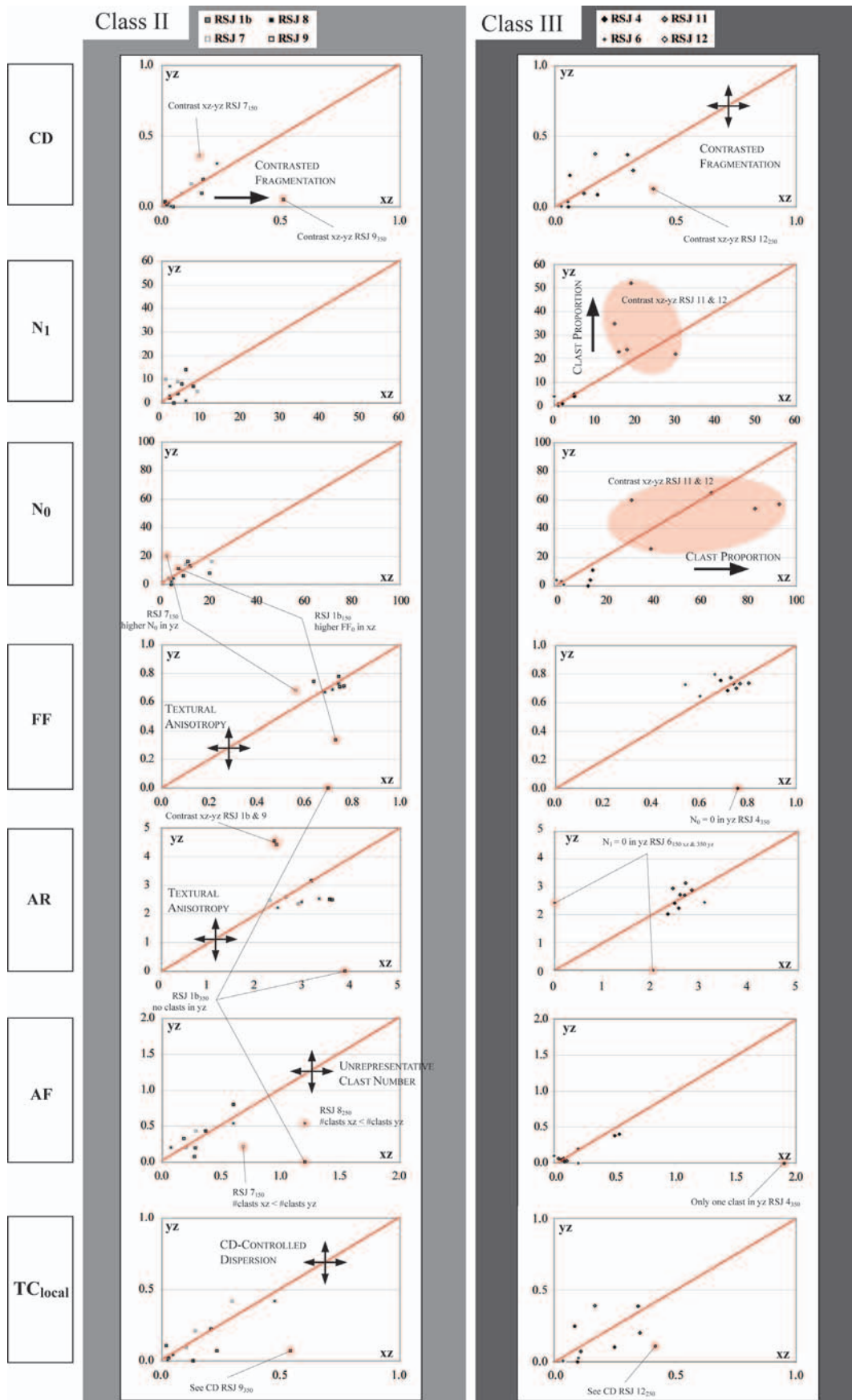


Fig. 13.1 Variability in the constitutive parameters of TC observed on the *RSJ* samples. Evidence from determinations made on the frontal (*xz*) and sagittal (*yz*) planes, e.g. 2 orthogonal planes parallel to the direction of applied triaxial load. Relation to the identity line (textural homogeneity) and interpretation of the observed dispersions. Double arrow is only a symbol to evidence deviation from homogeneity; accordingly the physically translated reasons for the observed deviations are indicated for each parameter. See text for further explanations. Corresponding binary masks on which the different determinations have been made can be found in **Appendix IV-I**.

it is observed from the *RSJ* serie that not all samples allow the determination of CD (see sample of *Class I* and partly *Class II*). For them, an extreme value of TC has been adopted (e.g. $TC = 0$). CD has “genetic” character.

- 2) Descriptive parameters: represented by the respective numbers of isometric and elongated clasts ($AR > 2$), given as N_0 and N_1 in the TC equation. They are parameters descriptive of the extent of fragmentation respectively of clast packing and can be used to define the transition between *clast-* and *matrix-controlled* cataclastic flows. In this sense, they are a global measure of rock heterogeneity.
- 3) Directional parameters: represented by the angular relationship between elongated clasts AF_1 and the roundness of isometric ones FF_0 , which are both directional parameters. In clastic materials they allow the definition of preferred orientations and textural anisotropies.

Fig. 13.1 shows the observed variations between *xz-* and *yz-*determinations for samples of *Class II* & *III*. The observed dispersions between local determinations of TC on *xz-* and *yz-*CT slices indicate limitations in describing several *RSJ* rock cores with the TC. They are summarized hereafter for each constitutive parameter of the TC:

For CD, deviation from the identity line referring to textural homogeneity is interpreted as related to *rock fragmentation*, with samples showing evidence of stronger fragmentation in one of the considered planes (*RSJ* 7, 9 & 12).

For N_0 and N_1 , difference in *xz* and *yz* determinations indicates *textural variability*. It is particularly affecting samples *RSJ* 11 & 12, which are the 2 most clastic specimens of the serie (with N_0 and N_1 values by far above other *RSJ* samples). Other *RSJ* samples are found improperly characterized by the current TC approach as they can barely be considered as corresponding to clastic materials, what questions the domain of validity of the TC parameter for preferentially fractured cataclastic specimens (at the medical XRCT resolution).

FF_0 , AR and AF_1 between *xz* and *yz* views are in relatively good agreement but this also reflects the often restricted amount of clasts in the analyzed samples, as these parameters will only have a physical meaning if a representative (minimum) clast population can be analyzed. Nevertheless, deviation from the identity line can be interpreted as an indication of *textural anisotropy*, as represented by samples *RSJ* 1b, 7, 8 & 9. The approach of the TC reaches obviously a limit when considering sample *RSJ* 4 that only depicts one elongated clast in the *yz* plane view.

By considering the variations in the local TC (e.g. slice by slice), the observed deviations are interpreted being primarily a function of the clast density CD as the scatter observed with TC is almost identical with the one observed for CD. This shows again that the TC parameter used for characterization purposes requires an adequate rock material (e.g. clastic) to find its full interest.

13.1.1.2 Parameters constitutive of the MC

Similarly to TC, the MC parameters represent 3 categories.

- 1) “Characteristic parameters”: represented by the linear roughness R_L , which is a parameter accounting for fracture types and their surface conditions. R_L is a function of rock composition and can be related to how damage through cataclasis manifests. Accordingly, fracture types function of petrological content could be used as cataclastic material diagnosis. It also has a “genetic” character.

- 2) Descriptive parameters: represented by the trace line length T_{LL} and the trace line density T_{LD} which are descriptive of the extent of damage (fracturing) and allow quantifying overall damage development. It is diagnostic for the degree of cataclasis (e.g. indicates heterogeneity) and marks the transition from *fracture-* to *clast-controlled* cataclastic flows.
- 3) Directional parameters: represented by the number of discontinuity set n and the orientation factor δ from which preferred orientations and in this case structural anisotropy can be inferred.

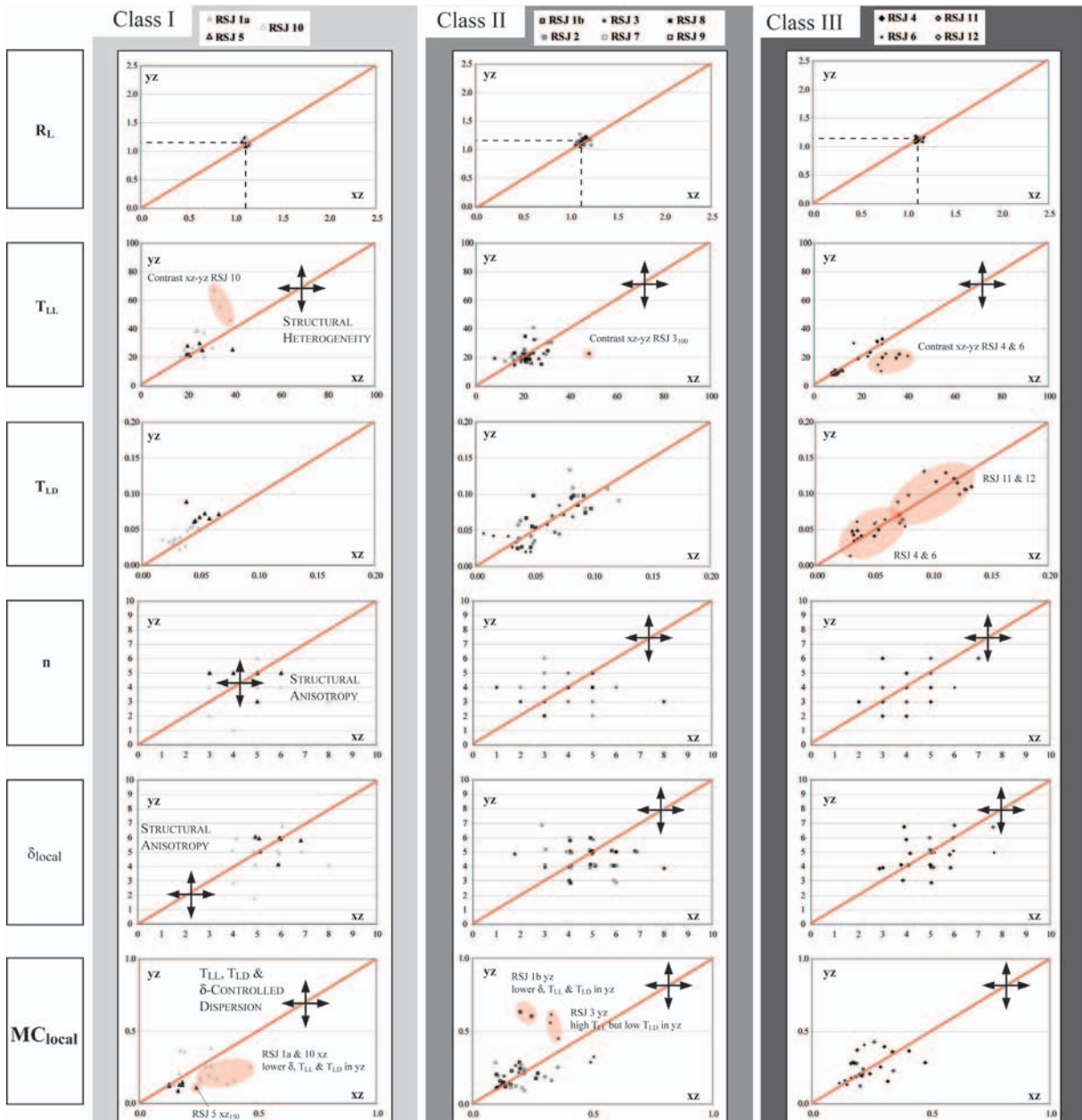


Fig. 13.2 Variability in the parameters constitutive of MC as observed on the *RSJ* samples. Evidence from determinations made on the frontal (*xz*) and sagittal (*yz*) planes, e.g. 2 orthogonal planes parallel to the direction of applied triaxial load. Relation to the identity line (structural homogeneity) and interpretation of the observed dispersions. Double-arrow symbol to indicate dispersion from homogeneity and physical meaning. See text for further explanations. Corresponding binary masks on which the different determinations have been made can be found in **Appendix IV-II**.

On the contrary to the preceding remarks for TC, MC can be applied to virtually all types of materials. However, as observed on the RSJ samples, the meaning of MC in terms of strength prediction changes from predominantly *fractured* (Class I) to predominantly *clastic* (Class III) materials. In fractured materials, the discontinuities correspond to entities diagnostic of damage in a petrographically still “intact” rock matrix (see terminology in **section 2.4**). In clastic materials, the analyzed discontinuities concern an already “fully damaged” rock matrix, for which intact rock characteristics can’t be assumed (with an exception for the *intra-clasts* fractures). Such characteristics of the damaged rock domain have already been evidenced in **Fig. 4.2** based on binary representations of descriptive rock mass elements. They will now be discussed for their effect and implication on rock core characterization by means of indirect image analysis.

Fig. 13.2 presents the observations made for the *Class I-III* samples. Dispersions in xz- and yz-determinations for each parameter constitutive of the MC are commented in the light of the “*characteristic*”, *descriptive* and *directional* parameters:

The parameter R_L is consistent for all samples, reflecting the similar fracture shapes in *RSJ* (or the same imprecision from hand drawing of the binary masks based on CT slices, see the note above). R_L can therefore be assumed reflecting the typical *fracturing mode* of carbonatic cataclasites.

Variation in T_{LL} and T_{LD} between xz and yz views is found reflecting the absence of discontinuity trace lines in xz (*RSJ 10*) and yz directions (*RSJ 3*) at the medical CT resolution. The particularity of samples *RSJ 4 & 6* (two petrographic rock core faces, i.e. clay and limestone, see **Appendix IV-II**) seems also to introduce contrasted values. Moreover T_{LD} for the two clastic samples *RSJ 11* and *12* produce higher values reflecting their more generalized fragmentation (side of clasts taken as discontinuities for MC determination, in analogy to *Bürgi*, 1999). Therefore in Class III, T_{LD} reflects material nature and contrasted type of discontinuities: *strong* discontinuities in *RSJ 4 & 6* that characterize the hard rock portions vs. *weak* discontinuities in *RSJ 11 & 12* that correspond to the interface between clast and fully damaged (clay-rich) matrix. It is interpreted therefore that T_{LL} and T_{LD} allow inferring on *structural* heterogeneity, as they relate to the persistence and generalization of fracturation inside the rock core volume.

The directional parameters n and δ clearly present the widest scatter. The *RSJ* samples display an amount of 1-6 discontinuity families per sample. Interestingly by considering the *RSJ* samples, it is clear that they represent a very different structural type than schistose rocks. Accordingly, preferred orientations are not uniquely defined (criterion “schistosity plane”) and should be classified accordingly. The deviation from the identity line is interpreted as indicative of *structural anisotropy*. The observed wide scatter is also interpreted as indicative of the general complex morphology and topography of discontinuity surfaces in fractured rocks. This remark points out the need to perform a full 3D analysis of discontinuity surfaces to optimally address rock core characterization in geotechnical studies (influence of pre-existing discontinuities on the resulting deformation mechanism).

By considering the variations in the local MC (e.g. slice by slice), the observed deviations are interpreted being primarily a function of T_{LL} , T_{LD} and their spatial description by means of δ . In sample *RSJ 1a & 10*, low MC in yz are related to the concurrent effect of low values of T_{LL} , T_{LD} and δ . In sample *RSJ 3*, the high MC values in yz are produced by the low T_{LD} in slices 300-400, despite of high values of T_{LL} . In sample *RSJ 1b*, an important contrast between values for T_{LL} , T_{LD} and δ is observed between yz and xz views.

13.1.1.3 Synthesis from TC & MC determinations

Fig. 13.1 & 13.2 introduce criteria for the determination of textural and structural heterogeneity and anisotropy at the rock core scale. Based on pseudo-3D TC & MC determinations, it is found that the *RSJ* samples correspond to differently fractured and fragmented materials involving diverse manifestations of heterogeneity and anisotropy. A full automatized 3D determination is estimated in this context capable of increasing the level of interpretation that can be expected from a TC & MC type analysis but requires at this stage further developments in terms of image analysis on medical XRCT rock core acquisitions.

For both TC & MC determinations, constitutive parameters can be differentiated into three indicative categories of “*characteristic*”, “*descriptive*” and “*directional*” parameters. Doing so, a physical meaning to each of the parameter is attributed in terms of its effect on rock texture and structure, which further relate to rock strength.

Globally, *Bürgi* (1999) mentions for the TC that high values of AR, AF_1 & CD have a positive effect in terms of rock strength, while a high value of FF_0 is negatively influencing the mechanical resistance. Moreover *Howarth & Rowlands* (1986) mention that as TC increases, so does the number of grains, shape complexity and randomness of orientation. Translated in fracturing mode, a rock with low grain volume and low TC will depict preferentially inter-granular deformation, while a rock with a high grain volume and high TC will deform by intra-granular processes (enhanced comminution). On the other hand for MC, a high R_L is acting positively on strength while high T_{LD} , T_{LL} & δ are expected reducing resistance. Considering **Fig. 13.1 & 13.2**, following can be said:

- Texturally, determination of a degree of rock fragmentation can be found with CD. It is diagnostic for the determination of *clastic* vs. *fractured* rock rheologies. Moreover, N_0 and N_1 provide a mean to evaluate *isotropic* vs. *anisotropic* rock textures. Anisotropy is further quantified by the parameter AF_1 . According to *Howarth & Rowlands* (1986), a minimum of 30-50 elongated clasts ($AR > 2$) are however required to obtain a meaning for AF_1 . Most of the TC determinations performed on CT slices from the *RSJ* samples show in this sense a practical limitation in the use of the TC parameter in its current formulation. For fractured specimens (but still not fragmented), a textural analysis should be preferentially made to assess the different fracture surface conditions. A modified TC parameter to be used in the MSI should accordingly be developed for such type of samples.
- Structurally, T_{LD} is indicative of the development of fracturing inside rocks and together with R_L it provides evidence for fracturing conditions (pure shear, yielding, or abrupt material failure, e.g. “texture” of discontinuities). T_{LL} is indicative of the persistence of fractures and can be used to determine a *degree of fragmentation* through sustained cataclastic fracturing. It further provides evidence for *partial* vs. *generalized* fracturing. The directional parameters n & δ are used to evidence structural anisotropies and they are found representing the widest scatter in the *RSJ* samples. In this context, a possible full 3D determination of δ (tensorial definition of the orientation factor) was already mentioned by *Bürgi* (1999) as constituting an important potential improvement that would enable a more accurate correlation with mechanical properties (problem of comparing scalars with tensors in the actual MSI formulation, see also **section 12.1.2**).

Fig. 13.3 shows further a conceptual model for the tectonically induced variability depicted by the *RSJ* samples. It can be understood as the result of fault zone activity (i.e. cataclasis) through a progressive fragmentation of the intact rock material (cataclastic gradient), which leads at the end to a clast-matrix assemblage where grain comminution becomes the most important deformation

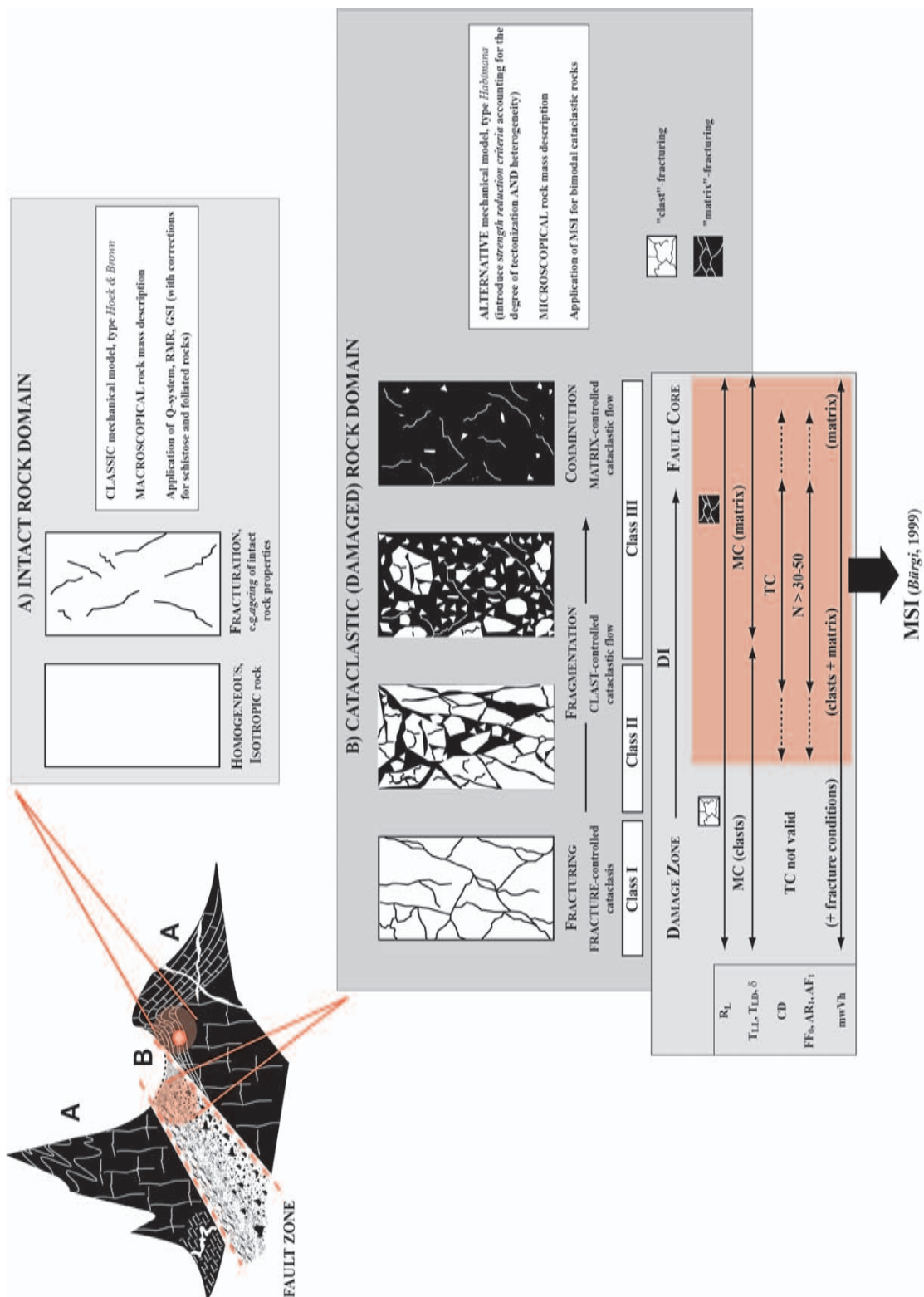


Fig. 13.3 Conceptual model for cataclastic diagnosis in rock cores as a result of their provenance from either the damage zone (fracturing and progressive fragmentation) or the fault core (predominant clast comminution through fracturing, grinding and crushing processes). Differentiation between the *intact* and *fractured* rock domains, following considerations from Fig. 4.2. **A)** Illustration of rock cores of the intact rock domain, characterized by ideally homogeneous and isotropic rock properties. Fracturation in the intact rock domain is interpreted preferentially as reflecting material ageing, e.g. the corresponding rock materials are not issued from a dynamic rock transformation process (fault zone activity). For engineering studies, such materials are characterized using classical rock mechanical models and their geotechnical description is made on the base of macroscopic evidences. **B)** Rock cores resulting from the progressive damaging in fault zone through fracturing, fragmentation and comminution (idealized evolution from *Class I* to *Class III* samples), leading to a progressive increase in the damage index DI. Such materials require alternative mechanical models that take into account their heterogeneous nature. A pragmatcal way follows consideration of *Habimana* (1999) and introduces the concept of *strength reduction criteria* reflecting the effect of tectonization on

Fig. 13.3 (continued) mechanical resistance (parameter t in the modified Hoek & Brown rupture criterion). Accordingly, ponderation factors into classical mechanical models can be introduced. Proper characterization of damaged rock structures require this time investigations at the microscopical scale to be accordingly related with the respective emplacement of the rock core in the fault zone architecture. Below the binary representations of characteristic rock cores, is a table introducing the MSI constitutive parameters (Bürgi, 1999) that allow evaluating their relevance according to rock core characteristics.

mechanism. Accordingly, the transition between the *fracture-* and *clast-controlled* cataclastic flows can be assessed, as well as evidence for the initiation of *matrix-controlled* cataclastic flow found. Reference rock cores for the structural and textural development in fault zones are represented from a binary perspective. Although no direct relationship is observed between the geological and mechanical characterizations in terms of DI (**Fig. 11.1 & 12.4**), the model ideally represents *Class I-III* samples to be related with the preferential *brittle*, *intermediate* and *ductile* modes of deformation. It assumes therefore that such a correspondence could become increasingly valid at a larger scale of observations (considerations of the entire rock mass). At the sample scale however, additional considerations of the orientation of geological structures should be absolutely made in a triaxial test interpretation to perform a correlation in between geological and mechanical properties.

Fig. 13.3 allows consideration about the validity of the MSI index proposed by Bürgi (1999), which will be the object of the next section.

13.1.1.4 Implications of a cataclastic gradient for MSI determinations

As stated in Bürgi (1999), the MSI approach in its current formulation is restricted to kakirites with a certain structural and mineralogical homogeneity at the scale of thin sections and triaxial tests. Based on the different values of TC & MC obtained on the *RSJ* samples, and together with the values for *mwVh* determined in **Chap. 11**, the relationship between the local MSI parameters and both the defined geological and mechanical classes is explored in **Fig. 13.4** and highlights the heterogeneity depicted by the *RSJ* samples.

The variation of the 3 parameters constitutive of the MSI introduces characteristic evolutive trends that can be explained using considerations presented in **Fig. 13.3**. The main observations are summarized hereafter:

For **mwVh**, no clear distinction can be made between the *Class I-III* and *brittle-ductile* sample groups. They both reflect a logical decrease in expected rock strength towards increasingly damaged materials. The strength control of the bulk mineralogy (i.e. XRD) is therefore only fixing a general strength limit. By considering the different structural characteristics depicted in **Fig. 13.3**, it is evident that a rock core characterization of fractured and slightly fragmented materials will benefit from more detailed mineralogical knowledge of localized alteration processes affecting the “hard” rock components and of mineralogical constraints on fracture conditions (as the deformation of such cataclastic rocks will be mostly controlled by the fractures in presence and the weakness zones resulting from weathering). For highly fragmented and comminuted materials, both the mineralogy of the clast fractions and of the “weak” matrix (evidencing alteration processes, for example resulting from fluid-rock interaction) will be of interest.

For **MC**, an interesting evolution from both the *Class I-III* and the *brittle-ductile* groups is evidenced, with *Class II* (intermediate) samples depicting the lowest values. It has already been mentioned in the description of the indirect XRCT technique that the petrographical diagnostic of fracture conditions based on indirectly resolved images constitutes a problem. On the contrary to thin section, a petrographical uncertainty arises when evidencing discontinuity trace lines in an image analysis procedure based on CT-slices. For the *RSJ* samples, it is therefore interpreted

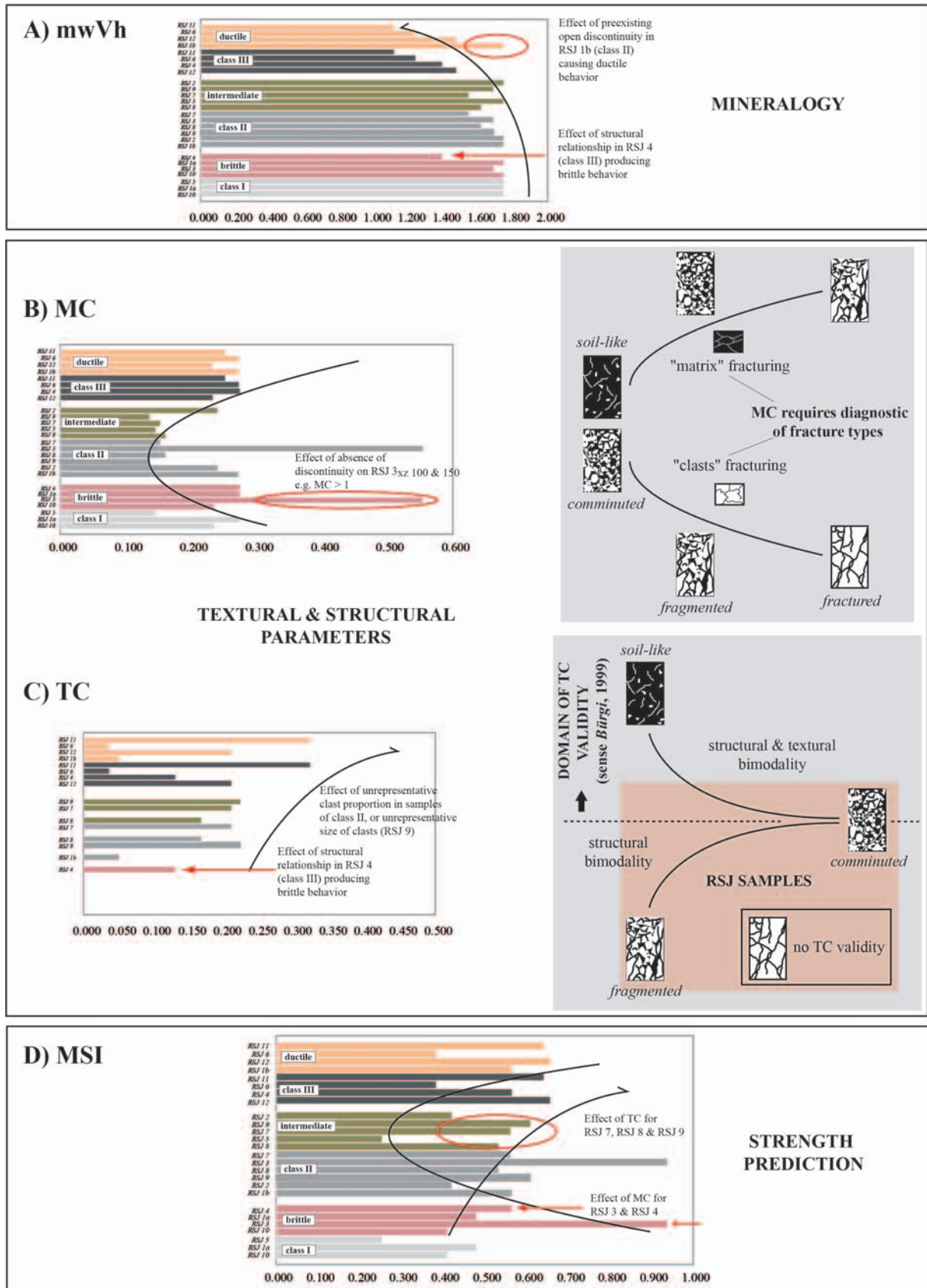


Fig. 13.4 Evolution of the MSI constitutive parameters for the *RSJ* samples classified either geologically (*Class I-III*) or mechanically (*brittle-ductile*). For all MSI constitutive parameters, evolutive trends can be understood as reflecting a transition between preferential *clast-* and *matrix-controlled* cataclastic flows. **A)** *mwVh*: Mineralogical coherence, strength reduction towards more damaged materials. **B)** *MC*: structural paradox between *Class I & III* indicative of contrasting fracture properties. **C)** *TC*: textural paradox related to variably fractured and fragmented rocks, with several *RSJ* samples not adequately described by means of *TC*. **D)** *MSI*: strength prediction paradox introducing argument to define the validity of the *MSI* in the form envisaged by *Bürgi* (1999). See also **Fig. 13.3**.

that the high MC in the *Class I* (brittle) samples is due to the analysis of “strong” discontinuities (mainly recrystallized). On the contrary, trace lines analyzed in *Class III* (ductile) samples correspond to “weak” discontinuities. This is schematically represented in **Fig. 13.4** making use of the characteristic cataclastic fault rocks from **Fig. 13.3**. It becomes accordingly evident that a MC-type strength reduction criterion requires a diagnostic on fracture properties to find relevance in terms of mechanical prediction. Accordingly proper ponderation factors should be attributed in the structural analysis to account for the nature of the discontinuities. Two trends are accordingly proposed:

- Evolution from *fractured* to *comminuted* materials, based on the structural relationship of “hard” discontinuities.
- Evolution from *fragmented* to *soil-like* materials, based on the study of “weak” discontinuities. This second trend corresponds to the cataclastic domain where the MSI is valid in its current form.

For **TC**, a general increase is observed between samples of both *Class I-III* and *brittle-ductile* behaviors. It has to be reminded that not all *RSJ* rock cores allow a textural clast analysis (*Class I* samples and partly *Class II*). For them a value of $TC = 0$ has been attributed to translate the fact that structural strength reduction is in these cases all accounted for by the discontinuities. However this seems not logical, since extreme samples of soil-like nature will also be attributed a value of $TC = 0$. As a consequence, the strength prediction based on the MSI is biased by the inappropriate use of **TC** in *Class I* and partly *Class II* samples, producing at the end unrepresentatively low MSI determinations. Moreover the high **TC** values for *Class II* samples are not physically meaningful due to the limited clast amount on which they have been determined (uncomplete fragmented nature, see **Appendix IV-I**). By considering the model of **Fig. 13.3**, it appears that the *RSJ* samples are inappropriate to be fully characterized by the MSI approach of *Bürgi*. Clearly, the **TC** has a meaning for fragmented materials at an already advanced stage. The schematic applicability domain of the **TC** is accordingly highlighted on **Fig. 13.4**. This domain can be understood as the onset of a structural and textural bimodality in rocks, e.g. the presence of two clearly separated rock phases disconnected structurally from each other (clastic and granular natures). As a consequence of their different fragmentation degree, most of the *RSJ* samples do not correspond to such a picture. They correspond to a state of damaging where intact rock elements still offer an important contribution in the deformation. Damage indicators can indeed be evaluated and structurally characterized in terms of their potential control on the resulting rock core cataclasis (resulting eventually to a generalized classification and a bimodality *sensu Bürgi*, 1999). Characterizing fractured and slightly fragmented rock cores by mean of the MSI is therefore estimated not accurate for a prediction in terms of strength in the current index formulation.

As a result of the preceding structural and textural observations and their interpretation in terms of rock cataclasis, the MSI values can't be translated objectively in terms of effective rock core strength. As a matter of fact, the textural and structural strength ponderations envisaged by *Bürgi* by means of the **TC** & **MC** parameters to «reduce» the resistance of a given mineralogical assemblage have only limited validity for the *RSJ* samples. Paradoxally, *Class I* samples have lower MSI than *Class III* samples, indicating the respective effect of **1**) the inappropriate clast-matrix approach (**TC**) for *Class I* and partly *Class II* samples, and **2**) a **MC** value determination for those samples that doesn't differentiate between petrographically weak and strong (e.g. recrystallized) discontinuities. As already mentioned, the study of frontal and sagittal CT slices from medical XRCT makes such a petrographical diagnostic currently not possible.

Based on the results of MSI values obtained on the *RSJ* samples, the different material characteristics described in **Fig. 13.3** (*fractured*, *fragmented* and *comminuted* materials) have been proposed. Accordingly, the *RSJ* samples are indicative of a high natural heterogeneity which will control the way a specific rock core deforms. Depicting different levels of fracturation and fragmentation, preferred orientation can be assessed (parameters AF_1 and δ) and related to material anisotropy, indicative of the ease with which the material will deform. In terms of a strength prediction based on the MSI, the mineralogy stays a major element that fixes overall conditions for fracture initiation and rock deformation.

Consequently, based on ideas of **Fig. 13.3**, it is demonstrated that the determination of the MSI proposed by *Bürgi* (1999) has only a limited domain of validity. In fault zone, the bimodal clast-matrix approach *sensu* *Bürgi* (1999) is valid only at an already high degree of rock fragmentation, under which textural criteria should be modified (e.g. more accurate textural analysis of fractured and slightly fragmented materials). It is therefore proposed to differentiate between different rock fragmenting stages leading to the definition of validity domains for the index in its current formulation. Adaptations have to be envisaged based on an adaptative weighting of the 3 considered characterization elements (mineralogy, structure and texture) in order to describe the entire fault zone development with the pertinent MSI approach (damage zone + fault core).

To account for the contrasted cataclastic fabric resulting in function of initial petrology both *Chaignat* and *Veuve* (2007) have proposed corrections for the mineralo-structural parameters constitutive of the MSI. Accordingly, a modification of *Bürgi*'s index formulation could be addressed according to the nature of the initial rock protolith (e.g. rock end members "porous" and "crystalline" of **Fig. 2.7**, e.g. preferentially undergoing yielding or an abrupt failure). A separated text presenting their considerations can be found in **Appendix IV-IV**. In the current stage, such considerations towards a more general MSI determination requires further research and more numerous data from petrologically contrasted cataclastic rock samples. Results of *Chaignat* and *Veuve* have been presented in **Chap. 3, section 3.3.3**.

13.1.1.5 Attempt of correlation between the MSI and triaxial strength

Fig. 13.5 shows the resulting relationship between the averaged MSI_{XRCT} from local determinations on both frontal and sagittal CT slices and the peak triaxial strength values of the *RSJ* rock cores presented in **Table 12.1** (the figure reproduces for indication *Bürgi*'s correlation *sensu* **Fig. 3.8**). For this task, due to the specific problem of *Class I* (\pm *Class II*) samples mentioned in the previous section, an upper bound value of $TC = 1$ has been reattributed to all samples for which no TC could be defined (samples that do not depict a clastic nature, e.g. for which a bimodal clast-matrix approach is found not valid). This is done with respect to the logic of *Bürgi*'s index stating that the MSI should increase together with material quality. Resulting changes in *RSJ*-MSI values are presented in **Table 13.1**. It has to be noted though that taking $TC = 1$ for non-clastic specimen is a strong assumption that indicates the need in terms of material characterization to probably adapt the MSI formulation for such type of cataclasites still characterized by a high proportion of intact rock elements (see the considerations of the preceding section).

The MSI values are plotted on **Fig. 13.5** according that the *RSJ* samples have been tested at a confining pressure σ_3 of 2 respectively 4 MPa. In such a confrontation, it has to be kept in mind that the presented values are based on the alternative medical XRCT technique (MSI_{XRCT}) that offers currently a lower resolution and permits a less accurate petrographical diagnostic compared to thin sections (MSI data from *Bürgi*, 1999). The *RSJ*-MSI values are therefore affected by some imprecision related to how the textural-structural analysis could be conducted. The interest of such a determination is certainly that MSI_{XRCT} values have a volumetric character (average of several

MSI determinations taken in orthogonal directions for one same sample). With this regard, the heterogeneous character of the tested samples can be better taken into account in their mineralo-structural characterization. Using in this context the concepts presented in **Fig. 13.3**, it can be assumed that the idealized cataclastic development in fault zones (*Class I* to *Class III* samples) is effectively related with a mechanical evolution from brittle towards more and more dominated ductile deformations, implying a general decrease in strength of the rock material (see arrow on **Fig. 13.5**). This is to explain as a result of the progressive development of new damage structures in the rock mass (progressive fragmentation leading to the apparition of new cataclastic rock matrix and of a soil-like material, reducing strength and modifying the mode of deformation).

It is found from **Fig. 13.5** that the correlation attempt between the geological and mechanical data derived in this research presents indeed good correlation coefficients of 0.8214 (samples tested at 2 MPa confining pressure) and 0.7591 (samples tested at 4 MPa confining pressure). This apparent result, that seemingly strongly supports the correlation envisaged by *Bürgi* (1999), has to be however criticized from a mechanical perspective. Namely, by taking a closer look at the correlation curves, it is found that the mechanical strength for samples tested at $\sigma_3 = 2$ MPa are similar or even higher than for samples tested at $\sigma_3 = 4$ MPa, leading to the conclusion that the *mechanical strength is independent of the confining pressure but directly linked to the MSI-value!* Such a statement is obviously wrong and at this stage of research following has to be said:

- The new MSI values used in this research derive from the XRCT analysis of the *RSJ* samples on frontal and sagittal CT slices. These values are averaged and still not permit to properly take into account the effect of singular pre-existing discontinuities in the mechanical failure

| | | MSI global (Table 11.6) | MSI local (TC = 0) | MSI local (TC = 1) |
|------------------|---------------|----------------------------|-----------------------|-----------------------|
| Class I | RSJ 10 | 0.524 | 0.412 | 2.160 |
| | RSJ 1a | 0.402 | 0.481 | 2.230 |
| | RSJ 5 | 0.337 | 0.256 | 2.004 |
| Class II | RSJ 1b | 0.608 | 0.566 | 0.858 |
| | RSJ 2 | 0.340 | 0.422 | 2.171 |
| | RSJ 9 | 0.643 | 0.611 | 0.611 |
| | RSJ 8 | 0.552 | 0.534 | 0.534 |
| | RSJ 3 | 0.585 | 0.939 | 2.630 |
| | RSJ 7 | 0.755 | 0.563 | 0.563 |
| Class III | RSJ 12 | 0.647 | 0.658 | 0.658 |
| | RSJ 4 | 0.834 | 0.566 | 0.798 |
| | RSJ 6 | 0.385 | 0.385 | 0.385 |
| | RSJ 11 | 0.688 | 0.643 | 0.643 |

Table 13.1 Mean global and local MSI values determined in this research on 13 *RSJ* samples implementing frontal and sagittal CT-slices. The different MSI_{global} correspond to the averaged values in between frontal and sagittal determinations presented in **Table 11.6** (given only for reference to the characterization performed in **Chap. 11** and for comparison with values discussed in this chapter). Such MSI's are *global* in the sense that for them, a global orientation factor δ has been used in the determination of the MC coefficient (see **section 11.3.1** and the global MC parameters in **Appendix IV-II**). Next, averaged *local* MSI-calculations implementing this time local MC parameters are given for two scenarios: **1)** Case where the 5 *RSJ* samples that cannot be characterized by the bimodal clast-matrix approach (e.g. *Class I ± II* samples) have been attributed a TC = 0. **2)** Case where TC is set for them equal to 1 (the concerned MSI-values are highlighted). Note that for *RSJ 1b* & *4* –that do permitted a TC calculation- the presented values differ between these 2 scenarios. This is to explain by the fact that they both contain a CT-slice for which a new attribution of TC = 1 had to be made (slices *RSJ 1b_{yz350}* & *RSJ 4_{yz350}*, see **Appendix IV-I**). The MSI values calculated on the base of TC = 1 for the non-clastic specimen have been taken for the confrontation with triaxial strength (**Fig. 13.5**).

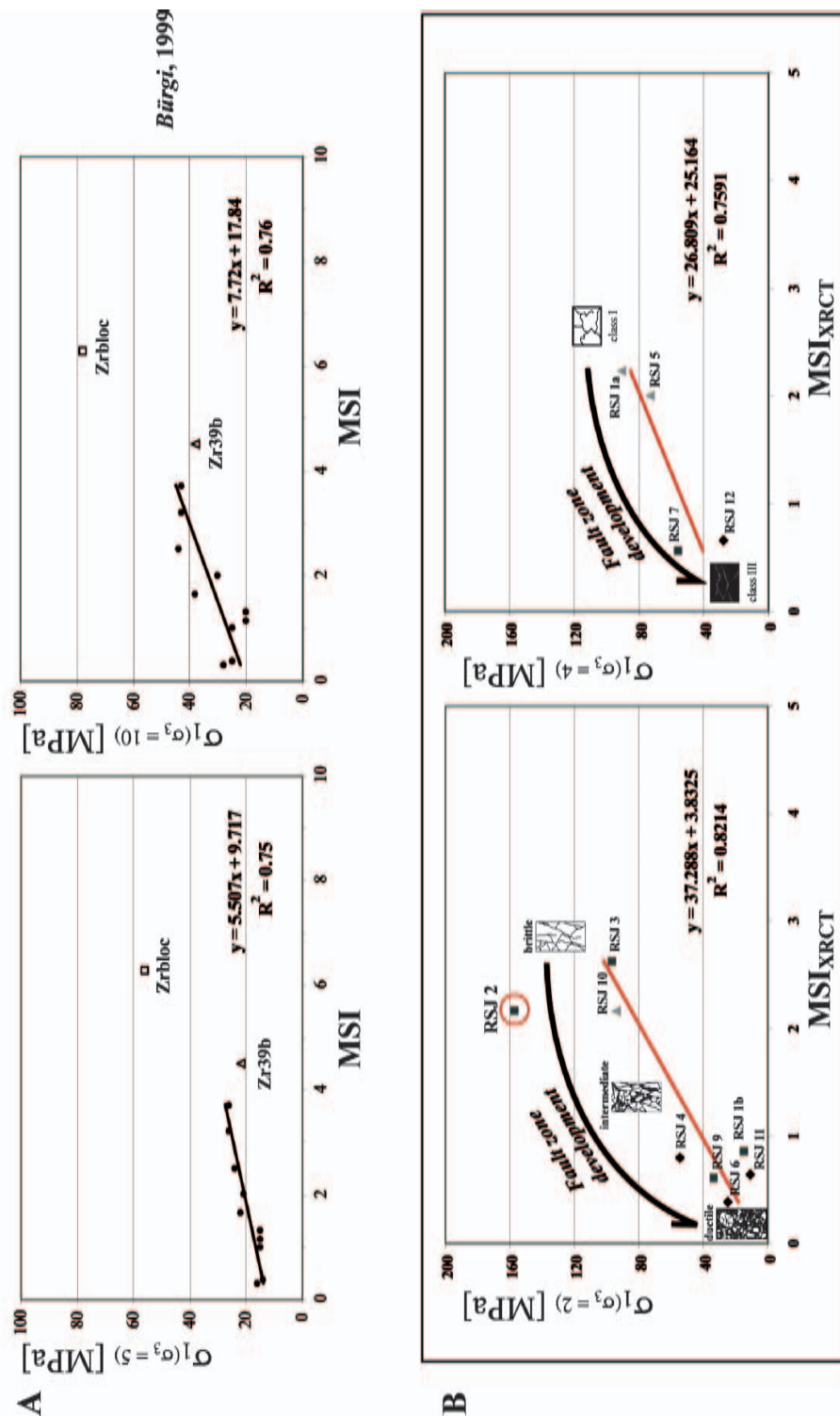


Fig. 13.5 A Bürgi's relationship between the MSI and triaxial strength data for two levels of confining pressure (5 & 10 MPa) as observed on quartzphyllitic samples from Cleuzon-Dixence. Correlation coefficients are indicated. Data from Bürgi (1999). Compare with Fig. 3.8. **B** Relationship between triaxial peak strength data determined on the RSI samples and their averaged MSI_{XRCT} from local TC & MC determinations. Note the difference in scale between A) and B). The RSI samples have been regrouped according to the level of confining pressure used in triaxial test (either 2 or 4 MPa). Values of MSI_{XRCT} have been recalculated using a TC = 1 (upper bound value) for samples that were found not accurately characterized by means of the texture coefficient (e.g. preferentially fractured specimens, corresponding to Class I ± Class II samples). Symbols are as for Fig. 11.4. Note the ambiguous position of Class II samples, showing either Class I or Class III affinity. Sample RSI 2 has been omitted from the correlation due to a strong control from a pre-existing discontinuity during triaxial test. Additionally on B), a consideration about the idealized fault zone development in terms of mechanical behaviors and geological classes is made, based on the conceptual model of Fig. 13.3. The mechanical resistance of RSI samples is found not varying significantly with regard to the level of confining pressure. See text for a critic of such a correlation.

of such materials (would require an “oriented 3D MSI” approach and the definition of tensor entities to be integrated in the MSI formulation).

- The MSI determinations have been made without the possibility to perform a detailed petrographical investigation of the analyzed damage structures (problem of discontinuities that are characterized by contrasting strength properties, see above). Therefore the binary masks used for TC & MC determinations regroup different petrographical entities analyzed in the current approach without distinction of their respective effect on rock strength (only the aspects of *feature density*, *shape*, *size* and *orientation* are considered, the aspect of the *feature-type* is lacking).
- The mineralogical content of the *RSJ* samples could only be estimated on the basis of the analysis performed by *Veuve* (2007) on an intact portion of *RSJ* material; therefore, only a rough mineralogical composition could be attributed to the different *RSJ* samples by considering their respective proportion of weak mineral phases (clay) based on the indirect XRCT technique. This procedure is not satisfying (indirect evaluation of mineral phases based only on their density contrast, no proper chemical analysis addressed) and a more detailed mineralogical analysis of the different samples should absolutely be undertaken with state of the art procedures, as the *mwVh* parameter has a strong influence on the resulting MSI value.
- The amount of data stays limited and the *RSJ* samples are found affected by a high structural variability. This fact would require to adapt the MSI in function of the type of samples that are characterized (fractured, fragmented or comminuted). A domain of validity of the MSI in its current form has been proposed in **Fig.13.3**. To investigate the correlation proposed by *Bürgi* (1999) which concerns structurally homogeneous kakirites (see **section 3.3.2**) and find arguments for an index adaptation, it would make more sense to define a correlation between samples of a same geological class instead of confronting samples at different evolutive stage (introducing an uncertainty in the characterization procedure).

Further research and more elaborated data sets are therefore required to explore the interest of *Bürgi*'s index (and its needed adaptations) with more confidence. The index's ability to characterize cataclastic rock cores from a geotechnical perspective could find a direct practical meaning. In terms of the improved characterization of cataclastic materials and of their better understanding, the mentioned limitations of the approach (inappropriate MSI formulation for *Class I* ± *Class II* samples in terms of TC, and also the problem of the comparison of scalars with tensors, see **section 13.1.1.3**) should be absolutely considered in the future to permit a more robust correlation in between the determined geological and mechanical parameters from rock cores. An implementation of tomographic DI reconstructions taking into account the petrographical nature of the indirectly evidenced geological features is expected therefore highly interesting to go in the direction of a 3D MSI definition. Accordingly, it is expected to reduce the degree of uncertainty that affects the prediction of cataclastic rock mass behavior based on mineralo-structural evidences from rock cores taken through the spatially heterogeneous fault zone development.

13.2 MECHANICAL ROCK CORE CHARACTERIZATION

The mechanical characterization of cataclastic rock cores introduces difficulties related to their inherent heterogeneity. Thus a resulting lack of representativity is often claimed in mechanical tests performed on such rock types. Moreover, an interpretation using mechanical models developed for the description of intact rock properties introduces uncertainties and inconsistencies when

applied to cataclastic materials. The damaged rock mass characterization and its particular rheology require therefore that additional parameters from geology are implemented next to the adopted parameters of classical mechanical studies.

In practical geotechnical studies, the possibility to perform numerous triaxial tests is often limited due to their excessive costs. Therefore, the high amount of data that would be required to develop a state of the art mechanical model (intrinsic determinations) in cataclastic formations is seldom attainable. To overcome this difficulty, the concept of *strength reduction criteria* for cataclastic fault rocks is introduced in this study. Based on them, the rock core characterization procedure is expected more accurate by taking into account the real material nature (heterogeneity, structural characteristics, and mineralogical constraints), even in cases where a limited sample amount is available.

With the use of the XRCT technique, important (geological) evidences of rock cores can be assessed previous to triaxial test. The possibility to perform XRCT acquisitions from a same rock core, e.g. *before* and *after* it underwent triaxial deformation, opens a wide perspective to assess the control of textural and structural elements on rock deformation. Accordingly, positioning XRCT as a bridge technique in between geology and rock mechanics seems logical and beneficial for an improved understanding of the behavior of cataclastic rock masses.

13.2.1 Use of XRCT Models Before and After Triaxial Tests

As visible from a geological rock core characterization, the assumption of a cataclastic failure localized on a single rupture plane is barely valid. The inherent damaged structure of such materials most likely introduces more complex stress transmission patterns that are difficult to assess from direct triaxial test evidence without a proper visual monitoring support.

As a matter of fact, the fault zone development presented in **Fig. 13.3** indicates that cataclastic fault rocks will depict evolutive mechanical properties from «intact» rock character in the slightly damaged zone (ideally *brittle*), to an overall fractured rock rheology in the fragmentation stage that combines contrasted mechanical modes (ideally *intermediate*), to reach finally granular characteristics in the fault core (ideally *ductile*). This development is evidenced in **Fig. 13.6** on the base of 3 *RSJ* samples that are characteristic for each stage (*RSJ 10, 9 & 11*).

It has been shown in **Chap. 11 & 12** that XRCT acquisitions *before* and *after* triaxial tests can be confronted through segmentation of *damage indicators* by means of the index DI (respectively DI_{triax}). Values of DI are progressively increasing towards the fault core. The 3D reconstructed segmented models (tomographic representation of DI) present interesting structural and textural relationships that can be correlated with the observed mechanical responses. It has been proposed in this sense to introduce a factor FI_{triax} corresponding to a *triaxially induced fracturation index* for cataclastic rock cores. Considering **Fig. 13.6**, FI_{triax} can be understood as providing a mean to evaluate effective fracturing vs. more ductile (internal) deformations in rock cores. It can be related to the intensity of damage propagation (through fracturing) in a given structure. For perfectly bimodal rock cores (e.g. structural disconnection between a clast- and a matrix phase), FI_{triax} has limited application, since for such rock cores, DI and DI_{triax} are found quasi-identical. Thus, determination of *strength reduction parameters* should in this case consider the inverse segmentation of DI, providing more information in the assessment of deformation characteristics (control of clast topography and morphology, strength increasing fabric elements). Inverse DI models of clastic materials would moreover provide the possibility to perform a TC type calculation on a 3D basis. Image analysis codes for such types of determination based on high-resolution XRCT data (facilitating greatly the segmentation of petrographically contrasted geological elements) have already been implemented

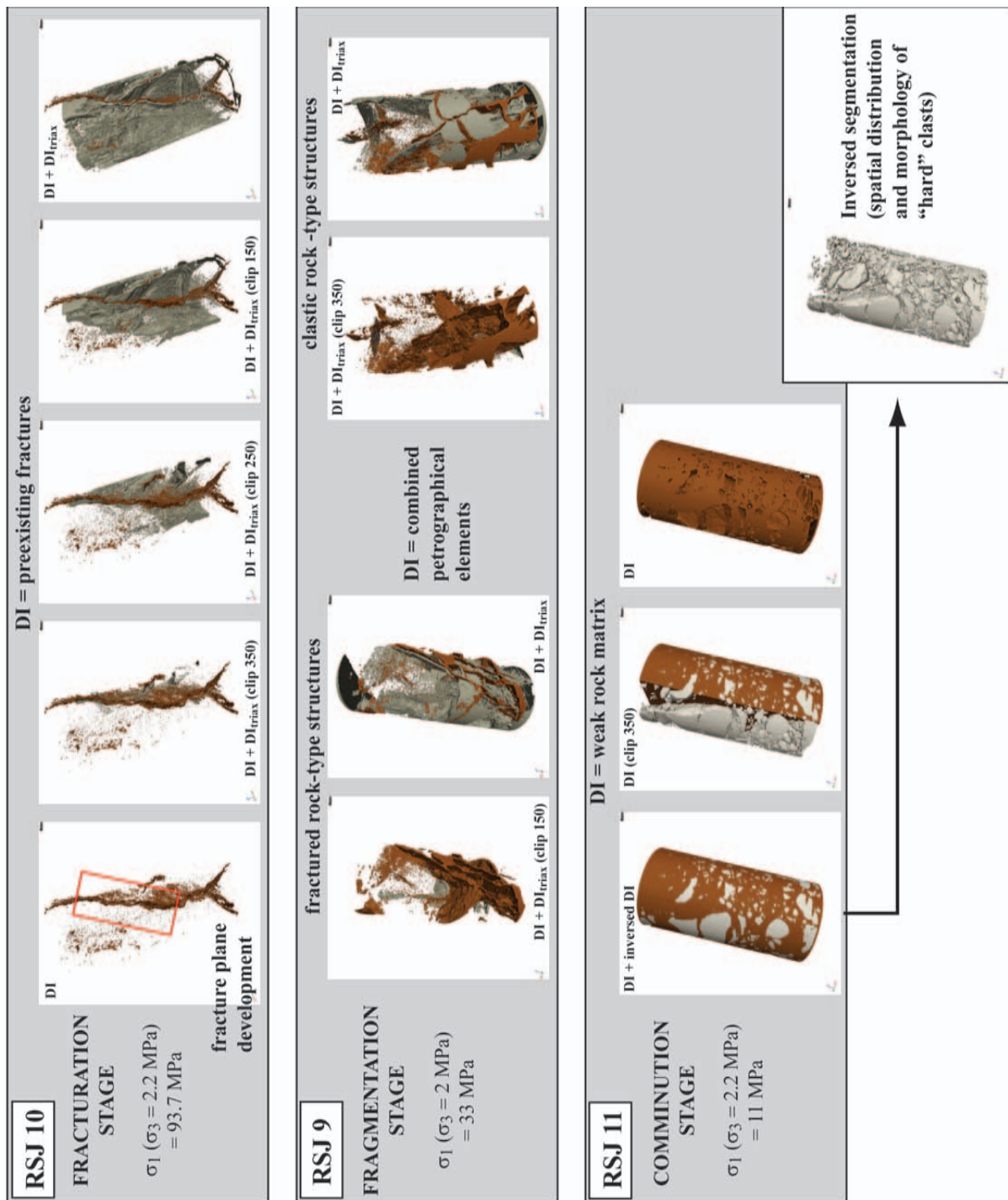


Fig. 13.6 Presentation and validation of structural types indicative of *fractured*, *fragmented* and *comminuted* materials introduced with **Fig. 13.3**. Different physical meaning of DI has to be considered. *RSJ 10*: Low cataclastic samples with intact rock character. Rupture plane develops along a pre-existing discontinuity affecting the limestone structure, as indicated by the DI model (brown). Besides this clear rupture plane, a generalized fracturing through the “intact” matrix is developed (DI_{riaux} , grey model cropped at 5 different positions to better depict its relationship with initial DI). Rupture angle α_{XRCT} is in agreement with the Mohr-Coulomb determination. *RSJ 9*: Combination of *brittle* (*fractured-rock* type, 2 first images) and *ductile* elements (*elastic-rock* type, 2 last images) that is indicative of a transitional rock structure inside fault zone. These contrasted types of structural elements will influence each in a specific way rock core deformation. Determination of rupture angle α_{XRCT} requires obviously more than the consideration of one single rupture plane. *RSJ 11*: Clastic sample corresponding to a bimodal rock assemblage *sensu Bürgi* (1999) with deformation proceeding by internal processes (mineralogical control of DI in this case). Note that only DI is presented, the light grey color corresponding here to the inverted model of the DI segmentation (brown). For such samples, strength reduction criteria would have to be found by considering the clast distribution and shape (clast morphology, e.g. 3D TC retranscription represented by the light grey color). α_{XRCT} gives better values than rupture interpretation by means of the Mohr-Coulomb approach. See 3D indirect visualizations of the original rock cores in **Appendix V-I**.

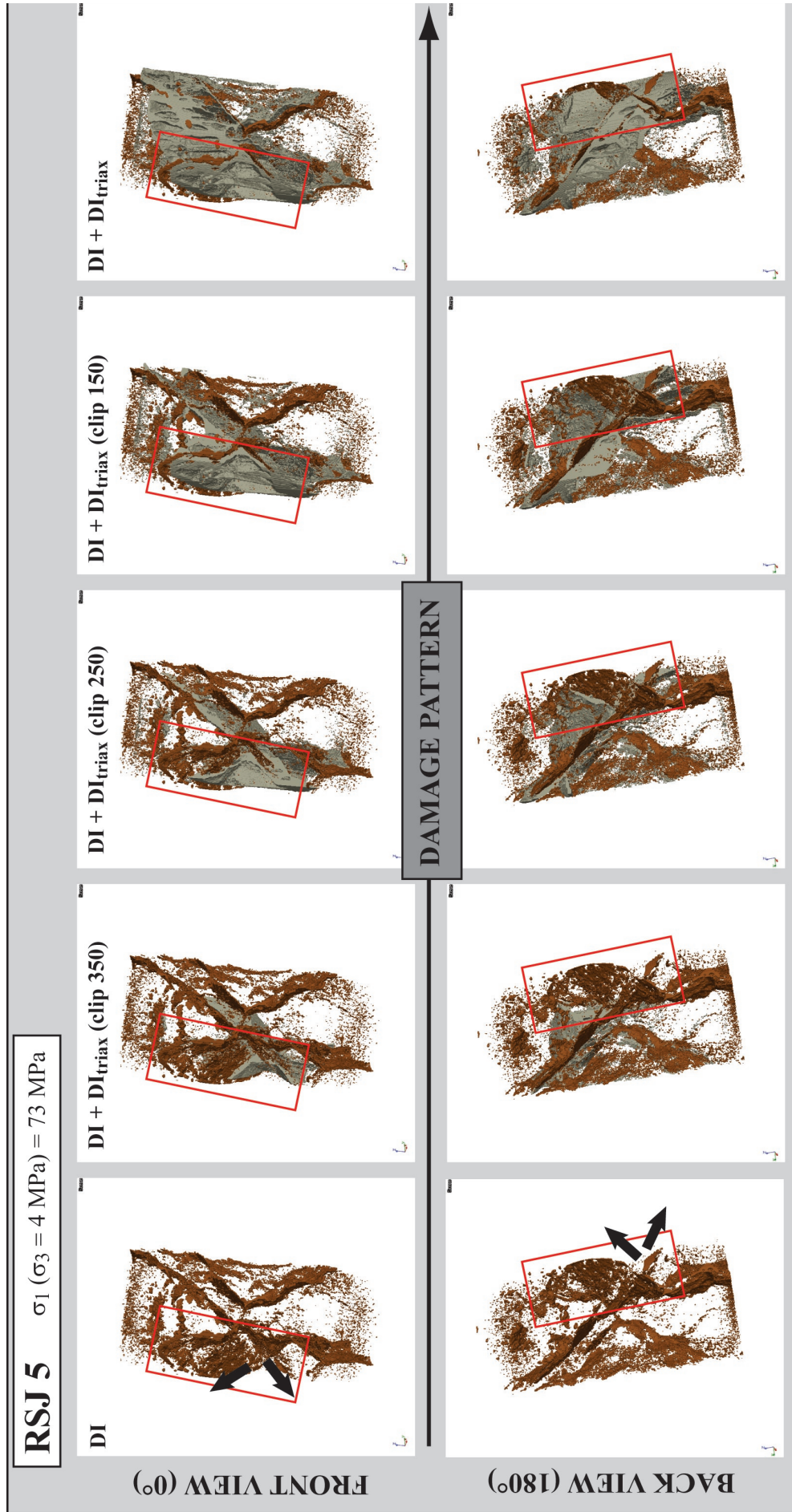


Fig. 13.7 Structural particularity of sample *RSJ 5* representative of “true” intermediate mechanical behavior (see **Fig. 12.2**). The figure illustrates the resulting damage pattern produced during triaxial test (DI_{triax} , grey color) compared to the initial spatial configuration of pre-existing discontinuities (DI , brown color). Front and back views of the segmented models are presented for a comparison. The sample is texturally indicative of *Class I* however it corresponds to an intermediate mechanical behavior. It is interpreted as reflecting stress deflection and movements along a combination of both *weak* and *hard* discontinuities in complex spatial relationship (conjugate pattern at about 45°). Rock matrix alteration might already be more advanced than for other *Class I* samples. See text for further explanations. Determined angle by means of XRCT is 49° (45° from visual inspection after removal from the triaxial cell, see **Table 12.4**). Arrows indicate the development of the corner visible in **Appendix V-I** in the indirect imaging of *RSJ 5* before segmentation.

by some authors (see Blob 3D, *Ketcham*, 2005). However the nature of the medical XRCT data used in this research introduced major problems in the straightforward application of such codes.

For rock cores depicting high FI_{triax} values (brittle samples), preferential fracturing in the hard rock portions vs. fracturing according to preexisting discontinuities should be absolutely considered. Currently at the medical XRCT resolution, it is recognized that a petrographical diagnostic is difficultly made without further analysis technique (i.e. thin section). The effect of preexisting discontinuities on rock core deformation is particularly visible for sample *RSJ 5*, as depicted with **Fig. 13.7**. An initial DI configuration (brown color on **Fig. 13.7**) corresponding to a conjugate crack system at about 45° is found influencing to a major extent the resulting test induced damage pattern (grey color). Despite the *Class I* textural character of sample *RSJ 5*, the triaxial test indicates a characteristic intermediate mechanical behavior (see **Fig. 12.2**). From the detailed geological characterization, *RSJ 5* is found affected by a low MC, no TC, which results in a low MSI value (0.337), contrasting with a peak triaxial strength of 73 MPa. Obviously, this sample is affected by numerous combinations of both *weak* and *hard* discontinuities (causing the low MC value) that interplay in a complex manner and influence to a large extent stress transmission during triaxial test. Moreover, the degree of weathering affecting the *RSJ 5* rock matrix might already be more advanced than for other *Class I* samples, influencing the development of new fractures. In this context, this sample is interpreted as corresponding to the onset of the *fragmentation* stage, leading progressively to the production of weak rock matrix through sustained cataclasis (increase in DI). This example supports the assumption that the control of preexisting discontinuities in various spatial orientations and of contrasted mechanical characteristics is a predominant aspect in cataclastic rock deformation, providing an additional argument that a mechanical interpretation assuming stress transmission along one singular structure is limited and potentially leading to a mechanical misinterpretation. Accordingly, a prediction of such a mechanical behavior would require a numerical approach (e.g. finite elements) based on **1**) the 3D description of preexisting rock structures (segmented DI models) and **2**) a detailed petrographical analysis and mechanical categorization of the evidenced preexisting structures (to be developed based on the current state of research, probably implying a distinct segmentation for each type of preexisting discontinuities).

13.2.2 Relevance of a Rupture Angle Determined by XRCT

Chap. 12 introduced the determination of α_{XRCT} for the re-interpretation of rupture conditions in the *RSJ* samples and introduction of an alternative rupture angle in the Mohr-Coulomb analysis. Orthogonal planes have been taken parallel to rock core axis to evaluate the rupture kinematics in the different samples. Determination of a main structure has been addressed for which angular measurements have been performed. Using the stereographic projection, reconstruction of the plane of maximum dip has been realized.

It has been shown that the XRCT-based rupture determinations can be in close agreement with the derived angle from the residual Mohr circle analysis (tendentially for *brittle* samples developing a single rupture plane). However, differences result for more complex samples (see **Table 12.4**). For them, the rupture angle based on residual Mohr circles should be re-defined in cases where the rock core can support a visualization once extracted from the triaxial cell (oriented failure criterion for rocks).

As experienced with the *RSJ* samples, heterogeneous rocks often don't allow such examinations after test. With a high level of inherited fractures, strong sample dislocations result making any examination by eye impossible. Given such conditions, the indirect recording from the tested sample structure *before* and *after* deformation constitutes an important source of information for an improved triaxial test interpretation.

It is interesting to notice that generally, samples affected by *ductile* mechanical behavior seem to be better represented when rupture conditions are assessed from the XRCT visualization (**Fig. 12.2**). On the contrary, *intermediate* samples introduce a difficulty, as for them the confident determination of a main structure controlling deformation is quite ambiguous. For that reason, it is suggested that the α_{XRCT} should be measured on a XRCT acquisition directly after peak rupture (end of first loading cycle). Accordingly, structural and geometrical «corruption» from the two second loading cycles (realized to permit a Mohr-Coulomb determination based on 3 residual Mohr circles) would be avoided.

It has to be said that in one way or the other, the approach corresponds to characterizing rupture only by its spatial orientation (assumed linear rupture plane). Provided the tomographic representation of DI, it is however obvious that morphological constraint from the true rupture structures could deliver important mechanical information for an improved characterization of cataclastic rocks. The spatial and morphological analysis of DI in fractured specimens could therefore be related to a 3D determination of the MC parameter. **Fig. 13.8** suggests such a consideration based on the segmented model of sample RSJ 7 (DI & DI_{triax} reconstructions for evaluation of damage propagation).

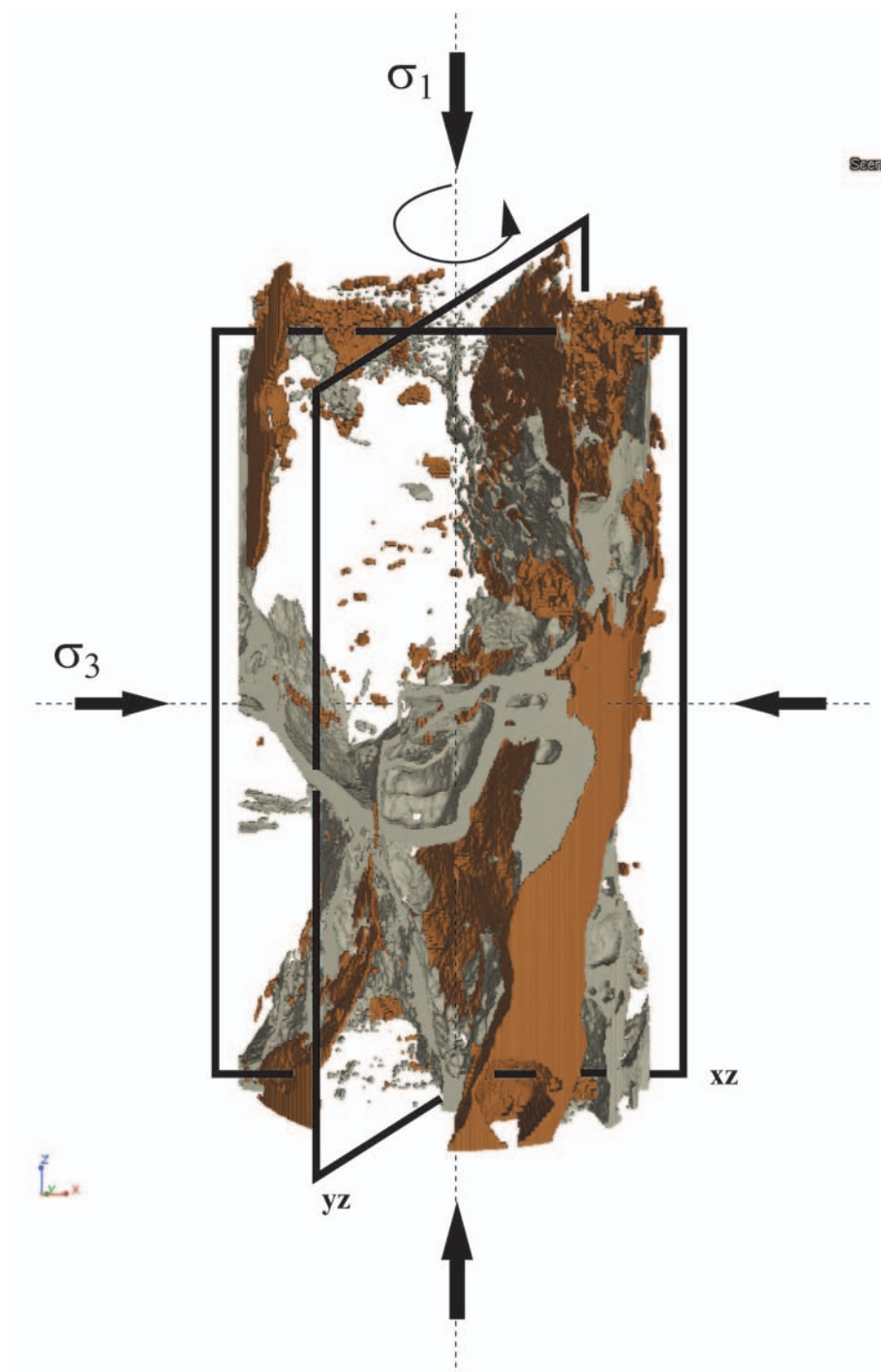


Fig. 13.8 Schematic representation of the two orthogonal planes from which α_{XRCT} is measured and relationship to effective damage by consideration of the DI model of sample *RSJ 7* (slightly fragmented, brown = DI, grey = DI_{triax} clipped at slice xz 150). The stereographic reconstruction of the (linear) plane of maximum dip will only be approximative with regard to the structural complexity inherent to heterogeneous rock samples. A 3D analysis of the DI model is expected providing a more realistic support for the 3D spatial analysis of effective rupture conditions and determination of the mechanical behavior by considering the effect of pre-existing geological features inside the volume.

14

CONCLUSIONS & PERSPECTIVES

« Tu en es encore à la tentation d'Antoine. L'ébat du zèle écourté, les tics d'orgueil puéril, l'affaissement et l'effroi.

Mais tu te mettras à ce travail : toutes les possibilités harmoniques et architecturales s'émouvront autour de ton siège. Des êtres parfaits, imprévus, s'offriront à tes expériences. Dans tes environs affluera rêveusement la curiosité d'anciennes foules et de luxes oisifs. Ta mémoire et tes sens ne seront que la nourriture de ton impulsion créatrice. Quant au monde, quand tu sortiras, que sera-t-il devenu ? En tout cas, rien des apparences actuelles. »

Arthur Rimbaud, *Illuminations*

At this stage of research several conclusions can be drawn roughly following the order of the chapters constituting this dissertation. They are summarized in the first part of this chapter.

Second a perspective is drawn questioning the possible 3D structural and textural analysis of rock cores based on the tomographic DI models. This perspective – although at a preliminary stage of research - already establishes promising considerations about how to better translate the cataclastic specificity into a characterization procedure able to predict rock strength (and at a more advanced stage rock behavior) on the base of geological evidences.

14.1 INPUTS FROM THE THESIS

Cataclastic rocks still constitute **a problematic material in underground engineering constructions**. On one hand, the prediction of their presence is difficultly made on the sole base of reconnaissance drilling and can be often overseen (type example: N16 Moutier tunnel). On the other hand, if cataclastic rocks are found during drilling operations, their implementation in geotechnical studies is often problematic due to the bad structural quality of the recovered samples.

During preliminary geotechnical site studies, geological field investigations and **understanding of the global tectonic setting** provide critical informations regarding the presence of potential fault zones susceptible to impair on the underground excavation project. The use of a **conceptual model for the presence and development of fault rocks at shallow crustal conditions** can help in translating local observations from outcrop or reconnaissance drilling into a more objective picture to be integrated in the rock mass characterization. Distinction between intact and damaged rock masses is an essential aspect. A geotechnical classification for cataclastic fault rocks is however still expected. Such a classification has to be based on petrological considerations, as the initial intact rock protolith will strongly influence the resulting cataclastic mineralogy, textures and structures. With this regard, **fundamental research in structural geology and mineralogy can greatly assist and alimient specific needs of applied studies** by providing a translation tool between sample evidences and the regional rock mass architecture. Accordingly, recognition of characteristic cataclastic samples in reconnaissance drillings can already allow inferring on the possible development of a fault zone based on the critical analysis of textures and micro-structures at the sample scale.

Thus, it seems evident that **the problem of weak rock masses has to be analyzed from a global perspective down to the sample (and further microscopical) scales**. Accordingly, this research considers the fault zone architecture and its control on the development of variably damaged rock masses, from the fault external part towards the fault core. Mechanical arguments addressing a characterization of the contrasted cataclastic behaviors can be better defined with regard to geological inputs. In this sense, it is proposed to evidence specific **damage indicators** (geology) affecting cataclastic rocks to be translated in terms of **strength reduction criteria** (mechanics). These ideas have been stimulated by research papers that present in this sense interesting insights on rock fracturing and development of fault zones. Indicative mechanical models for porous and crystalline rocks are presented in *Schultz & Siddharthan* (2005). An interesting correspondence is found with the mechanical models proposed by *Habimana* (1999). It has to be said that the concept of **damage indicators** is not restricted to studies at the sample scale. **Fig. 4.2** already introduces the analogy of the fracturing process on a scale-independent basis when a binary representation is considered.

This research has been performed at the sample scale. Thus the quality of the data at disposition for engineering design purposes strongly depends from the quality of the samples available for

laboratory analysis. The **possibility to obtain high quality cataclastic samples representative of *in situ* conditions** has been demonstrated by experience with a portative triple tube core driller. Rock core extraction becomes facilitated and the technique is found promising to address detailed studies of cataclastic environments. Particular attention during extraction from the rock mass is a prerequisite and proper sample conditioning should not be avoided. Cataclastic sampling on the field should moreover be made according to a dense drilling array, in order to gain a representative sample population in a given tectonized rock mass context. By doing so, best chances to properly evaluate rock mass heterogeneity and anisotropy can be found, as well as arguments for the observed variability in mechanical behaviors.

Using the concept of *damage indicators* to be translated into *strength reduction criteria*, it is supported within this study that the **determination of additional mechanical parameters accounting for the contrasted tectonization degrees of the tested materials** (e.g. *Habimana*, 1999) is pertinent. Accordingly, cataclastic rock mass description can be performed on the base of modified classical mechanical models for intact rocks (e.g. Hoek & Brown) that integrate ponderation factors accounting for the level of cataclasis underwent by a given sample under investigation (e.g. tectonization degree).

The Mineralogical and Structural Index MSI has been proposed by *Bürgi* (1999) as a **strength prediction index for cataclastic rocks**. It is based on mineralogical, structural and textural evidences determined from thin section image analysis. Values of triaxial tests determined by *Habimana* (1999) on quartzo-phyllitic rocks from Cleuzon-Dixence have been found to correlate with the MSI. This correlation has been further investigated in this research on carbonatic rock cores by confronting their triaxial strength with results of a detailed geological characterization based on indirect 2D images from medical X-ray computerized tomography (XRCT). The approach is however **still judged not convincing** due to too limited data and the often very heterogeneous nature of cataclastic rocks involving singular preexisting geological damage structures in orientation susceptible to strongly control rock strength. Main critics expressed on *Bürgi*'s approach relate to **1)** the fact that different samples were used for the mechanical and geological characterization and to **2)** the fact that the structural and textural determinations derive from a 2D analysis support. The MSI and its expected potential to predict cataclastic rock strength has therefore been restricted by *Bürgi* to cataclasites with a certain structural and mineralogical homogeneity at the scale of thin sections and triaxial tests (problem of frequently observed structural heterogeneities at the mesoscopic scales). However, a correlation between a MSI-type determination and mechanical strength should not be underestimated for its interest in geotechnical studies. Ideally with the approach, a first estimate in terms of strength could be realized on excess samples that would not be integrated in a mechanical study, subsequently increasing the level of input data at disposition for studies addressing the geotechnical characterization of cataclastic rock masses.

Stimulated by recent developments of the XRCT technique in geosciences and rock core analysis, this study has considered the 3D indirect investigation of cataclastic rock cores from geotechnical site studies at the medical scanner resolution (0.215 x 0.215 x 0.6 mm). Industrial scanners offer nowadays far better resolution potentials, however the possibilities to study sample sizes corresponding to rock cores from reconnaissance drilling operations still introduce a limitation. In this research sample reshaping in smaller sizes was made impossible due to the cataclastic nature of the rock cores. **Medical XRCT has therefore been found an ideal and most rapid analysis technique able to accommodate sample size up to 10 cm diameter**. Acquisition improvements are reached at low cost (elimination of beam hardening artifact with a pre-filtering support).

Based on samples from contrasted petrological contents it is found that the medical XRCT is

able to depict several type-geological features introducing important considerations for any rock core characterization. Consequently, an **image analysis tool permitting the optimized segmentation of geological elements at the medical XRCT resolution** has been developed and implemented for the indirect geological and geomechanical characterization of heterogeneous rock cores (CARact3D). Results are promising and require to be further tested and possibly developed profiting from expert knowledge in image analysis. To reach a fully operational 3D petrographical and spatial analysis with the medical XRCT will indeed be probably long and requires active research on the subject. Example of 3D petrographical analysis of rock components recorded using high-resolution XRCT (10-200 μm) is however already found in *Ketcham* (2005). With such an image quality, it is to expect that the possibilities of segmentation offered by CARact3D will increase concurrently.

Based on the XRCT database of 13 tectonized limestones collected at the N16 Roche St Jean tunnel in the Jura Mountains, a **pseudo-3D determination of the MSI** has been tested. The approach makes use of several 2D CT slices per sample taken in orthogonal planes (frontal and sagittal) on which the MSI is each time determined. Then the different MSIs are averaged to define a mean MSI value for the rock core expected to characterize the sample from a more global perspective (accordingly the derived MSI gets a volumetric character and is better able to take into account rock core heterogeneity). The frontal and sagittal planes from the XRCT acquisitions are preferentially chosen because they are in a direction parallel to the load application in triaxial tests. Based on this approach, a conceptual model describing the structural and textural evolution of rock materials within fault zones could be proposed. The **domain of validity of the MSI in the formulation by Bürgi (1999)** is highlighted. It shows that the MSI approach is valid for bimodal materials, described as composed of a clast and a matrix phase. It is found with the *RSJ* samples that such a bimodal approach fails to describe properly predominantly fractured cataclasites that still haven't fully develop into clastic materials (slightly cataclased samples from more external domains of the fault zone). Also in case of fluid-rock interaction susceptible to recement clasts by means of mineral precipitation, precise knowledge about the nature of discontinuities analyzed with the index (differentiation between "hard" and "soft" discontinuities) is required.

An indicative interpretation of sample deformation has also been made in this research through a similar pseudo-3D approach (analysis of several frontal and sagittal CT slices per sample) by **confronting XRCT acquisitions before and after triaxial tests** so as to define a "true" rupture angle. The exercise, performed on two orthogonal planes parallel to rock core axis, addressed the indirect visual analysis of trace lines corresponding to an interpreted "main" fracture. Reconstruction of the true dip of the fracture has then been realized by stereographic projection. XRCT-determined values have been confronted with a classical evaluation by means of a "soil" Mohr-Coulomb approach (determination of the rupture angle based on linear regression on the residual Mohr circles). Even if simplistic at this stage, **the confrontation questions potential source of errors in the mechanical interpretation made on cataclastic materials** and would require to be explored with a more relevant model (oriented failure criterion that considers the influence of pre-existing geological structures on the observed mechanical response). The *RSJ* samples show moreover that their complex (pre-existing) structural states are most likely to produce a rupture governed by multiple fractures in different orientations, which is not taken into account with the Mohr-Coulomb approach. The interest of α_{XRCT} determinations performed in this research was therefore the ability to **visualize effective rupture conditions** susceptible to provide important source of information in mechanical studies. At this stage, only one main rupture structure could be considered, what should be improved in the future to more accurately describe effective cataclastic rupture conditions and take into account the interplay between several fractures.

Using XRCT data with a pseudo-3D approach reveals therefore the interest in **developping proper image analysis tools able to quantify rock core structures and textures fully in 3D**. Provided the fact that XRCT permits the geological characterization on the exact same rock cores that are tested mechanically, the *morphology* of pre-existing geological features (i.e. *damage indicators*), together with their *spatial distribution*, offer strong potential constraints on the resulting triaxial test interpretation. Segmentation results using CARact3D have proposed in this sense to introduce the indices **DI** & **DI_{triax}** to define the structural characteristics of rock cores and their level of damage. These indices provide a scalar determination of the amount of damage present in a rock by comparison of rock core volumes *before* and *after* triaxial test. For geological studies, DI ranges can accordingly be established to classify samples of a given petrology (e.g. attribution in *Class I, II* & *III* as a function of DI). Based on DI, possible correlations would then have to be investigated between contrasted petrological contents to assess the manifestation of damage in different context and the general relevance of the method for rock core characterization purposes. For mechanical studies, test rupture conditions as well as the evaluation of triaxial test results can be precised by confronting DI with **DI_{triax}**. An **additional index FI_{triax}** has in this sense been proposed in this research. Preferential modes of deformation can be evidenced in this way (preferential fracturing and splitting vs. preferential compaction leading to comminution). Again, the approach would at this stage benefit from observations performed on additional petrological contents to be validated. An interesting aspect for the improvement of the proposed rock core characterization procedure is that both **DI** & **DI_{triax}** permit a tomographic reconstruction of *damage indicators* in 3D. Accordingly, spatial analysis tools could be implemented (tensorial determination of material heterogeneities and anisotropies, modellisation of rock core deformation under a given stress field, precise determination of failure modes and geometries).

The implementation of medical XRCT in the characterization procedure of cataclastic rock samples is therefore susceptible to **strongly reduce source of errors in any correlation attempts between their geological and mechanical properties**. In this sense the medical XRCT positions itself as a bridge analytical technique between the geological and geomechanical sciences. From a geological perspective, it permits to increase the level of accuracy of any textural-structural investigations by providing a 3D visualization of a rock core structure and its constitutive elements. It provides an ideal mean to perform a rock core classification by indirectly evidencing different degrees of degradation that are quantified and spatially visualized in terms of DI. From a mechanical perspective, it removes a certain “black-box” character to triaxial tests by effectively assessing damage development into cataclastic rock structures. Thus, interpretation of mechanical tests gets closer to real mechanisms that should be evaluated for their **effect and implications at the scale of the rock mass**. The study of contrasting deformation modes characterizing cataclastic rocks as well as the possibility to determine the cause of these variations (structural control of pre-existing geological features) is an important input to assess heterogeneity within a cataclastic horizon at the level of the underground work.

14.2 TOWARDS A CHARACTERIZATION OF CATACLASTIC ROCK CORE PROPERTIES BASED ON 3D XRCT DATA

Credit should be absolutely given to the quality of XRCT reconstructions at the medical resolution, as the technique bears many practical advantages (readiness of use, low time consumption, flexibility to accommodate different sample sizes and shapes). Developments of 3D analysis tools fitting the medical CT data for the structural and textural characterization of the segmented damage indicators are expected possible in a realistic time-scale profiting from expert knowledge in image analysis. An adaptative coordinate sytem should be developped for such models that would permit the geo-referentiation of a given DI configuration in a numerical code. Accordingly morphological and directional characteristics of geological features could be properly quantified and used to understand the sample deformation mode. Mineralogical constraints derived from appropriate analytical procedures (XRD, EM, thin sections) would have moreover to be taken into account for their respective control on rock strength.

Looking forward, an analysis protocol for cataclastic rock cores comparable to the protocols used in medicine for internal investigations of the human body could be possibly developped in the future.

The preceding remarks demonstrate the interest of the approach implementing medical XRCT for a combined geological and geomechanical study of cataclastic rock cores. Such a combined approach can in particular be performed on the exact same sample, potentially reducing source of errors between any correlation attempts.

Parameters from geology determined on rock cores prior to mechanical test (*damage indicators*) are indicative of material nature and its respective degree of cataclasis. By adding information from the indirect visualization after triaxial tests, influence of given textural and structural parameters can be assessed for their control on mechanical deformations. Accordingly, the relevance of XRCT models in a geological and mechanical confrontation introduces the concept of *strength reduction criteria*. They can be introduced in a triaxial test interpretation performed on the base of classical rock mechanical models. Accordingly, the influence of heterogeneity and anisotropy can be better addressed based on geological criteria.

Following the considerations from **Chap. 13** and based on the several parameters proposed after study of the XRCT-analyzed *RSJ* samples, their potential implementation in cataclastic rock mass characterization from both a geological and mechanical perspective is discussed. In particular the scalar (DI) and tomographic (3D segmented XRCT models) representations of *damage indicators* are evaluated for their practical interest in geotechnical studies.

It is said that these perspectives must be regarded as corresponding to a very preliminary stage of development. They are given for direction in further research aiming the characterization and prediction of tectonized rock masses in underground engineering works.

14.2.1 Parameters of the MSI vs. Damage Indicators from XRCT

The textural and structural parameters constitutive of the MSI have been evaluated from a pseudo-3D approach based on frontal and sagittal CT-slices (**Fig. 13.1 & 13.2**). As a result, it is shown that for TC and MC local determinations, the greatest variations inside rock cores relate to *shape* and *orientation* of rock elements (e.g. clasts and discontinuities).

When studied on a 2D basis, these variations can only be indicatively accounted for, as an uncertainty prevails regarding the full spatial development of rock elements. This is not to be underestimated as the complex organization of structures in cataclastic rocks leads to a high level

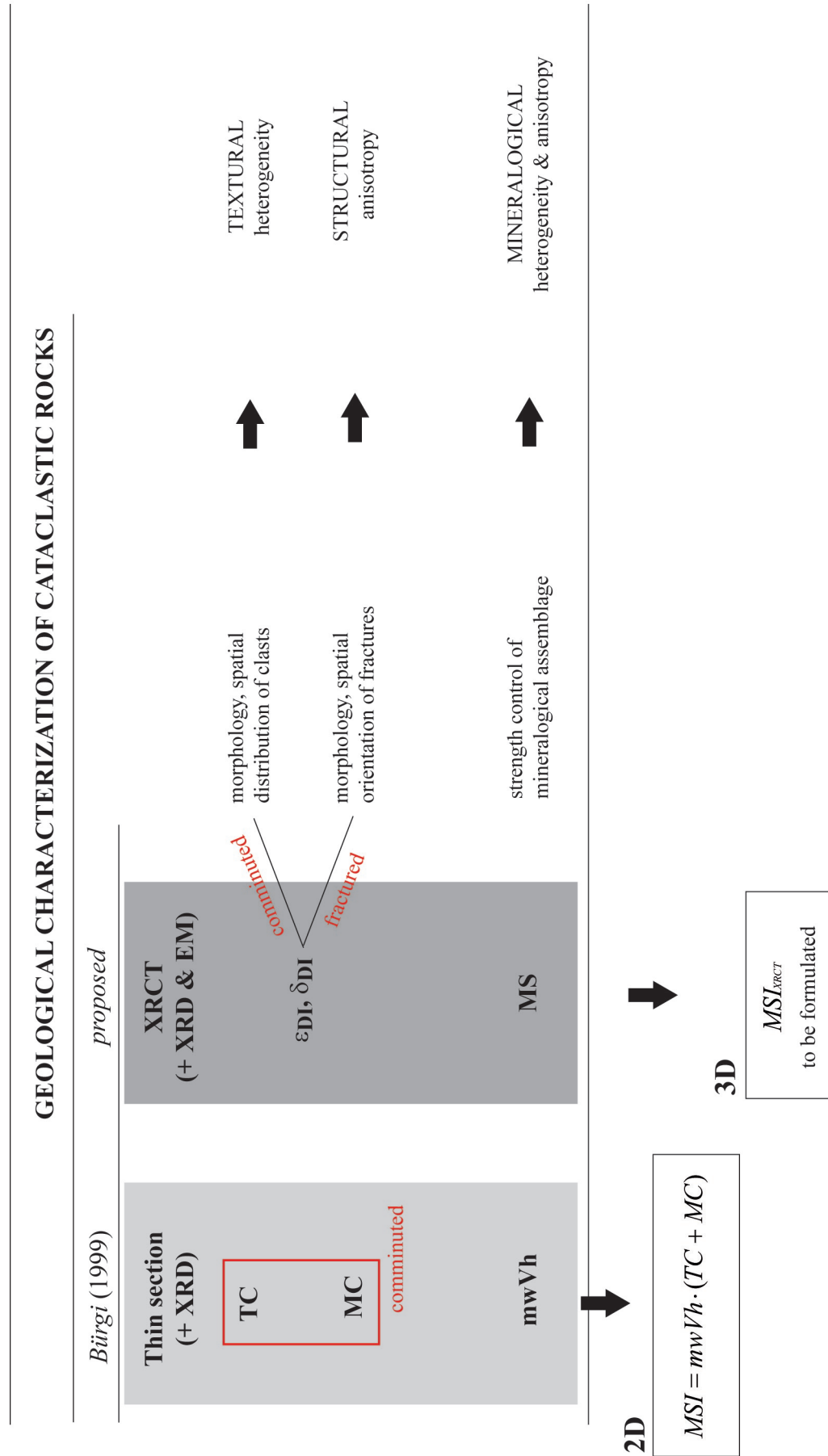


Fig. 14.1 Physical meaning of the TC & MC parameters proposed by Bürgi (1999) and proposition for a 3D retranscription based on segmented XRCT data. Implications for the determination of the Mineralogical and Structural Index MSI and its possible retranscription in 3D. Reference to different sources of heterogeneity & anisotropy susceptible to affect cataclastic rocks: *mineralogical, textural and structural*. Note that for determination of a mineralogical anisotropy, electron microscopy techniques are of great interest provided the possibility to perform surface mapping on uncovered thin sections. Such determinations can highlight preferred zones of alteration within the rock structure.

of heterogeneity and anisotropy. *Bürgi* (1999) already pointed out the fact that in case of MC, the orientation factor δ would benefit from a tensorial determination for best representativity (see sections 12.1.2 & 13.1.1.3).

Using the *RSJ*-XRCT data, segmentation of damage indicators and their 3D reconstruction permit to quantify and visualize preexisting structures (e.g. damage) spatially. Using considerations of **Fig. 13.3**, a physical meaning can be given to a characteristic DI spatial distribution and accounted for in terms of material characteristics (preferentially fractured vs. clastic specimens). It is evident that all informations related to critical structures and textures can be assessed in that way. If a coordinate system could be developed to establish a spatial referencial for the DI models, the structural and textural analysis could be basically performed on a full 3D basis. Form and shape of DI as well as their spatial orientation would have to be determined with proper image analysis tools. Moreover, difference in DI and DI_{triax} (leading to the determination of the *triaxially induced fracture index* FI_{triax}) could be more objectively quantified in terms of the resulting *fracture propagation* that effectively develops during triaxial deformation.

Fig. 14.1 establishes a retranscription of the parameters constitutive of the MSI with the additional determinations made possible by means of XRCT data segmentation.

14.2.2 Inputs for a XRCT Formulation of the MSI

The *RSJ* samples widely studied in this research correspond to different degree of cataclasis through tectonically induced processes of rock *fracturing*, *fragmentation* and *comminution*. The observed contrasts in TC & MC determinations from frontal and sagittal views are diagnostic of a type of material heterogeneity where the MSI has a limited validity in its current formulation (fractured vs. clastic samples). A spatial uncertainty affects moreover 2D determinations of preferred orientations and anisotropies. Thus, a 3D determination of parameters describing TC & MC on a volumetric basis would be welcomed, as suggested in **Fig. 14.1**.

The MSI, by considering structural and mineralogical rock parameters, regroups important mineralo-structural information needed to translate geological parameters into a strength prediction model. Based on what has been said, it is suggested that a determination of the MSI based on XRCT segmented models could be reached (e.g. MSI_{XRCT}). Profiting from tomographic reconstructions of geological features indicative of damage, it should become possible to go one step further in the characterization procedure by quantifying rock heterogeneity and anisotropy based on tensor formulations.

A proper formulation for the MSI_{XRCT} is however premature at the end of this research. At this stage, referring to the concept of *strength reduction criteria* introduced in this study, it is indicatively suggested to derive the MSI_{XRCT} from following tensorial determinations for a better description of the specific mechanical behavior of heterogeneous-anisotropic rock materials:

“MS” = strength of the overall *mineralogical assemblage*, that should integrate the effect of localized alteration zones and of discontinuity surface conditions (requires currently additional evidences from thin section or electron microscopy, see **Fig. 11.7**). This tensor is proposed to describe the effect of both *mineralogical heterogeneity* and *anisotropy*.

“ ϵ_{DI} ” = strength reduction criterion accounting for the 3D *texture* of damage indicators. In the case of predominantly comminuted materials, it should describe the *morphology* of clasts. In the case of predominantly fractured materials, it would correspond to a description of the *morphology* of fractures. This tensor is proposed to characterize rock core *heterogeneity*.

“ δ_{DI} ” = strength reduction criterion accounting for the 3D *structure* of damage indicators. For predominantly comminuted materials, it should describe the *spatial distribution* of clasts. In the case of predominantly fractured materials, the *spatial orientation* of fractures would have to be assessed. This tensor is proposed to characterize rock core *anisotropy*.

These 3 tensors, formulated in an appropriate manner, could be used to improve both the MSI approach and the determinations of the parameters a , m_b , s and t of the modified failure criterion proposed by *Habimana* (1999, **Eq. 3.2**, see also **Table 3.3**).

ACKNOWLEDGEMENTS

I address my thanks to the Swiss National Science Foundation (SNF) for the financial support over the 4 years that have been needed to realize the project Cataclasite II.

My gratitude goes to Prof. Dr Aurèle Parriaux, my *main* PhD advisor, for initiating research projects in very stimulating subjects and for his constant effort to maintain the role of the geologist in a central position in civil engineering works. He gave me his trust to perform and manage this project and for sure it was for me a life-forming experience. Dr Pascal Turberg at GEOLEP has been a central actor of this research and he had some of these subtle “right words at the right moment” that have been decisive in the finalization of my work. Laurent Tacher is thanked for the geoshaped implementation of a rose diagram software that effectively helped me in seeing *la vie en rose*. Dr Vincent Labieuse, my *second* PhD advisor, who confronted me with another world, improved my knowledge in rock mechanics and allowed me to transgress some borders that in my eyes shouldn't be borders. At LMR, Jean-François Mathier has been a source of answers to many day to day problems that a geologist like me encounters in a laboratory of rock mechanics. Laurent Gastaldo supervised the analyses in the lab and I'm thankful for his very relaxed manner in performing complex laboratory manipulations and for all his help and smiles. At LMS, Gilbert Gruaz helped me greatly for a few manipulations; I thank him for his humanity and electricity, I guess it has connected me with something...

Special thank to Prof. Dr Reto Meuli at the CHUV in Lausanne and Prof. Dr Eberhard Lehmann at the PSI in Villigen for providing me access to the XRCT and NT facilities in the framework of this research. Working at CHUV I was pleased to meet with following people whom I thank especially for their open-mindedness and patience with a dirty geologist in a white shirt environment: Prof. Pierre Schnyder, Martine Bernasconi, Grégoire Haengaertner, Francis Verdun, Christel Elandoy and Patric Hagmann. At PSI, I have to thank Dr Peter Vontobel, who followed me in the realization of the NT test and was an important source of strength for the finalization of my first published scientific paper. François Aguet at EPFL, for discussions on 3D image analysis. Yvon Desnoyers from Nancy Mining School, France, who has realized a very successful summer scholarship at EPFL in 2006.

I have to thank my contacts from field work: First Pascal Chollet (HILTI) and Frank Socquet (TechniDrill DGA) for technical support and numerous advices with the portative rock core extractor. *Vallorbe*: Pierre-Yves Jeannin, Pierre Behrli. *Montier*: Nath Challandes, Tito Haarpaintner, Daniel Rohrer, Alain Koenig, Stefan Lütolf, Markus Inniger. *Roche St Jean*: François Flury, Romain Christe, Laurent Bugnon, Pascal Mertenat, Bernard Menozzi. *Ceneri*: Diego Pozzorini, Edwin Drack. *Amsteg*: Beat Frei, Roger Moore. *Glion, Vièges, Honergrin*: Bureau Norbert SA. Moreover I thank: Dieter Fellner for his comments and insights on the subject of tunneling and geological prognosis. Laurent Chaignat and Christophe Veuve for the brilliant work they have realized during their Master theses and for all the good moments we have spent together on the field and elsewhere. Dario Carrea, Emmanuel Wick and Clément Michoud for their precious help with last minute TC determinations. Jean-Marc Terraz, Michel Teuscher, and Pierre Loesch for all the technical support I needed during this PhD. With great professionalism and creativity they were always ready to solve issues that may have looked desperate for many. Chantal Vicari-Strickler gave me her support and help on a playground that was not supposed to be mine.

Next to the scientific advice obtained by these different people all over these 4 years, I've obtained many insights on other (tectonic) aspects of life by several persons which I'd like to thank hereafter:

At GEOLEP and surrounding labs, past and present: f.* , Beppe, Seb, Thierry, Koen, Damien, Marguerite, Saskia, the *international postgraduate team 2003-04* (Mehdi, Tutu, Truffiño, JB, Jean & Laurie, Hubert, Manu, Etienne, Béné, Armande, Fanta, Marcelo), Isabelle, Robert, Laurence, *Stéphanie*, Pascal, Marco, Adrien, Séverine, Aude, Pierrick, Pascal, Dani, Simone, Gilles, m'sieur Matti, David, Diana, Julien, Cornelia, Alina, Mike, Jianong, Popov, Valérie & Yannick, Hazad, Rafal, Marta, Mathieu, Hervé, Rafael, Amparo, Claire, Claire, Stefano, Irene, Laurent, Bob, Patrick, Chinatown, Gérard, PanPan, Ruben, Jean, Djano, Marc. Stefan Schmid. The CHGEOL committee. The EFG council, in particular Leo Luzieux, Thomas Imbach, Dirk de Coster, Edmund Nickless, Ruth Allington, Manuel Rigueiro and Fionnuala Collins. Robert Font of the AIPG. Dr Harold Eisner, Nicolas Bolletta and my other “healers” who brought me to deep considerations about *quality* vs. *quantity*. Corinne, *für mehr Meer*. My Andorran friends who welcome me since many years and where I've found this special Andorran touch in the preliminary redaction of my manuscript. It's indeed always special in Andorra. My climbing friends, *for balance & momentum*: Fred, Matthieu, Martin, Damien, Pascal, Véro, Bernard & la Cat, Peter, Kirsten (& Yannis & Anouk), Ale, Thomas, Regula, Ago, Flo, Shandip (& B-nergy), Beni, Flip, Rolf, Tobi, Lars, Yann, Raph, Suppa, Enrico, Krister, Cédric, Alexandre, Richard, panStructure, Elie, Ryan, Tony, Alex, Ingo, Alain, BipBip, Arnaud, Les Nomades, Sabine, Canna, Diedro, Caro, Jeff, Ulric, Costa. And *Phil*, who has been settling the route. Of course: Alex, Christine, Ratheesh, Tia, Karen, Chris, Nono, Dessi *for flexibility*; Manu, Hugo, Nadia, Bert, *for freedom*; Elma, Sabina, Simon, Alex, Frank, Luki, Marki, Tobi, Katy, Carla, David le Rouge, Miu, Nate, Natalie, Evelyne, Muq, Dave, Adi, Adrian, Michi, Ina, Dani-El, Patrick, Achim, Andrea, Mauricio, Ronan, Sébastien, Callum, Thorsten, Bernhard, Nico, Senecio, Matthias, Kamil, Niels, Friedl, Nynke, *James*, Sebastian, Maurus, Pierre, Willy, Capi, Dov, Yves & Fabienne, Selma & Dani, Pete, *for being*.

I have especially to thank my family, in Jura and Holland, for their constant love and support; they have taught me to question and to self-question, *for the best*.

BIBLIOGRAPHY

- Aguet, F., Jacob, M. & Unser, M. (2005). Three-Dimensional Feature Detection Using Optimal Steerable Filters. *Proceedings of the 2005 IEEE International Conference on Image Processing (ICIP'05)*, Genova, Italy, September 11-14, 2005, pp. II-1158-II-1161.
- AFTES (2003). Recommandations relatives à la caractérisation des massifs rocheux utile à l'étude et à la réalisation des ouvrages souterrains. *Tunnels et ouvrages souterrains*, **177**, 138-186.
- Alshibli, K. A., Sture, S., Costes, N. C., Franck, M. L., Lankton, M.R., Batiste, S. N., Swanson, R. A. (2000). Assessment of localized deformation in sand using X-ray computed tomography. *Geotechnical Testing Journal*, **23**, 274-299.
- Amberg, W. (1999). Konzepte der Ausbruchsicherung für tiefliegende Tunnels, *Bauingenieur*, **74**.
- Bakoyannis, Y. (2005). Safety in tunnelling. In: *Kolymbas, D. & Laudahn, A. (Ed.), Rational Tunnelling. 2nd Summerschool, Innsbruck*, 291 pp.
- Barton, N. (2002). Some new Q-value correlations to assist in site characterization and tunnel design. *Int. J. Rock Mech. And Mining Sciences*, **39**, 185-216.
- Barton, N., Lien, R., Lunde, J. (1974). Engineering classification of rockmasses for the design of tunnel support. *Rock Mech*, **6(4)**, 189-236.
- Berger M. J., Hubbell J. H., Seltzer S. M., Chang J., Coursey J. S., Sukumar R., Zucker, D.S. (1998). XCOM: Photon Cross Sections Database. *National Institute of Standards and Technology*, NIST Standard Reference Database **8** (XGAM).
- Bésuelle, P., Rudnicki, J.W. (2004). Localization: shear bands and compaction bands. *Mechanics of Fluid-Saturated Rocks*, Guéguen, Y., Boutéca, M. (Eds.), Elsevier, Amsterdam, pp. 219- 321.
- Bésuelle, P., Viggiani, G., Lenoir, N., Desrues, J., Bornert, M. (2006). X-ray micro CT for studying strain localization in clay rocks under triaxial compression. In Desrues, J., Viggiani, G. & Bésuelle, P. (eds) 2006. *Advances in X-ray tomography for Geomaterials*, ISTE, 452 pp.
- Bieniawski, Z. T. (1973). Engineering classification of jointed rock masses. *Trans S. Afr. Inst. Civ. Engrs*, **15**, 335-344.
- Bieniawski, Z. T. (1974). Geomechanics classification for rock engineering and its application in tunnelling. In *Advances in Rock Mechanics*, Nat. Acad. Sci., Washington D.C., **2A**, 27-32.
- Bieniawski, Z. T. (1976). Rock mass classification in rock engineering. In Bieniawski, Z. T. (eds). *Exploration for Rock Engineering, Proc. of the Symposium*, **1**, Cape Town, Balkema, 97-106.
- Bieniawski, Z. T. (1978). Determining rock mass deformability: Experience from cases stories. *Int. J. Rock Mech. Min. Sci. & Geomech. Abstr.*, **15**, 237-247.
- Bieniawski, Z. T. (1979). The geomechanics classification in rock engineering applications. *Proc. 4th Congr. ISRM Montreux*, **2**, 41-48.
- Bieniawski, Z. T. (1984). Rock mechanics design in mining and tunnelling. *Balkema*, 272 pp.
- Bieniawski, Z. T. (1989). Engineering rock mass classifications. A Complete Manual for Engineers and Geologists in Mining, Civil, and Petroleum Engineering. *Wiley & Sons*, New York, 272 pp.
- Billi, A., Salvini, F., Storti, F. (2003). The damage zone-fault core transition in carbonate rocks: implications for fault growth, structure and permeability. *Journal of Structural Geology*, **25**, 1779-1794.
- Billi, A. (2005). Grain size distribution and thickness of breccia and gouge zones from thin (<1 m) strike-slip fault core in limestone. *Journal of Structural Geology* **27**, 1823-1837.
- Billi, A., Storti, F. (2004). Fractal distribution of particle size in carbonate cataclastic rocks from the core of a regional

Bibliography

- strike-slip fault zone. *Tectonophysics* **384**, 115–128.
- Blenkinsop, T.G. (1991). Cataclasis and processes of particle size reduction. *Pure and Applied Geophysics* **136**, 59–86.
- Borja, R.I. (2002). Bifurcation of elastoplastic solids to shear band mode at finite strain. *Computer Methods in Applied Mechanical Engineering*, **191**, 5287– 5314.
- Bucher, K. & Frey, M. (1994). Petrogenesis of metamorphic rocks, 6th Edition. *Springer-Verlag*. 318 pp.
- Bürgi C. (1999). Cataclastic fault rocks in underground excavations: a geological characterisation. *Thèse EPFL GC N° 1975*. 107 pp.
- Bürgi C., Parriaux A., Franciosi G. (2001). Geological characterization of weak cataclastic fault rocks with regards to the assessment of their geomechanical properties. *Quarterly Journal of Engineering Geology and Hydrogeology* **34**, 225-232.
- Calembert, T., Popescu, C., Popescu, M., Schroeder, C. (1980). Relationships between the petrographic and mineralogical properties of soils and rocks and their mechanical properties. *Bulletin Int. Assoc. Eng. Geol.*, **22**, 167-172.
- Carlson W. D. & Denison C. (1992). Mechanisms of porphyroblast crystallization: results from high-resolution computed X-ray tomography. *Sciences* **257**, 1236-1239.
- Chaïgnat, L. (2007). Etude géotechnique de roches cataclisées ou bréchiques dans des ouvrages souterrains basée sur l'interprétation de lames minces et d'images tomographiques à rayons X (XRCT) Caractérisation structurale, implications mécaniques et comparaison des méthodes. *Master ELSTE d'ingénieur géologue. Laboratoire de Géologie de l'ingénieur et de l'environnement de l'EPFL & Département de géologie de l'université de Lausanne*. Unpublished. 145 pp.
- Christe, P. (2004). Évaluation d'une approche pétrographique tridimensionnelle pour la caractérisation géologique et géomécanique des roches cataclastiques. *Thèse de diplôme « Formation postgrade internationale en Géologie de l'Ingénieur et de l'Environnement 2003-04 »*, EPFL, 64 pp, unpublished.
- Christe, P., Bernasconi, M., Vontobel, P., Türberg, P., Parriaux, A. (2007). Three-dimensional petrographical investigations on borehole rock samples: a comparison between X-ray Computed- and Neutron Tomography. *Acta Geotechnica*, **2(4)**, 269-279.
- Conroy G. C. & Vannier M. W. (1984). Noninvasive three-dimensional computer imaging of matrix-filled fossil skulls by high-resolution computed tomography. *Science* **226**, 456-458.
- Dalgıç, S. (2003). Tunnelling in fault zones, Tuzla tunnel, Turkey. *Tunnelling and Underground Space Technology*, **18**, 453-465.
- de Bresser, J. H. P., Peach, C. J., Reijs, J. P. J., Spiers, C. J. (1998). On dynamic recrystallization during solid state flow: effect of stress and temperature. *Geophysical Research Letter*, **25**, 3457-3460.
- de Bresser, J. H. P., Ter Heege, J. H., Spiers, C. J. (2001). Grain size reduction by dynamic recrystallization: can it result in major rheological weakening? *International Journal of Earth Science*, **90**, 28-45.
- Desrues, J., Viggiani, G., Bésuelle, P. (2006). Advances in X-ray tomography for geomaterials. *ISTE*, 452 pp.
- Dube, A. K. & Singh, B. (1972). Effect of Humidity on Tensile Strength of Sandstone. *Journal of Mines Metals and Fuel*, **20** (1), 8-10.
- Duncan, J. M. & Chang, C. Y. (1970). Nonlinear analysis of stress and strain in soils. *J. Soil Mech. Found. Div., Proc. ASCE*, **96**, N° SM5, 1629-1653.
- Ehrbar, H. (2004). Alptransit Gotthard – Sedrun – Vortriebskonzept in druckhaften Zonen – Vom Projekt zur Ausführung, Eurock 2004 & 53rd Geomech. Colloquium, Salzburg.
- Escuder-Virueite, J., Carbonell, R., Pérez-Soba, C., Martí, D., Pérez-Estaún, A. (2004). *Geological, geophysical and geochemical structure of a fault zone developed in granitic rocks : Implications for fault zone modeling in 3D*. *Int J Earth Sci*, **93**, 172-188.
- Evans, B., Kohlstedt, D.L. (1995). Rheology of rocks. In: *Abrens, T.J. (Ed.), Rock Physics and Phase Relations—a Handbook*

Bibliography

of *Physical Constants*, *American Geophysical Union Reference Shelf*, **3**, 148–165.

Fairhurst, C. (1964a). On the validity of the “Brazilian” test for brittle materials. *Int. J. Rock Mech. Mining Sci.*, **1**, 535-546.

Fairhurst, C. (1964b). Laboratory measurements of physical properties of rocks. *Rock Mech. Min. Sc.*, **1** (4), 533-546.

Fellner, D. (2003). Geotechnische Erfahrungen und Herausforderungen im Abschnitt Sedrun des Gotthard-Basistunnels, *Felsbau*, **3**.

Fellner, D. (2005). Engineering decisions based on hazard assessment. In: *Kolymbas, D. & Laudahn, A. (Ed.)*, Rational Tunnelling. 2nd Summerschool, *Innsbruck*, 291 pp.

Gunsallus, K. L., Kulhawy, F. H. (1984). A Comparative Evaluation of Rock Strength Measures. *Int. J. Rock Mech. Min. Sci. & Geomech. Abstr.*, **21**(5), 233-248

Habimana J. (1999). Caractérisation géomécanique de roches cataclastiques rencontrées dans des ouvrages souterrains alpins. *Thèse EPFL GC N° 1945*. 196 pp.

Habimana J., Labieuse V., Descoedres F. (2002). Geomechanical characterisation of cataclastic rocks: experience from the Cleuson-Dixence project. *International Journal of Rock Mechanics & Mining Sciences* **39**, 677-693.

Hadizadeh, J. & Johnson, W. K. (2003). Estimating local strain due to comminution in experimental cataclastic textures. *Journal of Structural Geology*, **25**, 1973-1979.

Hadizadeh, B. & Rutter, E.H. (1983). The low temperature brittle-ductile transition in quartzite and the occurrence of cataclastic flow in nature, *Geologische Rundschau*, **72**, 493–509.

Hayman, N. W. (2006). Shallow crustal fault rocks from the Black Mountain detachments, Death Valley, CA. *Journal of Structural Geology*, **28**, 1767-1784.

Heilbronner, R. (2000). Automatic grain boundary detection and grain size analysis using polarization micrographs or orientation images. *Journal of Structural Geology*, **22**, 969-981.

Heilbronner, R. & Keulen, N. (2006). Grain size and grain shape analysis of fault rocks. *Tectonophysics*, **427**, 199-216.

Heitzmann, P. (1985). Kakirite, Kataklasite, Mylonite – Zur Nomenklatur der Metamorphite mit Verformungsgefügen. *Eclogae Geologicae Helvetiae*, **78**(2), 273-286.

Higgins, M. W. (1971). Cataclastic rocks. *U. S. Geol. Survey Prof. Paper*, **687**.

Hirono, T. (2005). The role of dewatering in the progressive deformation of a sandy accretionary wedge: constraints from direct imagings of fluid flow and void structure. *Tectonophysics*, **397**, 261-280.

Hoek, E. (1994). Strength of Rock and Rock Masses. In Hoek, E., Kaiser, P. K. & Bawden, W. F. (Eds). *Support of Underground Excavations in Hard Rock*, Balkema, Rotterdam, 300 pp.

Hoek, E. & Brown, E. T. (1997). Practical Estimates of Rock Mass Strength. *Int. J. Rock Mech. Min. Sci.*, **34**, 1165-1186.

Hoek, E. & Marinos, P. (2006). A brief history of the development of the Hoek-Brown failure criterion. *RocLab's software documentation*. 1-8

Hoek, E., Marinos, P., Bennis, M. (1998). Applicability of the geological strength index (GSI) classification for very weak and sheared rock masses. The case of the Athens Schist Formation. *Bull. Eng. Geol. Env.*, **57**, 151-160.

Hoek, E., Marinos, P. G., Marinos, V. P. (2005). Characterisation and engineering properties of tectonically undisturbed but lithologically varied sedimentary rock masses. *International Journal of Rock Mechanics & Mining Sciences*, **42**, 277-285.

Holler, P. & Kögler, F.-C. (1990). Computer Tomography: a non-destructive, high-resolution technique for investigation of sedimentary structures. *Marine Geology*, **91**, 263-266.

- Homberg, C., Angelier, J., Bergerat, F., Lacombe, O. (2004). Using stress deflections to identify slip events in fault systems. *Earth and Planetary Science Letters*, **217**, 409-424.
- Hounsfield G. N. (1972). A method of and apparatus for examination of a body by radiation such as X- or Gamma-radiation, *London, British Patent No. 1,283,915*.
- Howarth, D. F. & Rowlands, J. C. (1986). Development of an index to quantify rock texture for qualitative assessment of intact rock properties. *Geotechnical Testing Journal*, **20**, 57-85.
- Hubbell, J. H., Veigle, W. J., Briggs, E. A., Brown, R.T., Cromer, D. T., & Howerton, R. J. (1975). *Atomic Form Factors, Incoherent Scattering Functions, and Photon Scattering Cross Sections*, *J. Phys. Chem. Ref. Data* **4**, 471-538.
- Ismat, Z., Mitra, G. (2001). Folding by cataclastic flow at shallow crustal levels in the Canyon Range, Sevier orogenic belt, west-central Utah. *Journal of Structural Geology*, **23**, 355–378.
- Ismat, Z., Mitra, G. (2005). Folding by cataclastic flow: evolution of controlling factors during deformation. *Journal of Structural Geology*, **27**, 2181–2203.
- Jain, A. K. (1989). Fundamentals of digital image processing. *Prentice Hall*, 592 pp.
- Jeng, F. S., Weng, M. C., Lin, M. L., Huang, T. H. (2004). Influence of petrographic parameters on geotechnical properties of tertiary sandstones from Taiwan. *Engineering Geology*, **73**, 71-91.
- Kaiser (2006). In Löw, S. (ed.): *Geologie und Geotechnik der Basistunnels am Gotthard und am Lötschberg. Tagungsband zum Symposium Geologie AlpTransit*, Zürich 26.-28. September 2005, 311 pp.
- Kavvas, M. (1996). Discussion: Tunnelling in weathered rock - Rock or soil mechanics approaches? In Mair & Taylor (eds). Balkema, Rotterdam.
- Ketcham R. A. & Carlson W. D. (2001). Acquisition, optimization and interpretation of X-ray computed tomographic imagery: applications to the geosciences. *Computers & Geosciences* **27**, 381-400.
- Ketcham, R. A. (2005). Three-dimensional grain fabric measurements using high-resolution X-ray computed tomography. *Journal of Structural Geology*, **27**, 1217-1228.
- Knipe, R. J. (1989). Deformation mechanisms – recognition from natural tectonites. *Journal of Structural Geology*, **11** (1/2), 127-146.
- Kolymbas, D. & Laudahn, A. (2005), Rational Tunnelling. 2nd Summerschool, *Innsbruck*, 291 pp.
- Kovári, K. (2003). History of the sprayed concrete lining method-part II: milestones up to the 1960s. *Tunnelling and Underground Space Technology*, **18**, 71-83.
- Kulhawy, F. H. (1975). Stress deformation properties of rock discontinuities. *Eng. Geol.* **9**, 327-350.
- Landis, E. N. (2006). X-ray Tomography as a Tool for Micromechanical Investigations of Cement and Mortar. In Desrues, J., Viggiani, G. & Bésuelle, P. (eds) 2006. *Advances in X-ray tomography for Geomaterials*, ISTE, 452 pp.
- Laubscher, H.P. (1979). Elements of Jura kinematics and dynamics. *Eclogae Geologicae Helvetiae*, **72**, 467–483.
- Laws, S. (2001): Structural, geomechanical and petrophysical properties of shear zones in the eastern Aar massif, Switzerland. ETHZ Thesis.
- Lee, H.-K., Kim, H. S. (2005). Comparison of structural features of the fault zone developed at different protoliths: crystalline rocks and mudrocks. *Journal of Structural Geology*, **27**, 2099–2112.
- Lehmann E. H., Pleinert H, Wiezel L. (1996). Design of a neutron radiography facility at the spallation source SINQ. *Nuclear Instruments and Methods* **A 377**, 11-15.

Bibliography

- Lehmann E. H., Vontobel P., Wiezel L. (1999). Properties of the Radiography Facility NEUTRA at SINQ and Its Potential for Use as a European Reference Facility. *Proceedings of the 6th World Conference on Neutron Radiography, Osaka, 1999*. 151-158.
- Lombardi (2006). In Löw, S. (ed.): *Geologie und Geotechnik der Basistunnels am Gotthard und am Lötschberg. Tagungsband zum Symposium Geologie AlpTransit*, Zürich 26.-28. September 2005, 311 pp.
- Lützenkirchen, V.H. (2002): Structural Geology and hydrogeology of brittle fault zones in the central and eastern Gotthard massif, Switzerland. ETHZ Thesis.
- Manaker, D. M., Turcotte, D. L. & Kellogg, L. H. (2006). Flexure with damage. *Geophys. J. Int.*, **166**, 1368–1383.
- Mancktelow, N. (1985). The Simplon line: a major displacement zone in the western Lepontine Alps. *Eclogae Geologicae Helvetiae*, **78**, 73-96.
- Marinos, P. & Hoek, E. (2001). Estimating the geotechnical properties of heterogeneous rock masses such as flysch. *Bull Eng Geol Env*, **60**, 85-92.
- Marinos, P., Hoek, E., Marinos, V. (2006). Variability of the engineering properties of rock masses quantified by the geological strength index: the case of ophiolites with special emphasis on tunneling. *Bull Eng Geol Env*, **65**, 129–142.
- Marinos, V., Marinos, P., Hoek, E. (2005). The geological strength index: applications and limitations. *Bull Eng Geol Environ*, **64**, 55–65
- Micarelli, L., Benedicto, A., Wibberley, C. A. J. (2006). Structural evolution and permeability of normal fault zones in highly porous carbonate rocks. *Journal of Structural Geology*, **28**, 1214-1227.
- Mosar, J., Stampfli, G. S., Girod, F. (1996). Western Préalpes Médiannes Romandes: timing and structure. A review. *Eclogae Geologicae Helvetiae*, **89** (1), 389-425.
- Muzi, L., Lyons, A. P., Pouliquen, E. (2004). Use of X-ray computed tomography for the estimation of parameters relevant to the modeling of acoustic scattering from the seafloor. *Nuclear Instruments and Methods in Physics Research*, **B 213**, 491-497.
- Nakashima Y. (2000). The use of X-ray CT to measure diffusion coefficients of heavy ions in water-saturated porous media. *Engineering Geology*, **56**, 11-17.
- Neubauer, F. (2005). Fault zone properties and fault classification: the role of fault history. *Geophysical Research Abstracts*, **7**, 02393.
- Nishikawa, O., Saiki, K., Wenk, H.-R. (2004). Intra-granular strains and grain boundary morphologies of dynamically recrystallized quartz aggregates in a mylonite. *Journal of Structural Geology*, **26**, 127-141.
- Olsen, P. A. & Børresen, T. (1997). Measuring differences in soil properties in soils with different cultivation practices using computer tomography. *Soil & Tillage Research*, **44**, 1-12.
- Palmstrom, A., Milne, D., Peck, M. (2001). The reliability of rock mass classification used in underground excavation and support design. *Int. Soc. Rock Mech. News*, **6(3)**, 40-41.
- Pandita, S. D. & Verpoest, I. (2003). Prediction of tensile stiffness of weft knitted fabric composites based on X-ray tomography images. *Composites Science and Technology*, **63**, 311-325.
- Passchier, C. W. & Trouw, R. A. J. (1996). *Microtectonics*. Springer Verlag, Berlin, Heidelberg. 289 pp.
- Paterson, M. S. (1978). Experimental rock deformation. The brittle field. *Minerals and Rocks*., Springer Verlag, Berlin, P. J. Wyllie ed., **Vol. 13**.
- Re, S. & Scavia, C. (1999). Determination of contact areas in rock joints by X-ray computer tomography. *International Journal of Rock Mechanics and Mining Sciences*, **36**, 883-890.
- Roscoe, K.H., Schofield, A.N., Thurairajah, A. (1963). Yielding of clays in states wetter than critical. *Géotechnique* **13**,

Bibliography

211-240.

Roscoe, K.H., Schofield, A.N., Wroth, C.P. (1958). On the yielding of soils. *Géotechnique* **8**, 22–53.

Rudnicki, J.W (2000). Geomechanics. *International Journal of Solids and Structures*, **37**, 349-358.

Russo, G. (1994). Some considerations on the applicability of major geomechanical classifications to weak and complex rocks in tunnelling. *Bollettino Assoc. Mineraria Subalpina, Anno XXIX*, **4**, 63-70.

Sandrone, F. (2008). Analysis of pathologies and long term behaviour of the swiss national road tunnels. *Thèse EPFL N° 4019*. 238 pp.

Schmid, S. M. (1982). Microfabric studies as indicators of deformation mechanisms and flow laws operative in mountain building. In K. J. Hsü ed., *Mountain Building Processes*, Academic Press, New York, 95-110.

Schmid, S. M. & Handy, M. R. (1991). Towards a genetic classification of fault rocks: geological usage and tectonophysical implications. In D. W. Müller et al. (eds) 1991. *Controversies in modern geology*. Academic Press Limited, London, 339-361.

Schreurs, G., Hänni, R., Panien, M., Vock, P. (2003). Analysis of analogue models by helical X-ray computed tomography. In Mees, F., Swennen, R., Van Geet, M. & Jacobs, P. (eds) 2003. *Applications of X-ray Computed Tomography in the Geosciences*. Geological Society, London, Special Publications, **215**, 213-223.

Schubert (2006). In Löw, S. (ed.): *Geologie und Geotechnik der Basistunnels am Gotthard und am Lötschberg. Tagungsband zum Symposium Geologie AlpTransit*, Zürich 26.-28. September 2005, 311 pp.

Schultz, R. A., Siddharthan, R. (2005). A general framework for the occurrence and faulting of deformation bands in porous granular rocks. *Tectonophysics*, **411**, 1 –18

Schwarz D., Vontobel P., Lehmann E. H., Meyer C. A., Bongartz G. (2005). Neutron Tomography of internal structures of vertebrate remains: a comparison with X-ray Computed Tomography. *Palaeontologia Electronica* Vol.8, **2A**, 10p.

Séné, Aliou (2007): Corrélations multiples entre les propriétés géologiques et géomécaniques des roches cataclisées à faciès gréseux. *Master ELSTE d'ingénieur géologue. Laboratoire de Géologie de l'ingénieur et de l'environnement de l'EPFL & Département de géologie de l'université de Genève*. Unpublished. 89 pp.

Sibson, R. H. (1977). Fault rocks and fault mechanisms. *Journal geol. Soc. London*, **133**, 191-213.

Singh, B., Goel, R. K. (2006). Tunnelling in weak rocks. *Elsevier Geo-Engineering Book Series*, John A. Hudson ed., **5**, 489 pp.

Stipp, M., Stünitz, H., Heilbronner, R., Schmid, S. (2002). The eastern Tonale fault zone: a 'natural laboratory' for crystal plastic deformation of quartz over a temperature range from 250 to 700°C. *Journal of Structural Geology*, **24**, 1861-1884.

Storti, F., Billi, A., Salvini, F. (2003). Particle size distributions in natural carbonate fault rocks: insights for non-self similar cataclasis. *Earth and Planetary Science Letters* **206**, 173–186.

Thomas, G. & Govindan, V. K. (2006). Computationally efficient filtered-backprojection algorithm for tomographic image reconstruction using Walsh transform. *Journal of Visual Communication & Image Representation*, **17**, 581-588.

Tourenq, C. (1966). La dureté Vickers des minéraux et des roches, quelques applications. *Bulletin Liaison Lab. Ponts et Chaussées*, **19**, 1-12.

Twiss, R. J. & Moores, E. M. (1992). *Structural Geology*. W. H. Freeman and Company, New York, 532 pp.

Van Geet, M., Swennen, R., Wevers, M. (2000). Quantitative analysis of reservoir rocks by microfocus X-ray computerised tomography. *Sedimentary Geology*, **132**, 25-36.

Van Geet, M., Swennen, R., Wevers, M. (2001). Towards 3-D petrography: application of microfocus computer tomography in geological science. *Computers & Geosciences*, **27**, 1091-1099.

- Verhelst, F., David, P., Fermont, W., Jegers, L., Vervoort, A. (1996). Correlation of 3D-computerized tomographic scans and 2D-colour image analysis of Westphalian coal by means of multivariate statistics. *International Journal of Coal Geology*, **29**, 1-21.
- Veuve, C. (2007). Caractérisation minéralogique de roches cataclastiques de différents contenus pétrologiques. *Thèse Master ELSTE d'ingénieur géologue. Laboratoire de Géologie de l'ingénieur et de l'environnement de l'EPFL & Département de géologie de l'université de Lausanne*. Unpublished. 165 pp.
- Viggiani, G., Lenoir, N., Bésuelle, P., Di Michiel, M., Marelli, S., Desrues, J., Kretschmer, M. (2004). X-ray microtomography for studying localized deformation in fine-grained geomaterials under triaxial compression. *C. R. Mécanique*, **332**, 819-826.
- Vinegar, H. J., de Waal, J. A., Wellington, S. L. (1991). CT studies of brittle failure in Castlegate sandstone. *International Journal of Rock Mechanics and Mining Sciences*, **28**, 441-448.
- Wellington S. L. & Vinegar H. J. (1987). X-ray computerized tomography. *Journal of Petroleum Technology* **39**, 885-898.
- Wenk, H. R. & Bulakh, A. (2004). Minerals: Their Constitution and Origin. *Cambridge: Cambridge University press*. 646 pp.
- Wheeler, J., Jiang, Z., Prior, D. J., Tullis, J., Drury, M. R., Trimby, P. W. (2003). From geometry to dynamics of microstructure: using boundary lengths to quantify boundary misorientations and anisotropy. *Tectonophysics*, **376**, 19-35.
- Wise, D. U., Dunn, D. E., Engelder, J. T., Geiser, P. A., Hatcher, R. D., Kish, S. A., Odom, A. L., Schamel, S. (1984). Fault-related rocks: suggestions for terminology. *Geology*, **12**, 391-394.
- Wyder, R. F. & Mullis, J. (1998). Fluid impregnation and development of fault breccia in the Tavetsch basement rocks/Sedrun, Central Swiss Alps. *Tectonophysics*, **294 (1/2)**, 89-107.

CURRICULUM VITAE

PERSONAL DATA

Surname, Name: Christe Pierre Guillaume
Birthday: June 7th 1978, in Porrentruy (JU)
Nationality: Swiss
Address: Route du Signal 17, 1018 Lausanne
Languages: French, German, Swiss German, English
basics in Spanish & Italian
E-mail: pierre@altitude.ch
Phone number: +41-79-201 86 41

EDUCATION

2004-present PhD candidate at GEOLEP & LMR of EPFL, Switzerland.
2003-2004 International Postgraduate Course in Engineering and Environmental Geology (partnership EPFL Lausanne, ENSMP Paris, ULG Lièges & PolyMtl Montréal).
1996-2002 Study and Master degree in Earth Sciences at the Department Erdwissenschaften of the University of Basel, Switzerland. Specialisation in Volcanology & Magmatic Petrology
1993-1996 Federal maturity type B (latin-english), Lycée Cantonal de Porrentruy (JU)
1982-1993 Obligatory school in Rossemaison and Delémont (JU)

PROFESSIONAL EXPERIENCE

2006-present Committee member of the Swiss Association of Professional Geologists (CHGEOLOG), swiss delegate for the European Federation of Geologists (EFG)
January-August 2003 Assistant work at GEOLEP, EPFL.
Summer 1999 & 2001 Geological fieldwork in south-western Colorado, San Juan Volcanic Field, USA (collaboration with Dr P. W. Lipman, US Geological Survey).
Summer 1998 Paleontological fieldwork in Esperaza, Aude, France (under supervision of the Musée des Dinosauriens, Esperaza and CNRS, Paris).

PROFESSIONAL INTERESTS

Natural hazards, risk assessment, complexity of natural systems. Relationship between the fundamental and applied researches and its implication for society, environment and economy.

APPENDIX I-I

(Appendix related to Chap. 3)
after *AFTES*, 2003

Q-ROCK MASS CLASSIFICATION SYSTEM *(Barton et al., 1974)*

INDICE Q DE BARTON

RQD (Rock Quality Designation)

| | |
|--|---------------|
| Très médiocre | RQD = 0 – 25% |
| Médiocre | 25-50 |
| Moyen | 50-75 |
| Bon | 75-90 |
| Excellent | 90-100 |
| Notes : | |
| (i) Quand la valeur du RQD est < 10 (y compris 0), on utilise une valeur nominale de 10 pour évaluer Q | |
| (ii) Les intervalles RQD de 5, i.e. 100, 95, 90, etc ... sont suffisamment précis | |

Jn (indice des familles de joints)

| | |
|--|--------------|
| Rocher massif, joints rares ou absents | Jn = 0.5 - 1 |
| Une famille de joints | 2 |
| Une famille + joints erratiques | 3 |
| Deux familles | 4 |
| Deux familles + joints erratiques | 6 |
| Trois familles | 9 |
| Trois familles + joints erratiques | 12 |
| Quatre familles ou plus, joints erratiques, | 15 |
| Rocher broyé, meuble | 20 |
| Notes : (i) pour les intersections de tunnel, utiliser (3.0xJn), (ii) pour les têtes d'accès, utiliser (2.0xJn) | |

Jr (Indice de rugosité des joints)

| | | | |
|--|--------|--|----------|
| a) Epontes en contact | | c) Epontes hors contact après cisaillement | |
| b) Epontes en contact après cisaillement de - de 10 cm | | | |
| Joint discontinu | Jr = 4 | Zone argileuse d'épaisseur suffisante pour empêcher le contact | Jr = 1.0 |
| Joint ondulés, rugueux ou irréguliers | 3 | Zone sableuse, graveleuse ou broyée d'épaisseur suffisante pour empêcher le contact | |
| Joint ondulés, lisses | 2 | | |
| Joint ondulés, striés (lisses, luisants, polis) | 1.5 | | |
| Joint plans, rugueux ou irréguliers | 1.5 | | |
| Joint plans, lisses | 1.0 | | |
| Joint plans, striés | 0.5 | | |
| Note : (i) les descriptions se réfèrent à des éléments de petites ou moyennes dimensions, dans cet ordre. | | Notes : (i) ajouter 1.0 si l'espacement moyen des joints est supérieur à 3 m. (ii) Jr=0,5 si les joints plans et striés comportent des linéations et que celles-ci sont orientées de telle sorte qu'elles peuvent amorcer une rupture. | |

Ja (Indice d'altération des joints)

| Epontes en contact | Caractère du joint | | Conditions | Eponte |
|----------------------------|-------------------------------------|---|---|--|
| | Joint propres | Joint serré, recimenté | Remplissage de quartz, épidote, etc | Ja = 0.75 |
| | | Epontes non altérées | Pas d'enduit, taches superficielles | 1 |
| | | Epontes légèrement altérées | Enduit minéral non radoucissant, grains sans argile | 2 |
| | Enduits ou remplissage | Enduits à frottement | Sable, silt, calcite, etc (non radoucissant) | 3 |
| | | Enduits à cohésion | Argile, chlorite, talc, etc (radoucissant) | 4 |
| Epontes en ou hors contact | Remplissage | Type | Epontes à contacts Remplissage léger (< 5 mm) | Epontes hors contact Remplissage épais |
| | Matériaux frottant | Sable, silt, calcite, etc | Ja = 4 | Ja = 8 |
| | Remplissage fortement surconsolidé | Remplissage compact d'argile, chlorite, talc, etc | 6 | 5 - 10 |
| | Remplissage légèrement surconsolidé | Surconsolidation légère ou moyenne d'argile, de chlorite, talc, etc | 8 | 12 |
| | Remplissage d'argiles gonflantes | Matériaux gonflants (ex montmorillonite) | 8 - 12 | 13 - 20 |

Jw (Influence de l'eau en charge)

| | | |
|---|---------------------------|------------|
| Excavation à sec ou faibles venues d'eau (< 5 l/mn localement) | $P_w < 1 \text{ kg/cm}^2$ | $J_w = 1$ |
| Venues d'eau ou pressions faibles, débouillage occasionnel au droit d'un joint | 1 – 2.5 | 0.66 |
| Fortes venues d'eau ou pression importante dans du rocher à joint sans remplissage | 2.5 – 10 | 0.5 |
| Fortes venues d'eau ou pression importante, débouillages fréquents | 2.5 – 10 | 0.3 |
| Très fortes venues d'eau lors des tirs, diminuant ensuite avec le temps | > 10 | 0.2 – 0.1 |
| Très fortes venues d'eau ou pressions très importantes sans réduction notable avec le temps | > 10 | 0.1 – 0.05 |

Notes : (i) les 4 derniers indices sont des estimations grossières. Augmenter la valeur de J_w en cas de mise en place d'un dispositif de drainage.
(ii) les problèmes particuliers liés à la formation de glace ne sont pas pris en compte.

SRF (Stress Reduction Factor)

| | | | | |
|--|---|--|--|-----------|
| Ouvrage recoupant des zones de faiblesse provoquant la décompression du rocher lors du percement | Zones de faiblesse fréquentes, contenant de l'argile ou du rocher décomposé chimiquement, rocher environnant très décomprimé (toutes profondeurs) | | | SRFR = 10 |
| | Zones de faiblesse individuelles, contenant de l'argile ou du rocher décomposé chimiquement (prof. de l'excavation < 50 m) | | | 5 |
| | Zones de faiblesse individuelles, contenant de l'argile ou du rocher décomposé chimiquement (prof. de l'excavation > 50 m) | | | 2.5 |
| | Nombreuses zones de cisaillement en rocher sain, sans argile (toutes profondeurs) | | | 7.5 |
| | Zones de cisaillement individuelles en rocher sain, sans argile (prof. de l'excavation < 50 m) | | | 5 |
| | Zones de cisaillement individuelles en rocher rigide, sans argile (prof. de l'excavation > 50 m) | | | 2.5 |
| | Joints ouverts, rocher très fracturé et décomprimé, " morceaux de sucre ", etc ... (toutes profondeurs) | | | 5 |

Note : (i) réduire l'indice SRF de 25 à 50% si les zones de cisaillement influent sur l'excavation mais ne la traversent pas.

| | | S_c / σ_1 | σ_q / σ_c | SRF |
|--|--|------------------|-----------------------|-----------|
| Rocher sain, problèmes de contraintes in situ | Contraintes faibles, excavation peu profonde | > 200 | < 0.01 | 2.5 |
| | Contraintes moyennes | 200 - 10 | 0.01 – 0.3 | 1 |
| | Contraintes importante, structure très serrée (condition normalement favorable à la stabilité mais peut être défavorable à la tenue des piedroits) | 10 - 5 | 0.3 – 0.4 | 0.5 – 2 |
| | Mouvements de toit modérés (rocher massif) | 5 - 3 | 0.5 – 0.65 | 5 – 50 |
| | Quelques " chutes de toit " (rocher massif) | 3 - 2 | 0.65 - 1 | 50 - 200 |
| | " Chutes de toit " importantes (rocher massif) | < 2 | > 1 | 200 - 400 |

Notes : (ii) Si l'état de contraintes initiales est fortement anisotrope (si mesuré) : pour $5 < \sigma_1/\sigma_3 < 10$, réduire σ_c à 0.75 σ_c . Pour $\sigma_1/\sigma_3 > 10$, réduire σ_c à 0.5 σ_c .
(iii) il est rare que la hauteur de couverture au-dessus du toit soit plus faible que la largeur de l'ouvrage. Si c'est le cas, il est suggéré de porter l'indice SRF de 2.5 à 5.

| | | | σ_θ / σ_c | SRF |
|----------------------------|--|------------------|----------------------------|---------|
| Rocher " poussant " | Déformation plastique du rocher sous l'action de fortes contraintes naturelles | Moyenne pression | 1 - 5 | 5 – 10 |
| | | Forte pression | > 5 | 10 – 20 |
| Rocher " gonflant " | Action chimique en fonction de la présence d'eau | Moyenne pression | | 5 – 10 |
| | | Forte pression | | 10 - 15 |

APPENDIX I-II

(Appendix related to Chap. 3)
after *AFTES*, 2003

RMR-CLASSIFICATION SYSTEM *(Bieniawski, 1989)*

CLASSIFICATION RMR DES MASSIFS ROCHEUX DE Z. T. BIENIAWSKI

| A. PARAMETRES DE CLASSIFICATION ET NOTATIONS CORRESPONDANTES | | Plages de valeurs | | | |
|---|---|------------------------------|----------------------------------|-------------------------------|------------------------------|
| Paramètres | | 4 - 10 MPa | 2 - 4 MPa | 1 - 2 MPa | 5 - 25 MPa MPa |
| 1 | Résistance de la roche (matrice) Indice Franklin I_s Résist. compr. uniax. σ_c | > 10 MPa | 2 - 4 MPa | 1 - 2 MPa | 5 - 25 MPa MPa |
| 2 | Notation | 15 | 7 | 4 | 0 |
| 3 | ROB | 90% - 100% | 50% - 75% | 25% - 50% | < 25% |
| 4 | Espacement des discontinuités | 20 | 13 | 8 | 3 |
| 5 | Nature des discontinuités (voir E) | 20 | 10 | 8 | 5 |
| 6 | Notation | 30 | 20 | 10 | 0 |
| 7 | Débit sur 10 m de longueur de tunnel (l/min) | Aucun | 10 à 25 l/min | 25 à 125 l/min | > 125 l/min |
| 8 | Ratio : pression eau / contr. princ. σ_1 | 0 | 0,1 - 0,2 | 0,2 - 0,5 | > 0,5 |
| 9 | Conditions générales | Complètement sec | Humide | Mouillé | Suissant |
| 10 | Notation | 15 | 10 | 7 | 4 |
| RMR = Somme des notations des paramètres 1 à 5 | | | | | |
| B. AJUSTEMENT DE LA VALEUR DE RMR EN FONCTION DE L'ORIENTATION DES DISCONTINUITES (voir F) | | | | | |
| Direction et pendage | Très favorable | Favorable | Moyen | Défavorable | Très défavorable |
| Notation | 0 | -2 | -5 | -10 | -12 |
| | 0 | -2 | -7 | -15 | -25 |
| | 0 | -5 | -25 | -50 | -60 |
| C. CLASSES DE MASSIF ROCHEUX DETERMINEES PAR LE RMR | | | | | |
| Valeur du RMR | 100 ← 81 | 80 ← 61 | 60 ← 41 | 40 ← 21 | < 21 |
| Classe | I | II | III | IV | V |
| Description | Très bon rocher | Bon rocher | Rocher moyen | Rocher médiocre | Rocher très médiocre |
| D. PROPRIETES GLOBALES ATTRIBUEES AU MASSIF ROCHEUX EN FONCTION DES CLASSES | | | | | |
| Classe | I | II | III | IV | V |
| Temps de tenue sans soutènement | 20 ans pour une portée de 15 m | 1 an pour une portée de 10 m | 1 semaine pour une portée de 5 m | 10 h pour une portée de 2,5 m | 30 mn pour une portée de 1 m |
| Cohésion du massif rocheux (kPa) | > 400 kPa | 300 à 400 kPa | 200 à 300 kPa | 100 à 200 kPa | < 100 kPa |
| Angle de frottement du massif rocheux (°) | > 45° | 35° à 45° | 25° à 35° | 15° à 25° | < 15° |

| E. INDICATIONS POUR LA NOTATION "NATURE DES DISCONTINUITES" | | | | | |
|--|---------------|------------------------|------------------------|------------------------|------------------------|
| Longueur des discontinuités | < 1 m | de 1 à 3 m | de 3 à 10 m | de 10 à 20 m | > 20 m |
| Notation | 6 | 4 | 2 | 1 | 0 |
| Ouverture des discontinuités | aucune | < 0,1 mm | de 0,1 à 1 mm | de 1 à 5 mm | > 5 mm |
| Notation | 6 | 5 | 4 | 1 | 0 |
| Rugosité des épontes des discontinuités | Très rugueuse | Rugueuse | Légèrement rugueuse | Lisse | Lustrée |
| Notation | 6 | 5 | 3 | 1 | 0 |
| Altération des épontes | Non altéré | Légèrement altéré | Moyennement altéré | Très altéré | Décomposé |
| Notation | 6 | 5 | 3 | 1 | 0 |
| Matériau de remplissage des discontinuités | Aucun | Remplissage dur < 5 mm | Remplissage dur > 5 mm | Remplissage mou < 5 mm | Remplissage mou > 5 mm |
| Notation | 6 | 4 | 2 | 2 | 0 |

Nota : Certaines conditions sont mutuellement exclusives. Par exemple, si du matériau de remplissage est présent, il n'est plus pertinent de considérer la rugosité dans la mesure où son effet sera effacé par celui du remplissage. Dans ce cas utiliser directement la notation du tableau A 4.

| F. INFLUENCE DE L'ORIENTATION ET DU PENDAGE DES DISCONTINUITES POUR LA STABILITE DES TUNNELS | |
|---|--|
| Horizontale du plan de discontinuité perpendiculaire à l'axe longitudinal du tunnel (creusement en travers bancs) | |
| Pendage 45° à 90° : très favorable | Pendage 20° à 45° : favorable |
| Creusement dans le sens du pendage | |
| Pendage 45° à 90° : moyen | Pendage 20° à 45° : défavorable |
| Creusement contre le sens du pendage | |
| Pendage 0° à 20° et orientation quelconque : moyen | |

APPENDIX I-III

(Appendix related to Chap. 3)

GSI-ROCK MASS CLASSIFICATION SYSTEM

(Hoek & Brown , 1997; Hoek et al., 1998; Marinos & Hoek, 2001; Hoek et al., 2005; Marinos et al., 2006)

The significant contribution of *Hoek & Brown* (1997) was to link the equation of the rock rupture criterion to geological observations. It was recognized very early in the development of the criterion that it would have no practical value unless the parameters could be estimated from simple geological observations in the field. By 1995 it had become increasingly obvious that Bieniawski's RMR is difficult to apply to very poor quality rock masses and it was felt that a system based more heavily on fundamental geological observations and less on 'numbers' was needed. This resulted in the development of the *Geological Strength Index*: GSI which continues to evolve as the principal vehicle for geological data input for the Hoek-Brown criterion (*Hoek & Marinos*, 2006).

The rock mass classification scheme envisaged by *Hoek & Brown* (1997) corresponds to a global approach in the sense that the rock mass is qualified as a whole with regard to its geomechanical behavior and tunnel support requirements. The criterion starts from the properties of intact rock and then introduced factors to reduce these properties on the basis of the characteristics of joints in a rock mass (e.g. this idea motivates the introduction in this study of specific *strength reduction criteria* for cataclastic rocks based on textural and micro-structural considerations). Accordingly, *undisturbed* and *disturbed* rock masses are defined and it is left to the user to decide which GSI value best described the various rock types exposed on a site.

Over the years, it has been decided that it would be profitable to allow the user to decide what sort of disturbance is involved and to allow users to make their own judgement on how much to reduce the GSI value to account for the strength loss (*Hoek & Marinos*, 2006). Therefore, different versions of GSI charts for a wide range of characteristic rock masses in different geological settings have been proposed. They are presented in this Appendix.

Basic idea of the GSI is to consider a (subjective) general rock impression that is function of the acquired experience in tunneling and which is defining the classes of the GSI system. It performs an estimation of the resistance of the deformability of fractured rock mass based on the:

- Uniaxial compression strength of the intact rock mass (« block » properties);
- Value for the constant m_i of the Hoek & Brown criterion for intact rock determined on the base of triaxial results;
- Value of the GSI determined at the outcrop.

Putting these parameters together one can determine the parameters a , m_b and s that will be needed to define a rupture criterion for the fractured rock mass. Practical use of the scheme by Hoek & Brown allows performing a good estimation for rock mass having $GSI > 25$ (*the value of 25 referring to the uniaxial compressive strength = 25 MPa*). When however GSI falls under the value of 25 (mostly the case for weak rocks), this scheme fails to characterize properly the rock mass.

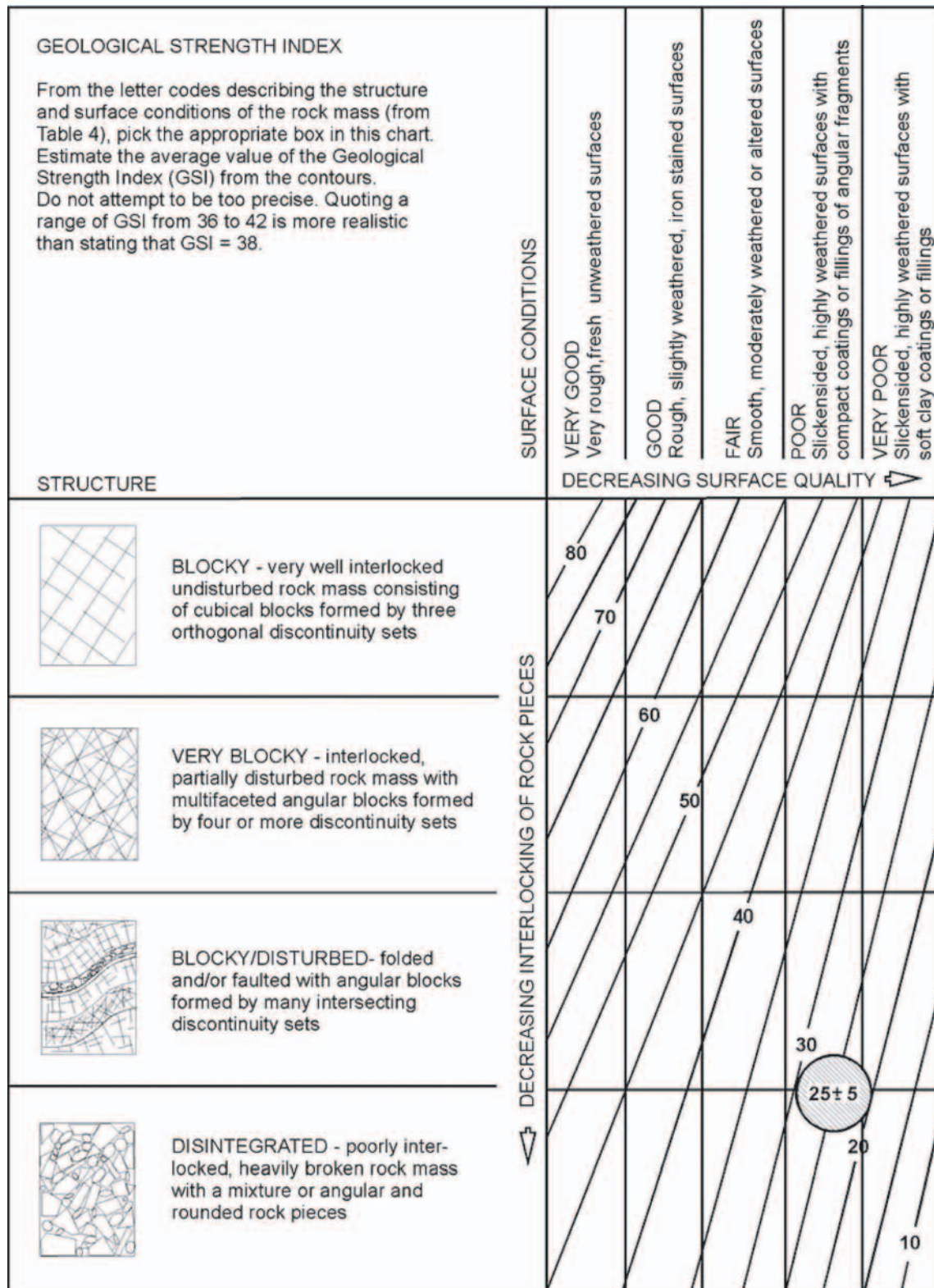
As stated in *Marinos et al.* (2005), the GSI has considerable potential for use in rock engineering because it permits the manifold aspects of rock to be quantified thereby enhancing geological logic and reducing engineering uncertainty.

Appendix I-III

Original GSI chart 1997

(Hoek & Brown)

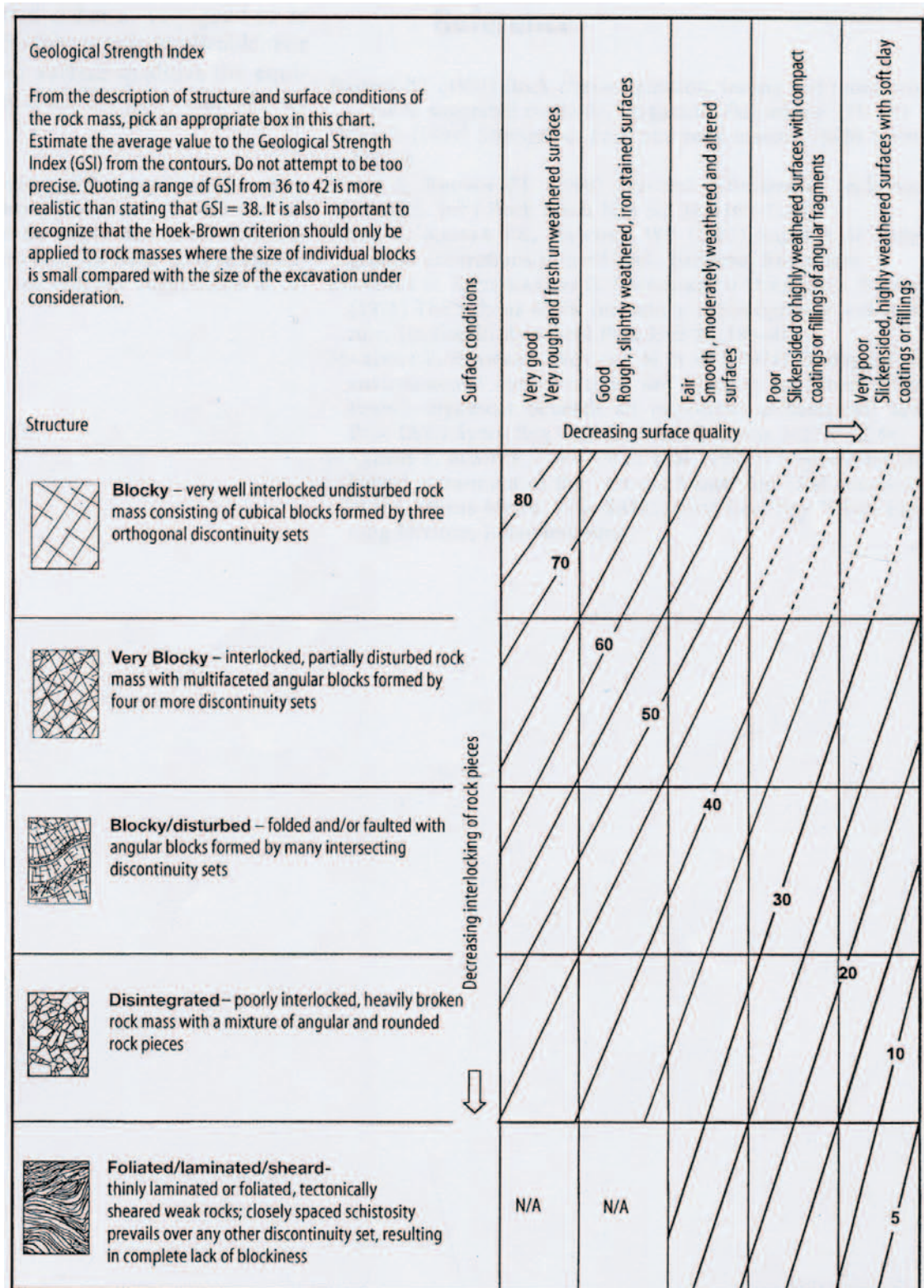
Note threshold value of 25 for index applicability.



GSI chart 1998

(Hoek, Marinos & Benissi)

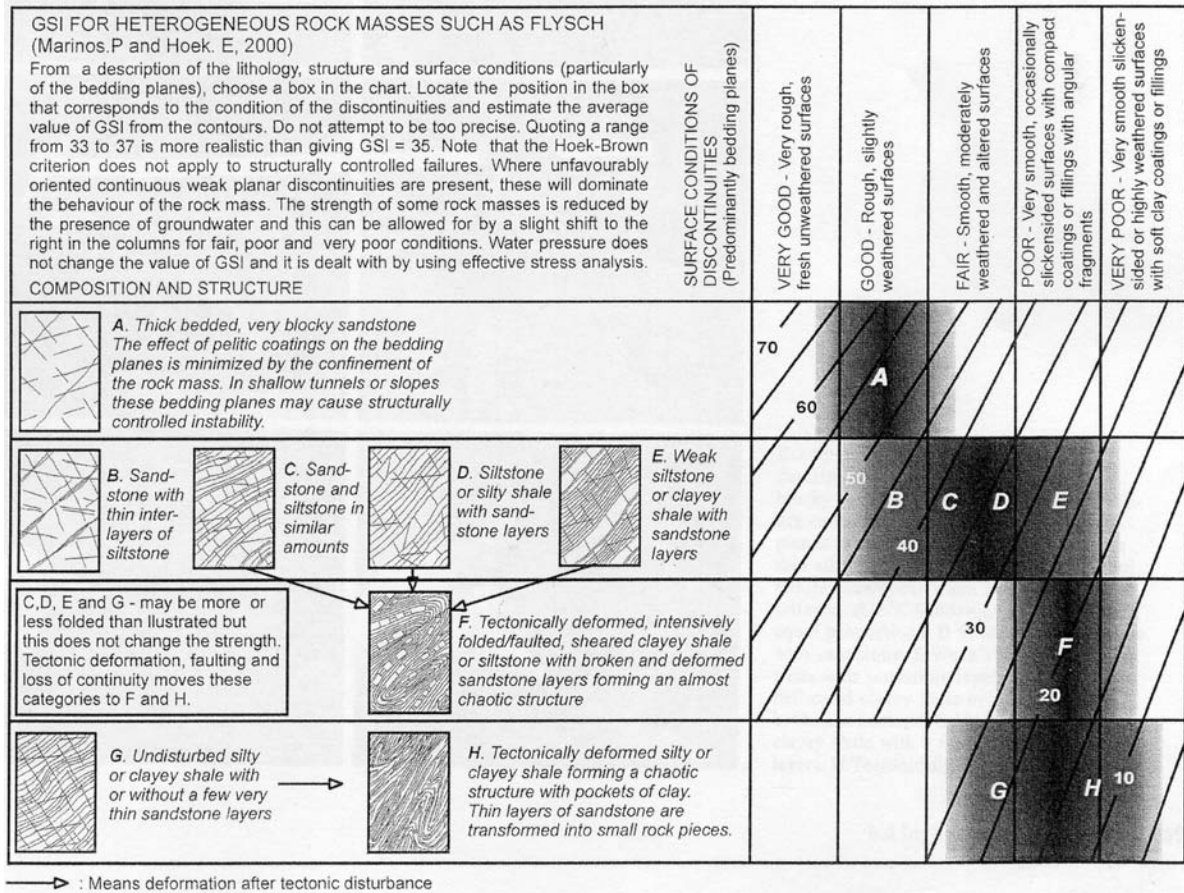
A class for *foliated/laminated/sheared* rock masses is introduced, based on observations made on the Athens Schist Formation

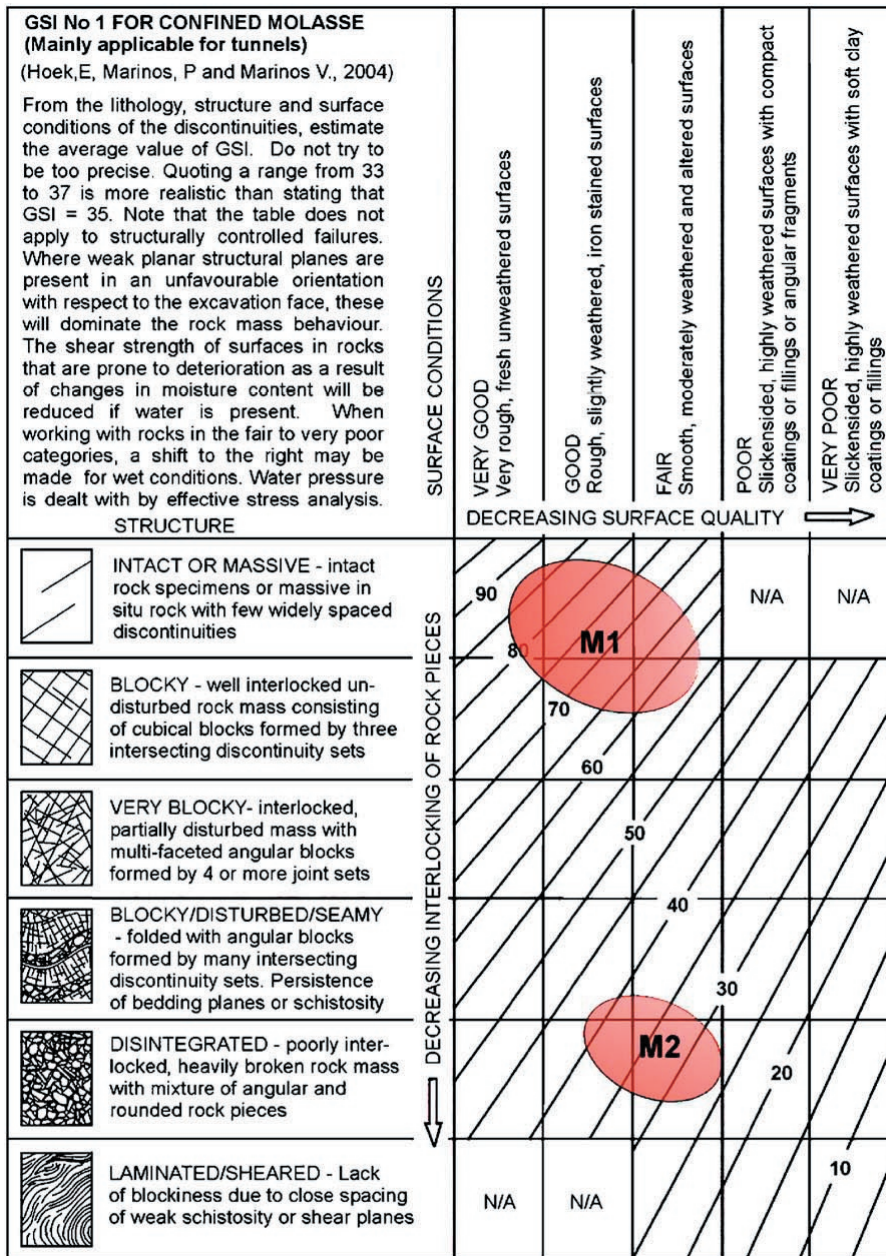


GSI chart 2001

(Marinos & Hoek)

Estimation for the geotechnical properties of heterogeneous rock masses such as flysch

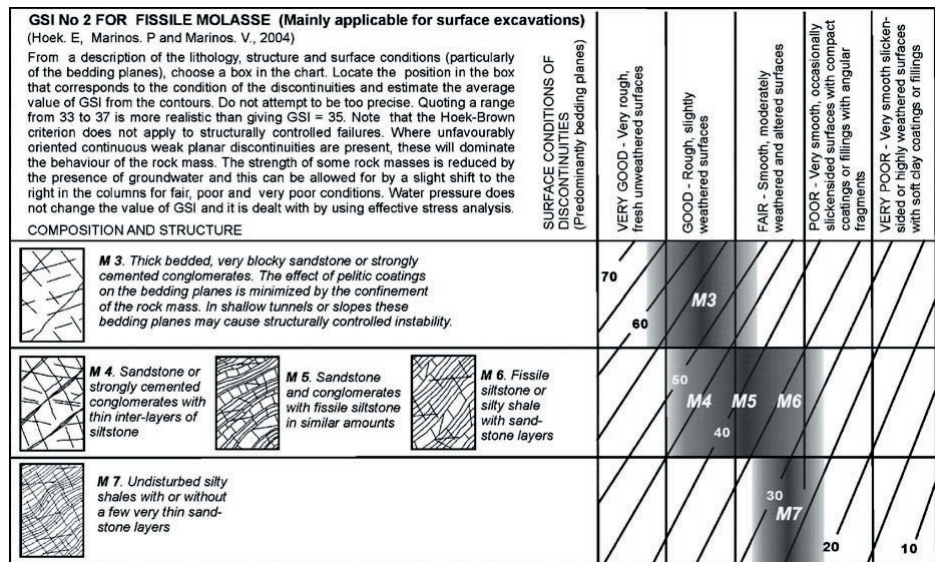




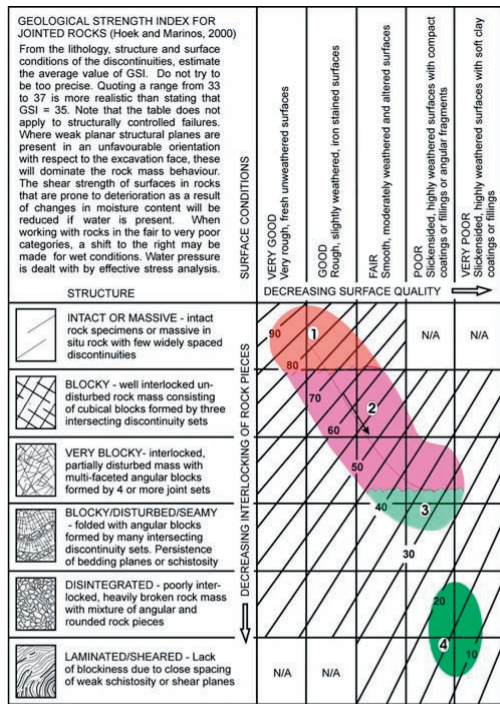
GSI version 2005

(Hoek, Marinos & Marinos)

Considerations of tectonically undisturbed but lithologically varied sedimentary rock masses, e.g. molasse



Appendix I-III



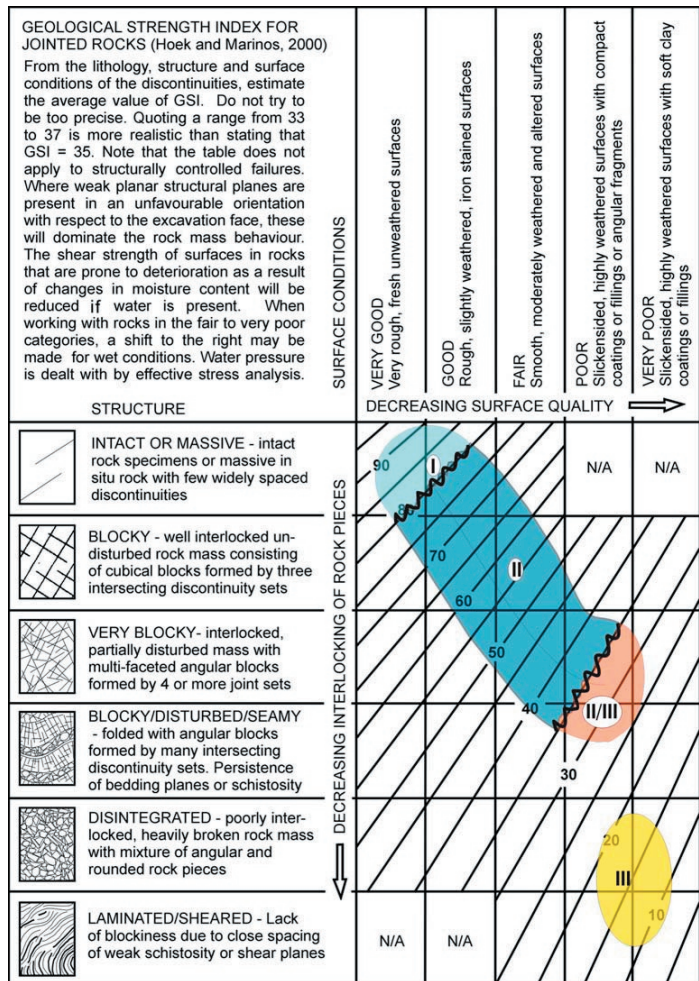
1. Massive strong peridotite with widely spaced discontinuities. The conditions of discontinuities are poorly only affected by serpentinisation
 2. Good to fair quality peridotite or compact serpentinite with discontinuities which may be severely affected from alteration.
 3. Schistose serpentinite. Schistosity may be more or less pronounced and their planes altered.
 4. Poor to very poor quality sheared serpentinite. The fragments consisting of weak materials
- Increase of presence of serpentines or other weak material (e.g talc) in joints or schistosity

Warning: The shaded areas indicate the ranges of GSI most likely to occur in these type of rocks. They may not be appropriate for a particular site specific case.

GSI version 2006

(Marinos, Hoek & Marinos)

Case of ophiolitic series with special emphasis on tunnelling.



I. Stable conditions; only at great depths possibility of rock burst failures

II. Stability mainly controlled by structural failures

II/III. Stability controlled by structural failures or mild overstraining.

III. Stability controlled by stress dependent rock mass

failure with significant squeezing at depth

Ravelling from the face may occur in masses corresponding in the low areas of zone II/III and in zone III

APPENDIX II

(Appendix related to Chap. 8)

RESEARCH PAPER Christe et al., 2007

**Three-dimensional petrographical investigations on
borehole rock core samples: a comparison between X-ray
computed- and neutron tomography**

Acta Geotechnica, 2(4), 269-279

Three-dimensional petrographical investigations on borehole rock samples: a comparison between X-ray computed- and neutron tomography

P. Christe · M. Bernasconi · P. Vontobel ·
P. Turberg · A. Parriaux

Received: 20 October 2006 / Accepted: 4 October 2007
© Springer-Verlag 2007

Abstract Technical difficulties associated with excavation works in tectonized geological settings are frequent. They comprise instantaneous and/or delayed convergence, sudden collapse of gallery roof and/or walls, outpouring of fault-filling materials and water inflows. These phenomena have a negative impact on construction sites and their safety. In order to optimize project success, preliminary studies on the reliability of rock material found on site are needed. This implies in situ investigations (surface mapping, prospective drilling, waterflow survey, etc.) as well as laboratory investigations on rock samples (permeability determination, moisture and water content, mineralogy, petrography, geochemistry, mechanical deformation tests, etc.). A set of multiple parameters are then recorded which permit better insight on site conditions and probable behavior during excavation. Because rock formations are by nature heterogeneous, many uncertainties remain when extrapolating large-scale behavior of the rock mass from analyses of samples order of magnitudes smaller. Indirect large-scale field investigations (e.g. geophysical prospecting) could help to better constrain the relationships between lithologies at depth. At a much smaller scale, indirect analytical methods are becoming more widely used for material

investigations. We discuss in this paper X-ray computed tomography (XRCT) and neutron tomography (NT), showing promising results for 3D petrographical investigations of the internal structure of opaque materials. Both techniques record contrasts inside a sample, which can be interpreted and quantified in terms of heterogeneity. This approach has the advantage of combining genetic parameters (physico-chemical rock composition) with geometric parameters resulting from alteration or deformation processes (texture and structure). A critical analysis of such 3D analyses together with the results of mechanical tests could improve predictions of short- and long-term behavior of a rock unit. Indirect methods have the advantage of being non-destructive. However, as it is the case with large-scale geophysical surveying, XRCT and NT are affected by several error factors inherent to the interaction of a radiation modality (X-ray or neutron beam) with the atomic structure of the investigated materials. Recorded signals are therefore in particular cases not artifact-free and need to be corrected in a subsequent stage of data processing.

Keywords Geotechnical sample sizes · Neutron tomography · Petrographical investigations · Structure · Texture · X-ray computed tomography

P. Christe (✉) · P. Turberg · A. Parriaux
Laboratoire de Géologie de l'Ingénieur et de l'Environnement,
Ecole Polytechnique Fédérale, Lausanne, Switzerland
e-mail: pierre.christe@epfl.ch

M. Bernasconi
Service de radiodiagnostic et radiologie interventionnelle,
Centre Hospitalier Universitaire Vaudois, Lausanne, Switzerland

P. Vontobel
Spallation Neutron Source Division, ASQ,
Paul Scherrer Institut, Villigen, Switzerland

1 Introduction

In the framework of a PhD project at EPFL, rock samples derived from recognition drilling were studied in order to investigate possible relationships between their geological and mechanical properties. This approach follows previous work by Bürgi [2, 3] and Habimana [6, 7]. It was found that geological parameters regrouped under a quality index called MSI (Mineralogical and Structural Index [2]) show

an apparent tendency to positively correlate with rupture values from triaxial compression [6]. Observations were made on quartzo-phyllic rock samples from the Cleuzon-Dixence dam project in Switzerland. Conclusions of this research are encouraging but further work is needed to get more reliable results. The current research project seeks therefore to test the proposed methodology for rocks of varying petrological content.

A major problem pointed out by Bürgi [2] is the 2D nature of their petrographical and structural analysis. Until recently, the majority of microstructural investigations on rock samples were made by thin sections under a crossed-polarized microscope. The geometrical relevance of such investigations can be improved using new techniques that have become available to earth scientists that allow 3D visualization of the rock interiors. Computed tomographic methods have been applied for several years to different research projects in the earth science community (e.g. [4, 5, 9, 12, 15, 17, 18]). Performing a mineralogical and structural analysis of rock samples on the basis of 3D petrographical and petrological evidence could therefore considerably increase the relevance of a characterization procedure of the type envisaged by Bürgi et al. [3].

Although there is no doubt that non-destructive techniques are powerful, they do not represent an investigation standard in the field of engineering geology and they are still expensive. Beam flux intensities for a particular investigation must be high enough to penetrate dense materials and provide reliable measurement statistics. Submillimeter resolution investigations are therefore often only possible on small samples in the order of 2×2 cm, for which desktop scanners have become easily available (see for example at <http://www.skyscan.be>). Specialized centers working on new techniques for indirect 3D rock imaging report today resolutions of up to 1/1,000 of object diameter on samples up to about 8 cm in diameter with 200–225 kV microfocal X-ray sources; specific higher-energy instruments providing beam energy of 420–450 kV have somewhat lower spatial resolution but nevertheless permit high-quality micro-analysis on decimeter-scale samples (see UTCT, University of Texas at Austin, USA). Breakthrough resolution for indirect rock visualization is obtained with synchrotron derived irradiation sources that are characterized by high brightness and high intensity, many orders of magnitude more than with X-rays produced in conventional X-ray tubes. Reports from experiments performed at such facilities indicate today resolution potentials close to the nanometer scale (see European Synchrotron Radiation Facility, Grenoble, France).

Samples tested in this study are cylindrical probes from geotechnical reconnaissance drilling and have dimensions of about 8×16 cm. Rock cores collected in such operations are often fragile when extracted in difficult

geological settings (see for example many drilling operations performed at the AlpTransit tunnelling sites in Switzerland, where cataclastic and kakiritic materials were frequently encountered) and require that there be minimal manipulation to preserve their structures and textures. Therefore, to keep a maximum of information from such rock samples, their initial shape and dimension are fixed parameters in indirect analysis aiming derivation of relevant 3D relationships at the represented scale to be combined with regional structural data. The samples presented hereafter were chosen for their contrasting petrological characters and for evaluating the potential of two irradiation techniques providing adequate beam flux intensities and energies for proper penetration of geotechnical rock core sizes. The first was the X-ray computed tomography facility found at the Radiodiagnostic Institute of the University Hospital in Lausanne (CHUV). Second, a neutron tomography station located at the Paul Scherrer Institute in Villigen (PSI) offered the possibility to perform tests on referenced materials. We present in this study observations made by both techniques on the same reference geotechnical samples. 3D reconstructed models will be presented as well as individual tomographic slices and the complementary nature of the two methods will be highlighted.

2 Presentation of rock samples

Four samples were chosen according to their contrasting structural characteristics as well as on their varying mineralogical compositions. Three samples were rock cylinders from reconnaissance drilling performed at the TRIDEL gallery site under construction in Lausanne that were tested at the EPFL under uniaxial compression (e.g. showing important fracturing). The last sample was drilled during field work near Vallorbe in the Jura Mountains. We present a short description of each sample:

2.1 CT1-co

CT1-co is a sample of reinforced concrete from the upper part of a drillhole at the TRIDEL site in Lausanne. Diameter of core is 84.5 mm and length is 160 mm. The clastic nature of concrete (aggregate) and the metallic iron fibers are easily recognized by eye in hand specimen. The sample was fractured under uniaxial compression at the Laboratory of Rock Mechanics of the EPFL (LMR) and gave resistance value of $\sigma_c = 30$ MPa.

Sample composition is a standard concrete of gravel and sand from Lausanne area, cement and a water content of about 35%.

2.2 CT2-sa

CT2-sa is a sample of medium-grained sandstone from the Lausanne grey molasse formation taken during drilling operation at the TRIDEL site in Lausanne. Sample diameter is 80 mm and length is 160 mm. Fracture testing under uniaxial compression at the LMR gave a peak resistance value of $\sigma_c = 9$ MPa. Fracture networks are recognizable on the outer surface of the sample.

Sandstone composition is about 40% detrital quartz, 20% CaCO_3 , and smaller proportions of feldspar, Fe–Mg–, and micaceous minerals with structural formulas of type $(\text{K,Na,Ca})_2(\text{Al,Mg,Fe,Ti})_{4-6}(\text{Si,Al})_8\text{O}_{20}(\text{OH,F})_4$.

2.3 CT3-ma

CT3-ma is a sample of tectonized marl from a further reconnaissance drilling at TRIDEL site, Lausanne. Marls have a high proportion of clay minerals and tend to be very fine-grained. Moreover clays have a strong geotechnical meaning as they can capture water into their mineralogical structure allowing a strong swelling potential in case where smectite is present causing with time potential damage on geotechnical structures. Diameter of sample is 82 mm and length is 160 mm. Sample was fractured under uniaxial compression at the LMR and broke at $\sigma_c = 3.7$ MPa. Irregular surface shape and decompression fractures due to drying processes at the contact with ambient air affect the sample.

Marl composition is about 17% SiO_2 , 43% CaO and 35% H_2O at saturation with minor proportions of Al_2O_3 , Fe_2O_3 , MgO , K_2O and Na_2O .

2.4 CT4-li

CT4-li is a tectonically fractured micritic limestone of Jurassic age collected along the Pontarlier fault zone near Vallorbe, in the Jura Mountains. Sample diameter is 76 mm and length is approximately 200 mm with irregular bases. Uniaxial resistance performed on a 55 mm wide sample from the same formation gave a σ_c value of 60 MPa. A set of fractures that are partly recrystallized with calcite, partly filled with clay materials, is visible by eye.

Limestone composition is about 80% CaCO_3 , 2% H_2O and minor proportions of SiO_2 , Al_2O_3 , MgO , K_2O , Na_2O and FeO .

3 Analytical principles and methods

Tomography refers to the cross-sectional imaging of an opaque object from either transmission or reflection data

collected by illuminating the object from different directions using a particular radiation modality (here either X-rays or neutrons). Recording of intensity signals from different projections angles (e.g. sinograms) and combination of these projections all together allows the reconstruction of a 3D tomographic image of the investigated structure. In the strict sense of the word, a projection at a given angle is the negative logarithmic transmission image in the direction specified by that angle, what can be expressed as the object internal properties derived from the transmitted intensities. The conversion of intensity signals into an image requires reconstructing a function from its projections. This can be achieved with the use of so-called convolution-backprojection algorithms [8, 13, 14].

Tomographic methods are based on attenuation measurements of an incident beam intensity through a material of a given composition. The recorded final intensity I is related to the initial intensity I_0 through a linear attenuation coefficient defined as μ in the case of X-rays or as Σ in the case of thermal neutrons. Beer's Law, relating I to I_0 , is expressed for a homogeneous material as follows:

$$I_{(x)} = I_0 e^{-\mu x} = I_0 e^{-\Sigma x}.$$

The physical properties of the source radiation control the interaction that will result with the atomic structure of the investigated material. X-rays are emitted as a polychromatic beam (i.e. containing a spectrum of energies) and interact mainly with the electron shells of atoms. This leads to a CT map of linear attenuation coefficients that are dependent on material density, element composition and radiation energy. A CT scan detects in that sense density and chemical contrasts between adjacent components. Energy dependent total linear X-ray attenuation coefficients μ including photon absorption and scattering can be derived from tabulated X-ray mass attenuation coefficients μ/ρ from, e.g. <http://physics.nist.gov/PhysRefData/XrayMassCoef/cover.html> by multiplying with material density ρ .

In NT polychromatic neutrons interact with the nucleus of an atom. Scattering and absorption effects in NT are therefore a function of the effective cross sectional area that an atom of a specific isotope presents to a given neutron flux. In that sense, neutrons are very sensitive to detection of light elements like hydrogen, boron or lithium, meaning that such elements present big neutron cross-sections and are therefore very attenuating. Contrary to X-rays, neutrons will penetrate dense materials with minimal attenuation. Although XRCT and NT differ in their detection potential, they are complementary methods in the sense that each technique will have advantages for a given detection purpose. As a rule of thumb, however, one can keep in mind that elements with similar atomic number Z

are better discriminated by neutrons than by X-rays. Table 1 is a list of common chemical elements found in rocks for which X-ray and neutron properties are listed together with solid state densities, atomic number and atomic weight.

As expressed before, 3D investigations of a structure are achieved by combining different radiation paths taken under different incremental angular projections using tomographic reconstruction algorithms. Acquisition is achieved by placing the sample on a rotary table rotating in small angular steps over 180° in the case of parallel beam projection in NT. For our XRCT measurements, sample orientation remains fixed while the source rotates over 360° around the sample placed on a table moving through the gantry, resulting in continuous helical data acquisition.

Final beam intensities are recorded on highly sensitive detectors specially designed for X-ray or neutron detection. They capture the 2D ray field perpendicular to the ray path. The geometry of the detector system must be appropriate in order to catch the entire rays. Scattering effects must be minimized in the case of NT due to device design (optimization between distance of sample from source and distance to detector). Signal records are finally converted in a slice image via the above mentioned convolution-back-projection algorithms.

Table 2 presents common rock-forming minerals classified by density for which linear attenuation coefficients were calculated for both XRCT and NT irradiations. Figure 1 makes a graphical comparison of these different attenuation

coefficients and highlights the specific behavior of hydrated phases that are strongly opaque under NT investigation.

In the following we present the facilities we have used for XRCT and NT investigations.

3.1 X-ray computed tomography (XRCT)

XRCT measurements were performed at the University Hospital in Lausanne (CHUV) at the radiodiagnostic institute. CT scans were performed using a LightSpeed VCT from GE Medical Systems (<http://www.gehealthcare.com>). Detector is a 40 mm-wide HiLight® Matrix III Scintillator with isotropic design. It contains 64-channel detector rows made of 58,368 cells (912 detectors per row) with a thickness in the z -direction of 0.625 mm each, providing an isotropic resolution of 0.35 mm. Lighting angle of the detector is 56 degrees. Dynamic range is 16 bit and reconstructed density maps are 512×512 pixels. X-ray parameters were set to 120 kVp voltage and 640 mA tube current for a focal spot size of 1.2 mm. Acquisition was achieved in a helical mode corresponding to a continuous rotation of the CT gantry (X-ray source and detector) during the displacement of the sample at a constant speed of 25.8 mm/s. A full rotation was performed in 0.8 s and image reconstruction step was set to 0.3 mm providing a voxel size of $0.3 \times 0.215 \times 0.215$. A reconstruction algorithm with a medium edge enhancement effect was used (DETAIL CT algorithm from GE Medical Systems).

Table 1 List of common chemical elements found in rocks for which total scattering and attenuation properties under X-ray and neutron irradiations are given, together with atomic number, atomic weight and solid state densities

| Chemical element | Atomic number | Atomic weight (g mol ⁻¹) | Density (g cm ⁻³) | X-ray mass attenuation coefficient (cm ² g ⁻¹) 120 keV | X-ray attenuation coefficient (cm ⁻¹) 120 keV | Neutron scattering cross section (cm ² g ⁻¹) 1.8 Å, 25 meV | Neutrons attenuation coefficient (cm ⁻¹) 1.8 Å, 25 meV |
|------------------|---------------|--------------------------------------|-------------------------------|---|---|---|--|
| H | 1 | 1.0079 | 0.09 | 0.282 | 0.025 | 49.013 | 4.411 |
| C | 6 | 12.011 | 2.26 | 0.144 | 0.325 | 0.278 | 0.629 |
| O | 8 | 15.999 | 1.43 | 0.146 | 0.209 | 0.159 | 0.228 |
| Na | 11 | 22.99 | 0.97 | 0.146 | 0.142 | 0.086 | 0.083 |
| Mg | 12 | 24.305 | 1.74 | 0.154 | 0.268 | 0.092 | 0.160 |
| Al | 13 | 26.982 | 2.7 | 0.153 | 0.413 | 0.034 | 0.091 |
| Si | 14 | 28.086 | 2.33 | 0.163 | 0.380 | 0.046 | 0.112 |
| S | 16 | 32.066 | 2.07 | 0.174 | 0.360 | 0.019 | 0.040 |
| K | 19 | 39.098 | 0.86 | 0.191 | 0.164 | 0.030 | 0.026 |
| Ca | 20 | 40.078 | 1.55 | 0.206 | 0.319 | 0.043 | 0.066 |
| Ti | 22 | 47.867 | 4.54 | 0.210 | 0.953 | 0.055 | 0.248 |
| Fe | 26 | 55.845 | 7.87 | 0.269 | 2.117 | 0.125 | 0.986 |

Note that the level of the irradiation energy strongly differs between the X-ray (120 keV) and the neutron data (25 meV), but correspond to effective scan parameters for each technique. X-ray mass attenuation coefficients taken from <http://physics.nist.gov/PhysRefData/Xcom/html/xcom1.html> [1] and total neutron cross sections calculated for a wavelength of 1.8 Å corresponding to a thermal neutron energy of 25 meV from <http://www.ncnr.nist.gov/resources/n-lengths/list.html> [16]. Attenuation coefficients include both coherent and incoherent scattering and absorption

Table 2 Calculated attenuation coefficients for relevant mineral species present in the studied samples and classified by density

| Compound | Chemical formula | Density (g cm ⁻³) | X-ray linear attenuation coefficient (cm ⁻¹) 120 keV | Neutrons attenuation coefficient (cm ⁻¹) 1.8 Å, 25 meV |
|------------|--|-------------------------------|---|---|
| Air | O ₂ | 0.00 | 0.00000 | 0.00000 |
| Water | H ₂ O | 1.00 | 0.16100 | 5.38000 |
| Microcline | KAlSi ₃ O ₈ | 2.56 | 0.40448 | 0.24275 |
| Kaolinite | Al ₂ Si ₂ O ₅ (OH) ₄ | 2.60 | 0.39780 | 2.26568 |
| Albite | NaAlSi ₃ O ₈ | 2.62 | 0.39824 | 0.27165 |
| Quartz | SiO ₂ | 2.65 | 0.40810 | 0.28241 |
| Chlorite | (Mg,Fe,Al) ₁₂ [(Si,Al) ₈ O ₂₀](OH) ₁₆ | 2.65 | 0.49555 | 1.16772 |
| Smectite | (Na,Ca)Al ₄ [(Si,Al) ₈ O ₂₀](OH) ₄ ·2(H ₂ O) | 2.70 | 0.41850 | 1.26832 |
| Calcite | CaCO ₃ | 2.71 | 0.46070 | 0.34373 |
| Illite | (K,H ₃ O) [(Si,Al) ₃ O ₁₀](OH) ₂ | 2.75 | 0.43175 | 1.89746 |
| Anorthite | CaAl ₂ Si ₂ O ₈ | 2.76 | 0.44160 | 0.26307 |
| Muscovite | KAl ₃ Si ₃ O ₁₀ (OH) ₂ | 2.83 | 0.44148 | 0.97482 |
| Rutile | TiO ₂ | 4.25 | 0.78625 | 0.41071 |
| Ilmenite | FeTiO ₃ | 4.79 | 1.01548 | 0.54514 |
| Pyrite | FeS ₂ | 5.01 | 1.09218 | 0.34386 |
| Magnetite | Fe ₃ O ₄ | 5.20 | 1.22200 | 0.70055 |
| Hematite | Fe ₂ O ₃ | 5.30 | 1.22960 | 0.71837 |

Structural formulas are given for each compound. X-ray attenuation coefficients for energies of 120 keV, neutrons attenuation coefficients for a wavelength of 1.8 Å corresponding to a thermal energy of 25 meV

In order to minimize beam hardening effects (preferential attenuation of low-intensity X-rays by crossing the sample due to the polychromatic nature of the X-ray beam) a sample holder made from a Cu-sheet surrounding a 2 cm thick PVC cylinder was used to pre-filter X-rays before entering the sample.

3.2 Neutron tomography (NT)

NT measurements were performed at the Paul Scherrer Institute (PSI) in Villigen at the Neutron Transmissions Radiography Station (NEUTRA, [10, 11]). Neutrons are

generated at PSI through a proton accelerator by sending a 590 MeV proton beam at a target of heavy metal (lead). From there neutrons are ejected in a moderator tank and slowed down to thermal energy of approximately 25 meV (“SINQ”, Swiss Spallation Neutron Source). Extraction of neutrons for radiographic and tomographic use is made through a flight tube forming a collimator that bundles neutron rays to a slightly divergent beam of about 35 cm diameter that is directed to the sample holder. Attenuated neutrons are then recorded on a 0.25 mm thick ⁶Li-doped ZnS based neutron scintillator screen and imaged with a 1,024 × 1,024 pixel CCD camera. Acquisition times lasted 1.5 h (300 angular projections over 0.6° increments, 18 s

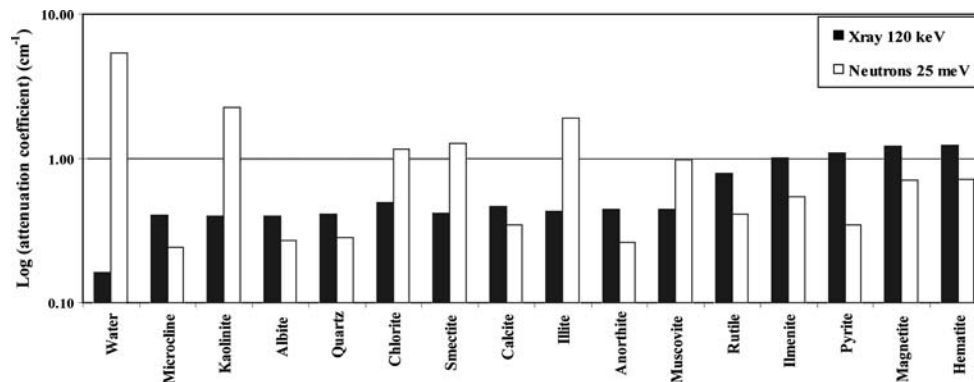


Fig. 1 Graphic presentation of the linear attenuation coefficients for X-rays (120 keV) and neutrons (1.8 Å and 25 meV) for the mineral species listed in Table 2. Clay minerals and hydrated mineral species become particularly well highlighted in the neutron data

illuminations for each view). Three additional exposures without sample (flatfield views) and one exposure without neutron beam (CCD noise background) were taken. These are used to derive the transmission values I/I_0 from the sample projection images.

Rock samples were placed at position 2 of NEUTRA providing a collimation ratio L/D of 350 and a field of view of 97×97 mm using a 50 mm objective (Pentax 50 mm F 1.2). Neutron flux is $5.0 \times 10^{-6} \text{ cm}^{-2} \text{ s}^{-1}$ per mA. Nominal resolution is 0.095 mm per pixel (0.215 mm per pixel in the case of XRCT). Geometric distortion due to distance from sample to scintillator was evaluated to be 0.143 mm.

Due to the size of the rock samples only about one half of their volume could be visualized at NEUTRA (300 images), as opposed to the 560 images encompassing the entire volumes acquired via XRCT.

4 Results and discussion

XRCT and NT data were edited at NEUTRA with the help of VGStudio MAX software (<http://www.volumegraphics.com>) for voxel data visualization and analysis. 2D visualizations of individual tomographic “slices” were performed with the freeware ImageJ™ (rsb.info.nih.gov/ij).

Quality and displayed contrasts differ strongly between both methods. Table 2 presents comparative attenuation coefficients for X-rays and thermal neutrons for the typical mineral species found in the four rock samples CT1-co, CT2-sa, CT3-ma and CT4-li.

Sample CT1-co is representative of a clastic texture where individual components can be visualized in a cement matrix. This type of material can be seen as a bimodal structure, where matrix properties will have a strong influence at the early stage of any deformation process before clast deformation will initiate. Recognition of fractures or voids in the matrix is therefore crucial to better characterize a deformation process, as well as clast shapes. The XRCT model of CT1-co provides good 3D information on the entire sample thickness whereas discrimination of individual particles is only possible by means of NT investigations on a peripheral area. This is probably due to the amount of hydrated components present in the matrix cement used for concrete preparation but also on an inappropriate sample size for proper neutron penetration in such materials (Fig. 2).

Decimeter-scale concrete is therefore too attenuating for neutrons to penetrate properly. The high hydrogen content in concrete leads to a low neutron transmission. The high scattering probability of neutrons induces additional blurring and a strong deviation from the exponential attenuation law.

On the contrary, densities of aggregate components and hydrated cement are in a good range for X-ray penetration

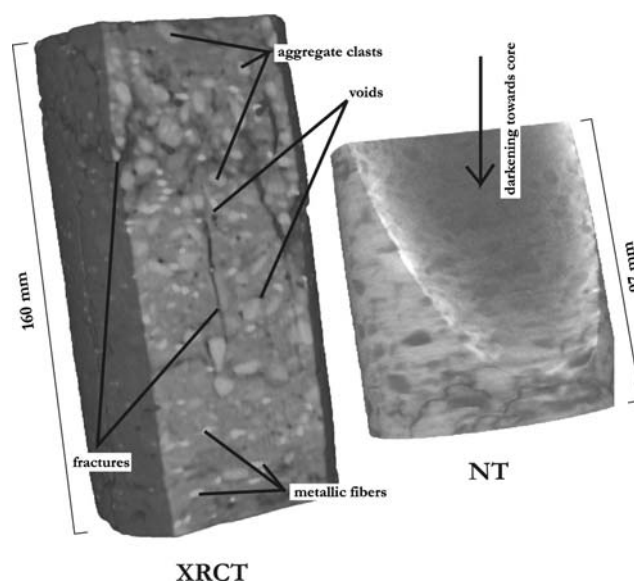


Fig. 2 XRCT (left) and NT (right) 3D reconstructions of fractured sample CT1-co. Main features of sample are pointed out on the XRCT model. Note decreasing recorded information towards the core of sample CT1-co in the NT image, as indicated by a shadow zone (arrow)

for the given sample size. The 1 mm bright metallic fibers used in this concrete type for enhanced mechanical performance are displayed with a strong saturation level on XRCT images whereas they are practically invisible on NT images (Fig. 3). Fractures present in sample CT1-co are only discernable on the outlines of the NT model, whereas they are strongly contrasting in the internal parts of the XRCT model (Fig. 3).

Sample CT2-sa is homogeneous mid-grained sandstone with grain sizes in the millimeter to submillimeter range. Grain packing in the matrix is therefore only slightly visible on XRCT or NT scans as we get close to the limits of resolution of both techniques. Sample CT2-sa is interesting in terms of differentiation between rock matrix and fracture patterns. The sandstone is mainly composed of detrital quartz and feldspar grains for which X-rays and neutrons attenuation coefficients are quite similar (Table 2). The porous nature of sandstone permits only little water to remain in the rock structure if material has time to dry under ambient air conditions. Therefore, neutron penetration in CT2-sa is about as good as in the case of X-rays (Fig. 4).

Structures of interest like fractures offer good contrasts with both methods. Figure 5 shows a 3D reconstruction from the NT scan. Fracture outlines are similarly detected with XRCT (Fig. 4). Sample CT2-sa is therefore representative of a material that is productively investigated with both methods.

Sample CT3-ma is a material that is in between a rock and a soil (“soft rock-hard soil”). It has a plastic

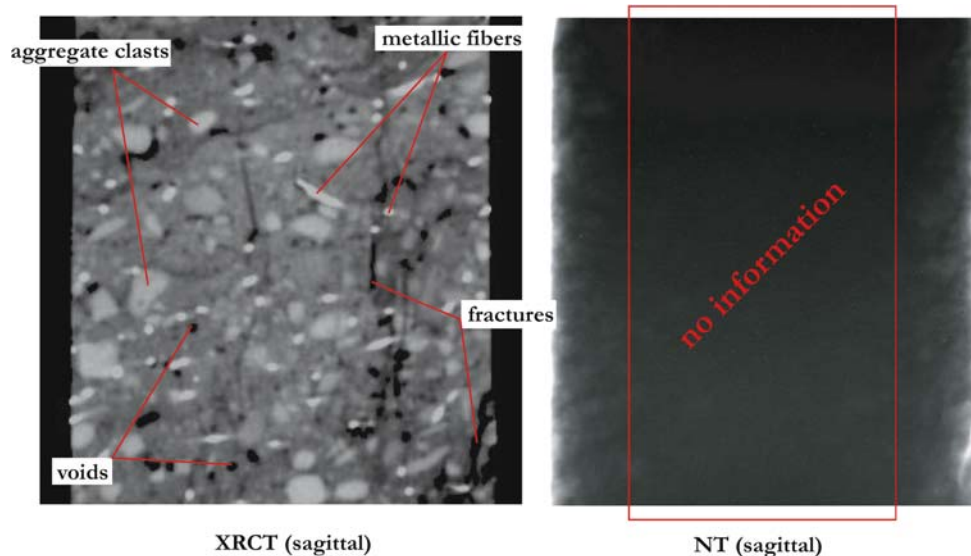


Fig. 3 Individual sagittal XRCT (*left*) and NT (*right*) slices of fractured sample CT1-co. Due to the limited field of view of our NT instrument only about 70% of sample length is presented here. Different components are pointed on the XRCT picture. The NT slice is poorly resolved in the internal sample parts due to inappropriate sample dimensions for neutron penetration and the presence of hydrated species in the cement matrix

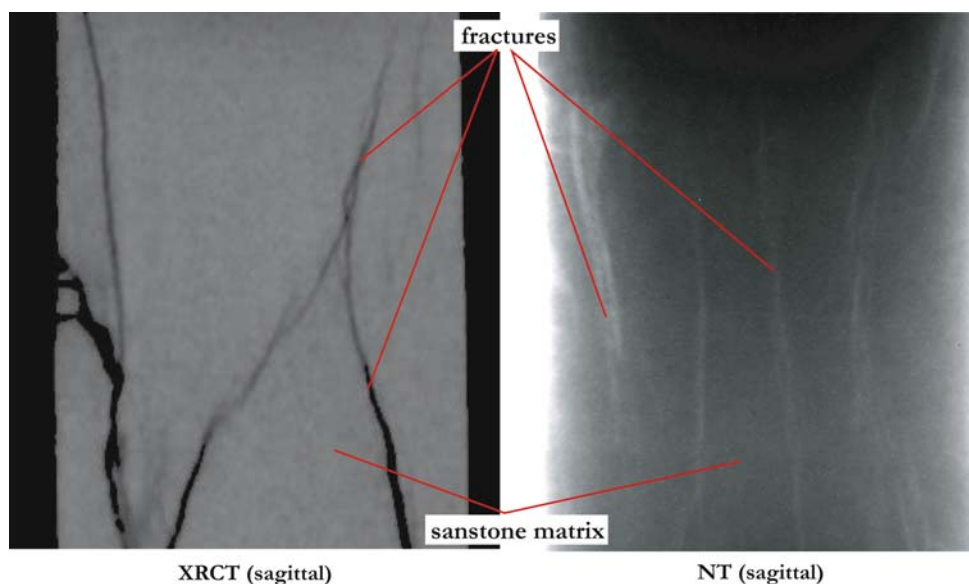


Fig. 4 Comparative sagittal XRCT and NT slices of fractured sample CT2-sa. In the case of dry sandstone, neutron penetration is achieved across the entire sample thickness and gives result in good concordance with XRCT visualization

mechanical behavior that is controlled by important proportions of clay minerals and by the effective water content of the sample. In such materials, void features like fractures will tend to seal easily when wet, implying a very low permeability. However, crack patterns caused by decompression will form when the material is submitted to a drying process. The fractures visible on the surface of sample CT3-ma result from prolonged contact with

ambient air contracted during storage after completion of the uniaxial compression test.

The significant abundance of hydrated mineral species like clays makes any neutron radiography or tomography on such materials inefficient for large samples (Table 2; Fig. 6). Investigations of the inside parts of the sample are instead possible with X-rays. The very fine-grained nature of such marls is however a big problem for the resolution

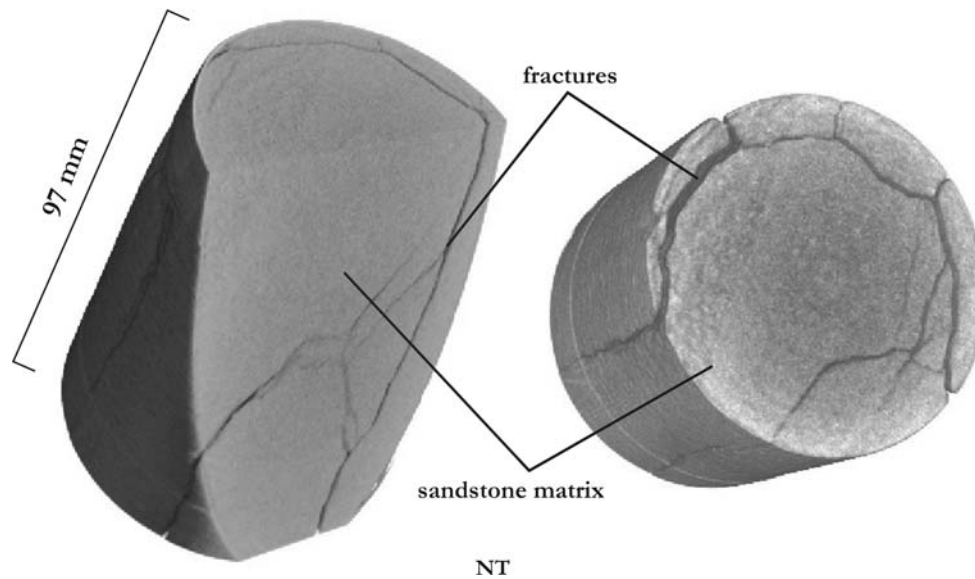


Fig. 5 Reconstructed NT models of fractured sample CT2-sa. As the rock matrix is very homogeneous, features like fractures are highly contrasting and easily detected in a tomographic image

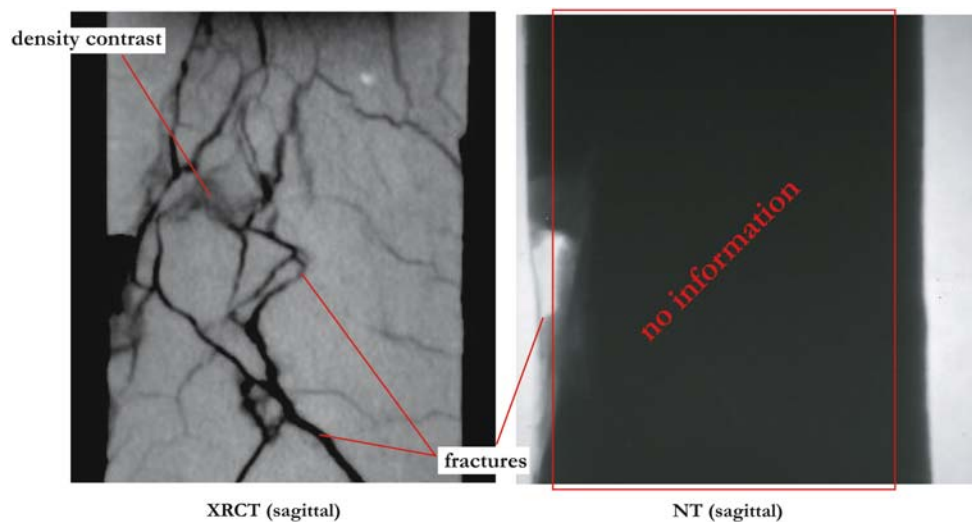


Fig. 6 Comparative sagittal XRCT (*left*) and NT slices (*right*) of fractured sample CT3-ma. Neutron penetration is very poor due to significant quantity of hydrated mineral species inside the sample as well as sample dimensions

of features of interests other than penetrative fractures. CT slices show however regions of contrasting densities reflecting a probable modification of the internal structure of the sample that could eventually be linked to alteration processes (increase in overall microporosity, Fig. 6). Reconstructed NT images were compared with the XRCT scan on a broken surface at the sample outline. The NT model is strongly blurred compared to the XRCT model according to detection of fine fractures but renders the general core shape accurately (Fig. 7).

Sample CT3-ma is therefore characterized as an extreme material where both methods run up against some detection

limits. However, individual CT slices reflecting density contrasts related to alteration states and/or material heterogeneities present the possibility of detecting mechanically important features that would remain hidden by classical investigation techniques.

Clays are on the other hand an interesting contrasting agent for NT detection if only present in small proportions inside a sample. As for the case of sample CT4-li, which represents again a homogeneous rock matrix separated by different cracks, structures like clay-filled fractures are very nicely displayed on an NT model (Fig. 8). The entire limestone matrix appears quite transparent to neutrons but

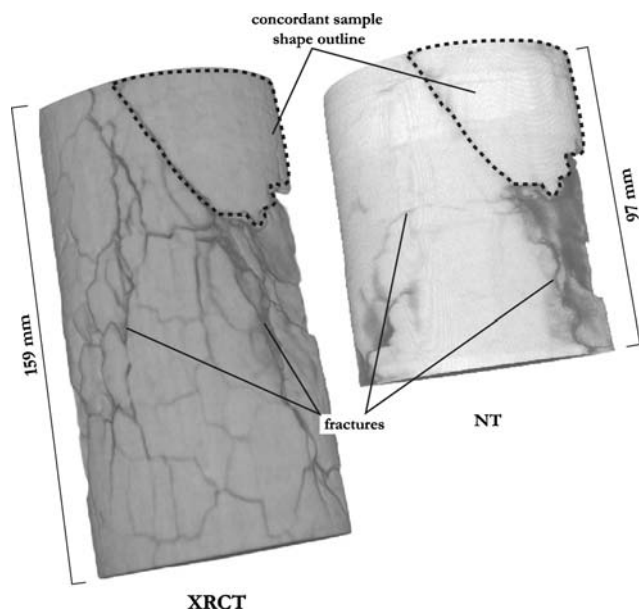


Fig. 7 3D models reconstructed for fractured sample CT3-ma. Left is an XRCT view and right the poorly resolved NT view. Both techniques give concordant results in the visualization of the *broken outline* of the sample represented by a *dashed surface area*. However, resolution of fractures patterns due to drying of the sample at ambient air is poorly realized in the case of NT investigation

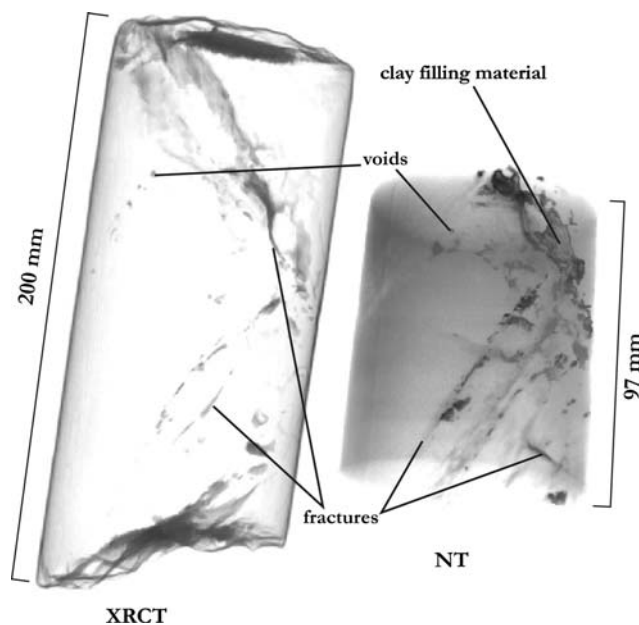


Fig. 8 3D models of sample CT4-li. NT reconstruction (right) permits nice visualization of clay materials inside cracks (*dark grey spots*) and displays with better contrast than XRCT a presumed fracture patterns inside the sample

clays in small proportions give a very high contrast on NT scans due to the amount of bounded water present in the mineralogical structure (Fig. 8). This is apparently better

achieved with NT than with XRCT but would need to be properly quantified.

Fracturing of limestones under tectonic processes involves circulation of calcite-enriched fluids. These fluids will preferentially precipitate inside open cracks and will eventually seal the existing fractures modifying their mechanical properties. Because of identical densities between precipitating calcite and limestone matrix, these features will tend to become invisible by XRCT investigation. NT scans are apparently more promising for the detection of such sealed fractures (Fig. 9).

For a geomechanical interpretation it is indeed important to detect such features as they could influence the whole mechanical behavior of a rock sample.

5 Conclusions

In the case of samples of similar shapes and size, as it is the case for this study, a direct comparison of X-ray Computed- and Neutron Tomography can be achieved. Differences in image contrasts result primarily from different attenuation properties of X-rays and neutrons by crossing a given material but also from optimization of the device parameter settings for a particular investigation (irradiation time, X-ray voltage and beam focal spot size, sample distance from neutron source, etc.). Although not especially designed for our investigation purpose, a rapid access to the two techniques could be obtained at a medical XRCT facility and at a NT facility providing test measurement opportunities. XRCT and NT were therefore applied in order to qualitatively determine which technique would better permit a rapid 3D imagery of quality that could be integrated in the process of rock mass characterization during geotechnical reconnaissance drilling operations. Prerequisites were to keep the rock core sizes unmodified (implying adequate parametrization of the XRCT and NT scanners to reach a penetration depth of <10 cm) and to get a resolution potential precise enough to highlight geological relevant features for a geomechanical 3D analysis. In that sense, XRCT seems to be more versatile than NT for producing imagery of interest independent of the petrological type of the analyzed sample. NT however, has some advantages when small proportions of the volume like clay-filling materials must be tracked precisely. The strong attenuation induced by hydrated species provides a contrast of high-quality on NT scans that looks more precise than on comparative XRCT-scans. Different interactions of these two irradiation modalities with a material of given composition mean that the two techniques could be used as complimentary analytical methods.

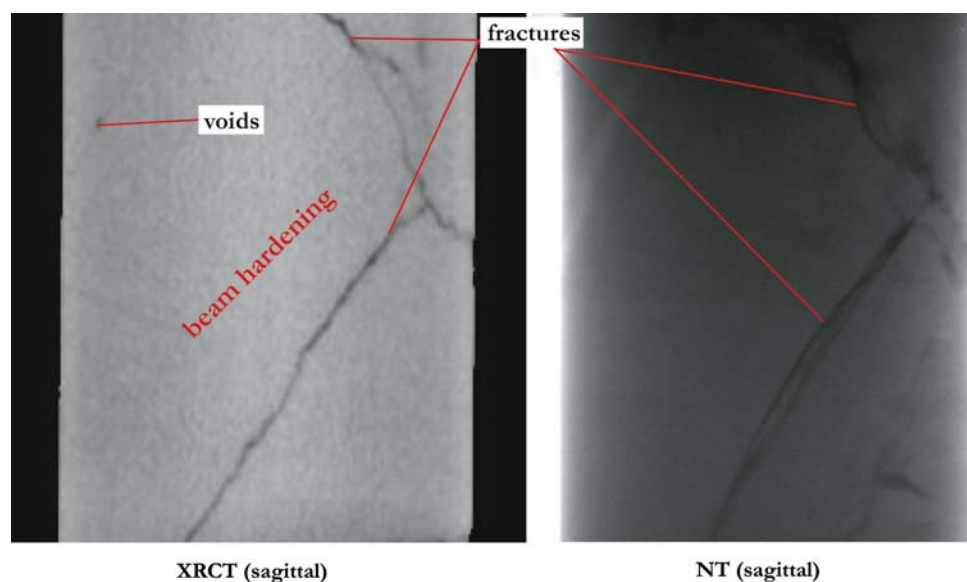


Fig. 9 Comparative sagittal XRCT (*left*) and NT (*right*) slices of sample CT4-li. XRCT slice is of medium quality, as hardening effects are visible towards central parts of the image. Calcite-filled fractures tend to be masked under X-ray investigation. The NT slice however shows more promising results in terms of structure visualization

Previous measurement tests made with medical XRCT already convinced us to properly pack the rock core sample before completion of the scan into an absorbing material that would minimize beam hardening effects. Image quality was improved considerably but very dense materials like sample CT4-li are still not artifact free. It seems that calcium, when present in strong proportion into a structure, induces some problems for proper X-ray penetration. This is particularly true when the investigated body is of the size of a geotechnical rock core. But in general, XRCT for rock investigation gives good results, as contrasting structures and textures can be visualized to a resolution of about 0.625 mm. Different components of sample CT1-co were therefore very nicely displayed on XRCT models. Problems arise with very fine-grained samples for which microstructures detection would require a finer resolution, as in the case of CT3-ma. However, apparent density contrasts inside a fine-grained matrix can be detected with XRCT and should be evaluated in terms of possible sample heterogeneity implying an eventual preferred mechanical deformation locus under stress application.

A particular weakness of XRCT is that, because it records density contrasts, features of different nature but similar densities will be masked on the resulting model. In particular, calcite-cemented fractures in sample CT4-li give a good illustration of this phenomenon.

NT investigation on borehole samples gave variable results in terms of image quality. If the proportion of hydrated mineral species is high or there is a high water

content as in concrete or marl, NT scans will show almost nothing, as expected from the very high attenuation coefficient of H under neutron irradiation. This is particularly true for decimeter-scale sample sizes that are too thick for proper neutron transmission. In the case of smaller samples and smaller diameters, neutrons can give more detailed internal information that is complementary to X-ray investigation results.

On the other hand and as expressed before, if the spatial extent of hydrated minerals is comparatively low, NT tomography will provide very precise detections of H-rich zones inside the material. Sample CT4-li, consisting of a homogeneous H-poor rock matrix crossed by millimeter-wide fractures filled with hydrous minerals, would therefore be a candidate for NT investigations.

In the case of dry and H-poor samples, as is the case with CT2-sa, XRCT and NT investigations gave similar results.

For the time being, an additional advantage of XRCT is that variable volume sizes can be visualized whereas NT scan parameters as optimized for this study limit the field of view to 97×97 mm. Moreover, the near-parallel geometry of the neutron beam will present a persistent size-limitation in comparison to X-ray irradiation.

Acknowledgments We would like to thank Dr R. Meuli at the CHUV in Lausanne and Prof. Dr E. Lehmann at the PSI in Villigen for providing us access to the XRCT and NT scanners in the framework of this research as well as for their helpful comments during preparation of this manuscript. Dr V. Labiouse from the Laboratory of

Rock Mechanics (LMR) at the EPFL is thanked for his support in the mechanical part of the research and comments on the manuscript. Financial support for P. Christie is provided by the Swiss National Science Foundation (SNF No. 2100-63'640.00).

References

- Berger MJ, Hubbell JH, Seltzer SM, Chang J, Coursey JS, Sukumar R, Zucker DS (1998) XCOM: photon cross sections database. National Institute of Standards and Technology, NIST Standard Reference Database 8 (XGAM)
- Bürgi C (1999) Cataclastic fault rocks in underground excavations: a geological characterisation. Thèse EPFL GC No. 1975
- Bürgi C, Parriaux A, Franciosi G (2001) Geological characterization of weak cataclastic fault rocks with regards to the assessment of their geomechanical properties. *Q J Eng Geol Hydrogeol* 34:225–232
- Carlson WD, Denison C (1992) Mechanisms of porphyroblast crystallization: results from high-resolution computed X-ray tomography. *Sciences* 257:1236–1239
- Conroy GC, Vannier MW (1984) Noninvasive three-dimensional computer imaging of matrix-filled fossil skulls by high-resolution computed tomography. *Science* 226:456–458
- Habimana J (1999) Caractérisation géomécanique de roches cataclastiques rencontrées dans des ouvrages souterrains alpins. Thèse EPFL GC No. 1945
- Habimana J, Labiouse V, Descoedres F (2002) Geomechanical Characterisation of cataclastic rocks: experience from the Cleuson-Dixence project. *Int J Rock Mech Min Sci* 39:677–693
- Hounsfield GN (1972) A method of and apparatus for examination of a body by radiation such as X- or Gamma-radiation. London, British Patent No. 1,283,915
- Ketcham RA, Carlson WD (2001) Acquisition, optimization and interpretation of X-ray computed tomographic imagery: applications to the geosciences. *Comput Geosci* 27:381–400
- Lehmann EH, Pleinert H, Wiezel L (1996) Design of a neutron radiography facility at the spallation source SINQ. *Nucl Instrum Methods A* 377:11–15
- Lehmann EH, Vontobel P, Wiezel L (1999) Properties of the radiography facility NEUTRA at SINQ and its potential for use as a European Reference Facility. In: Proceedings of the sixth World Conference on Neutron Radiography, Osaka, pp 151–158
- Nakashima Y (2000) The use of X-ray CT to measure diffusion coefficients of heavy ions in water-saturated porous media. *Eng Geol* 56:11–17
- Radon J (1986) On the determination of functions from their integral values along certain manifolds. *IEEE Trans Med Imaging* 5(4):170–176
- Ramachandran GN, Lakshminarayanan AV (1971) Three-dimensional reconstructions from radiographs and electron micrographs: Application of convolution instead of Fourier transforms. *Proc Natl Acad Sci USA* 68:2236–2240
- Schwarz D, Vontobel P, Lehmann EH, Meyer CA, Bongartz G (2005) Neutron tomography of internal structures of vertebrate remains: a comparison with X-ray computed tomography. *Palaeontol Electron* 8(2A):10
- Sears VF (1992) Neutron scattering lengths and cross-sections. *Neutron News* 3(3):29–37
- Van Geet M, Swennen R, Wevers M (2000) Quantitative analysis of reservoir rocks by microfocus X-ray computerized tomography. *Sediment Geol* 132:25–36
- Verhelst F, Vervoort A, De Bosscher P, Marchal G (1995) X-ray computerized tomography: determination of heterogeneities in rock samples. In: Proceedings of the eighth international congress on Rock Mechanics, Sept. 25–30, 1995. Balkema, Amsterdam

APPENDIX III

(Appendix related to Chap. 10)

CARact 3D: CODE FOR THE IMPROVED SEGMENTATION OF GEOLOGICAL FEATURES RESOLVED BY MEDICAL XRCT.

To be implemented in ImageJ™
rsbweb.nih.gov/ij/

Appendix III

```
import ij.*;
import ij.plugin.filter.PlugInFilter;
import ij.process.*;
import java.awt.*;
import ij.gui.*;

public class CARact_3D implements PlugInFilter {

    /*global values input*/
    ImagePlus imp;
    ImageStack stack;
    boolean canceled, treatment, elimination;
    int matrix, damage, criterion, number, densitymin;

    /*internal commands*/
    public int setup(String arg, ImagePlus imp) {
        if (arg.equals("about")) {
            showAbout();
            return DONE;
        }
        stack = imp.getStack();
        return DOES_16+SUPPORTS_MASKING;
    }

    /*CARact_3D detection*/
    public void run(ImageProcessor ip) {
        short[] pixels; //definition of a vector containing all the analyzed image
                        //informations

        int nSlices = stack.getSize(); //slice number in a stack
        getDetails(); //display window, introduction of variables
        if (canceled) return;

        int width = ip.getWidth(); //size of window
        Rectangle r = ip.getRoi(); //consider ROI size for calculation

        int offset, i, nw, n, ne, w, c, e, sw, s, se; //setting of local variables
        for (int slice = 1; slice <= nSlices; slice++) { //progression over entire stack
            IJ.showStatus("Running analysis : "+slice+"/"+nSlices); //indication of progress
            pixels = (short[])stack.getPixels(slice); //vector integration of values

            for (int y=r.y; y<(r.y+r.height-2); y++) { //progression inside vector matrix
                offset = y*width; //pixel localization in the first line
                                //y of the column vector
                n = pixels[offset] & 0xffff; //initialization: n (north) takes
                                //corresponding value in 16-bit
                ne = pixels[offset+1] & 0xffff; //same for ne (north-east)
                for (int x=r.x; x<(r.x+r.width-1); x++) { //progression over line
                    i = offset + x; //localization i of pixel during
                                //treatment
                    nw = n; //offset of values
                    n = ne; //same
                    ne = pixels[i+1] & 0xffff; //values update
                    w = pixels[i+width-1] & 0xffff;
                    c = pixels[i+width] & 0xffff;
                    e = pixels[i+width+1] & 0xffff;
                    sw = pixels[i+2*width-1] & 0xffff;
                    s = pixels[i+2*width] & 0xffff;
                    se = pixels[i+2*width+1] & 0xffff;
                    if (c < ((matrix+4*damage)/5))
                        pixels[i] = (short)(damage); //primary segmentation
                    else if (elimination && (c > densitymin))
```

```

        pixels[i] = (short)(matrix); //elimination of overdensity if
                                   required
    else if ((w+e-2*c) > ((matrix-damage)*criterion/1000))
        pixels[i] = (short)(damage); //E-W detection
    else if ((n+s-2*c) > ((matrix-damage)*criterion/1000))
        pixels[i] = (short)(damage); //N-S detection
    else if ((nw+se-2*c) > (2*(matrix-damage)*criterion/1000))
        pixels[i] = (short)(damage); //NW-SE detection
    else if ((ne+sw-2*c) > (2*(matrix-damage)*criterion/1000))
        pixels[i] = (short)(damage); //NE-SW detection
    else pixels[i] = (short)(matrix); //remaining image parts
                                   set as matrix
    }
}

/*treatment of isolated pixels, after segmentation*/
if (treatment)
for (int y=(r.y+r.height-1); y>r.y+1; y--) {
    offset = y*width;
    s = pixels[offset] & 0xffff;
    se = pixels[offset+1] & 0xffff;
    for (int x=r.x+1; x<(r.x+r.width-1); x++) {
        i = offset + x;
        sw = s;
        s = se;
        se = pixels[i+1] & 0xffff;
        w = pixels[i-width-1] & 0xffff;
        c = pixels[i-width] & 0xffff;
        e = pixels[i-width+1] & 0xffff;
        nw = pixels[i-2*width-1] & 0xffff;
        n = pixels[i-2*width] & 0xffff;
        ne = pixels[i-2*width+1] & 0xffff;
        if ((nw+n+ne+w+e+sw+s+se) > ((7-number)*matrix+(number+1)*
damage))
            pixels[i] = (short)(matrix);
        else pixels[i] = (short)c;
    }
}
;
}

}

/*user interface*/
void getDetails() {
    GenericDialog gd = new GenericDialog("CARact_3D");
    gd.addMessage("Primary segmentation");
    gd.addNumericField("Matrix density : ", 35000, 0);
    gd.addNumericField("Feature density : ", 32000, 0);
    gd.addMessage("Secondary segmentation");
    gd.addNumericField("Detection : ", 20, 0, 6, "/ 1000");
    gd.addCheckbox("Noise elimination", false);
    gd.addNumericField("Neighbours (0-7) : ", 0, 0);
    gd.addCheckbox("Overdensity elimination", false);
    gd.addNumericField("Minimal density to erase : ", 35000, 0);

    gd.showDialog();
    if (gd.wasCanceled()) {
        canceled = true;
        return;
    }
    matrix = (int)gd.getNextNumber();
}

```

Appendix III

```
        damage = (int)gd.getNextNumber();
        criterion = (int)gd.getNextNumber();
        treatment = gd.getNextBoolean();
        number = (int)gd.getNextNumber();
        elimination = gd.getNextBoolean();
        densitymin = (int)gd.getNextNumber();
    }

    void showAbout() {
        IJ.showMessage("About CARact_...",
            "This sample plugin filter detects\n" +
            "damage indicators\n" +
            "with 16-bit grayscale images\n" +
            "so as to give indication of a damage extent inside the rock."
        );
    }
}
```

CD = $\frac{\text{clast's surface}}{\text{image surface}}$

Clast density

Diagnostic for:

- Fractured vs. Clastic rock determination
- Extent of fragmentation through cataclasis

For perfectly clastic material:
rock strength ↗ when CD ↗

N₁

Number of elongated clasts (AR > 2)

N₀

Number of isometric clasts

FF = $4\pi \frac{\text{clast's surface}}{(\text{clast perimeter})^2}$

Form factor, deviation from circularity (calculated only for isometric clasts, \overline{FF}_0)

For perfectly clastic material:
rock strength ↘ when FF ↗

AR = $\frac{\text{major axis}}{\text{minor axis}}$

Aspect ratio of clasts (calculated only for elongated clasts, \overline{AR}_1)

AF = $\sum_{i=1}^n \left[\frac{X_i}{N_i(N_i - 1)} \right] \cdot i$

Angular differences between elongated clasts (AF₁)

Diagnostic of:

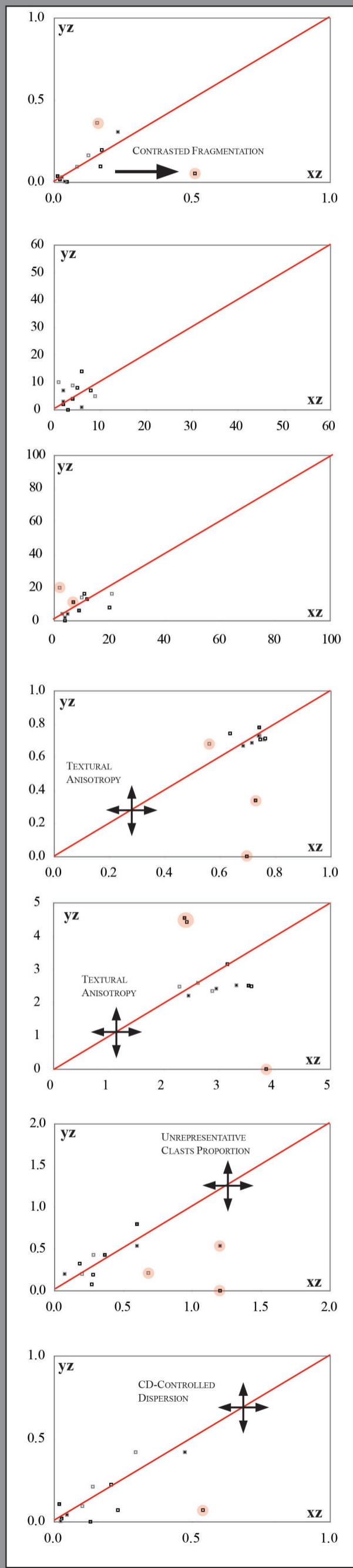
- Spatial distribution of elongated clasts
- Development of textural preferred orientations

For perfectly clastic material:
rock strength ↗ when AF ↗ & AR ↗

local TC

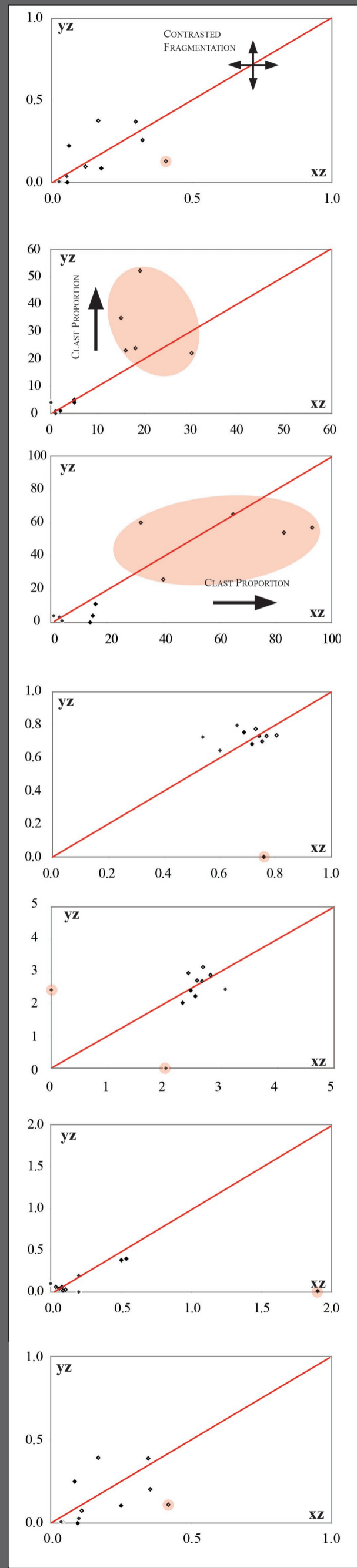
Class II

■ RSJ 1b ■ RSJ 8
□ RSJ 7 □ RSJ 9



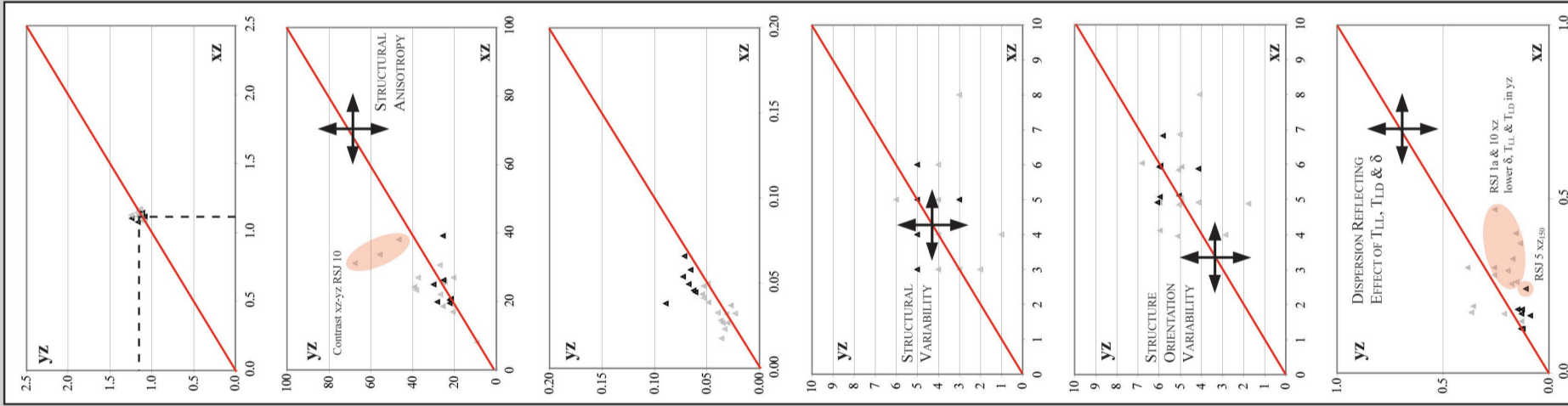
Class III

◆ RSJ 4 ◆ RSJ 11
♦ RSJ 6 ♦ RSJ 12



Class I

▲ RSJ 1a △ RSJ 10
 ▲ RSJ 5



R_L = $\frac{\text{length of trace line}}{\text{length of projected trace line}}$
 Linear roughness
 Diagnostic for:
 - Fracturing mode (dilatation vs. compaction)
 - Fracturing propagation & geometry
 For fractured material:
 rock strength \nearrow when $R_L \nearrow$

T_{LL}
 Total trace line length in the reference area (CT slice)
 Diagnostic for:
 - Persistence of fracturing
 For fractured material:
 rock strength \searrow when $T_{LL} \nearrow$

T_{LD}
 Trace line density
 Diagnostic for:
 - Extent of fracturing
 - Level of fragmentation
 For fractured material:
 rock strength \searrow when $T_{LD} \nearrow$

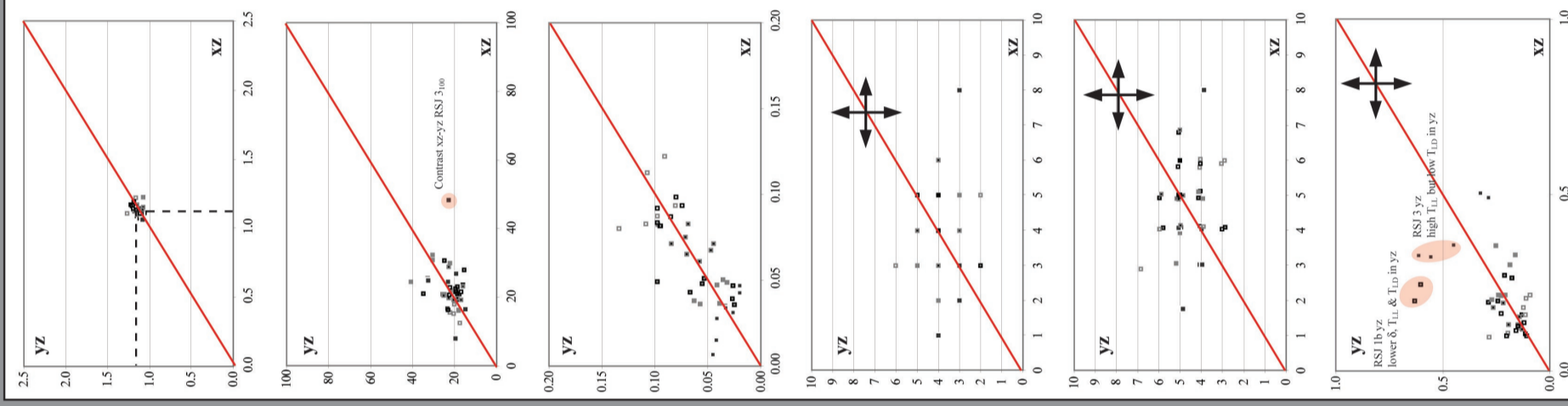
n
 Number of discontinuity sets (classified in 18 families of 10° width each)

δ_{local}
 Orientation factor (number, individual length and preferred orientation of discontinuities)
 Diagnostic for:
 - Spatial distribution of discontinuities
 - Development of structural preferred orientations
 For fractured material:
 rock strength \searrow when $\delta \nearrow$

local MC

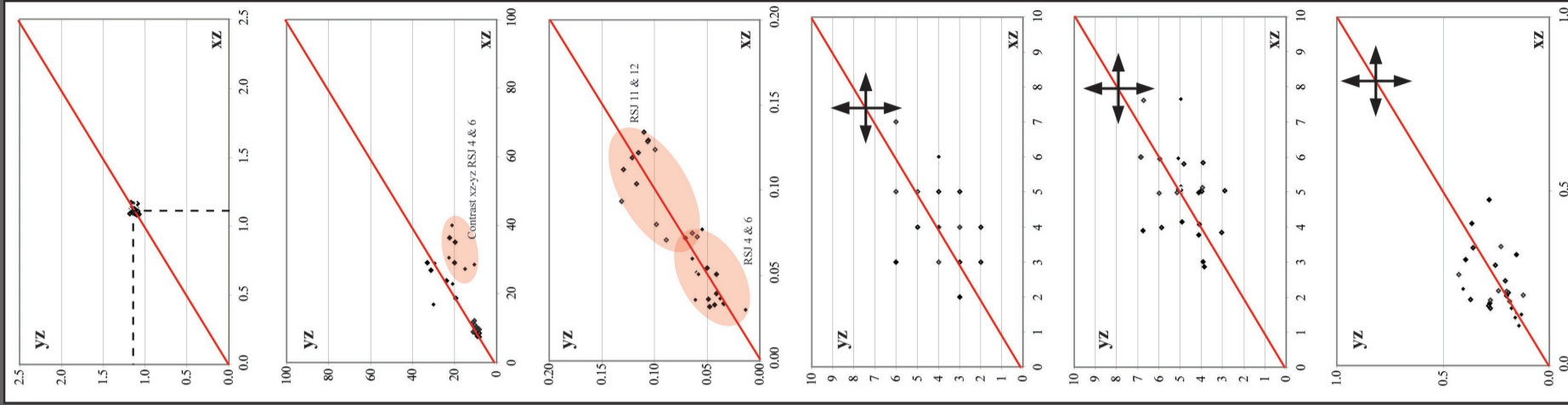
Class II

■ RSJ 1b ■ RSJ 3 ■ RSJ 8
 ■ RSJ 2 □ RSJ 7 □ RSJ 9



Class III

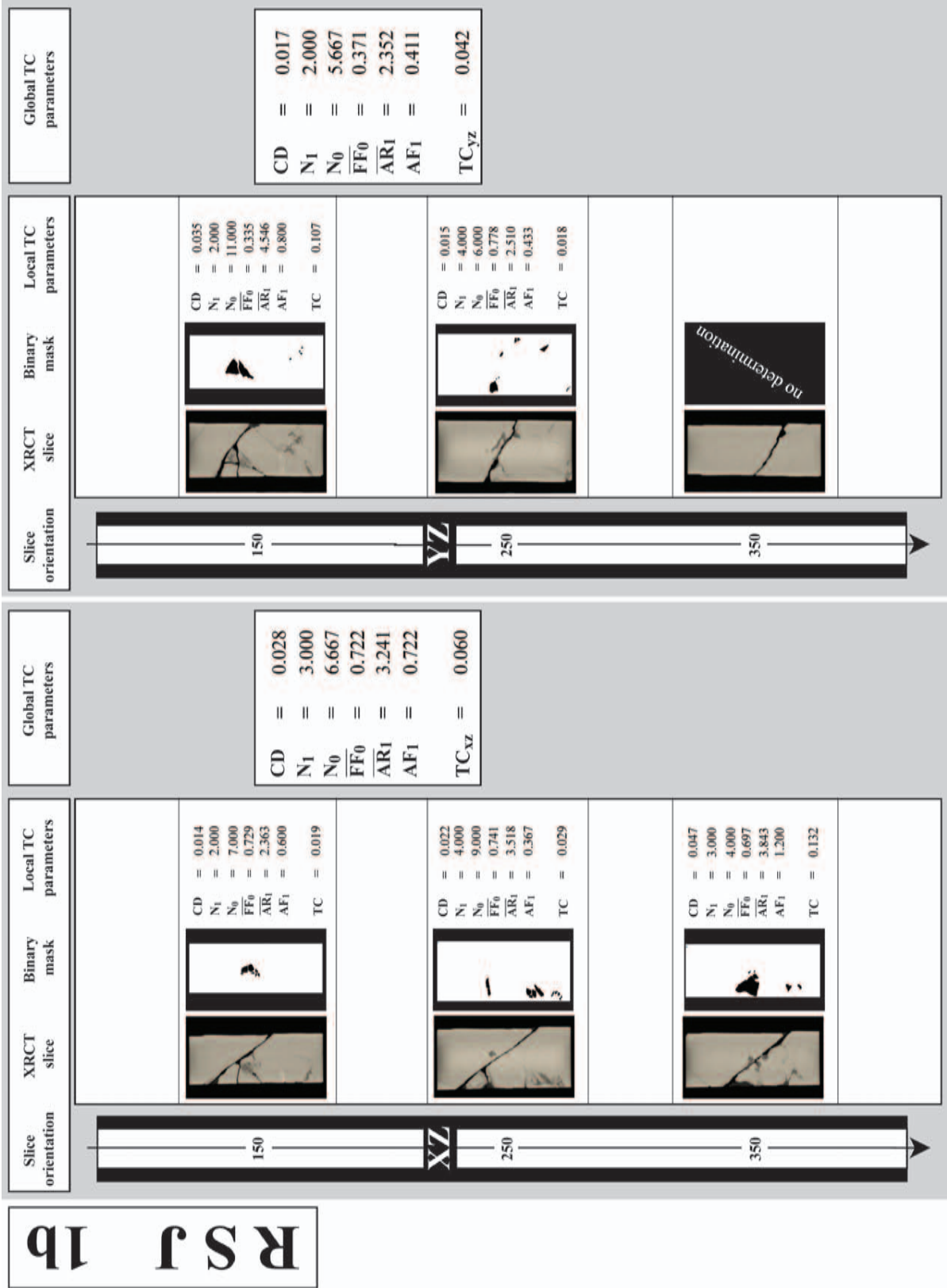
◆ RSJ 4 ◆ RSJ 11
 ◆ RSJ 6 ◆ RSJ 12

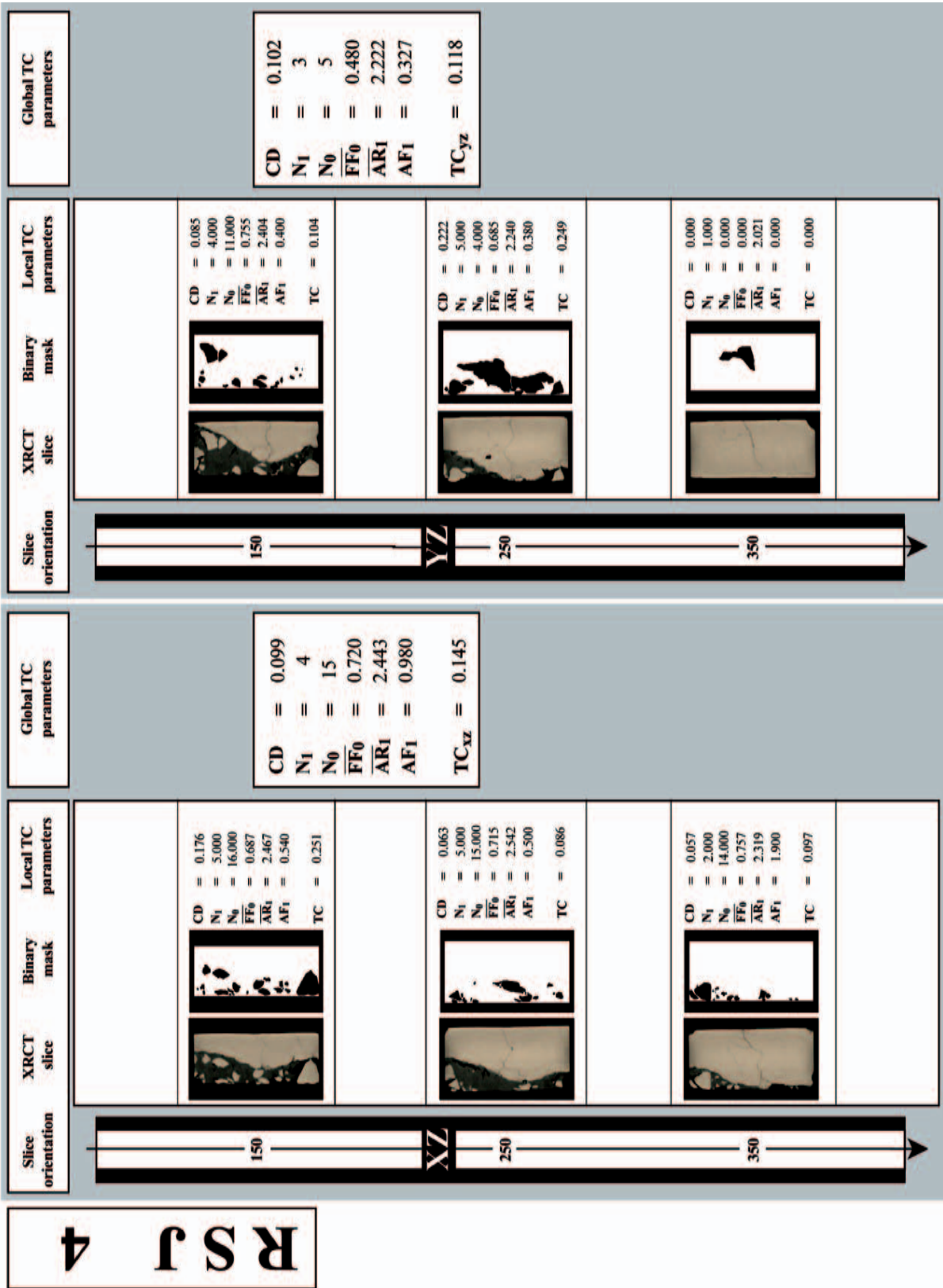


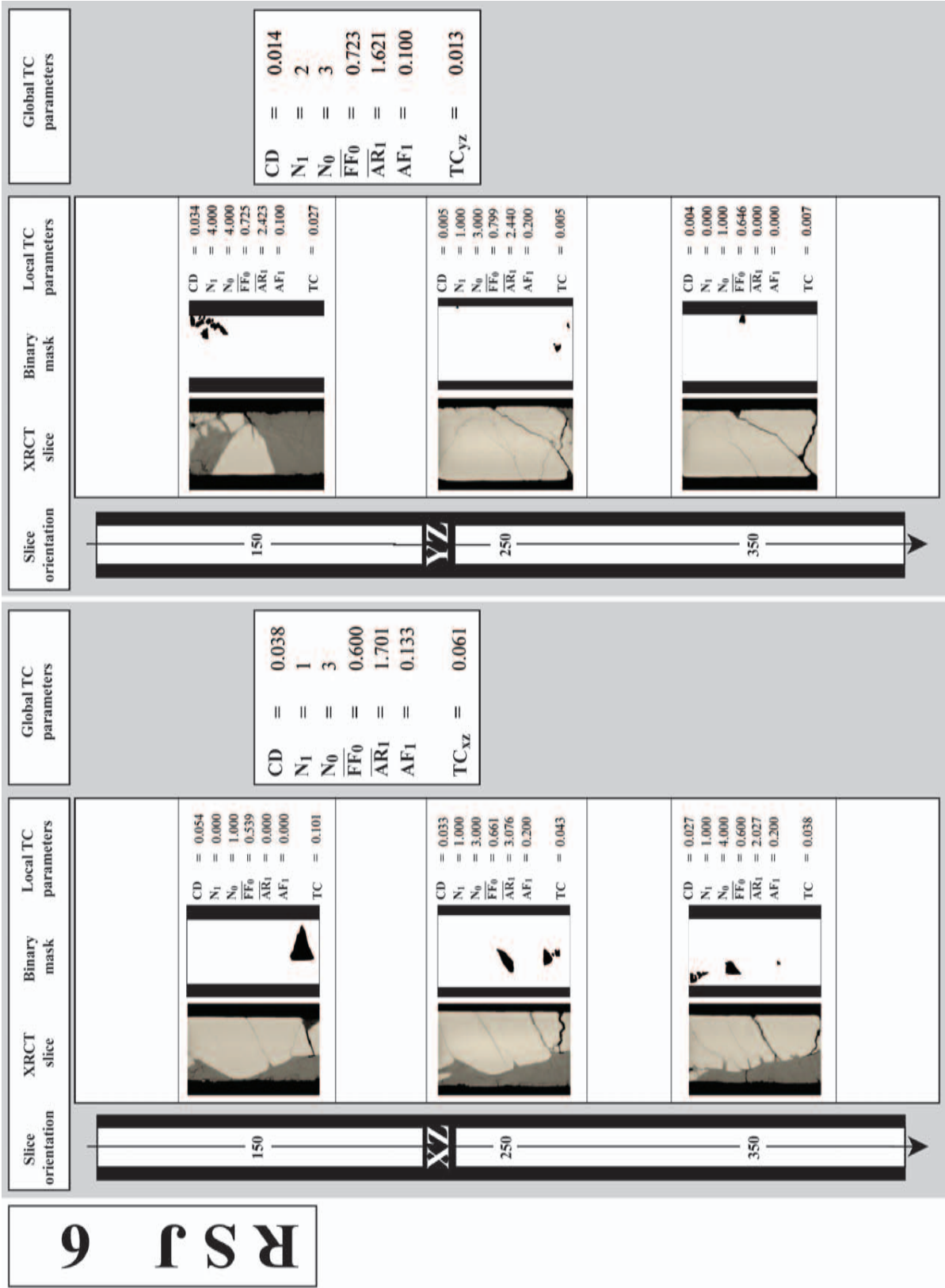
APPENDIX IV-I

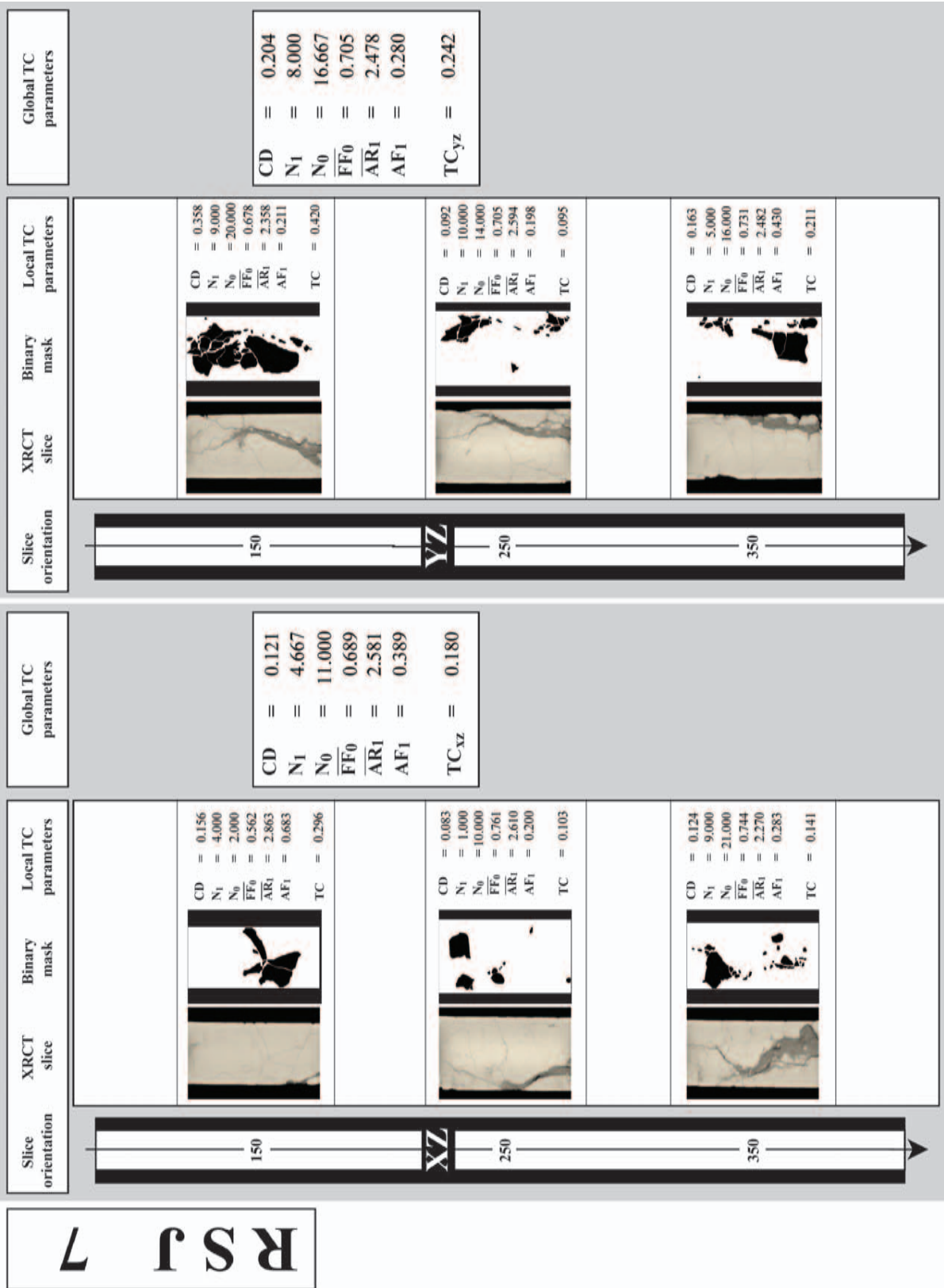
(Appendix related to Chap. 11 & 13)

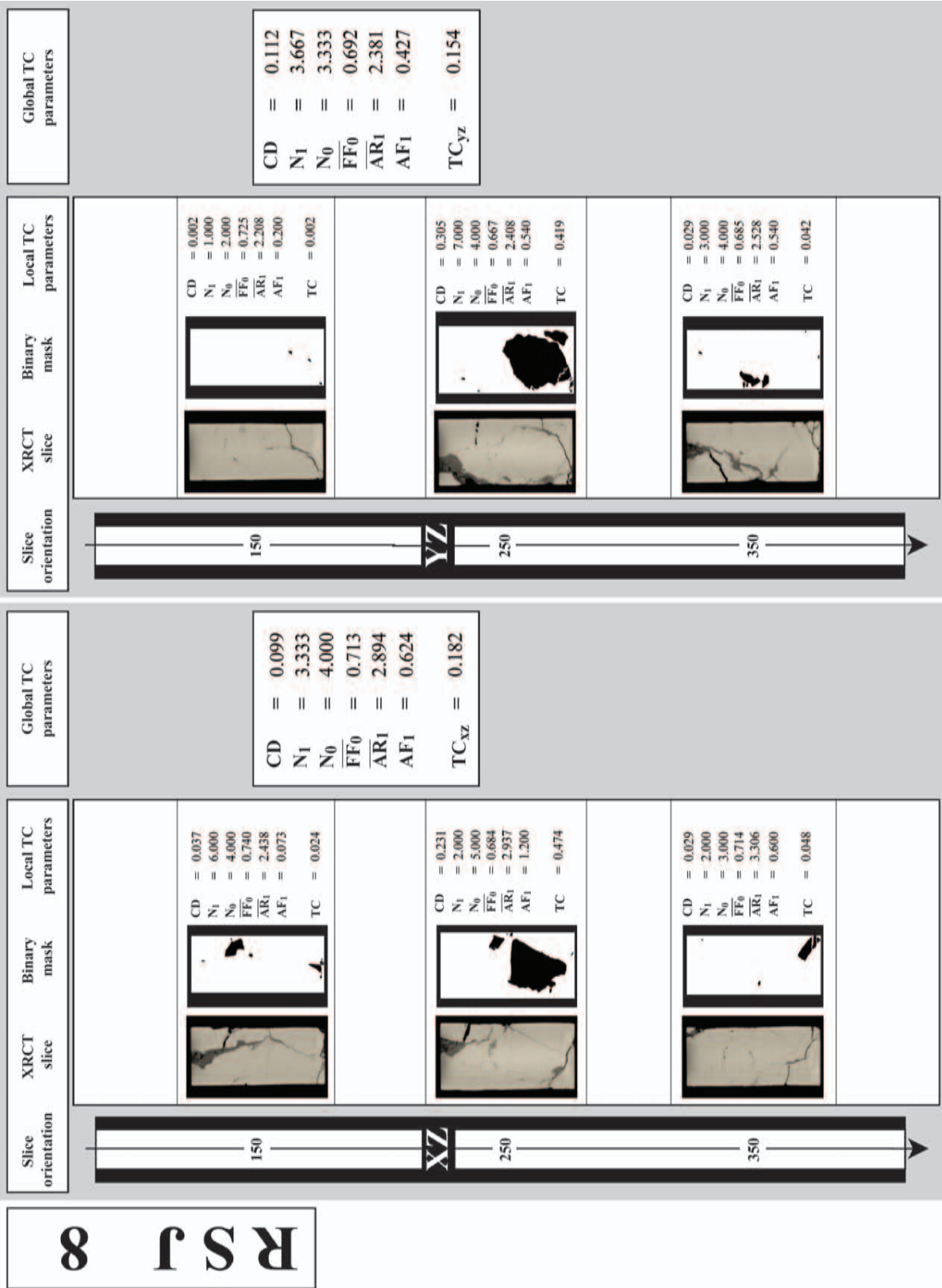
DETERMINATION OF TC BASED ON FRONTAL AND SAGITTAL CT-SLICES

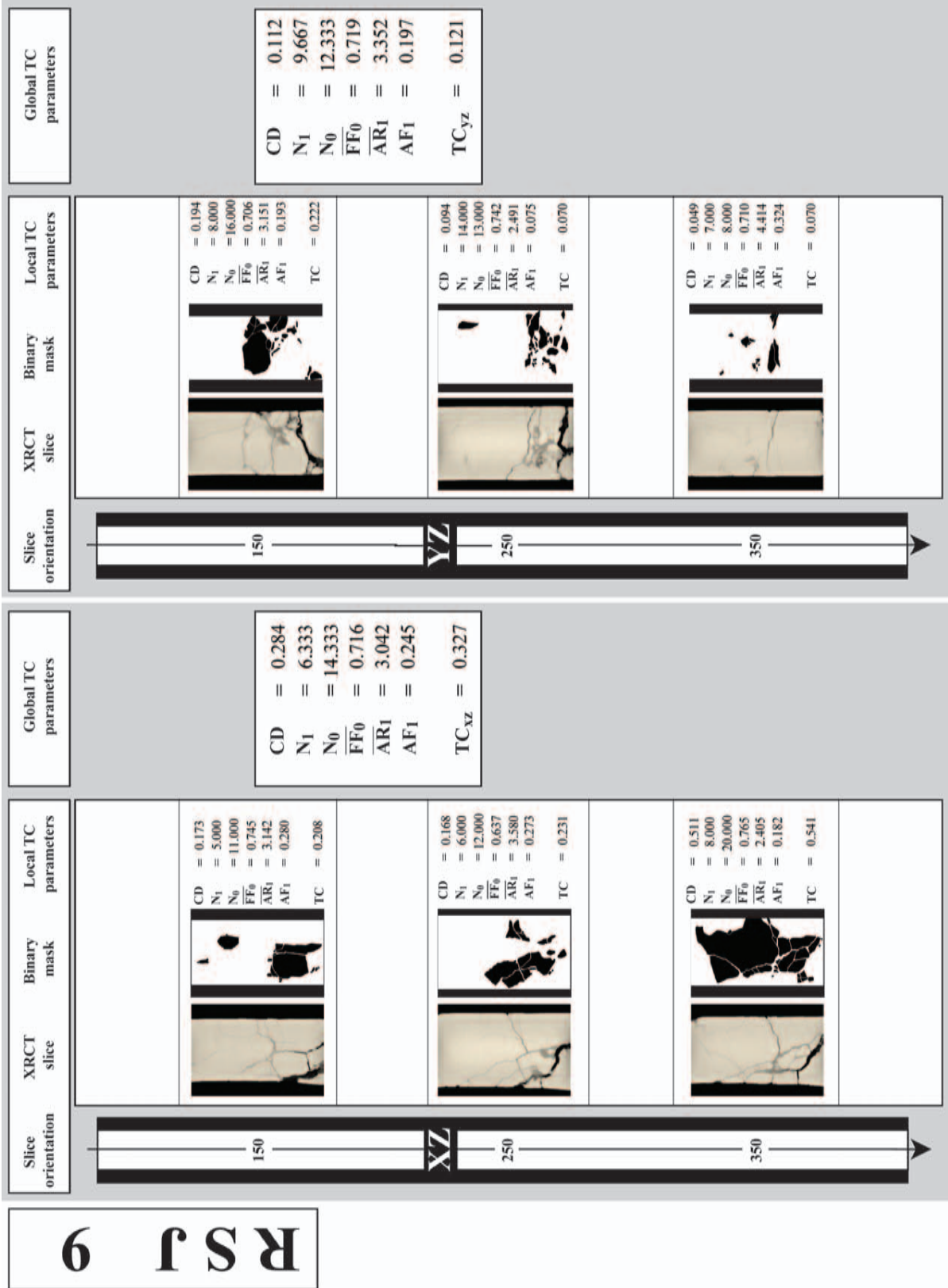


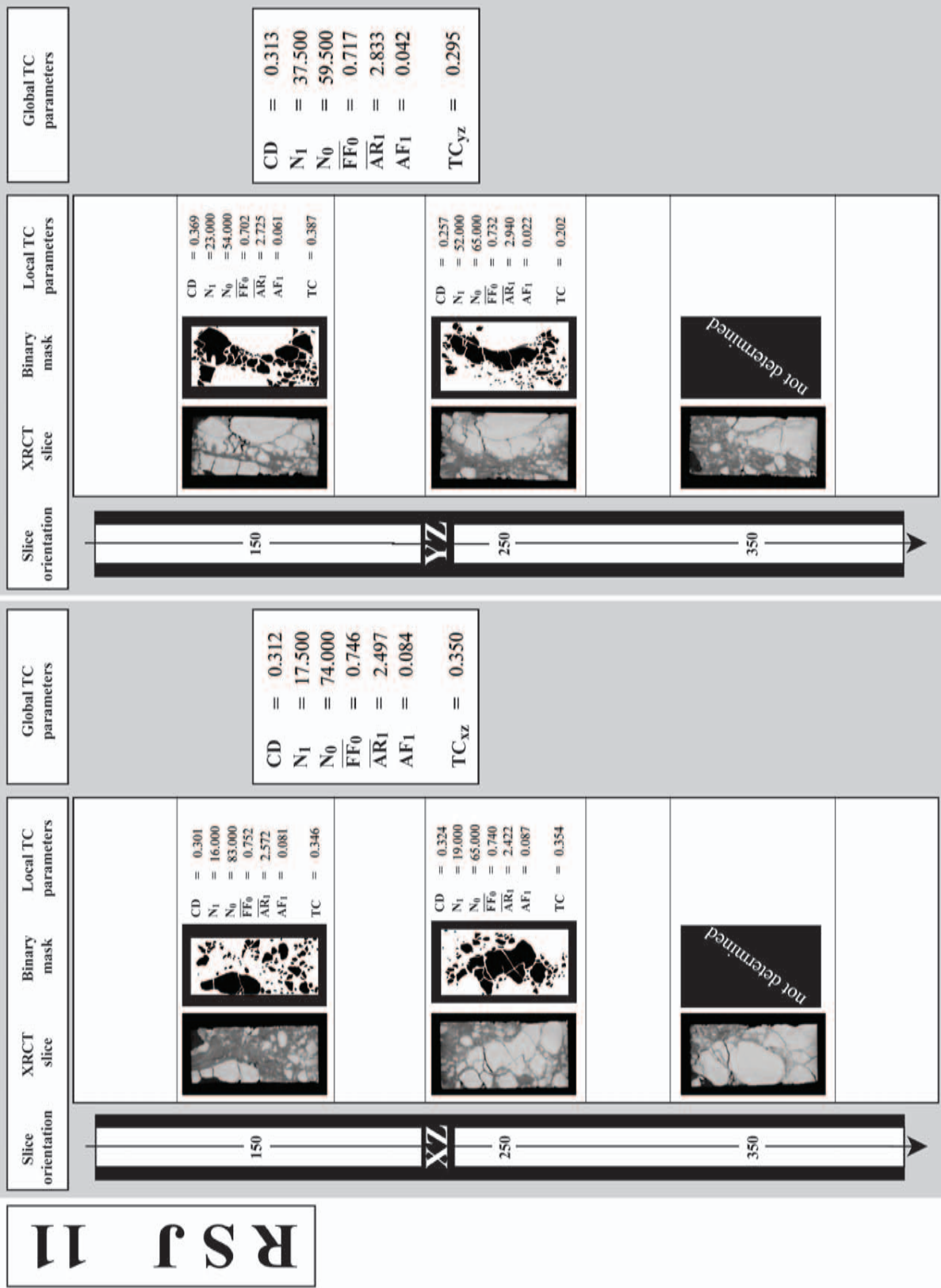


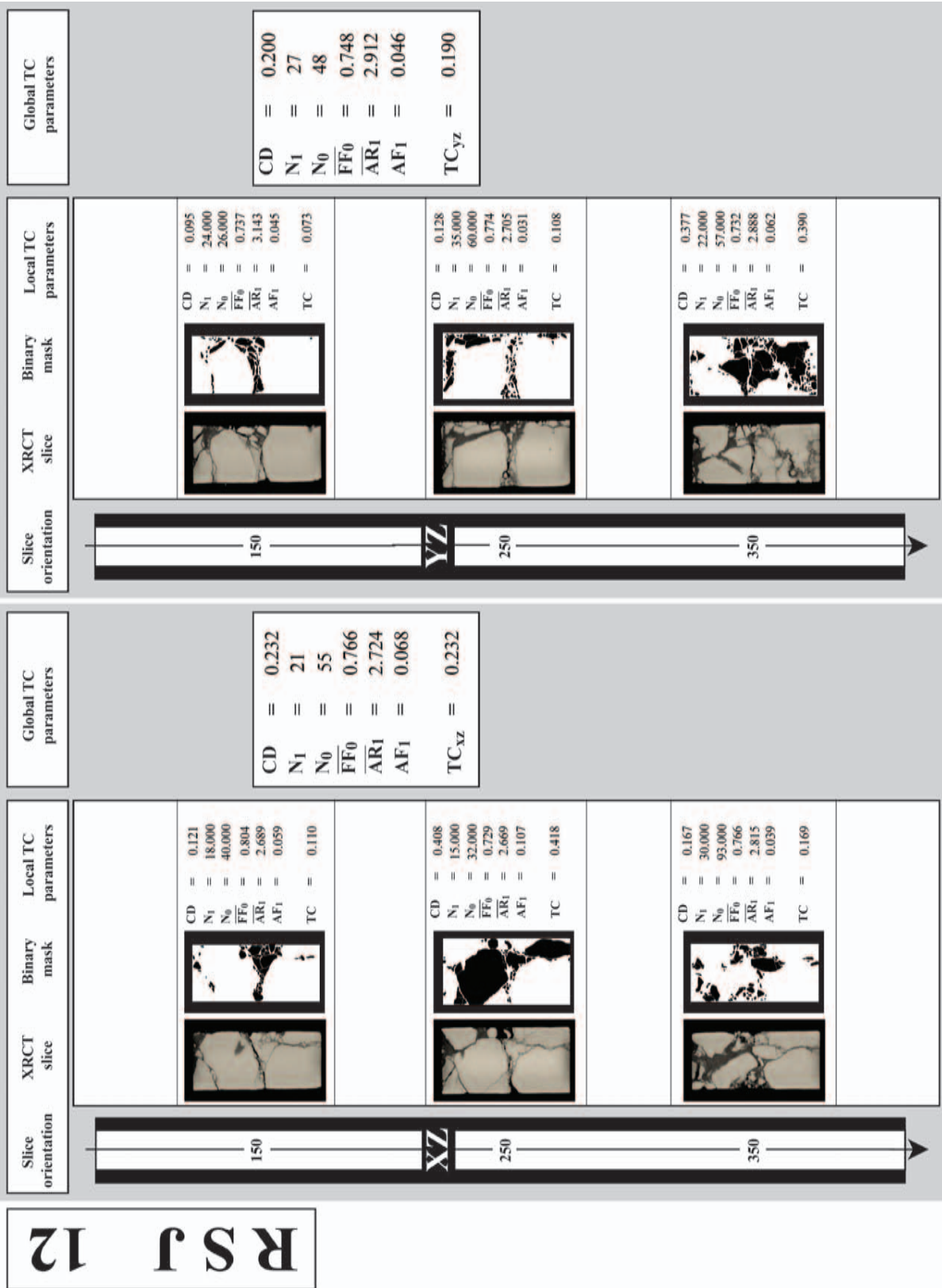








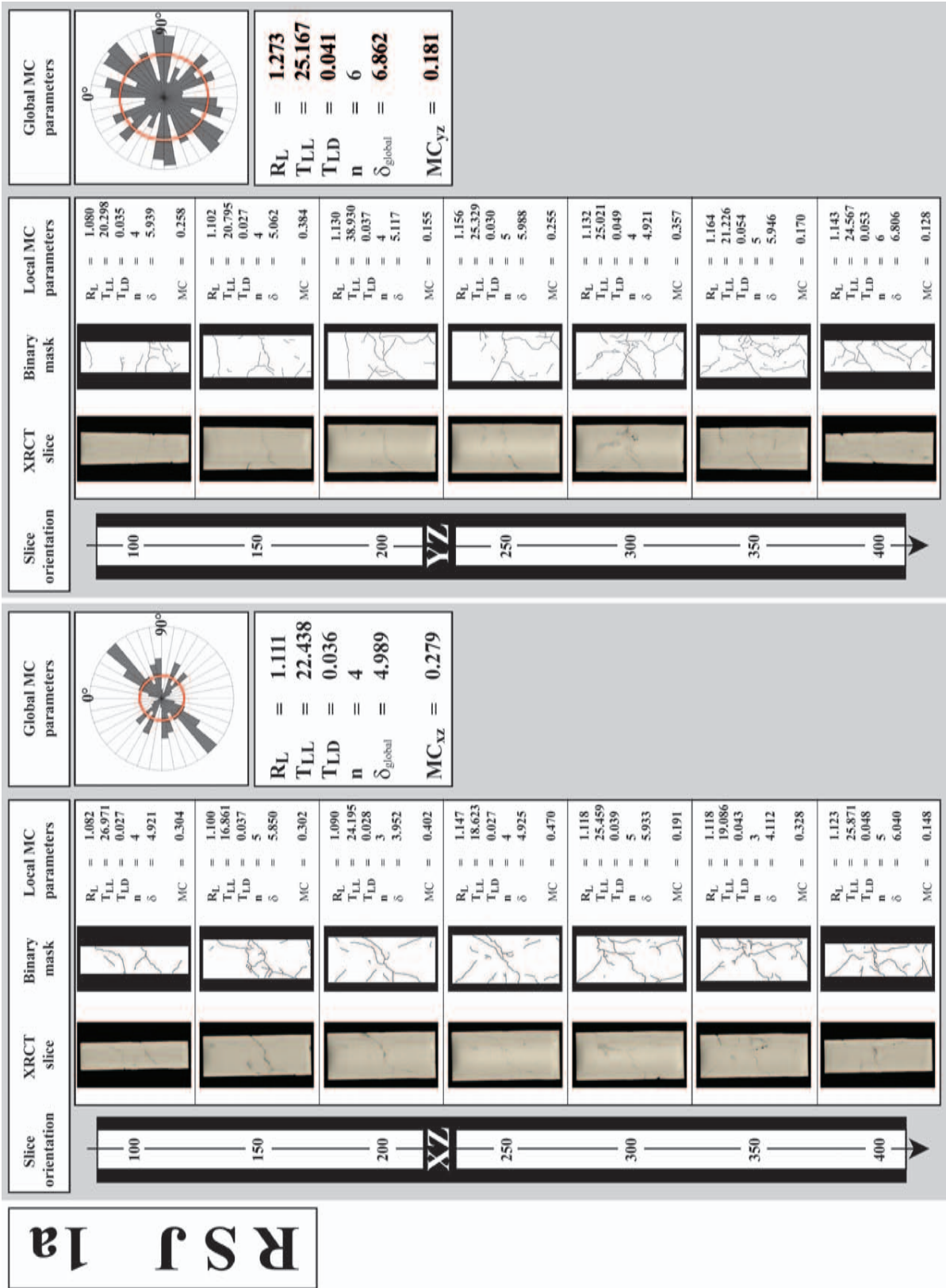


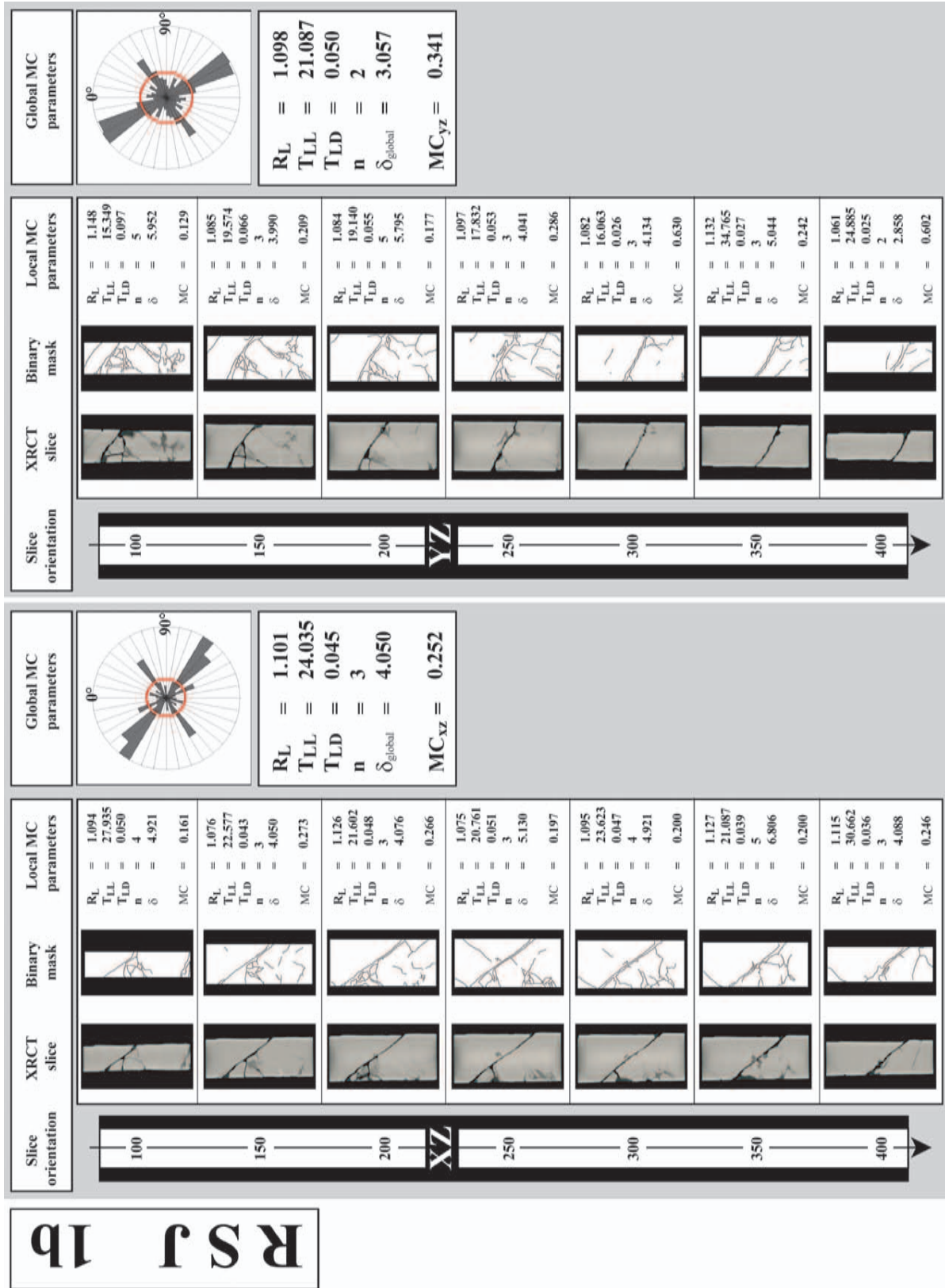


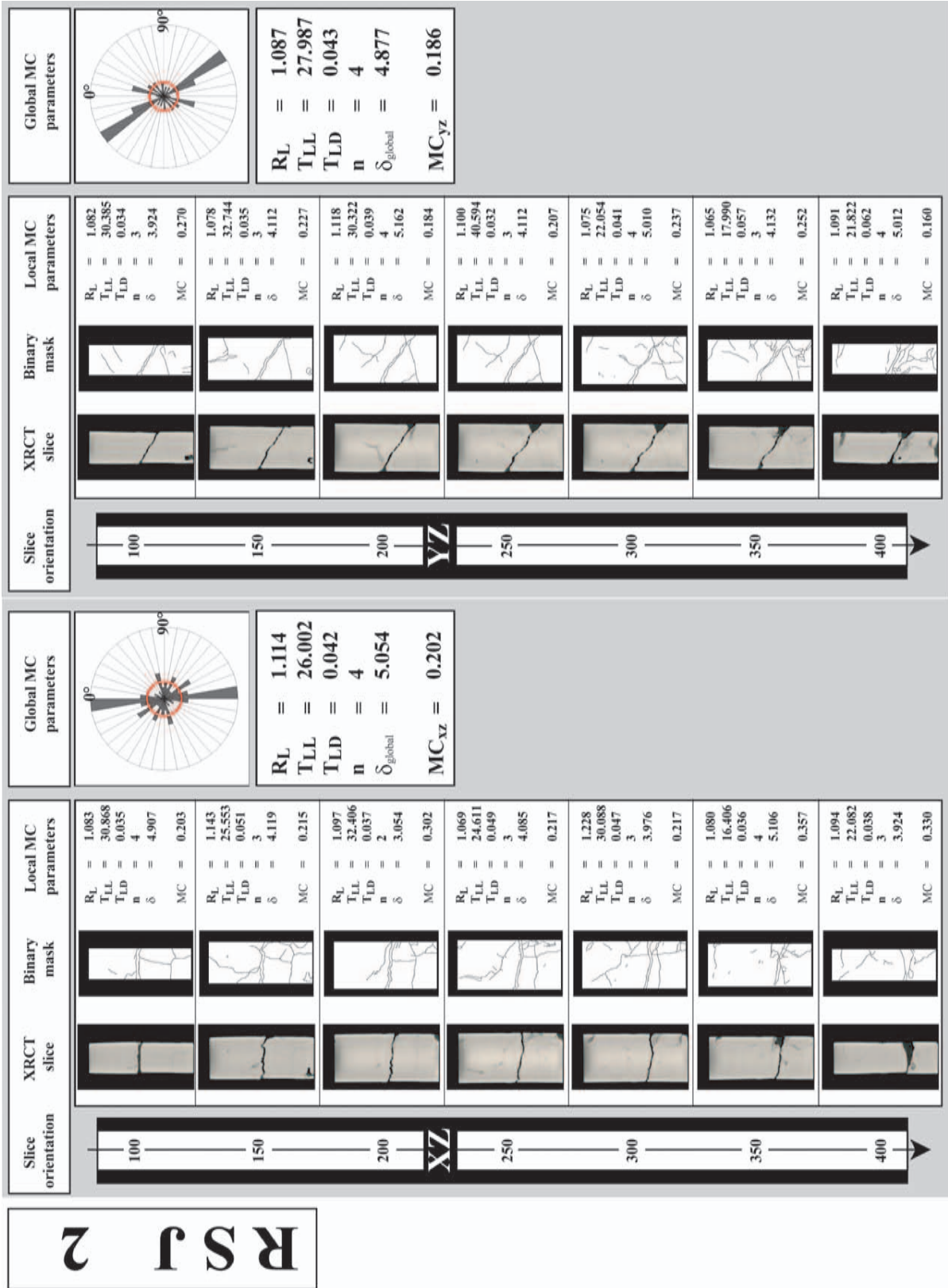
APPENDIX IV-II

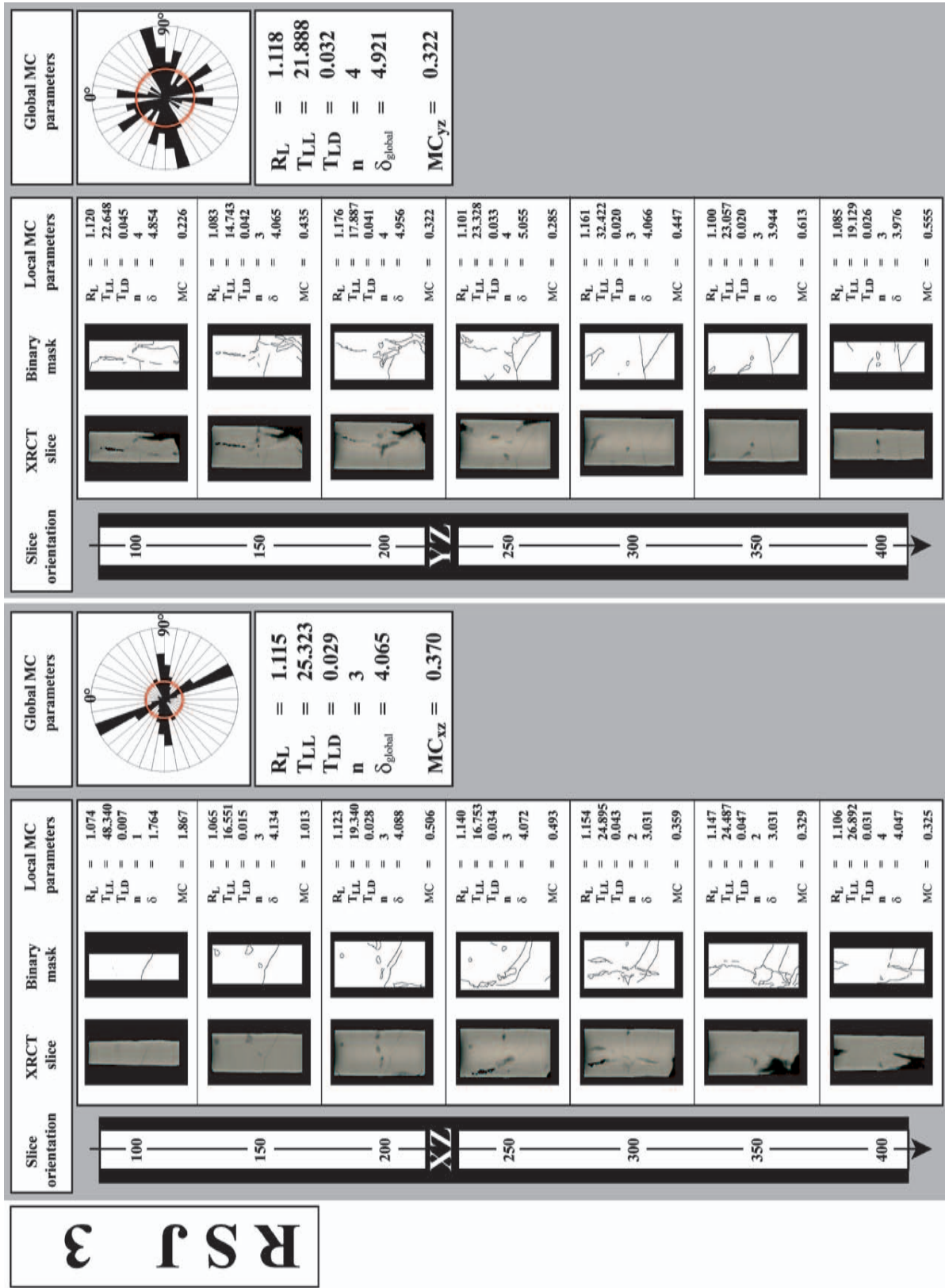
(Appendix related to Chap. 11 & 13)

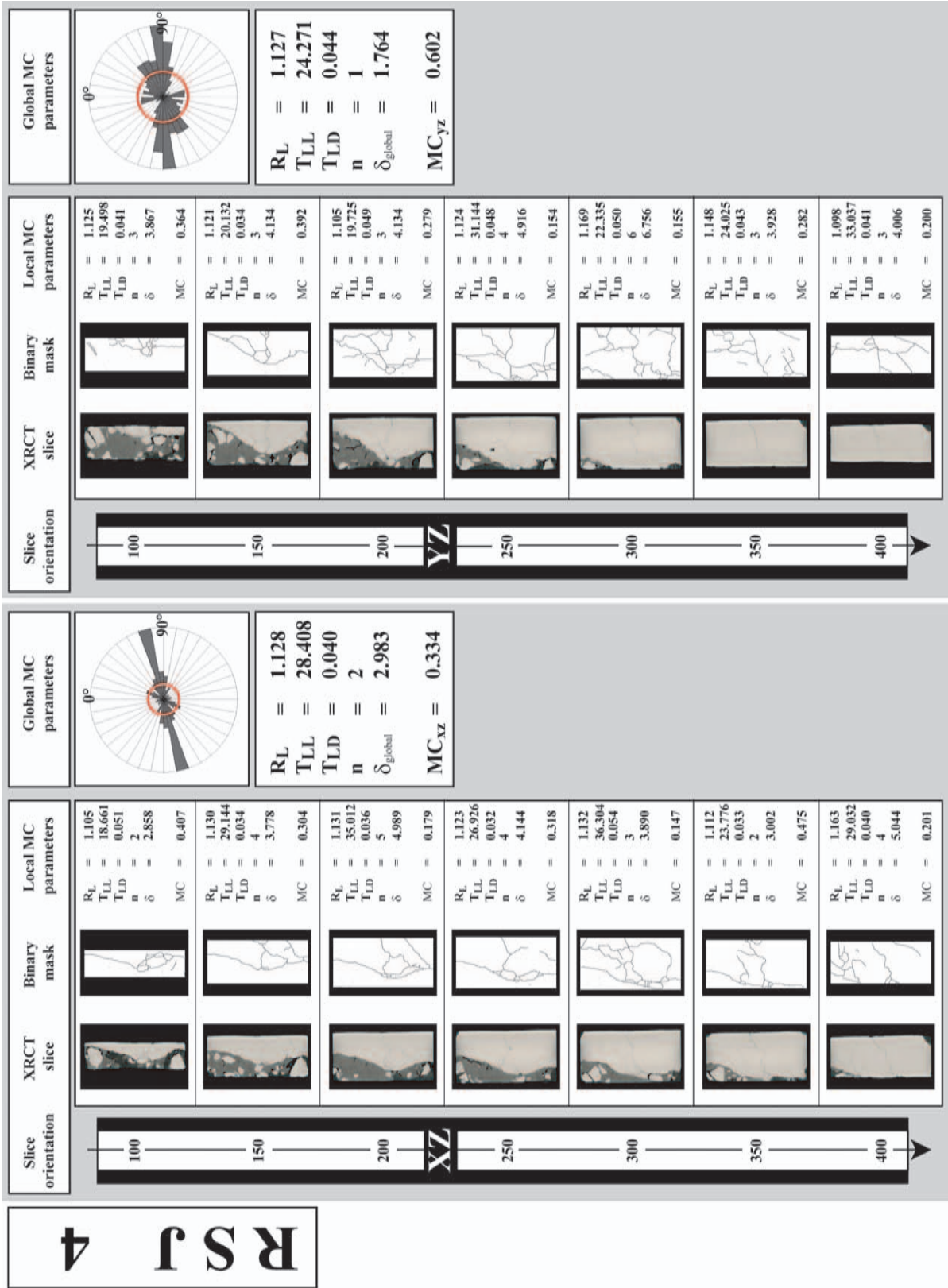
DETERMINATION OF MC BASED ON FRONTAL AND SAGITTAL CT-SLICES

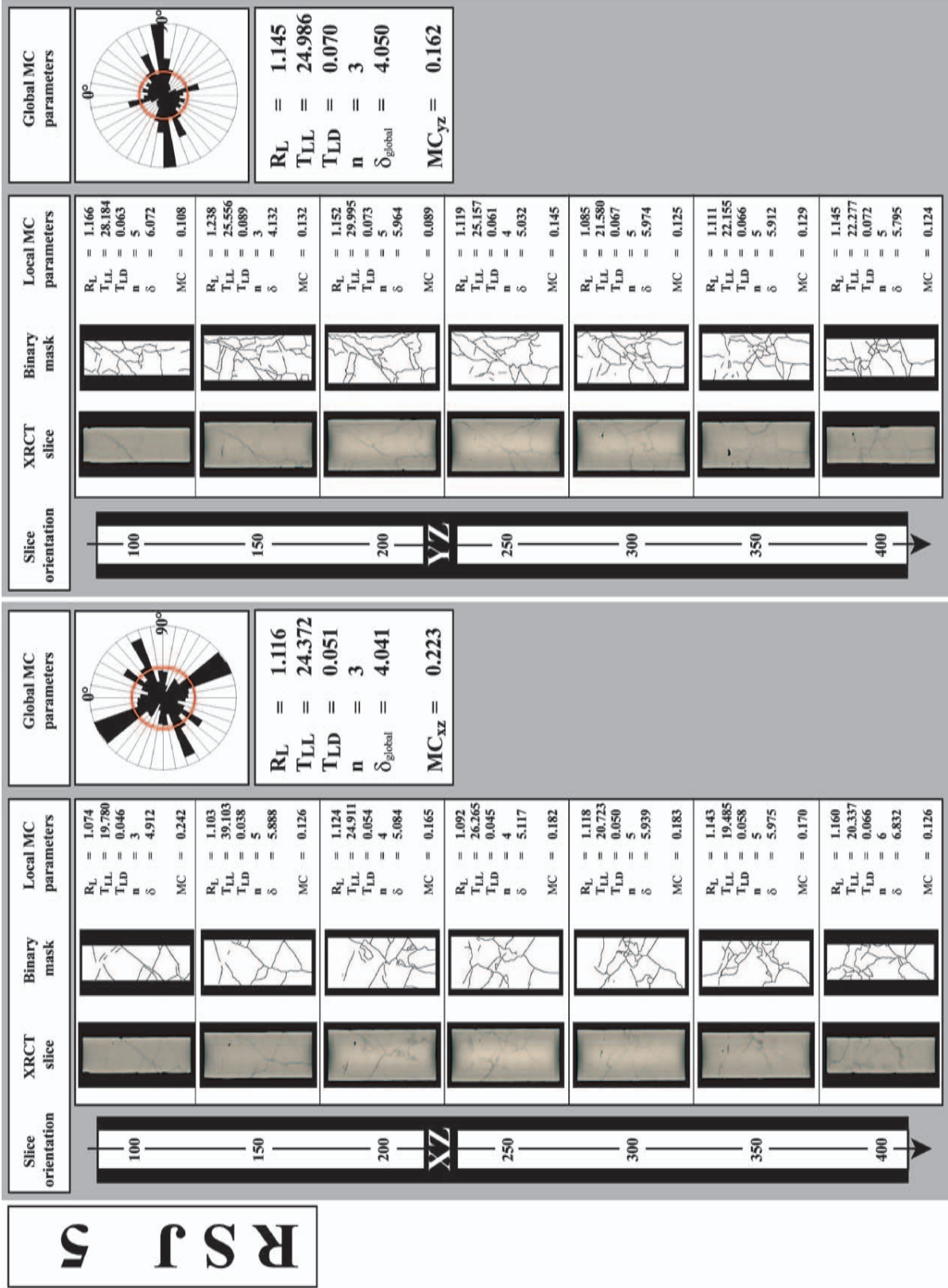


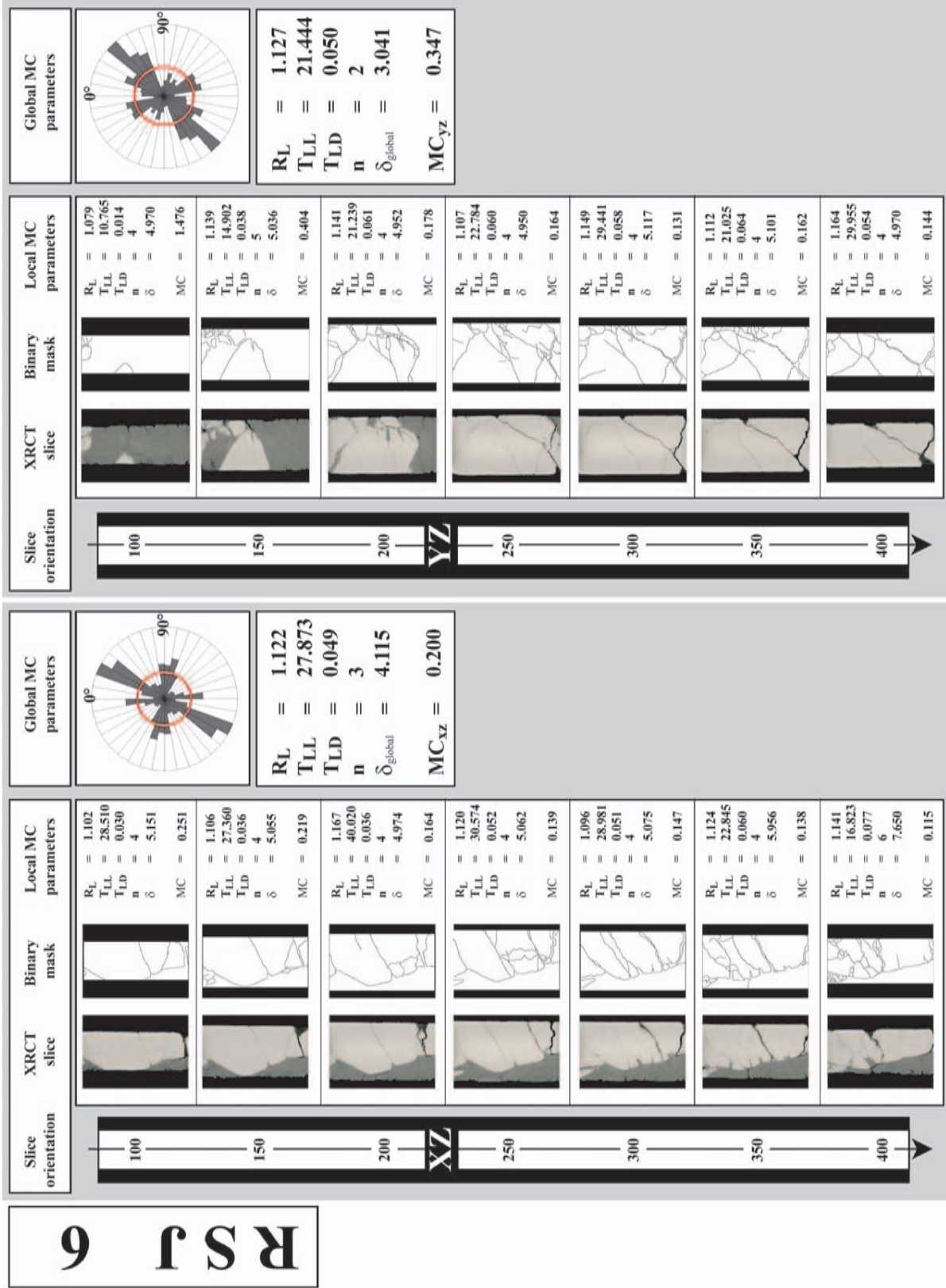


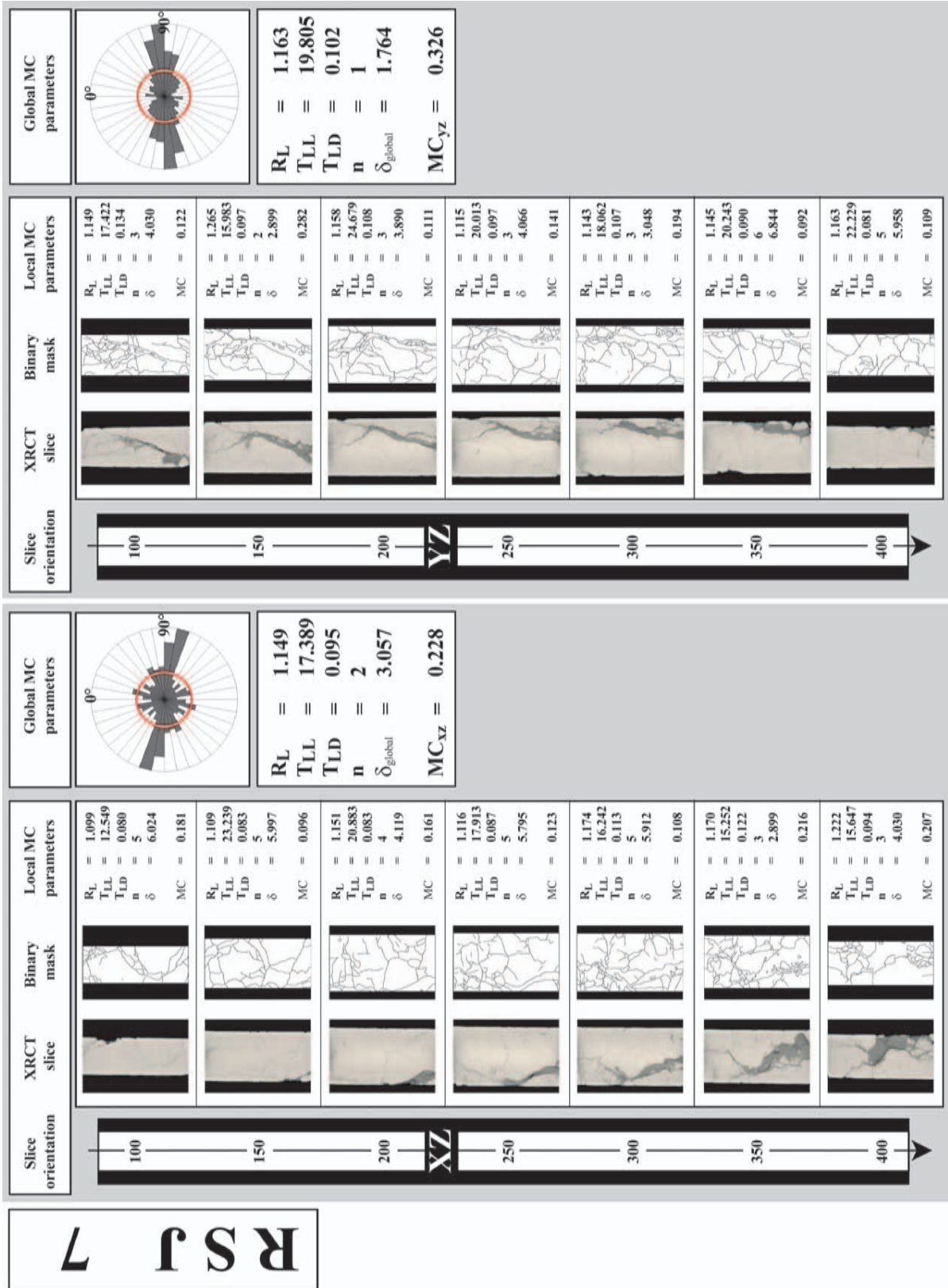


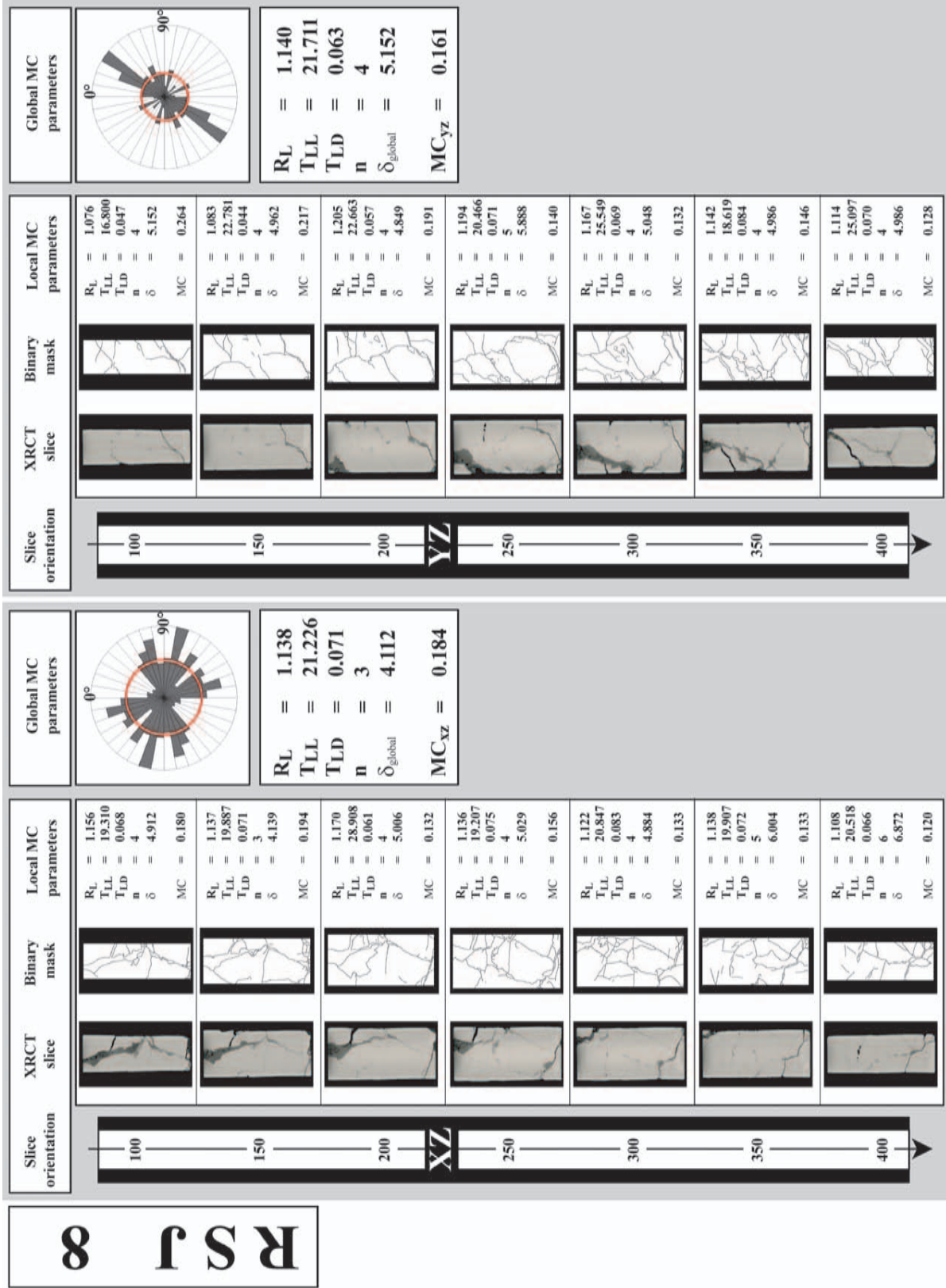


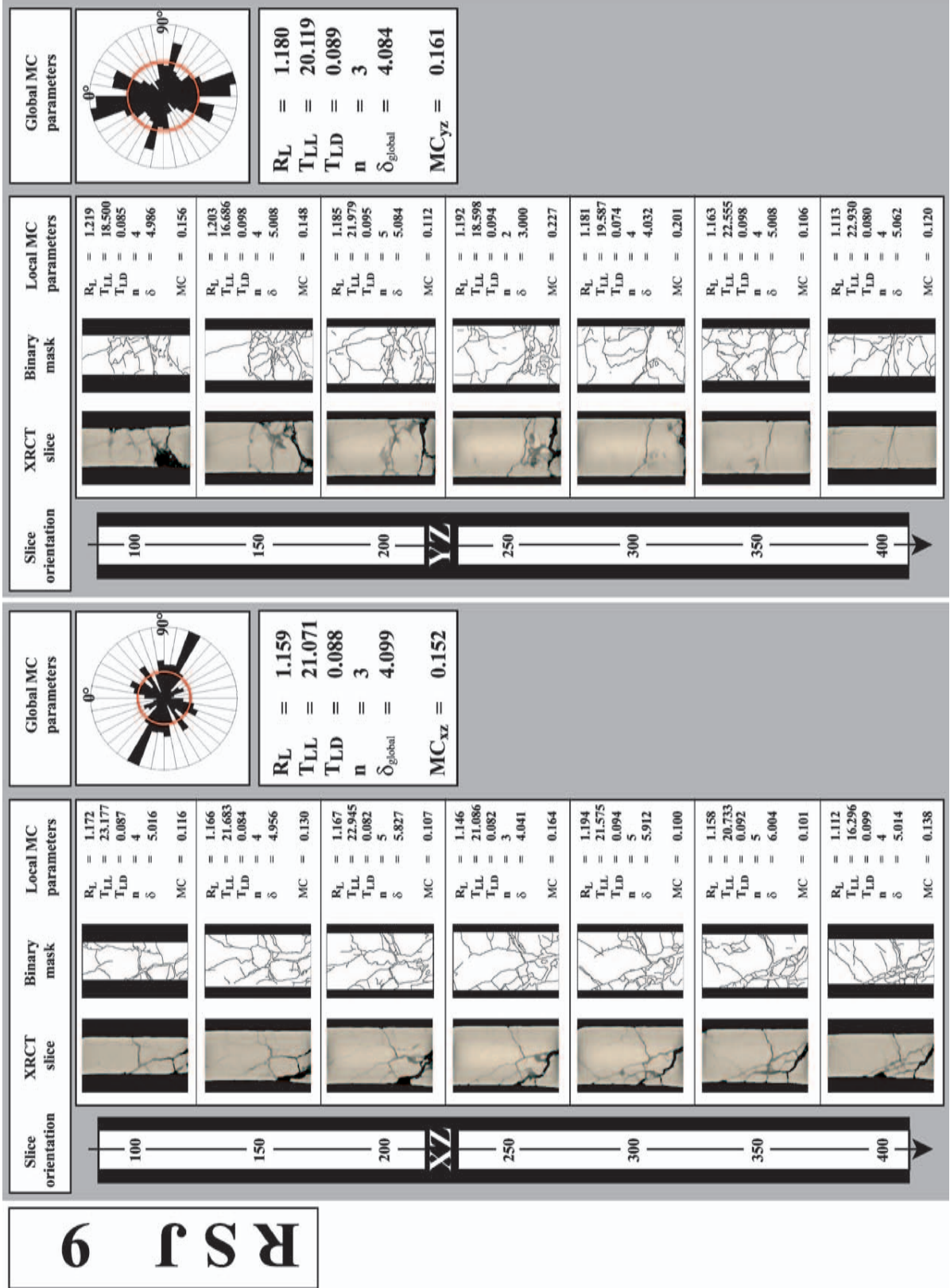


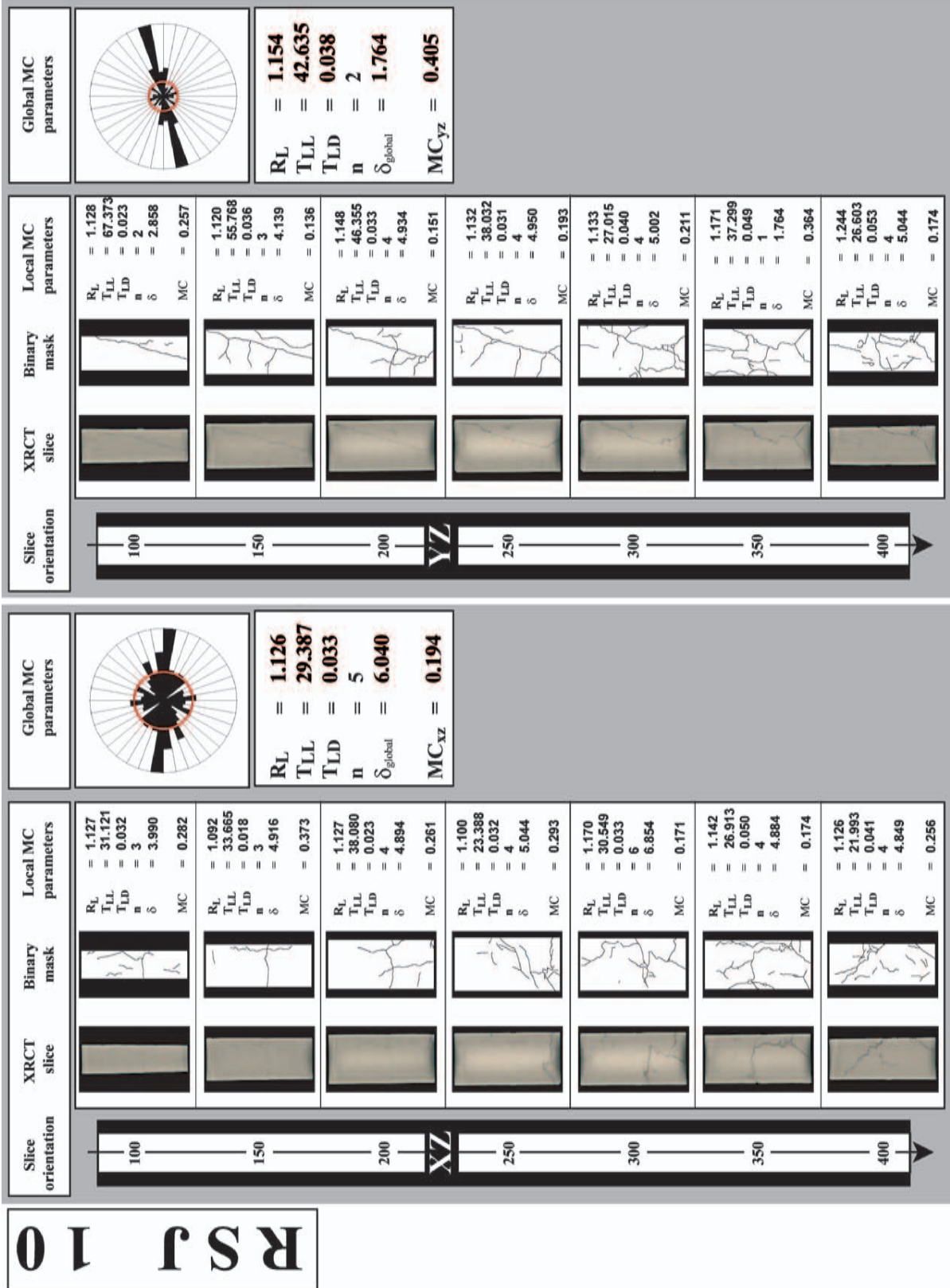


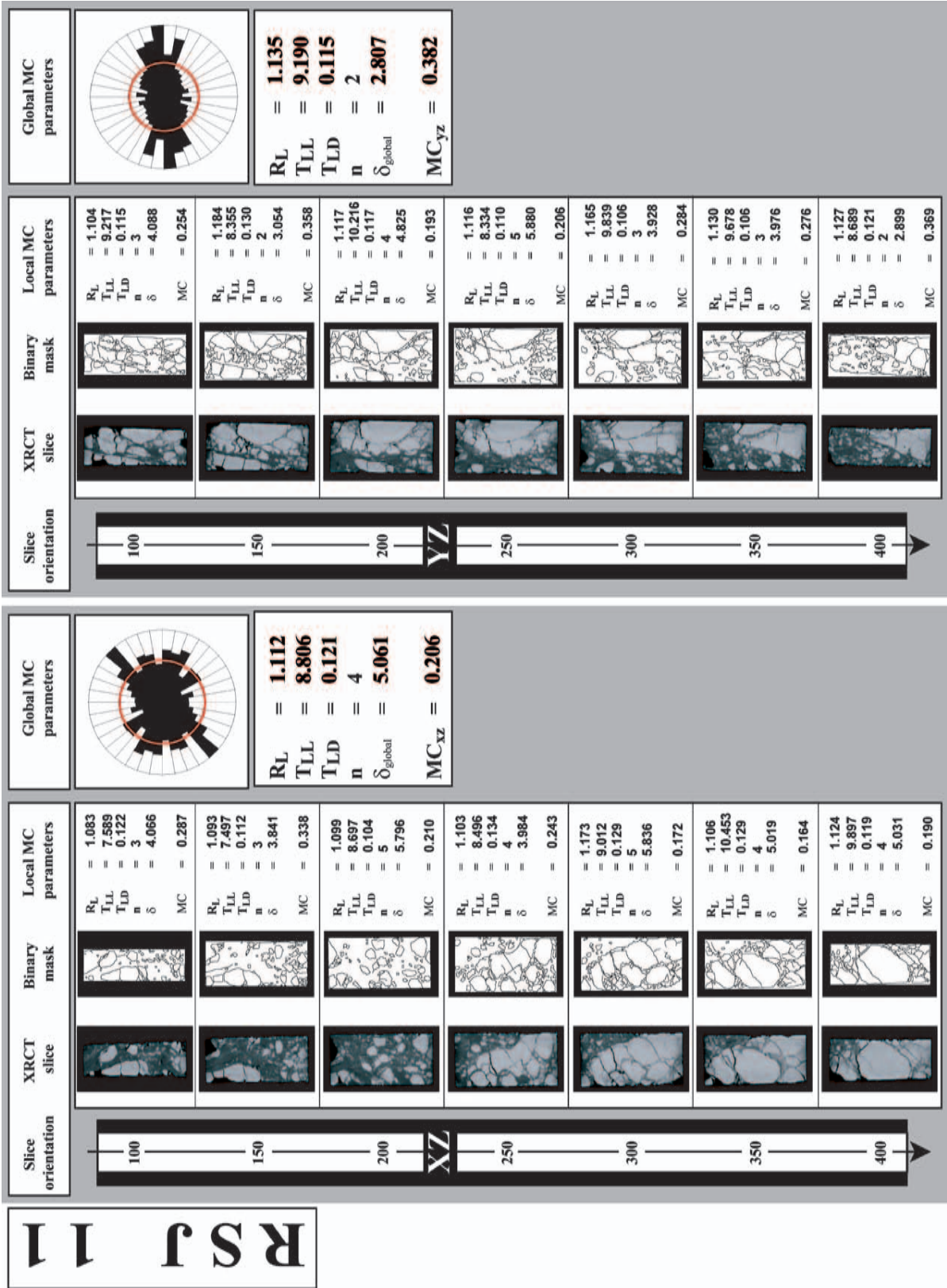


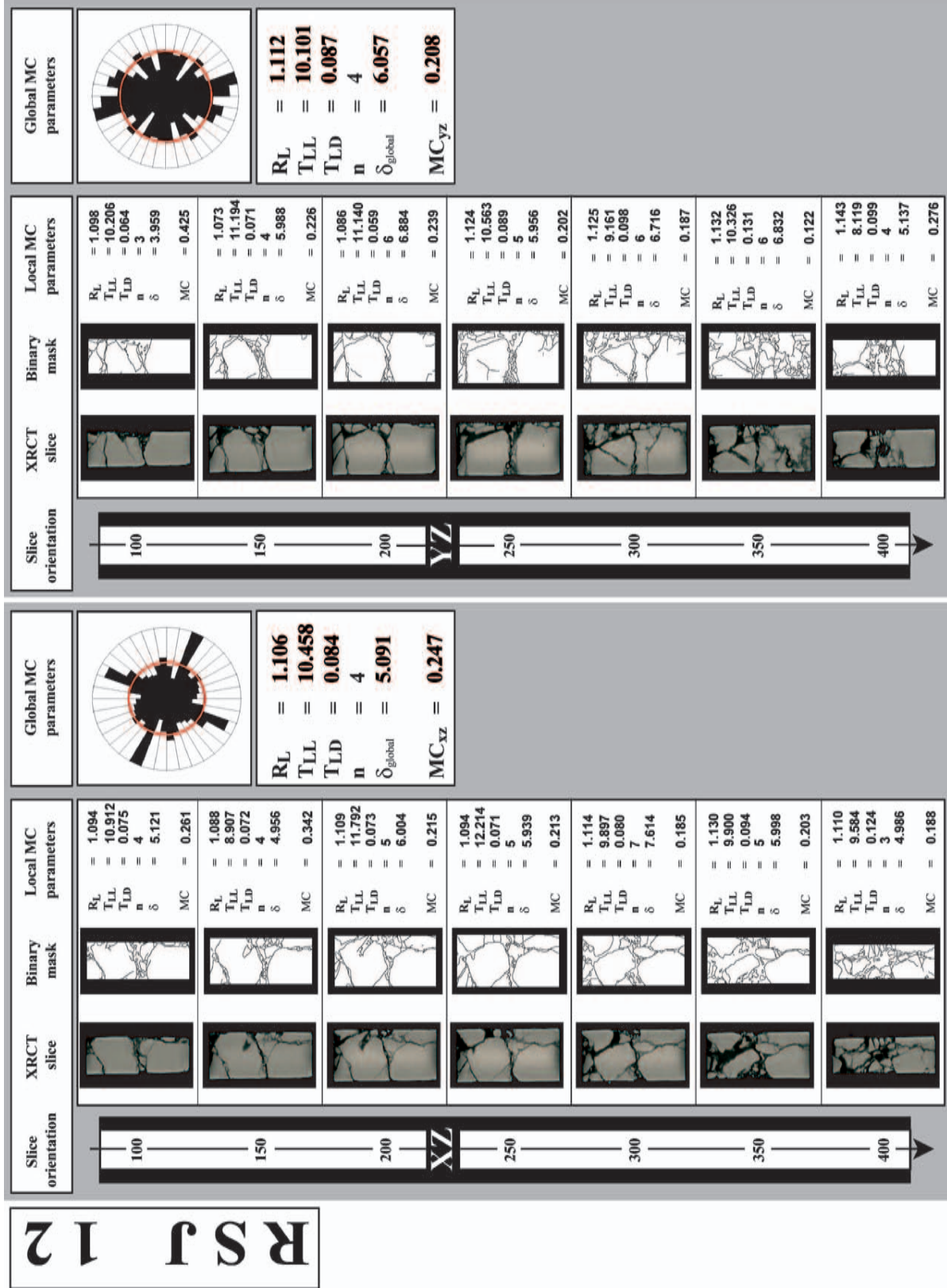








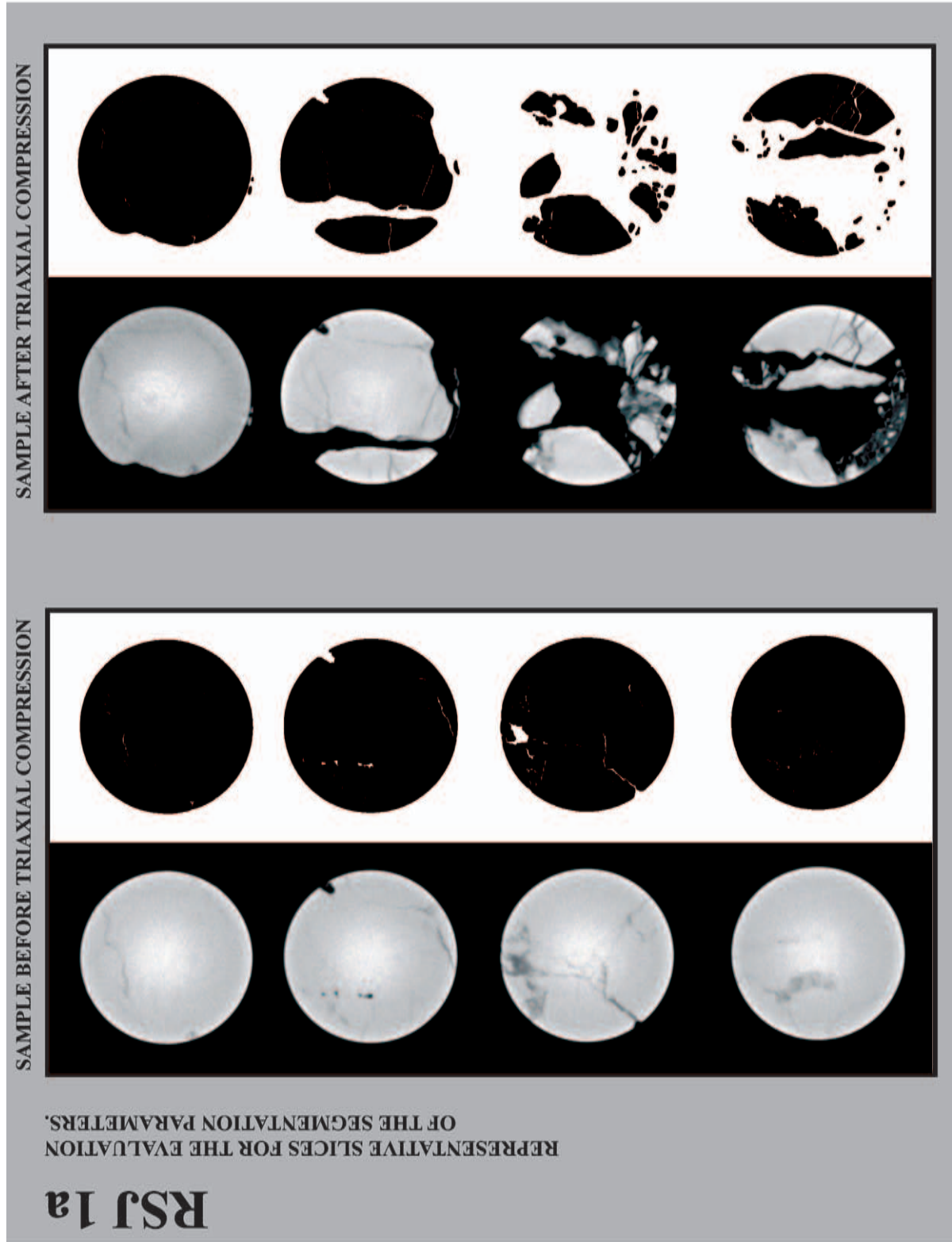


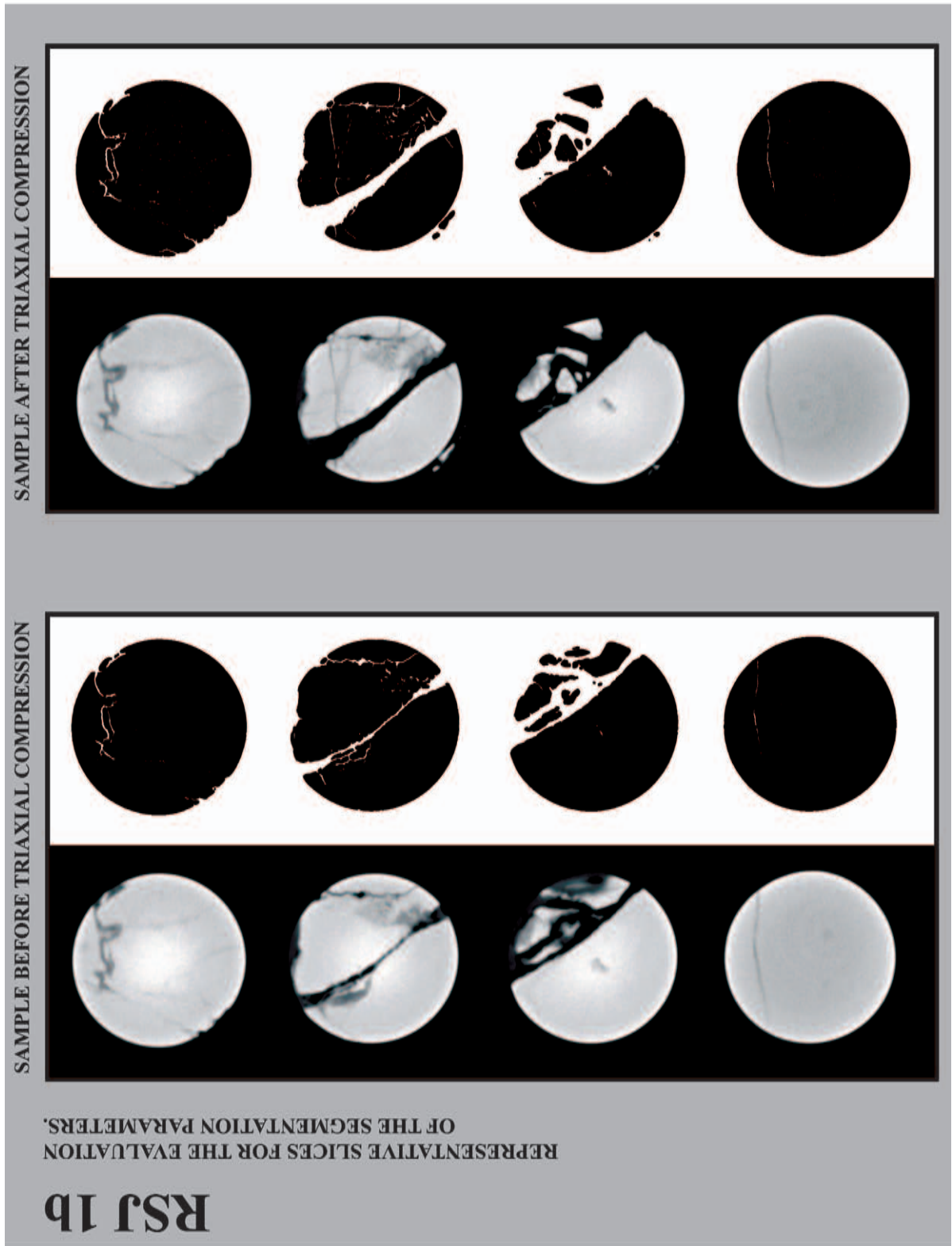


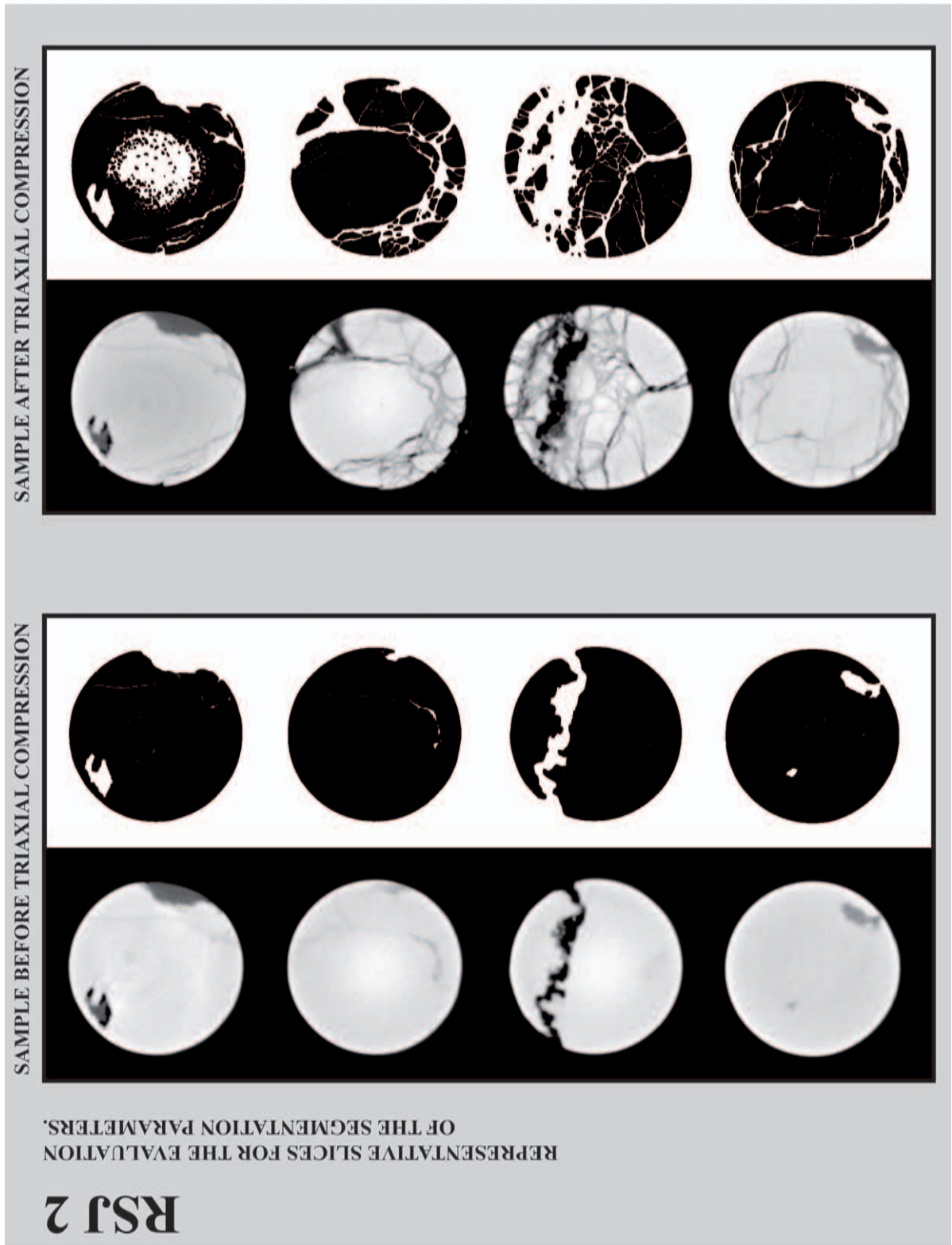
APPENDIX IV-III

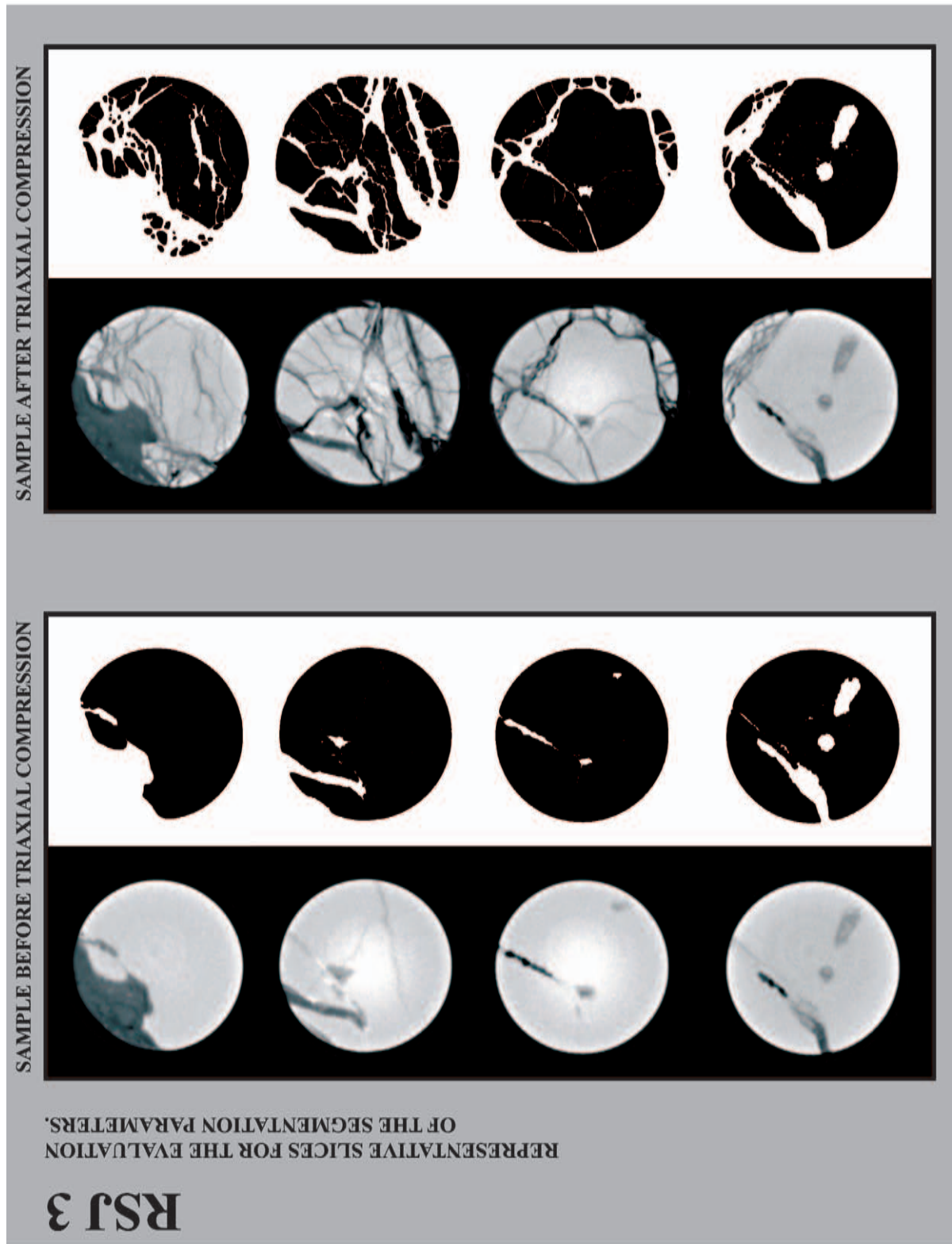
(Appendix related to Chap. 11 & 12)

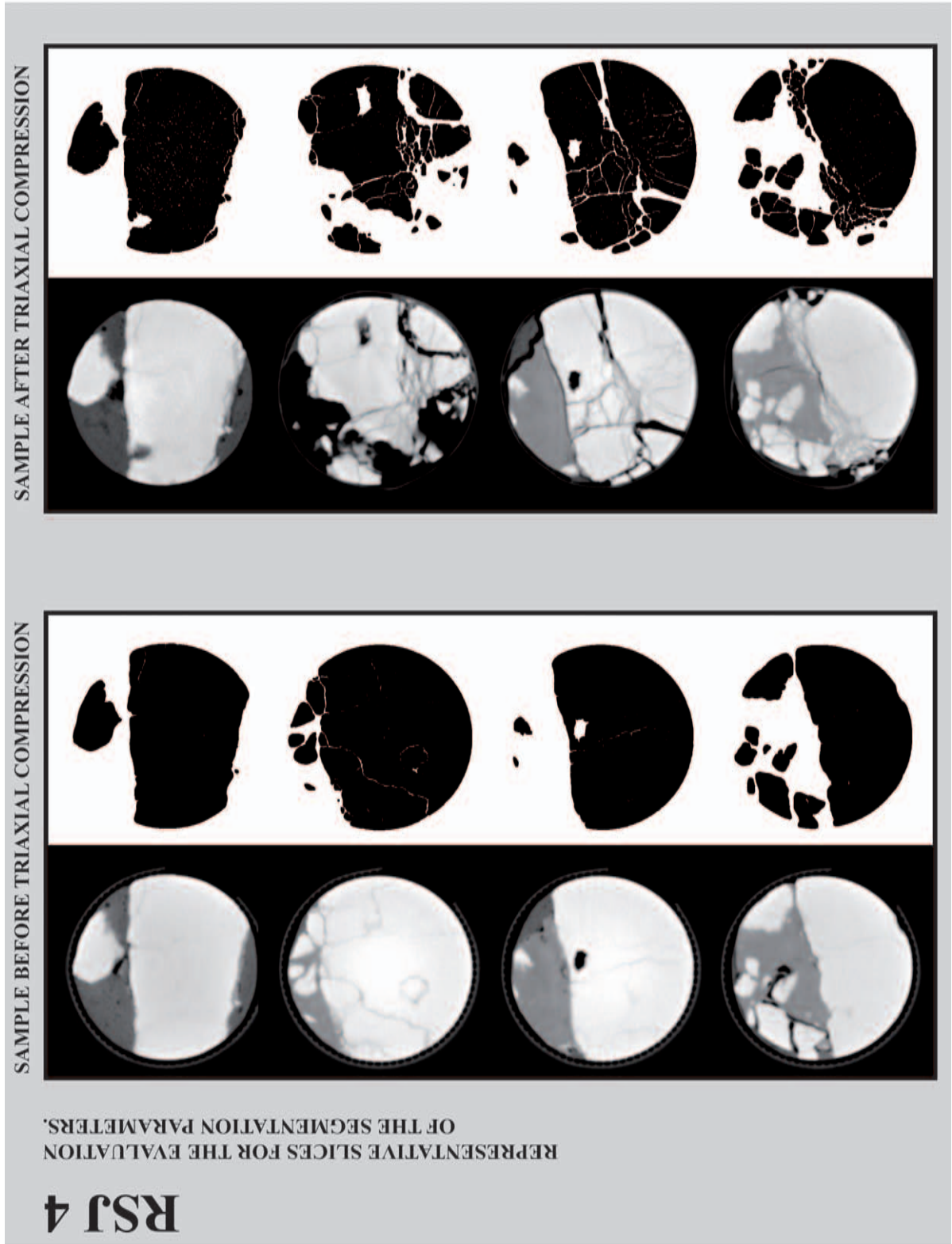
CT-SLICES USED FOR CALIBRATION OF THE BEST-FIT SEGMENTATION OF THE RSJ XRCT DATA

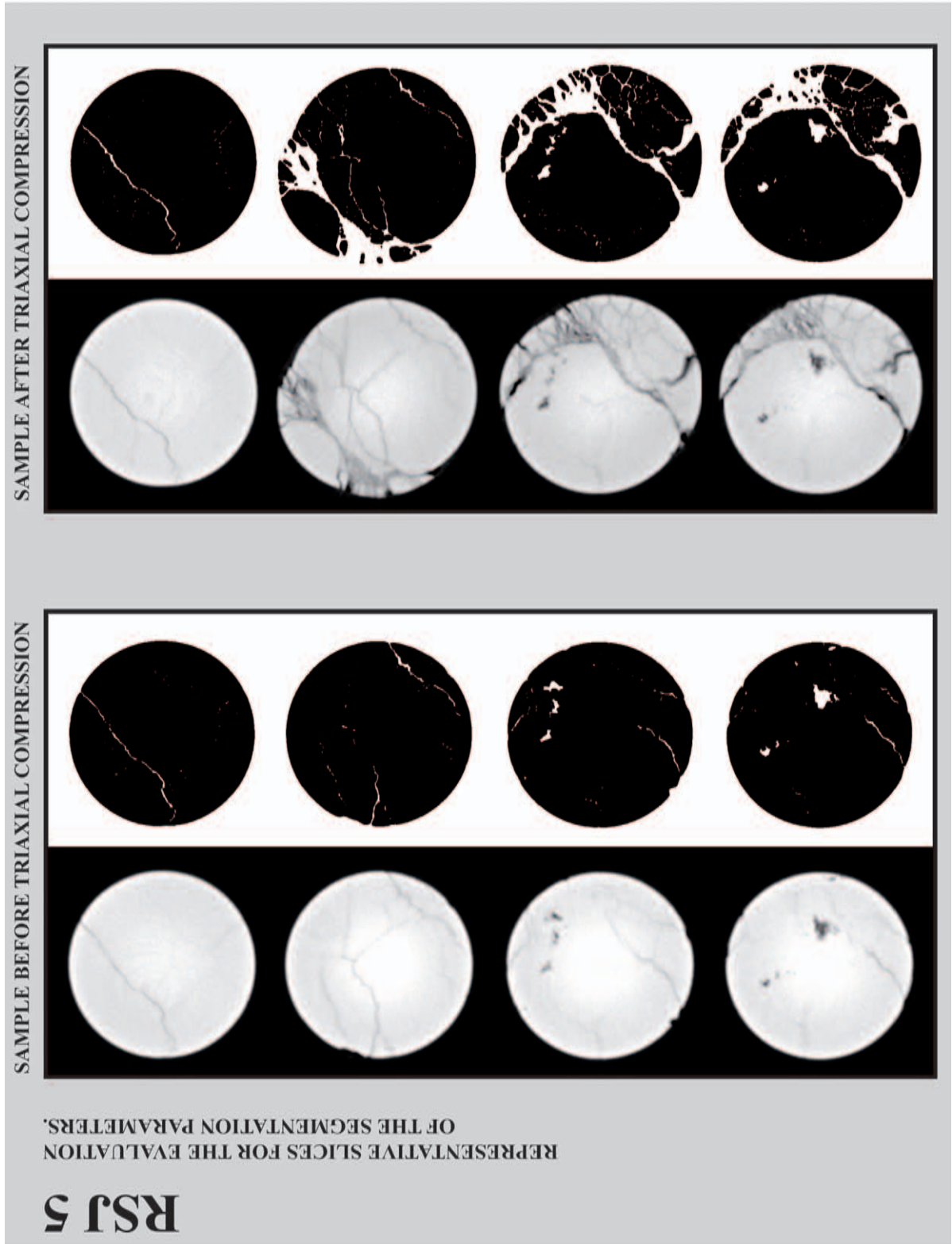


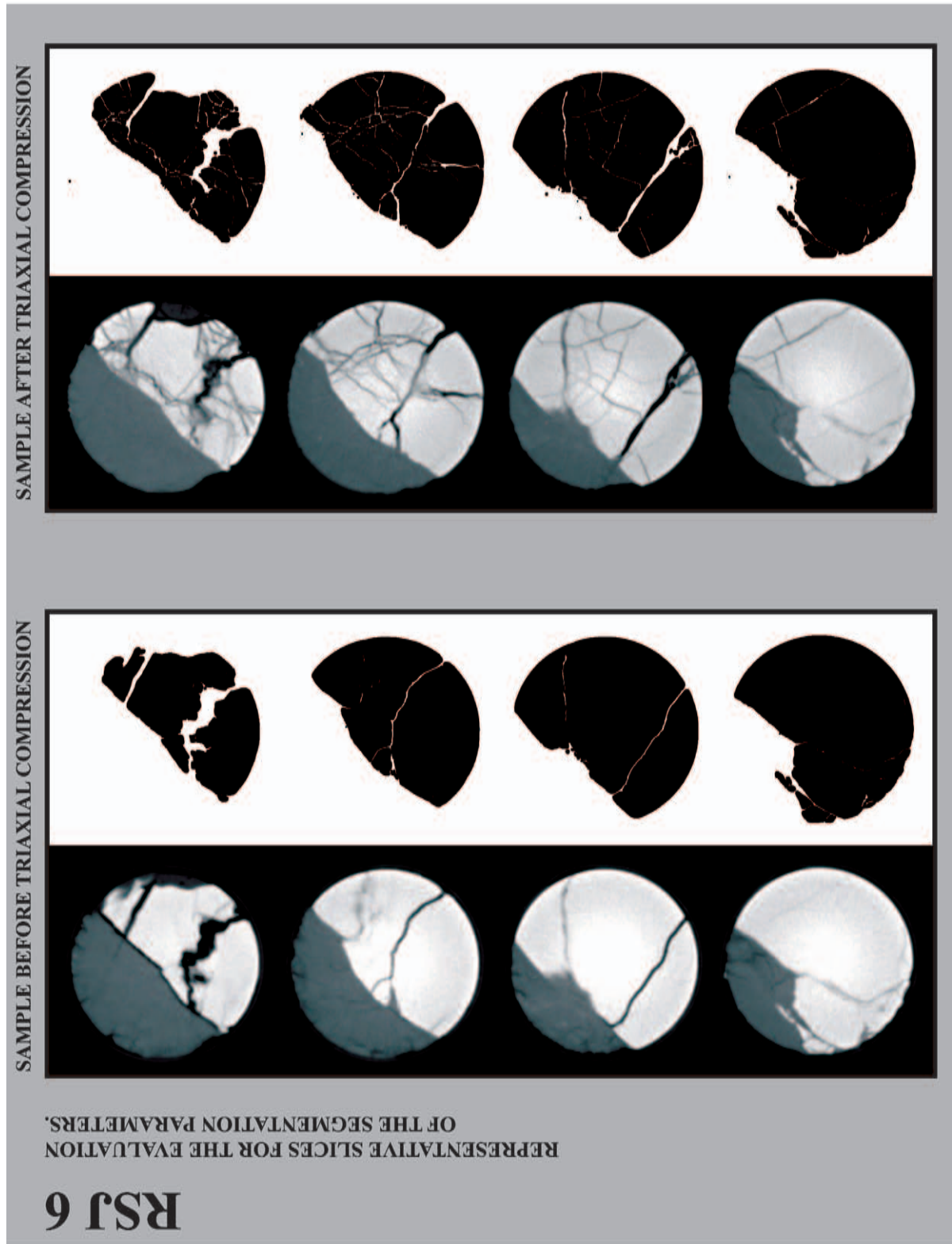


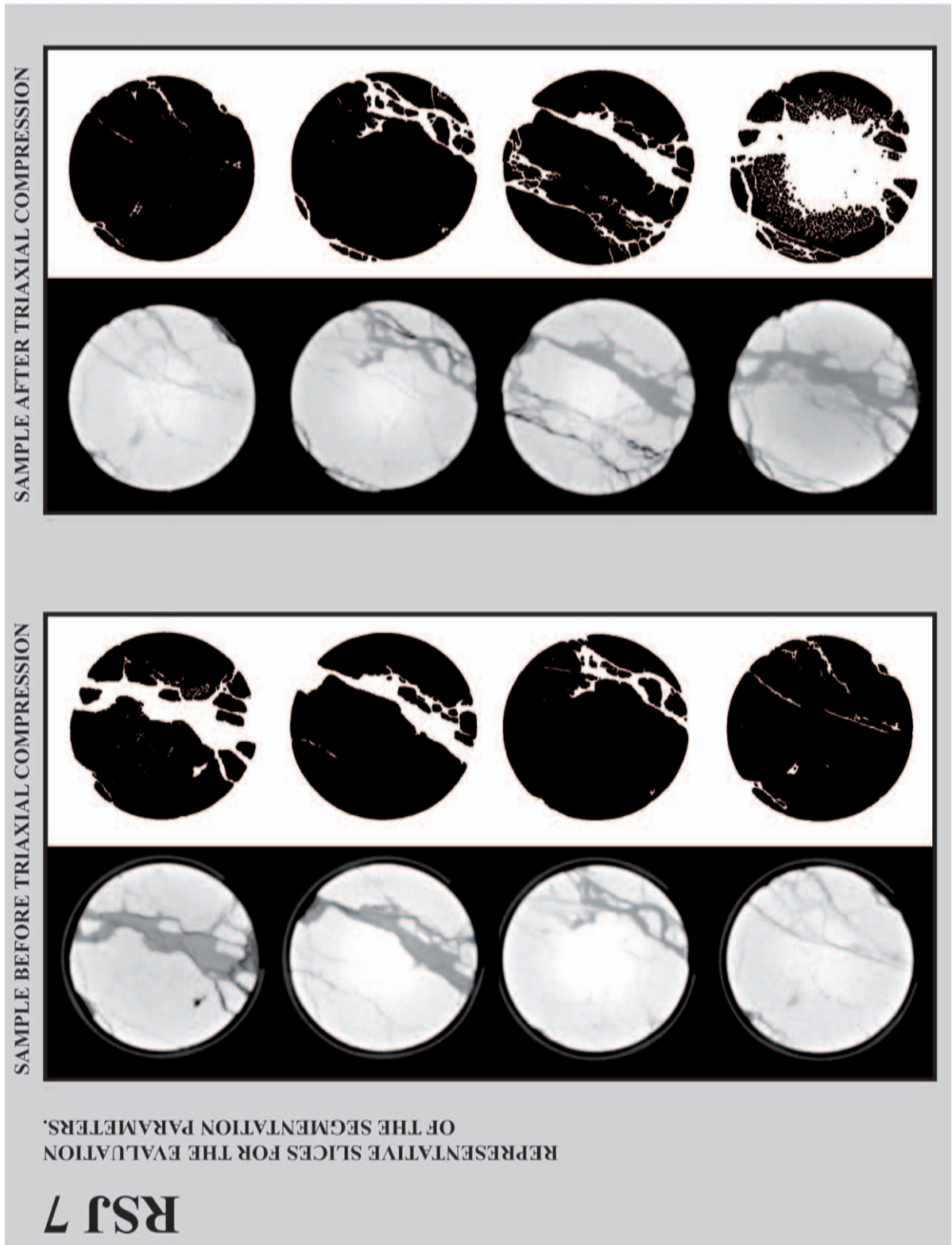


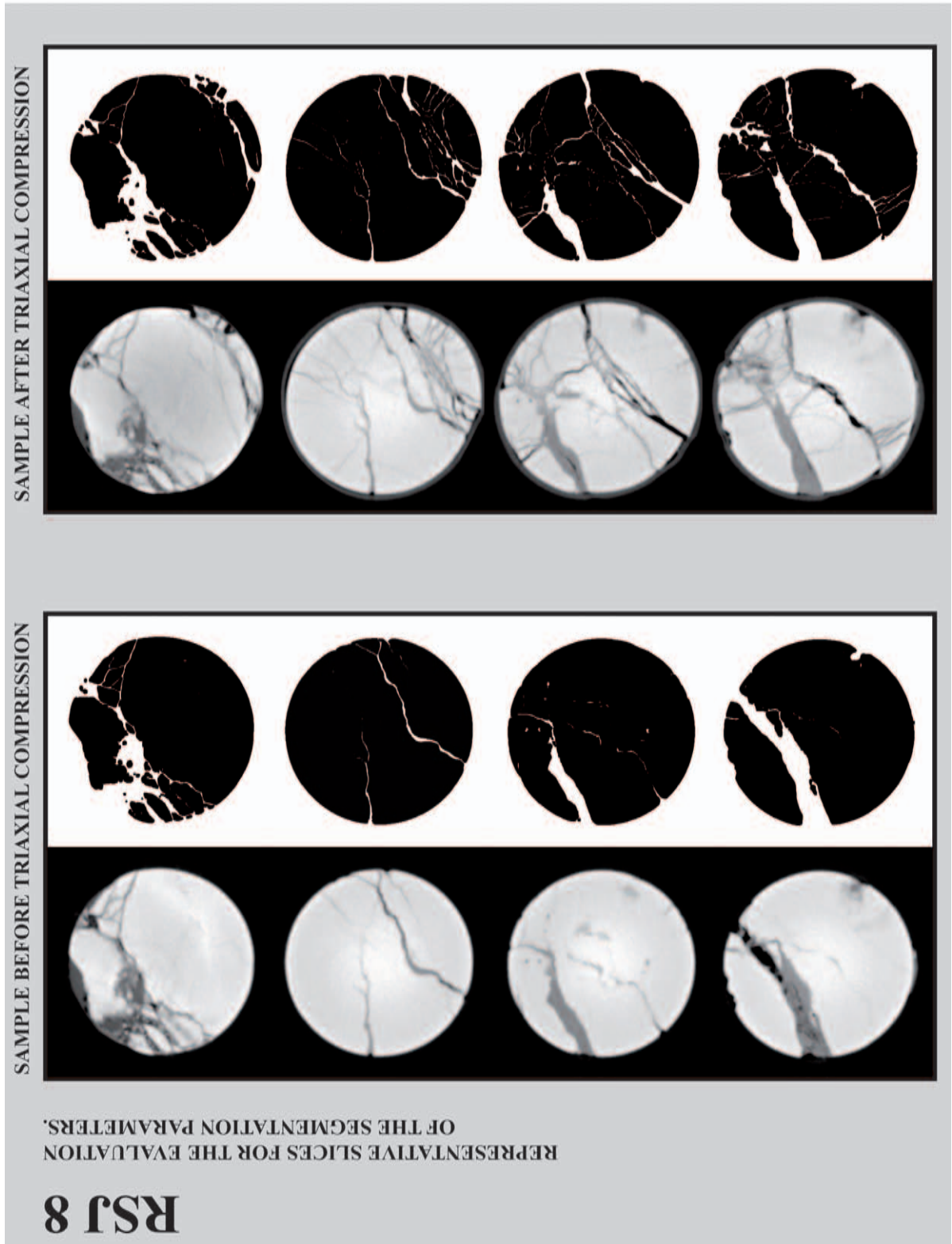


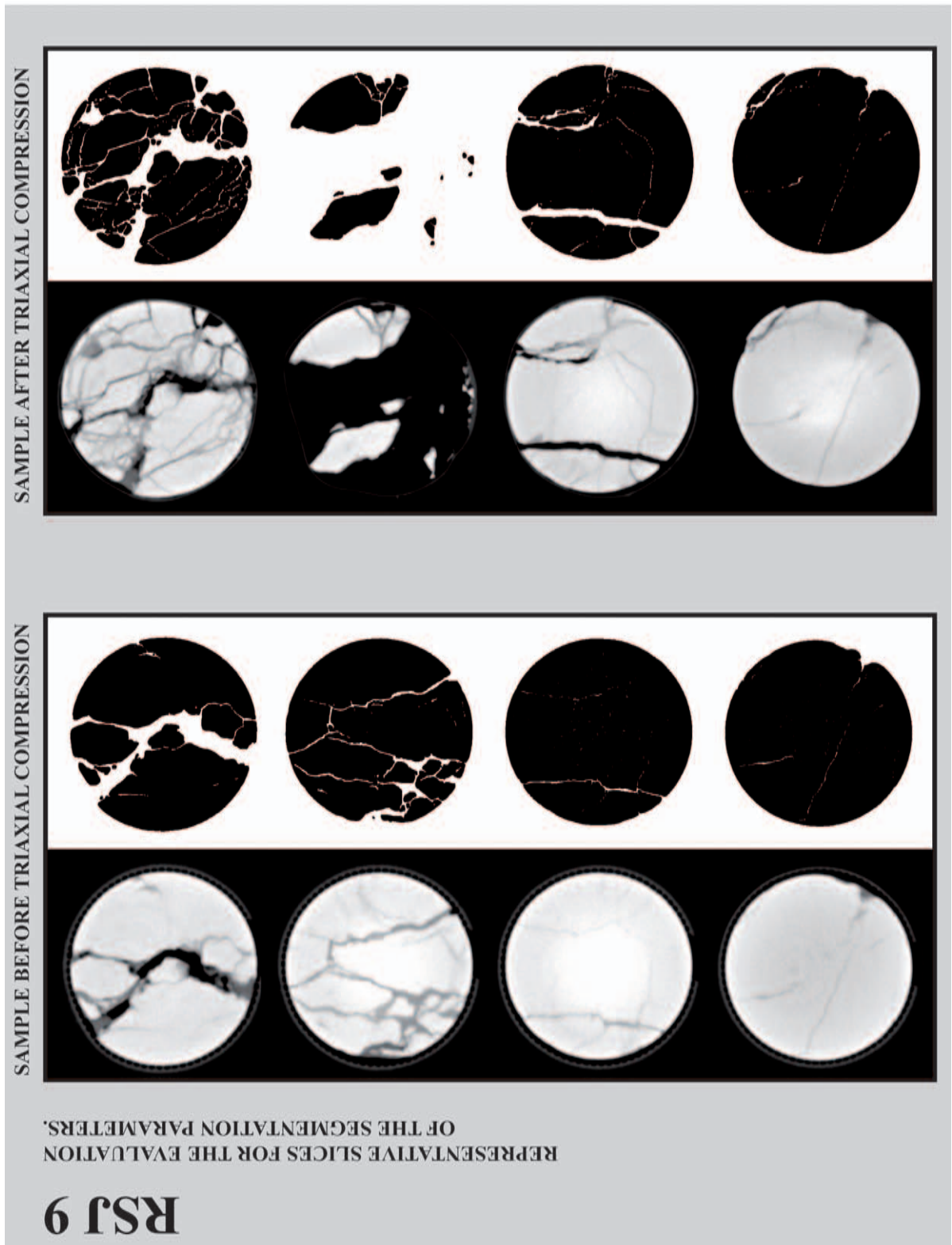


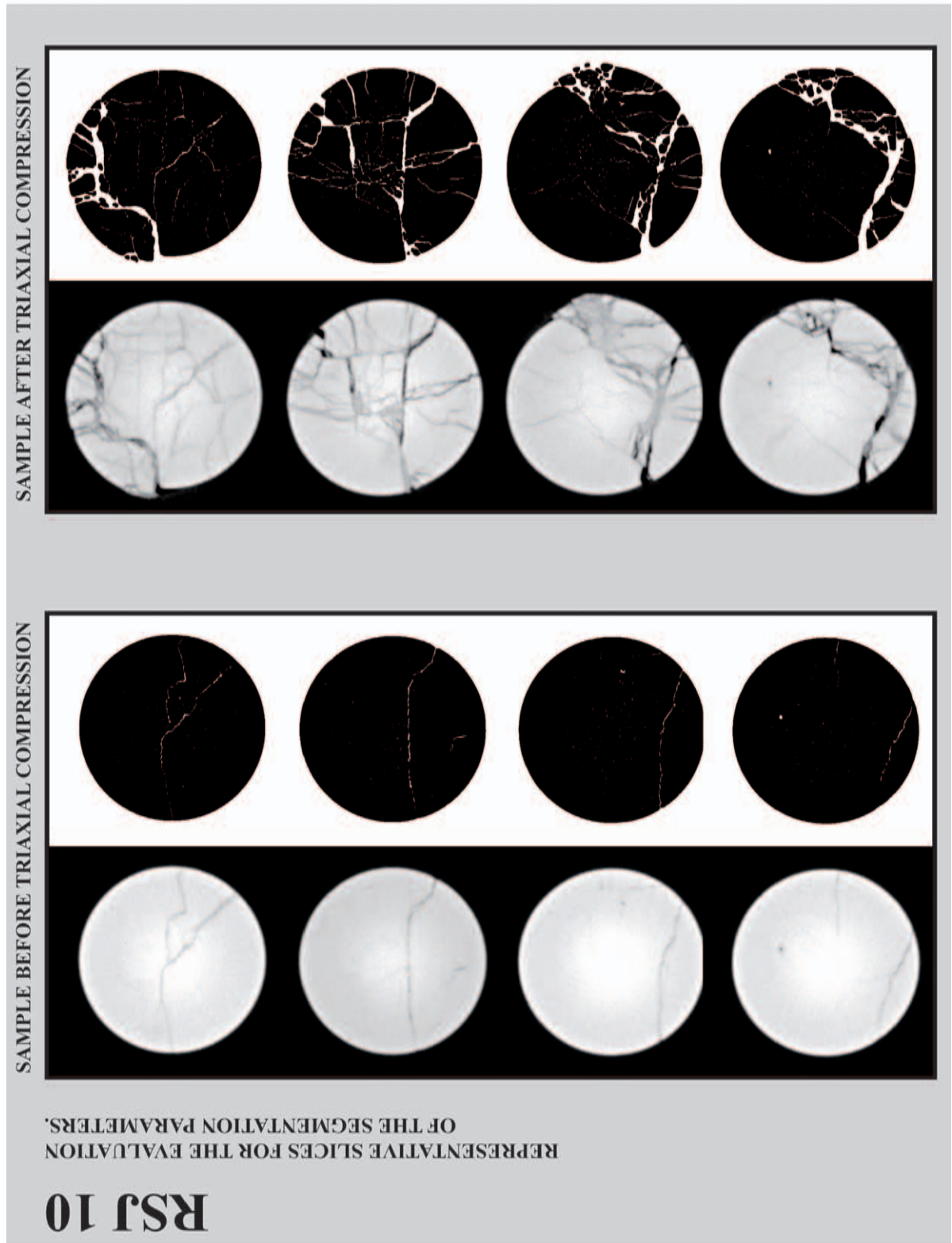


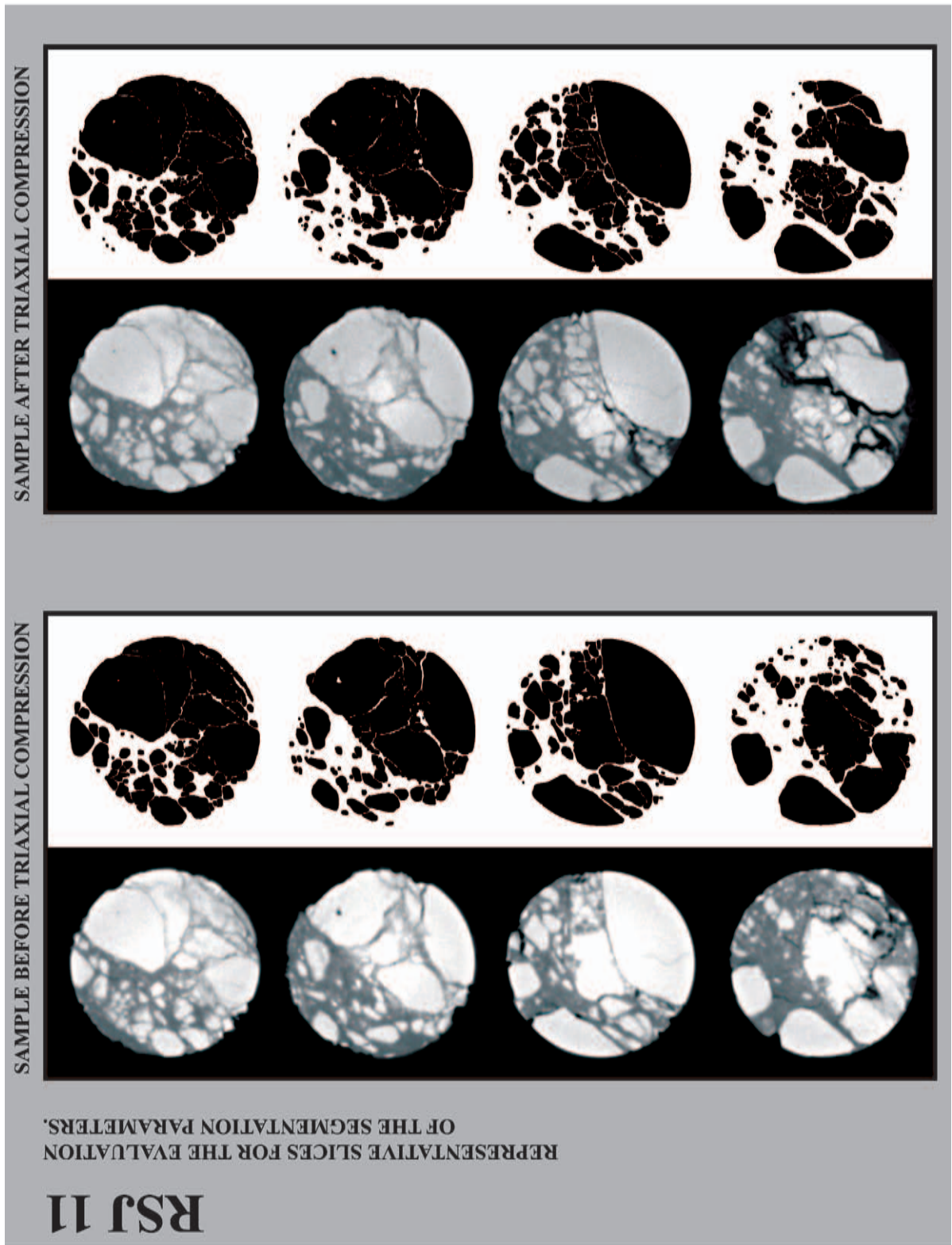


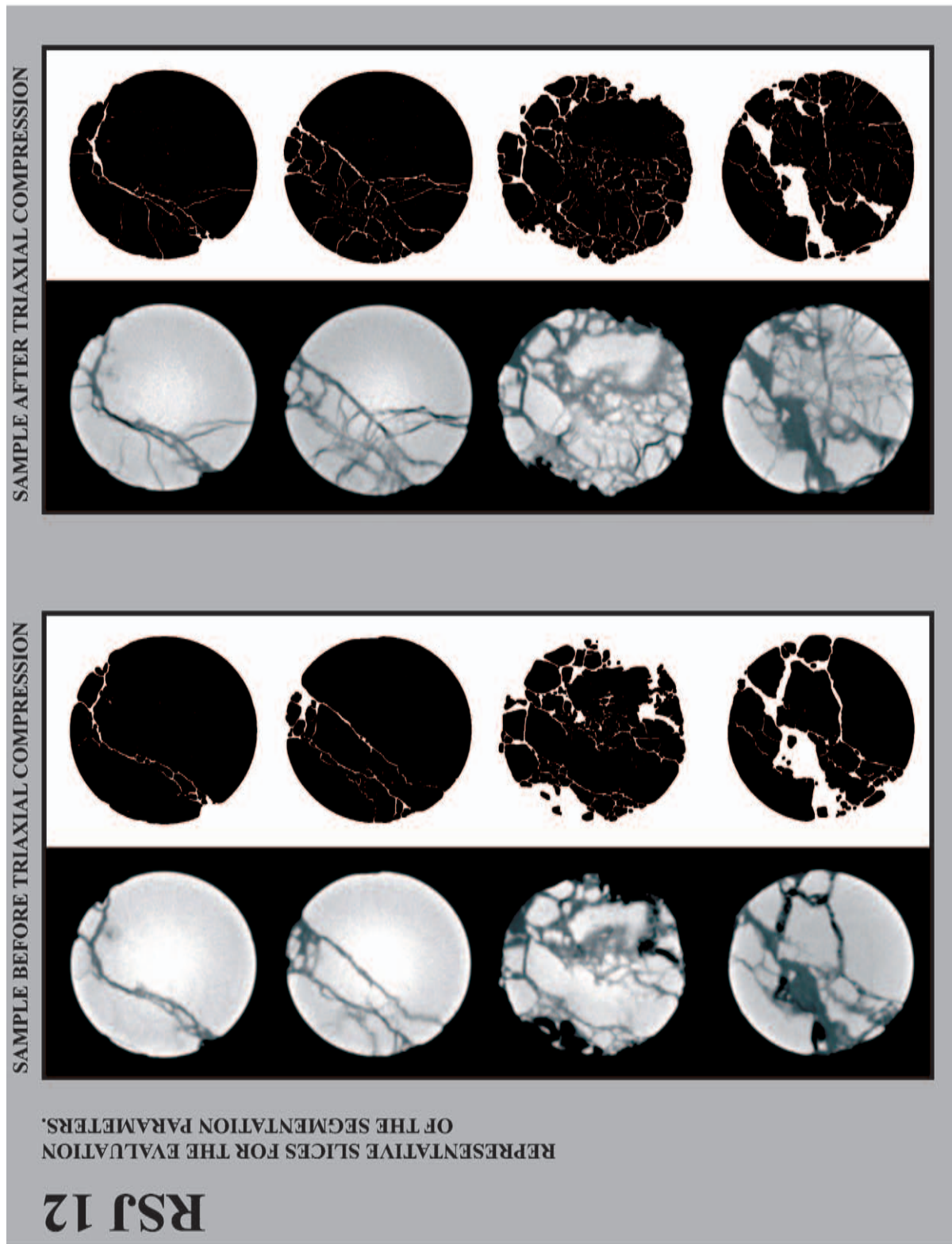












APPENDIX IV-IV

(related to Chap. 13, section 13.1.1.4)

PROPOSITION OF CORRECTIONS FOR THE TC AND MC PARAMETERS OF THE MINERALOGICAL AND STRUCTURAL INDEX MSI FOR CATACLASTIC ROCKS

**Perspectives from the supervised Master Theses of *Chaignat* and *Veuve*
(2007)**

Correction for MC (Chaignat, 2007)

Profiting from observations on contrasted petrological content, the influence of characteristic void spaces has quantitatively been assessed by *Chaignat* (2007). Accordingly, a void coefficient VC has been defined to improve the MC determination. Such a consideration seems important as it is known from literature that ongoing cataclasis introduces an important porosity reduction mechanisms able to decrease rock strength and to produce flow barrier in extreme compaction shear zones (*Bürgi*, 1999; *Neubauer*, 2005; *Micarelli et al.*, 2006). On the other hand, the presence of pores in a given rock structures has a negative effect on rock strength and influences strongly the resulting fracturing mode (*Jeng et al.*, 2004; *Schultz & Siddharthan*, 2005).

In rock petrology where cataclasis leads to the development of an important void space proportion, like it is the case in carbonates, the void coefficient VC is defined in analogy to the textural coefficient TC. Accordingly, void spaces are geometrically treated in a binary image according to their shape analogy to clasts, with the difference that void spaces have no strength and cohesion to offer against stress. VC is given by following relationship:

$$(Eq. 1) \quad VC = VD \left[\left(\frac{N_o}{N_0 + N_1} \overline{FF_o} \right) + \left(\frac{N_1}{N_0 + N_1} \frac{1}{\overline{AR_1} \cdot \overline{AF_1}} \right) \right]$$

where

- VC = void coefficient [-]
- VD = void density [%]
- N_o = number of isometric void spaces (AR < 2)
- N₁ = number of elongated void spaces (AR > 2)
- $\overline{FF_o}$ = mean form factor of isometric void spaces
- $\overline{AR_1}$ = mean aspect ratio of elongated void spaces
- $\overline{AF_1}$ = angular factor of elongated void spaces

With regard to the equation of TC by *Bürgi* (1999, **Eq. 7.2**), two differences are noticeable. First the mean form factor $\overline{FF_o}$ is directly multiplied to the first term of the equation taking into account the shape of void spaces (inverse of $\overline{FF_o}$ is taken in the TC equation). This is done because it is assumed that -contrary to elongated clasts who are expected to strengthen rock mass- elongated void spaces will have a more negative influence on rock strength than isometric ones (e.g. preferred nucleation of new discontinuities). Second, the inverse of the product $\overline{AR_1} \cdot \overline{AF_1}$ is taken in the case of void spaces to reflect that an increase of elongated void spaces at high angular differences is more susceptible to penalize rock strength than to increase it. This second hypothese of *Chaignat* (2007) seems however questionable as high angular differences between elongated void spaces will offer a higher degree of freedom for rock components to accommodate stress during deformation, e.g. the possibility of indentation of “blocks” will increase, leading at the end to a probable positive effect on rock strength.

Using VC, the MC term of the MSI is corrected in following way to take into account the strength reduction produced by voids:

$$(Eq. 2) \quad MC' = MC - (x \cdot VC \cdot MC)$$

where

- MC' = matrix coefficient after correction for void spaces (VC)
- x = ponderation factor function of petrological content

Eq. 2 shows that if void spaces tends towards the value of 0, the MC' will be equal MC. Ponderation factor x is an empirical parameter given in percent that has to be determined according to the petrological content investigated. It reflects the influence of pore spaces on the variation of uniaxial strength of a rock mass, assumed to be related by a linear function (*Dube & Singh, 1972*). It can be seen as the percentage in rock strength reduction caused by a given pore space fraction.

Note: This approach is pertinent but requires that values for x would be available for the different petrological contents studied. *Chaignat (2007)* choose therefore to use a serie of uniaxial compression tests that have been performed at the LMR in 2006 on samples from the Eyholz tunnelling site (**Chap. 5**) in the framework of a mandatory contract. Based on a correlation that resulted between pic strength values σ_c and the different sample porosities, he found a value of $x = 12.397\%$ that has been used by default for the other petrological content under study.

Correction of mwVh (*Veuve, 2007*)

Determinations of mwVh by *Veuve (2007)* from XRD or TEM mineralogical analyses have demonstrated to vary in a significant manner. In particular, XRD resolution being limited to 5% of mineral phase, some critical components can be overseen in cataclasites of particular petrologies (see for example presence of localized clay into tectonized limestones). Despite recommendations by *Bürgi (1999)* to use at least 200 g of rock material ground down mechanically to a grainsize of about 10 μm to ensure mineralogical homogeneity of the analysed fault rocks, ineffective mineralogical determinations in terms of strength can easily result from XRD analyses.

It has been recognized that in quartzophyllitic rocks (*Bürgi 1999*), the most populated phase is quartz with only minor proportions of the main components feldspars \pm calcite. All other phases have been regrouped into a non-quantified mineralogical assemblage considered to be composed mainly of phyllosilicates (mica + chlorite) and for which the Vh of muscovite has been taken (850 MPa). This undifferentiated phase is expected penalizing at most fault rock strength. The presence of minor proportion of accessory minerals such as e.g. sphene, turmaline, or opaque minerals is not considered by *Bürgi (1999)* to influence the mechanical behavior of fault rocks significantly.

However in terms of strength reduction, the most critical mineralogical phases are weak mineral phases that -even if present in small proportions- act negatively on overall rock strength due to unfavorable structural distribution (e.g. for example microcrack-filling with clay minerals). Therefore, by considering the important variation in Vickers hardness between mineral phases (see **Table 7.2**), *Veuve* expressed the need to better ponder their weight in the calculation of the MSI, so as to avoid overestimation of the influence of “hard phases” like quartz and underestimation of “weak phases in critical structural relationships” like phyllosilicates and clay. Accordingly, a suggestion to take the logarithmic values of Vh is made. The mineralogical term of the MSI becomes therefore:

$$\text{(Eq. 3)} \quad \text{mwVh} = \sum v_i \cdot \log(\text{Vh}_i)$$

$\log(\text{Vh}_i)$ = logarithmic value of the Vickers hardness for mineral phase i
 v_i = amount of mineral phase i in the sample

As cataclasis induces materials of important rheological contrasts and have been described by *Bürgi & Habimana (1999)* as “*somewhere between the properties of soils and rocks*”, the weighting of the different mineral phases and their objective translation in terms of strength reduction should at this stage be investigated in details. Improvements in the general understanding of cataclastic behavior and fracture propagation are expected. An appropriate balance between “strength enhancing mineral phases” vs. “strength decreasing mineral phases” is needed to account for the description of

Appendix IV-IV

observed deformations. Next to it, by implementing SEM, correction factors accounting for the alteration/weathering affecting rock structure could be determined and used as descriptor of mineralogical anisotropy.

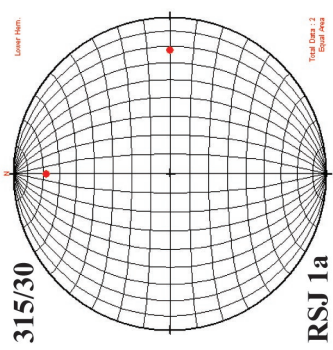
APPENDIX V-I

(Appendix related to Chap. 12 & 13)

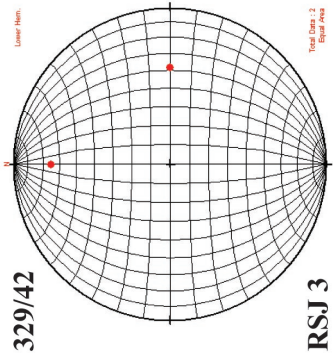
DETERMINATION OF α_{XRCT} BASED ON FRONTAL AND SAGITTAL CT-SLICES OF RSJ SAMPLES CLASSIFIED BY MECHANICAL BEHAVIOR

Legend for all **Appendices V-I**:

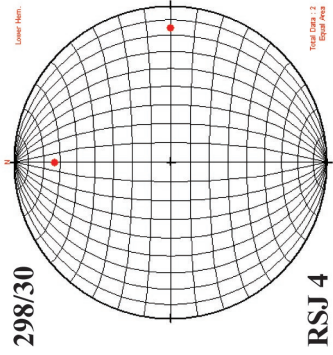
XRCT evidence for *RSJ* samples *before* and *after* triaxial test. Each plate presents the stress-strain curve of the triaxial test, 3D reconstructions of XRCT acquisitions (*undeformed* and *deformed* according to 2 different scene views at 180°) as well as 3 clipping positions (150, 250 & 350) inside the volume according to the frontal (xz) and sagittal (yz) planes. Distance between clipping planes corresponds to about 20 mm. Based on such visualization, an interpretation of the rupture mechanism during triaxial test is evaluated (see **Table 12.3, Chap. 12**). Accordingly, a “major” discontinuity has been evaluated. Accordingly the rupture angle α_{XRCT} for the re-interpretation of triaxial stress data is determined from stereographic projections of the averaged frontal and sagittal trace lines. Mohr-Coulomb parameters are then calculated based on α_{XRCT} and confronted with values resulting from the Mohr circle analysis.



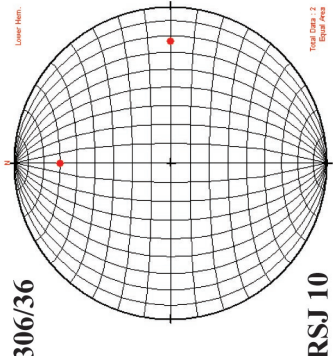
RSJ 1a



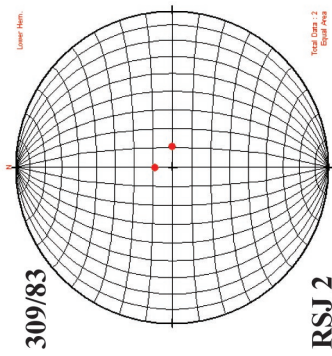
RSJ 3



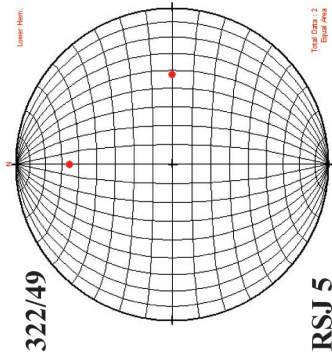
RSJ 4



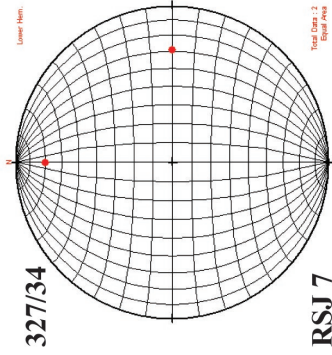
RSJ 10



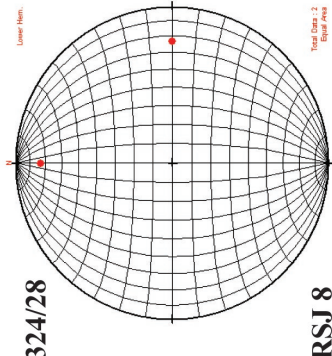
RSJ 2



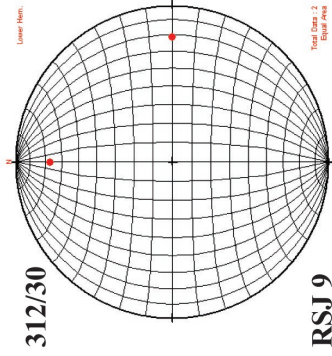
RSJ 5



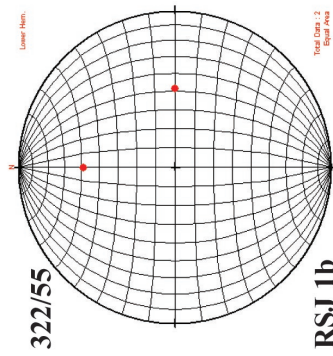
RSJ 7



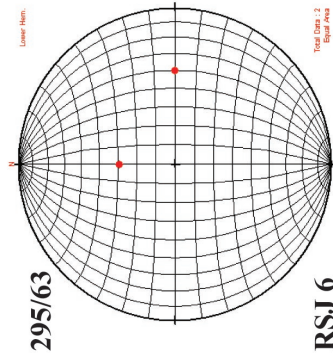
RSJ 8



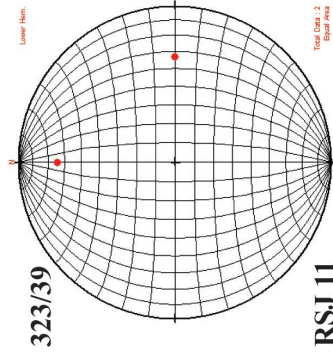
RSJ 9



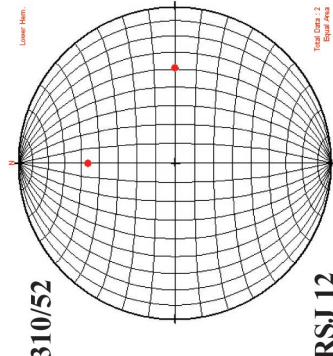
RSJ 1b



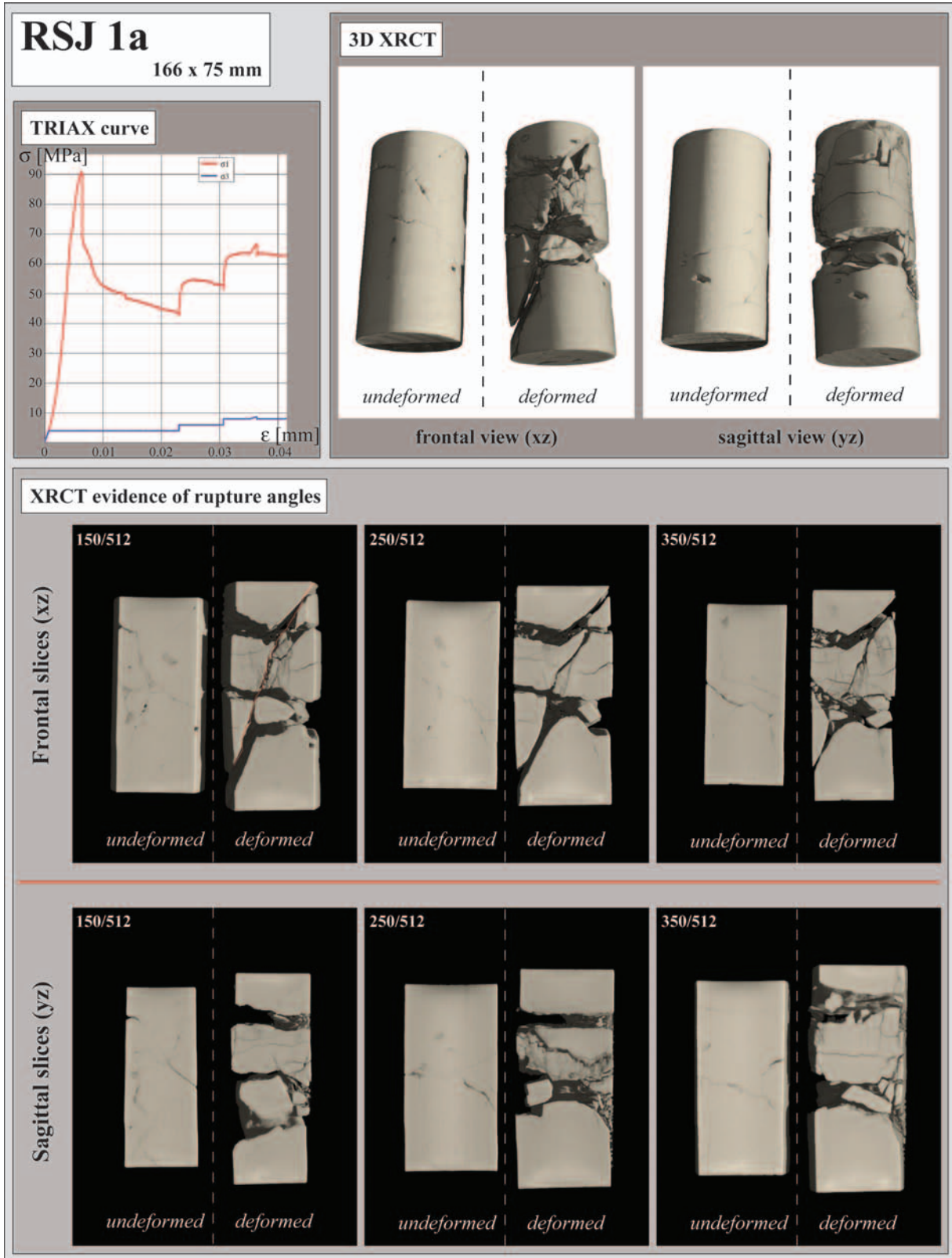
RSJ 6

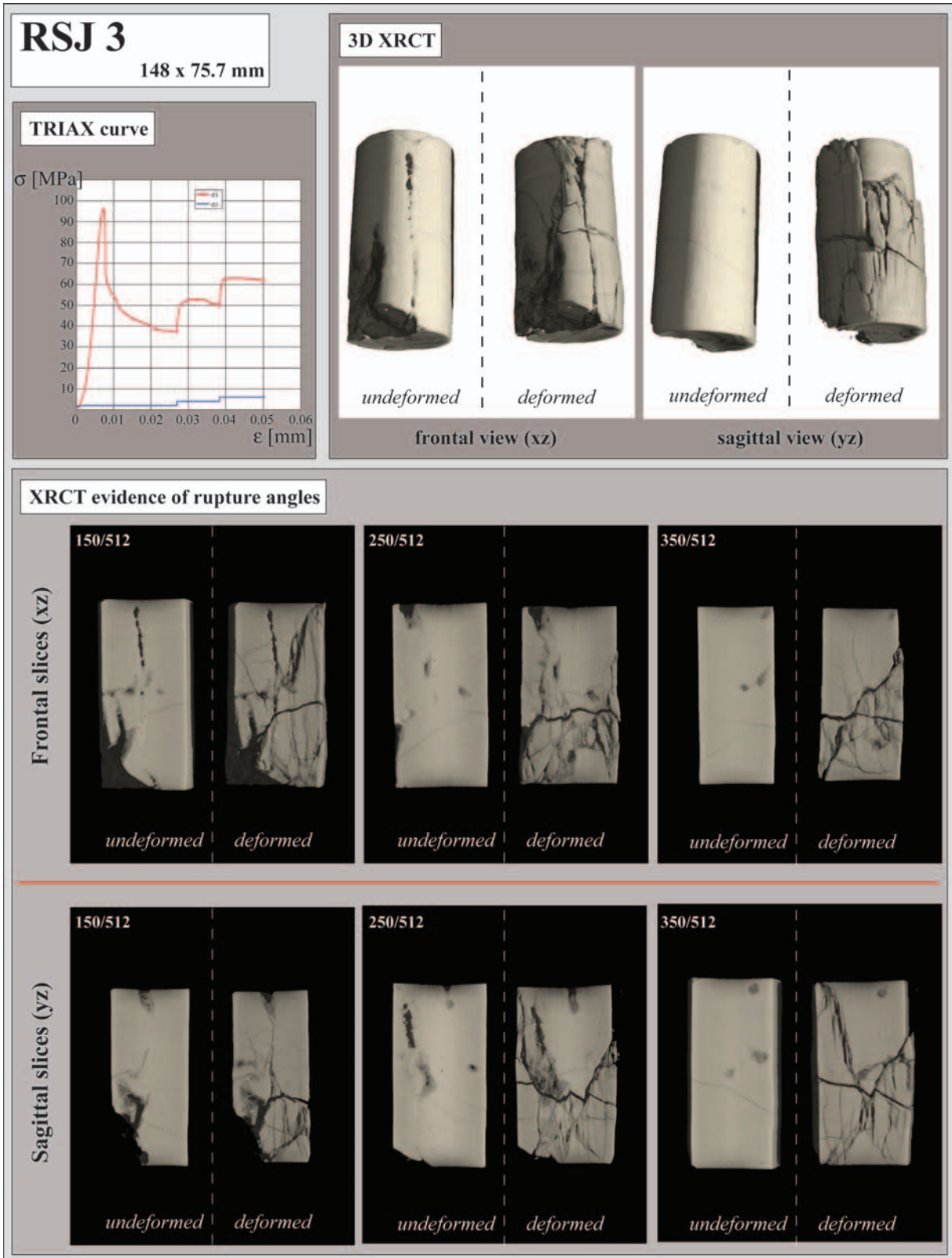


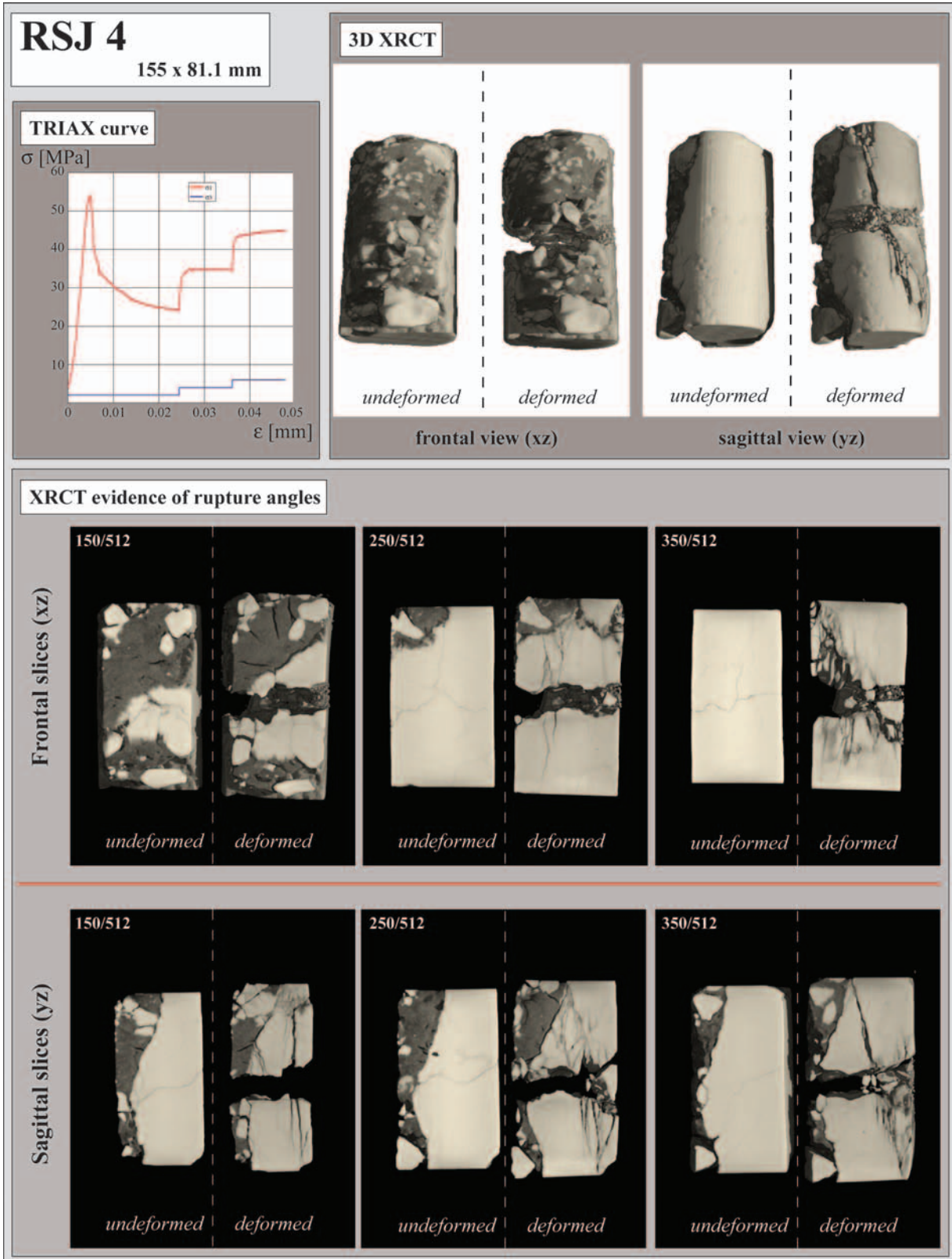
RSJ 11

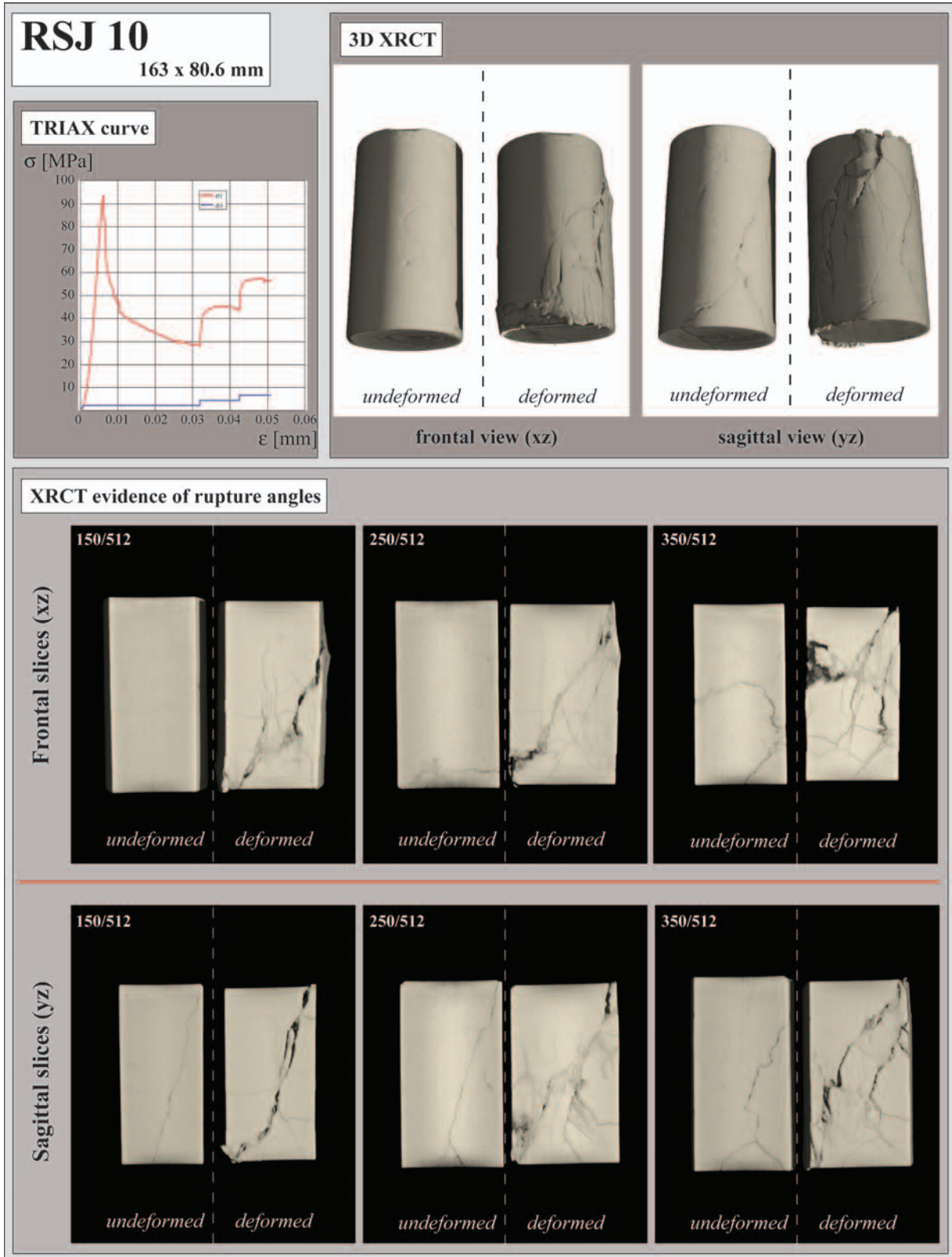


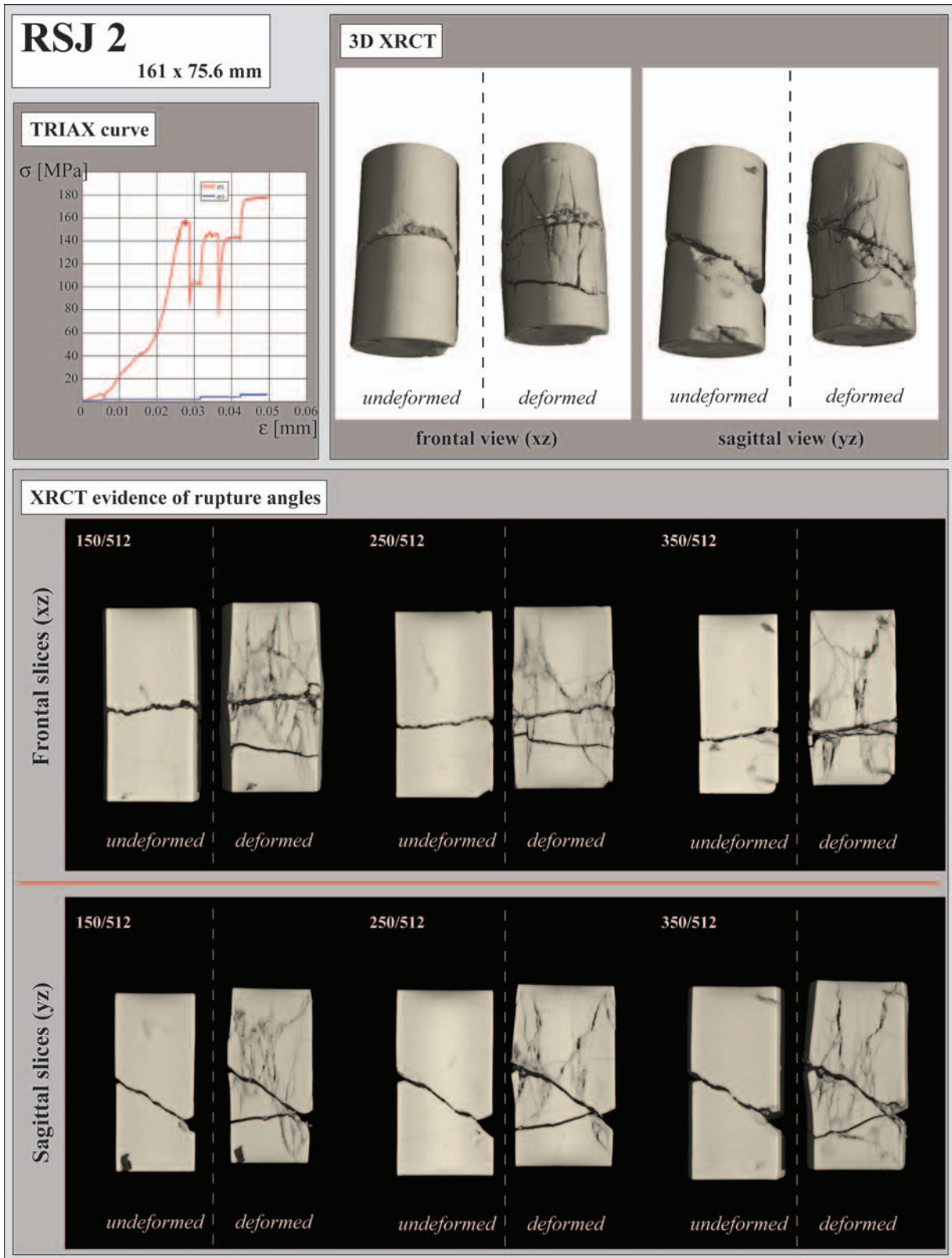
RSJ 12

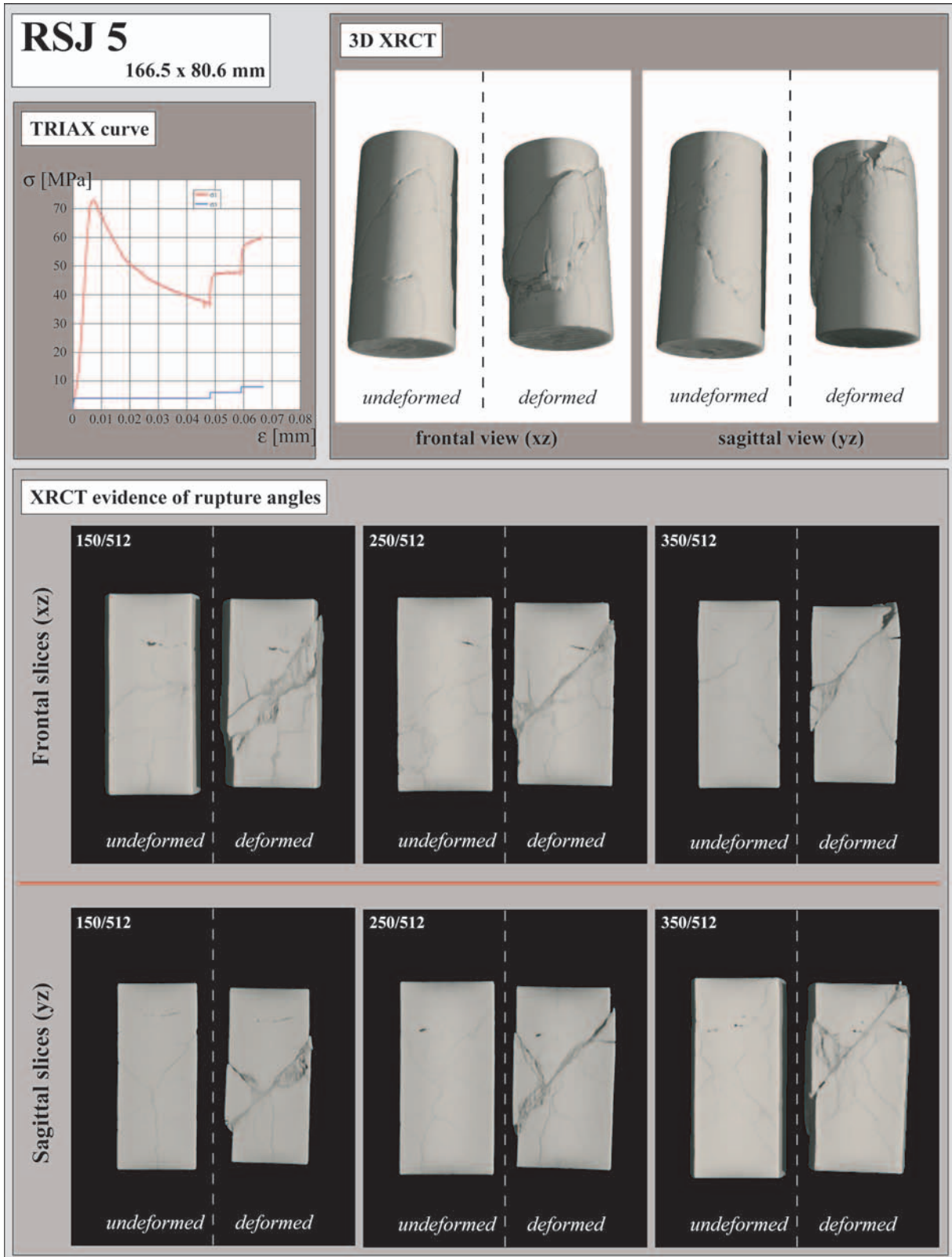


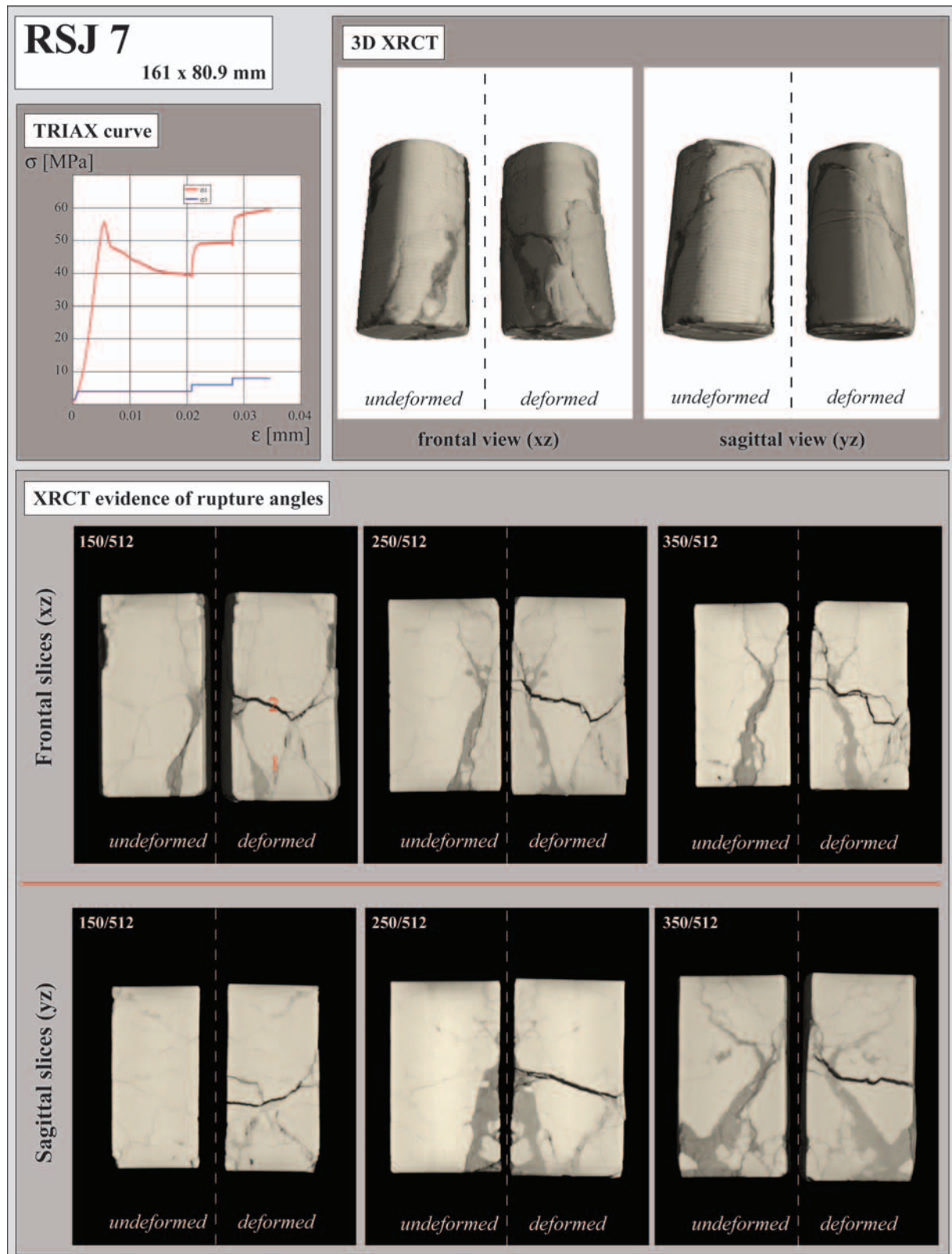


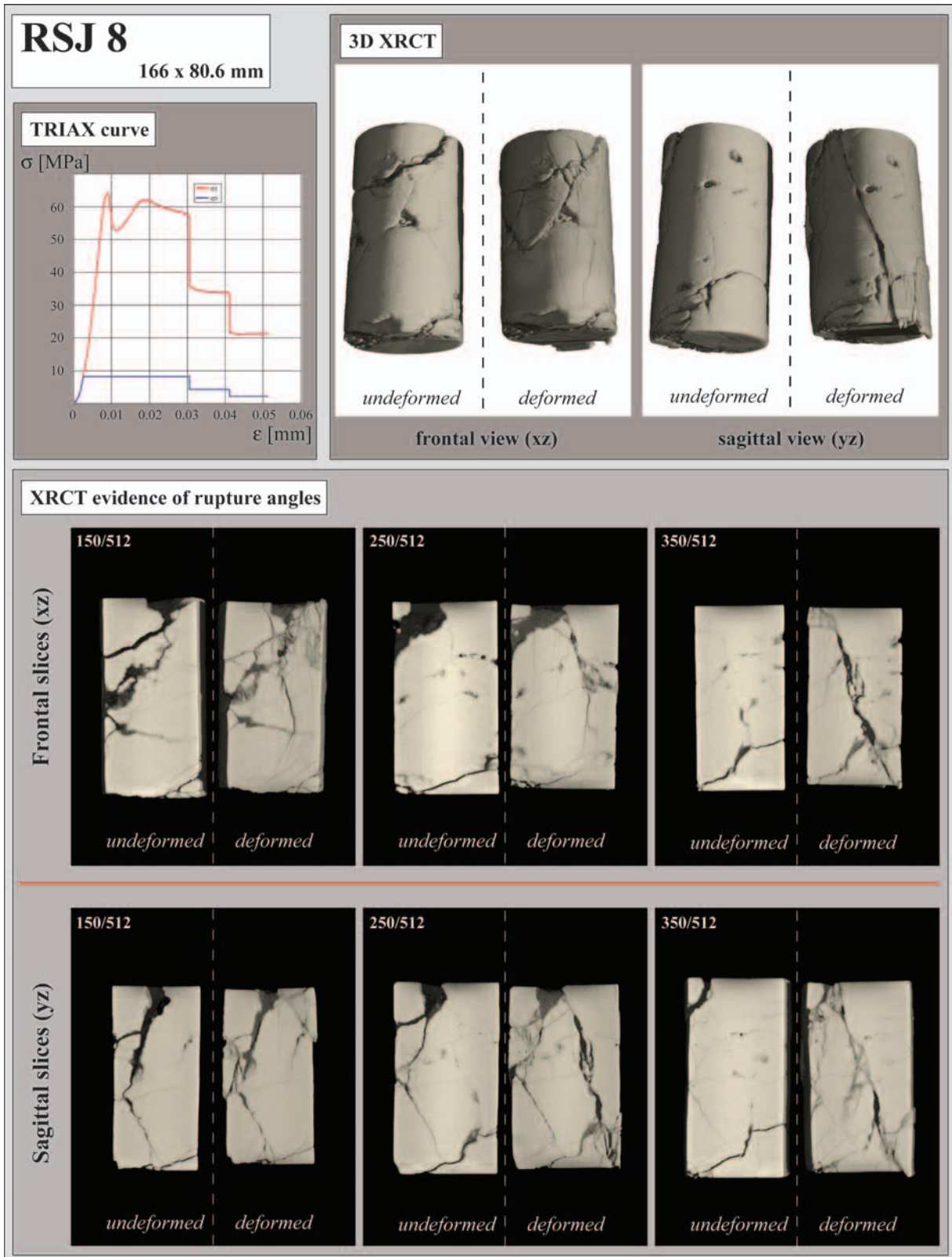


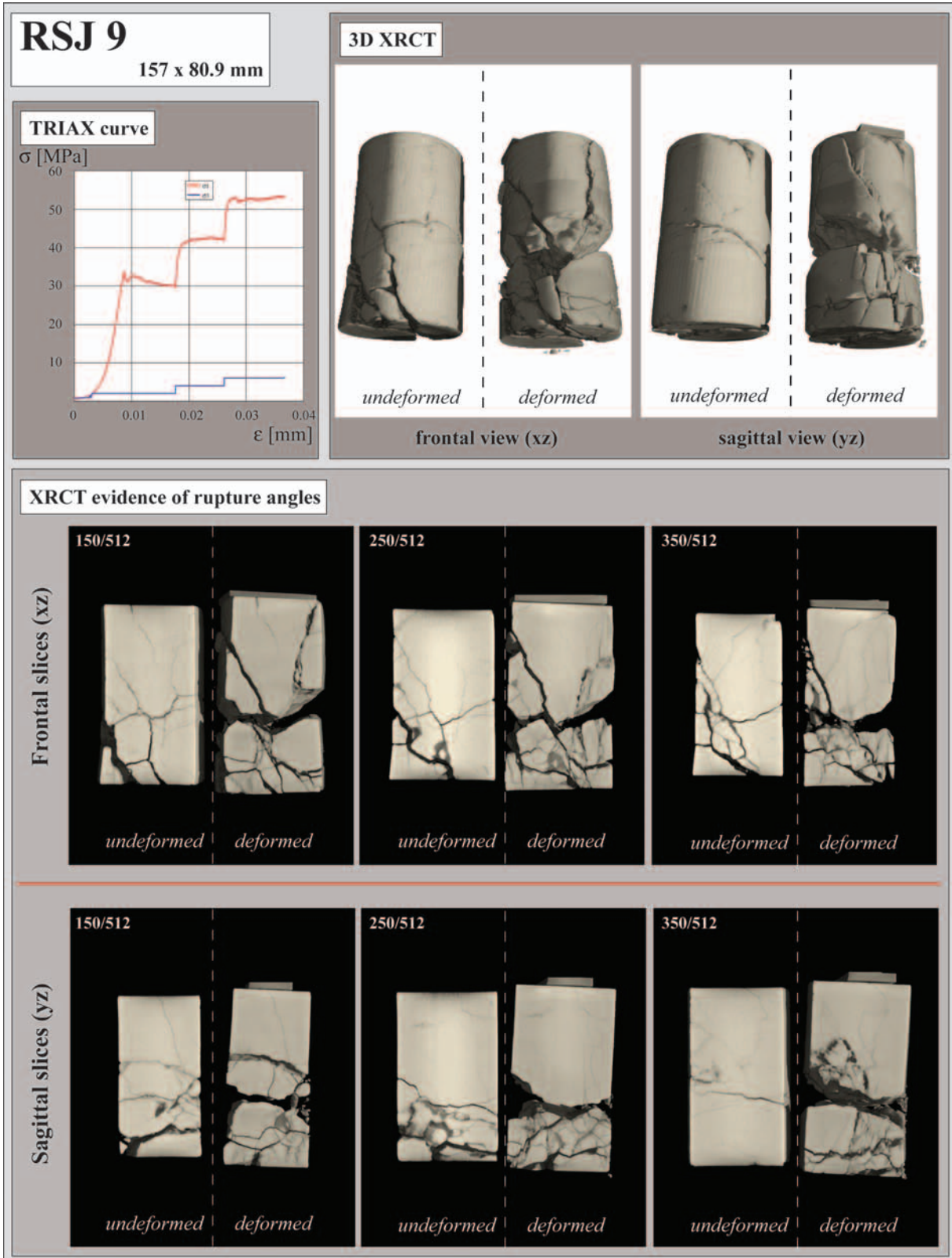


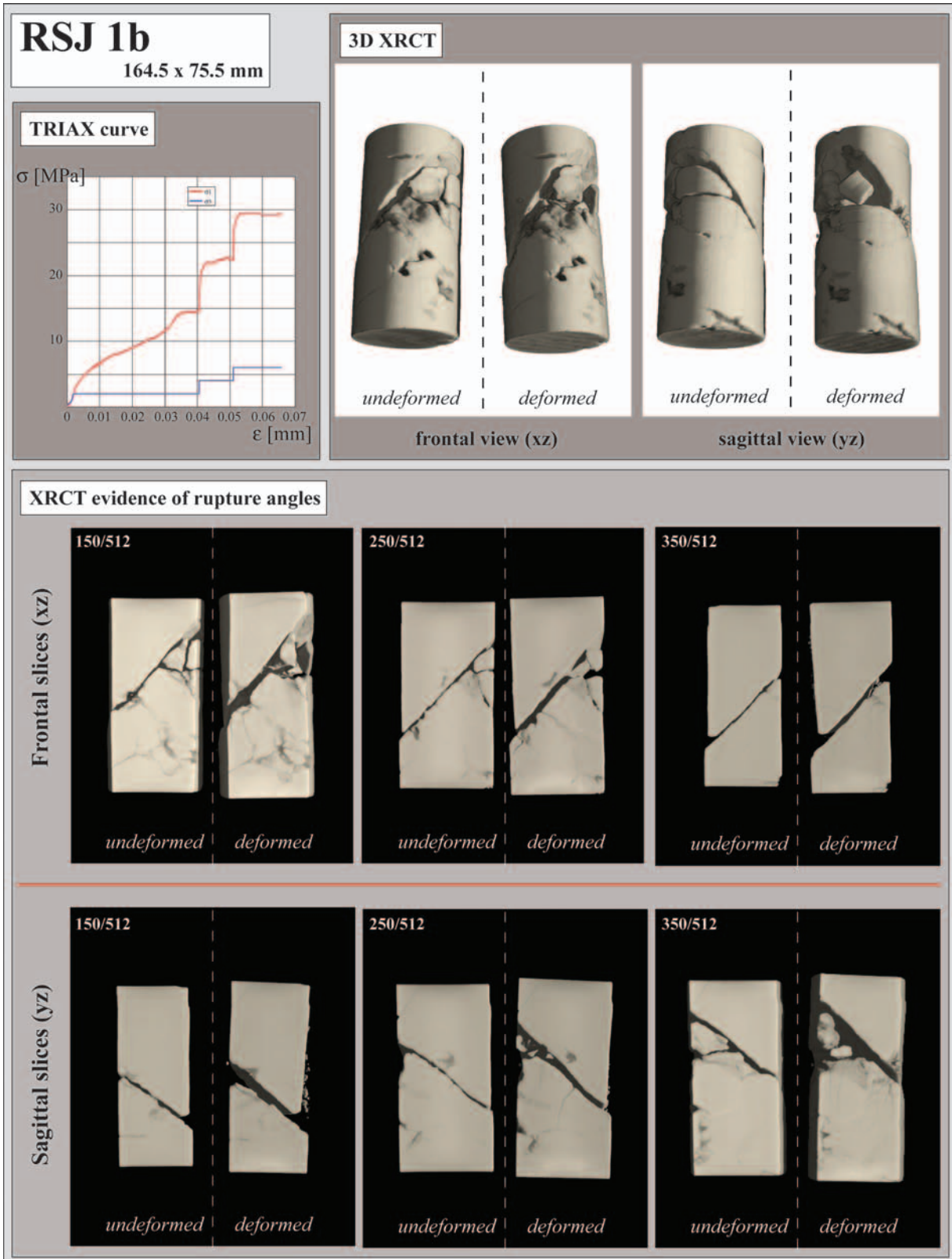


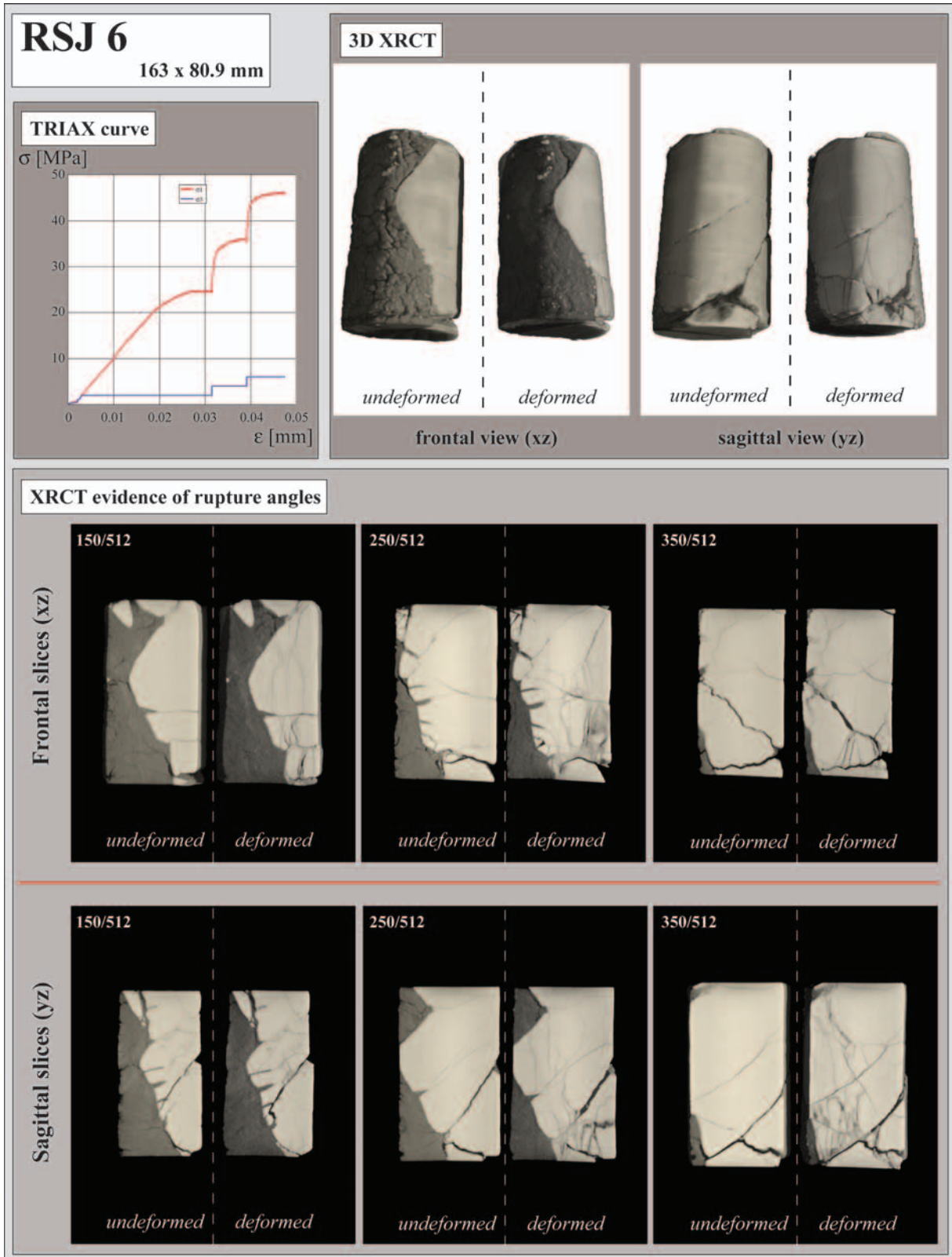


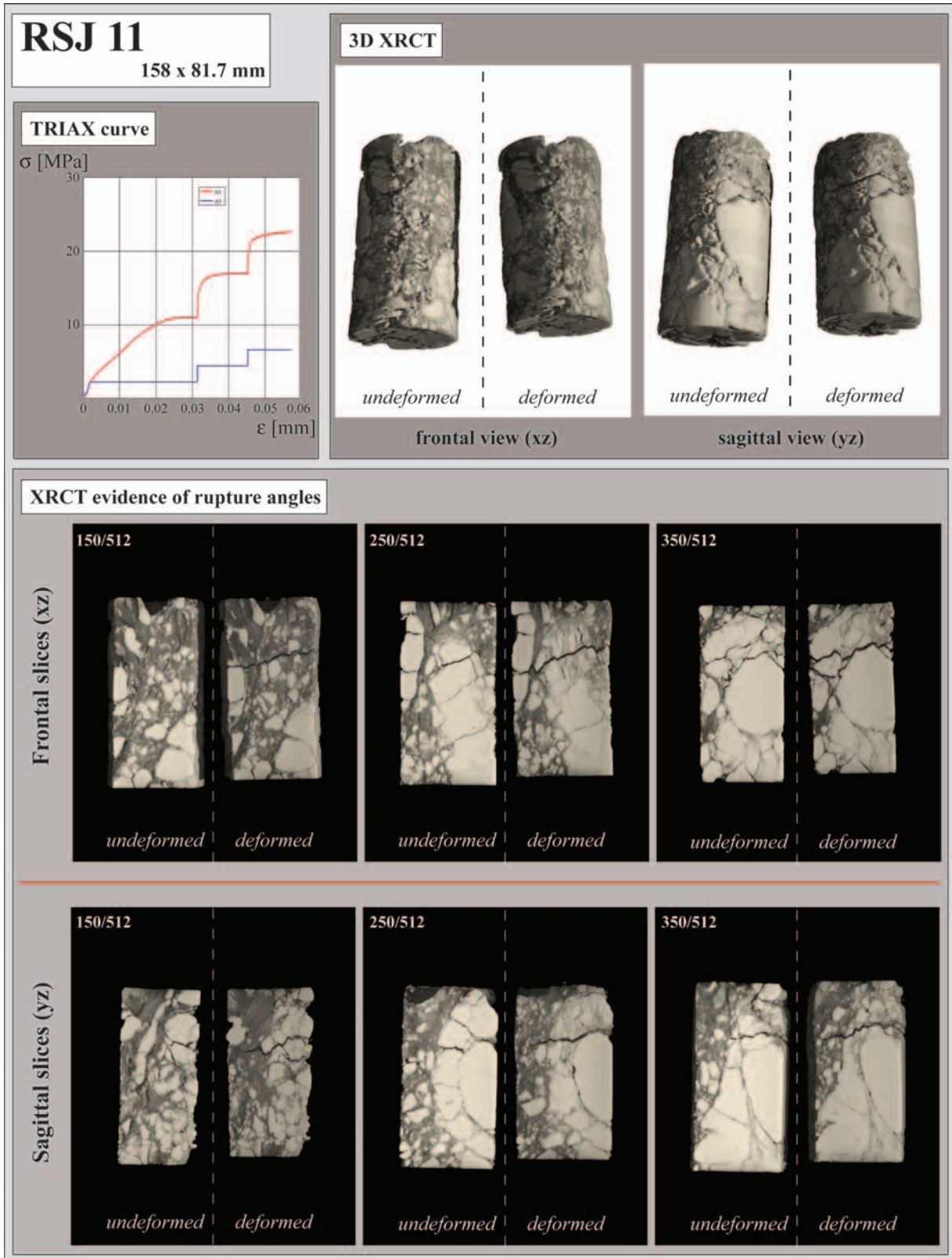


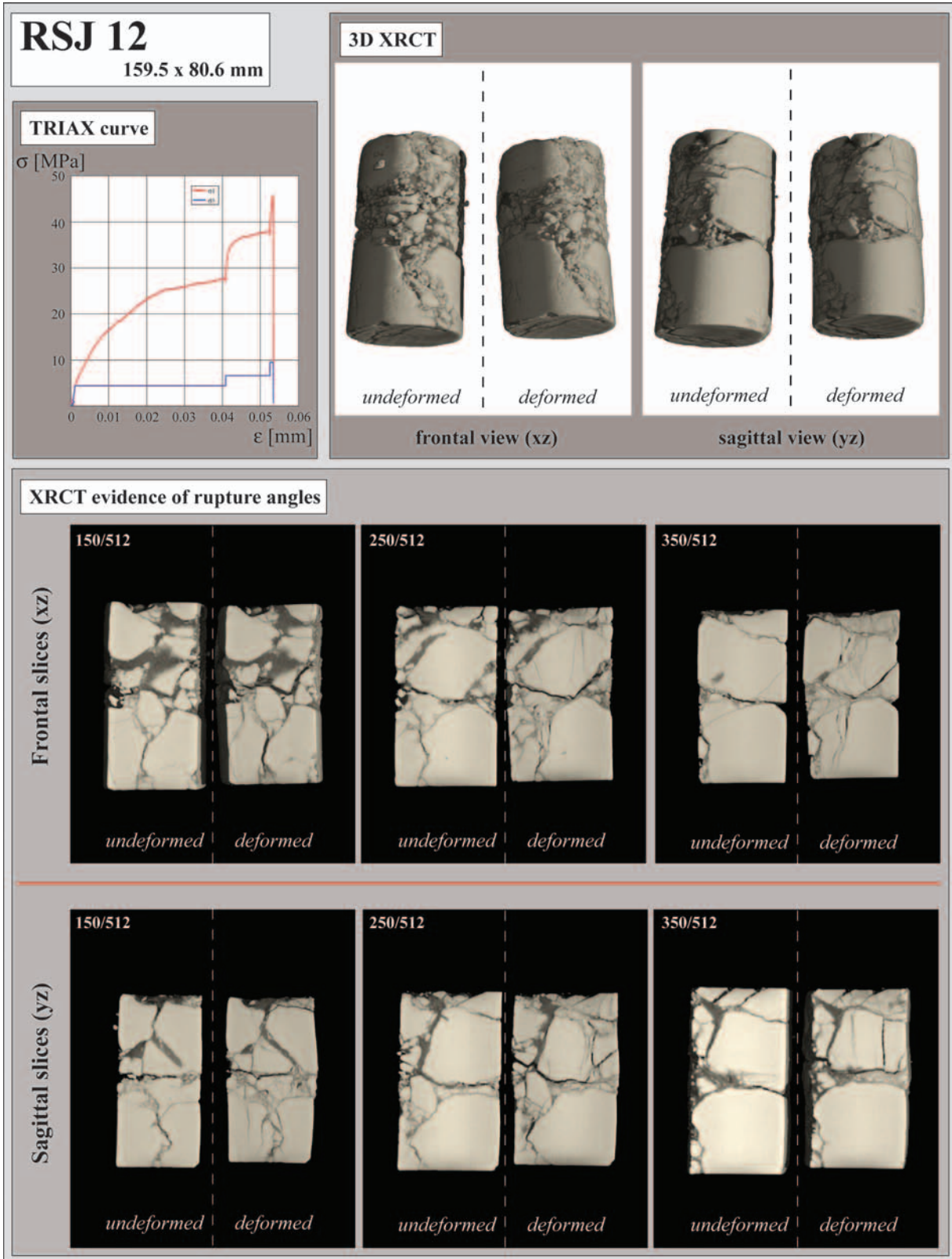








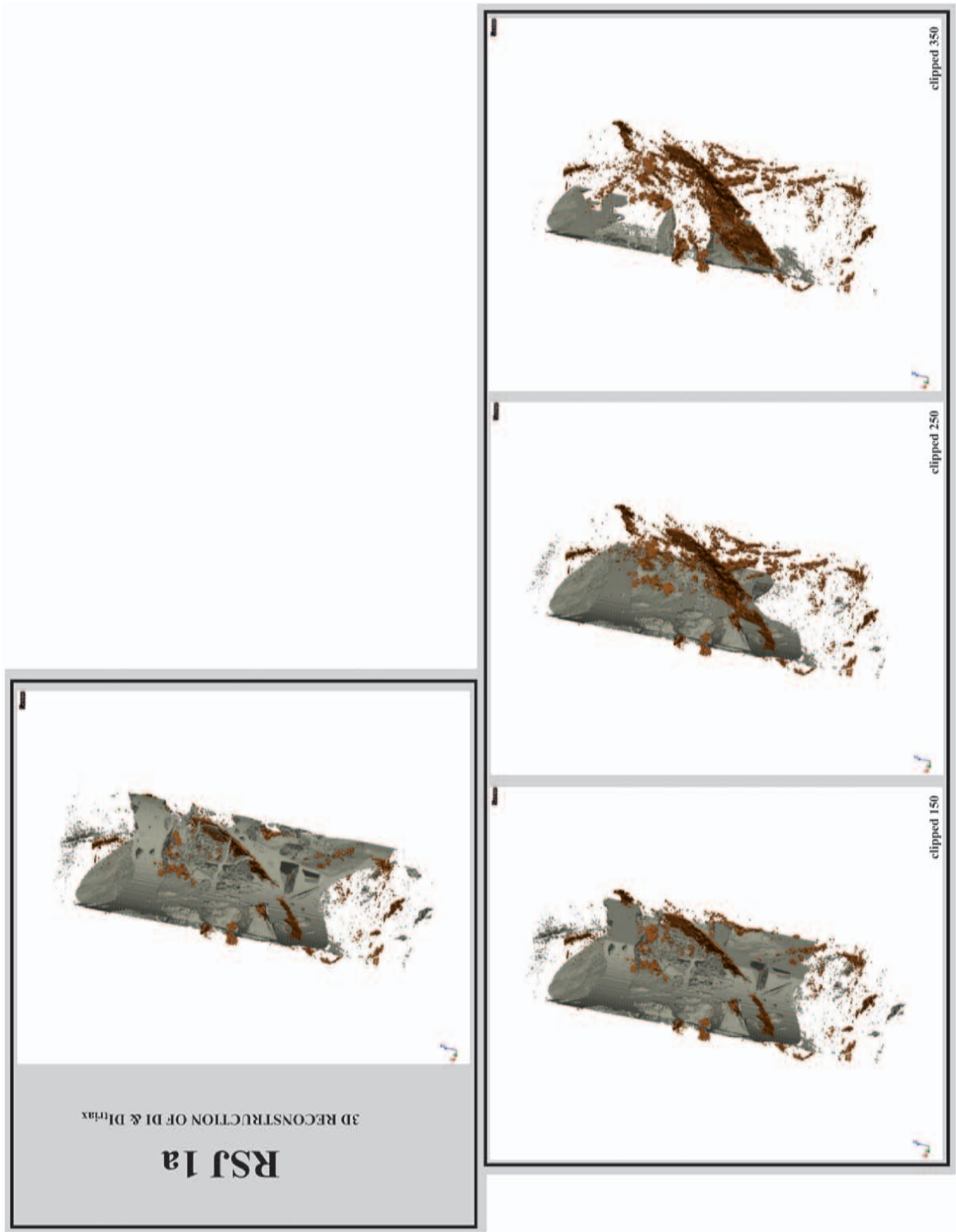




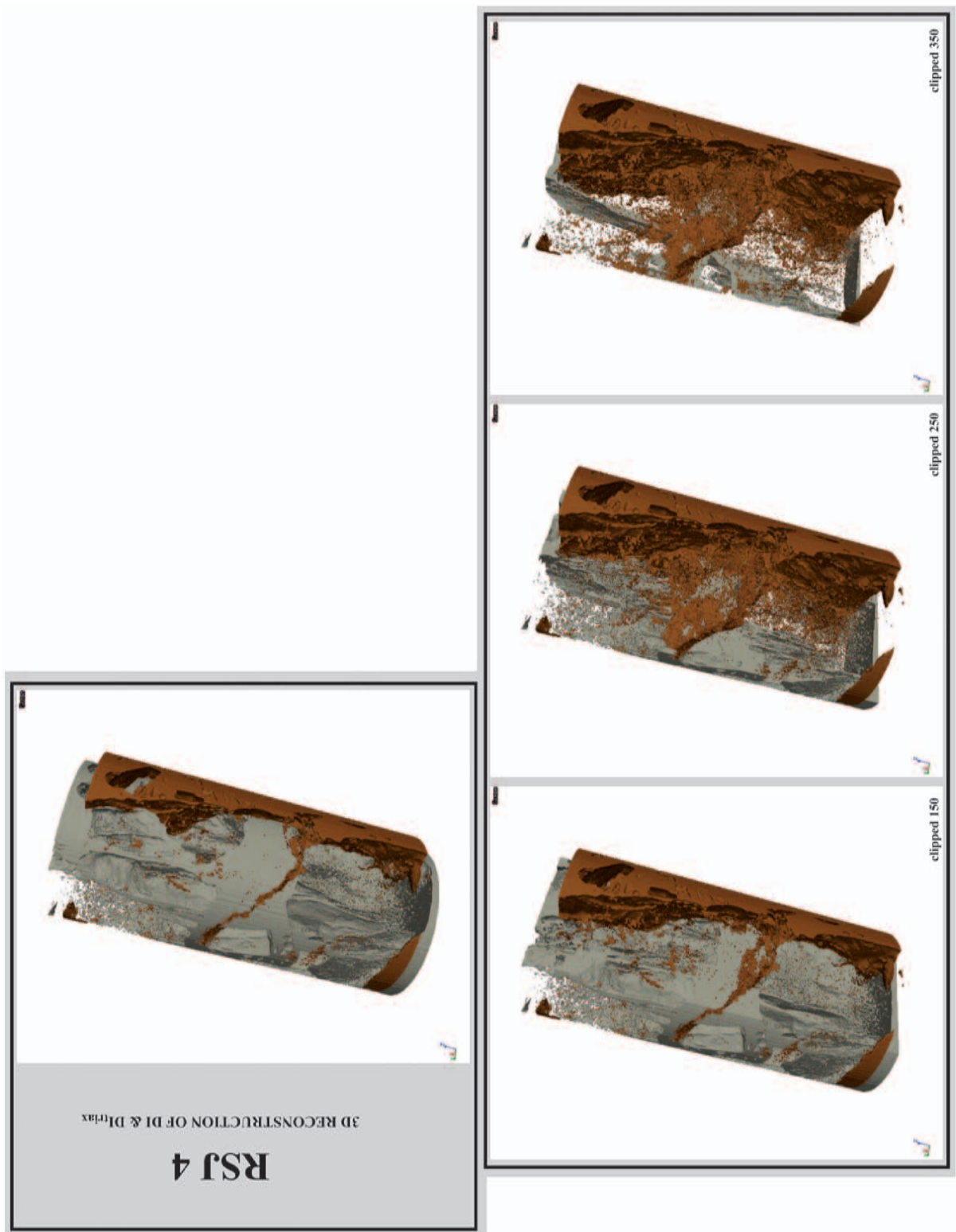
APPENDIX V-II

(Appendix related to Chap. 12 & 13)

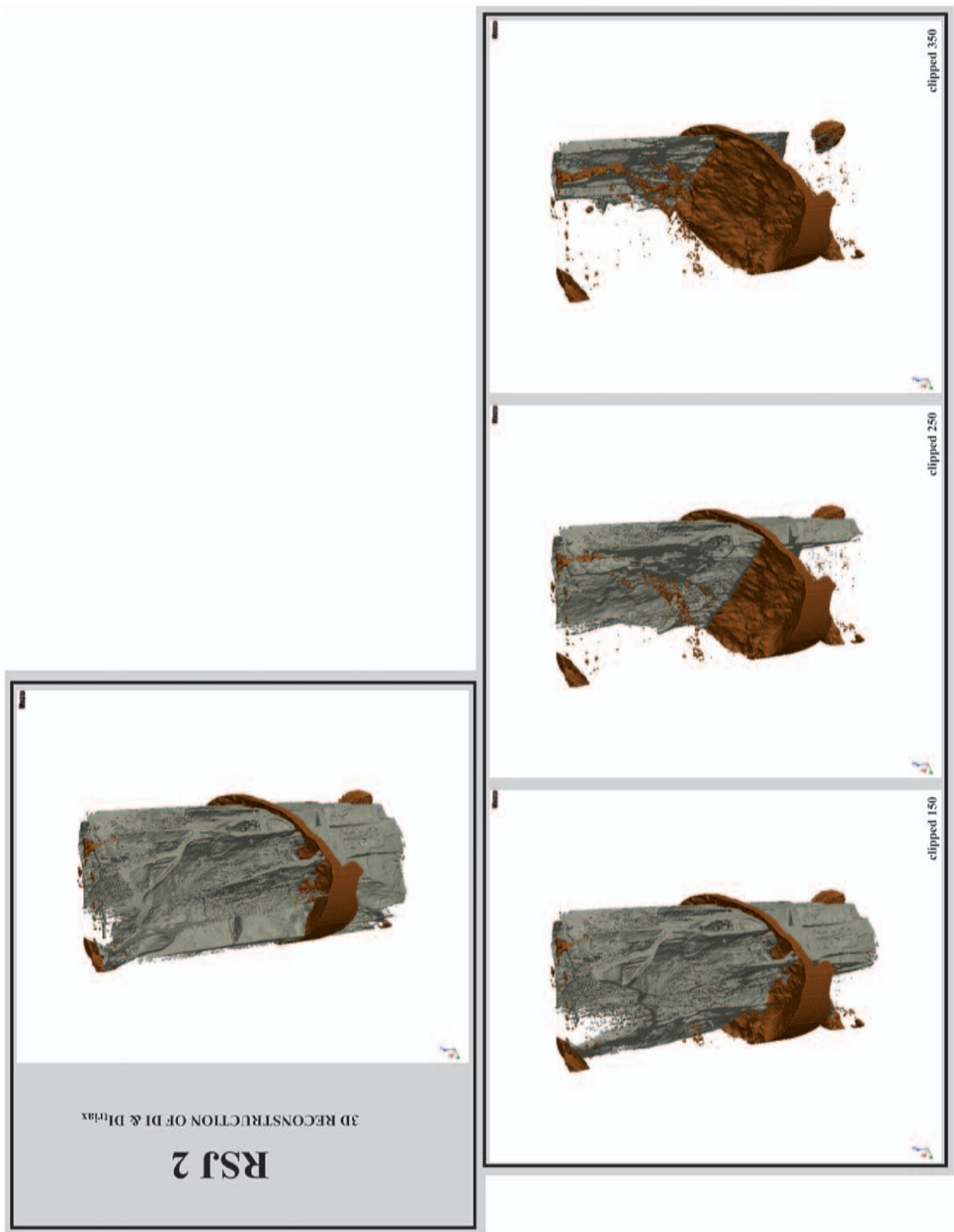
3D RECONSTRUCTION OF DI_{triax} WITH SUPERPOSITION OF INITIAL DI (RSJ SAMPLES CLASSIFIED BY MECHANICAL BEHAVIOR)

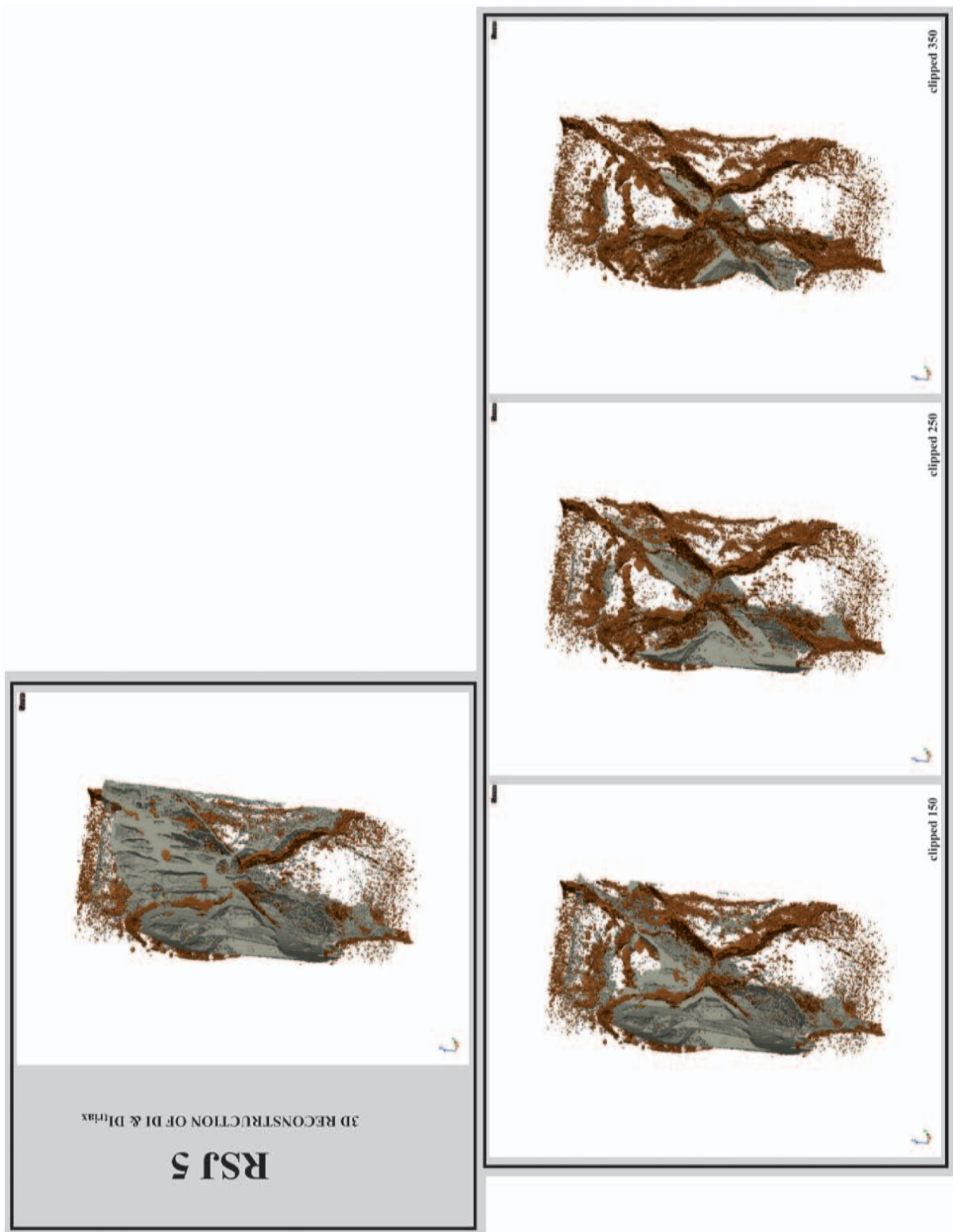


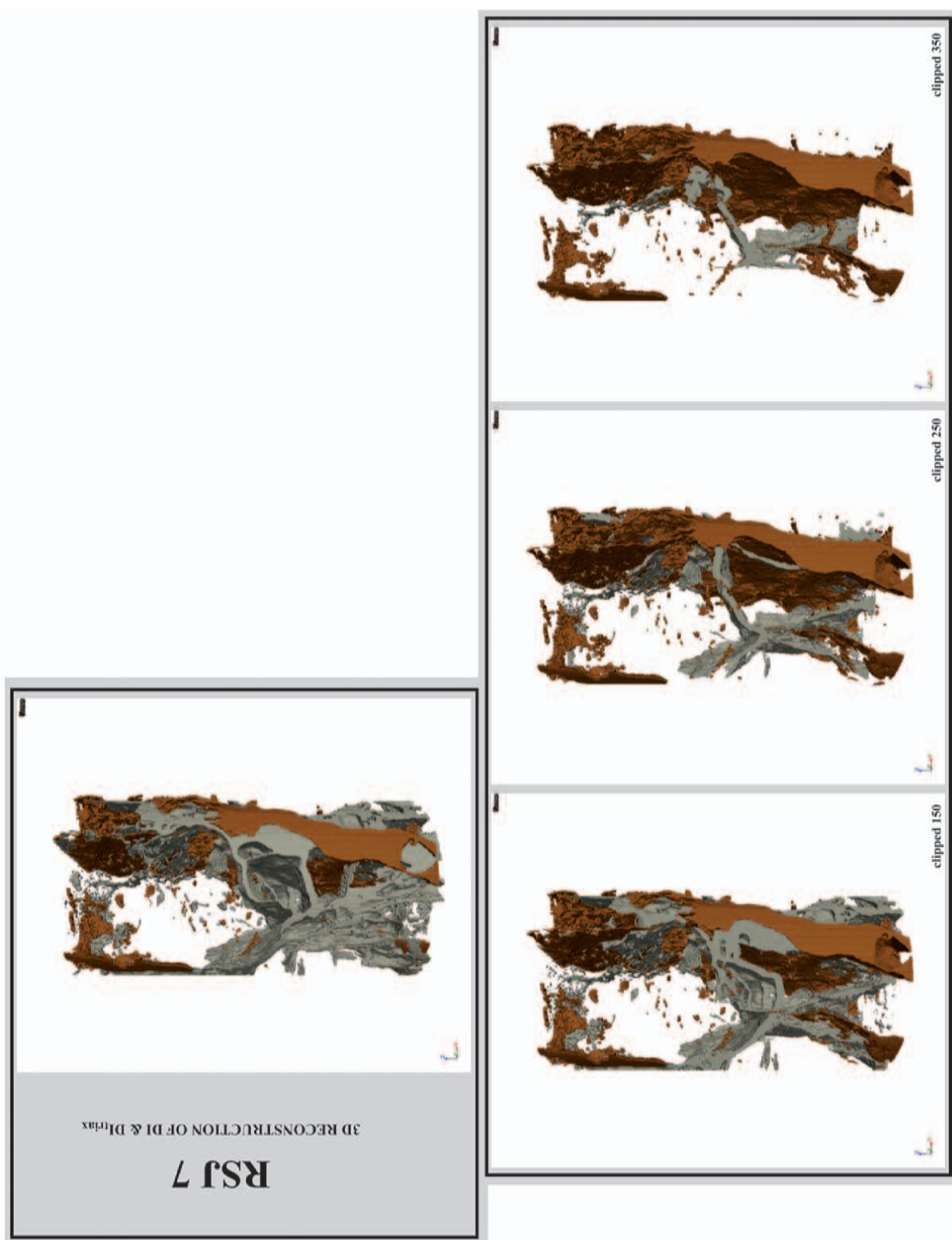




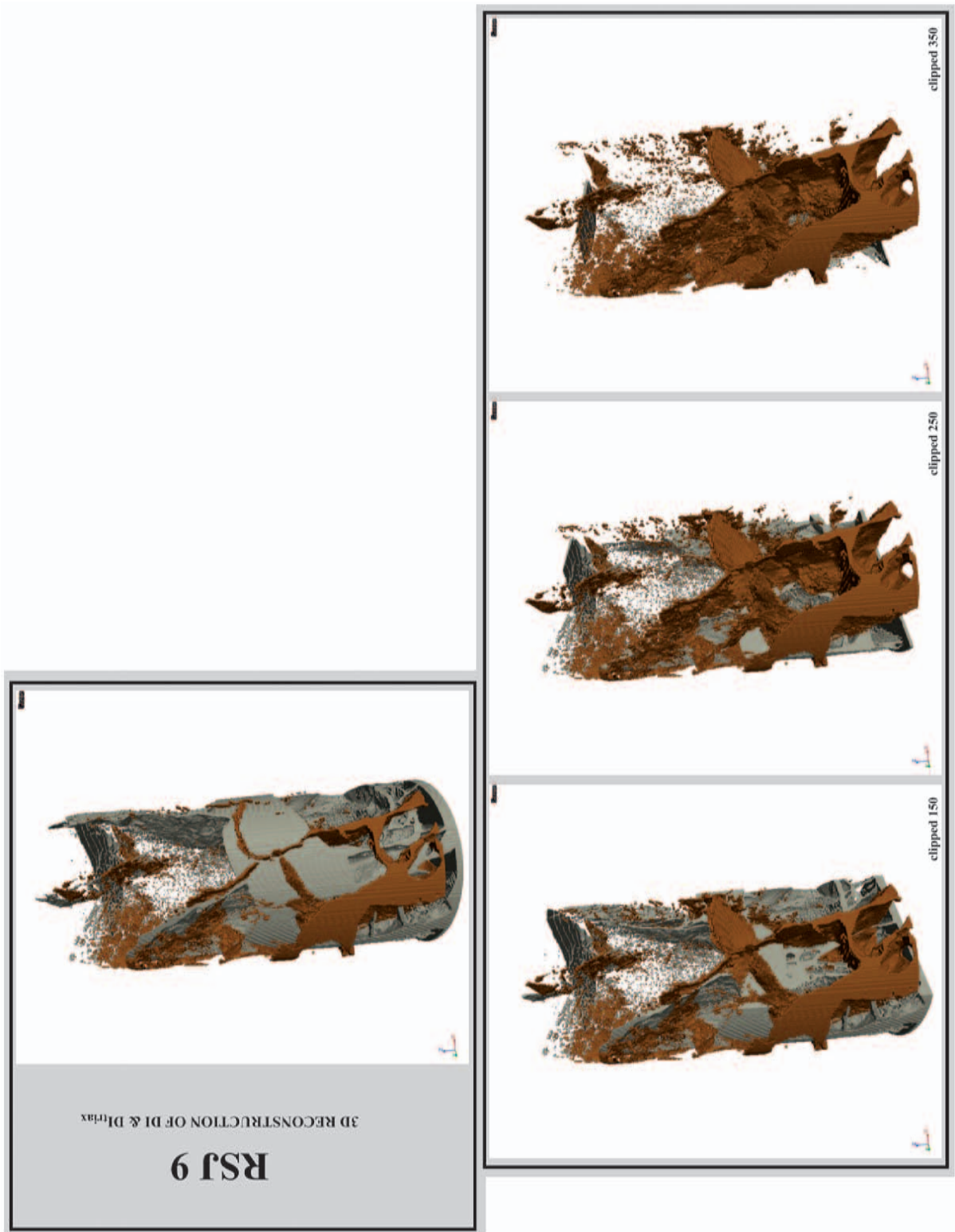


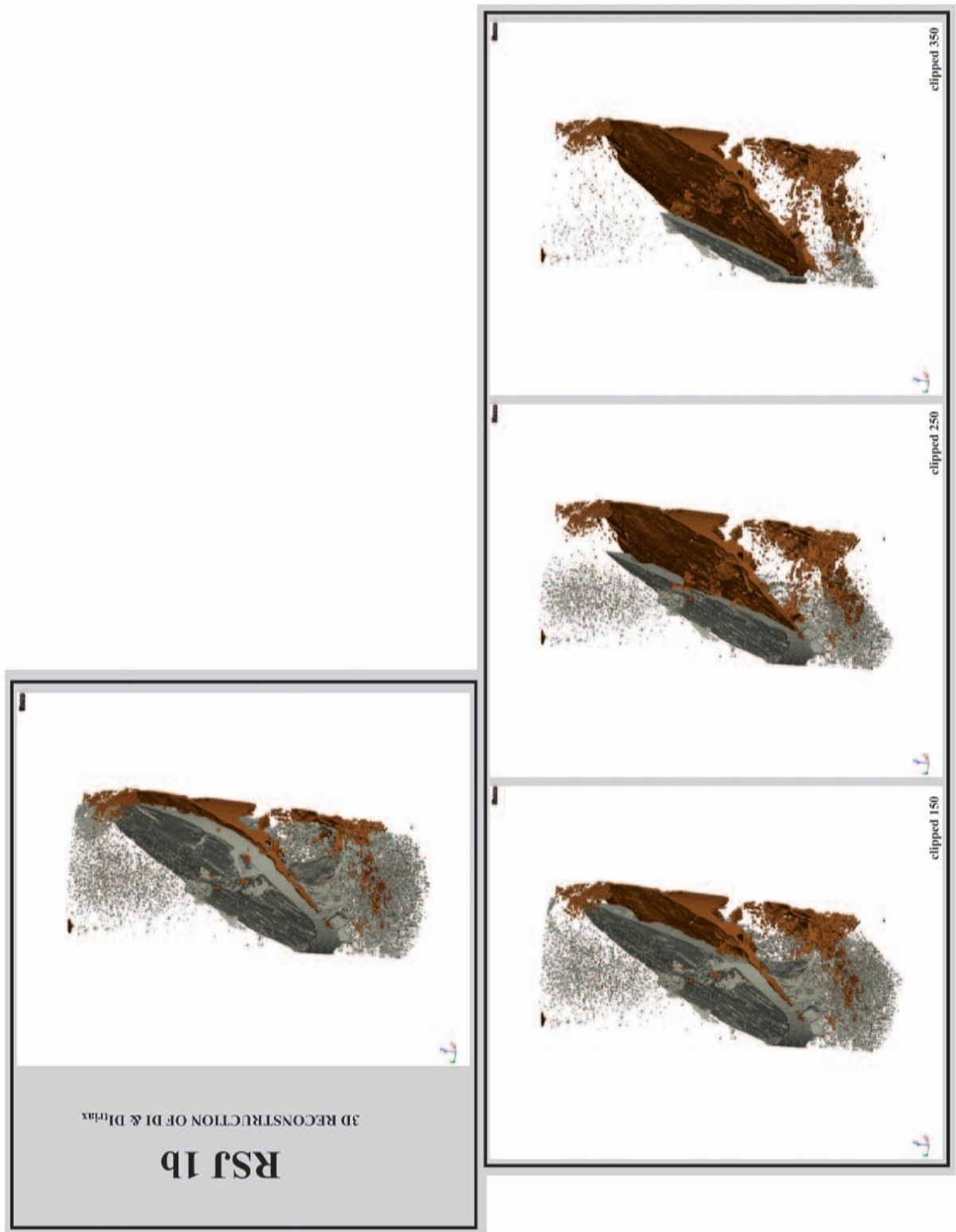


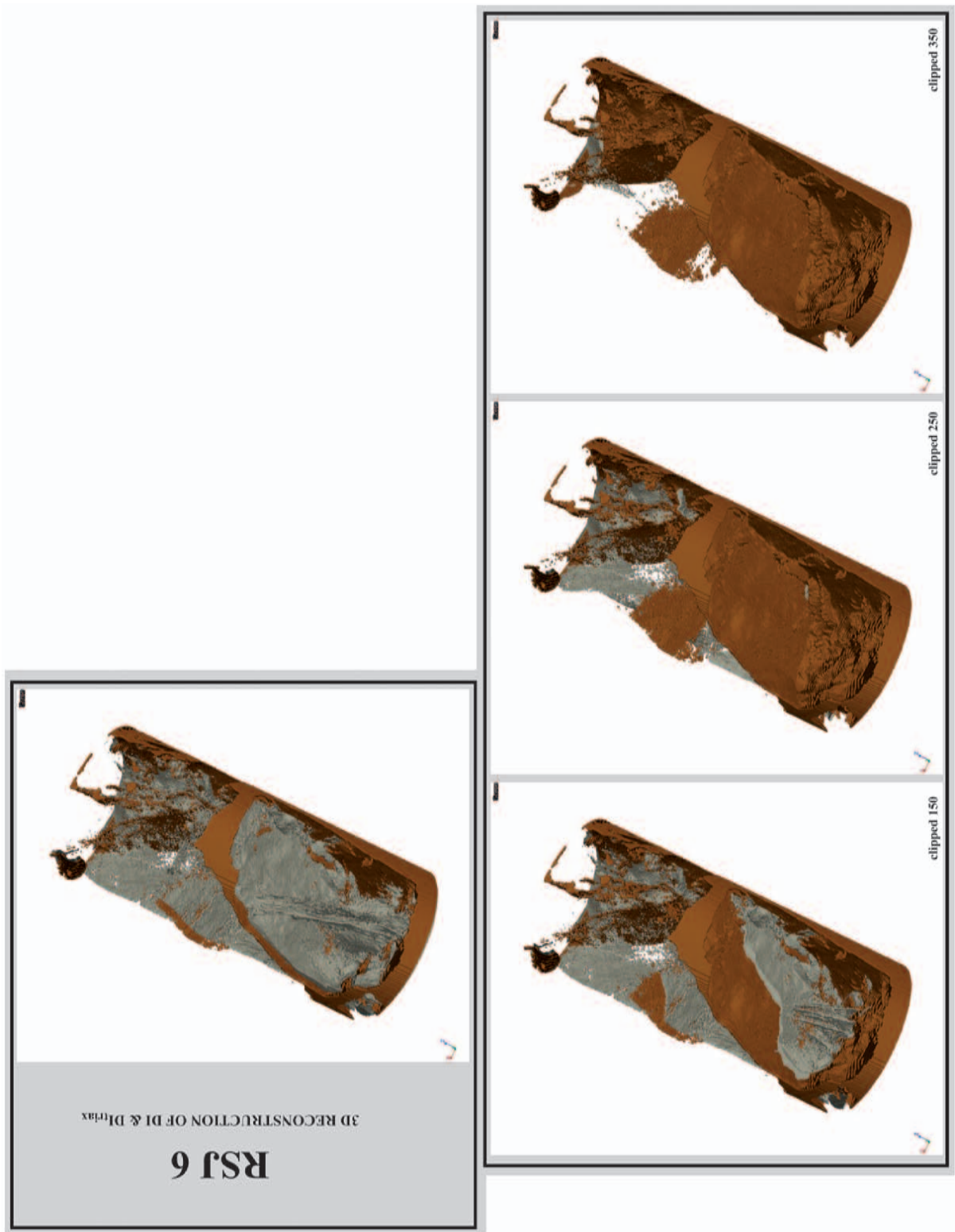


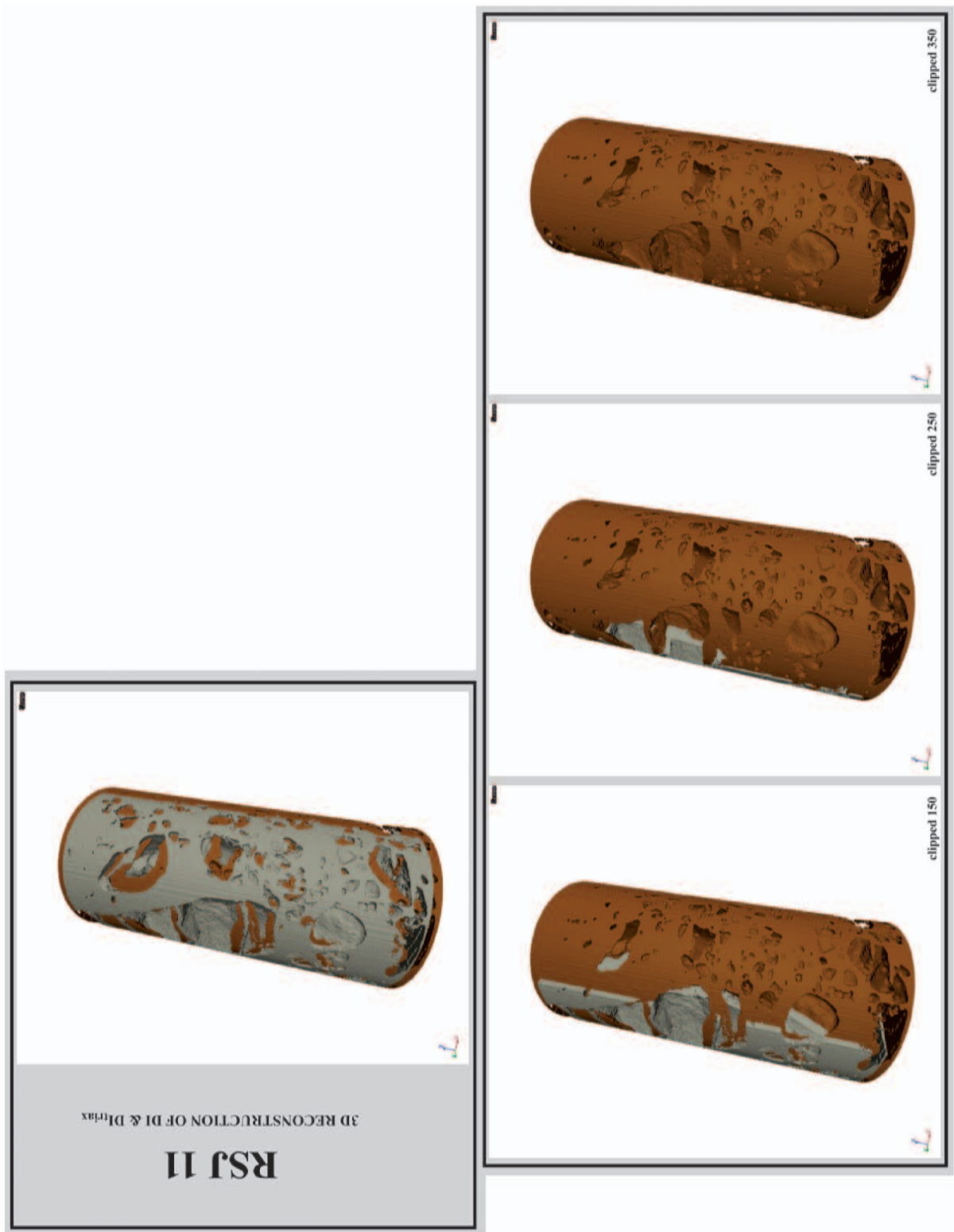


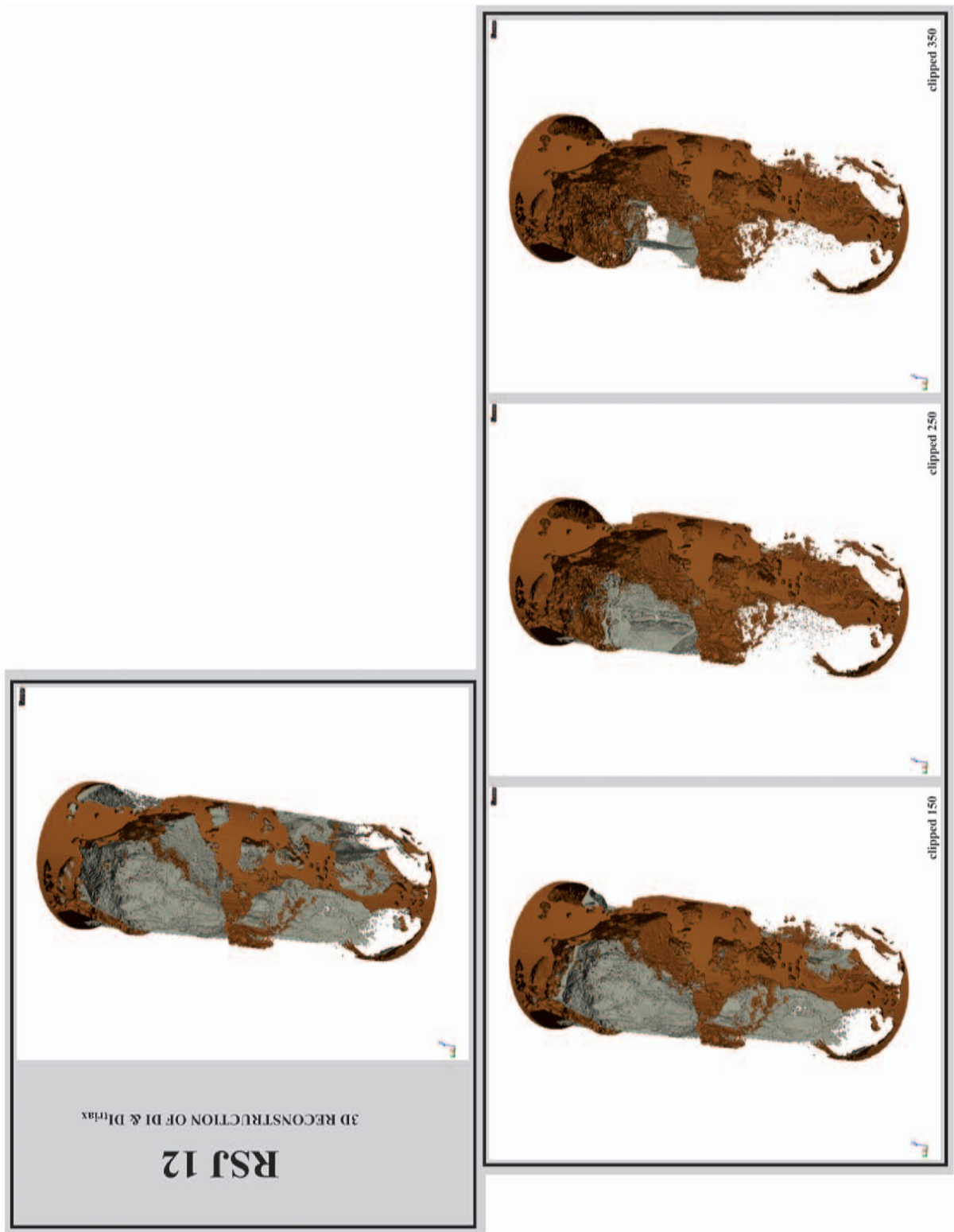




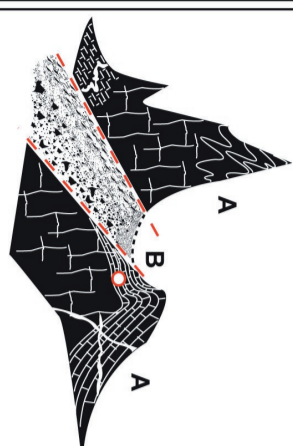












Fault-Zones at shallow crustal condition, brittle deformation & cataclastic flow. SCALE-INDEPENDENT BINARY REPRESENTATION OF FRACTURATION PROCESS. COMPARATIVE CHART.

| MODEL | LEVEL OF OBSERVATION (FAULT PROCESS DIAGNOSIS) | PARAMETERS (DAMAGE INDICATORS) | IMPLICATION FOR ROCK MASS | TERMINOLOGY FOR ROCK MASS ELEMENTS |
|--|--|---|---|--|
| <p>REGIONAL kilometers</p>  <p>OUTCROP meters</p>  | <p>FRACTURE = FAULT ZONE</p> <ul style="list-style-type: none"> - Fault Zone Type - Fault Zone Anatomy - Fault Zone Thickness & Depth - Fault Zone Composition - Fault Zone Mechanisms - Tectonic Evolution of Fault Zone - Implication of Fault Zone on the hydrological & hydrothermal regime - Relationships to Host (intact) Rock Mass <p>FRACTURE = FAULT</p> <ul style="list-style-type: none"> - Fault Type - Fault Geometry & Structure - Fault Variability; Fault Core vs. Damaged Zone, Gradational Profile - Composition of Fault Materials - Dry vs. Wet Faults, Weathering - Relationships to Host (intact) Rock Mass | <ul style="list-style-type: none"> - Compressional vs. Extensional Setting - Shear Rate - Shear Amount - Shear Conditions - REGIONAL Stress Field - Offsets - Strain Level, Localization & Accomodation - Type of Deformations - Implications of Deformations (Stability, Fluid Circulation, Large-Scale Inhomogeneities) <p>FRACTURE = FAULT</p> <ul style="list-style-type: none"> - Shear vs. Rock Mass - Density/Persistence of Discontinuities - LOCAL Stress Field - Offsets - Degree of Structural Complexity - Type of Deformations - Implications of Deformations (Stability, Fluid Circulation, Small-Scale Inhomogeneities) | <p>A) INTACT Rock Mass (Peripheral Strain)</p> <p>B) DAMAGED Rock Mass (Penetrative Strain)</p> <p>HOMOGENEOUS</p> <ul style="list-style-type: none"> - brittle deformation - fracturing <p>HETEROGENEOUS</p> <ul style="list-style-type: none"> - brittle deformation - cataclastic flow through fracturing, crushing and rotation of rock fragments <p>INTACT Rock Rheology</p> <p>FRACTURED Rock Rheology (e.g. no more direct function of lithological composition)</p> <p>ELASTIC & PLASTIC DEFORMATIONS</p> <p>VISCO-ELASTIC & VISCO-PLASTIC DEFORMATIONS</p> <p>"BLOCK - DISCONTINUITY" Model</p> <p>"CLASTS IN FINE-GRAINED MATRIX" Model</p> | <p>A) INTACT Rock Mass ("petrogenetic")</p> <p>B) DAMAGED Rock Mass ("detritic")</p> <p>ROCK MATRIX</p> <p>FINE-GRAINED MATRIX (e.g. Cataclastic Matrix)</p> <p>DISCONTINUITIES / FRACTURES</p> <p>DISCONTINUITIES / FRACTURES</p> <p>BLOCKS / CLASTS / FRAGMENTS OF</p> <p>BLOCKS / CLASTS / FRAGMENTS OF:</p> <p>1) DAMAGED Rock (e.g. Cataclastic Blocks, internally disturbed)</p> <p>2) INTACT Rock (e.g. Intact Blocks, no internal deformation)</p> |
| <p>SAMPLE centimeters</p>  <p>XRCT millimeters</p>  <p>THIN SECTION micrometers</p>  | <p>FRACTURE = FAULT BAND, FAULT PLANE</p> <ul style="list-style-type: none"> - Intact Rock Materials vs. Damaged Rock Materials - Categorization of Structural State of Rock Materials - Structural and Textural Evidence of Fracture Types - Other Structures - Assumptions on Isotropic/Anisotropic Nature of Material <p>INDIRECT OBSERVATION (X-ray irradiation):</p> <ul style="list-style-type: none"> - on Intact or Damaged Rock Material - BEFORE or AFTER mechanical testing - Based on Density Contrasts (Features Of Interest (FOI) vs. Undifferentiated Matrix) - 2D & 3D Visualization of Structural/Textural Relationships <p>MICROSCOPIC OBSERVATION (polarized light):</p> <ul style="list-style-type: none"> - on Intact or Damaged Rock Material - Petrographical Nature of Materials - Equilibrium/Disequilibrium Mineral Assemblages - Interpretation of Microstructures - 2D Visualization of Structural/Textural Relationships | <ul style="list-style-type: none"> - Cracks (open, filled, recrystallized) - Joints, Joint surfaces - Veins, Anastomosing Fractures - Shear Bands - Stylolith (transpressive) - Slickenside (transmissive) - Schistosity - Foliation - Breccia Texture - Gouge Texture - Grain Size Variability - Clay content <p>Directional Anisotropy</p> <p>ADDITIONAL</p> <ul style="list-style-type: none"> - Primary Pores, Voids - Determination of Porosity/Permeability - Consistency - Alteration Zone, Physico-Chemical Weathering, Mineral Grains Zonations - Density Contrasts - Preferred Orientation of Mineral Grains (for example Quartz c-axis) <p>To be translated into STRENGTH REDUCTION PARAMETERS Mechanical Strength Analysis (Compressive vs. Extensive Strength)</p> | | |

